

University of Warwick institutional repository: <http://go.warwick.ac.uk/wrap>

A Thesis Submitted for the Degree of PhD at the University of Warwick

<http://go.warwick.ac.uk/wrap/59733>

This thesis is made available online and is protected by original copyright.

Please scroll down to view the document itself.

Please refer to the repository record for this item for information to help you to cite it. Our policy information is available from the repository home page.

Library Declaration and Deposit Agreement

1. STUDENT DETAILS

Please complete the following:

Full name: Jason Blair Jones

University ID number: 0962715

2. THESIS DEPOSIT

2.1 I understand that under my registration at the University, I am required to deposit my thesis with the University in BOTH hard copy and in digital format. The digital version should normally be saved as a single pdf file.

2.2 The hard copy will be housed in the University Library. The digital version will be deposited in the University's Institutional Repository (WRAP). Unless otherwise indicated (see 2.3 below) this will be made openly accessible on the Internet and will be supplied to the British Library to be made available online via its Electronic Theses Online Service (EThOS) service.

[At present, theses submitted for a Master's degree by Research (MA, MSc, LL.M, MS or MMedSci) are not being deposited in WRAP and not being made available via EThOS. This may change in future.]

2.3 In exceptional circumstances, the Chair of the Board of Graduate Studies may grant permission for an embargo to be placed on public access to the hard copy thesis for a limited period. It is also possible to apply separately for an embargo on the digital version. (Further information is available in the *Guide to Examinations for Higher Degrees by Research*.)

2.4 If you are depositing a thesis for a Master's degree by Research, please complete section (a) below. For all other research degrees, please complete both sections (a) and (b) below:

(a) Hard Copy

I hereby deposit a hard copy of my thesis in the University Library to be made publicly available to readers (please delete as appropriate) EITHER immediately OR after an embargo period of ... 2 years months/years as agreed by the Chair of the Board of Graduate Studies.

I agree that my thesis may be photocopied. YES / ~~NO~~ (Please delete as appropriate)

(b) Digital Copy

I hereby deposit a digital copy of my thesis to be held in WRAP and made available via EThOS.

Please choose one of the following options:

EITHER My thesis can be made publicly available online. ~~YES~~ / ~~NO~~ (Please delete as appropriate)

OR My thesis can be made publicly available only after[date] (Please give date) **1 January 2016**
YES / ~~NO~~ (Please delete as appropriate)

OR My full thesis cannot be made publicly available online but I am submitting a separately identified additional, abridged version that can be made available online.
~~YES~~ / ~~NO~~ (Please delete as appropriate)

OR My thesis cannot be made publicly available online. ~~YES~~ / ~~NO~~ (Please delete as appropriate)

3. **GRANTING OF NON-EXCLUSIVE RIGHTS**

Whether I deposit my Work personally or through an assistant or other agent, I agree to the following:

Rights granted to the University of Warwick and the British Library and the user of the thesis through this agreement are non-exclusive. I retain all rights in the thesis in its present version or future versions. I agree that the institutional repository administrators and the British Library or their agents may, without changing content, digitise and migrate the thesis to any medium or format for the purpose of future preservation and accessibility.

4. **DECLARATIONS**

(a) I DECLARE THAT:

- I am the author and owner of the copyright in the thesis and/or I have the authority of the authors and owners of the copyright in the thesis to make this agreement. Reproduction of any part of this thesis for teaching or in academic or other forms of publication is subject to the normal limitations on the use of copyrighted materials and to the proper and full acknowledgement of its source.
- The digital version of the thesis I am supplying is the same version as the final, hard-bound copy submitted in completion of my degree, once any minor corrections have been completed.
- I have exercised reasonable care to ensure that the thesis is original, and does not to the best of my knowledge break any UK law or other Intellectual Property Right, or contain any confidential material.
- I understand that, through the medium of the Internet, files will be available to automated agents, and may be searched and copied by, for example, text mining and plagiarism detection software.

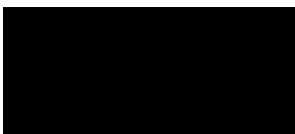
(b) IF I HAVE AGREED (in Section 2 above) TO MAKE MY THESIS PUBLICLY AVAILABLE DIGITALLY, I ALSO DECLARE THAT:

- I grant the University of Warwick and the British Library a licence to make available on the Internet the thesis in digitised format through the Institutional Repository and through the British Library via the EThOS service.
- If my thesis does include any substantial subsidiary material owned by third-party copyright holders, I have sought and obtained permission to include it in any version of my thesis available in digital format and that this permission encompasses the rights that I have granted to the University of Warwick and to the British Library.

5. **LEGAL INFRINGEMENTS**

I understand that neither the University of Warwick nor the British Library have any obligation to take legal action on behalf of myself, or other rights holders, in the event of infringement of intellectual property rights, breach of contract or of any other right, in the thesis.

Please sign this agreement and return it to the Graduate School Office when you submit your thesis.

Student's signature:  Date: 6 January 2014

Investigation of Laser Printing for 3D Printing and Additive Manufacturing

Jason Blair Jones

A thesis submitted for the degree of
Doctor of Philosophy

Warwick Manufacturing Group (WMG)
The University of Warwick
Coventry, United Kingdom

Sept 2013

© 2013. All rights reserved.

Table of Contents

Table of Contents	i
List of Samples	viii
List of Tables	x
List of Figures	xii
Acknowledgements	xxiii
Declaration	xxiv
Summary	xxv
Research Outputs	xxvi
Abbreviations and Definitions	xxxii
1. Introduction	1
1.1. Dry Toner, Not Liquid Ink	2
1.2. Aims and Objectives	3
1.3. Funding For This Research.....	3
1.4. Overview of the Research	4
Literature Review	7
2. Additive Manufacturing	9
2.1. Introduction	9
2.2. Layer by Layer Concept.....	10
2.3. The Digital Step: Patterning Energy or Material	11
2.4. Drive Toward AM of Multi-material Parts/Systems	14
2.5. Empowering 3D Printing with 2D Printing	15
3. Electrophotography	17
3.1. Introduction to Electrophotography	17
3.1.1. Materials Overview	17

3.1.2.	Brief History.....	20
3.1.3.	EP Process Overview: 7 steps.....	26
3.2.	Toner and Carrier Preparation and Measurement	29
3.2.1.	Toner Materials and Composition	30
3.2.1.1.	Non-conductive Toner	32
3.2.1.2.	Conductive Toner.....	38
3.2.1.3.	Photoconductive Toner	40
3.2.1.4.	Discussion of toner materials.....	42
3.2.2.	Pulverised Versus Polymerised	43
3.2.3.	Toner Size	47
3.2.3.1.	Classification	48
3.2.4.	Tribocharging Toner with Carrier.....	49
3.2.4.1.	Predicting Tribocharge Polarity – Triboelectric Series 52	
3.2.4.2.	Predicting Tribocharge Magnitude	55
3.2.4.3.	Measuring Toner Charge	57
3.2.4.4.	Non-uniform Nature of Toner Charging	59
3.3.	EP Physics and Principles	62
3.3.1.	Forces at Work in EP	62
3.3.1.1.	Electrostatic	63
3.3.1.2.	Electrodynamic (including van der Waals)	64
3.3.1.3.	Gravity	66
3.3.2.	Effect of Humidity and Temperature.....	66
3.4.	EP Process Steps and Hardware	68
3.4.1.	Charging and Corona	69
3.4.1.1.	Limitations of Corona Charging.....	71
3.4.2.	Exposure and Photoreceptor.....	72
3.4.2.1.	Trapped charges.....	75
3.4.3.	Development.....	77
3.4.3.1.	Fringe Field Effects = Edge Growth	82
3.4.4.	Transfer	86
3.4.4.1.	Effect of Transfer Gap and Geometry on Field Strength 91	
3.4.4.2.	Effect of Final Receiver on Electrostatic Transfer ...	91
3.4.4.3.	Transfer Challenges with Inherently Conductive Toners 93	
3.4.5.	Fusing	98

3.4.6.	Cleaning and Erasing	100
3.5.	EP (Toner) versus Inkjet (Liquid Ink)	101
4.	Convergence of EP and AM	107
4.1.	Transfer Method Evolution Toward AM by EP	107
4.2.	Indirect Use of EP in AM	108
4.2.1.	Cubital Ltd, Israel	109
4.2.2.	Kira Corporation, Japan	113
4.2.3.	Liu and Jang	114
4.2.4.	Sintermask	116
4.2.5.	Tan and Chua	117
4.3.	Electrostatic Transfer/Deposition	118
4.3.1.	Conventional Electrostatic Transfer	119
4.3.1.1.	Kumar et al.	119
4.3.1.2.	PEPperPRINT – Biochip printing	121
4.3.1.3.	Critical Review of Conventional Electrostatic Transfer Approaches	125
4.3.2.	Top Charging	127
4.3.2.1.	Kumar et al.	127
4.3.2.2.	Büttner and Krüger	130
4.3.2.3.	Critical Review of Top Charging	131
4.3.3.	Repulsion	133
4.3.3.1.	Jethon	134
4.3.3.2.	Wimpenny and Banerjee	135
4.3.3.3.	Critical Review of Repulsion	137
4.3.4.	Related approaches	140
4.3.4.1.	Nanoxerography	140
4.3.4.2.	Electrokinetic imaging	142
4.4.	Non-electrostatic Final Transfer (Heat and Pressure) 143	
4.4.1.	Bynum Proposes “Tackification”	144
4.4.2.	Grenda	146
4.4.3.	Cormier et al.	148
4.4.4.	Metal Printing Process (MPP) by Sintef	149
4.4.5.	Wimpenny et al.	151
4.4.5.1.	Scoping and feasibility trials	152
4.4.5.2.	Samples made by CTG PrintTec GmbH	155

4.4.5.3. Selective Laser Printing (SLP) Development Rig..	161
4.4.5.4. Laser Printed Electronics	168
4.4.6. Stratasys	168
4.4.7. Critical Review of Non-electrostatic Transfer Approaches	170
4.5. Others Who Have Considered EP and Related Techniques for AM	174
4.6. Summary and Analysis of Prior Art	176
4.6.1. AM Endeavours Using Direct Deposition by EP	179
4.6.2. AM by EP Challenges	181
4.7. Conclusions	184
Experimental Work	187
5. Toners and Printing Apparatuses	189
5.1. Toner Materials	190
5.2. Development	193
5.3. Printer Selection	194
5.4. Sample Shape and Size	195
5.5. Sample Set Populations and Analysis	198
5.5.1. Sample Set Population Size	198
5.5.2. Representation of Error in Graphs	199
5.6. Sample Substrates	200
5.7. Explanation of the Selective Laser Printing (SLP) Development Rig	200
5.7.1. Stage 1 – As Built in Custom-fit (Early 2009)	201
5.7.1.1. Infrared Heater and Temperature Sensor	205
5.7.1.2. Surface Potential Measurement	207
5.7.1.3. Pulsed DC Corona Device	211
5.7.1.4. Two-component Printers	213
5.7.1.5. Deposited Layer Height Measurement	218
5.7.1.6. Ambient Temperature and Humidity (not shown)	220
5.7.1.7. Platform and Substrate Arrangements	220
5.7.2. Stage 2 – After Refurbishment of Printers	221
5.7.2.1. AC Fan Ionizer	224
5.7.2.2. Heater Orientation	224
5.7.2.3. Two-component printers	225
5.7.2.4. Platform and Substrate Arrangements	228

5.7.3.	Stage 3 – Print to Ground and Build Sleeve	230
5.7.3.1.	Two-component printer with shifted voltages	230
5.7.3.2.	Enclosed build sleeve and Z-axis stiffening	233
5.8.	Explanation of the Electro-Magnetic Brush Evaluation Rig (EMBER) test rig	235
5.8.1.	Surface potential measurement.....	240
6.	Scoping Trials	243
6.1.	Further Analysis of Legacy Samples	243
6.1.1.	Manufacture of Legacy Samples	244
6.1.2.	Analysis of Legacy Samples	247
6.1.3.	Results and Discussion of Legacy SLP Sample Analysis	249
6.1.4.	Results and Discussion of EMB Sample Analysis .	252
6.1.5.	Conclusions From Legacy Sample Analysis.....	256
6.1.6.	Unanswered Questions from Legacy Sample Analysis	258
6.2.	Assessing the Performance of EP in Inert Atmospheres	260
6.3.	Evaluating Printers	261
6.3.1.	Two-component Printer Evaluation	261
6.3.1.1.	Multilayer Height Limit of Printing on Paper	262
6.3.1.2.	Post-print Assembly and Consolidation.....	267
6.3.1.3.	Conclusions from Two-Component Printer Trials .	275
6.3.2.	Single Component Printers	276
6.4.	Exploring a Range of Toner Composition	276
6.4.1.	Conventional toner	277
6.4.2.	Ceramics.....	277
6.4.2.1.	Commercial “Ceramic” Toner	278
6.4.2.2.	Ceramic Powder as a Negative Single Component Toner	280
6.4.2.3.	Ceramic Powder as a Positive Mono Component Toner	283
6.4.2.4.	Sand & Sugar	284
6.4.3.	Legacy Toner Materials Revisited.....	285
6.4.3.1.	Somos 201	285
6.4.3.2.	Epoxy	286

6.4.4.	High Performance Polymers	286
6.5.	Conclusions	286
7.	Discovery and Substantiation of Defect Causes.....	289
7.1.	Using Non-electrostatic Transfer	290
7.1.1.	Defects Using Conventional Toner	290
7.1.2.	Characterizing Surface Potential	293
7.1.2.1.	Discussion of Surface Potential (Non-electrostatic Transfer) 311	
7.1.3.	Considering Surface Energy and Pressure	320
7.1.4.	Summary of Defects Arising with Non-electrostatic Transfer.....	323
7.2.	Using Electrostatic Transfer.....	323
7.2.1.	Theoretical Modelling of Height Limitation	324
7.2.2.	Conventional Electrostatic Transfer	332
7.2.2.1.	Effect of Breakdown on Deposition	333
7.2.2.2.	Counteracting the Repulsive Effect of Residual Charge 335	
7.2.2.3.	Using Intermediate Conductive Layers.....	354
7.2.3.	Variations on Top Charging	371
7.3.	Pressure-free Electrostatic Transfer	376
7.4.	Summary and Conclusions	385
8.	Approaches to Controlling Charge	389
8.1.	Accumulating Residual Toner Charge	389
8.1.1.	Unexpected Evidence of Residual Charge	389
8.1.2.	Intentional Charge Trapping	392
8.1.3.	Proposed Model of Charge Trapping	409
8.2.	Approaches to Charge Neutralization	412
8.2.1.	Preliminary Exploration of Neutralizing Methods and Measurements.....	412
8.2.2.	Layer by Layer Neutralization	420
8.2.3.	Discussion of Neutralization Approaches	437
8.2.4.	Summary and Conclusions	438
9.	Assimilating Charge Neutralization and Electrostatic Transfer.....	441
9.1.	Conventional Electrostatic Transfer to 0V	442

9.1.1. Discussion of Printing to "Ground"	448
9.2. Feasibility of Repulsion with Neutralization	449
9.2.1. Discussion of Repulsion Feasibility	454
10. Conclusions and Further Work.....	457
10.1. Summary of Novelty	460
10.2. Summary of the Contribution to Knowledge:.....	462
10.3. Future Work	463
Appendix A: Timeline of AM and EP Convergence.....	471
Appendix B: Elucidating the Influence of Pressure Uniformity.....	472
Appendix C: The Influence of the Heater on Defect Formation	476
Appendix D: Two Interesting Facts About Electrophotography	479
Appendix E: 3D Photocopying Poster	480
References	483
Annex: Related Publications by the Author	501

List of Samples

Sample 6-1 The Largest Volume SLP Sample from Custom-fit	244
Sample 6-2 The Tallest SLP Sample from Custom-fit	246
Sample 6-3 EMB Sample Exceeding the 3mm Height Limit	247
Sample 6-4 Multilayer Two-component Print on Paper	262
Sample 6-5 Post-print Stacking and Sintering of Transfer Paper	270
Sample 6-6 Stack and Sinter Bulk Alumina between Paper	273
Sample 6-7 Pure Alumina as a Negative Toner	281
Sample 6-8 Surface Coated Alumina as a Negative Toner	282
Sample 6-9 Surface Coated Alumina as a Positive Toner	283
Sample 7-1 Registration Trials with Commercial Toner	290
Sample 7-2 Baseline for Sample with 5mm Shift Print Pattern	295
Sample 7-3 10min Delay Between Layers	298
Sample 7-4 Grounded Conductive Platform	301
Sample 7-5 Print Blank Images First	304
Sample 7-6 Grounded Conductive Substrate and Platform	307
Sample 7-7 Plasma Treated Toner Layers	320
Sample 7-8 First Layer Defects	333
Sample 7-9 First Conventional Transfer	338
Sample 7-10 Half Conventional/Half Tackification Transfer	340
Sample 7-11 Maximum 3,000V Transfer	342
Sample 7-12 Print All Day Long	343
Sample 7-13 Doubling the Distance to the Counter Electrode	347
Sample 7-14 Printing onto Taped Down Al Foil	355
Sample 7-15 Printing onto Glued and Taped Al Foil	355
Sample 7-16 Printing onto Al Plate with Low Voltage	356
Sample 7-17 Printing onto Al Foil Covered by Tape	357
Sample 7-18 Printing onto a Stack of Copper-clad Board	359
Sample 7-19 Capacitively Coupling to Conductive Layers	360
Sample 7-20 Embedding Wires	364
Sample 7-21 Insulated Wires at the Build Surface	365
Sample 7-22 Gold Sputtering	367
Sample 7-23 Conductive Polymer Layers	368
Sample 7-24 Brine Layers	369
Sample 7-25 Top Charging with Positive Pulsed DC Corona	371
Sample 7-26 Top Charging with Negative Pulsed DC Corona	372
Sample 7-27 Top Charging with Field Attracted Positive Ions	373

Sample 7-28 Conventional Electrostatic Transfer onto Conductive Substrates	376
Sample 7-29 Conventional Electrostatic Transfer onto Non-conductive Substrates	379
Sample 7-30 Top Charging by Tribocharging	381
Sample 7-31 Selective Contact Charging of the Substrate	383
Sample 7-32 High Voltage Global Contact Charged Sample	384
Sample 8-1 Macroscale Simulation of Residual Toner Charge Decay	392
Sample 8-2 Print onto Film	394
Sample 8-3 Printing onto Tape	395
Sample 8-4 Toner on Tape	396
Sample 8-5 More Toner on Tape	399
Sample 8-6 Volume Charged Cantilever	402
Sample 8-7 Measuring Residual Charge in Legacy Samples	406
Sample 8-8 Neutralize by Contact with Grounded Al Plate	413
Sample 8-9 Neutralize by High Voltage Discharge Through a Body	413
Sample 8-10 Neutralize by AC Discharge Through a Body	413
Sample 8-11 Neutralize by Immersion in a Liquid	414
Sample 8-12 Neutralize Surfaces by AC Fan Ionizer	416
Sample 8-13 Neutralize by AC Ionizer before Fusing	416
Sample 8-14 Non-contact Electrostatic Voltmeter Measurements	417
Sample 8-15 Neutralize by Flame	419
Sample 8-16 Baseline Sample without Neutralization	421
Sample 8-17 Neutralize by AC Ions Only	422
Sample 8-18 Neutralize by AC Ions and Transfer Corona	422
Sample 8-19 Neutralize by Transfer Corona Only	422
Sample 8-20 Blank Prints then No Neutralization	425
Sample 8-21 Prime by Conventional Transfer, No Neutralization	426
Sample 8-22 Conventional Transfer with Flame Neutralization	430
Sample 8-23 Pseudo-Piezoelectric Behaviour of Toner	436
Sample 9-1 Print onto Grounded Conductive Substrate	442
Sample 9-2 Print onto Non-conductive Substrate (Near Ground)	443
Sample 9-3 Print onto Non-conductive Substrate (Away from Ground)	444
Sample 9-4 Transfer Corona Near and Away from Ground	445
Sample 9-5 Defects from Touching the Underside of the Substrate	449
Sample 9-6 Intentionally Repelling Toner Off the Substrate	450
Sample 9-7 Repulsion with and without a Counter Electrode	452

List of Tables

Table 1.1 – Tabular Overview of the PhD	5
Table 2.1 – The Digital Step of AM Process Categories	12
Table 3.1 – Triboelectric Series*	54
Table 3.2 – Comparing* Inkjet and EP	102
Table 4.1 – Summary of AM Approaches Utilizing EP for Direct Deposition	177
Table 4.2 – Summary of Challenges Encountered	178
Table 5.1 – Typical Printer Settings: Polyester Toner	216
Table 5.2 – Typical Printer Settings: Epoxy Toner.....	228
Table 5.3 – Summary of 1 st Printer Voltage Shift and Re-wiring	231
Table 5.4 – Progress Toward Printing with Voltage Shift	232
Table 6.1 – EDS of contamination in Sample 6-3.....	254
Table 6.2 – EDS of Fired Portion of Sample 6-5	272
Table 6.3 – EDS of Fired Portion of Sample 6-6	275
Table 7.1 – Printer Settings: Commercial Polyester Toner	291
Table 7.2 – Experimental Regime for Surface Potential Characterization.....	295
Table 7.3 – Summary of Surface Potential Characterization Results.....	311
Table 7.4 – Values for Figure 7.17.....	326
Table 7.5 – Values for Figure 7.19.....	330
Table 7.6 – Experimental Regime using Conventional Electrostatic Transfer	337
Table 7.7 – Sample 7-9 Preparation and Results	338
Table 7.8 – Sample 7-10 Preparation and Results	340
Table 7.9 – Sample 7-11 Preparation and Results	342
Table 7.10 – Sample 7-12 Preparation and Results	344
Table 7.11 – Sample 7-13 Preparation and Results	348
Table 7.12 – Summary of Conventional Electrostatic Transfer Results	349
Table 7.13 – Sample 7-14 Results and Discussion	355
Table 7.14 – Sample 7-15 Results and Discussion	356
Table 7.15 – Sample 7-16 Results and Discussion	357
Table 7.16 – Sample 7-17 Results and Discussion	358
Table 7.17 – Sample 7-18 Results and Discussion	360
Table 7.18 – Sample 7-19 Results Compared to Sample 7-13	362
Table 7.19 – Sample 7-20 Results and Discussion	365
Table 7.20 – Sample 7-21 Results and Discussion	366
Table 7.21 – Sample 7-22 Results and Discussion	367
Table 7.22 – Sample 7-23 Results and Discussion	368
Table 7.23 – Sample 7-24 Results and Discussion	369

Table 7.24 – Sample 7-25 Results and Discussion	372
Table 7.25 – Sample 7-26 Results and Discussion	373
Table 7.26 – Sample 7-27 Results and Discussion	374
Table 7.27 – Sample 7-28 Preparation Parameters	377
Table 7.28 – Sample 7-28 Results and Discussion	378
Table 7.29 – Sample 7-29 Preparation Parameters	379
Table 7.30 – Sample 7-29 Results and Discussion	380
Table 7.31 – Sample 7-30 Results and Discussion	381
Table 7.32 – Sample 7-31 Results and Discussion	383
Table 7.33 – Sample 7-32 Results and Discussion	384
Table 7.34 – Summary of Defects Substantiated in §7	386
Table 8.1 – Sample 8-2 Results and Discussion	395
Table 8.2 – Sample 8-3 Results and Discussion	396
Table 8.3 – Sample 8-4 Results and Discussion	397
Table 8.4 – Summary of Sample 8-5 Specimens	399
Table 8.5 – Sample 8-5 Results and Discussion	400
Table 8.6 – Results of Sample 8-5 Specimens on Day 2	401
Table 8.7 – Sample 8-6 Results and Discussion	404
Table 8.8 – Sample 8-7 Results and Discussion	407
Table 8.9 – Sample 8-10 Results and Discussion	414
Table 8.10 – Sample 8-11 Results and Discussion	415
Table 8.11 – Sample 8-14 Results and Discussion	418
Table 8.12 – Sample 8-15 Results and Discussion	420
Table 8.13 – Matrix to Evaluate Neutralization by Transfer Corona and AC Ionizer	421
Table 8.14 – Results and Discussion for Sample 8-16 to Sample 8-19	423
Table 8.15 – Sample 8-15 Results and Discussion	426
Table 8.16 – Results and Discussion: 60-layer Sample 8-21	427
Table 8.17 – Results and Discussion for Sample 8-22	431
Table 8.18 – Evidence of Toner Leaving 40-layer Sample 8-22	435
Table 9.1 – Sample 9-2 Results and Discussion	443
Table 9.2 – Sample 9-3 Results and Discussion	445

List of Figures

Figure 2.1 – AM Technology families by patterning method.....	13
Figure 2.2 – Volume/value of system output by patterning method.....	13
Figure 3.1 – Optical microscope images of toner in the laser printed word “toner”	18
Figure 3.2 – Illustration of photoconductive behaviour in light and darkness.....	20
Figure 3.3 – First image developed and preserved using the principles of EP, courtesy of Xerox Corporation [44].....	24
Figure 3.4 – The Xerox 914, the first automatic office copier to make copies on plain paper, courtesy of Xerox Corporation [45]	25
Figure 3.5 – Xerox Telecopier 200: First laser, plain-paper fax machine (left) [47]; Xerox 9700: First xerographic laser printer (right) [48], both courtesy of Xerox Corporation	26
Figure 3.6 – Illustration of the charging and exposing steps in EP	27
Figure 3.7 – Illustration of the development, transfer and fusing steps in EP	28
Figure 3.8 – Illustration of all 7 steps used in a typical EP device.....	29
Figure 3.9 – 100X magnification of toner showing the black pigments in a partially melted (and resolidified) translucent polymer matrix.....	32
Figure 3.10 – Electron behaviour in a conductor and dielectric material resulting in charge separation and dielectric polarization respectively.	35
Figure 3.11 – Figures 3-5 from US Patent 3,764,312 [104] showing the spraying of fused toner to achieve a conductive state.....	42
Figure 3.12 – Conventionally pulverized vs. chemically polymerized toner preparation (after [112])	45
Figure 3.13 – Mechanically pulverized toner (left [37] and lower right [113]) compared to chemically polymerized toner (upper right [113]).....	45
Figure 3.14 – Illustration of toner on carrier (left), and SEM image [37] of toner on a large carrier bead (right)	52
Figure 3.15 – Scatter Plot of 4000 toner particles showing charge versus size [155]	59
Figure 3.16 – SEM images of high adhesion (top row), light adhesion (middle row) and stacked toner particles (bottom) by Whitney & Kemp [164].....	61
Figure 3.17 – Electrical resistivity of a powder at elevated temperature and humidity [172]	67
Figure 3.18 – Schematic of EP printing [173].....	68
Figure 3.19 – The Paschen discharge limit in air as a function of gap size [46].....	71
Figure 3.20 – Map showing available and most used (indicated within the rhombus) development options (after [194]).....	77
Figure 3.21 – A two-component magnetic brush developer (after [108])	78

Figure 3.22 – Toned carrier on the magnetic brush (inspired by [62]).....	79
Figure 3.23 – Perpendicular electric field component at the centre of a line charge plotted versus the width of the line (From reprint of [202] in [108, 205])	83
Figure 3.24 – Latent image charge on the photoreceptor and its influence on line versus solid area development (after Figure 1 in [204])	83
Figure 3.25 – Image showing the solid area field strength without an electrode (a), with a grounded electrode (b), and with a biased electrode (c) (Fig 2.7 from [108])	85
Figure 3.26 – Conventional electrostatic transfer developed by Schaffert (Adapted from [215])	87
Figure 3.27 – Cross-section through a sheet of paper ~90µm thick showing the simulated magnitude of the z-component of the electric field (top) and SEM image (bottom) [225]	92
Figure 3.28 – Behaviour of conductive powder particles in between conductive and insulative electrode surfaces (After figure 5-13 from [181])	96
Figure 3.29 – Electrostatic repulsion created by an encapsulated polarized conductive toner particle during an electrostatic transfer step - After Walker et al. [103]	97
Figure 4.1 – Timeline: Development of Additive Manufacturing by Electrophotography ..	107
Figure 4.2 – Conventional electrostatic transfer onto flexible (left) and rigid (right) substrates (© Society for Imaging Science and Technology [244])	109
Figure 4.3 – Overview of the solid ground curing (SGC) process [252]	110
Figure 4.4 – Image showing the use of a mask (#58) to selectively cure the top layer (#62) of a part, Figure 1C from [246]	112
Figure 4.5 – Image showing the use of toner on a glass slide (#264) as a mask for UV curing a layer in a cross-shaped part, Figure 1.18 from [245]	112
Figure 4.6 – Laminated object manufacture using laser printed toner as an adhesive [255]	113
Figure 4.7 – Liu and Jang [256] patent (Figure 3) showing the use of electrostatically deposited toner as a binder on a powder bed.....	115
Figure 4.8 – Image showing the use of toner on a glass slide as a mask for IR sintering the upper-most layer of a part in a powder bed [258]	116
Figure 4.9 – Repulsion transfer of toner onto a powder bed (after [259]).....	118
Figure 4.10 – Electric field strength versus print height [261].....	120
Figure 4.11 – Illustration of the synthesis of a multilayer peptide array on a glass slide [274]	122
Figure 4.12 – Printer schematic and array of printers for biochip fabrication [274].....	123
Figure 4.13 – Self-limiting nature of multilayer printing when using a conventional electrostatic final transfer step where voltage is fixed (by the dielectric breakdown strength of air) (modified from author’s original, in [244])	126
Figure 4.14 – Top Charging transfer method steps as employed by Kumar et al. (© Society for Imaging Science and Technology [244]).....	128

Figure 4.15 – Repulsion transfer deposition steps a) attract the toner off of the photoconductor and onto the transfer belt; b) repel the toner off of the belt and onto the stacked layers..... 134

Figure 4.16 – Schematic of a Laser Printer Concept for AM where the toner is repelled off of the transfer belt using a strong field [279]..... 135

Figure 4.17 – Repulsion transfer efficiency as demonstrated by Banerjee [211]..... 136

Figure 4.18 – Nanoxerography charging means (left); Nanoparticle assembly module (right) [282] 141

Figure 4.19 – Detail from Figure 4.18 showing nanoparticles attracted to charged areas (left); Actual accumulation of nanoparticles on substrate with a 300nm width [282] 141

Figure 4.20 – Discrete components patterned using electrokinetic imaging [287]..... 143

Figure 4.21 – Apparatus for the direct transfer and lamination of powdered layers as proposed by Bynum (FIG 2A from [288]) 145

Figure 4.22 – Conceptual illustration of the final transfer step by Bynum based on making layers tacky or sticky (© Society for Imaging Science and Technology [244])..... 145

Figure 4.23 – Schematic of a 3D Laser Printer Concept by Grenda [291]..... 147

Figure 4.24 – 3D Laser Printer test rig and parts by Grenda [291] 147

Figure 4.25 – Cormier’s Colour 3-D Laser Printer Configuration [60]..... 148

Figure 4.26 – Metal Printing Process schematic [229]..... 150

Figure 4.27 – Support material strategy for MPP (adapted from [229]) 151

Figure 4.28 – Early test rig for laser printing multiple layers of non-conductive toner 153

Figure 4.29 – Overview of EMB coating process [300] 155

Figure 4.30 – Detail of EMB coating process (modified from [300]) 156

Figure 4.31 – Multilayer epoxy sample produced by EMB coating process 158

Figure 4.32 – Laser printed ziggurat shaped object exceeding the 3mm theoretical height limit for conventionally transferred laser printing (© Society for Imaging Science and Technology [236] also available without modification from [211])..... 160

Figure 4.33 – Selective Laser Printing (SLP) development rig being fabricated at MTT Technologies Ltd (now Renishaw PLC Additive Manufacturing Products Division)..... 161

Figure 4.34 – SEM image of Somos 201 [61] 164

Figure 4.35 – Charge distribution of classified Somos 201 powder with 0.5 wt.% of FCA .. 165

Figure 4.36 – Removal from platform and stretching of a Somos 201 tensile specimen.... 166

Figure 4.37 – Drawing of an EP based 3D printer utilizing service loops for a transfer belt [306] 169

Figure 5.1 – Charge distribution of thermosetting epoxy toner..... 192

Figure 5.2 – Charge distribution of Samsung PolyJZ polyester toner 193

Figure 5.3 – Selective Laser Printing (SLP) development rig as built in the Custom-fit project 202

Figure 5.4 – SLP rig showing major components and instrumentation added for this PhD (note: print sequence is from right to left)..... 203

Figure 5.5 – Stage 1 SLP rig schematic layout showing instrumentation and typical cycle timings (note: print sequence is from left to right)	204
Figure 5.6 – Default orientation and print direction (looking up from underneath) of sample passing under medium wave (left) and short wave (right) infrared heaters.....	205
Figure 5.7 – Setup for measuring the sensitivity of the field mill to charged area.....	209
Figure 5.8 – Surface potential measured by field mill vs. charged area	209
Figure 5.9 – Surface potential (of a fixed area) measured by field mill vs. stand-off distance	211
Figure 5.10 – Pulsed DC corona device installed on the SLP rig with the field mill located after the printers (platform motion is from right to left in this image).....	212
Figure 5.11 – CTG PrintTec GmbH printer configuration with typical voltages.....	215
Figure 5.12 – Detailed illustration of the pressure applied during the transfer step	216
Figure 5.13 – View of the laser stripe used for height measurement (arrow on left); and alternate position for the field mill after the 2 nd printer (initially installed at its recommended stand-off distance)	219
Figure 5.14 – SLP rig showing major components and instrumentation added for Stage 2 of this PhD (note: print sequence is from right to left)	222
Figure 5.15 – Stage 2 SLP rig schematic layout showing instrumentation and typical cycle timings (note: print sequence is from left to right)	223
Figure 5.16 – Rotation of medium wave infrared heater to improve heating uniformity ..	225
Figure 5.17 – View of the underside of the refurbished CTG PrintTEC GmbH printers showing corotron devices before and after the final transfer roller	226
Figure 5.18 – Viewing window in the refurbished printers (left), and view through the window showing the back of the transfer roller (right); arrow shows roller rotation (print direction is right to left).....	226
Figure 5.19 – Typical voltages used inside the CTG GmbH printers after refurbishment ...	227
Figure 5.20 – Stage 2 SLP rig platform supporting a stack of ceramic plates on top of the original glass substrate on silicone matting.....	229
Figure 5.21 – Close up view of a typical substrates stack (including charge plate) on the platform as it passes under the transfer roller	229
Figure 5.22 – Voltages shifted -900 V so the CTG GmbH printers would print to ground ..	230
Figure 5.23 – Examples of development quality on the transfer roller (including defects) experienced during the 55 trials toward achieving high density printing to ground	233
Figure 5.24 – Adjusted position of the laser height measurement device (partially under the stainless reflecting surface) in order to be centred on the new cylindrical build volume.....	234
Figure 5.25 – Original cantilevered platform (left); redesigned build sleeve (right)	235
Figure 5.26 – Views of the build sleeve as designed and installed in the SLP rig by Renishaw PLC	235
Figure 5.27 – EMBER rig for testing electrostatic transfer effectiveness	236

Figure 5.28 – EMBER rig schematic showing printing mode (left); and optional compacting/consolidation step (right)..... 237

Figure 5.29 – EMBER CAD model showing the developer & platen (left); and platform (right)..... 237

Figure 5.30 – EMBER rig transfer step close up: showing an 0.2mm gap between the developer and substrate during a deposition cycle 239

Figure 5.31 – Gold-leaf electroscope for detecting net charge imbalance showing no charge (left) and net charge on an acrylic substrate (right)..... 241

Figure 5.32 – Inducing charge separation in a gold-leaf electroscope [315]..... 241

Figure 6.1 – Sample 6-1, a bespoke helmet insert (the largest volume SLP sample produced in the Custom-Fit project)..... 245

Figure 6.2 – Sample 6-2, the tallest SLP sample from the Custom-Fit project (© Society for Imaging Science and Technology [244]) 245

Figure 6.3 – Sample 6-3, EMB sample from Custom-Fit project exceeding the theoretical height limitation proposed by Kumar and Dutta in [261] 247

Figure 6.4 – Result from dimensional analysis of Sample 6-1 (largest volume SLP sample)..... 249

Figure 6.5 – Optical and SEM (both at 200x) comparison of the resumed build interface on Sample 6-2 (tallest SLP sample) 250

Figure 6.6 – SEM (100x) of cross-section from Sample 6-2 (tallest SLP sample) showing the layers which were deposited initially and those deposited in the resumed build 251

Figure 6.7 – SEM of the interface between the initial and resumed build in Sample 6-2. Left image at 500x and right image at 1,000x..... 251

Figure 6.8 – SEM image of cross-section through Sample 6-3 produced by EMB technique 253

Figure 6.9 – EDS of contamination particle found in Sample 6-3 (EMB sample)..... 254

Figure 6.10 – Optical and SEM comparison (both at 300x) of the contamination particles in Sample 6-3 (EMB sample)..... 255

Figure 6.11 – Carrier banding evident in Sample 6-3 (EMB sample) 256

Figure 6.12 – ASTM F2036 pattern printed on paper; an example from the Sample 6-4 series (Multilayer Printing on Paper) 262

Figure 6.13 – Cross-sectional optical microscopy from the Sample 6-4 series, comparing the stack height between single (left) and 15 layer prints (right) (© Society for Imaging Science and Technology [244])..... 263

Figure 6.14 – Graph of the Sample 6-4 series showing the paper thickness versus the fused toner thickness 263

Figure 6.15 – Cross-sectional optical microscopy comparison of the fused toner height from the entire series of Sample 6-4 at 1,2,3,4,5,10 and 15 prints (Note: lines and boxes in this figure show optical microscopy measurements graphed in Figure 6.14) 264

Figure 6.16 – Optical microscopy images from the Sample 6-4 series showing the deviation in image registration when the paper is recirculated 15 times . 269

Figure 6.17 – Images showing the post-print assembly steps for Sample 6-5 prior to firing 270

Figure 6.18 – Sample 6-5 after firing (left) and SEM image of resulting body (right)..... 271

Figure 6.19 – Sample 6-6 assembled stack (left) and result after firing (right) 273

Figure 6.20 – SEM of a sintered portion of Sample 6-6 showing light necking 274

Figure 6.21 – Optical image during Raman spectroscopy of commercially available “ceramic” toner exhibiting a strong florescence background 279

Figure 6.22 – Loading pure ceramic into a LaserJet 5 cartridge (left); and the resulting print on paper, Sample 6-7 (right)..... 281

Figure 6.23 – Surface coated alumina printed on paper (inside dashed rectangle) as Sample 6-8 (left); and text printed on overhead transparency (right). 282

Figure 7.1 – Large detail of the deposition from registration trials (Sample 7-1) with view of the entire substrate inset; yellow arrow indicates the printing direction 292

Figure 7.2 – Surface quality of Sample 7-2 where successive prints (with each layer shifted 5mm to the right), were transferred layer-on-layer using only heat and pressure 297

Figure 7.3 – Graph of average post-print surface potential vs. average cumulative maximum print thickness for set of samples including Sample 7-2 (© Society for Imaging Science and Technology from [236])..... 297

Figure 7.4 – Surface quality of Sample 7-3 where a 10 min delay was introduced between successive prints (with each layer shifted 5mm to the right) 299

Figure 7.5 – Graph of post-print surface potential and surface potential after 10min delay vs. average cumulative maximum print thickness for Sample 7-3... 299

Figure 7.6 – Image showing the conductive aluminium cover plate used to cover the nonconductive former glass substrate and silicone matting 302

Figure 7.7 – Graph of post-print surface potential vs. cumulative maximum print thickness for Sample 7-4 302

Figure 7.8 – Graph of post-print surface potential vs. the area printed for each layer 304

Figure 7.9 – Graph of post-print surface potential of Sample 7-5 following 20 consecutive blank ‘prints’ and then a surface potential vs. average cumulative maximum print thickness printed immediately afterwards on the same substrate..... 306

Figure 7.10 – Image of the surface quality and “eye” shaped defects of Sample 7-6..... 308

Figure 7.11 – Graph of post-print surface potential vs. average interpolated cumulative thickness for Sample 7-6 309

Figure 7.12 – Result of placing a sheet of paper on top of Sample 7-6 for layer 20..... 310

Figure 7.13 – Sheet of paper as placed on top of Sample 7-6 during the printing of layer 20. Note: toner transferred near to the image stack as background (upper right hand corner), but not directly over it; this is evidence that residual toner charge in the image stack was repelling incoming toner. Also, the paper is folded back to show the defect pattern on the top surface of the sample. (Note: image adapted from [236] with shadow of folded back paper edge enhanced for better reproduction)..... 316

Figure 7.14 – Photomicrograph of developed thermoplastic surface from [204]. The size of the deformation cells is about 2µm..... 318

Figure 7.15 – Photomicrograph of developed thermoplastic surface from [204]. The size of the deformation cells is about 2µm..... 321

Figure 7.16 – Parallel plate illustration of powder transfer from photoconductor to build platform [Adapted from 261]..... 325

Figure 7.17 – Required platform voltage to maintain a 3MV/m transfer field strength at the top surface of a given part height (using conventional transfer) based on Equation (7-2). 326

Figure 7.18 – Electric field strength versus deposited print thickness, using Equation (7-1) with the charge per unit volume of the fused toner equal to 0-100% of the fresh toner value used by Kumar and Dutta [261]. 328

Figure 7.19 – Electric field strength versus deposited print thickness, using Equation (7-1) with the charge per unit volume of the fused toner equal to 0-100% of the fresh commercial polyester toner value and no voltage applied to the platform. 330

Figure 7.20 – Substrate and platform configuration enabling an aluminium plate to be charged with a high voltage wire to effect electrostatic transfer methods 333

Figure 7.21 – “Fish scaling” defects in polyester toner layer due to air breakdown..... 334

Figure 7.22 – “Fish scaling” defects in epoxy toner layer due to air breakdown 334

Figure 7.23 – Image of Sample 7-9 (800V transfer voltage) with general pitting, but some areas of reduced pitting 339

Figure 7.24 – Graph of post-print surface potential vs. average interpolated cumulative thickness for Sample 7-9 339

Figure 7.25 – Charge plate configuration for Sample 7-10 (note: the exposed area on the charged plate shown here was covered during printing to avoid breakdown) 340

Figure 7.26 – Image of Sample 7-10 with significantly reduced pitting in areas above the charged plate 341

Figure 7.27 – Graph of post-print surface potential vs. average interpolated maximum cumulative thickness (for the half over the charged plate) for Sample 7-10 341

Figure 7.28 – Image of Sample 7-11, without pitting defects..... 342

Figure 7.29 – Graph of post-print surface potential vs. average interpolated cumulative thickness for Sample 7-11 343

Figure 7.30 – Image of Sample 7-12 with 176 layers and very few surface defects as built on the SLP rig (before removal from platform); print direction was to the left..... 345

Figure 7.31 – Image comparing repetitions from Sample 7-12: 176 layers printed with transfer voltage of 3,000V (left) vs. 229 layers printed with transfer of 2,500V (right) 345

Figure 7.32 – Graph of pre-print surface potential vs. average interpolated cumulative thickness for Sample 7-12 346

Figure 7.33 – Image of Sample 7-13, exhibiting general pitting defects and low deposition area on the left.....	348
Figure 7.34 – Graph of post-print surface potential vs. average interpolated cumulative thickness for Sample 7-13	349
Figure 7.35 – Sample 7-14 with surface pitting above the foil and defect-free surface elsewhere	355
Figure 7.36 – Sample 7-15 showing sparking during sample preparation (above) and global surface quality defects (below)	356
Figure 7.37 – Image during the fusing of Sample 7-16, showing defects forming in early layers deposited on the Al plate	357
Figure 7.38 – Sample 7-17 defect free deposition over substrate and foil covered with insulating tape (on left side)	358
Figure 7.39 – Illustration of transfer voltage coupling for Sample 7-18	359
Figure 7.40 – Sample 7-18 defect-free deposition over 4mm high	360
Figure 7.41 – Graph of pre- and post-print surface potential vs. average interpolated cumulative thickness for Sample 7-19.	361
Figure 7.42 – Showing Sample 7-13 compared to the reduced defects in Sample 7-19.....	362
Figure 7.43 – Comparing Sample 7-19 (left) with a sample build on top of a 2mm taller capacitively coupled stack (right).....	363
Figure 7.44 – Sample 7-20 showing wires carrying transfer voltage (above) and resulting deposition pattern (bottom)	365
Figure 7.45 – Sample 7-21 with red insulated wires at the build surface carrying the transfer voltage, charged inductively showing a) good deposition on wires and poor deposition on silicone and b) detail of the same on a sample without silicone matt.....	366
Figure 7.46 – Sample 7-22 showing poor surface quality deposition throughout 20 layers including onto a sheet of paper	368
Figure 7.47 – Sample 7-23 showing poor wetting/application of PEDOT:PSS onto a substrate prior to toner deposition	368
Figure 7.48 – Sample 7-24 showing a) application of brine solution onto the ceramic plate underlying the sample substrate, b) foil coupling to the brine solution (false coloured in green), c) resulting deposition with false colour indicating the position of the underlying foil (blue) and brine solution (green), d)photo showing reduced defects in sample centre.....	370
Figure 7.49 – Sample 7-25 showing extensive surface defects without any noticeable improvement due to the positive ions; the arrow indicates the print direction	372
Figure 7.50 – Sample 7-26 showing extensive surface defects without any noticeable improvement due to negative ions.....	373
Figure 7.51 – Sample 7-27 showing a) reduced surface pitting; b) this sample (right) compared to another sample prepared identically, except without ions; c) detail comparing the two samples showing improved surface quality with field attracted ions	374

Figure 7.52 – Image of the EMBER rig just after a printing cycle to deposit black toner onto the substrate. For more information on the EMBER rig, see §5.8 377

Figure 7.53 – Sample 7-28 showing the layer fusing step with hot air gun (above), and the resulting fused surface quality (below) 378

Figure 7.54 – Sample 7-29 showing a) no toner transfer after printing using a developer bias of -1,000V, b) very light toner transfer using a developer bias of -2,000V, c) slightly darker transfer when using -3,000V bias..... 380

Figure 7.55 – Sample 7-30 showing a) the toner transferred after the first rubbing, b) more substantial deposition after the second rubbing, c) toner deposition and texture after 14 fused layers..... 382

Figure 7.56 – Sample 7-31 showing toner deposit after contacting the substrate with high voltage using a piece of metal (above), and the resulting toner deposit after contacting the substrate with high voltage using a carbon brush (below) 383

Figure 7.57 – Sample 7-32 showing a) substrate pre-print treatment in a high voltage field which induced breakdown; b) toner deposition including “bubble” defects; c) repeat of treatment with lower field strength eliminated “bubbles” but resulted in a lower density of toner deposition 385

Figure 8.1 – Large image (right) viewing the underside of the charge plate clinging electrostatically to Sample 7-12 upon removal from the SLP rig 18 days after it was made. Overlaid on the left is a small image of the same, viewed from above..... 390

Figure 8.2 – Plot showing the drop off rate for the tribocharged beads electrostatically suspended from the acrylic window of Sample 8-1; periodic photos of beads inset 393

Figure 8.3 – Sample 8-2 clinging to the side of the SLP rig; the film substrate wrinkled during processing which precluded further layer deposition..... 395

Figure 8.4 – Fabrication of Sample 8-3, printing over Kapton tape (entirely covering two pieces of tape inside rectangles and covering only a portion of the tape in the circled corners)..... 396

Figure 8.5 – a) Unpeeled tape which secured Sample 8-3; b) harvested section with tape folded back on itself and cut; c) physically lifting the tape up using a field..... 397

Figure 8.6 – a) Areas harvested for Sample 8-5; b) harvesting the specimens; c) specimen placement without a field; d) B and C lifting due to the field ... 400

Figure 8.7 – “Failed” tensile sample from the Custom-fit project; the circled portion was used as Sample 8-6 403

Figure 8.8 – Sample 8-6 in a 4mm gap with a) no applied field, b) with a field of -0.75 MV/m, and c) with a field of 0.75 MV/m applied 404

Figure 8.9 – Sample 8-7 showing a) residual charge testing; b) the strategy for testing the static dissipation of the material; c-d) testing 407

Figure 8.10 – Simplified model of toner charge based on the assumption that residual toner charge is neutralized during fusing 410

Figure 8.11 – Improved conceptual model of charge trapping, showing non-uniform shape and charge distribution of toner prior to fusing, and charge rich interlayers thereafter	411
Figure 8.12 – Early attempt to transfer from an intermediate substrate (lower plate) onto the final receiver (upper plate).....	414
Figure 8.13 – Attempted neutralization by immersion in water	415
Figure 8.14 – Acrylic substrate neutralized by AC fan ionizer	416
Figure 8.15 – Non-contact electrostatic voltmeter measurement of the surface potential on Sample 8-14 in different areas	418
Figure 8.16 – Neutralizing the surface potential on Sample 8-15 using a flame.....	420
Figure 8.17 – Sample 8-16 shown in the lower right hand side of this image with reduced surface pitting along the top edge.....	423
Figure 8.18 – Four samples showing the effect of neutralization by ac fan ionizer and use of transfer corona.....	423
Figure 8.19 – Graph showing the surface potential before each layer printed for all four samples illustrating the effect of neutralization by AC fan ionizer and transfer corona.....	424
Figure 8.20 – Smooth defect-free surface of Sample 8-21	426
Figure 8.21 – 60 layer version of Sample 8-21 showing ridges and surface pitting defects.....	427
Figure 8.22 – Graph of the surface potential versus the build height during the production of the 60 layer version of Sample 8-21.....	428
Figure 8.23 – Graph of the surface potential and laser height measurement for the two sets of different flame neutralization regimes of Sample 8-22	431
Figure 8.24 – Photo of Sample 8-22 which was flame neutralized each layer (left) and another which was flame neutralized only after all 10 layers were deposited (right).....	431
Figure 8.25 – Graph of the cumulative toner weight added for each layer in the repeat of Sample 8-22 showing much lower deposition rate for samples neutralized layerwise	432
Figure 8.26 – Graph of a repeat of Sample 8-22 prepared without flame neutralization except for three instances when the surface potential troughed at 530, 650, and 620V as labelled on the graph.....	433
Figure 8.27 – Differential plot of the graph in Figure 8.26 showing the change in (Δ) surface potential, height, and weight effected by each layer deposited ..	434
Figure 8.28 – Evidence of toner leaving the 40-layer Sample 8-22 by snowballing (above) and back transfer (below)	435
Figure 8.29 – Height of unfused 40-layer toner stack measured with and without 3,000V on the charge plate over time.....	436
Figure 9.1 – Sample 9-2 showing areas of non-deposition (above), which correlated to counter bores in the underlying platform (below)	443
Figure 9.2 – Non-conductive spacer which lifted the ceramic substrate 13.5mm above the grounded platform.....	444

Figure 9.3 – Sample 9-3 showing reduced deposition (above) and compared to Sample 9-2 (below)	445
Figure 9.4 – Sample 9-4 sets laid out in rows	446
Figure 9.5 – Weight and height of sets in Sample 9-4	447
Figure 9.6 – Defect in a flower or fan pattern which was caused by a finger contacting the underside of the substrate-charge plate pair	450
Figure 9.7 – Sample 9-6 showing toner intentionally repelled off of the substrate by a finger contacting the underside of the substrate	451
Figure 9.8 – Sample 9-7 showing the edge of a sample substrate (painted black) as printed with white epoxy toner (above) and the same edge after toner has been repelled off (see area by arrows) by using the charge plate at -3,000V without a counter electrode.....	453
Figure 9.9 – Sample 9-7 shown with the underlying charge plate at -3,000V causing toner to collect on a grounded socket head cap screw (acting as the counter electrode)	454
Figure 10.10 – Overlapping photographs showing the same toner image on each imaging member from the OPC to the transfer roller (TR) to two different samples both with the same waviness defect pattern	473
Figure 10.11 – Tekscan pressure sensor readings showing non-uniform pressure (left); improved distribution (middle); a map of entire substrate after improvement (right); and a force vs. time plot (below)	474
Figure 10.12 – Image showing the medium wave length heater elements aligned to the waviness defects	476

Acknowledgements

My family: My dearest wife and three children, parents, in-laws and siblings

Greg Gibbons and David Wimpenny

CASE award generously sponsored by Renishaw PLC and UK tax payers through the Engineering and Physical Sciences Research Council (EPSRC)

Anonymous donor

Renishaw PLC Additive Manufacturing Products Division: Simon Scott, Ben Ferrar, Jake Ufton, Chris Sutcliffe, Peter Nun, and Richard Pointon

Rupesh Chudasama, De Montfort University

The SPRINT Project Collaborators: Renishaw PLC, De Montfort University, Parker KV, MTT Technologies Ltd and the UK Technology Strategy Board

CTG PrintTEC GmbH: Andreas Schoenberger, Dieter Jung and Christian Hornickel

Beat Zobrist, Zobrist Engineering and Consulting (ZEAC)

De Montfort University: Soumya Banerjee, Sameet Raut, Susheel Juvanapudi, Adam Moroz, John Watts, and Andrea Tallis

Collaborators from the Laser Printed Electronics and Custom-fit Projects

Declaration

I declare that this thesis is presented in accordance with the regulations for the degree of Doctor of Philosophy. It has been written by myself and has not been submitted previously for a degree at any other university. All data generated and analysis shown herein has been undertaken by me unless stated otherwise. As noted in the text, several sections of this work have been the basis for conference and journal publications.

Jason Blair Jones

September 2013

Summary

Additive Manufacturing (AM), popularly called “3D printing,” has benefited from many two-dimensional (2D) printing technology developments, but has yet to fully exploit the potential of digital printing techniques.

The very essence of AM is accurately forming individual layers and laminating them together. One of the best commercially proven methods for forming complex powder layers is laser printing, which has yet to be used to directly print three-dimensional (3D) objects above the microscale, despite significant endeavour.

The core discovery of this PhD is that the electrostatic charge on toner particles, which enables the digital material patterning capabilities of 2D laser printing/photocopying, is disabling for building defect-free 3D objects after the manner attempted to date. Toner charge is not mostly neutralized with fusing as previously assumed.

This work characterizes and substantiates the accumulation of residual toner charge as a primary cause for defects arising in 3D printed bodies. Next, various means are assessed to manage and neutralize residual toner charge. Finally, the complementary implementation of charge neutralization with electrostatic transfer methods is explored.

Research Outputs

Outputs arising in part or whole from this research include:

- The following Papers

Note: The author's version of selected* publications has been annexed to this thesis following the references.

- *J. B. Jones, D. I. Wimpenny, G. J. Gibbons, and C. Sutcliffe, "Additive Manufacturing by Electrophotography: Challenges and Successes," in *IS&T's NIP26 and Digital Fabrication 2010*, Austin, Texas, 2010, pp. p. 549-553.

Abstract: 3-D printing of complex structures by selective deposition is currently dominated by direct write and inkjet technologies (as utilized in Stratasys, Objet, ZCorp, Voxeljet, and Solidscape systems). Dry toner systems, despite their high productivity and maturity in 2D digital printing, have only been used indirectly for Additive Manufacture (AM) of objects above the micro scale. For over 3 years a European consortium has sought to overcome the inherent challenges of multilayer printing by electrophotography to enable its use in mainstream AM which promises increased deposition efficiency and a means of utilizing materials not amenable to liquid ink formulations. This paper reviews the challenges addressed and demonstrates the progress made including development of a bespoke thermoplastic elastomer toner and the specialized hardware configuration used to print and fuse it into tensile specimens over 50 layers thick which elongated over 500% before failure. Additionally, seeking to reduce oxidation during toner fusing, electrostatic printing and fusing was unsuccessfully attempted in a vacuum and in argon; while printing in a partial vacuum (above 50 kPa) and nitrogen was possible.

- J. B. Jones, D. I. Wimpenny, R. Chudasama, and G. J. Gibbons, "Printed Circuit Boards by Selective Deposition and Processing," in *22nd Solid Freeform Fabrication Symposium*, Austin, TX, USA, 2011, pp. 639-656.

Abstract: With electronic applications on the horizon for AM, comes the dilemma of how to consolidate conductors, semi-conductors, and insulators in close proximity. To answer this challenge, laser printing (selective deposition) was used in tandem with fiber laser consolidation (selective processing) to produce PCBs for the first time. This combination offers the potential to generate tracks with high mechanical integrity and

excellent electrical conductivity (close to bulk metal) without prolonged exposure of the substrate to elevated temperatures. Herein are the findings of a two-year feasibility study for a "one-stop" solution for producing PCBs (including conductive tracks, dielectric layers, protective resists, and legends).

- *J. B. Jones, G. J. Gibbons, and D. I. Wimpenny, "Transfer Methods toward Additive Manufacturing by Electrophotography," in *IS&T's NIP27 and Digital Fabrication 2011*, Minneapolis, Minnesota, USA, 2011, pp. 180-84.

Abstract: 3D printing of complex structures by selective deposition is currently dominated by inkjet technologies. Dry toner systems, despite their high productivity and maturity in 2D digital printing, have only been used indirectly for Additive Manufacture of objects above the micro scale. Although electrophotography (EP) promises increased deposition efficiency and a means of utilizing materials not amenable to liquid ink formulations; this potential cannot be achieved using conventional electrostatic transfer methods.

This paper reviews the problems associated with conventional transfer in multilayer printing (including height limitation and defect exaggeration) and demonstrates alternative transfer principles which promise to unlock the potential of Additive Manufacturing by EP.

- J. B. Jones, D. E. Cooper, D. I. Wimpenny, and G. J. Gibbons, "SME Technical Paper TP12PUB36: Gateways Toward Dissimilar Multi-material Parts," presented at the *RAPID 2012 and 3D Imaging Conferences & Exposition*, Atlanta, GA, USA, 2012.

Abstract: Nature provides a pattern of complex systems in which materials with vastly dissimilar properties grow together and function in close proximity. Although the gap between biological and existing AM systems cannot be overstated, the aspiration for AM to mimic this capability of nature has been widely admired (but is currently limited to multi-material parts made from families of like materials). The recent ASTM F2921 standard provides the first standardized framework to identify anisotropic properties of printed parts. This research highlights how understanding and quantifying the anisotropies between and within layers of printed parts provides foundational understanding to begin to emulate nature's pattern by consolidating dissimilar multi-material parts in AM which promises future potential to supersede conventional part assembly with integral printed systems.

- *J. B. Jones, D. I. Wimpenny, and G. J. Gibbons, "The Influence of Residual Toner Charge on 3D Laser Printed Objects," in *IS&T's NIP28 and Digital Fabrication 2012* Quebec City, Canada, 2012, pp. 327-331.

Abstract: The recent advances in digital fabrication have nearly become synonymous with the formulation of functional inks and inkjet printing. Conversely, dry toner systems, despite their high productivity and maturity in 2D digital printing, have scarcely been utilized for 3D printing and digital fabrication, despite significant endeavor.

This paper reviews the advantages that laser printing offers digital fabrication (over inkjet) and provides insights to overcome the technical barriers which to date have prevented it from gaining traction as a 3D printing technique.

- R. Chudasama, J. B. Jones, and D. I. Wimpenny, "Synthesis of an Electrophotographic Toner for Additive Manufacturing," in *DAAAM International Scientific Book 2012*, B. Katalinic, Ed., Vienna Austria: DAAAM International, 2012.

Abstract: Despite the increasing use of fine polymeric powders in AM since 1987 (Selective Laser Sintering), only a limited number of polymers have been introduced in the last 25 years, with even fewer engineering polymers. The initial production of these materials has generally been via granulation and reduction to micro-scale powder using mechanical grinding until sufficient demand for the material/technology has justified more sophisticated production methods with better process control and yield.

This migration from mechanical reduction toward higher efficiency means of powder production parallels the history of toner development for photocopying and laser printing. Presumably, feedstock powder materials for new developmental AM techniques, such as those based on electrophotography (i.e. laser printing), would also follow the same pattern; however, mechanical milling of many engineering polymers result in low yields (due to their tough nature). This creates a dilemma for developing a range of technically suitable thermoplastic engineering powders using the resources that can be sustained by the incipient demand for AM.

This paper will review the limitations of traditional mechanical milling methods employed for polymer manufacture and report yields when applied to a variety of engineering polymers. The initial results of an alternative powder preparation method based on polymerization will also be reported which promises higher yields and better control over properties for AM materials generally, which could also enable electrophotography to gain traction as a definitive fabrication technology. This is the first time that electrophotographic toners have been polymerised for use in AM.

- J. B. Jones, D. Büttner, R. Chudasama, D. Wimpenny, and K. Krüger, "Laser Printing Circuit Boards and Electronics," *Journal of Imaging Science and Technology*, vol. 56, pp. 040503-1 – 040503-11, 2012.

Abstract: Although significant progress has been made toward digital printing of electronics using inkjet technologies, the potential of laser printing for digital fabrication has been largely overlooked. Despite their speed and resolution capabilities toner-based systems are often regarded as incapable of handling conductive materials. This research reports recent laser printing development and its potential to replace conventional printed circuit board manufacturing steps, including conductive track deposition. The research had a dual focus, demonstrating proof of concept with conventional office laser printers (for artwork masks, etch resists, and seed layers for overplating), and used industrial laser printers with developmental toners to support direct production of electronics (conductive tracks, dielectric layers, and legends). The results confirm that laser printing can complement other digital printing approaches for directly depositing resists and conductive tracks.

- J. B. Jones, D. I. Wimpenny, and G. J. Gibbons, "[In Press, Accepted Manuscript] Additive Manufacturing under Pressure," *Rapid Prototyping Journal*, vol. 20, issue 6, Accepted 2013.

Abstract: Purpose – Although Additive Manufacturing (AM), also known popularly as 3D printing, has set a new standard for ease of use and minimal restraint on geometric complexity, the mechanical part properties do not generally compare with conventional manufacturing processes. Contrary to other types of polymer processing, AM systems do not normally use (in-process) pressure during part consolidation. This research investigates the effects on material properties of layer by layer application of pressure during fabrication of polymeric parts by AM.

Design/methodology/approach – Tensile specimens were produced in Somos 201 using conventional laser sintering and Selective Laser Printing (SLP) - a process under development in the UK, which incorporates the use of pressure to assist layer consolidation.

Findings – Mechanical testing demonstrated the potential to additively manufacture parts with significantly improved microstructure and mechanical properties which match or exceed conventional processing. For example, the average elongation at break and ultimate tensile strength of a conventionally laser sintered thermoplastic elastomer (Somos 201) increased from $136 \pm 28\%$ and 4.9 ± 0.4 MPa, to $513 \pm 35\%$ and 10.4 ± 0.4 MPa respectively, when each layer was fused with in-process application of pressure (126 ± 9 kPa) by SLP.

Research limitations/implications – These results are based on relatively small sample size, but despite this, the trends observed are of significant importance to the elimination of voids and porosity in polymeric parts.

Practical implications – Layerwise application of pressure should be investigated further for defect elimination in AM.

Originality/value – This is the first study on the effects of layerwise application of pressure in combination with area-wide fusing.

- 2 UK/PCT Patent applications
 - Additive Building
(GB1109045.3, WO2012164015); Priority date: 31 May 2011
 - Improved Electret Manufacture
(GB1213585.1, PCT/EP2013/065694); Priority date: 31 July 2012

- 1 Poster “3D Photocopying”
 - 2011 1st Place Warwick Post-grad poster and
 - 2011 1st Place Regional Competition Winner, the highest award for any post-grad poster competition nationwide
 - A copy of the poster is available in Appendix E

Abbreviations and Definitions

Bold abbreviations are used most frequently

AM Additive Manufacturing

[*sic*] term (Latin) indicating something incorrectly written was intentionally transcribed as it was in the original

§ symbol for "section"

°C degrees Celsius

μA microamperes

μm micrometres

Å angstroms or angstrom, equals 10^{-10} meters

AC alternating current

aka also known as

Al aluminium

AMPD Additive Manufacturing Product Division of Renishaw PLC

at.% atomic percentage

Au gold

back transfer undesirable adhesion of toner to printer components (normally the photoreceptor or transfer roller) after it has gone through the transfer step

background (transfer) additional unintentional toner transfer onto what should be the clean "background" of the image, i.e. where the latent image is not

C Coulombs, SI derived unit of electrical charge

C toner concentration, expressed as a wt.% of the ratio of toner to carrier in the developer mix

CAD Charged Area Development

CAD Computer-Aided Design (Figure 5.29 only)

CCA Charge Control Agent

c_e electric susceptibility, degree a material polarizes in a field

cf. abbreviation of the Latin word meaning "compare"

charge acceptance measure of a photoreceptor's ability to have its surface charged uniformly

charge neutralization see charge recombination

charge recombination	process where net charge imbalance recombines with additional opposite polarity charge to achieve a net zero charge on a toner particle or body with a volume charge, used synonymously with charge neutralization
charge relaxation	the natural neutralization of charge imbalance, where opposite charges recombine
CNC	Computer Numerically Controlled (machine tools)
cold offset	when the toner is not heated sufficiently to flow, then it does not adhere well to the paper during the fixing step
CRT	Cathode Ray Tube
CT	Computer Tomography, a 3D volumetric scanning method which takes a series of X-ray images through an object
CTG	abbreviation for the flatbed laser printer manufacture CTG PrintTec GmbH (Alsdorf, Germany)
<i>d</i>	thickness of the fresh toner layer for Kumar's equations
DAD	Discharged Area Development
dark decay	a measure of the ability of a photoreceptor's surface to hold a uniform charge on its surface in the dark
DCD	Dual-Component (aka two-component) Development
dielectric polarization	the redistribution of electrons in the outer valence shells of a dielectric molecule due to influence from a field
dusting	a condition arising from a wide PSD where undesired and uncontrolled toner deposition occurs inside the printer
<i>e-</i>	symbol for electrons (the "-" means a negative charge)
<i>E or E_f</i>	field strength (V/m)
e.g.	abbreviation for "exempli gratia" (Latin) meaning "for the sake of example"
EDS	Energy dispersive X-ray spectroscopy
electret	the electrostatic equivalent to a permanent magnet
ELM	Electrophotographic Layered Manufacturing
EMB	Electro Magnetic Brush
EP	electrophotography
ERP	Electrophotographic Rapid Prototyping
ESD	Electrostatic Discharge
ESFF	Electrophotographic Solid Freeform Fabrication
FCA	flow control agent (which also influence charge)
FDM	Fused Deposition Modelling – an additive manufacturing approach in which polymer is selectively extruded
g	grams

hot offset	when toner flows too much (typically due to overheating) then it splits like a drop of water when exiting the fusing nip, leaving only half of it on the paper while the other half adheres to the fusing roller
i.e.	abbreviation for "id est" (Latin) meaning "that is"
image stack	the 3D equivalent to a growing "pile" height as used in conventional 2D printing terms
IPA	IsoPropyl Alcohol
JKR	Johnson–Kendall–Roberts equation for vdW forces
K_f	relative permittivity of the fresh layer of toner for Kumar's equations
K_p	relative permittivity of the printed (fused) layers of powder for Kumar's equations
kS/m	kilosiemens/metre
latent image	charge pattern formed on a photoreceptor by exposure
lateral conductivity	a measure of the stability of a photoreceptor's surface charges with a latent image on it, ensures image stability
LEDs	Light Emitting Diodes
LOM	Laminated Object Manufacture, a type of AM system
min	minutes
min ⁻¹	per minute (as in a heating rate of 5°C min ⁻¹)
mm	millimetres
mN/m	millinewtons per metre, a measure of surface energy
MV/m	Megavolts/metre (unit for field strength)
nip	pinch point between two rollers (or roller and substrate)
OPC	Organic PhotoConductor, OPCs (plural)
p	printed (fused) toner height for Kumar's equations
PBT	polybutylene terephthalate
photoinduced discharge	measure of the ability of a photoreceptor's surface to neutralize charge on its surface when exposed to light
PLC	programmable logic controller
PLC	Public Limited Company, As in Renishaw PLC
PMMA	poly(methyl methacrylate)
PSD	particle size distribution
PTFE	polytetrafluoroethylene
Q or q	symbol for charge
q/d	charge-to-diameter ratio
q/m	charge-to-mass ratio
r	volume resistivity

residual image	a defect arising in photoreceptors where charge is trapped in the photoconductive layers
RH	relative humidity
s	seconds
S/m	Siemens/metre
SE	Secondary Electron (detection mode for SEM)
SEM	Scanning Electron Microscope
SGC	Solid Ground Curing, a type of AM system
SLA	StereoLithography Apparatus, a photopolymer vat AM process which uses an energy source to selectively cure a photopolymer resin in a vat
SLP	Selective Laser Printing , an AM process based on laser printing, as described in §4.4.5.3
SLS	Selective Laser Sintering, a powder bed fusion AM process based on selectively fusing powder layers using a high energy point source, such as a laser
takt time	The meter or pace of sub-operations in manufacturing
T _g	glass transition temperature for polymer
thermoplastic xerography	a process related to conventional EP where a global deposition of thermoplastic powder is selectively charged with a latent image, and softened (typically by heat or vapour), and then solidifies with a surface texture which varies with the latent image charge
V ₀	DC voltage applied to the build platform for Kumar's equations (§7.2.1)
VDC	Volts of direct current
vdW	van der Waals forces
vol.%	volume percentage
vs.	versus
w.r.t.	with respect to
wt.%	weight percentage
Δ	(uppercase Greek letter "delta") signifying "difference" or "change in" as in the change in weight per layer printed
ε ₀	absolute permittivity of a vacuum, 8.8541 × 10 ⁻¹² F/m
ε _r	relative permittivity, compared to the absolute permittivity of a vacuum (free space)
κ	relative dielectric constant, alternative term for relative permittivity
ρ _f	charge per unit volume in the fresh toner layer in Kumar's equations (§7.2.1)
ρ _p	charge per unit volume in the printed (fused) toner layer for Kumar's equations (§7.2.1)

1. Introduction

The increasingly popular use of the term “3D printing” to describe Additive Manufacturing (AM) techniques implies that they are derived directly from 2D printing technology. Although 2D has paved the way for many advances inherited by AM, the minority of 3D systems actually use digital printing technology directly for build material deposition (§2.3). However, the term 3D printing may, in fact, foreshadow impending convergence of digital printing with AM systems (§2.5, §4.1). Aspirations for accelerating build speeds and printing smart products (including digital fabrication and printing integral electronics) are fuelling a shift towards high throughput methods for digitally patterned material deposition.

This shift toward higher speeds and multi-materiality oblige re-evaluation of material deposition means, including further upscale of digital printing technologies such as inkjet and electrophotography (EP) for 3D applications. Although ink and aerosol jetting technologies (wet approaches) have found a definitive footing in 3D (§3.5), EP (the basis for laser printing and photocopying) has only been used indirectly for AM of objects above the microscale. EP’s high productivity, reliability and resolution have warranted significant attention by various researchers (§4), but reliable realization of AM parts has proven elusive.

This thesis examines the aspects of EP which currently impede its use in AM. In particular, the limitations of conventional electrostatic and alternative transfer methods (including height limitation and defect exaggeration) are reviewed (§4), together with experimentally elucidated underlying causes (§6-7). Furthermore, the discovery and substantiation of the influence of residual toner charge trapped in a consolidated body is demonstrated (§7-9). These findings offer improved insights to more accurately model and overcome transfer limitations and manage residual toner charge to enable viable AM by EP.

1.1. Dry Toner, Not Liquid Ink

The technological focus of this work is the use of dry toner, not liquid ink, for AM. EP (also called *xerography* which literally translates as “dry writing”) is a completely dry digital printing process. It uses electrostatics to arrange small (microscale) particles into patterned layers, which are typically fused thermally or chemically. EP is the enabling technology for laser printing and photocopying, and is explained in detail in §3. For the scope of this document EP will refer to the use of dry toners typically in the diameter range of 5 to 60 μm .

1.2. Aims and Objectives

This research was aimed at up-scaling EP (laser printing) to become an effective AM or 3D printing process above the microscale.

Prior research undertaken to achieve this end culminated in a test rig and process called Selective Laser Printing (SLP), however it suffered from several problems. Overcoming these problems became the focus for this work. The objectives of this project, set with guidance from the industrial sponsor were to:

- Overcome the height limitation of the SLP process;
- Understand the cause of and eliminate the defects arising in parts produced using the SLP process;
- Produce fully dense parts using genuine engineering polymers (preferably thermoplastic) without contaminants (as opposed to faux materials which only mimic engineering materials, for example) with mechanical properties on par with injection mould grade polymers;
- Enable a production AM system for polymer parts with 600 dpi resolution and potential for reasonable production times.

1.3. Funding For This Research

The funding for this PhD was provided by a CASE award, generously sponsored first by MTT Technologies Ltd and then subsequently (through acquisition) by Renishaw PLC Additive Manufacturing Products Division based in Stone, Staffordshire, UK. The research follows on from

investigations by Professor David Wimpenny of De Montfort University with his blessing and support. This work was supervised by Dr. Greg Gibbons of the University of Warwick and focused on understanding and overcoming the height limitation and surface defects of multilayer laser printed samples.

In the spirit of transparency, it should be known that this PhD research was undertaken in parallel with another PhD candidate, Rupesh Chudasama of De Montfort University, who investigated the production of new toner materials (including thermoplastics by polymerization) and characterized the influence of pressure on defect formation in the SLP process. The research for both students was undertaken using the same equipment with some overlap in toner materials, and supported by the SPRINT project (project number: 100735; TP number: TP14IHVM/611IBD219A), funded in part by the UK Technology Strategy Board.

While the resources were shared, the research objectives were different and each student was responsible for their own work. The research reported herein pertains only to the work undertaken by the author unless otherwise noted as already declared.

1.4. Overview of the Research

Table 1.1 provides a tabular overview of this PhD indicating clusters of chapters with the major themes of the work.

Table 1.1 – Tabular Overview of the PhD

<i>PhD Content</i>	
Front Matter & Introduction	Contents
	Acknowledgements
	Declaration
	Summary
	Research Outputs
	Abbreviations and Definitions
Literature Review	Ch. 1 Introduction
	Ch. 2 AM
	Ch. 3 EP
	Ch. 4 Convergence of AM & EP
Experimental Work	Ch. 5 Toners and Printers (Methods and Materials)
	Ch. 6 Scoping Trials
	Ch. 7 Discovery and Substantiation of Defects
	Ch. 8 Approaches to Controlling Charge
	Ch. 9 Assimilating Charge Neutralization with Electrostatic Transfer
Conclusions & End Matter	Ch. 10 Conclusions and Future Work
	Appendices
	References
	Annex (Related Articles by the Author)

For the reader desiring to have an abbreviated synopsis of this work, review of the conference papers delivered annually by the author from 2010-2012 at the Digital Fabrication Conference, co-sponsored by the Society for Imaging Science and Technology (IS&T) and the Imaging

Society of Japan (ISJ), is recommended. For convenience, the author's version of these publications is included in the Annex.

Literature Review

2. Additive Manufacturing

This chapter introduces the general concept of Additive Manufacturing (AM) and overviews why utilizing digital printing for AM is relevant to its advancement.

2.1. Introduction

Throughout history, various approaches for adding and subtracting materials have been used to make things. Early subtractive processes include cutting, carving, grinding, milling, etching, etc. Traditional additive processes include clay sculpture/pottery, weaving, extrusion, forming, sand casting, welding and, especially, manual assembly.

Since the Industrial Revolution, which began in England in the late 18th Century, the automation of these different processes has advanced at an asymmetrical rate. Subtractive methods, especially milling, have been readily automated, first using water/steam power, then electricity and since the 1960's – 70's, CNC (i.e. microprocessor/computer controlled) milling has gained traction as the first fully digital production technique [1]. From the 18th Century until the mid-1980's, the automation of additive techniques advanced at a slower pace, remaining largely operator reliant and assembly oriented [2, 3].

2.2. Layer by Layer Concept

In more recent decades, the partial and full automation of additive techniques has substantially closed the gap created during the asymmetrical development of the prior two centuries. Precursors to conventional AM approaches included semi-automated methods to produce or scan 3D objects in layers, including L. D. Beckerle's 1969 patent for producing 3D models as a series of stacked layers [4] and M. Takada's 1983 patent for recognizing solid object shapes and recording them in stacked layers [5]. Classical AM, as known today, first emerged in the mid-1980's with Charles Hull's stereolithography apparatus (SLA) which used a laser to cure a photopolymer resin into stacked layers [6, 7]. By the late 1980's, Carl Deckard's selective (laser) sintering method for thermally fusing stacked layers [8, 9], and Scott Crump's (fused deposition) modelling apparatus (FDM) for extruding a series of stacked layers [10, 11] had also been added to the AM landscape. For the last 25 years, a plethora of technologies which use additive building, normally by stacking and laminating flat layers one upon the next, has been developed and commercialized.

The ability to consistently and reliably print/deposit and stack high quality layers is the first step to develop new AM systems. *Due to the inherent challenges that EP introduces for layer stacking, this entire work is dedicated to achieving that end.*

Owing to the conceptually simple objective of this work (of stacking toner layers), this chapter gives limited attention to conventional AM processes and historic development. For more detailed treatment of the basics and evolution of AM, the reader is referred elsewhere [12-15]. All known AM systems which relate to EP are explained in §3.5. The remaining subsections in this chapter outline how EP can contribute to the development of AM.

2.3. The Digital Step: Patterning Energy or Material

Since its inception in the mid-1980's, AM processes have been capable of producing objects digitally (direct from a computer model without any fixed tooling). The digital step is achieved using a variety of technologies and is often referred to as being the "selective" step, as in "selective laser sintering" or SLS. Understanding how this digital step is achieved provides critical insight into understanding why exploration of EP is relevant to the future of AM.

C. Williams et al. have simplified the types of digital steps into two basic categories: the patterning of energy (i.e. patterned exposure to energy such as by a mask or its digital equivalent) or the patterning of material (selective deposition) [16]. For example, some systems selectively deposit (pattern) material while others scan a laser (patterning energy) to selectively cure or melt some of the material in a powder layer. Table 2.1 lists the families of AM processes (as per ASTM F2792 [17]) and

designates what type of digital step is implemented. (The only processes which digitally control both material deposition and energy exposure fully independently [i.e. double section] are non-commercial [18].)

Table 2.1 – The Digital Step of AM Process Categories

<i>AM Process Category:</i>	<i>Digital Step (What is being patterned?):</i>
photopolymer vat	energy
material jetting	material
binder jetting	material
material extrusion	material*
powder bed fusion	energy
sheet lamination	energy (i.e. cutting energy)
directed energy deposition	energy*

* In both of these processes the material is thermally heated just prior to or during deposition, therefore by changing the heat input into the material/substrate, it can be argued that both the energy and the material are being patterned, albeit that one is normally being patterned indirectly.

Representing Table 2.1 as a pie chart (Figure 2.1) indicates that technologies which pattern material are slightly more prevalent than those which pattern energy. However, it is asserted here that the estimated value and volume of AM parts produced worldwide (based on [19]) by energy patterning systems are far more dominant as shown in Figure 2.2.

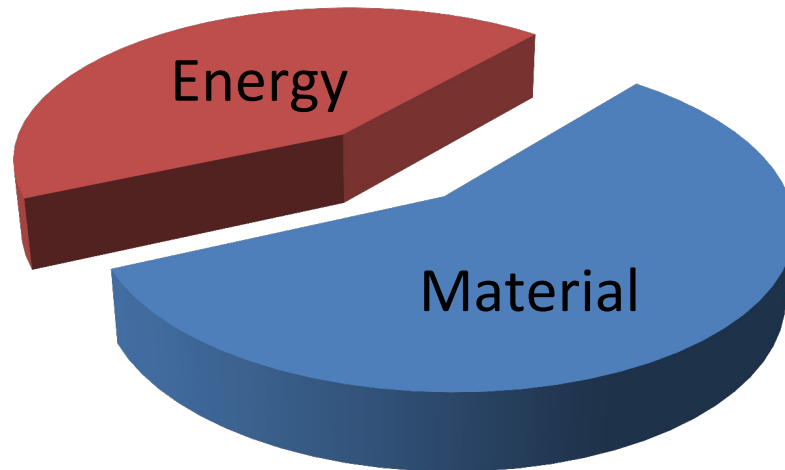


Figure 2.1 – AM Technology families by patterning method

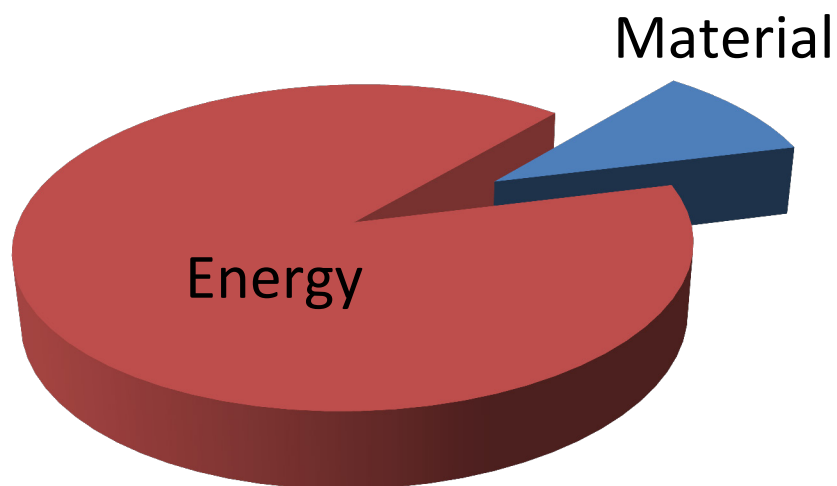


Figure 2.2 – Volume/value of system output by patterning method

One of the core reasons that systems which pattern energy have become the mainstay for high value AM, and of end-use products in particular, is the drive for maximum productivity. Energy is generally faster and easier to move around (laser beams, electron beams, etc.) than physical material (powders, resins, filaments etc.); therefore, patterning the

energy enables higher production yields. This trend is to be expected for products where the basis of competition continues to be speed and (topologically optimized) geometry.

2.4. Drive Toward AM of Multi- material Parts/Systems

One of the drawbacks of patterning only energy is that the final product can typically be made in only one material. Although this is not problematic per se, it precludes the potential to vary individual part composition. As the author has detailed elsewhere [20], a new basis of competition is emerging where full optimization of the composition as well as topology of printed objects will be required [21]. Essentially this entails a shift from printing parts to printing integral assemblies, and is a form of biomimicry [20]. This trend is foreshadowed by early multi-material AM systems (such as Objet's inkjet based Connex system and multi-feed/nozzle material extrusion systems). Furthermore, the expansion of research activities from the 2D printing world into "digital fabrication" reinforces this notion, and convergence with AM is inevitable [22-24]. This new basis of competition requires the patterning of material.

To date, the early examples of direct printing of integral functional systems/assemblies have been achieved largely using the flexibility of material extrusion systems, such as fab@home [25-27] or Nscript [28]; and aerosol jetting [29]. Patterning material enables global consolidation

steps (such as by using IR heaters), which can make thermal fusing faster than scanning with point sources. Despite the superior flexibility of extrusion systems, their limited deposition speed (even with multiple heads) has prompted exploration of additional technologies to pattern material.

2.5. Empowering 3D Printing with 2D Printing

The search for highly mature scalable fast deposition (material patterning) processes inevitably embraces consideration of 2D digital printing technologies for AM. Given the popular use of the term “3D printing” to describe AM, it is ironic that only the minority of these systems actually implement digital printing technology to build with (including material and binder jetting). However, as the basis of competition shifts toward printing “smart” products (integral printed systems/ assemblies of dissimilar materials), highly effective and efficient digital deposition (material patterning) technologies will be needed to synergize the fields of digital printing, digital fabrication and AM [20].

The two most dominant printing technologies for conventional text and image printing are inkjet and EP as explained in §3.5. Of these two, only inkjet has found a definitive role in the AM/digital fabrication landscape [30-36]. This work does not intend to detract from the merits of inkjet, however it is not ideally suited for deposition of all materials (as explained more fully in §3.5).

To date, EP has only been used indirectly in AM (§4.2). The reasons why EP has not been implemented for directly patterning build material in AM are reviewed in §4.3 to §4.6. Herein is the window of opportunity which motivates this research.

3. Electrophotography

This chapter acquaints the reader with the fundamental materials and principles of electrophotography (EP). The introductory section (§3.1) includes an overview of EP and a brief history. Subsequent sections revisit the materials and process steps in more technical and theoretical detail.

3.1. Introduction to Electrophotography

EP is the underlying technology which has enabled photocopiers and laser printers to produce and reproduce images normally using small polymeric powder particles called toner. A combination of specialised materials and processing steps allows toner to be moved around electrostatically in order to form a high resolution image as described below.

3.1.1. Materials Overview

EP is enabled by two fundamental classes of materials: toner and photoconductive materials.

Toner is fundamentally a fine powder (with a typical particle diameter of 5 to 20 μm) which can be electrostatically charged. Figure 3.1 shows the word "toner" laser printed (using a LaserJet 5500, Hewlett-Packard, USA)

about 5mm long on a sheet of paper. The inset images show magnified views of the print which illustrate the scale and shape of the manufacturer's standard black toner composing the letters. Careful inspection of the highest magnification image reveals that toner is not homogeneous. Here a translucent polymer forms a matrix containing black pigmented particles (and other constituents).

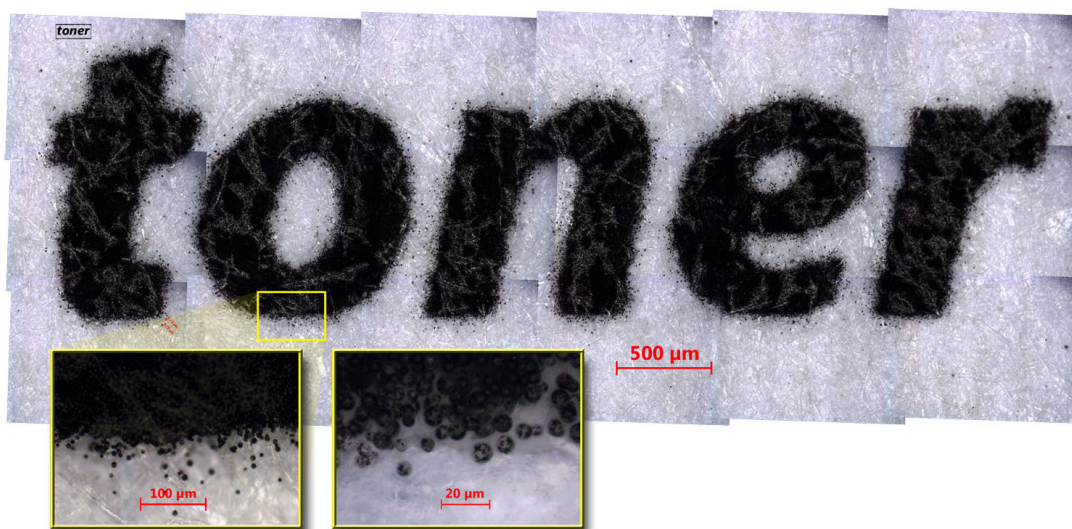


Figure 3.1 – Optical microscope images of toner in the laser printed word "toner"

Toner is normally made from insulating materials which are charged by rubbing (i.e. tribocharging). A macroscale analogy for charging by rubbing has been experienced by many children when rubbing a balloon against their hair. The balloon "steals" electrons from hair resulting in a net negative charge on the balloon and a net positive charge on hair. The net negative charge of the balloon allows it to cling to objects with a positive charge, such as the wall. Essentially the same phenomenon at microscale is used to charge toner (see §3.2 and §3.4.1 for more details). When a toner particle has a non-zero net charge, then it can be

moved around in an electric field. It will be attracted to the opposite charge and repelled by the like charge. In this way it is similar to the way magnetism works.

In order to arrange toner into a pattern to form text or images, it is necessary to be able to create a patterned electric field, which is achieved by using photoconductive materials.

A photoconductive material is a class of materials that become more conductive when exposed to light. In practice this allows it to act like an insulator in the dark and a conductor in the light, as illustrated by Figure 3.2. By charging a photoconductive material in the dark and then selectively exposing a portion of that material to light, it is possible to create a charge pattern. Exposure to light switches the material into conductive behaviour which creates a path for static charge to leak away to ground. Early systems used conductive flat metal plates coated with photoconductive material, although coating conductive rollers/drums (Figure 3.2) has been favoured since then.

The unique properties of these two materials enabled the American inventor, Chester Carlson (1906-1968, New York) to demonstrate the feasibility of EP in the late 1930s.

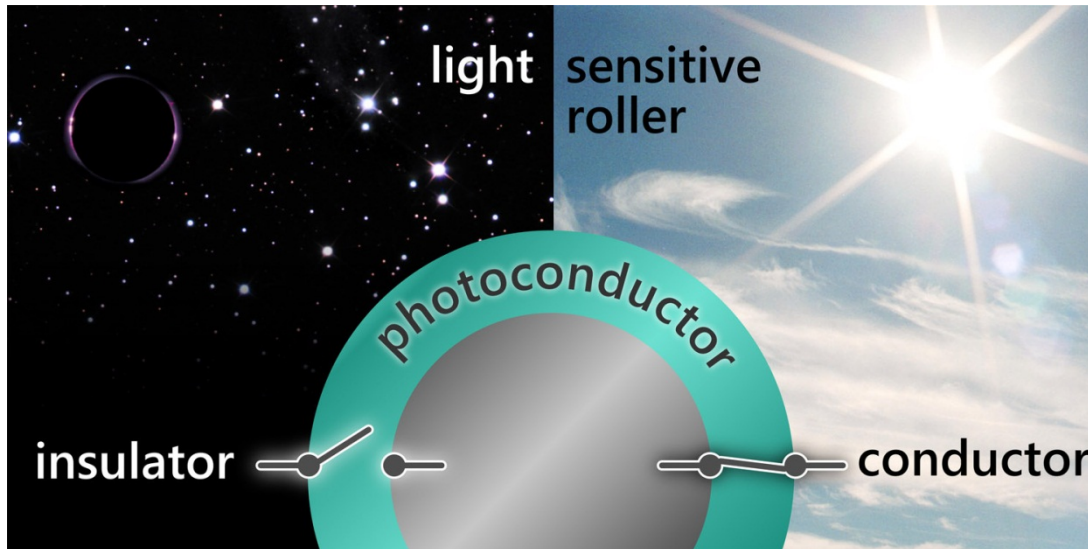


Figure 3.2 – Illustration of photoconductive behaviour in light and darkness

3.1.2. Brief History

The purpose of including the history of EP here is that unique insights into up-scaling EP to 3D can be gained by deconstructing historic decisions which enabled 2D EP, as will be highlighted in subsequent discussions.

The underlying scientific understanding to enable EP was observed in the 18-19th centuries. Benjamin Franklin demonstrated the fundamental principles of charge and electrostatics used in EP, such as coronas, insulator charge exchange and electrostatic adhesion [37]. Furthermore, the phenomenon of photoconductivity had already been observed in an element called Selenium (Se) as published by English electrical engineer, Willoughby Smith in 1873 [38]. It was noticed again by Heinrich Hertz in 1887 and more fully explained by Albert Einstein in 1905 [39].

The EP concept was born in 1938 when Chester Carlson combined electrostatics and photoconductivity; which previously had been unrelated. Dr. Harold E. Clark of Battelle Memorial Institute in Columbus Ohio, USA (and later a Xerox physicist) summarized Carlson's genius of unintuitive combination as follows:

Electrophotography had practically no foundation in previous scientific work. Chet put together a rather odd lot of phenomena, each of which was obscure in itself and none of which had previously been related in anyone's thinking. The result was the biggest thing in imaging since the coming of photography itself. Furthermore, he did it entirely without the help of a favorable scientific climate. There are dozens of instances of simultaneous discovery down through scientific history, but no one came anywhere near being simultaneous with Chet. I'm as amazed by his discovery now as I was when I first heard of it. [40]

Carlson perceived the problem which EP would ultimately solve in 1936-37, while working on patents at the patent division of the electronics firm P. R. Mallory (now the Duracell division of Proctor and Gamble) in New York City, NY, USA, during the day and studying law in the evenings and on the weekends at the New York Law School [41]. He spent much of his study time at the New York Public Library on Fifth Avenue, copying long passages out of law books that he couldn't afford to buy [39]. Since his father was crippled by spinal arthritis, it was not surprising and very distressing that the long hours sitting caused his back to hurt [39]. Furthermore, his hand would frequently become so cramped that he could not write [39]. These conditions motivated Carlson to think about a copy machine which he believed would solve all of his problems [39].

Carlson was already familiar with the copying techniques of his day and their shortcomings from his work at the law office. He studied photography, chemistry and any other imaging principles that he could find. At length he learned about photoconductivity and after failed attempts to apply its use in an electrochemical context, his attention turned to high voltage (with low amperage) and the potential of electrostatics [39]. David Owen summarized Carlson's rationale, "Carlson realized that if he could devise a copying process based on voltage rather than amperage, he might be able to build a machine that would neither set paper on fire nor electrocute its operator" [39].

Carlson read a brief article by Hungarian physicist Paul Selenyi, who had used a directed beam of ions (charged particles) to create a charge pattern on an insulator (now known as a latent image) [39]. After the pattern was made, it was dusted with very fine particles which adhered to the charged areas to produce an image [39].

The process employed by Selenyi, coupled with Carlson's awareness of earlier image production techniques using dusting and electrostatics (by German Professor George Christoph Lichtenberg since 1777), were enough to inspire Carlson's own process, EP [39]. Carlson originally called the process "electron photography" and by 1942 had consolidated it to "electrophotography" [42, 43].

After filing a patent in late 1937 (which was expanded and granted in 1942 [43]), he set about demonstrating the practicality of his invention with great difficulty [39]. One particularly annoying problem was that the pure sulphur crystals (sulphur is a weakly photoconductive material related to Selenium) that he was trying to melt onto a zinc plate frequently caught fire filling the apartment building with the smell of rotten eggs and alienating him from those who had to endure the odour [39].

Due to the inconveniences he caused with his experiments at home, eventually he rented the second floor of a house in Astoria, Queens, to use as a makeshift laboratory and hired an assistant, Austrian physicist Otto Kornei, to help him with his experimental work [39, 41]. Nearly one year after filing his initial patent, he and Kornei finally achieved the breakthrough they had been working toward. In a darkened room, Kornei charged the photoconductor uniformly by rubbing the sulphur coating on the zinc plate with a cotton handkerchief. Next, he placed a transparent cellulose ruler with black scale marks over the sulphur and turned on a photo flood lamp about 1 foot away for approximately 10 seconds (forming a latent image) [39]. Then he dusted the plate with yellow spores called lycopodium powder and then gently blew away the loose powder to reveal a perfect replica of the ruler's markings. The powder was then wiped off the plate and the process was repeated, but a glass slide with the date and place written on it was used instead of the ruler [39]. The resulting image was preserved by transferring the powder onto wax paper and heating the wax paper to fix the lycopodium powder in

place (Figure 3.3) [39]. This demonstration was repeated countless times in order to attract the investment needed to fully develop this approach into a working machine.



Figure 3.3 – First image developed and preserved using the principles of EP, courtesy of Xerox Corporation [44]

The ensuing efforts to technically mature and commercialize this process spanned many years and several institutions, as detailed by other authors [39, 41], but the foremost champion of this technology throughout the commercialization process was Joe Wilson who was the president of Haloid, the company which would become Xerox. Perhaps most amazing was that based on the usage of the existing offerings, Wilson risked everything on a product that people would “use only a few times a day” [39].

At length, the first fully automatic copier to make copies on plain paper was released in 1959 as the Xerox 914 as shown in Figure 3.4.

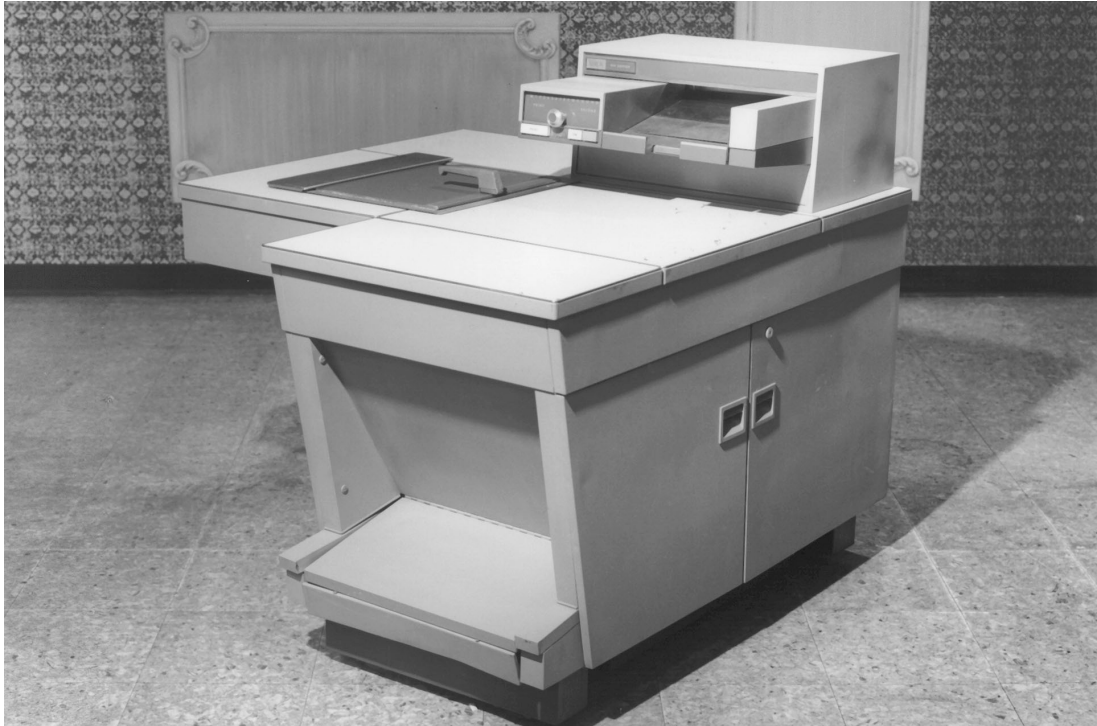


Figure 3.4 – The Xerox 914, the first automatic office copier to make copies on plain paper, courtesy of Xerox Corporation [45]

In the mid-1970's, EP was the enabling technology to move from analogue copying processes to the original digital printing process when it was coupled with a laser that traced a pattern directly onto the photoconductive material, resulting in laser printing. Laser printers are now used at many scales from small offices printing only in black and white to full colour digital printing presses [46].



Figure 3.5 – Xerox Telecopier 200: First laser, plain-paper fax machine (left) [47]; Xerox 9700: First xerographic laser printer (right) [48], both courtesy of Xerox Corporation

The first laser printer was the Xerox Telecopier 200 (roll fed) released in 1975, which was followed by the high speed Xerox 9700 (sheet fed) (See Figure 3.5) a couple of years later [49].

3.1.3. EP Process Overview: 7 steps

Building on the review of the historic inventive steps for EP (§3.1.2), this section gives an overview of the process steps as they have evolved into standard practice today (which were remarkably well anticipated by Carlson’s initial patents [39]).

The first step in EP is to uniformly **charge** the surface of a drum coated with a thin layer of photoconductive material (known as a photoconductor or photoreceptor) in the dark (Figure 3.6). This is normally done by using a corona wire or charge roller which emits ions (charged particles) (for more information see §3.4.1). Additionally the toner is tribocharged, typically by agitation in parallel to this step.

Second, the photoreceptor is discharged in the pattern desired for printing by selective **exposure** to a low power laser or an array of light emitting diodes (LEDs) (Figure 3.6). The resulting charge pattern is called a latent image.

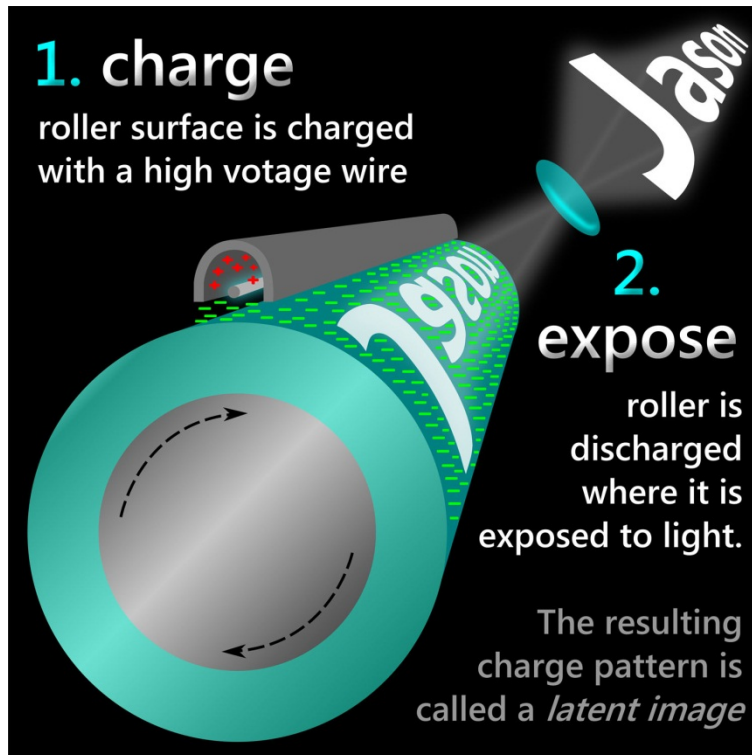


Figure 3.6 – Illustration of the charging and exposing steps in EP

Third the image is "**developed**" by presenting charged toner particles to the photoreceptor. This term seems to have been adopted from the wet chemical photographic development process, even though in this case it is based on physics and not on chemistry. Where charge remains on the photoreceptor surface, the toner is repelled. Where the charge has been eliminated (through exposure to light) the toner adheres by electrostatic forces (as illustrated in Figure 3.7), this is called discharged area development (DAD). In some printers the development process is

reversed so that toner adheres to an opposite charge left on the surface of the photoreceptor, this is called charged area development (CAD).

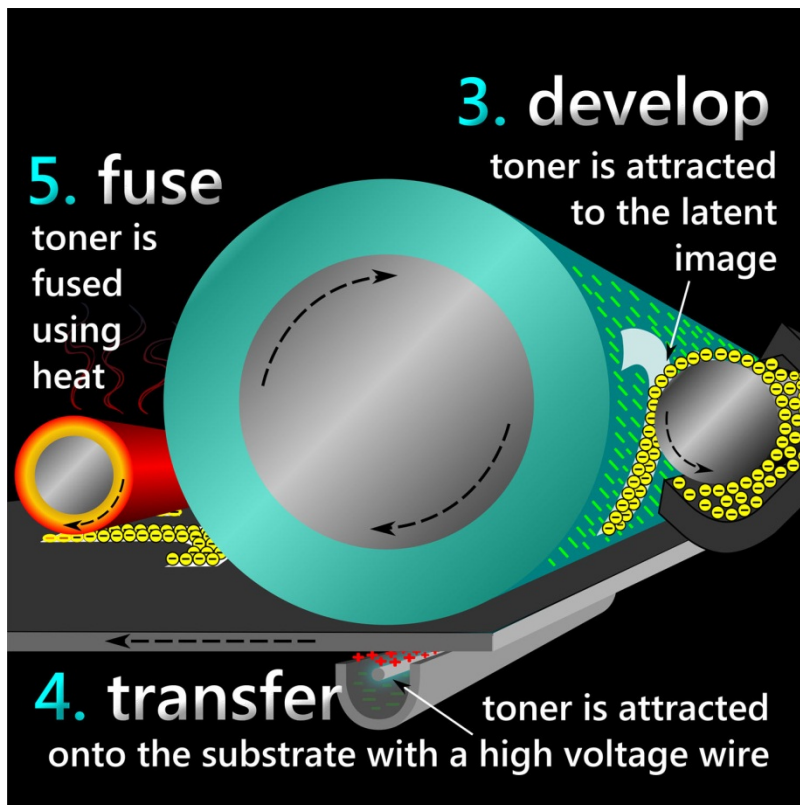


Figure 3.7 – Illustration of the development, transfer and fusing steps in EP

Step four is to **transfer** the toner off of the photoreceptor and onto the paper (or other substrate). Normally this is achieved by creating an electrostatic field between the photoreceptor and a high voltage wire on the backside of the paper. The field strength is adjusted to be stronger than the electrostatic forces holding the toner onto the photoreceptor. The positive charge on the backside of the paper electrostatically “tacks” the toner in place on the paper until it can be permanently **fused** in place, most often using a heated roller, which is the fifth step in the process. The sixth and seventh steps **clean** any residual toner off of the

photoreceptor and **erase** any residual charge by exposing the entire surface of the photoreceptor to light.

In modern laser printers and photocopiers, these seven steps are executed continuously and in parallel as shown in Figure 3.8.

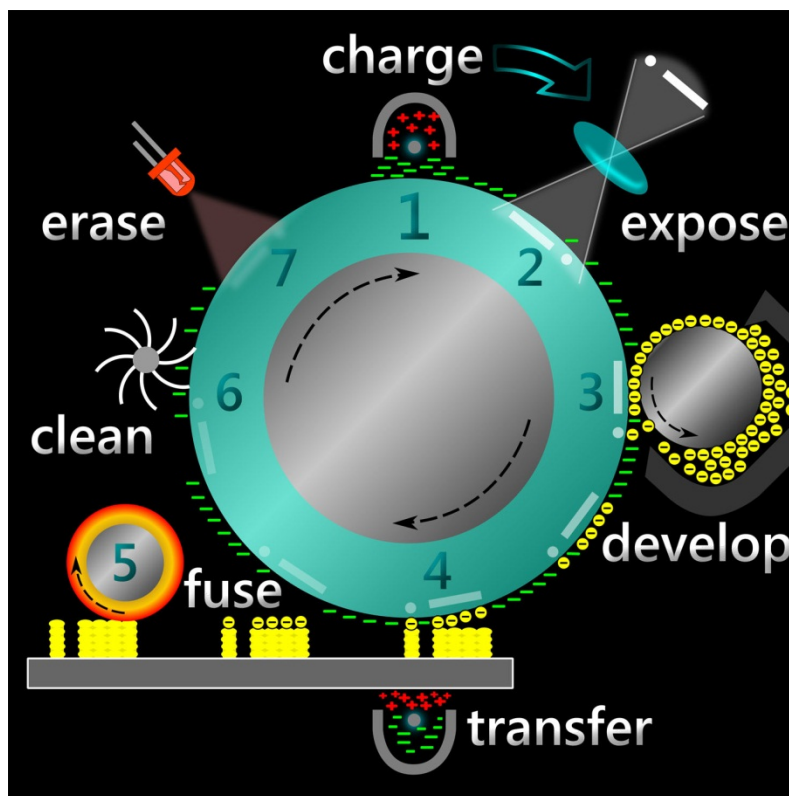


Figure 3.8 – Illustration of all 7 steps used in a typical EP device

3.2. Toner and Carrier Preparation and Measurement

In the early days of Xerox, the extreme difficulty of producing good toner earned it the nickname “black gold,” and many supposed that toner development alone would act as a barrier to competition [41]. This

theory was validated in the 1970's when anti-monopoly pressure mounted in many countries and at least in some cases, legislation required the separate supply of toner and machines [50]. Incidentally, the author asserts that the enduring complexity and expense of producing lab and pilot scale batches of customised toners and fusing them (particularly in comparison with ink formulation for inkjet) may still be the primary factor why EP has not yet matured as a direct deposition technique in digital fabrication or AM.

Understanding the difficulties and implications of toner production and yield (and circumventing them at least to some degree) is essential in order to enable AM by EP. To that end, this subsection reviews the dominant production techniques and characteristics desired in toner.

3.2.1. Toner Materials and Composition

A typical full-page (A4 or US letter) single-sided EP print can precisely place in excess of 10,000,000,000 (10^{10}) individual toner particles in a matter of seconds; where each toner particle is typically 7-10 μ m in diameter and has a charge in the range of 10^{-15} - 10^{-14} C [46, 51]. This triumph of engineering has only been possible through highly mature production and characterization techniques on a relatively narrow range of toner materials. Conventional EP applications (involving the printing of text and images) are fully invested in the optimized performance of incumbent toner formulations and have little incentive to change.

The original "toner" used by Chester Carlson was lycopodium powder (as related in §3.1.2) [52]. The yellow-tan coloured powder is a naturally occurring spore from certain club mosses with a relatively spherical isometrical shape and a median size (d_{50}) of $\sim 32\mu\text{m}$, and a naturally occurring narrow particle size distribution (PSD) (d_{10} and d_{90} of $10\mu\text{m}$ and $52\mu\text{m}$ respectively) as measured by Živcová et al. [53]. Both the round shape and narrow PSD contributed to the success of Carlson's early demonstrations; however the relatively light colour did not provide good contrast when deposited on white paper and a practical method of making the image permanent had yet to be conceived.

The toner development team at Haloid (later Xerox) tested hundreds of materials searching for the ideal toner material from grains including "Gaines Dog Food", minerals, and virtually every natural and artificial polymer known [54]. The material needed to charge adequately during the EP process and then fuse permanently on the paper. Ultimately it was determined that to make the process viable, a semi-crystalline polymer with a low melting point was essential for the fusing step. Referring to the 914, John Rutkus would later remark, "If we hadn't accomplished the lower-melt toner, we wouldn't have had a product" [39]. This led to the standardized use of non-conductive polymer materials for most toner applications as described below. Alternative toner material formulations, including conductive and photoconductive materials have been proposed for niche applications, and will also be explained briefly.

3.2.1.1. Non-conductive Toner

The diverse requirements of toner traditionally have led to a choice of matrix material (typically composing 40-60 wt.% or 75-90 wt.% for magnetic and non-magnetic toners respectively) restricted to a narrow range of dielectric polymers, especially styrene-acrylate co-polymers (used in an estimated 80% of toners) and polyester [55]. These matrix materials are loaded with pigments (See Figure 3.9), charge control agents (CCAs), internal waxes (typically to aid fusing), and magnetite (especially for magnetic toners). Surface additives, often called flow control agents (FCAs) on the exterior of toner particles enhance toner flow, help control charge and help to reduce toner adhesion [55]. Incidentally, the FCAs are typically nanoscale metal oxides, which makes the toner behaviour of EP a nano-enabled technology. Figure 3.9 shows toner after fusing and indicates the degree of particle melt with standard black toner and print settings (LaserJet 5500, Hewlett Packard, CA, USA).

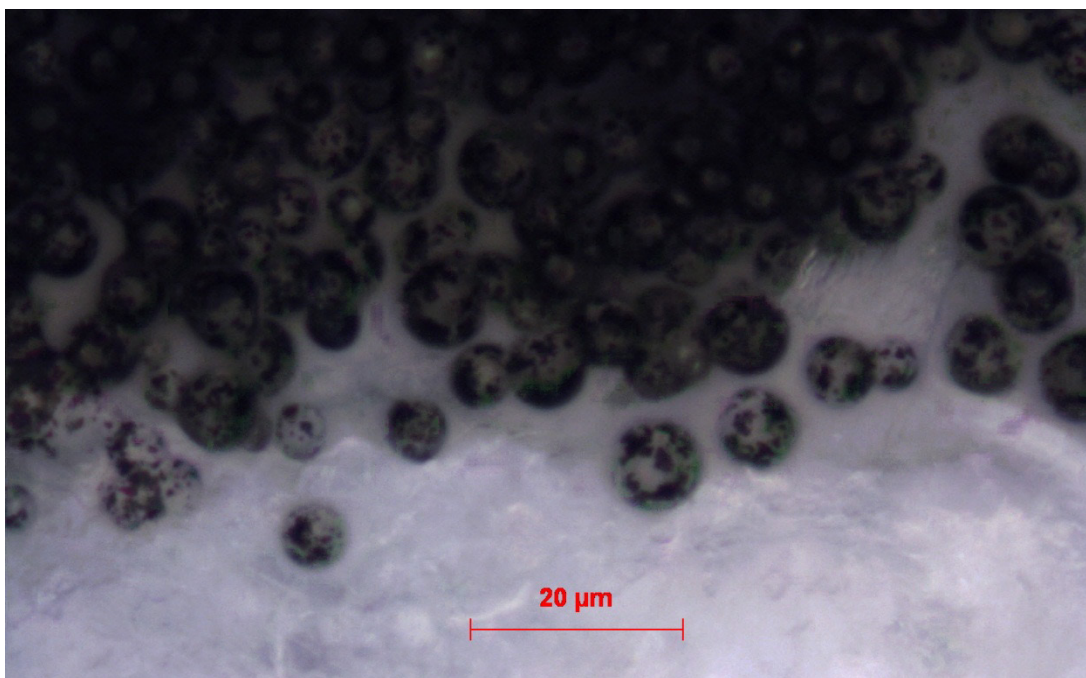


Figure 3.9 – 100X magnification of toner showing the black pigments in a partially melted (and resolidified) translucent polymer matrix

It is noteworthy that virtually all of the early toner materials were reduced in size by fracturing (See §3.2.2) [51]. Therefore brittle polymers (including styrene-acrylate co-polymers and polyester) were favoured due to their low specific cost for size reduction. Although chemical polymerization methods are capable of producing fine powders in non-brittle polymers, the development of chemically produced toners has been driven by maintaining compatibility with the status quo, therefore the range of polymers produced chemically tend to have a very similar formulation to those which can be reduced mechanically.

Initially Xerox used a positively charging toner due to the type of photoreceptor that they used. Then the development of low cost organic photoconductors (OPCs) in the 1980's (which were sensitive to the $\sim 780\text{nm}$ wavelength of low cost solid state lasers for laser printing), led the industry to favour toner materials that tend to triboelectrically charge with a negative affinity [56, 57]. Economies of scale for the lower cost hardware components, and increased production of negative toners, resulted in most EP equipment being standardized for negative toners. Consequently, the modern availability of pigments, CCAs, FCAs, and other toner additives for modifying materials is better for negatively charging toners [55].

Despite the predominant use of a narrow range of polymers, researchers have demonstrated the potential for EP to print a much wider range of materials. These materials include: high and low density polyethylene, polyvinyl acetate, polypropylene, nylon, thermoplastic elastomers, a

soluble acrylic material, polyether ether ketone (PEEK), polyamide-imides, polytetrafluoroethylene (PTFE) and others known to the author, but not publically disclosed at this time [58-61].

Beyond polymers, ceramics have been used in industrial and research contexts. To date the printing of pure and nearly pure ceramic has been primarily restricted to a research context [62-64]. Since most ceramics tend to tribocharge positively [65-68] and are highly abrasive, exploration of their use may be impeded due to the difficulty of obtaining suitable EP printing devices to use them for toner. The highest ceramic content toner commercially available is loaded with ceramic pigments and used for decoration of ceramic tiles and other fired products as experimented with in §6.3.1.2.2. These toners are typically printed onto transfer paper using a conventional two-component printer and then transferred onto the ceramic substrate for subsequent firing. Suppliers for these toners tend to be relatively small specialized organizations including FotoCeramic (UK), mz Toner Technologies GmbH (Germany) and Ceramic Digital (UK) [64, 69]. The FotoCeramic toner has an estimated ceramic content of 40 to 70 wt.% with the remainder being composed mostly of polymer and wax for fusing [70].

3.2.1.1.1. *Dielectric Behaviour (Including Polarization) and Properties*

The concept of dielectric behaviour and related material properties in an insulating material will be important to understanding triboelectric charging and future discussions in this work, therefore it is introduced

here with Figure 3.10 showing a simplified representation of atoms (showing only outer shell electrons) in a conductor and atoms within molecules of a dielectric insulator. In contrast to metals, where the outer valance electrons are free (or nearly free) to move around the object (such as to achieve maximum distribution around the object's surface according to Gauss' law [Figure 3.10 upper left] or re-distribute due to induced charge separation [as shown in Figure 3.10 lower left]), the electrons in non-conductive materials are bound to their nuclei and cannot move around freely.

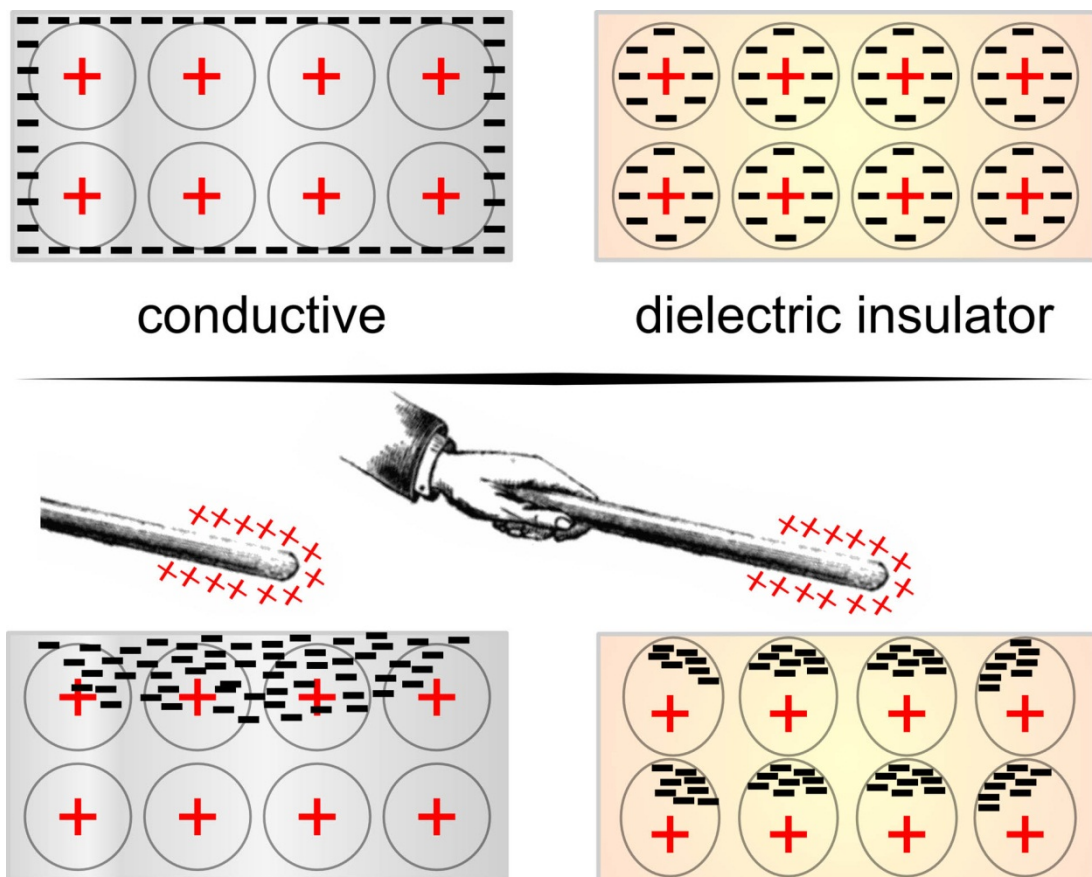


Figure 3.10 – Electron behaviour in a conductor and dielectric material resulting in charge separation and dielectric polarization respectively.

Despite the limited electron mobility in an insulator, polarization can occur at a molecular level, where electrons re-distribute within the bounds of the electron shells (Figure 3.10 lower right). This re-distribution of electrons is referred to as *dielectric polarization* which can occur in virtually any material and manifests itself as electric dipoles, and is especially pronounced in polar molecules [71-74]. A material in which there are permanent electric dipoles is called an electret and behaves as an electrostatic analogue to the permanent magnet (which has permanent magnetic dipoles) [75, 76]. The degree of material polarization (which can also cause molecular reorientation in weakly bonded molecules) caused by a field is called *electric susceptibility*, c_e , and increased polarization typically enables electric fields to pass through a material more easily [77].

Related to the electric susceptibility is a material's electromagnetic *permittivity*, ϵ_r , which is the measure of a material's resistance to allowing an electromagnetic wave or electric field to form in or pass through it [78]. The response to a field is "expressed as the ratio of its electric displacement to the applied field strength" [79], measured in Farads per metre (F/m). The *absolute permittivity* of a vacuum, ϵ_0 , is 8.8541×10^{-12} F/m. Standard practice is to compare the permittivity of all other materials (at a given temperature and frequency) to the absolute permittivity of a vacuum which is defined to have a relative permittivity of 1.0 [80]. Therefore the *relative permittivity* ϵ_r or κ (also known as a relative dielectric constant) is the ratio of the amount of electrical energy stored in a material by an applied voltage compared to

that stored in a vacuum [81, 82]. Counter intuitively, the higher a material's ϵ_r , in general, the more it slows down electromagnetic waves/fields propagating through it [83, 84]. Typically the higher a material's ϵ_r , the less it polarizes, thereby resisting the flux (rate of a field passing through it). That means the higher a material's ϵ_r , the weaker the total electric field is inside the dielectric [84, 85]. Toner production method and scale has been shown to affect the ϵ_r ; which tends to be higher for production scale than pilot scale batches, probably due to the more heterogeneous mixing of the extruders at smaller volumes [86]. Incidentally dipoles created by nature tend to be much stronger than those in manmade materials, for example water typically has $\kappa \sim 80$, while most toner polymers are ~ 3 (with a few approaching 10) [54, 55, 80, 86]. Materials with a high ϵ_r , are desired for miniaturizing capacitors because the more insulating capacity a material has, the less of it is required in the gap to achieve the same capacitance [87]. Generally, ceramics have very high $\epsilon_r > 100$ compared to polymers which are typically < 4 [87, 88].

A material's insulating ability is described by its *dielectric strength*, which is a measure of the maximum field strength, measured in volts per meter (V/m) it can withstand without breaking down (allowing electrons to flow, typically as a spark) [89, 90]. When a solid material breaks down, the field is so strong that it frees bound electrons to create a conductive path to ground which typically destroys (or at least significantly degrades) the material's insulating ability [89]. For many bulk ceramics and polymers, the dielectric strength is inversely proportional to its relative permittivity

[91]; typically where ceramics have relatively low dielectric strength of <50kV/mm compared to polymers which have high dielectric strengths >300kV/mm [87, 88].

The *volume resistivity*, r , (also known as electrical resistivity) as defined by ASTM D257 [92] has been summarized as, "...the resistance to leakage current through the body of an insulating material. The ratio of the potential gradient parallel to the current in a material to the current density. In SI, volume resistivity is numerically equal to the direct-current resistance between opposite faces of a one-meter cube of the material (Ohm-m)" [93]. Contrary to conventional measures of resistance, which vary with the length and cross-section of a wire, resistivity is the specific resistance of a bulk material. Typical toner materials have a resistivity between 10^8 - 10^{14} $\Omega\cdot\text{m}$ which has been demonstrated to effect the deposition rate (measured by weight) per area in EP which, according to at least one study, correlates to deposition rates of 0.9 and 0.3 mg/cm² respectively [86].

3.2.1.2. *Conductive Toner*

Given the objectives of this research, it may seem irrelevant to discuss conductive toners; however the problems arising during transfer (See §4.6) lead to the natural consideration of using conductive toners. For that reason the composition of 'conductive' toners is included here and an explanation of its implications on development and transfer in §3.4.4.3.

The term 'conductive toner' is used indiscreetly and can refer to toner composed of a *polymer matrix* loaded with conductive particles, a polymer *encapsulated* conductive powder, or toner in which the matrix material (and therefore the outer surface) is *inherently conductive*. The former has been investigated recently for two-component development where a *polymer matrix* conductive toner has been loaded with silver flakes and beads [94, 95]. The toner behaves essentially like an insulator during the printing process, due to its polymer matrix which isolates its conductive content (although the presence of some metals does influence the deposition rate and tendency for reverse bias development to a greater extent than the volume resistivity according to some [96]). After fusing, the toner is typically fired, which removes the polymer matrix material and sinters the silver to become functional for electronics [94, 95, 97-101].

Encapsulation by a dielectric material (such as polymer) has been widely used to electrostatically deposit materials from metals to pharmaceuticals. The ethos behind encapsulating something with a shell is that, "...a universal shell material is provided for use with various variable core compositions, permitting alterations to the components in the core without affecting electrostatic application of the powder materials to a substrate" [102]. Although theoretically this seems like the ideal solution, in practice it is not that simple. Specifically when trying to encapsulate solder powder with a dielectric coating, Walker et al. explained how the thickness of the shell impacted on the effectiveness of tribocharging. They succinctly summarized the relationship as follows:

In triboelectric charging of insulators, the electrons and protons are polarized. Also, the strength of the attraction depends on the Coulomb force between the two materials. The Coulomb force increases as the charge increase [sic]. This charge is directly proportional to the number of electrons available. Therefore, the thickness of the coating can be varied to supply the needed electrons to produce adequate charges [103].

By encapsulating conductive materials with an appropriate thickness shell, they can be charged and printed as insulators and later post processed to achieve bulk conductivity in a similar way as the polymer matrix-based 'conductive' toner explained above. As explained in §3.4.4.3 a substantial thickness of shell is required to overcome the tendency of the conductive core to polarize thereby repelling itself from a conductive substrate as shown in Figure 3.29.

The development of *inherently conductive toners*, made primarily from pure metals or solder pastes, has been attempted with limited and rumoured success [18], however to the author's knowledge its use has been restricted primarily to deposition in monolayers onto non-conductive substrates, or for use in processes such as ionography as used in the Metal Printing Process (MPP) described in §4.4.4.

3.2.1.3. Photoconductive Toner

Discussion of photoconductive toners may seem out of scope in this study. However, the problems arising when attempting to upscale the transfer step for multilayer/3D printing (See §4.6) lead to the natural consideration of using photoconductive toners.

The proposed use of a photoconductive material based toner was first published in 1963 in Japan, and its proposed use to form a photoconductive shell around a transparent core was filed in 1969 [104]. The post-treatment of each layer to maintain conductivity was published in 1973 [104] for reasons explained in the following paragraph. More recently, the use of materials yielding improved photosensitivity in toner [105], and even some which reverse their charge in an applied electric field when illuminated have been published [46, 106].

Honjo explained that the photoconductivity of the toner with transparent core was compromised by the fusing step for each layer because the continuity of the shell material was disrupted/diluted by the highly insulating core material [104]. Fully photoconductive toners suffered a height limiting phenomenon in that multiple fused layers absorbed the radiation thus effectively shielding underlying layers from light, thereby limiting the depth of conductivity. The compromised photoconductivity in both cases limited the number of layers which could be electrostatically transferred image-on-image, because even though the freshly deposited toner could be irradiated (achieving a conductive state) the poorly irradiated underlying fused layers acted as an insulator, thereby isolating the fresh layer from ground and thus inhibited charge neutralization [104, 107]. For that reason Honjo proposed globally treating each layer by spraying it with a conductive compound after deposition in order to maintain consistent conductivity with each layer printed, thereby counteracting the highly insulative nature of the toner, as shown in Figure

3.11 [104]. Although the rationale for his approach is well explained, it seems to negate the advantages of using a photoconductive toner.

FIG. 3

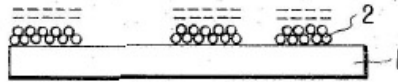


FIG. 4

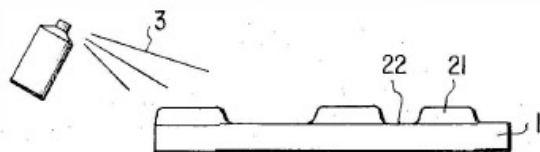


FIG. 5

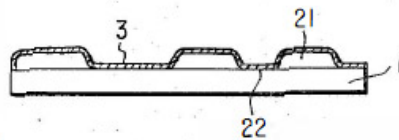


Figure 3.11 – Figures 3-5 from US Patent 3,764,312 [104] showing the spraying of fused toner to achieve a conductive state

3.2.1.4. Discussion of toner materials

As illustrated by the foregoing, non-conductive non-magnetic toner provides a good compositional match with the objectives of this research to print “pure” polymer (See §1.2). This class of materials has been printed extensively and is therefore the best studied and understood toner [108].

Conductive toners represent unique possibilities for applications with alternative transfer challenges §3.4.4.3, however the conductive

components can be challenging to print, and be regarded as contamination when the objective is to produce parts in “pure” thermoplastic materials.

Although the photoconductive toners provide a unique way to neutralize residual toner charge on a layer by layer basis, they suffer from height limitation when using an electrostatic transfer, and also compromise the ability to print pure thermoplastics by contaminating them with semi-conductive materials.

In line with the objectives of this research, which stipulate the use of “pure” thermoplastics, non-conductive non-magnetic toners charged by two-component development will be the focus of the remainder of this work (for further selection rationale see §5.1).

3.2.2. Pulverised Versus Polymerised

Toner production for EP has undergone substantial improvement since EP was first commercialized. Understanding the production methods gives an appreciation for the historic choice of toner materials which still heavily influences modern toner composition.

The first industrial toner production (Figure 3.12 left) was achieved by melt mixing the toner ingredients in an extruder to form pellets which were subsequently pulverized by a grinding process (normally by air jet milling) and classified to achieve a relatively narrow particle size

distribution (PSD) [109, 110]. This method still accounts for ~40% of colour and ~80% of black toner production worldwide [111].

(Intentional page break to allow illustration and images on the next page to be viewed at the same time)

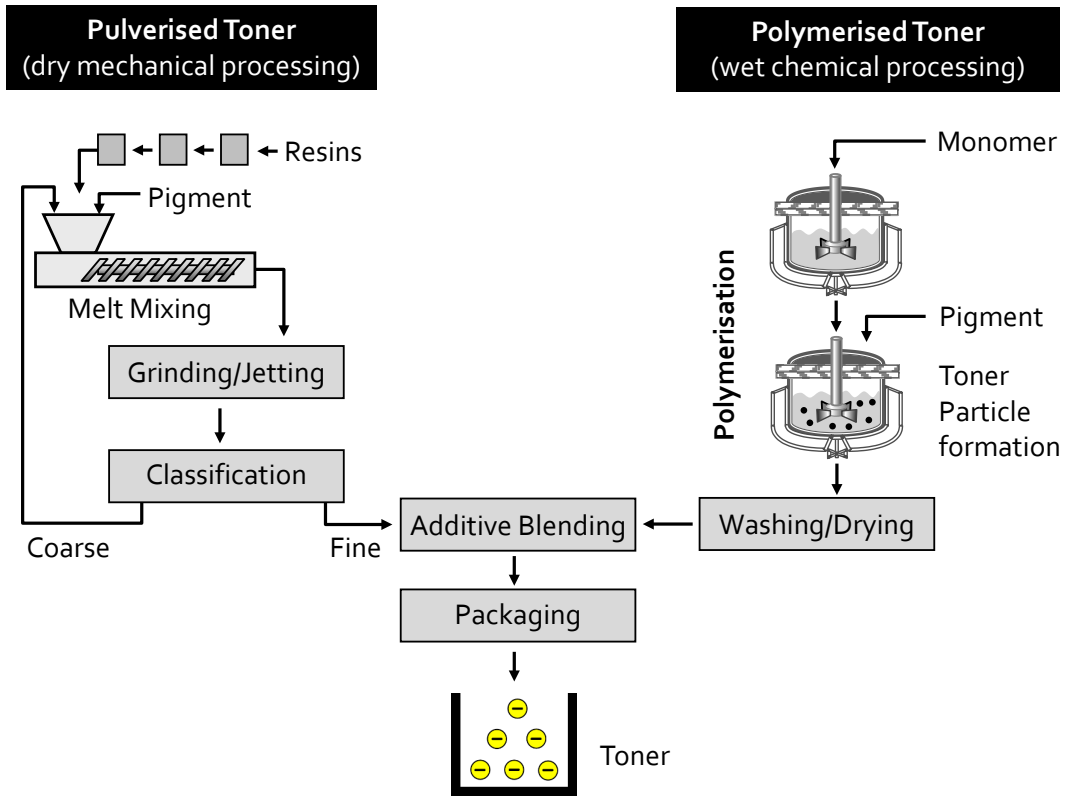


Figure 3.12 – Conventionally pulverized vs. chemically polymerized toner preparation (after [112])

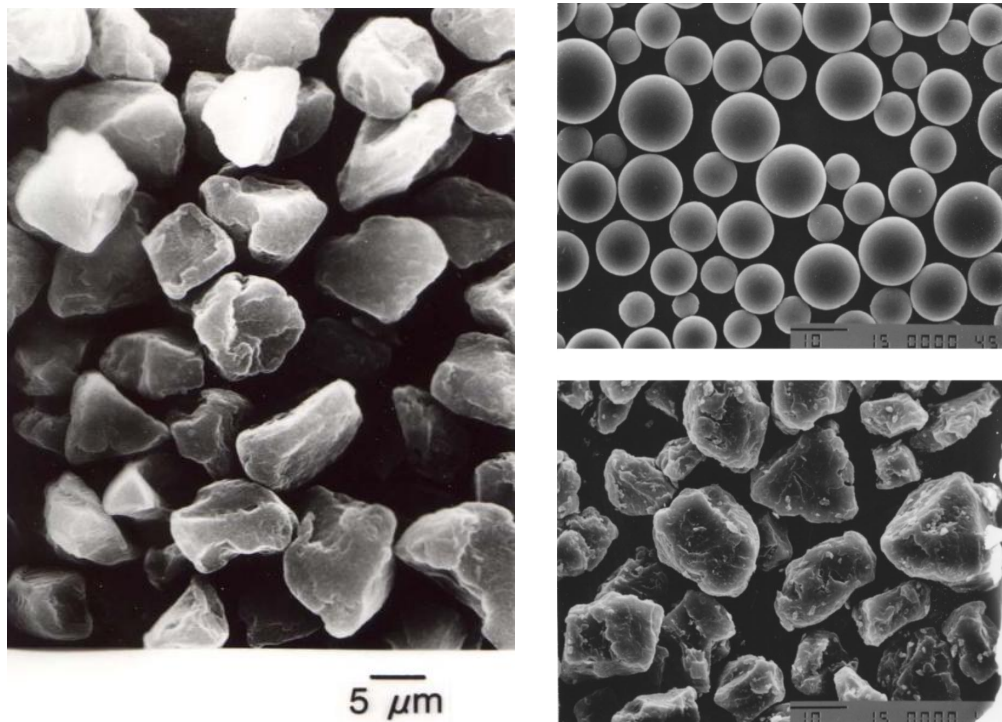


Figure 3.13 – Mechanically pulverized toner (left [37] and lower right [113]) compared to chemically polymerized toner (upper right [113])

In order to most efficiently reduce the pellets to fine particles, brittleness is desired in the toner matrix material. Toners produced by pulverization typically have irregular shapes with angular faces due to brittle fracture as shown in Figure 3.13 (left and lower right) [109, 110] with an estimated surface area typically less than a few m^2/g .

The toner industry is in widespread transition toward chemical production of toner (Figure 3.12 right), as evidenced by the fact that as of the last five years, the majority of colour toners ($\sim 60\%$) are being produced by chemical means [111, 114]. This transition is driven by the desire for higher resolution, which requires finer toner particles, which can be produced chemically with a narrower PSD, using less energy with less waste, than pulverized toner [111, 115]. A variety of polymerization techniques are used to produce toner [110]; but in a typical approach monomers, pigments and additives are dispersed and homogenized in an aqueous medium and then the mixture is polymerized in a reactor to form fine toner particles which are subsequently rinsed and dried [110, 113, 116]. The size of the particles can be adjusted by changing the monomer and by varying the polymerization conditions, especially the reactor mixing rate which heavily determines the degree of emulsion separation, which determines the toner size [117, 118]. Under optimized conditions the yield can approach 100% of particles in a usable size range [69]. The surface tension and other factors in the chemical production generally tend to produce spherical toner particles as shown in Figure 3.13 (upper right). The polymerization process does not oblige the use of brittle materials; however the coexistence of polymerized and

pulverized toners (in some cases even for the same printer) has led to the choice of similar chemistry polymer matrices in both. This trend may change as the market fully embraces chemically produced toner (obviating the need for “backwards compatibility” with pulverized toner) and environmental/sustainability priorities lead toward toners based on renewable plant oils [119].

3.2.3. Toner Size

Optimum toner size varies from printer to printer but is typically between 5-20 μm [54, 86]. A trend of reduced toner particle size has been driven by the desire for higher resolution prints/printers [95]. For example, a 600, 1200 and 2400 dpi print resolution correlates to square pixel sizes of 41.8, 20.4, and 10.2 μm . Since single pixel and single toner particle deposition have been demonstrated as impractical, toner diameters at a fraction of the pixel dimensions are required [120]. Incidentally, the pursuit of higher and higher resolution printing has driven premier quality printing toner particles below 5 μm which are handled suspended in a liquid (liquid EP) rather than as dry powders, for several reasons including prevention of health and safety concerns from airborne powders [121, 122]. Although a toner population may be centred on a desired toner size, it is the deviation from the centre (i.e. the tails of the PSD) that most impacts print quality, which provides a strong impetus to keep the PSD narrow [123]. A typical PSD for a “9 μm ” toner might have percentile particle diameters (d_5 , d_{50} , d_{95}) of 5.5, 9.1, and 13.6 μm .

3.2.3.1. Classification

Owing to the influence of particle size on its charging magnitude, accurate classification of toner size is essential. When the PSD is too wide, smaller particles have a higher charge-to-mass ratio than larger ones and as a result toner particles do not act in unison, thereby undermining development and transfer steps [86]. This condition can lead to undesired and uncontrolled toner deposition including accumulation on the surfaces inside a printer which is called *dusting* [110].

Originally the lycopodium spores used by Carlson had a naturally occurring narrow PSD which precluded the need for classification [53]. Manmade toner materials do not normally have this advantage, although some optimized chemical processes yield particles with such a narrow PSD that classification is unnecessary [69, 109, 110].

For pulverized and wide PSD polymerized toners, mechanical sieving has and continues to be an essential method for cutting the tails of a PSD. Where higher accuracy is desired, laser diffraction devices have become the dominant method for characterizing PSD expressed as a differential size distribution or a cumulative undersize distribution (also explained in ASTM F577 [124]) [125-127]. In fact, many air jet mills have an integrated classifier in order to extract only particles which have reached the right particle size range and let the others further reduce before they are removed from the mill [86, 109]. Even with laser diffraction, classifying particles $<5\mu\text{m}$ is very difficult, and frequently $1\text{-}4\ \mu\text{m}$

particles are mixed in with the final product; this difficulty reinforces the trend toward polymerized toners [113].

3.2.4. Tribocharging Toner with Carrier

The recognition that charging occurs when contacting and especially rubbing two materials together goes back to Greek times when silk rubbed amber attracted hay, feathers, or dry leaves [128, 129]. Indeed, the English word "electricity" is derived from the Greek word for "amber" and "tribo" from the Greek word to "rub" which combine into the term "triboelectricity" [129]. Even though these may be our earliest recorded observations, certainly the observation of tribocharging must predate those records because these phenomena can be observed in nature such as windblown (dry) snow [130] or sand [131] and more recently with lunar particles [132].

Charge on insulators is a surface dominated phenomenon because there is no mechanism or path for readily inducing the charge to travel into the bulk of the material. The depth that charge penetrates into polymers for example, has been debated between researchers, but is generally agreed to be between <10 angstroms and 30nm [54, 133]. In granular systems it has been noted that "...charging is generally such that smaller particles charge negatively while larger particles charge positively" [134]. This is an observation that holds true for many present day toner-carrier combinations [86].

EP was perhaps the first use of particle charging where the effect was intentionally produced on something other than waste (such as airborne contamination) [39]. In 1992 Dr. L. B. Schein characterized understanding of toner charging as being in the, "pre-scientific era, primarily based on empirical studies," he further emphasized that "toner charging, specifically, and insulator charging, generally, remain one of the least-understood branches of physics" [108]. Although significant progress has been made as reported herein, there are still many unanswered questions. Toner charging, according to Karner et al. [135], depends on many factors including: particle size, particle shape, surface roughness, nature and work functions, impurities, amorphicity, contact material, energy of contact and relative humidity.

A wide variety of development methods have been devised in order to effectively charge toner (§3.4.3), however the most widely implemented method (two-component insulating brush development) [108] has been selected for these trials (§5.2). In this development method (explained in §3.4.3), toner is brought into rubbing contact with a second material, selected specifically to achieve a target charge polarity and magnitude on the toner. The ability to tune the properties of the second *carrier* material, make this charging process extremely flexible. Nash explained that, "the use of carrier 'chemistry' to manipulate toner charging properties is potentially a most valuable tool for developer designers" thus enabling charging of toner with a wide range of chemistry by using different carriers [136].

In order to conveniently contact the toner surface, the second material is used to encapsulate larger spheres with soft or hard magnetic cores (For SEM image of carrier core see Figure 6.9) called *carrier or developer beads*. When mixed in appropriate ratios, and agitated together, triboelectric charging results in the toner particles electrostatically adhering to the outside of the carrier beads (Figure 3.14). The ratio in which agglomerates naturally combine is such that each carrier-toner agglomerate has a net zero charge. The electrically neutral carrier-toner agglomerate is reminiscent of an electrically balanced atom where nucleus and orbiting electrons correlate to the pseudo-fractal geometrical arrangement of the carrier and toner. Typical toner-to-carrier concentrations range from 3 to 10 wt.% of toner, with the balance of the mixture made from carrier beads. Maintaining a consistent toner concentration is critical to ensuring uniform charging [137]. Concentration is typically measured using a sensor in the developer.

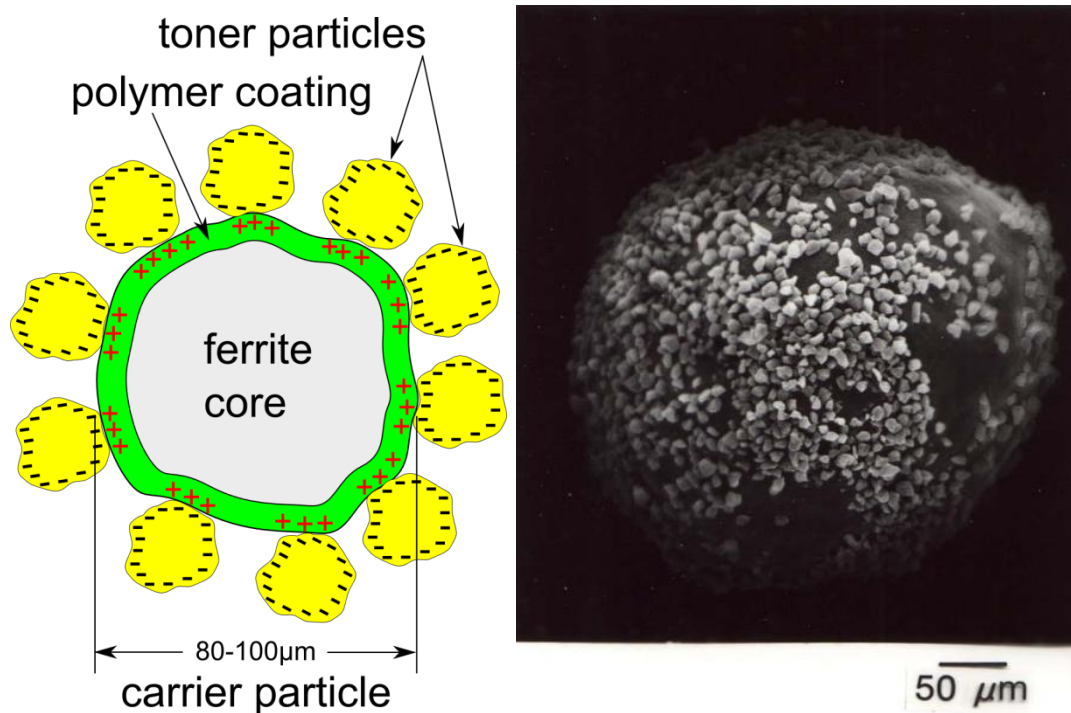


Figure 3.14 – Illustration of toner on carrier (left), and SEM image [37] of toner on a large carrier bead (right)

The reduction in the average size of carrier beads has kept pace with the trend of reduced toner particle size in order to provide the appropriate ratio of carrier surface area to toner surface area (where the smaller the carrier particle diameter, the higher the charge provided to the toner, due to the increased available surface area) [86, 95, 138]. Average carrier particle diameters from the 1980s, 1990s and 2000's correspond to 90, 60 and 35µm respectively with a trend away from metal cores toward hard or soft magnetic ferrite cores [138].

3.2.4.1. Predicting Tribocharge Polarity – Triboelectric Series

Material behaviour during triboelectric charging can be characterized by the likelihood of a material to donate or accept electrons. Nearly all materials can be forced to acquire either a net positive or negative

charge if rubbed with the right secondary material. The relationship between tribocharged materials is expressed by the triboelectric series in Table 3.1, which allows prediction of tribocharge polarity. When any two materials in the series are rubbed together the material listed closer to the negative end of the series will gain a net negative charge, while the other material will gain a net positive charge. Many triboelectric series have been developed exploring materials and the influence of additives on their charging tendencies [54, 108, 139-143]. The longest series known to the author is one by Battelle Memorial Institute (who worked with Chester Carlson on EP) which had more than 280 materials listed on it [54].

Many toner materials are intentionally selected from the middle of the triboelectric series so that with some additives the toner can be charged either positively or negatively.

Table 3.1 – Triboelectric Series*

+ POSITIVE END OF SERIES

Asbestos glass
Silicone elastomer with silica filler
Borosilicate glass, fire polished
Window **glass**
Polymethylmethacrylate
Ethylcellulose
Polyamide 11
Polyamide 6-6
Rock Salt (NaCl)
Melamine formol
Wool, Knitted
Silica, fire polished
Silk, Woven
Polyethylene glycol succinate
Cellulose acetate
Polyethylene glycol adipate
Polydiallyl phthalate
Cellulose sponge
Cotton, woven
Polyurethane elastomer
Styrene-acrylonitrile copolymer
Styrene-Butadiene copolymer
Polystyrene
Polyurethane flexible sponge
Borosilicate glass, ground state
Polyethylene glycol terephthalate
Polyvinyl butyral
Formo phenolique, hardened
Epoxide resin
Polychlorobutadiene
Butadiene-acrylonitrile copolymer
Natural rubber
Sulphur
Polyethylene
Polyvinyl chloride without plasticizer
Polytrifluoroethylene
Polytetrafluoroethylene (PTFE)

- NEGATIVE END

*(adapted from [54, 108]); bold items are frequently used in toner

3.2.4.2. **Predicting Tribocharge Magnitude**

Many researchers made contributions toward creating models capable of predicting the charge magnitude when tribocharging insulating/dielectric powders [65, 68, 144-148]. Frequently, discussions acknowledge the great difficulty in correlating measured values with ionization potential, dielectric constant, or dielectric strength [144]. Despite the challenges, Gutman and Hartmann of Xerox developed a two-component development tribocharge model that predicts the sign and magnitude of the charge-to-mass (q/m) ratio of a toner at concentration C , as published in the early 1990's and set forth below [136, 141, 149]. Nash summarized the formula by explaining: "Conceptually, toner triboelectric charging can be simply expressed as a product of terms related to the physics and chemistry of charging and to the mechanics of mixing" [141].

Tribocharge model by Gutman and Hartmann (Xerox)

$$q/m = \left(\frac{A'}{C + C_0} \right) \cdot (\phi_{toner} - \phi_{carrier}) \cdot (1 - \exp\{-\gamma \cdot t\}) \quad (3-1)$$

physics chemistry mechanics

Where

q/m is the charge to mass ratio

C is the toner wt.% concentration of the toner-carrier mixture

γ is the rate constant defined by the type of mixing

t is the mixing time

The other variables are determined by the following equations.

The A' term is defined for Equation (3-1) as follows [141]:

$$A' = \left(\frac{4 \cdot \pi \cdot R^2 \cdot \varepsilon_0}{M \cdot e \cdot d} \right) \quad (3-2)$$

Where

R is the radii of the carrier bead

ε_0 is the absolute permittivity of a vacuum (8.85×10^{-12} F/m or C²/J·m)

M is the mass of the carrier bead

e is the elementary charge (1.602×10^{-19} C)

d is the charge tunnelling cut-off distance (typically assumed to be 1nm)

The C_0 term is defined for Equation (3-1) by the following formula:

$$C_0 \approx \left(\frac{\rho_{toner} \cdot r_{toner}}{\rho_{carrier} \cdot R_{carrier}} \right) \quad (3-3)$$

Where

ρ is the density of the toner and carrier

r is the radius of the toner

R is the radius of the carrier bead

Since the surfaces of toner and carrier particles are typically composed of multiple components (such as binder, pigment, FCA, etc.), the Φ_{toner} and $\Phi_{carrier}$ terms in Equation (3-1) can be expressed as the sum of the surface-weighted characteristic charging factor contributions for each component as follows [141]:

$$\Phi = P_i \cdot \mu_i + P_j \cdot \mu_{ji} + \dots \quad (3-4)$$

Where

P_i, P_j , etc. are the fractional weights, with total sum equal to unity

μ_i, μ_j , etc. are characteristic charging factors for each surface component

Therefore the terms in Equation (3-1) can be summarized as follows:

The $\left(\frac{A'}{C+C_0}\right)$ term accounts for contribution to charging by the toner-to-carrier ratio and their respective physical characteristics (size, mass, density, etc.). Next the $(\phi_{toner} - \phi_{carrier})$ term accounts for the surface chemistry contribution to charging. Finally, the $(1 - \exp\{-\gamma \cdot t\})$ term parametrically represents the saturation of triboelectrical charge as a function of mixing time in the developer [136].

This formula is the best model developed to date, but its practical use is marginal as Nash explains, because some "considerations not explicitly accounted for" by the above equation are critical to the success of toner behaviour [136]. The reason is that equation (3-1) only deals with an average charge-to-mass ratio q/m , whereas in practice the non-average population of the toner distribution can compromise the ability of the particles with mean characteristics to print with EP [136]. For that reason, the industry relies principally on measuring charge empirically.

3.2.4.3. Measuring Toner Charge

Due to the difficulties of predicting the spectrum of charge that a toner will acquire (See §3.2.4.2), in practice most toner is paired with several carriers, and the response is measured empirically. As alluded to above, tribocharging is notoriously difficult to measure, largely because the magnitude of charge and mass involved is extremely small, making it hard to detect [54, 150]. The measurement methods used have improved substantially since the development of EP.

The optimum amount for toner to be charged varies with each EP system, but is typically between 2-25 μ C/g [108]. For reference one Coulomb (C) of charge is the equivalent to the electric charge in 6.24×10^{18} electrons and the average discharge of a bolt of lightning is ~ 15 C [151]. This means that a typical charged polyester toner particle of 10 μ m diameter ($\sim 7.33 \times 10^{-10}$ g, based on a density of 1.4g/cm³) has an excess of 32,510e⁻. Historically an average charge-to-mass q/m ratio was measured as specified in ASTM F1425 Standard Test Method for Determining the Tribocharge of Two-Component Developer Materials [152]; commonly known as the "blow-off method" because the toner is removed from the carrier using air and the change in mass and charge is measured to deduce the average charge-to-mass ratio on the toner.

More recent measurement techniques actually measure the charge-to-diameter ratio as a spectrum (Figure 3.15), rather than a simple average [153, 154]. This new method represents the charge of a toner population in a similar way that a PSD represents its size. By counting all of the particles measured, the charge distribution (Figure 5.1 and Figure 5.2) can be plotted as the frequency of q/d as a percentage of the population.

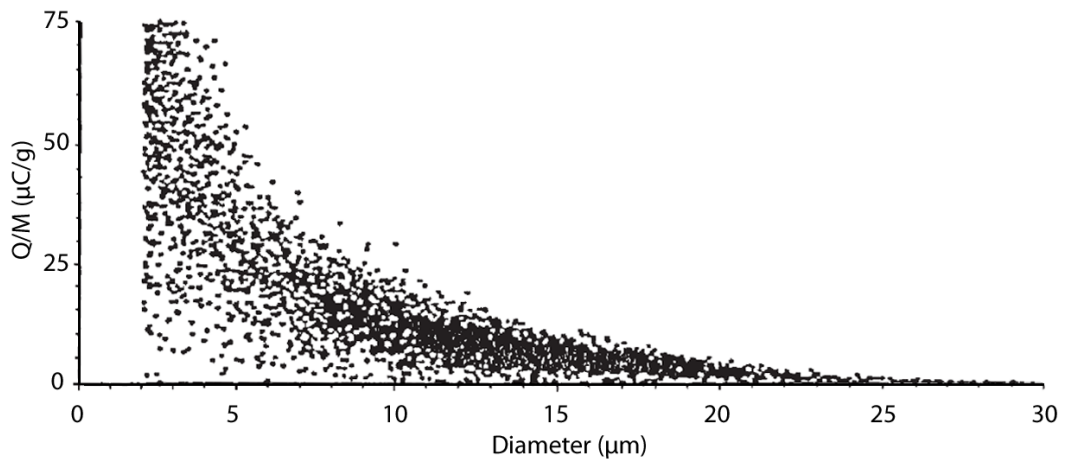


Figure 3.15 – Scatter Plot of 4000 toner particles showing charge versus size [155]

The average charge-to-mass ratio q/m is related to the mean charge-to-(particle) diameter ratio q/d for an idealized spherical toner particle by the following equations [86, 136, 156, 157]:

$$q/d = (q/m) \cdot \left(\frac{\rho \cdot \pi \cdot d^2}{6} \right) \quad (3-5)$$

Where

ρ is the density

d is the mean particle diameter

Solving for q/m gives:

$$q/m = (q/d) \cdot \left(\frac{6}{\rho \cdot \pi \cdot d^2} \right) \quad (3-6)$$

Using these formulas allows convenient conversion between the two most widely used charge characterization measurements.

3.2.4.4. *Non- uniform Nature of Toner Charging*

Although it is widely acknowledged that representing toner as a point charge or uniformly charged sphere is an oversimplification [51, 54,

158], widespread modelling of non-uniform particle shape/charging has not gained traction to date [54, 155, 158-161]. Outliers in experimental results can be explained as anomalies to the theory, caused by the oversimplification of the formulas. While recent advancements to provide an adequate theoretical model of toner adhesion [162, 163] are being assessed, a few practical examples are given as follows to support discussion points later in this work.

Firstly, not all toner charges with the intended polarity, as evidenced by the (small) proportion of positively tribocharged toner particles in Figure 5.1 and Figure 5.2.

Next, the multitude of factors influencing toner charge [135], virtually assures that charging magnitude across the entire surface of each toner particle is highly varied. To illustrate the influence that only particle shape may have on the uniformity of charge, Hays has taken a small stone from his back garden and rolled it around in a shallow container of paint [54]. He asserts that the patchy paint coverage on that stone may be used as a proxy to indicate for toner the areas of higher energy contact with the carrier which would help account for non-uniform tribocharging [54].

Lastly, Whitney and Kemp while at Lexmark International Inc. (Lexington, Kentucky, USA), documented toner behaviour using SEM, which they assert could only be explained by non-uniform tribocharging, as shown in Figure 3.16 [162, 164].

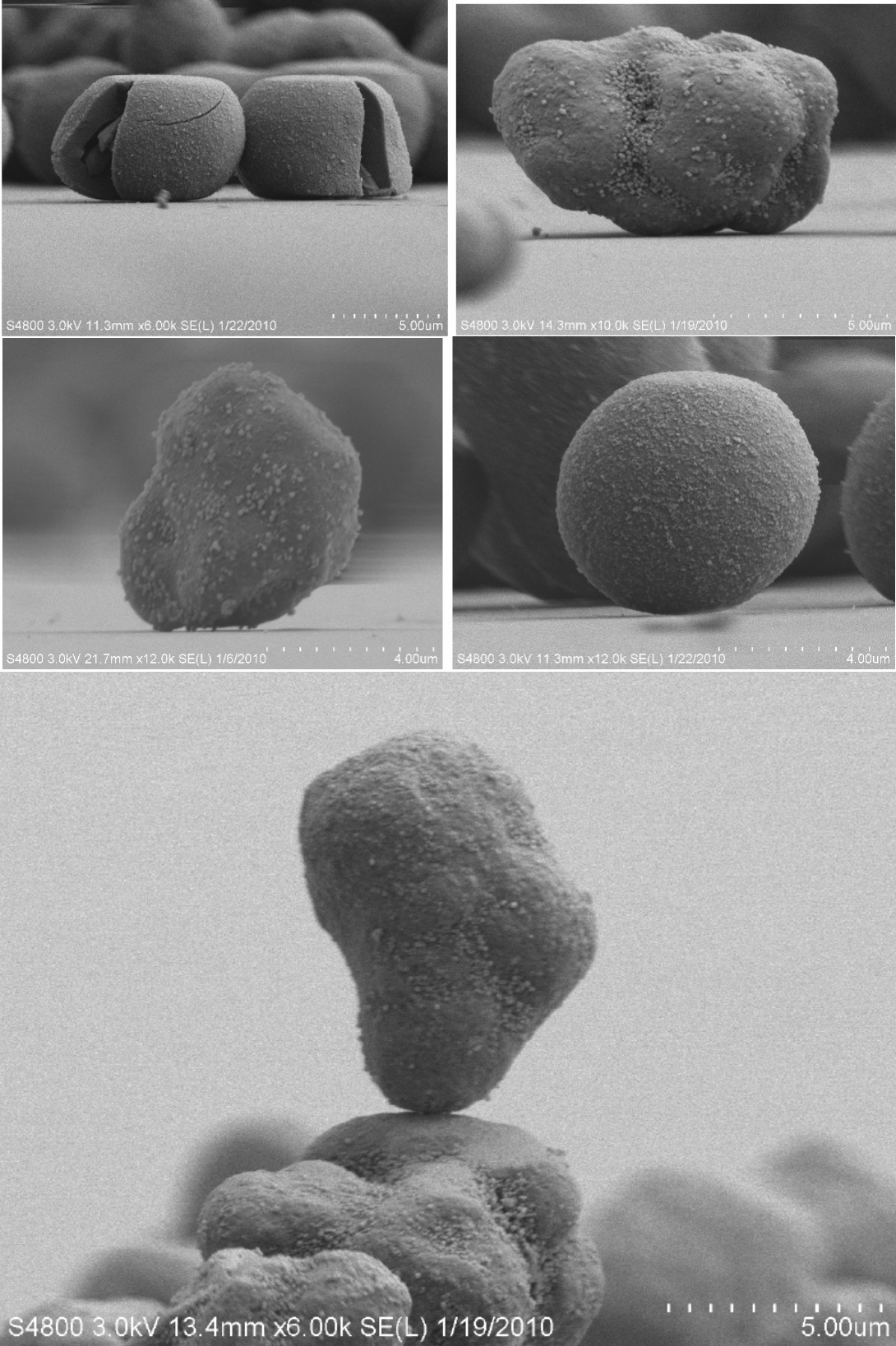


Figure 3.16 – SEM images of high adhesion (top row), light adhesion (middle row) and stacked toner particles (bottom) by Whitney & Kemp [164]

3.3. EP Physics and Principles

The study of EP embraces the interaction between several disciplines, including chemistry and many branches of physics (especially electrostatics, electromagnetism/electrodynamics). The remainder of this chapter will review established EP formulas relevant to this research, and measurement techniques used to verify theoretical calculations.

Toner behaviour is complicated due to a multitude of simultaneously interacting variables. In addition to factors influencing toner-carrier charging (as reviewed in §3.2.4), further factors influencing toner behaviour include: toner-to-toner interactions [155, 161, 165], fields used for development and transfer [46, 166], toner contact/adhesion with the surfaces of imaging members and substrates [166], and variations in the local environment [163]. The cumulative set of interactions is sophisticated enough that formulas alone typically still lack robust utility beyond research environments (as with carrier-toner charging §3.2.4), and oblige reliance on iterative empirical assessment rather than theoretical predictions [86, 160, 163].

3.3.1. Forces at Work in EP

At least three forces are at work in EP systems: electrostatic, electrodynamic and gravity. For most toner systems these forces have been listed in descending magnitude, however it is noteworthy that as

particles diminish in size the electrodynamic surface-dominated phenomenon play a more substantial role.

3.3.1.1. *Electrostatic*

Coulomb's Law (1785) (aka Coulomb's inverse square law) describes how particles with like charges repel each other and opposite charges attract. This law quantifies the magnitude of electrical force (F_e) between two particles (considered as point charges for this formula) which is proportional to the product of their charges (q_1 and q_2) and inversely proportional to the square of separation between them as shown in (3-7). Incidentally this relationship is essentially the same as gravitational force is to mass as described by Isaac Newton's law of gravitation [54, 167].

$$F_e = \frac{q_1 q_2}{4\pi\kappa\epsilon_0 r^2} \quad (3-7)$$

Where:

F_e is the magnitude of electrical force, measured in Newtons (N)

q_1 is the charge on particle 1, measured in Coulombs (C)

q_2 is the charge on particle 2, measured in Coulombs (C)

κ is the relative permittivity (aka dielectric constant relative to air); (1 in vacuum, ~ 1 for air and ~ 3 for most toner materials [54])

$\epsilon_0 = 8.8542 \times 10^{-12}$ F/m, the permittivity of free space (vacuum)

r is the distance separating the two charged particles

Electrostatic forces are considered to be "long range" (because they only decrease with the square of the distance), can be used to attract or

repel, are responsible for Coulombic repulsion between toner particles, and are generally used to transfer toned images onto the receiving substrate [46].

3.3.1.2. *Electrodynamic (including van der Waals)*

The second type of force on toner particles is “proximity force” or intermolecular forces which become significant when the distance between adjacent particles or a substrate is <10-30nm (100-300Å) [132, 163]. These forces are always attractive/cohesive for dry toners [46] and the finer the particle size, the larger the adhesion effects on the toner [86]. These forces are thought to arise from London or dispersion interactions “whereby an instantaneous dipole fluctuation in one particle polarizes a neighboring [*sic*] particle. The resulting dipole–dipole interaction is the dominant contribution to van der Waals interactions” [46, 168]. Although proximity forces may be an aggregate of several phenomena, the best known and largest established contributor is the van der Waals (vdW) force, so for simplicity this document will refer primarily to vdW force in connection with proximity forces.

The force needed to overcome these van der Waal forces F_{vdW} (assuming an elastic response to any stresses induced from these forces) is given by the Johnson–Kendall–Roberts (JKR) equation (3-8) as follows [163, 168]:

$$F_{vdW} = -\frac{3}{2} w_a \pi R \quad (3-8)$$

Where:

w_a is the work of adhesion

R is the radius of the toner particle

These forces can be substantial, particularly as particle sizes reduce to provide higher resolution prints; however, several practices in the toner industry help reduce these forces. For example, the standard practice of adding fumed silica (and/or other oxides) with high surface areas (typically 50-400 m²/g [55, 169] depending on agglomeration) as flow control agents (FCAs) to the surface of toner particles dramatically reduces the vdW force [51, 155]; the distancing effect from the substrate these surface additives provide is visible in Figure 3.16 (middle left). Furthermore, the use of a zinc stearate coating as a lubricant on photoreceptors also reduces the tendency of toner to stick to the photoreceptor by an estimated factor of 4-5x [46, 170]

vdW forces explain the conundrum of how it is possible to place like sign charged toner in close proximity. Considering only the Coulombic repulsion between charged particles (as described by Equation (3-7)), one could conclude that it would be impossible to deposit like sign charged toner particles in close enough proximity to produce high resolution images [51]. The repulsive force between toner particles is counteracted by cohesive vdW forces which allow like sign toner to reside in such close proximity [51].

3.3.1.3. Gravity

During the early days of EP it was observed that even when a selenium plate with a developed (or toned) image on it was dropped onto the floor edgewise, the toned image would not dislodge [39].

Various researchers have examined the magnitude of gravity in relationship to electrostatic and van der Waals forces and found that in many of the EP processes, its effect on the toner is negligible. The exceptions to this include its role in contributing to toner charge in cascade develop (which is not relevant to this work, apart from the legacy understanding imparted from its use), and toner adhesion to the surface(s) of the photoreceptor or final receiver [108, 163, 171].

3.3.2. Effect of Humidity and Temperature

One of the great difficulties experienced by Carlson and Kornei was the inability to reproduce their early experiments for no apparent reason [39]. The explanation for these difficulties was explained at least in part by the influence of humidity and temperature in electrostatics. One example of a problem caused by extremely dry conditions is that tribocharging effectiveness is increased to the point that electrostatic force binding the toner and carrier together will not let the toner leave the carrier [86]. The reason for this is that moisture typically decreases the resistivity of a material, thereby providing paths of lower resistivity along which charge can migrate [172]. Likewise, the effect of increasing temperature on dielectrics ultimately reduces their resistivity. The

interaction between these two effects on insulating powders can be significant, due to their relatively high surface area (compared to a bulk material) as shown in Figure 3.17.

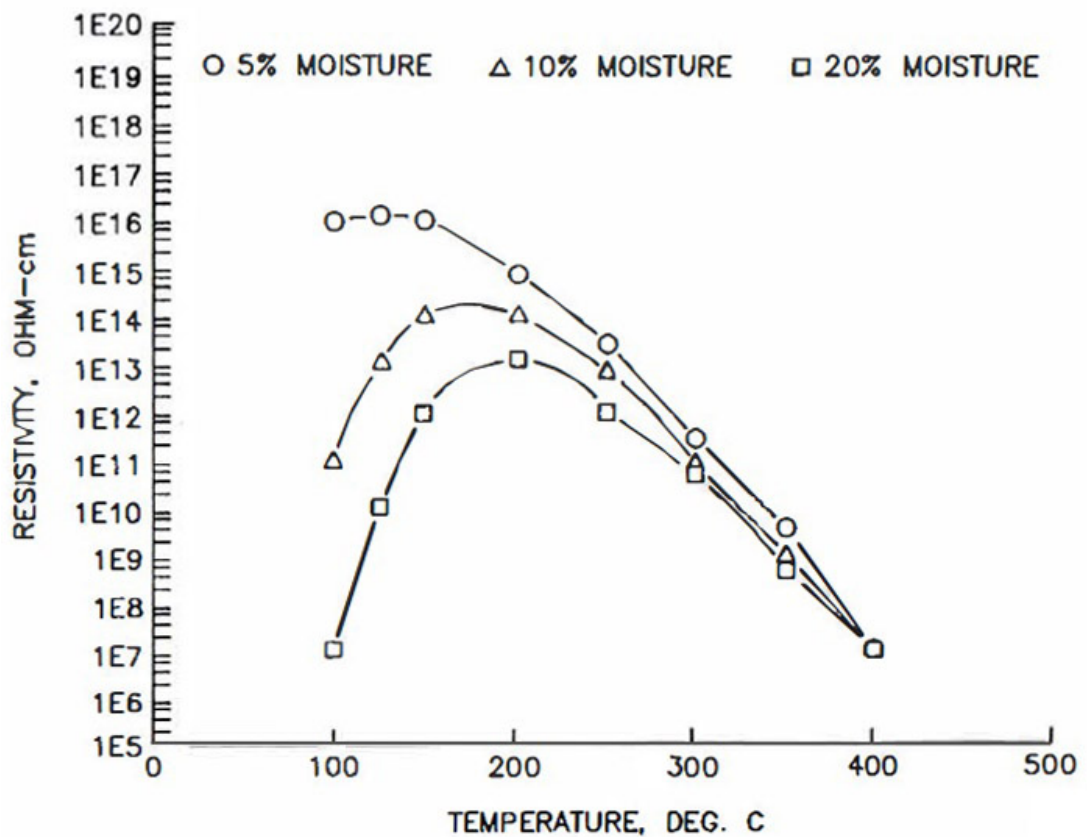


Figure 3.17 - Electrical resistivity of a powder at elevated temperature and humidity [172]

While the effects on the materials cannot be ignored, the practical implication of environmental factors on individual EP steps varies. For example, Whitney et al. [163] experimentally demonstrated that toner adhesion to a transfer belt increased with temperature (largely due to toner softening which increased the footprint on the substrate), but was not strongly affected by relative humidity.

Given the temperature controlled laboratory conditions in which the trials in this work were undertaken, the effect of environmental humidity and temperature changes were deemed to be slow enough that any effects would have been negligible for each set of consecutively deposited layers in a sample.

3.4. EP Process Steps and Hardware

This subsection reviews each EP step with sufficient technical detail to give the experimental work and related discussions context. For reference, an overview diagram of the main steps used in EP is given in Figure 3.18.

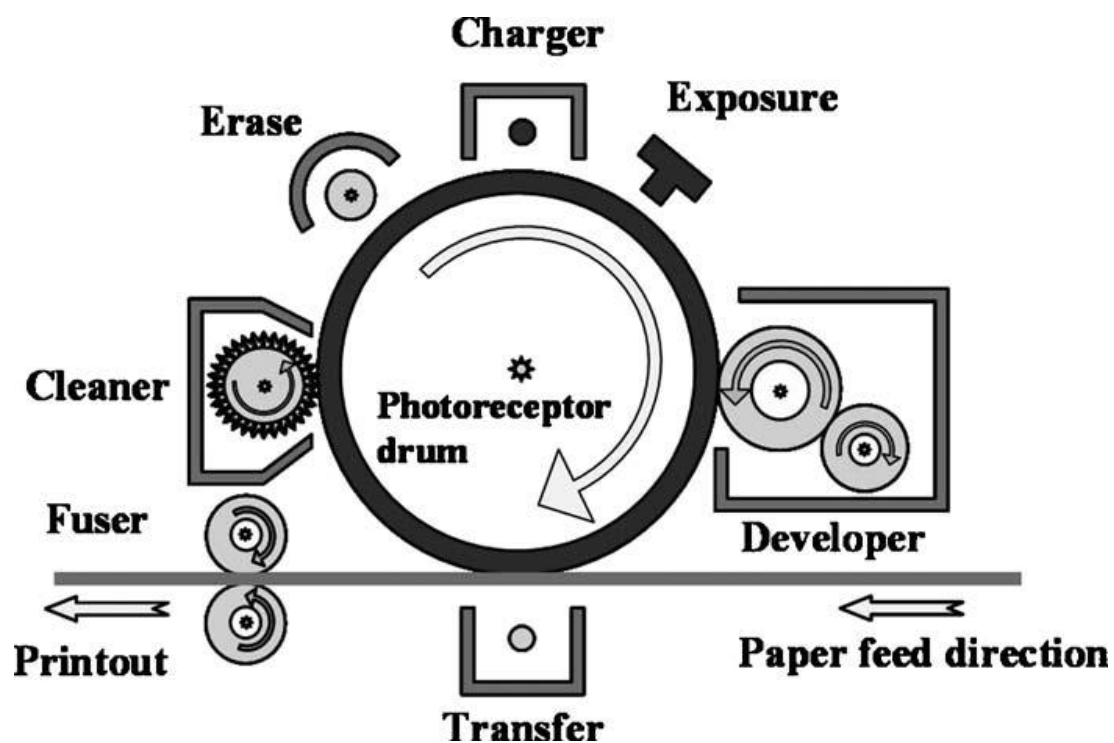


Figure 3.18 – Schematic of EP printing [173]

3.4.1. Charging and Corona

One of Carlson's key innovations was essentially inverting the application of charge as employed by Selenyi. Rather than selectively adding charge to a neutral background (by spraying a focused beam of ions in a pattern), Carlson globally charged the entire background and then selectively neutralized it (by the use of light on a photoconductive material) [39, 174]. Initially Carlson used manual tribocharging to charge the photoconductive plate, but automating the process called for a more robust charging method.

At least three types of charging have found industrial application: corona, induction, and contact/triboelectric charging [175]. A positive corona wire was implemented to provide a uniform covering of ions for the photoreceptor. Corona wires have a small diameter wire which is charged with several thousand volts and a grounded shield on one side. The high voltage causes a strong field in which nearby air molecules are separated into a corona or plasma of ions. The ions (sometimes referred to as free electrons), with the same sign charge as the wire, are repelled radially away from the wire, which is positioned to ensure that they shower down upon the surface of the photoreceptor. The ions with the opposite sign charge as the wire, are attracted to the grounded shield along with any same sign charge ions with a trajectory directed at or near to it. A noteworthy study characterizing the corona charging of organic photoreceptors has been made by Weiss et al. [176].

With advances in photoreceptor technology (§3.4.2), negative charging was desired. Typically the emission uniformity from positive coronas is adequate for printing, while the uniformity for negative coronas is very poor [177]. In order to uniformly charge a photoreceptor with negative charge, a scorotron was invented. A scorotron is a corona wire used with a screen between it and the photoreceptor surface, where the screen is charged to the potential desired on the surface of the photoreceptor. The bias of the screen is such that it homogenizes and limits the charge deposited on the surface of the photoreceptor [178].

Only an estimated 10% of ions produced by corona wires are utilized to charge/discharge the particles at each EP step, leaving the remaining 90% free to deposit alongside the others, making it difficult to assume homogeneity in deposition pattern [175]. This phenomenon observed in corona charging may contribute to the debated "mosaic-like" charging of dielectric surfaces [54, 179, 180].

More recently the use of a charge roller, a more energy efficient charging method, has become widely implemented. A charge roller directly touches the photoreceptor and supplies several hundred volts of charge and has become the most popular method for charging in printers [181]. Despite its popularity in office printers, digital presses and industrial laser printers (as used in this research) still require the larger charging capacity offered by corona charging [178].

3.4.1.1. Limitations of Corona Charging

A review of the forces at work in EP may lead to the false impression that charged toner particles can simply be moved around by use of fields with ever-increasing field strength; however the application of fields is limited by the breakdown strength of air, known as the Paschen limit [46, 168]. Paschen empirically measured the breakdown strength of air as a function of the gap size between and geometry of two electrodes as plotted in Figure 3.19.

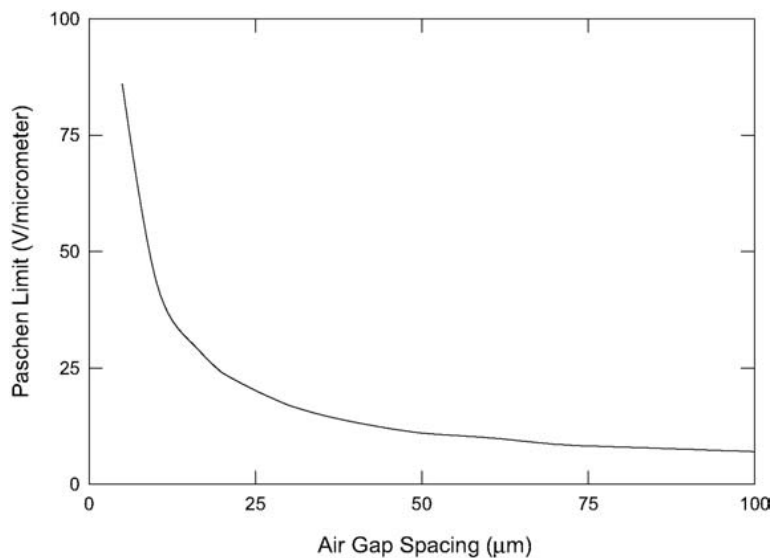


Figure 3.19 – The Paschen discharge limit in air as a function of gap size [46]

Except for air gaps below 25-30 μm , the maximum field strength in air is approximately 3.3 V/ μm . This limit imposes a narrow process window for using fields to manipulate charged toner particles. The implications of this limit for electrostatic transfers are discussed further in §3.4.4.

In addition to Paschen's limit, Hays has estimated that ion charging (from corona/scorotron wires) is half as effective as tribocharging [54]. This has implications for using ion sources to neutralize charge on printed

(and particularly fused) toners, as was attempted in the experimental work. Along the same theme, in 2006 Mazumder et al. identified shortcomings in state-of-the-art charge neutralization techniques and equipment and called for further research in this area [175].

3.4.2. Exposure and Photoreceptor

As already mentioned, one of Carlson's key innovations was to selectively neutralize a globally charged surface [39]. This "magical" step was achieved using a thin layer of photoconductive material on a conductive backing known as a *photoreceptor* or *photoconductor*.

A photoreceptor's performance can be evaluated against the quality and time required for at least five basic criteria: *charge acceptance*, *dark decay/discharge*, *photoinduced discharge*, *lateral conductivity*, and propensity to trap charge in a *residual image* [174]. A brief description of these criteria follows. For a quantitative review of these steps the reader is referred elsewhere [174].

Moving chronologically through the printing sequence, a photoreceptor should first easily accept surface charge (*charge acceptance*), generally from a corona device or charge roller (as described in §3.4.1). A sufficient net surface charge density should be accumulated to result in a surface potential of several hundred volts [108, 182]. After a photoreceptor is uniformly charged, it should not lose that charge quickly while in the dark. The rate at which charge is lost in the dark is called

dark decay. Next, it is selectively exposed using a laser or LED radiation (typically visible or near IR radiation). Where exposed, the photoconductive material generates and transports charge (or holes depending on its chemistry) in order to ground the surface charge; the rate at which it does this is called *photoinduced discharge*. The resulting pattern of charged and neutralized areas on the photoreceptor surface is called a *latent image*. The latent image must be stable for the print cycle duration because if charge relaxation occurs due to *lateral conductivity* it will result in an unstable blurred latent image (and subsequently blurred development). Sometimes photoconductive materials have a tendency to acquire a *residual image* by trapping charge which is undesirable and discussed further in §3.4.2.1. In some cases the photoreceptor is actively erased (§3.4.6), by exposing the entire surface of the photoreceptor to light prior to beginning a new print cycle.

As discussed (§3.1.2) the first images made using EP were produced using a photoreceptor made from fused sulphur on a zinc plate which was charged by rubbing with a cotton handkerchief and then exposed using a photo flood lamp. The relatively poor photosensitivity of sulphur would soon lead to the use of selenium, a much better photoconductor, as the semi-conductive coating on the photoreceptor.

Also, the productivity drive to execute process steps in parallel (Figure 3.8 and Figure 3.18) led to the use of cylindrical photoreceptors (since 1948 when the Copyflo was introduced), replacing the use of flat photoreceptors [39].

In early laser printers, photosensitive drums were required with a circumference which exceeded the length of the paper to be printed. This allowed the photoconductive coatings on the drum enough time to chemically recover before a new latent image was written for the next print [183]. A similar practice has been employed when using developmental toners to prevent variation in the print due to slow photoreceptor recovery or toner recoating.

Material developments have enabled the use of lower cost (often disposable) organic materials for photoreceptor drum coatings, first commercialized in 1970 by IBM [57]. Two excellent review articles summarize the last 40+ years of photoreceptor developments, including the transition to organic photoconductors (OPCs) [56, 57]. Phthalocyanine has emerged as one of the preferred OPC materials which accounts for the blue-green colour of many OPCs (as illustrated in Figure 3.8 and others) [176]. Charge injection into OPCs from negative corona charged surfaces is minimal because the primary charge carriers in OPCs are holes (rather than electrons) [57]. Additionally, the details of photoinitiated electron transfer have been explained in detail by Williams [184]. OPCs have historically been compatible with negatively charging toners which required a transition from positively charged toner as first commercialized by Xerox.

More recently, the wide availability and relatively low cost of OPC's has led to a market dominated by negatively charging toner materials (and

additives), although a few positive charging toner systems are still produced such as the systems by Kyocera which use amorphous silicon (ceramic/ceramic-like) photoreceptors which are more durable, but have had limited market penetration [57].

Further advances include the use of a zinc stearate coating as a lubricant on photoreceptors which reduces the force of toner adhesion to the photoreceptor by approximately 5x [46, 170].

Exposure resolution is routinely 600 to 2400 dpi (equating to square pixels measuring ~42-10 μ m) using lasers or high density LED strips. In practice the latent image stability on most photoreceptors (except for specialized photoconductors, such as high gamma photoconductors) combined with variations in toner size and behaviour often results in developed resolutions 2-4x lower than the exposed resolution (discussed further in §3.4.3) [57, 185].

All SLP experimental work described herein utilized OPCs (for negatively charged toners) with a charged surface potential of 720V and a fixed 40 μ s LED exposure with 600 dpi resolution.

3.4.2.1. Trapped charges

One of the potential defects in OPCs is that charges can get trapped in the photoconductive layer resulting in a *residual (latent) image* on the photoreceptor which is difficult if not impossible to remove. The concepts

of charge migration and (especially bulk) charge trapping are relevant to future discussion so it is briefly described here.

Fatigued OPCs are prone to charge trapping (resulting in a residual image) either at the interfaces between functional layers (such as at the charge generation layer (GGL) interface with the charge transport layer (CTL)) or trapping of space charge in the bulk of the OPC [57, 186, 187]. Typically this is caused when the OPC is exposed to light or heat before (or while) the surface is charged [176]. When charge is trapped, a new latent image with uniform charge cannot be formed. This means that even after a full cycle of charging and photoinduced discharge the photoreceptor retains some charge inside the photoconductive layer. This forms a defect which makes the charge acceptance of the photoreceptor non-uniform for subsequent print cycles.

Normally, trapped charges are not liberated by repeated charging and exposure cycles, although it has been demonstrated that elevated charging increases the applied field which sometimes facilitates charge release and migration [57, 174, 176].

Further to the propensity for charge to be trapped during migration through a photoconductive layer as described, charged or uncharged defects can also be found *in virtually all insulators*, as first discovered in the 1930's [188, 189]. According to Coudray [190], the abundance of these defects (or at least detection thereof) depends on "the stoichiometry, the doping, and the experimental elaboration and treatment conditions" implemented. When charge is trapped such that it

creates permanent dipoles, it becomes an electret as described previously (§3.2.1.1.1). Since nature abhors imbalance, natural forces cause charge imbalance to decay (recombine) toward neutrality over time [54]. Depending on the materials used and the thickness of material surrounding the charge imbalance, decay to neutral can take decades or even centuries [191, 192]. Although many of these defects go unnoticed, the use of polymers in electronics is increasing the detection of undesirable charge trapping in organic memory devices and will doubtless intensify with the uptake of polymer-based electronics [193].

3.4.3. Development

Probably deriving its terminology from a photographic heritage, the *development* step realizes the toner pattern on the photoreceptor surface by presenting the latent image with oppositely charged toner particles which adhere to it (Figure 3.7). A wide variety of development approaches have been devised as shown in Figure 3.20

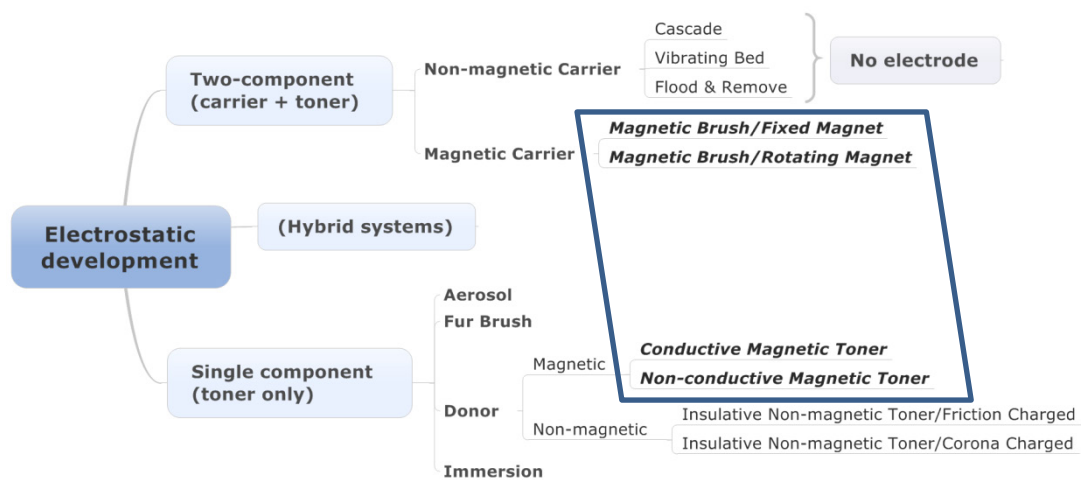


Figure 3.20 – Map showing available and most used (indicated within the rhombus) development options (after [194])

For reasons explained in §5.2, two-component magnetic brush (fixed magnet) development was predominantly used in this research. Two-component development is sometimes referred to as dual-component development or (DCD).

Since the concept of two-component tribocharging of toner has already been introduced (§3.2.4), including a model for quantifying charge magnitude (§3.2.4.2), this section reviews the principles used for mixing toner and carrier, and toning the image using a magnetic brush.

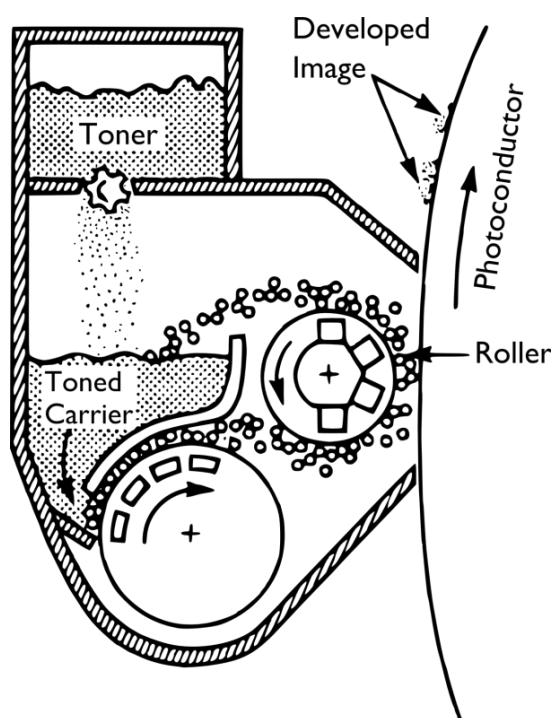


Figure 3.21 – A two-component magnetic brush developer (after [108])

Figure 3.21 shows a two-component magnetic brush developer. In this example the toner-carrier mixture recirculates in an anti-clockwise manner. Magnetic carrier beads are mixed with the toner by agitation and are transported through the developer by a series of rollers. At least one of the rollers, the developer roller, has magnets inside it and is located very close to the photoconductor surface.

The magnets inside the developer roller cause the magnetic carrier beads to form into bead chains which follow lines of magnetic flux as shown in Figure 3.22. A multitude of carrier bead chains in close proximity creates the appearance of "bristles" on a "brush" which gently rubs against the photoconductor drum surface, thus bringing the toner particles into close proximity with the latent image (Figure 3.22).

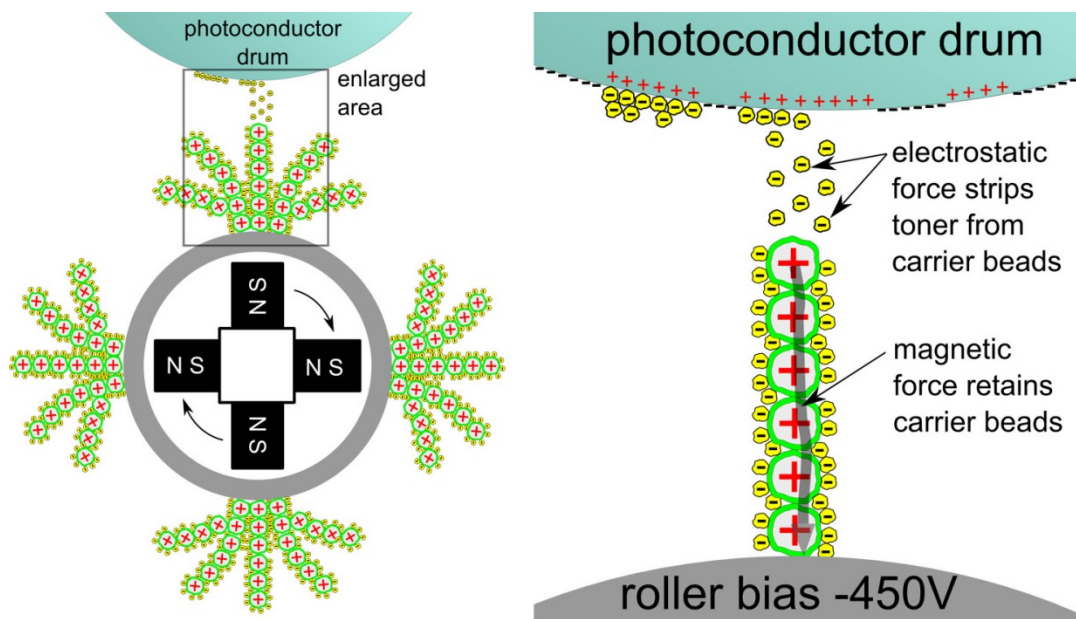


Figure 3.22 -Toned carrier on the magnetic brush (inspired by [62])

Normally the developer roller is charged with a bias voltage (of several hundred volts or more) in order to establish a field to help induce the toner particles to leave the magnetic brush. Where the latent image has the opposite sign charge as the toner particles (or at least, a substantially lower potential than the roller bias, making it electrostatically favourable for the toner to move) it draws the toner particles off of the carrier beads, thus developing or toning the latent image.

As previously mentioned (§3.4.2), the development resolution of conventional office printers and copiers is typically 2-4x lower than the exposure resolution (which is typically 600 to 2400 dpi or $\sim 42\text{-}10\mu\text{m}$ square pixels) resulting in developed images with a resolution of 100-150 μm [57, 95, 103, 120].

The undesired development of toner onto the background of the image (*background development* or simply "*background*"), can be caused by reverse sign toner charge, non-uniform particle sizes (particles found in the tail of an unacceptably wide PSD) or inappropriate development field strength. Similar to what is reviewed in the next subsection (§3.4.4), it is critical to control the factors affecting the electrostatic development field strength (between a magnetic brush and the photoreceptor) such as the air gap, developer roller bias, etc. The ceiling for development field strengths is subject to the Paschen discharge limit for air (§3.4.1.1), however the air gap is often small enough (Figure 3.19) that breakdown is typically avoided up to 15V/ μm which provides tremendous field strength in air to pull toner off the carrier beads [54, 195].

A variety of theories and models exist to describe two-component insulative brush development on the photoreceptor [108, 196-199]. Part of the difficulty of solving this problem is establishing an "effective" relative permittivity for the carrier-toner developer mix in their magnetic bead chains or brush "bristle" arrangement [108]. The most relevant mathematical model for using EP for AM applications is arguably the solid

area development model (3-9) because most 3D models have large solid printed areas.

Solid Area Development Model for Insulative Magnetic Brush [54]

$$\frac{m}{A} = \frac{-\varepsilon_0(v_p - v_b)}{(q/m) \left\{ \frac{t_p}{\kappa_p} + \frac{t_t}{\kappa_t} + \frac{(t_d - \delta)}{\kappa_d v} \right\}} \quad (3-9)$$

Where:

m/A is the mass over Area deposited on the photoreceptor

ε_0 is the relative permittivity of the air

v_p is the voltage on the surface of the photoreceptor

v_b is the voltage on the magnetic carrier bead chains (or brush bristles)

q/m is the average charge on the toner

t_p is the thickness of the photoconductive layer on the photoreceptor

κ_p is the relative permittivity (or dielectric constant) of photoreceptor

t_t is the thickness of the toner layer (accumulating on the photoreceptor)

κ_t is the relative permittivity (or dielectric constant) of the toner layer

t_d is the thickness of the developer mix (i.e. length of the bead chains)

κ_d is the relative permittivity (or dielectric constant) of the developer mix

$v = v_b/v_p$ or the potential difference between the brush and photoreceptor

Although in practice some of these values are hard to determine, noting that the q/m term is in the denominator means that the lower the toner charge, the greater the density of toner developed on the photoreceptor surface [54]. This insight into how the toner charge effects the rate at which the development electric field at the photoreceptor surface goes to

zero (or at least a constant value) can help one understand what could otherwise be counterintuitive [54, 196]. This also relates to the phenomenon of toners with a lower resistivity developing more densely (§3.2.1.1.1) [86].

3.4.3.1. *Fringe Field Effects = Edge Growth*

One problem experienced early with EP (especially when using cascade and other development approaches lacking an electrode) in relation to photoreceptors was that fine lines could be developed easily, but only the edges of large solid printed areas developed well (as illustrated in Figure 3.24e, and demonstrated in Figure 5.23c) [108, 200, 201]. This problem has been allegedly overcome for conventional printing requirements; however it is now time to be re-explored because the objectives are different for AM.

Examination of the perpendicular component of an electrostatic field from a line charge revealed that the external field strength diminished as a function of its width, as shown in Figure 3.23 [202, 203]. This explained the development behaviour for solid areas which can be considered to act like *very* wide lines; essentially leaving the centre of solid areas devoid of any external field to attract toner.

The difference between line and solid area development was elucidated by Thourson [204] which demonstrated that fringing fields gave rise to better development than large areas of uniform charge density as illustrated in Figure 3.24.

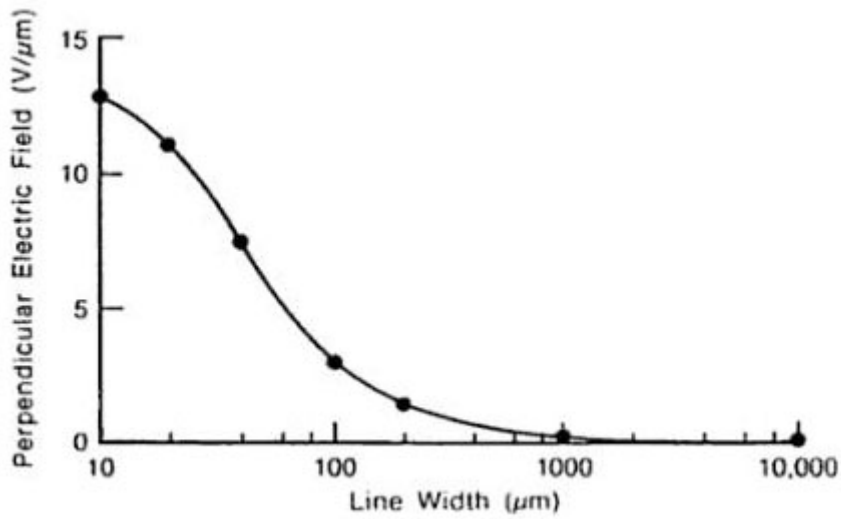


Figure 3.23 – Perpendicular electric field component at the centre of a line charge plotted versus the width of the line (From reprint of [202] in [108, 205])

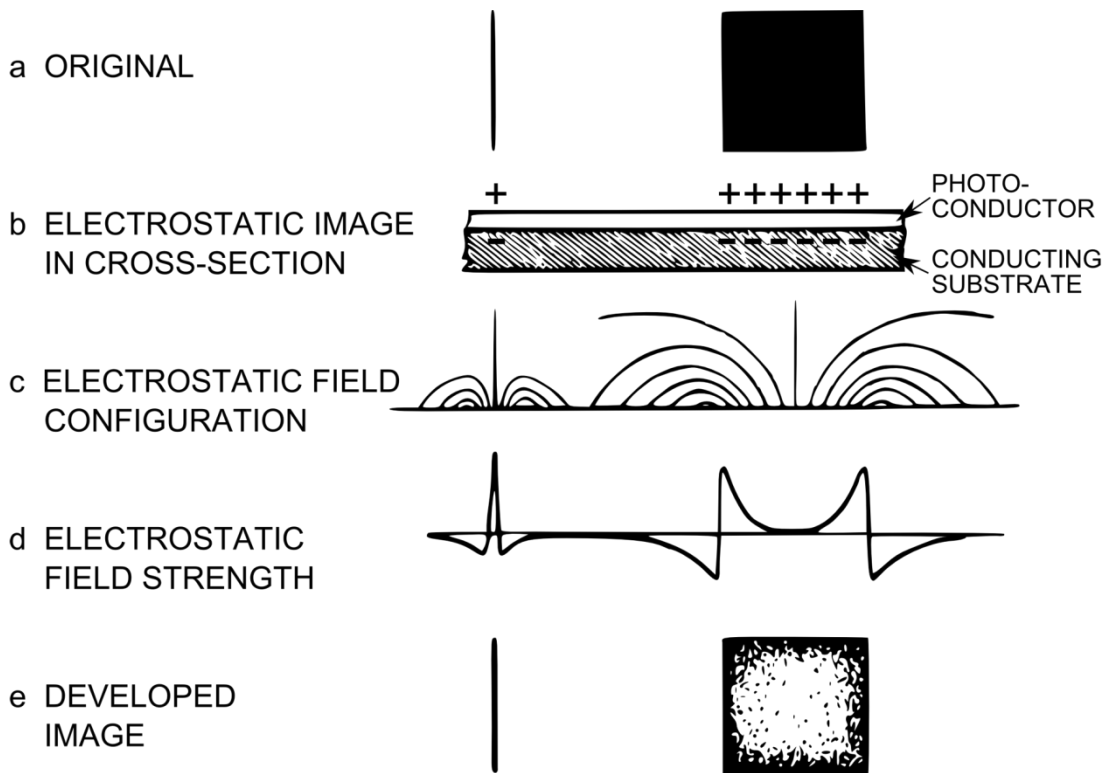


Figure 3.24 – Latent image charge on the photoreceptor and its influence on line versus solid area development (after Figure 1 in [204])

The charge density in the latent image (Figure 3.24b) on the photoreceptor, which is roughly proportional to the optical density of the original image (Figure 3.24a), produces fields which extend into space to act on the toner (Figure 3.24c) [204]. The fidelity of the fields to the latent image is best at the photoreceptor surface, and deviation increases (Figure 3.24c) with increased distance from the photoreceptor [204]. The uniform charge density in the solid print induces a charge of opposite polarity in the underlying conductive substrate thereby suppressing the magnitude of the external field (Figure 3.24d) (because most of the electric field exists within the photoreceptor due to the total charge configuration) [204]. For that reason development is best at the edges of the solid (Figure 3.24e), where the change in charge density is sudden, which gives rise to fringing fields which extend outside the photoreceptor, which correspond to the highest magnitude of external field strength [204].

It is also worth noting that the fields tend to be rectifying with respect to the field thus giving rise to fields of opposite polarity, surrounding the latent image islands (as shown in Figure 3.24d below the horizontal line). Since toner is monopolar (except for "defective" toner which has opposite sign charge) it is only attracted to the field with opposite polarity in the latent image.

This problem was largely solved using electroded development, which was first disclosed in a patent application filed in 1954 [206], and had gained widespread use by the mid-1970s [207]. Its use was widely

implemented with insulative and then conductive magnetic brush development (after proof of concept had been demonstrated with cascade development) using a bias voltage [108, 208]. In insulative magnetic brush development, the high density of carrier beads effectively acted as an electrode (or counter-electrode) which capacitively coupled some of the electric field to it [108, 208], thereby it reduced field strength suppression in solid areas (as in Figure 3.25 b-c) and allowed toner development.

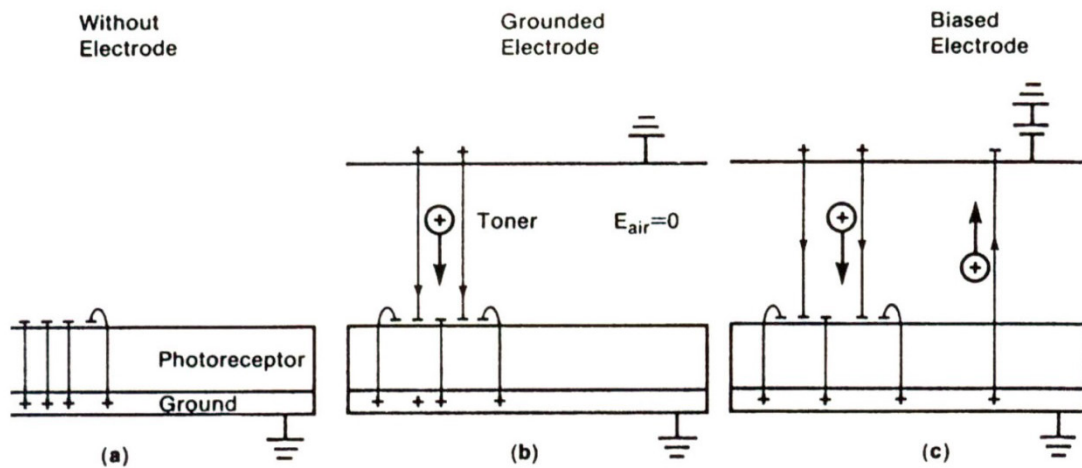


Figure 3.25 – Image showing the solid area field strength without an electrode (a), with a grounded electrode (b), and with a biased electrode (c) (Fig 2.7 from [108])

The magnetic brush enabled solid area development, but there is still a discrepancy between lines and solid areas (with insulating brush development), because "...electric fields due to lines are approximately twice as strong as the electric fields due to solids, and a 2:1 ratio of line to solid area toner mass per unit area is to be expected" [209]. This discrepancy has also been largely reconciled with conductive magnetic brush development, however it seems that it has had less widespread

implementation (as of the 1990's) than insulative magnetic brush development method, probably due to patent restrictions [108].

Even though the solid area development problem has been "solved" for conventional text and image printing, it has typically only been evaluated by optical density (as per ASTM F 2036 – 05^{E1} [201]), except in a few cases where evaluation by weight [147, 210, 211] and height measurement (by Coordinate Measuring Machine [CMM], [212]) has been undertaken. The experience of many researchers with "edge growth" and "surface defect exaggeration" (§4.6) when printing multiple developed toner images layer-on-layer has triggered re-investigation of this issue and several solutions have been proposed [212, 213].

3.4.4. Transfer

After developing their first successful image on a photoreceptor (See §3.1.2), Chester Carlson and Otto Kornei wanted to preserve the image that they had just developed. Carlson pressed some wax paper against the lycopodium spores which had been developed on the photoreceptor and most of them stuck to the wax paper. He then heated the wax paper in order to make the image permanent. Therefore the first transfer method ever employed did not use electrostatics, but relied on the adhesion of the spores when impregnated into softened wax [39].

Almost a decade later, Roland Schaffert and co-workers at Battelle Memorial Institute worked to develop Carlson's invention into a practical system. Initially they pursued the same approach as Carlson for transfer

by applying adhesives onto paper, looking at vacuum systems and even considering the use of grippers which would pull the paper through the EP steps [39]. Finally, in the mid-to-late 1940's [214] after nearly a year without success, they took a different tack. Schaffert reflected:

It all sounds pretty obvious today... but we worked a year before we thought of using static electricity to pull the image off the plate and onto the paper. Before that we tried all sorts of adhesives [40, 41].

Schaffert generated a field through the thickness of the paper (See Figure 3.26) with sufficient strength that the toner was induced to move from the photoreceptor toward the high voltage potential on the backside of the paper. Once transferred, the toner was held in position on the front side of the paper by oppositely charged ions on the backside paper until it was fused. This use of electrostatics to transfer the toner from the photoreceptor to the paper eliminated the need for sticky paper, is far more effective, and has proven highly reliable [39]. Electrostatic transfer has become a universal convention across nearly all EP processes.

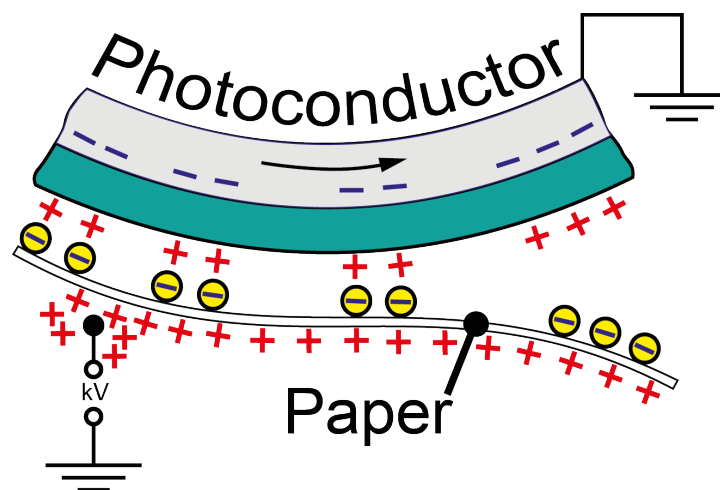


Figure 3.26 – Conventional electrostatic transfer developed by Schaffert (Adapted from [215])

The transfer field strength is carefully controlled to be strong enough to detach the toner from the photoreceptor (or final transfer roller) without creating sparks (air breakdown as introduced in §3.4.1.1 and discussed further in §3.4.4.1).

The toner velocity when jumping gaps (perpendicular to the surface of the imaging members) varies primarily with toner particle size, toner charge, and the transfer field strength. The minimum required toner velocity for printing 20 sheets min⁻¹ is typically claimed to be 1 m/s [216, 217] although toner velocities up to 10 m/s have been observed in typical transfer configurations [217]. The transfer field strength is essential to maintain toner velocity. Numerical simulation has shown that without a transfer field, an initial 1m/s toner velocity for 8µm diameter particles with typical charge jumping a 200µm gap would quickly slow due to air drag to ~0.2m/s on toner impact [216]. Transfer efficiency is typically about 85% but can be improved with strong transfer fields and high nip pressure [218].

Owing to the very large circumference of the photoreceptor (or final transfer roller) relative to the small nip, standard practice is to approximate transfer fields for EP using the formula for constant electric field strength (3-10) (as if it were measured between two parallel plates) [54, 108]:

Field Strength

$$E = V/d \quad (3-10)$$

Where:

E is the field strength

V is the potential difference between the two plates

d is the distance between the plates

Even when electrostatically favourable conditions exist for toner transfer, in practice there is still a small amount of toner which does not transfer and needs to be cleaned off of the OPC or final transfer roller. This residual toner which remains on the OPC can be explained by imperfections in surfaces of the imaging components, high electrodynamic forces, and variations in the toner shape and charging.

In the last five years, significant progress has been made toward more accurately modelling the force of toner adhesion on the photoconductor surface [162-164, 166, 219]. According to work by Kemp and Whitney, toner adhesion is best modelled by a cubic polynomial equation as follows:

Toner Adhesion Model by Kemp and Whitney [163, 219]

$$F_a = A + Bq + Cq^2 + Dq^3 \quad (3-11)$$

Where:

A is the van der Waals force of attraction

Bq is additional force due to non-uniform charges

Cq^2 is the Coulombic attraction from multiple particles

Dq^3 is the Van der Waal force of attraction that "is a function of the toner footprint from the Coulombic attraction forces" [163].

Using this model and correlating it with experimental work, Whitney & Kemp showed that the typical toner removal force from an intermediate transfer belt was 300-1,000nN for 6 μ m diameter toner charged at 4-10fC [163]. It is worthwhile bearing in mind that zinc stearate coatings on the OPC and FCA help reduce the force of toner adhesion to the photoreceptor to the lower half of that range [46, 170].

Sometimes an additional transfer roller will be used after the photoreceptor to facilitate more aggressive transfer parameters which could prematurely shorten the life of the photoreceptor. When a transfer roller is used, it is typically the final imaging member that the toner is carried on before being transferred to the paper or alternative final receiver. This is the case with the industrial laser printers used in this research (§5.7.1.3).

Some toner which is transferred onto the substrate can never leave the OPC or leave and return, resulting in *back transfer* onto the OPC (or last imaging member); this is electrostatically and electrodynamically analogous to a hot offset condition as described in the next sub-section (§3.4.5). This undesirable adhesion of toner materials to the photoreceptor or final transfer roller can generally be avoided by optimizing the transfer parameters and restricting toner to a narrow PSD.

3.4.4.1. Effect of Transfer Gap and Geometry on Field Strength

The potential for air breakdown varies depending on the gap between the imaging members and is geometry specific, as discovered and first recorded by Friedrich Paschen in 1889 [220] and shown in Figure 3.19. For example, air breakdown at atmospheric pressure is typically 1.2 V/ μm for needle points but up to 3.3 V/ μm for 100mm diameter spheres [221]. Therefore field strengths in transfer nips which have gaps of hundreds of microns or more (which allow air to readily pass in between them) are typically ~ 1.5 V/ μm (1.5MV/m) or less to avoid breakdown according to the Paschen limit [222]. When a minimal amount of air is present at the transfer nip (typically by limiting the gap to $<30\mu\text{m}$) spark generation is inhibited, due to the scarcity of air molecules (which increases the mean free path), meaning that even if an electron is freed by ionization it would not collide into neighbouring molecules with enough energy to start a chain reaction to make a spark (aka avalanche breakdown) [223]. Therefore, transfer field strengths up to 40-50 V/ μm can be used for nip gaps of $10\mu\text{m}$ [178]. It is noteworthy that even when nip gaps are below $30\mu\text{m}$, if the surface of the roller(s) is rough enough to allow additional air into the nip, breakdown can occur [224]. For that reason, most transfer fields are limited to 1.5-2V/ μm to avoid sparks (breakdown) with a margin of safety.

3.4.4.2. Effect of Final Receiver on Electrostatic Transfer

Another factor which affects conventional electrostatic transfer is the homogeneity of the relative permittivity (dielectric constant) of the final substrate/receiver, and whether its composition is subject to polarization

in a field. Various researchers have described how transfer fields are affected by various grades, thicknesses and fillers in paper [225, 226]. Cassidy et al. [225] (Figure 3.27) shows how the field strength varies with the non-uniformities in mass density and paper thickness. The bottom half of the image is a cross-sectional image through a sheet of paper obtained using SEM. The top half of the image shows the numerically simulated strength of the vertical element of the field in the transfer nip (modelled as if between two capacitor plates and ignoring the effects of toner) based on the digitized surface from the SEM. The greyscale in the top half of the image represents the field strength where dark correlates to lowest strength and white to the highest [225].

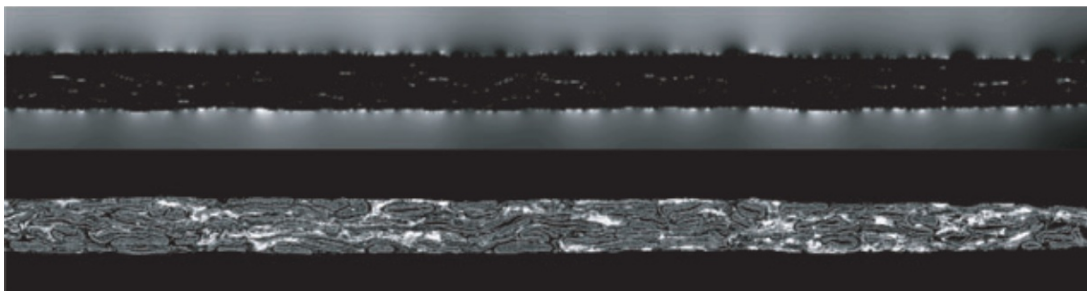


Figure 3.27 – Cross-section through a sheet of paper $\sim 90\mu\text{m}$ thick showing the simulated magnitude of the z-component of the electric field (top) and SEM image (bottom) [225]

The effects of heterogeneity in the substrate on the simulated transfer field strength are noteworthy because they give an indication of how conventional transfer field strength and homogeneity would be affected when passing through a fused multilayer toner body. Arguably the non-uniformities in an AM context would be more complex than the foregoing illustration for at least three reasons. Firstly, the addition of many layers would mean an accumulation of non-uniformities with each new print.

Second, in addition to the dependence on heterogeneity in the toner material, each layer printed would include differing proportions of build and support material (each with a different composition and relative permittivity) according to the variations in the cross-section of the model being printed. Third, since the layers would be composed of toner, residual toner charge and polarization would further complicate predicting the transfer field strength.

3.4.4.3. *Transfer Challenges with Inherently Conductive Toners*

This subsection has been added to support issues and discussions arising in §4.6 and §7-9 and is best understood after gaining an appreciation of multilayer transfer challenges.

Upon preliminary consideration, it may seem that using a conductive toner could resolve nearly all of the problems with multilayer transfer described in the literature (as reviewed §3.5). While the challenges detailed in §4.6 may cease to be an issue, depositing conductive toner introduces new challenges depending on the type of development system being used as described below. The comments in this section refer to the intended use of toner materials which are inherently conductive (such as metals).

Discharge in a Two-component Developer

A two-component developer (§3.4.3) is reliant upon attraction between toner and carrier due to tribocharging [103]. Although it is possible to

tribocharge metals, they discharge very easily due to their inherent conductivity making them impractical to handle in a conventional two-component developer [103]. For that reason, printing of metals using a two-component printer has been achieved by loading it into a polymer matrix toner or encapsulating it within a dielectric layer, which enables it to retain its charge throughout the printing process as has been discussed (§3.2.1.2) and demonstrated [95, 97]. It is noteworthy that the coating must be robust enough to survive hopper/developer mixing and be thick enough to be able to supply an adequate number of electrons to achieve electrostatic adhesion with the carrier (since the Coulomb force is directly proportional to charge, which is directly proportional to the number of electrons available) [103].

Bouncing of Conductive Toners between Charged Plates

Charge induction of conductive particles is one of the most widely implemented means of charging metal particles (including use in the Metal Printing Process §4.4.4). Given the use of toner which is inherently conductive prior to deposition, one could assume that it would continue to be conductive after consolidation. If this were the case, the build surface could be considered to behave effectively like a conductive plate. During the transfer step, this build surface is in close proximity with the surface of the photoreceptor which behaves like a conductor where it has been exposed, so therefore the toner behaviour in that gap (after printing the first monolayer of toner) can be modelled using two conductive plates arranged as shown in Figure 3.28.

Attempting an electrostatic transfer step requires a potential difference between the photoreceptor and the build surface. The potential difference sets up a field which induction charges conductive particles therein. Since the electrons in the particles are free to transfer out of each particle even with only brisk contact (conduction) with another conductor, unique "bouncing" behaviour is observed as described below.

When a conductive particle is in contact with a charged plate, charge will flow into the particle to exclude the electric field from its interior, thus redistributing electrons according to Gauss' law for a conductor (Figure 3.10) [108, 227]. Therefore, without mechanically restraining the particle, it will remain in contact only long enough to achieve the same charge as the plate, after which it is repelled away as shown in Figure 3.28 (left). This makes it nearly impossible to attract and hold particles onto consolidated charged layers. After arriving at the second, oppositely charged plate, the particle is not simply neutralized because, opposite charge flows from the second plate into the particle to null any internal electric fields [108]. Having exchanged charge to achieve the same charge as the second plate, it will be repelled back toward the first plate. Even if one of the plates is grounded, the charged plate (and resulting field) will induce charge separation in the grounded plate. This will result in an opposite polarity charge-rich surface on the grounded plate, which will supply charge into the particle to null the internal field (and distribute itself according to Gauss' law), thereby perpetuating the cycle. This cyclic attraction, contact exchange of electrons, and repulsion, creates an oscillation of the particle between the two plates. Each cycle actually

completes a circuit by transferring a small amount of charge across the gap (i.e. intermittent current flow) between the two plates [228]. Cho [227] showed that the average electric field on the surface of the charged particle on the plate compared to the electric field between the two plates was 1.65x higher [108]. This reciprocating motion between the two plates has been documented by various researchers, and is often referred to as the “bouncing” problem [54, 103, 108, 181].

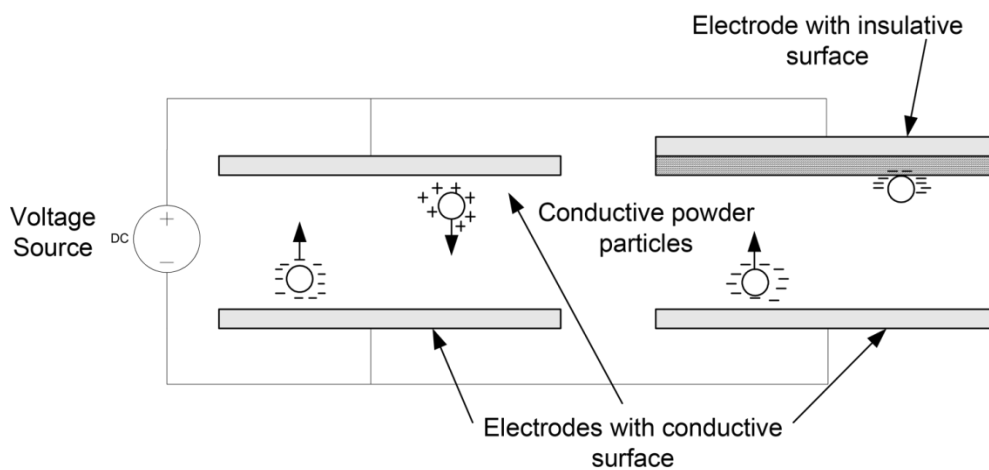


Figure 3.28 – Behaviour of conductive powder particles in between conductive and insulative electrode surfaces (After figure 5-13 from [181])

This issue may be avoided by covering one of the plates with an insulative material as shown in Figure 3.28 (right). This is the case for conductive toner printing where the paper acts as the dielectric (as long as humidity is low) and allows transfer of a monolayer of toner [108]. During part of the development of the Metal Printing Process (MPP) (§4.4.4), Sintef deposited wax onto a conductive plate relying upon its insulative and adhesive properties to develop an image using conductive and non-conductive powder [63, 229]. In order for this to solve the transfer problem, as identified in §4.6, it would be necessary to put an

insulating layer in between each layer of toner (essentially requiring the opposite action as suggested by Honjo [104] as shown in Figure 3.11); which undermines any practical or intended transfer benefits of printing inherently conductive toner layer-on-layer.

Challenges with printing encapsulated conductive particles

In view of the toner bouncing tendency described above, it may seem logical to “retreat” to encapsulating the conductive particles and triboelectrically charging them. While this offers the ability to develop them with a magnetic brush, it does not substantially improve the prospect of electrostatic transfer due to polarization (unless the shell is relatively thick around the core) [103].

Where a contact transfer is used, the conductive core of the particle becomes polarized on the photoreceptor which then repels it away from the substrate as shown by Walker et al. [103] in Figure 3.29.

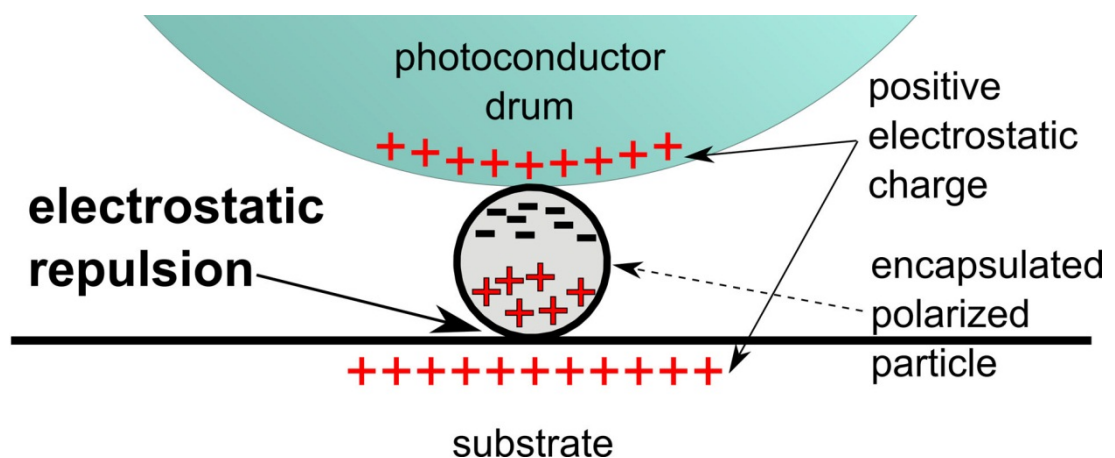


Figure 3.29 – Electrostatic repulsion created by an encapsulated polarized conductive toner particle during an electrostatic transfer step - After Walker et al. [103]

The author acknowledges that this principle has been illustrated using simple material classifications and there may be a window of opportunity for materials which are not as conductive as metals, but which are essentially electrostatically dissipating.

Furthermore, both Océ and Delphax have produced devices which use inherently conductive toner (using single component development and ionography respectively) and have dealt with this issue by implementing a thermal transfer and high pressure transfixing step (combining transfer and fixing in the same step) respectively to achieve consistent transfer irrespective of humidity (which enables paper to act as a conductor [54]) [108]. Both thermal input and pressure feature heavily in the more successful early proof of concept attempts as reviewed in §4.4 and analysed in §6.1.

3.4.5. Fusing

Except in the case of transfixing operations which combine transfer and fixing, toner is fixed to the paper using a fusing means. The most popular method is to use a hot roller, although a range of options are used commercially including fusing by: solvent, radiant heaters, flash, cold rolling, etc. The factors governing fusing physics are typically: temperature, pressure and dwell time in the nip.

Historically, fusing temperatures of 150-180°C were routinely used (and still are for high production machines) as guided by the rule of thumb that fusing temperatures were typically 100°C above the glass transition

(T_g) temperature of the polymer; however the drive to be more energy efficient has led to development of toners which fuse below 100°C [230].

Typical nip pressures vary between 1-20 kg/cm² (14-142 psi) with the most common between 2-3 kg/cm² [231-234]. Typical dwell time in the heating nip is 20-50ms for a low-gloss black and white print and 30-100ms for a high-gloss colour print [230].

Fixing the toner by fusing is prone to two types of defects: *cold offset* and *hot offset*. When the toner is not heated sufficiently to flow, then it does not adhere well to the paper (or other final receiver) and typically stays on the final imaging member (photoreceptor or transfer roller) [230]. Conversely, when the toner flows too readily (typically due to overheating), hot offset can occur. Hot offset is when the toner particle is liquid enough that it splits into two halves upon exiting the fuser nip, thereby transferring partially onto the fusing roller and partially remaining on the paper [230].

When a transfixing step is used, toner that flows too readily can simultaneously cause hot offset and back transfer (§3.4.4) which can be damaging to the photoreceptor. For this reason printers which use transfixing operations often include a final transfer roller to prevent damaging the photoreceptor; however if overheated toner flow is not sufficiently reduced by the quenching effect of the transfer roller, then a double back transfer can occur fixing toner on the final transfer roller and also on the photoreceptor. A developmental toner-like material used in

early trials to assess the feasibility of AM by EP is thought to have caused double back transfer (due to fine particles which overheated) (§4.4.5.3).

Historically many fusing rollers were continuously coated with an oil-based release agent to help prevent the toner from adhering to it. More recently, the inclusion of wax inside the toner particle, which is released in the fuser, provides a lubricant which reduces the hot offset tendency of the toner to adhere to the hot roller [230]. Including wax inside the toner has become a far more widely implemented alternative to coating the fusing roller with oil [55]. This is palatable for printing text and images, but is not desirable for AM of 3D parts (unless wax were to be intentionally used as a support material).

It is also important to realize that a satisfactory degree of particle melt for imaging applications (as shown in Figure 3.9) can be relatively low and does not approach full density as known and needed in 3D polymer processing such as injection moulding or AM [235].

3.4.6. Cleaning and Erasing

Even when electrostatically favourable conditions exist for toner development and transfer, and physical conditions are optimal for fusing, in practice there is still a small amount of toner which is left behind at each step. For that reason each subsystem in the printer generally has a cleaning mechanism. Sometimes it is as simple as a wiping blade and other times it is as sophisticated as another magnetic brush designed to

remove particles from the surface of the photoreceptor for example. Having been cleaned the subsystems are ready for the next print cycle.

In addition to the need for physical cleaning, the photoreceptor needs to be erased using a general exposure to light in order to homogenise the surface charge before the next print. This facility was available in the industrial printers used in this research, however the rigour of the print cycle was not sufficient to warrant its use (§5.7.1.3).

3.5. EP (Toner) versus Inkjet (Liquid Ink)

In 1987, Larry Schein said, "Electrophotography is the technology used in virtually all copiers commercially available today and it promises to be the most prevalent printer technology of the 2000s" [108]. Ironically, the first digital printing process has been surpassed by more recent digital printing techniques (especially inkjet and aerosol jetting) for digital fabrication and AM applications. Although many digital printing methods are finding application space (such as thermal inkjet for wax printing and thermal print heads for fusing thermoplastics, as used in the Blue Printer, Denmark - www.blueprinter.dk), the prominence of piezoelectric ink-based printing systems in AM/digital fabrication merits brief mention in comparison with EP. For an explanation of applications where EP has significant advantages over inkjet, the reader is referred to the section titled, "Strengths of Laser Printing" in [236] (available in the Annex).

Table 3.2 overviews some of the major technical differences between inkjet and EP. This table is based on typical office-based systems excluding industrial scale EP or inkjet (such as UV curing/wide format).

Table 3.2 – Comparing* Inkjet and EP

	<i>Inkjet</i>	<i>EP</i>
Typical solids content in deposited media	<25vol.%	100%
Maximum solid particle size ¹	<5 μ m	20 μ m
Typical resolution	300-1200dpi	300-1200dpi
Typical deposition thickness	1 μ m	5 μ m
Requires solvents during deposition?	Yes	No
Amenability to printing:		
high dielectrics	Difficult	Easy
thermoplastics	Difficult	Easy
Thermosets	Easy	Easy
conductives	Easy	Difficult
Inherent moisture stability	Not water-fast	Water-fast
Difficulty/cost of scaling in X&Y	Low	High
Difficulty/cost of scaling volume deposition rate	High	Medium
Barriers to print media development	Lower	Higher
Barriers to system development	Lower	Higher

*based on typical office based printers, and the following sources: [34, 35, 37, 46, 108, 197, 209, 237, 238].

¹ assuming a minimum resolution of 300 dpi (85x85 μ m pixels), and for inkjet a 20:1 minimum nozzle diameter to jettable solid particle diameter ratio.

Although digital printing technologies have been reducing the amount of material they deposit over the last 25+ years (§3.2.3), driven by higher resolution requirements, the lack of carrier liquid in EP results in significantly more deposition than inkjet, by solids volume, which results in a thicker printed layer [239].

Owing to the need for carrier liquid in inkjet, the largest solid particles that can be carried is significantly lower than EP. It is noteworthy that EP is suitable for use with sub-5 μm particles, however these must be used inside a fluid or else they become aerosolized which presents a health risk [24]. However, when safely managed in a liquid (liquid EP) very fine toners can produce superior print resolution (such as HP Indigo printers); however the needs of this work encourage volume deposition, therefore larger scale dry toners were the focus.

The typical resolution used for office applications is 600 dpi. Office-based inkjet and laser printing devices are not generally optimized for precision deposition at higher resolutions than 1200dpi.

As mentioned above, the deposition thickness of EP is generally much thicker than inkjet. This difference is accounted for largely by the use of a carrier liquid in inkjet which also generally permeates into porosity in the substrate (such as paper). The carrier liquid also means that solvents, in addition to the pigment or other functional toner components, must be deposited onto the substrate. The choice of solvent and substrate determines if inkjet is water-fast or not. The use of solvents naturally facilitates the suspension and printing of nano-scale conductive inks, which is more difficult in dry toner applications. The larger solid mass of toner particles makes it easier to deposit high dielectric strength materials and thermoplastics with long polymer chains. Since EP is a dry process, deposited toner is immediately amenable to thermal fusing methods (without drying).

The precision and pressure required for reliable fusing in EP makes scaling EP in X&Y more difficult/costly than inkjet, which accounts for the dominance of inkjet in the wide-format printing market [230].

Scaling the volume deposition rate (without excessively compromising resolution) is inherently easier for EP because electrostatics can transport larger particles (up to $\sim 100\mu\text{m}$) without the constraint of passing them through a nozzle (which must be sized to avoid clogging) [240-242].

The capital equipment requirements to either polymerize or extrude and grind toner are typically higher than those for producing inks [55, 109, 243].

Lastly, EP hardware/software is not typically open source (perhaps in part due to the need to match the fuser to the toner characteristics) which is an additional barrier to entry compared to multiple inkjet systems/components which are open source.

Arguably, developing an inkjet-based digital printing system has lower barriers to entry than a toner-based one. Their co-existence in the 2D printing world is evidence of their complementary natures. It is proposed that sufficiently resourced endeavour can overcome the technical barriers to unlock the strengths of EP for 3D/digital fabrication applications, so both may co-exist there as well.

This chapter has set forth the foundational understanding needed to appreciate the motivations and implications of using EP for AM as will be reviewed in the next chapter.

4. Convergence of EP and AM

This section reviews the methods employed for printing multiple layers by EP toward AM. The focus is on EP based processes intended to impart shape and functionality beyond the application of colour (for text and images), excluding simple textures below 1mm high (such as for braille or fine art reproduction).

4.1. Transfer Method Evolution Toward AM by EP

Figure 4.1 (larger image available in Appendix A) is a timeline prepared by the author of key patents by date issued and known commercial and research initiatives toward the use of EP in AM systems. The patents are labelled with the inventor's name and research is shown with the name of the industrial or academic leader of the research inside a bar representing the duration of the initiative.

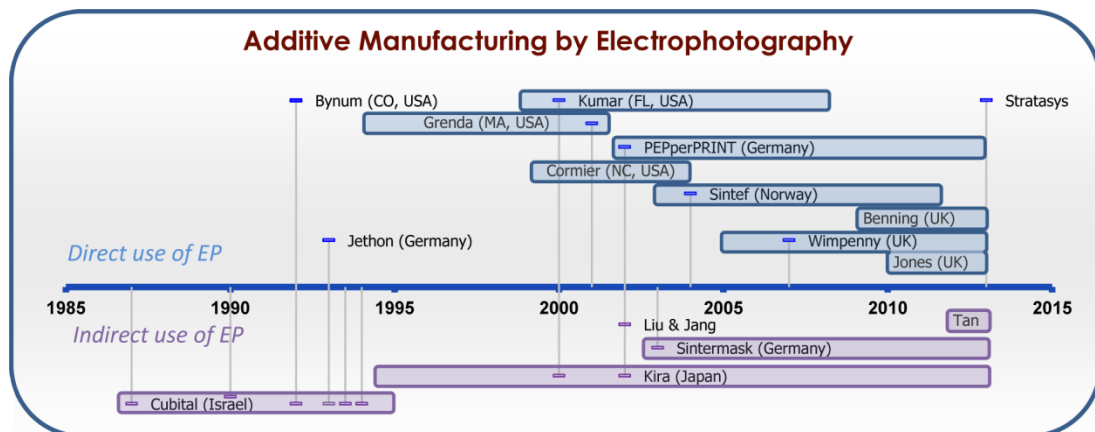


Figure 4.1 – Timeline: Development of Additive Manufacturing by Electrophotography

The activity mapped above the timeline (in blue) employed EP as a direct deposition process resulting in a final product composed of consolidated toner. The activity mapped below the timeline (in purple) used electrophotography indirectly in the fabrication process, such that products resulting from these processes are composed primarily of material(s) other than toner.

The clearest differentiator between the various research initiatives is the method of transferring toner out of the printer, therefore the prior art will be reviewed in groups sorted by the type of final transfer method implemented. Transfer method approaches are introduced chronologically in the order that they were first attempted in AM in the following groups:

- Electrostatic transfer used indirectly in AM (§4.2)
- Direct deposition by electrostatic transfer methods – conventional and alternative (top charging, repulsion, etc.) (§4.3)
- Non-electrostatic final transfers (primarily relying on heat and pressure) (§4.4)

4.2. Indirect Use of EP in AM

Although the intent of the current research is the use of EP for direct material deposition, a review of the indirect uses of EP follows for completeness and context.

As described in §3.4.4 the first commercially available transfer method used a transfer field through the back side of the paper to draw the toner off of the photoreceptor (or final transfer roller/belt where used). This remains the most widely used transfer approach for conventional laser printing and photocopying to date and has been adapted for multilayer printing on flexible media (Figure 4.2 left) as well as rigid substrates (Figure 4.2 right).

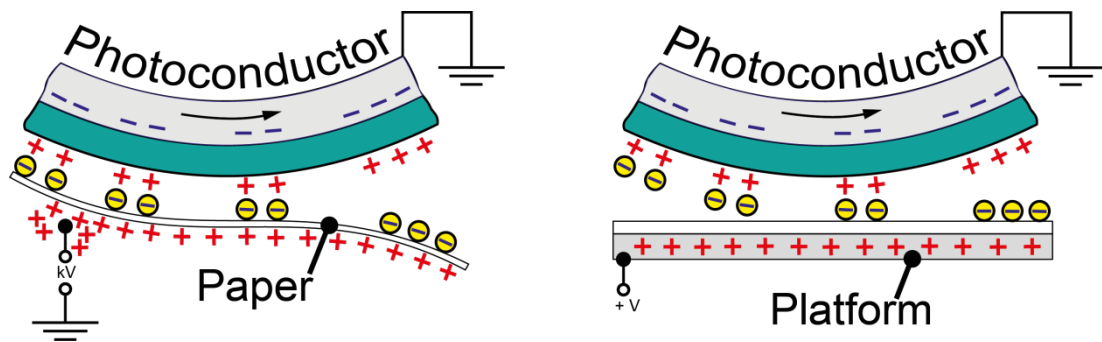


Figure 4.2 – Conventional electrostatic transfer onto flexible (left) and rigid (right) substrates (© Society for Imaging Science and Technology [244])

This section reviews approaches which used EP as an indirect means of fabrication, where the output of the process was composed primarily of something other than toner.

4.2.1. Cubital Ltd, Israel

The earliest use of electrophotography to support production of AM parts originated in Israel and was inspired by discoveries and research distilled into patents by Scitex Corporation Ltd, Israel [245, 246]. These

inventions led to the formation of Cubital Ltd in the mid-1980s which developed machines and additional patents until around 2000 [247-251].

Figure 4.3 shows an overview of the solid ground curing (SGC) process as commercialized by Cubital Ltd. The core competence of Cubital was chemical engineering of UV curable materials for fabricating 3D objects.

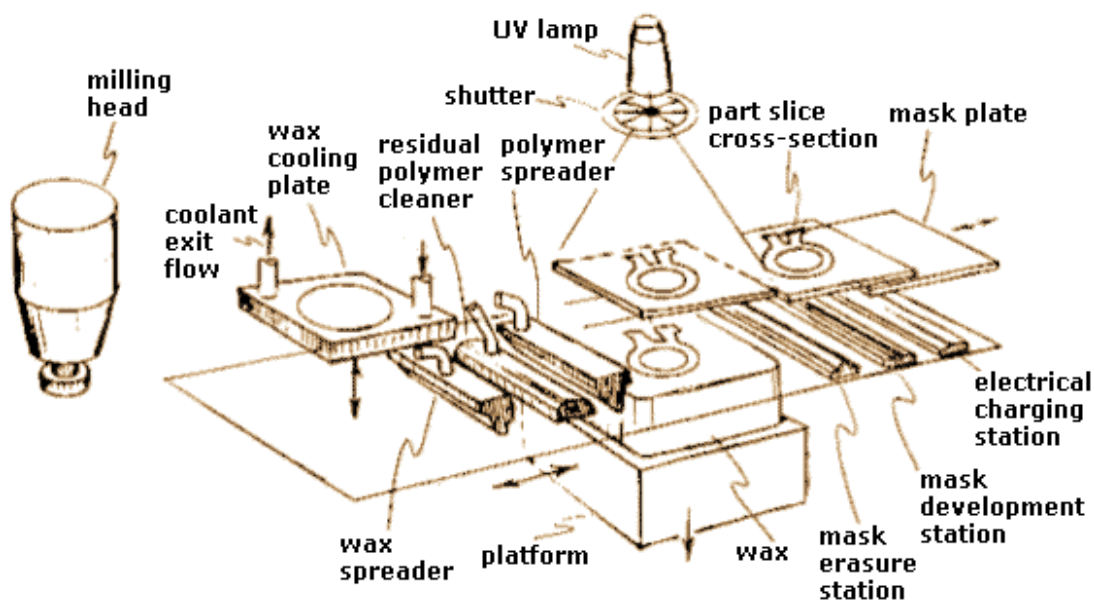


Figure 4.3 – Overview of the solid ground curing (SGC) process [252]

In the SGC process, an entire layer of photosensitive resin was spread to a desired layer thickness. That material was then selectively cured by UV exposure through a mask. EP was utilized to print a unique negative mask on a sheet of glass (mask pate) for patterning the UV exposure of each layer as shown in Figure 4.4-Figure 4.5.

Where the toner was deposited, the UV radiation was blocked, and where it was not, the resin beneath was exposed to UV through the glass which initiated a crosslinking chemical reaction. Once the desired portions of

the photosensitive resin layer were solidified by UV exposure, the uncured resin was vacuumed up and a molten wax support material flood filled all of the remaining area of the layer and was allowed to cool. Once solidified, the entire layer (wax and thermoset) was then milled flat providing an appropriate build surface upon which photosensitive resin for the next layer was spread. In the meantime, the toner was cleaned from the glass mask plate and the negative mask pattern for the next layer was printed in toner onto the glass. This sequence was repeated for each layer until the build was complete, after which the wax was heated until it liquefied and was removed from the part.

In this way, the SGC process relied on EP for the digital patterning of material, however the final component was composed of UV cured resin, not toner.

It is noteworthy that the photopolymer expertise of Cubital was brought together again in the company Objet (now merged with Stratasys), which successfully utilizes inkjet technology to pattern the resin as it is deposited (doing away with the need for a mask), rather than trying to pattern the UV exposure.

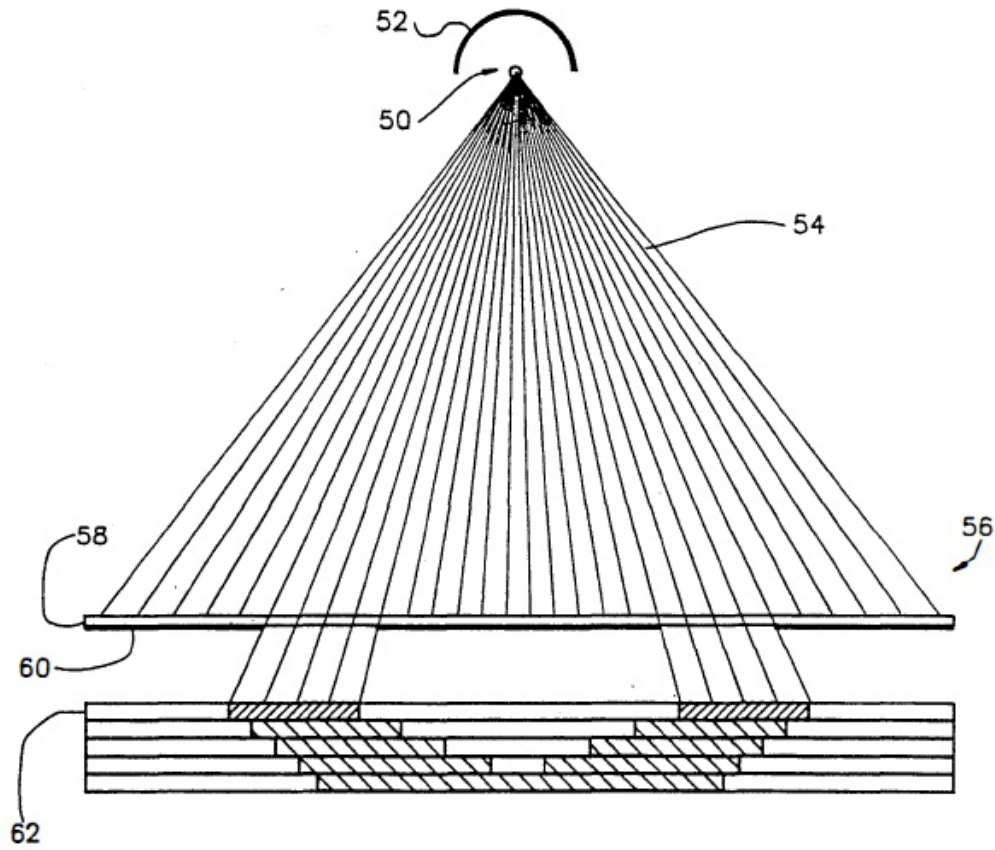


Figure 4.4 - Image showing the use of a mask (#58) to selectively cure the top layer (#62) of a part, Figure 1C from [246]

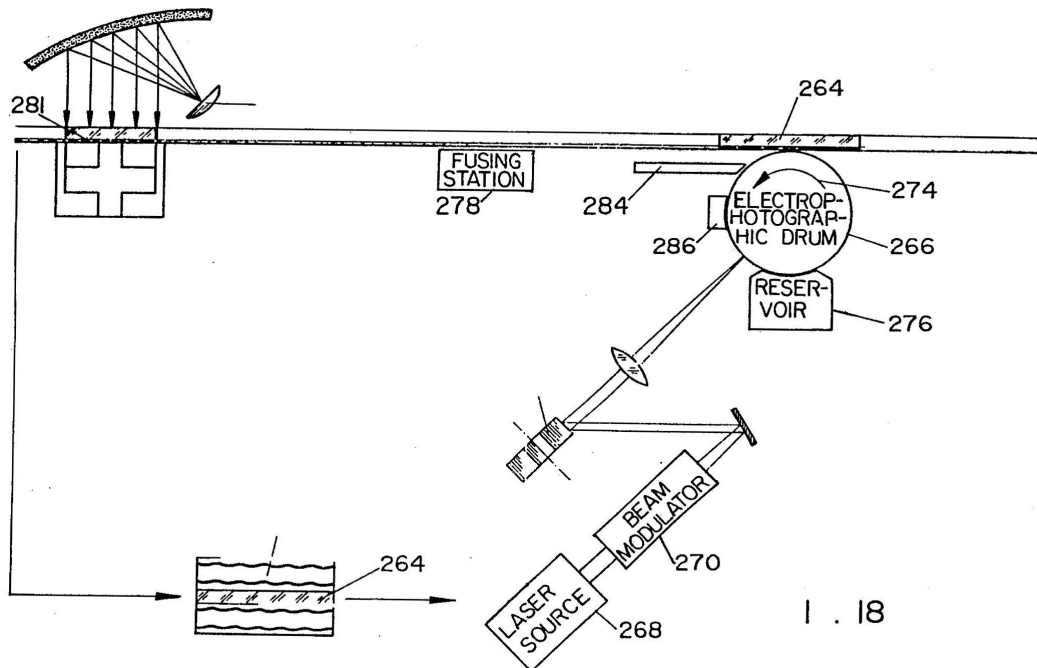


Figure 4.5 - Image showing the use of toner on a glass slide (#264) as a mask for UV curing a layer in a cross-shaped part, Figure 1.18 from [245]

4.2.2. Kira Corporation, Japan

Kira Corporation, Japan, was granted US patents in 2000 [253] and 2002 [254] and developed an AM system based on a layered object manufacture (LOM) approach which used paper as the primary build material and toner to “glue it” together. At least one version of their system used a modified printer (Kyocera, Japan). An illustration of their approach is shown in Figure 4.6.

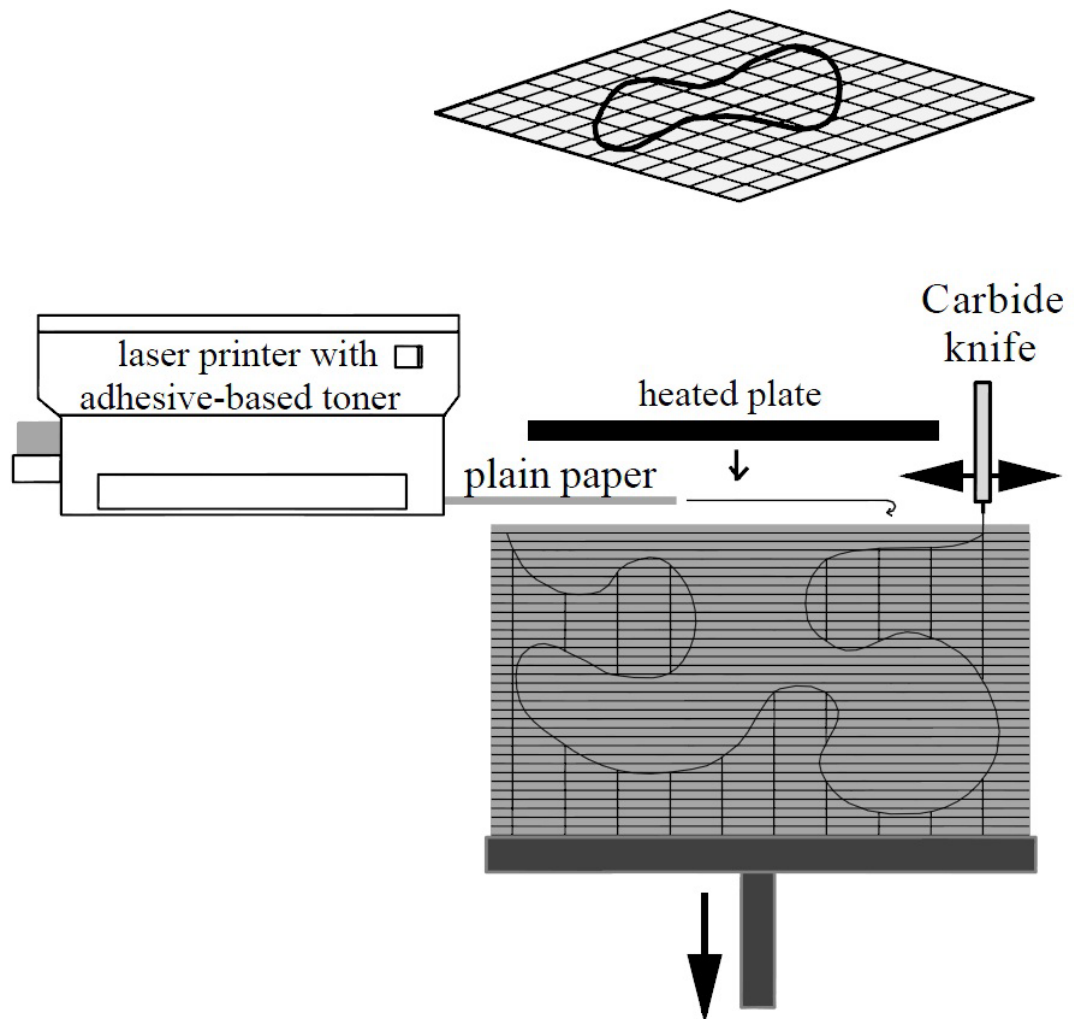


Figure 4.6 – Laminated object manufacture using laser printed toner as an adhesive [255]

Figure 4.6 shows that for each layer, toner was printed in the shape of a cross-section of the part and then laminated onto the paper stack using heat and pressure. A carbide knife then cut around the cross-section of the desired object. The knife also scored the paper in the areas outside of the part in each layer, which was left behind to serve as support material until the build was completed and it could be removed.

In this way, EP was used as an important part of the system, but the primary build material was paper. Apparently difficulties with the paper transfer to the hot plate and stack delamination tendencies led to alternate lamination techniques which did not rely on EP.

It is also noteworthy for future discussion that, according to Hays [54], paper is often considered to act like a conductor due to its tendency to absorb moisture (§3.4.4.3).

4.2.3. Liu and Jang

Liu and Jang [256] proposed and patented the use of EP to bind powder particles together.

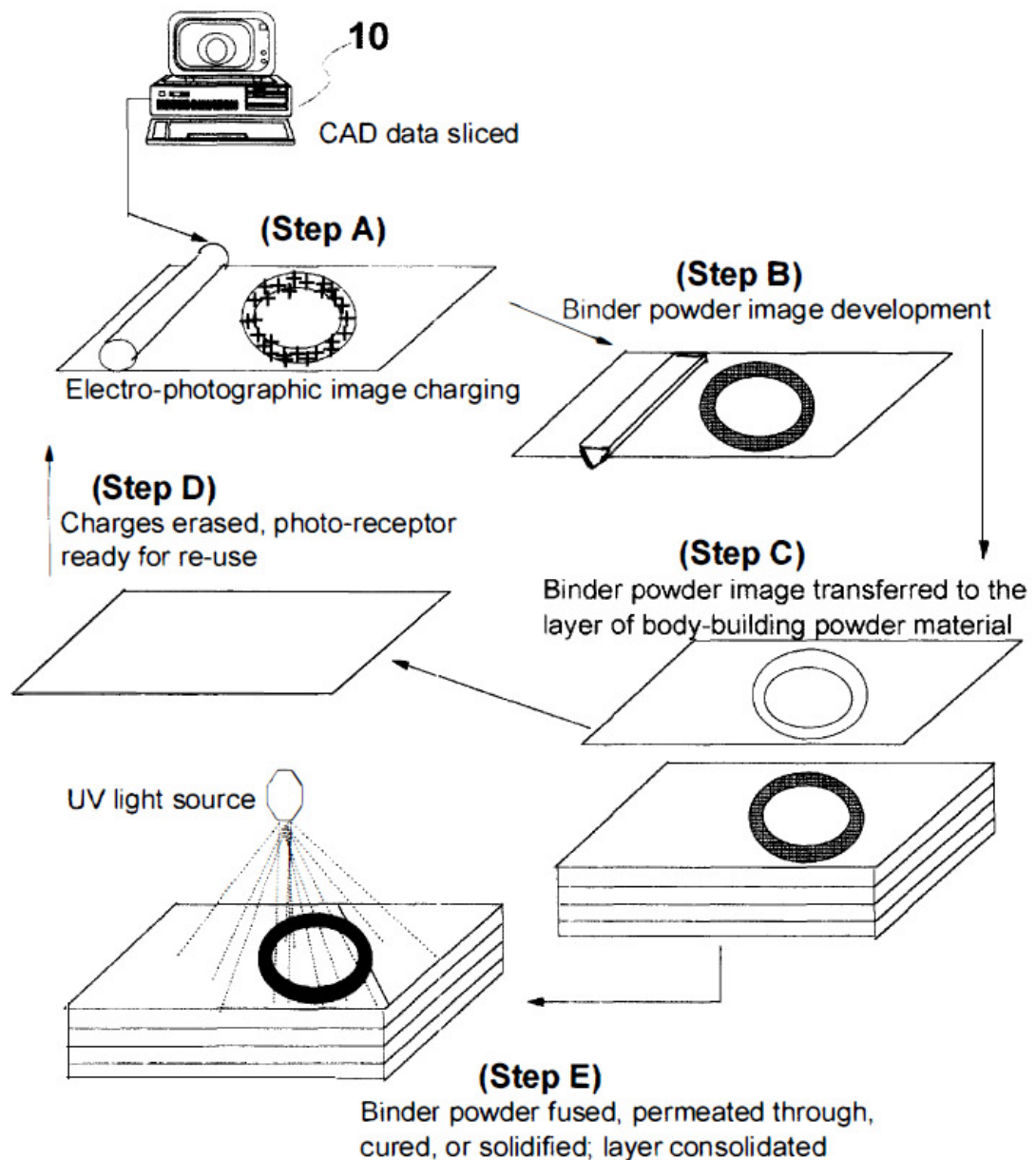


Figure 4.7 – Liu and Jang [256] patent (Figure 3) showing the use of electrostatically deposited toner as a binder on a powder bed.

This process is analogous to binder jetting (§2.3) except that the binding is achieved/activated by the addition of a dry powder binder (which is later fused/cured) rather than a liquid binder. No substantive development work on this concept has been published by them, although some work by Kumar et al. (§4.3.2.1) and Tan and Chua (§4.2.5) appears to share the same general approach.

4.2.4. Sintermask

Sintermask FIT GmbH, Germany (formerly Speed Part RP AB, Sweden), is developing a powder bed fusion process which simultaneously sinters an entire layer using an infrared heater through a mask, as shown in Figure 4.8. For each layer, a unique mask is laser printed using ceramic toner which patterns the infrared exposure [257].

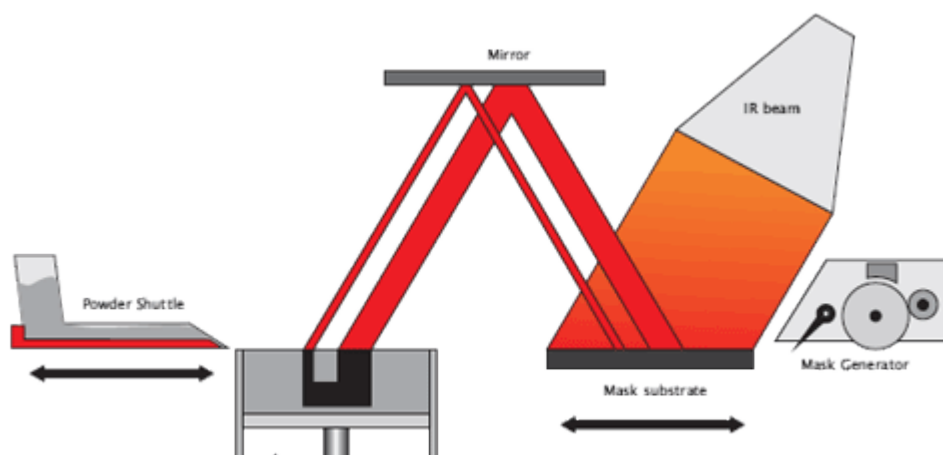


Figure 4.8 – Image showing the use of toner on a glass slide as a mask for IR sintering the upper-most layer of a part in a powder bed [258]

The use of EP to generate a unique mask for each layer is reminiscent of the approach used by Cubital (§4.2.1), except that in this case the mask blocks infrared, rather than ultraviolet radiation. Although substantial progress has been made developing this approach including the release of several beta systems, it does not seem to have reached stability technically or commercially as yet.

4.2.5. Tan and Chua

Tan and Chua [259] have published early work on a process which is also analogous to binder jetting (§2.3) and appears to iterate with some innovation on the approach proposed by Liu and Jang (§4.2.3). Similar to earlier work, the use of EP to deposit a dry binder onto a powder bed is proposed, except the use of an alternative repulsive transfer method akin to those discussed in §4.3.3 is planned. The new approach aims to overcome the few millimetres height limitation identified by Kumar et al. (§4.3.2.1) and Jones et al. [260]. Figure 4.9 shows how by using a controllable voltage source, a developed image can be transferred onto an intermediate transfer or “donor” member at position 1 (when the member is held at a potential with a polarity that is the opposite of the charge on the toner). Then it can be partially melted by a heater before its arrival to position 2, where the polarity of the potential can be reversed in order to repel the toner image off of the intermediate member and onto the surface of a powder bed. At this early stage it is not entirely obvious how much progress has been made to realize the proposed theory. While there is little evidence in the publication demonstrating the technical advantages of this approach over liquid binder jetting, it does reflect an improved understanding of the difficulties of effectively transferring toner in AM.

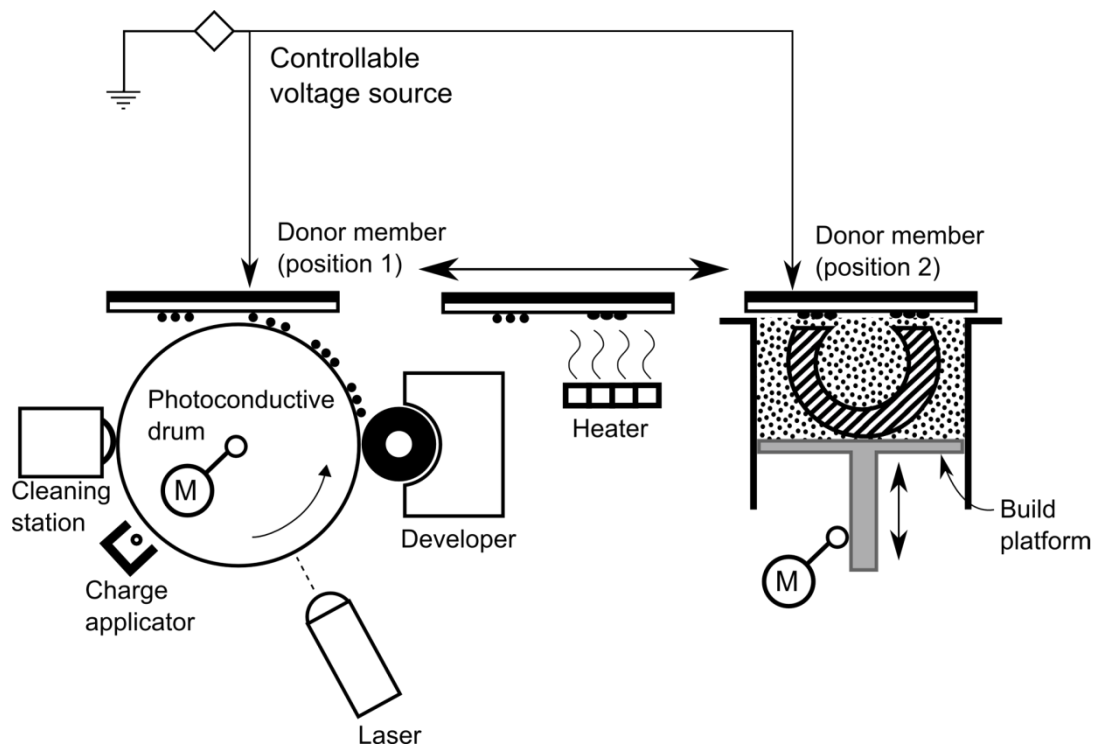


Figure 4.9 – Repulsion transfer of toner onto a powder bed (after [259])

4.3. Electrostatic Transfer/Deposition

The following initiatives used EP with an electrostatic final transfer step as a direct deposition means. In each case, the intention was to produce parts composed of consolidated toner. Each activity is introduced in subsections grouped by like transfer method. The subsections are sequenced chronologically from earliest implementation to show the evolution of the electrostatic final transfer step toward enabling multilayer printing.

4.3.1. Conventional Electrostatic Transfer

As described in sections 3.4.4 and 4.2, the conventional electrostatic transfer method has been the most widely adopted transfer approach for conventional 2D applications (text and image printing). This section reviews its use for multilayer functional printing applications.

Various researchers have acknowledged the potential of EP for functional applications [46], and attempts to achieve multilayer printing electrostatically as early as the 1950's [39] have implemented a conventional transfer method revealing its inherent shortcomings [244, 261, 262]. Defects develop when toner layers are stacked successively exceeding heights from 0.04 to ~3mm, however researchers have rarely illustrated the defects, and instead show proposed alternate transfer solutions [261]. Due to the lack of published examples, as part of this research, both the field dependent success of this transfer method (up to 15 layers thick, see §6.3.1.1) and its shortcomings as enumerated in the literature were demonstrated (see Table 7.34) in a preliminary study, which may be a useful frame of reference for comparison with the following approaches.

4.3.1.1. *Kumar et al.*

In 2003, Kumar and Dutta, of the University of Florida, were the first researchers to clearly publish the field strength limitation of conventional electrostatic transfer and correlate it with the maximum theoretical height of directly printed objects made from non-conductive toner as shown in Figure 4.10 [261, 263].

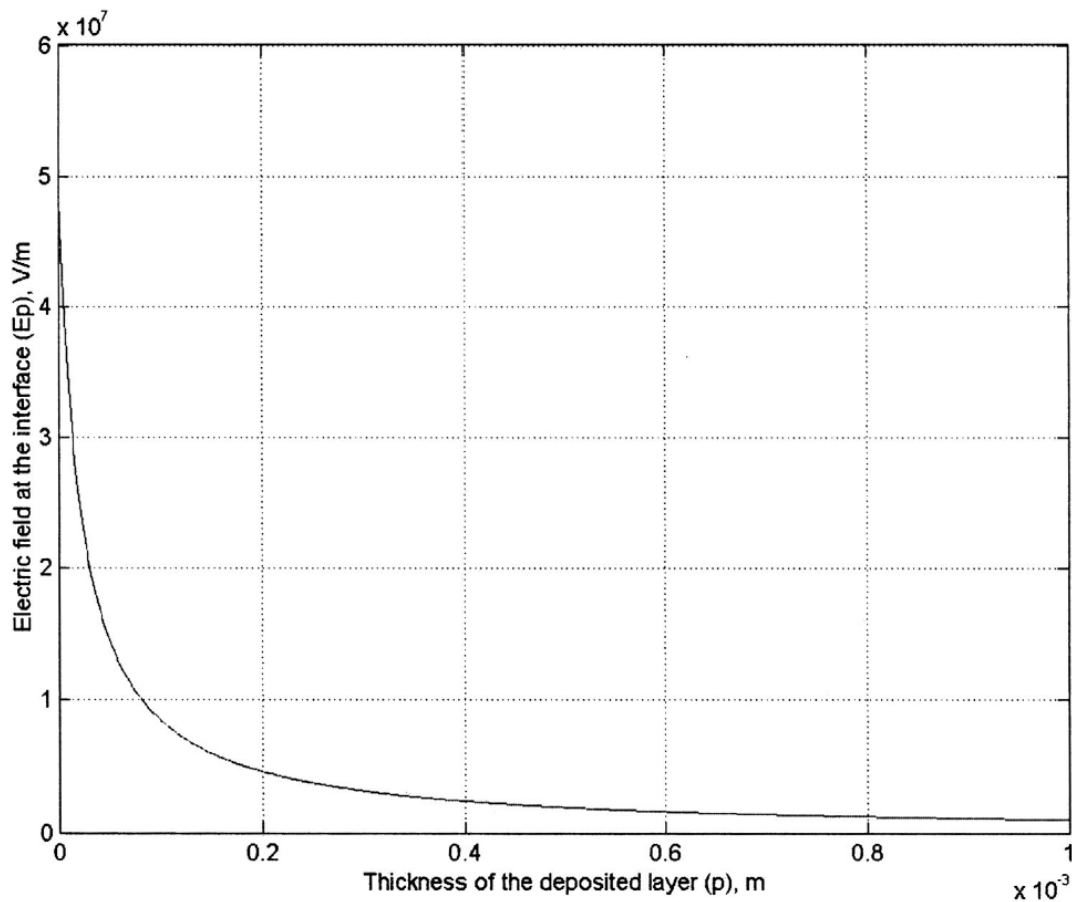


Figure 4.10 – Electric field strength versus print height [261]

The force on the toner particles exerted by the electrostatic field diminishes drastically with the deposition of the first 1mm of toner layers (Figure 4.10). It was also observed that with each successive print, the thickness of the fresh toner layer deposited dropped, which was a manifestation of the diminished critical field strength at the top surface of the part (which was less effective at attracting toner off of the photoconductor) [264]. Dutta summarized by explaining that stacking layers indefinitely was not possible because eventually there was a “cessation of transfer” [264]. The phenomenon is illustrated in Figure 4.13 (in §4.3.1.3). Despite these challenges it did prove viable for

building up layers initially because, “Even if the powder is non-conducting an electric field can be transmitted through the layers of powder up to a few millimeters [*sic*] thick” [261].

Ashok V. Kumar et al. were not satisfied with height limited builds and have researched and published prolifically about potential solutions to overcome the limitations of conventional transfer to enable AM by EP [181, 213, 261, 263-273] as discussed further in §4.3.2.

4.3.1.2. PEPperPRINT – Biochip printing

PEPperPRINT GmbH based in Heidelberg, Germany, is a spin-off company from the German Cancer Research Center which utilizes EP technology to produce peptide arrays used for developing new medical agents, vaccines, and disease diagnosis means [274]. The material printed in this process consists of activated amino acids which are “frozen” into the polymer matrix of toner particles. After printing, the toner is heated in order to melt the matrix which acts as a solvent and facilitates the coupling of the amino acids to the substrate. Up to 20 different amino acid toners can then be assembled into peptide arrays as shown in Figure 4.11.

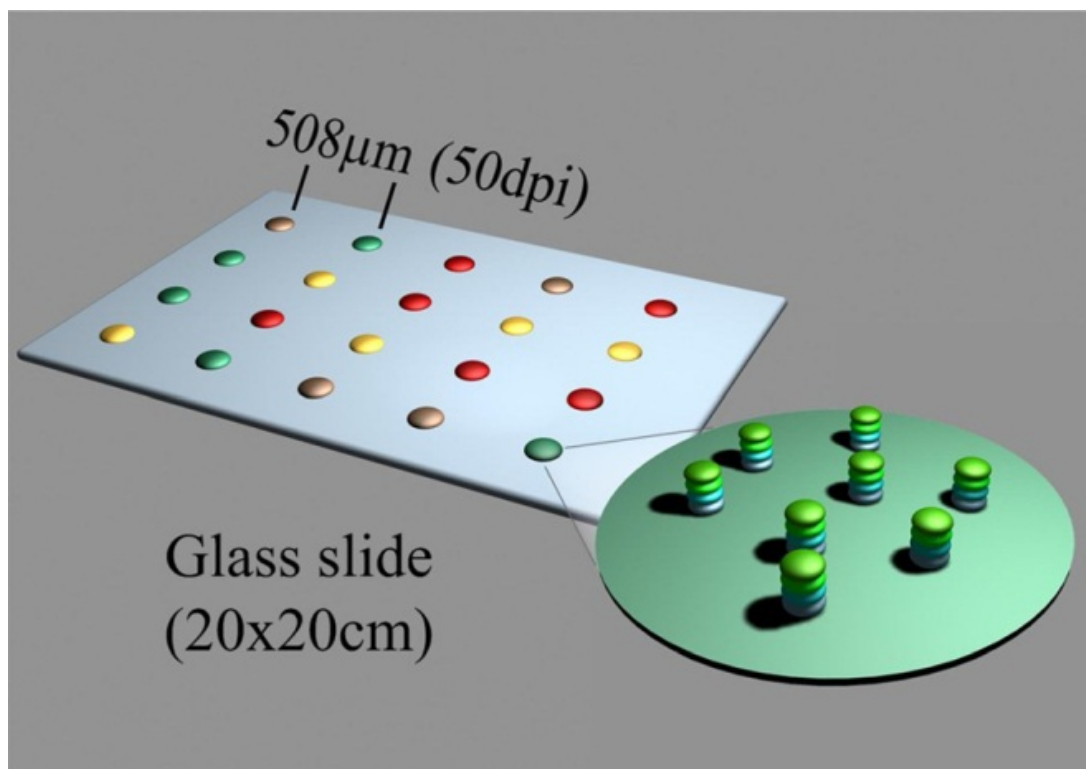


Figure 4.11 – Illustration of the synthesis of a multilayer peptide array on a glass slide [274]

These peptide arrays were first printed onto paper [275], and more recently onto glass substrates [274]. Figure 4.12 shows the peptide printing system which consists of 20 mono component printers which print one type of amino acid toner each [274].

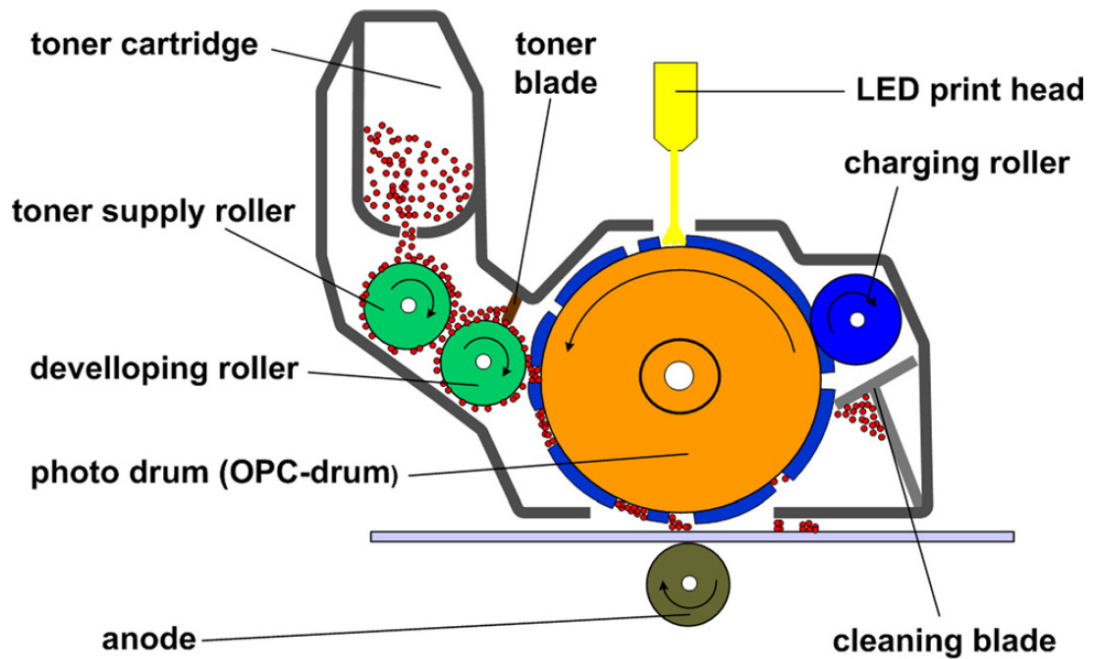


Figure 4.12 – Printer schematic and array of printers for biochip fabrication [274]

The final transfer step is achieved using a conventional electrostatic transfer where the field is generated through the 1mm thickness of the glass slide substrate using a transfer anode (roller made from static dissipative foam) with a voltage of $\sim 2.5\text{-}3$ kV which was the maximum admissible without suffering air breakdown (§3.4.1.1) [274].

In addition to peptide arrays, larger three dimensional shapes were attempted. Güttler et al. report challenges encountered during attempts to use EP to directly print biocompatible “functional surface” scaffolds in complex shapes by using a chemically degradable support material [262]. Since the printing hardware was not discussed, it is presumed that the system as described above (including conventional electrostatic transfer) was used for these trials. From the following quote, one can deduce that they first attempted simply to print toner layer-on-layer with conventional fusing in between which was unsatisfactory.

...toner layers can not [*sic*] simply be printed one above the other and fixed by melting in between. The 3D-structure distorts by the frequent melting processes and its top surface fast corrugates. This prevents the uniform deposition of additional layers of toner [262].

Güttler et al. explains that an alternative approach was devised to circumvent the surface degradation experienced previously [262]. To supplement thermal fusing, chemical bonding was proposed and patented by Grunze et al. [276]. Specifically, the initial monolayer was to be covalently bonded to the underlying substrate and the entire layer cross-linked in order to provide a smooth build surface for the subsequent layer and resist deformation during the deposition and consolidation of subsequent layers [276]. Trials revealed that even when supplemented with chemical bonding, obtaining a “highly uniform deposition of layers with different toners” was last reported to be a “major problem” [262].

Despite the lack of definitive progress toward classical AM applications, the effectiveness of EP (including a conventional electrostatic transfer) for biochip printing has been demonstrated and functional printing (with form above the microscale) has been attempted.

4.3.1.3. Critical Review of Conventional Electrostatic Transfer Approaches

The impracticalities of using conventional electrostatic transfer approaches for AM of non-conductive toners directly are undisputed in the literature. Kumar's statement that "the electric field strength at the top layer decreases as the part height increases" summarizes the primary weakness of this transfer method [261]. In practical terms, this means that the process is self-limiting in nature where "printing stops after the part height is around one millimeter [*sic*]" [181]. This is because layer growth insulates incoming toner from the effects of the transfer field (See Figure 4.13).

Further to the field strength reduction due to self-insulation, the uniformity of the field which is able to permeate through the substrate would be compromised by variations in the consolidated layers as discussed in §3.4.4.2.

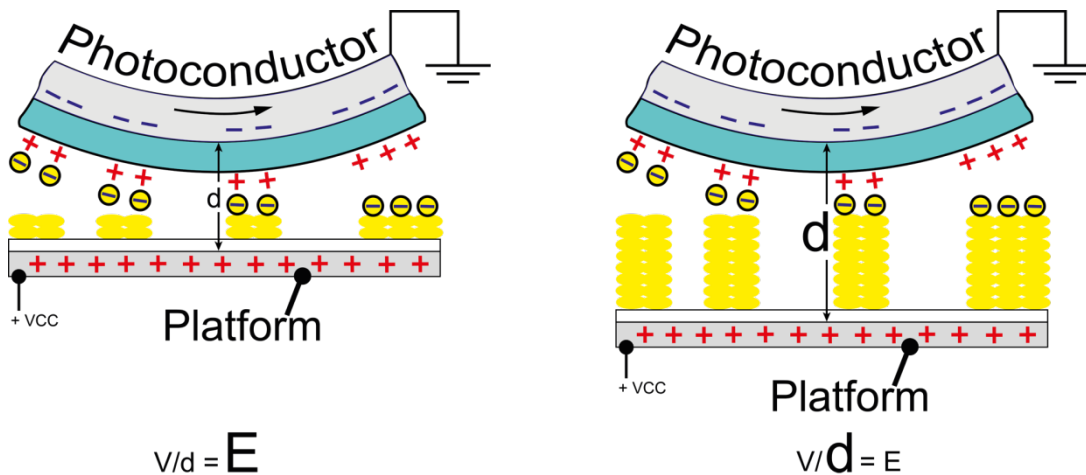


Figure 4.13 – Self-limiting nature of multilayer printing when using a conventional electrostatic final transfer step where voltage is fixed (by the dielectric breakdown strength of air) (modified from author’s original, in [244])

For the peptide array printing application a conventional electrostatic transfer was viable because the pile height (i.e. image stack or build height) of the printed toners did not grow beyond the critical transfer field strength, even though it appears to have been approaching that threshold since the transfer efficiency was noted to be considerably lower than commercially available colour printers [274].

Regarding the more classical AM application of printing scaffolds, the lack of demonstrated forward progress weakens the assertion by Güttler et al. that layer defects were caused by distortion induced from “frequent melting” opening the matter to reconsideration [262].

The shortcomings of the conventional electrostatic transfer step for multilayer printing above the microscale led to further innovation to enable uniform layer deposition with greater height.

4.3.2. Top Charging

Building on the outcomes of experimental work with conventional electrostatic transfer approaches as described in the last section, Kumar et al. developed and patented an alternative electrostatic transfer approach based on charging the top surface of deposited layers, known as “top charging”. This subsection describes their work in the context of related research and gives a technical critique.

4.3.2.1. *Kumar et al.*

Dr. Ashok V. Kumar and his colleagues based in the Department of Mechanical and Aerospace Engineering at the University of Florida have undertaken and published research in the area of Rapid Prototyping (now referred to as AM) and EP since 1999 [273]. They have developed their own printing system based on a single component Canon print engine and called the process Electrophotographic Rapid Prototyping (ERP) or Electrophotographic Solid Freeform Fabrication (ESFF) [181, 261].

After first understanding the field limited nature of conventional electrostatic transfer (see §4.3.1.1), a new approach was adopted and patented where an electrostatic field was generated between the upper surface of the layer stack and the photoreceptor as shown in Figure 4.14 [266]. This approach enabled a transfer field to be maintained which was “not affected by the thickness of the [fused] toner layer” [181].

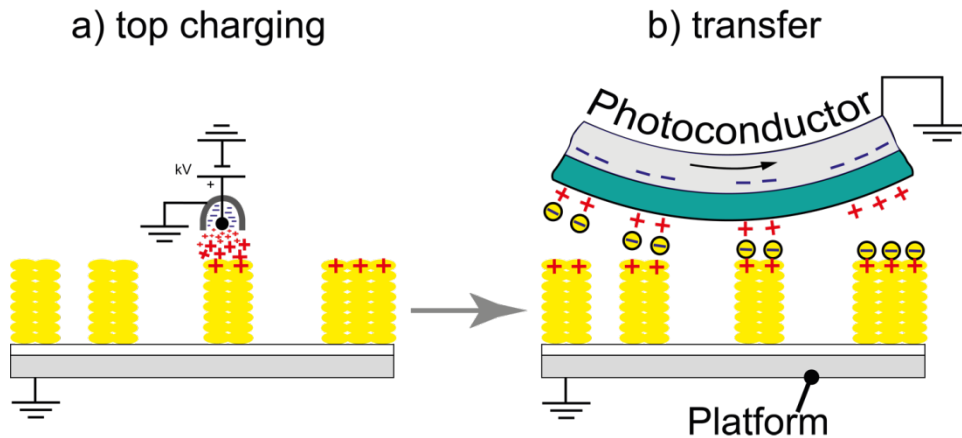


Figure 4.14 – Top Charging transfer method steps as employed by Kumar et al. (© Society for Imaging Science and Technology [244])

The author has previously described how this approach was realized:

Kumar et al. installed a corona wire to charge the top surface of the printed image stack before each print... [(Figure 4.14)] [261, 271]. By saturating the uppermost printed layer with [positive] ions it was intended that the electrostatic field induced between the fused toner and the photoconductor would be enough to transfer the toner... Theoretical calculations and [preliminary] empirical results by Fay and Dutta suggest[ed] that ‘...the part would continue to build indefinitely with adequate corona charging...’ as long as the resulting build stack could be consistently discharged [213, 264]. The top charging approach doubled the height of the printed image stack from 1mm to 2mm without noticeable surface degradation [264]. Although various trials showed image stack growth in excess of 2mm, surface defects formed thereafter which were exaggerated with each successive print” (© Society for Imaging Science and Technology from [244], referencing style updated).

The top charging approach proved helpful and theoretically solved the issues, however, in practice it did not provide a means of producing parts with unlimited height [263]. In his final report to the funding body of his

research, Kumar asserted that, "This low rate of printing [by top charging] can be improved by *more efficient removal of residual charge* from the previously printed layers and by increasing the charge density deposited by the corona charging device" [271] (emphasis added). The next year, the assessment was elaborated on by stating that, "The trapped volume charge in the printed part increases with every layer deposited and it can reach a value where the repulsion due to volume charge exceeds the attraction due to the fixed surface charge deposited by corona. This again creates a limitation on the part height... [and] suggests that *consistent complete discharge of the printed toner powder before fusing is necessary for building higher part thickness*" [181] (emphasis added).

Owing to the absence of definite reports on his progress, the author contacted Kumar to inquire about the final state of the development efforts. Kumar explained that they had the potential to print in excess of 5mm, however the development of surface defects at that height negated any incentive to do so [270]. They were not able to find applications for sub-2mm thick parts sufficiently compelling to attract further funding, therefore their research in this area was suspended.

Since his primary objective had eluded him, Kumar took a side-step to investigate indirect production of parts in a powder bed where laser printed toner was used as a binder [264, 272]. While preliminary feasibility was demonstrated, it did not impart substantial advantages over alternative methods and was therefore discontinued [272]. This

work to use toner as a binder, echoed the work of Liu and Jang (§4.2.3) and prefigured the subsequent attempts by Tan and Chua (§4.2.5).

Although Kumar et al. left the largest body of peer-reviewed and non-peer reviewed work on the subject, the lack of tall samples implies that understanding of the defect causes was not complete. While the field is indebted to them for their foundational work and the courage required to publish their failures (together with their successes), it is timely to question their assumptions and research in order to shore up and build on the foundation that they have laid and generously shared.

4.3.2.2. *Büttner and Krüger*

Büttner and Krüger of the Institute of Automation Technology, Helmut Schmidt University (Hamburg, Germany) published a top charging approach to printing conductive tracks on ceramic, albeit without the aspiration to produce tall parts [94, 97-101].

During the deposition of silver filled polymer toners, high voltage corotrons were used to oppositely charge the substrate in order to attract the toner onto it [100]. During follow-on trials, a surface preparation step was included which consisted of applying a sodium chloride-based “brine solution” intended to increase the conductivity of the substrate and thereby improve the transfer efficiency [94].

The use of the corotrons did increase deposition on the green unfired substrates [94, 100]. Apparently this surface treatment was less effective

on fired ceramic substrates, possibly due to lower moisture content in the substrates. Additional deposition was observed when the brine surface treatment was used, however "...it is unclear if the electrical properties of the brine or the tacky residue it left on the ceramic, or a combination of the two, contributed to the improvement" [95].

4.3.2.3. Critical Review of Top Charging

Perhaps the best critical review of the work by Kumar et al. is found in an insightful retrospective comment by one of his master's students surnamed Kumar Das. The statement and its implications are reviewed in the following quote:

In the final analysis, Kumar Das surmised that the surface defects were caused by the accumulation of residual [negative] toner charge which was not being fully dissipated prior to fusing each layer [181]. He acknowledged that the positive charge from the corona wire counteracted the residual toner charge in the early layers (when it was close to the platform), but its effectiveness diminished as the platform moved further away from the wire [181]. In essence this is a parallel problem to that of conventional transfer. The grounded platform was being shielded from the [corona] wire in proportion to the increasing toner thickness, therefore the surface deposited coronal charge was limited by the breakdown strength of the air [Paschen Charge Limit, Figure 3.19] and could no longer supply enough positive charge to fully neutralize each layer [181]. With the fusing of each new layer of negatively charged toner, an increasingly negative volumetric charge [was] accumulated in the printed image stack. When the repulsive force exerted by the volumetric charge on the incoming fresh toner exceeds the attraction created by the positive surface charge, defects form. Based on his attempts to fully discharge

printed layers Kumar Das observes that, 'Complete discharge of the volume charge of a printed insulator layer is very difficult to attain' [181]. Even though the top charging transfer method pushed the maximum image stack height to 2mm, mainstream additive manufacturing applications require increasing the image stack height by two or three orders of magnitude. The limitation of conventional transfer had been replaced by a new limiting phenomena induced by charge retention in the fused non-conductive toner layers (© Society for Imaging Science and Technology from [244], referencing style updated).

From Kumar Das' explanation, it was underestimating the *effect of residual toner charge* rather than any inherent weakness in the top charging transfer concept which accounted for the lack of quality samples exceeding 2mm high. This concept was not explicitly highlighted in any peer-reviewed publication, which may account for the lack of awareness of this notion. While theoretical calculations by Dutta [264], and physical evidence supporting this hypothesis were clear, empirical measurement of the residual charge does not feature in his master's thesis [181] or anywhere else to the author's knowledge. For such a substantial discovery/theory, this is surprising, particularly because the surface potential of at least one imaging member (the photoreceptor) was measured and reported in several sets of trials. Also, the rationale as to why the toner charge would need to be discharged or neutralized prior to fusing (as opposed to after) is unexplained.

The use of ions to counteract the residual charge initially imparted by tribocharging may have proven to be a non-starter since ion approaches are typically deemed less effective than tribocharging means (3.4.1.1).

Furthermore, it is not clear when the surface quality issues may have begun because the hot platen fusing method almost certainly would have masked early minor defects by "ironing them out".

Since Büttner and Krüger never attempted to produce anything with stacked layers in excess of the microscale, little can be concluded regarding the potential limitations to their approach if adopted for macroscale parts; however the surface treatment steps they used had relevance to the current research trials (Sample 7-24, Sample 8-11) undertaken *before* their work was published.

4.3.3. Repulsion

Aiming to avoid the difficulties of conventional electrostatic transfer or homogeneously top charging fused layers of non-conductive toner, researchers devised a transfer method based on "electrostatic repulsion" for multilayer deposition trials. The "repulsion" transfer concept essentially inverted the conventional electrostatic transfer (See §3.4.3). Instead of using a transfer field to attract (or pull) the toner off of the photoreceptor/transfer roller, a field with the same polarity as the tribocharged toner was used to repel (or push) toner off of the imaging members and onto the layer stack [277]. Figure 4.15 illustrates the steps

of this approach as implemented with a corona wire located inside a transfer belt (after [278]). Toner developed on the photoreceptor was first attracted onto a transfer belt using a field with opposite charge to the toner, as per convention (shown in Figure 4.15a). Further along the belt path, another field with the same polarity as the toner (shown in Figure 4.15 generated by a corona wire inside the belt) was used to repel the toner off the belt and onto the layer stack growing up from the platform (as shown in Figure 4.15b).

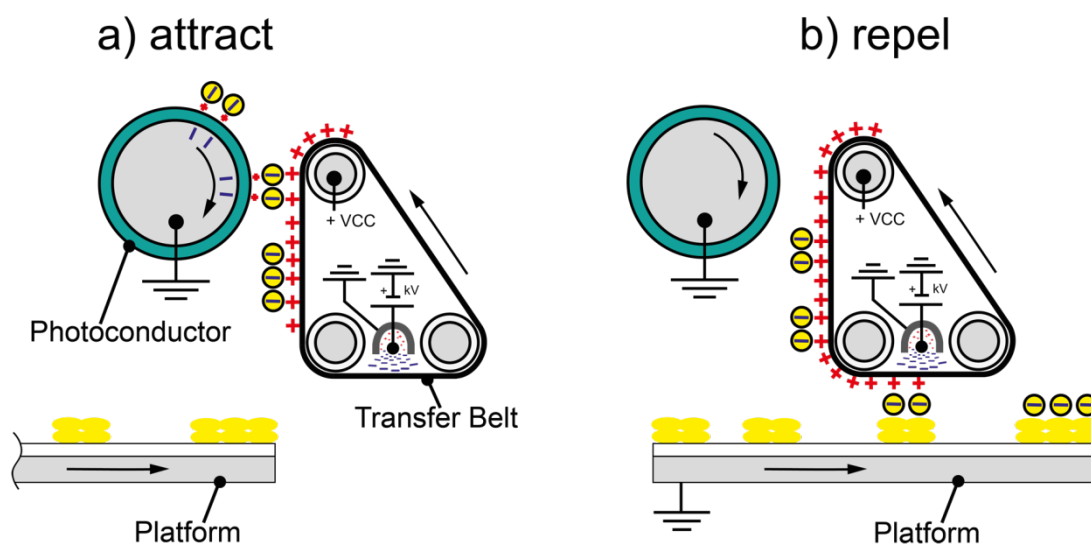


Figure 4.15 – Repulsion transfer deposition steps a) attract the toner off of the photoconductor and onto the transfer belt; b) repel the toner off of the belt and onto the stacked layers

4.3.3.1. *Jethon*

Rolf Jethon first introduced the idea of pushing toner off of the transfer belt and onto a multilayer image stack in his German patent filed in 1991 [279]. Figure 4.16 clearly illustrates the presence of a corotron (labelled

as "M") inside the transfer belt. This corotron would have to be charged with the same polarity as the toner in order to "push" it off of the belt.

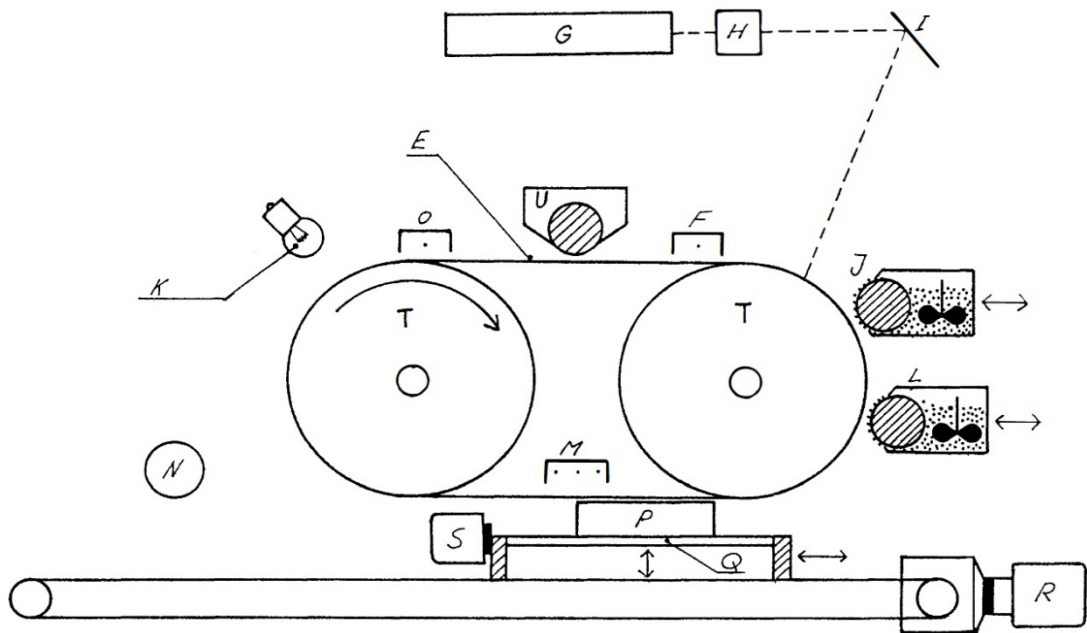


Figure 4.16 – Schematic of a Laser Printer Concept for AM where the toner is repelled off of the transfer belt using a strong field [279]

Although Jethon clearly illustrated his approach conceptually, there is no record of any further work to demonstrate his approach.

4.3.3.2. *Wimpenny and Banerjee*

As explained in §4.3.3.1 the principles of a repulsion transfer were implicitly expressed in the drawings of a patent granted in 1993 to Jethon [279] and later intended for a glass coating/decorating system patent in 2000 [278]. Despite evidence that repulsion principles were considered valuable enough to protect with patents, it wasn't until approximately 20 years after they were first elucidated, that Soumya Banerjee published the only results in the public domain (known to the author) of multilayer

printing by repulsion in 2011 [211]. Wimpenny and Banerjee devised this approach without awareness of the early work by Jethon.

Banerjee showed a nearly linear growth of the sample weight over the course of 150 layer-on-layer prints transferred by repulsion, while the weight of deposition on his standard control samples (produced using conventional electrostatic transfer) did not maintain linear growth as shown in Figure 4.17 [211].

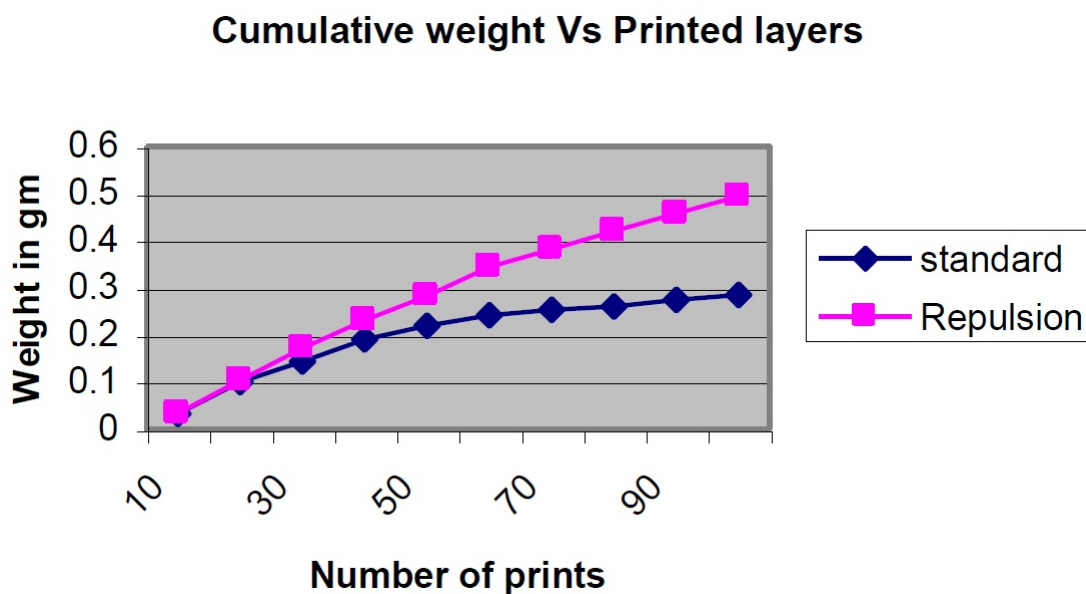


Figure 4.17 – Repulsion transfer efficiency as demonstrated by Banerjee [211]

The implied reasoning for the continued effectiveness of repulsion was that the thickness of the transfer belt (through which the “repulsive field” was passing) did not change, while in a conventional transfer the ever-growing consolidated layer stack acted like an insulator reducing the effective field strength on the incoming toner (as long as the voltage supplied to the transfer field remained constant) as per Figure 4.13.

Despite the apparent promise shown and a patent filed [277], this approach was abandoned in preference for a “hot tack” transfer (or “tackification”) which is described in §4.4. Banerjee never realized parts above 2mm and cited the reason “lack of time” for moving on to an alternative transfer method [211]. Banerjee further explains that tackification provided thicker layers and more material composition flexibility [211].

4.3.3.3. Critical Review of Repulsion

The state of the art of repulsion transfer techniques in §4.3.3 demonstrates that researchers understood the challenge of accumulating multiple stacked layers of non-conductive toner, however there is no tangible evidence to date that this transfer method can be practically implemented above the microscale.

Jethon – The invention disclosed by Jethon demonstrates originality of thought, but little more can be said because no further research has been found.

Banerjee – The research presented by Banerjee was admittedly part of his scoping trials, however it has not been published with sufficient detail to allow independent verification of the conclusions he asserts.

For example, Banerjee mentions that the voltage applied to produce the repulsive field was varied between 1.8 and 3kV, however he does not

explain what voltages were used for generating the conventional field for his control sample, nor where the field was generated [211]. Additionally, he omits any indication of whether the voltage remained constant throughout each build. It is unclear if his use of the term "initial voltage" implied that the voltage was increased throughout the experiment (such as after each layer) or whether it was part of a regime of experimentation at multiple fixed voltages. This is a critical point, because if there had been a need to increment the voltage throughout the deposition process, it could imply that the deposition rate was field strength dependent. If it were field strength dependent, then presumably it could not practically build defect-free objects above a few millimetres high, as was the case for Kumar et al.

Unfortunately, the height of the samples made does not answer this question either. Banerjee stated that the layer thickness was between 7 and 10 μm per print [211] which would have given a cumulative height of between 1.05 and 1.5mm which is still relatively close to the grounded platform. The growth up to this point is no guarantee that surface defects would not have developed above 2mm as was the case for Kumar et al. [181] which would have hampered growth in the Z direction in due course.

From the above discussion, it is evident that the repulsion technique works to build up objects made from non-conductive materials, but perhaps only until the print thickness insulates the substrate from the effect of the (corona or otherwise induced) field as demonstrated by

Kumar in §4.3.2.1. Alternatively, residual toner charge may be a limiting phenomenon for this approach as can be inferred by the statement in the published patent application that, "it may be preferable that any residual charge of the top surface of the previously deposited powder layer is discharged before the deposition of the subsequent layer" [277]. Unfortunately, there is not enough information to come to a well-supported conclusion on this point.

Furthermore, Banerjee's rationale for discontinuing this approach in favour of tackification (See §4.4.1) based on claims of the improved thickness of the deposited layer were not fully explained or supported. He did not acknowledge that the improved layer thickness may have been primarily due to an increase in the toner diameter used, from $\sim 5\mu\text{m}$ for the Lexmark printer to $\sim 30\mu\text{m}$ for the two-component development in the CTG PrintTEC GmbH printers [211].

Having elucidated that this approach may be electrostatically limited, one can conclude that parts attempted by this method may suffer a similar self-insulating fate with image stack growth above the microscale, even though this was not experimentally verified by Banerjee.

Although Banerjee's intention for further trials was evident in a request that the printers for the Selective Laser Printing (SLP) rig (See §4.4.5.3) be built incorporating the potential for a repulsive transfer (which proved impractical to manufacture according to CTG GmbH [280]), the lack of detail reported, and discontinuation of its investigation diminishes the

credibility that it was considered to be definitively more effective than top charging or conventional transfer.

4.3.4. Related approaches

The following approaches use the fundamental principles of EP as a material patterning means, but do not share the same scale or system architecture as traditional toner systems. They are included here for completeness and also to give further context.

4.3.4.1. Nanoxerography

Jacobs et al. of the University of Minnesota have demonstrated the use of electrostatics to arrange nano-scale particles from an aerosol or liquid suspension into a pattern of lines $<1\mu\text{m}$ wide which is approximately two orders of magnitude better than conventional office-based EP [281-286]. The technique was enabled by using a multi-contact electrode which is essentially used to create the equivalent of a latent image (as discussed in §3.4.2) by contact charging an 80nm thick film of polymethylmethacrylate (PMMA), making it an electret (See Figure 4.18 left).

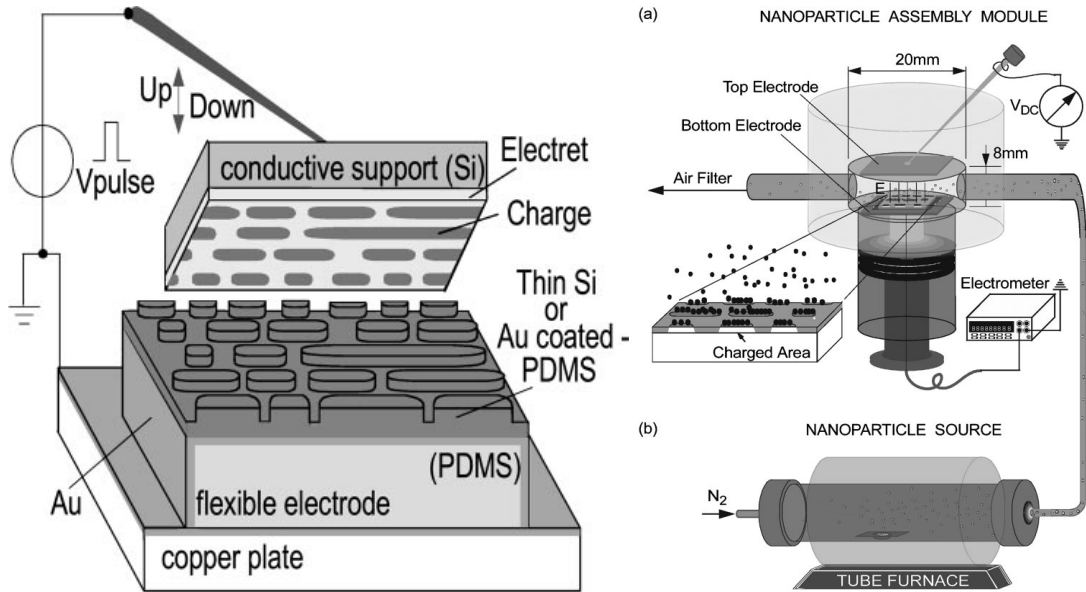


Figure 4.18 – Nanoxerography charging means (left); Nanoparticle assembly module (right) [282]

Once the charge pattern was stored in the PMMA, nanoparticles were presented to its surface and were attracted to the charged areas only as shown in Figure 4.19.

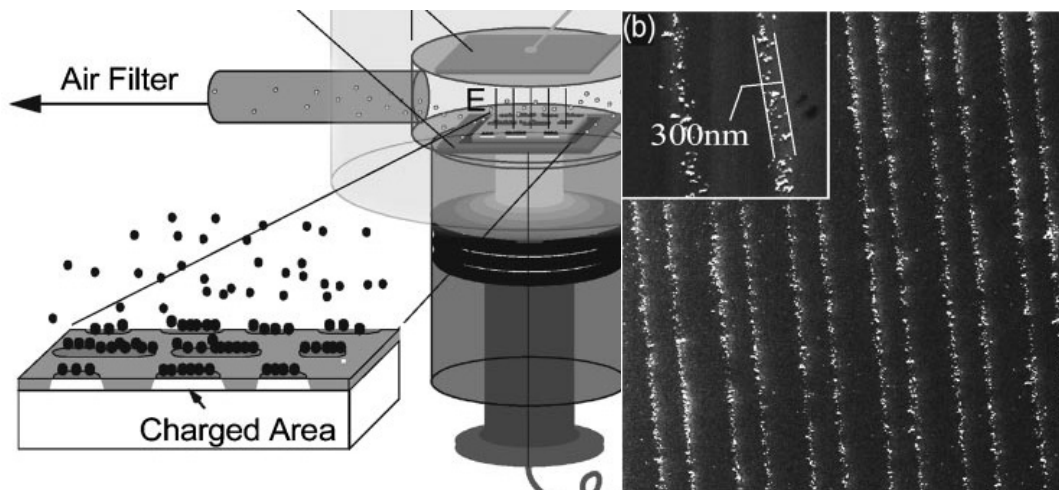


Figure 4.19 – Detail from Figure 4.18 showing nanoparticles attracted to charged areas (left); Actual accumulation of nanoparticles on substrate with a 300nm width [282]

Although nanoxerography is not on the scale which is considered part of AM at this time, convergence of AM with digital fabrication and

nanotechnology may make it more relevant in time. Additionally, it shows the flexibility in both scale and implementation of the principles of EP.

4.3.4.2. *Electrokinetic imaging*

Electrox Corp (NJ, USA) has demonstrated and patented a process called electrokinetic imaging which essentially implements the principles of EP as a guided self-assembly means useful for coated particles from a few microns to 100 μ m in diameter suspended in a dielectric fluid [222, 287].

Similar to nanoxerography (§4.3.4.1), this is not a digital process, but relies on a physical dielectric mask that is laminated to a conductive substrate. The mask is then charged in an external field such that it stores charge, becoming an electret. The field from the stored charge in the mask essentially makes the mask a semi-permanent latent image. The particles to be assembled are coated with a material which imparts them with an electrochemical charge, allowing them to move in an electric field. Once prepared, the masked substrate is immersed typically for 5 to 20s, in a bath filled with the dielectric liquid containing the desired particles for assembly. The liquid is agitated allowing the dispersed material to come within the influence of the field emanating from the mask. Since particles can be preferentially charged on one side or another, their orientation and placement can be controlled via a process analogous to discharged area development (DAD) as illustrated in Figure 4.20.

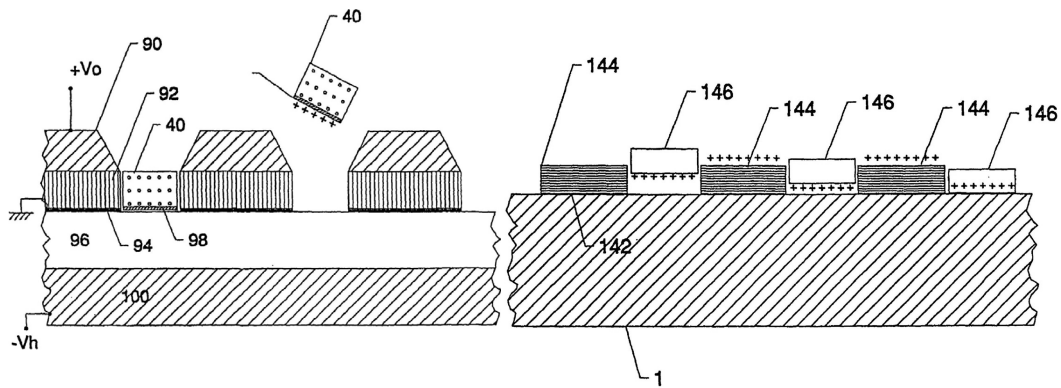


Figure 4.20 – Discrete components patterned using electrokinetic imaging [287]

Neither nanoxerography nor electrokinetic imaging is a digital process (they both require a physical electret mask) and therefore they currently have limited appeal in AM. However, their implementations demonstrate the flexibility and scalability of EP principles which may become more relevant and useful as EP/electrostatics-based manufacturing techniques mature.

The shortcomings revealed in §4.3 have since led to development of transfer methods which are not reliant on electrostatics, such as heat and pressure, as discussed in §4.4.

4.4. Non- electrostatic Final Transfer (Heat and Pressure)

Although the image development process inside an EP printing device is always based on electrostatics, the final transfer step may not be. This section reviews EP research where the final transfer step does not explicitly utilize electrostatics to add toner to the image stack/pile. The most common approach has been the combined use of heat, pressure,

and friction; however, solvent or chemical bonding has also been attempted.

4.4.1. Bynum Proposes “Tackification”

In 1989 David Bynum, of Colorado, became the first to file a patent to use EP for forming “lamina” or layers which were to be laminated together using heat and pressure [288]. The final transfer step involved making the powdered lamina “tacky by the application of external heat, solvent vapor [*sic*] or induction heating” as illustrated in Figure 4.21 and Figure 4.22 [288]. As the author has written elsewhere:

The fresh toner in the developed image would stick to the tacky layer beneath and after the transfer was complete, a platen press applied enough pressure to fully densify the printed image stack [288]. In essence, Bynum’s transfer approach operated in the absence of electrostatics and harked back to the earliest adhesion transfer method employed by Carlson and Kornei. [as discussed in §3.1.2 and §3.4.4] (© Society for Imaging Science and Technology from [244], referencing style and punctuation updated).

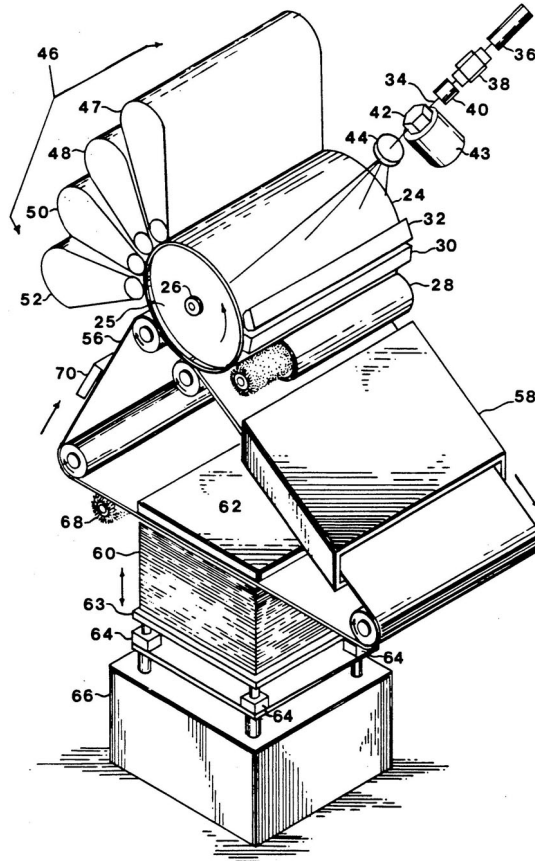


Figure 4.21 – Apparatus for the direct transfer and lamination of powdered layers as proposed by Bynum (FIG 2A from [288])

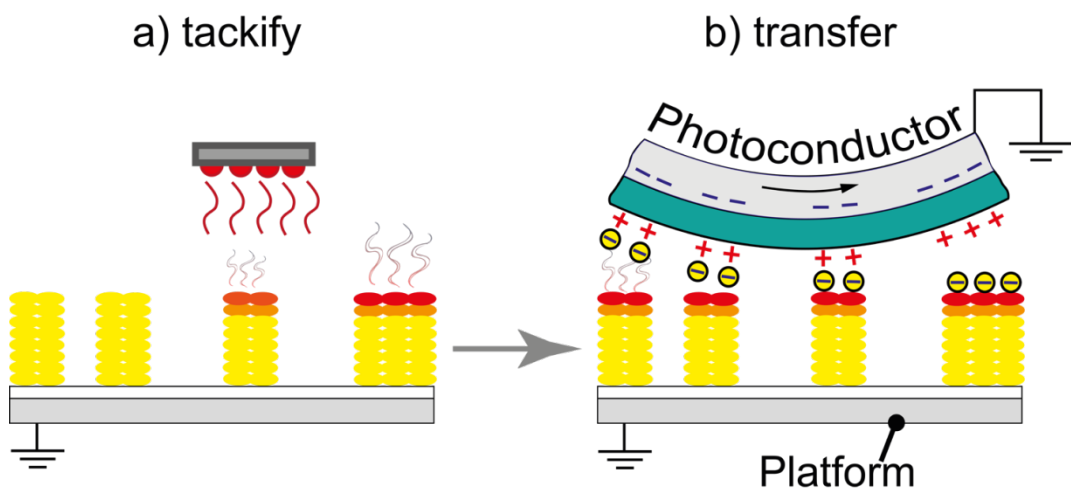


Figure 4.22 – Conceptual illustration of the final transfer step by Bynum based on making layers tacky or sticky (© Society for Imaging Science and Technology [244])

Bynum was the first person on record to envision the use of EP as a direct means of manufacturing above the microscale. His patents also anticipated the ability to create multi-coloured objects, and even the potential to produce multiple discrete parts in a fully-assembled configuration (similar to in-mould assembly [20, 289]) [288].

The next year, Bynum followed up his first patent with another that explicitly incorporated a scanning means to capture an object which would then be reproduced by his proposed EP printing system with some refinements [290]. Although his clarity of thought and planning is evident in the patents filed, no indication of experimental work has been found. Despite this, a plethora of transfer means have since been predicated on the “tackification” approach he proposed as is recorded hereafter.

4.4.2. Grenda

Ed Grenda's research led to the first test rig which employed laser printing directly as a deposition process in AM using heat and pressure (i.e. “tackification” in Bynum’s terms) for the final transfer step. Grenda stated in 1997 [291] that the key patent for his process had been licensed (possibly Bynum’s) and other patents had been applied for including US patent 6,206,672 filed in 1994 [292].

The initial test rig concept is illustrated in Figure 4.23 wherein the image is developed into a powder layer using conventional EP and then that

layer is carried on a platen to a fusing station where the layer is fused onto the part using heat and pressure.

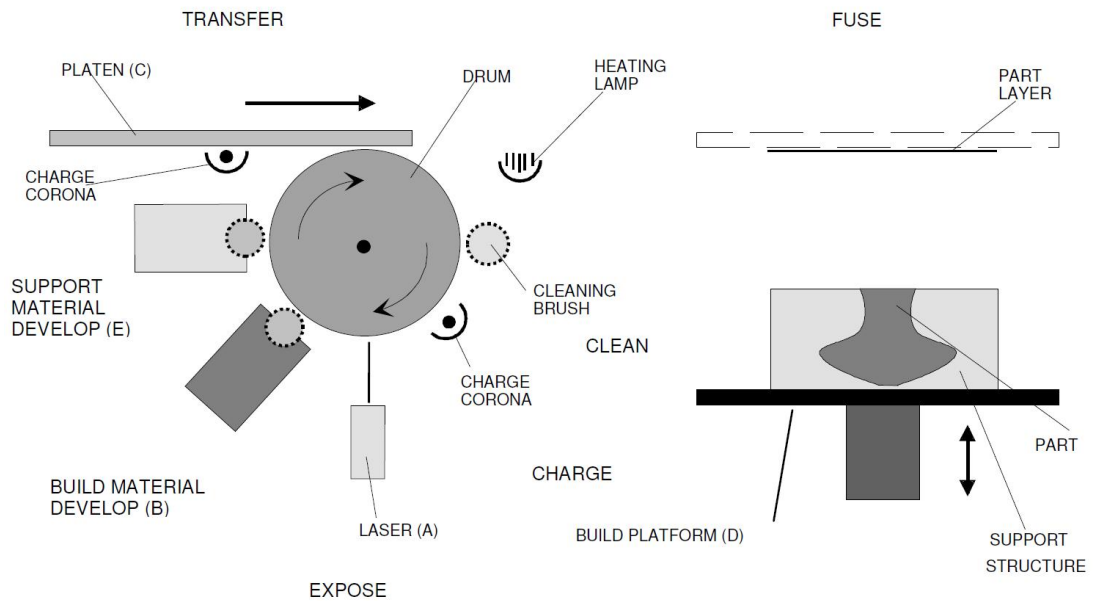


Figure 4.23 – Schematic of a 3D Laser Printer Concept by Grenda [291]



Figure 4.24 – 3D Laser Printer test rig and parts by Grenda [291]

Figure 4.24 shows the 3D Laser Printer test rig (left) and also some parts produced by Grenda et al. Grenda was the first to publish images of 3D parts directly printed using EP, and from the successful tone of his writings, it is not clear why his efforts were not continued.

4.4.3. Cormier et al.

Denis Cormier and his students at North Carolina State University undertook a variety of experiments aimed at utilizing EP for directly printing polymers including the ability to selectively colour three-dimensional parts [60, 210, 293, 294]. This was the first time selectively coloured parts were produced by EP even though the capability had been anticipated by Bynum and Grenda [288, 291]. The trials used conventional office-based laser printers (Laserjet 2100 and LaserJet 4500, Hewlett Packard, CA, USA) loaded with a variety of experimental toner/powdered materials. The configuration of the printer used for the colour experiments is shown in Figure 4.25.

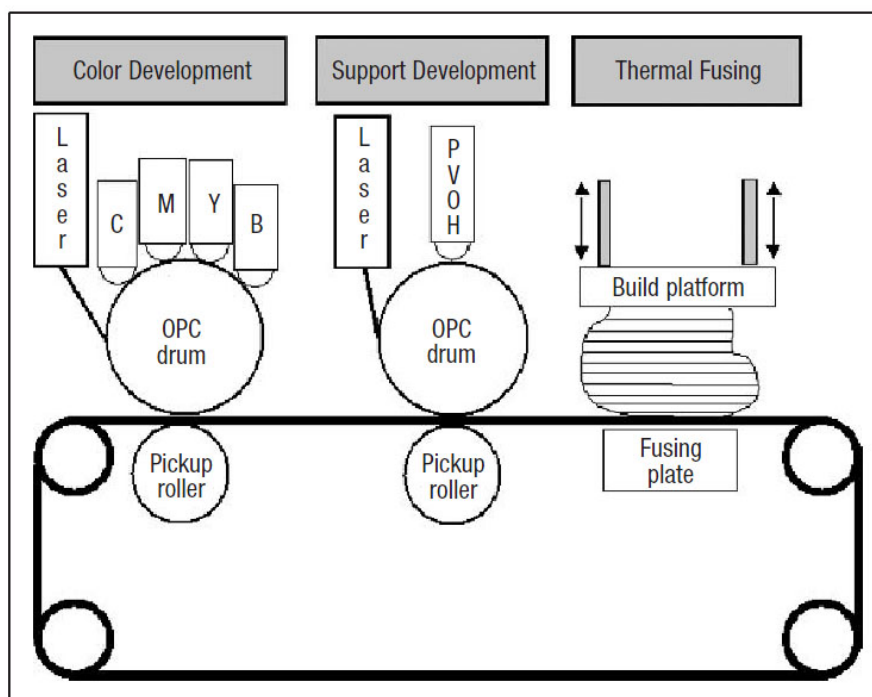


Figure 4.25 – Cormier's Colour 3-D Laser Printer Configuration [60]

Cormier's work indicated good potential for EP in AM, but was not funded and therefore not sustained. No samples taller than a couple of millimetres were made. Cormier's familiarity with the same challenges experienced by others is evident in the following statement:

With regards to layered electro-photographic printing, perhaps the most significant technological challenge lies in inducing the printed image to leave the OPC drum and to be deposited onto the build platform [293].

Recently, there have been indications that Cormier's interest in this technology has been revived, however public dissemination of his activities are not yet available at the time of this writing.

4.4.4. Metal Printing Process (MPP) by Sintef

The Metal Printing Process (MPP) under development at Sintef in Trondheim, Norway, uses the principles of ionography for building metal parts supported by un-sintered ceramic powder which is deposited by EP [295, 296].

As implied by the name of the process, metal powder is used as the build material. The build material is assembled using ionography, which follows similar steps to EP as shown in Figure 4.26.

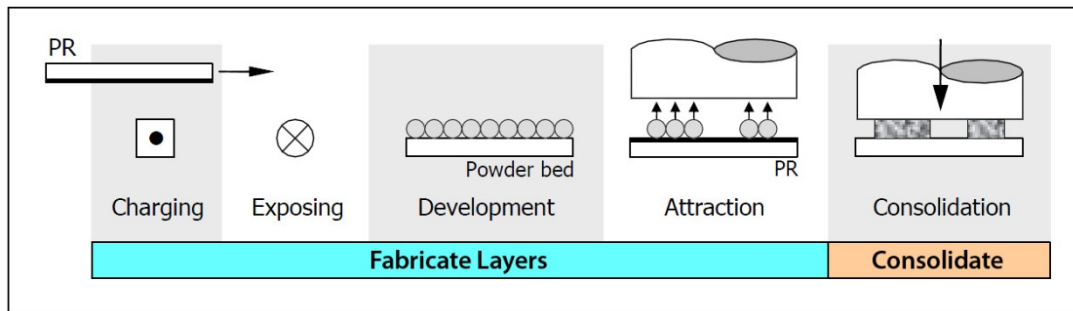


Figure 4.26 – Metal Printing Process schematic [229]

First, a powder bed of conductive metal powder is charged using an applied voltage and a photoreceptor is charged using a scrotron and then exposed to form a latent image [62, 296]. Next, a monolayer of charged conductive particles is then attracted onto the anode/photoreceptor which is flipped over (not shown in Figure 4.26) and powder is transferred to the punch “by electrostatic forces” [229], and in some cases assisted by the use of an electrically insulating wax coating on the punch [62]. The final transfer of the powder from the punch is achieved by pressing ($\sim 200\text{MPa}$) the powder onto the consolidated part which is held in a die at elevated temperatures ($\sim 600^\circ\text{C}$) [229].

After the metal printing portion of the process was proven technically, pursuit of the support strategy (as shown in Figure 4.27) required an inert material. Ceramic powder was selected as the appropriate support material; however the selection of a non-conductive powder caused a problem. Boivie et al. explains that it was virtually impossible to charge it in situ in a powder bed (as is possible with conductive particles), necessitating the use of alternative charging approaches such as tribocharging [229]. This adoption of an alternative charging step

qualified the support material deposition as a form of EP. The ability to charge and print ceramic powders was demonstrated, although the maximum build height achieved did not exceed a few millimetres [63].

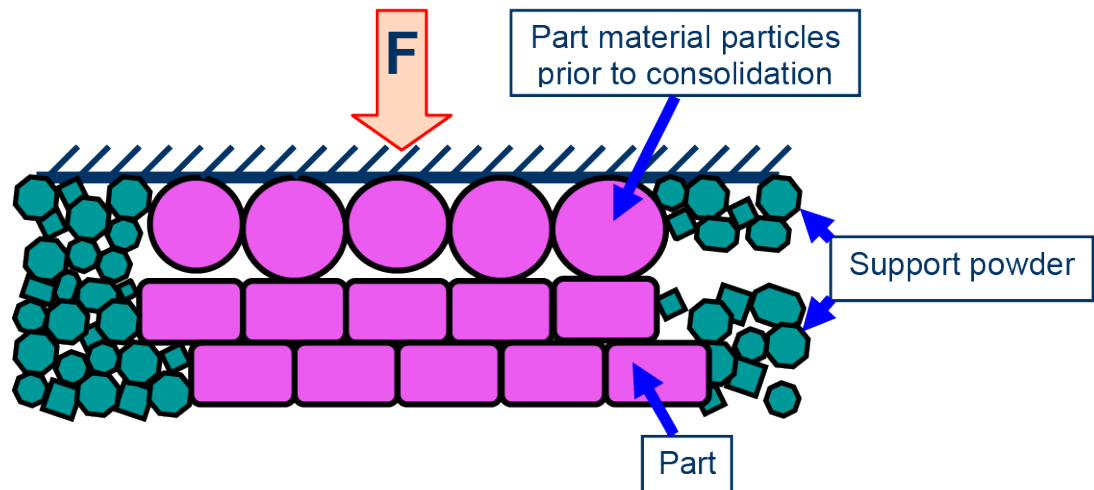


Figure 4.27 – Support material strategy for MPP (adapted from [229])

Although a variety of metal samples (without support material) were produced, substantial difficulties were encountered with the additional steps required for the ceramic support material. Furthermore, there was difficulty finding an appropriate material for the die which was prone to cracking. The future of this process is unclear, owing to the difficulty of managing material behaviour at high temperatures and pressures.

4.4.5. Wimpenny et al.

Professor David I. Wimpenny of De Montfort University, Leicester, UK and his research group members have undertaken EP-based experimental work for AM and published since 2006 [18, 58, 59, 61, 95, 116, 211, 236, 244, 260, 277, 297, 298]. Prof. Wimpenny's research approach was

highly collaborative (partially due to the nature of the funding attracted for the research) involving various partners across multiple overlapping research initiatives. Since the current research derives from the foundation laid by Prof. Wimpenny (et al.) a more detailed review of his endeavours follows. For clarity the various components which contributed to the overarching EP research theme directed by Prof. Wimpenny are described in the following subsections:

- Scoping and feasibility trials with Soumya Banerjee (§4.4.5.1)
- Proof of concept samples made by CTG PrintTec GmbH (§4.4.5.2)
- Selective Laser Printing (SLP) development rig by partners in the Custom-fit project (§4.4.5.3)
- Laser Printed Electronics (§4.4.5.4)

4.4.5.1. Scoping and feasibility trials

The early scoping and feasibility trials were largely undertaken by PhD candidate Soumya Banerjee under the direction of Prof. Wimpenny with support from the European Union Framework 6 Custom-fit project (No: 507437). The initial focus of the research was dominated by exploring materials which were amenable to formulation as toner particles, yet after fusing would perform as well as tough injection moulded polymers [58, 297]. Evaluation of material properties was predominantly performed on office-based laser printers (Laserjet 4, Hewlett Packard, CA, USA), where older printers were preferred because of their capability of depositing larger particles [95], resulting in thicker layers. The search expanded to non-conductive toners including assessing candidate support materials which were easy to remove [59].

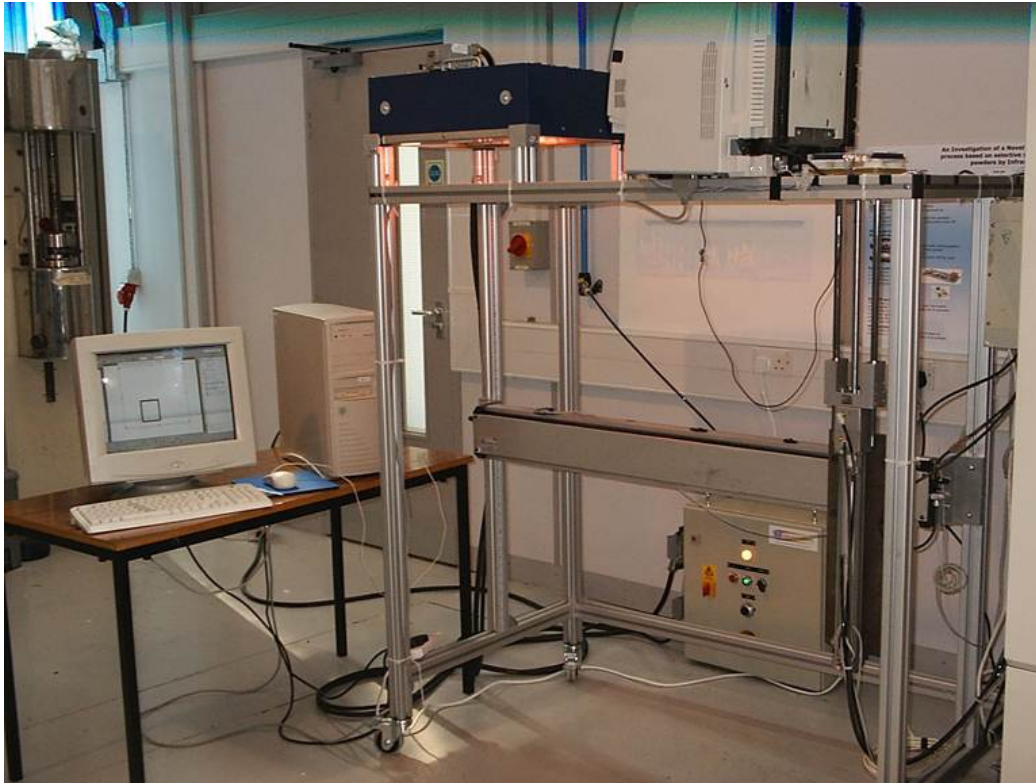


Figure 4.28 – Early test rig for laser printing multiple layers of non-conductive toner

Figure 4.28 shows the initial test rig built by Wimpenny and Banerjee in order to trial laser printing of multiple layers using an adapted office laser printer (C510, Lexmark, KY, USA) mounted on its side, which was not optimal for printing, but enabled exploration of the concept [299]. The most significant difference between the architecture of this and prior test rigs was the use of a non-contact infrared heater for fusing rather than a flat platen type heater, a trait which was passed on to the subsequent development rig (§4.4.5.3). As the interest in non-conductive toners intensified, two-component development became attractive (because it allowed more material flexibility than single component development – See also §5.2). Some trials were thus undertaken on an office laser

printer which used two-component development (Ricoh Aficio CL7000, Ricoh Company Limited, Tokyo, Japan).

By mid-2007, Wimpenny and Banerjee had begun to comprehend the challenge of effective transfer and proposed a transfer based on repulsion in a patent application [277]. After preliminary demonstration of the effectiveness of repulsion transfer (as reviewed in §4.3.3.2), Banerjee shifted his focus to using a “tackification” based transfer approach.

Initially, the application of glue to the build surface was explored as a means of achieving final transfer which was not height limited [299]. This practice was reminiscent of early transfer strategies explored by Roland Schaffert (§3.4.4). Although toner was successfully deposited in the absence of a transfer field (onto a non-conductive substrate 20mm thick), the practicalities of glue application after the deposition of each layer made an alternative means of making the build surface tacky attractive [299]. For this he resorted to heat and pressure, in line with Bynum’s approach.

The desire to use two-component printers to print onto a rigid flat substrate, coupled with the need to apply heat and pressure to deposit layers eventually led to collaboration with German printer manufacturer CTG PrintTEC GmbH.

4.4.5.2. *Samples made by CTG PrintTec GmbH*

CTG PrintTEC GmbH (CTG) based in Alsdorf, Germany, is a specialist printer manufacturer which was offering the market two-component printers for toners loaded with ceramic pigments for printing customized images directly onto glass or decorative tiles.

At the request of Wimpenny and Banerjee, CTG demonstrated the feasibility of depositing and fusing powder layer-on-layer to heights in excess of 8mm (See Figure 4.31) [244]. Initial proof of concept was accomplished using an electromagnetic brush (EMB) powder coating machine which utilizes some of the principles and hardware from EP as shown in Figure 4.29 and Figure 4.30 and described below.

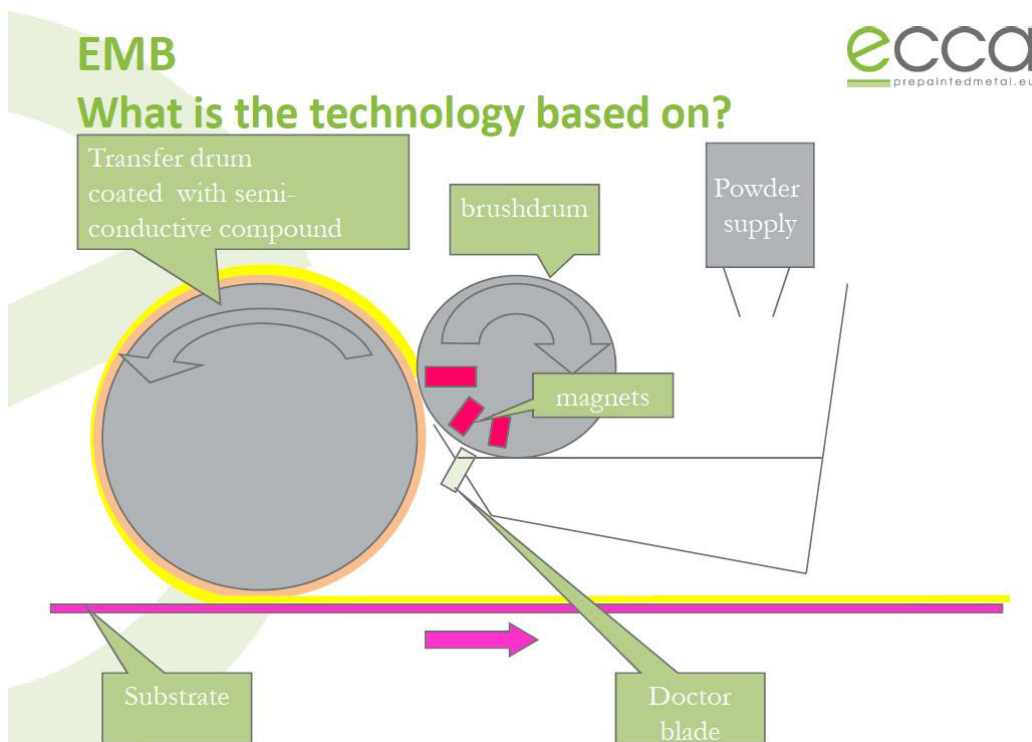


Figure 4.29 – Overview of EMB coating process [300]

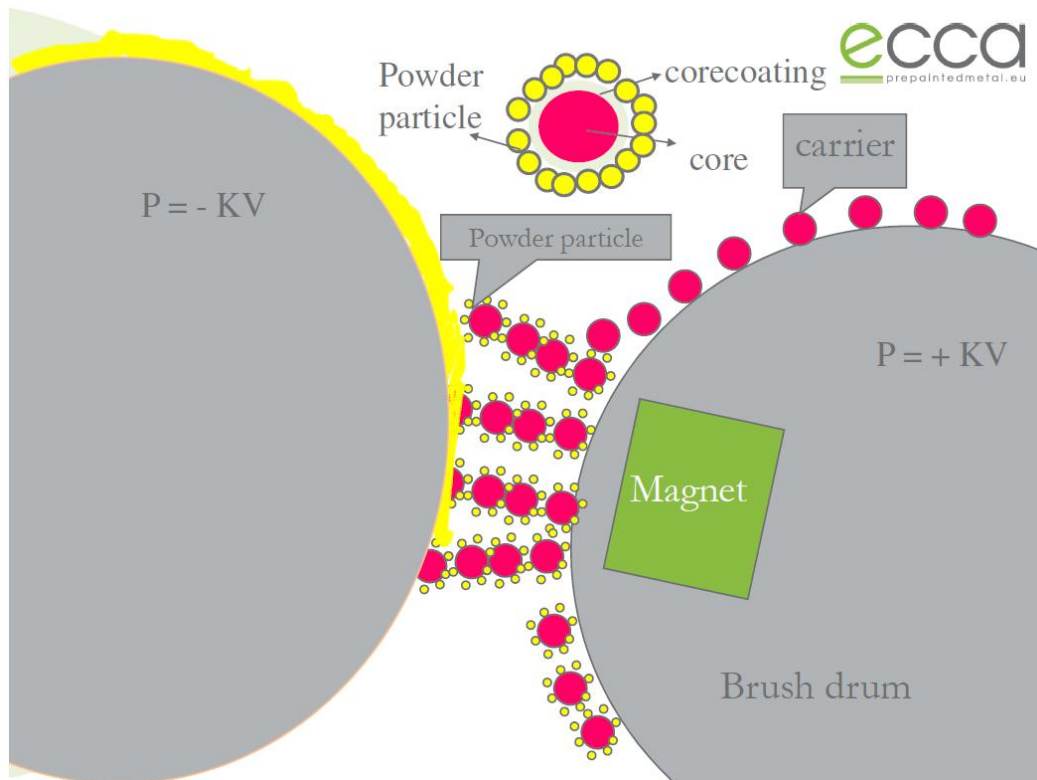


Figure 4.30 – Detail of EMB coating process (modified from [300])

Although this device is related to electrophotographic printing equipment, it is not capable of developing images (i.e. selective deposition) because it does not use a photoreceptor, nor any method for developing a latent image [301].

Deposition occurs as a single pass continuous operation across the entire width of the drum and can produce coatings as thick as $100\mu\text{m}$ [280, 300].

Standard EMB powder coating steps include the following [300, 302]:

1. A two-component developer with a bias voltage tribocharges the supplied powder and places it in proximity to the final transfer drum using a magnetic brush (Figure 4.30).
2. Once tribocharged, the powder is electrostatically attracted to the final transfer drum which is charged to attract the powder (Figure 4.30).
3. The powder is then deposited onto the substrate by means of electrostatic attraction or thermal transfer (a combination of heat and pressure).
4. Finally the powder is melted (generally using an infrared heater) and settles to create a uniform coating on the substrate.

A slightly modified EMB powder coating system was used to produce several sets of samples as shown in Figure 4.31. The feedstock powder was a high T_g thermosetting epoxy resin. Initial trials were undertaken without classifying the powder, however subsequent trials used feedstock powder classified with an average particle size distribution (PSD) centred at 47.7µm diameter and surface coated with FCA (ZEAC, Winterthur, Switzerland). Modifications to the equipment were required to allow multi-pass printing at different heights.

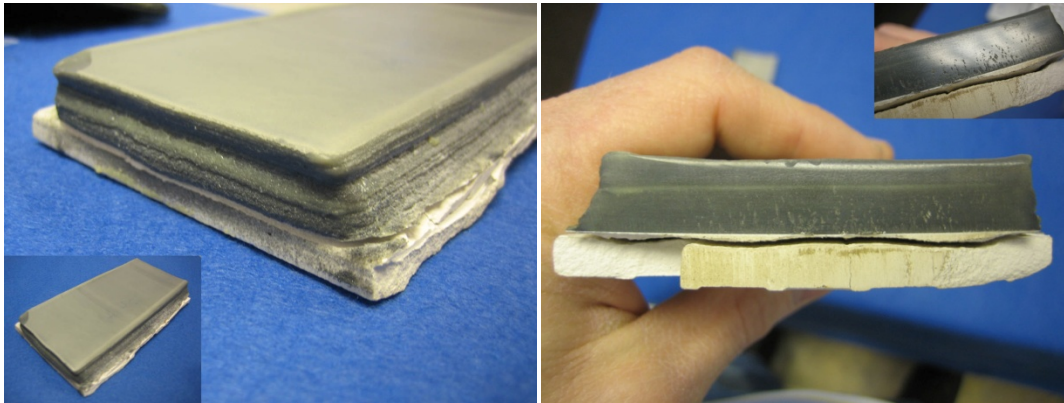


Figure 4.31 – Multilayer epoxy sample produced by EMB coating process

The samples were produced according to the following procedure [211, 244, 280, 303]:

1. A decorative ceramic tile was heated in an oven to $>150^{\circ}\text{C}$.
2. The tile was then mounted onto a platform and allowed to cool to "exactly" 150°C . It was then passed under the final transfer drum of the EMB powder coating machine which deposited material by means of thermal transfer (sometimes called "hot tack transfer" or "tackification") with substantially higher pressure than is used in conventional laser printing. Layer thickness was an estimated $100\mu\text{m}$. Electrostatic attraction was not used to transfer the powder onto the substrate and consolidated layers.
3. The entire tile with newly deposited epoxy powder layer was heated in an oven to $160\text{-}180^{\circ}\text{C}$.
4. The tile was then removed from the oven and mounted onto the platform, allowed to cool to 150°C and then a new layer was deposited on top of the last deposited layer. Approximately every five layers, the platform was mounted slightly lower to allow for height growth due to the newly deposited layers.

5. This process was repeated for each layer until a height in excess of 8mm was accumulated.
6. (Note: the time required to produce each layer was approx. 10-15 min)

It is worth noting that there was a substantial amount of manual manipulation of the sample during the build process. The layers had a tendency to curl up at the edges which were manually pushed back down before a new layer was deposited [303]. Despite the manual intervention required to continue the deposition process, the EMB samples are arguably the most significant exceptions to the 1-3mm theoretical height limit as described by Kumar and Dutta [261].

Having demonstrated image stack height growth in excess of the theoretical limit established by Kumar and Dutta [261] using the EMB coating technique, the next step was to demonstrate if the same achievement was possible using a fully-fledged laser printing system (which uses photoreceptors to develop images digitally).

Building on the success of the EMB produced sample, the same team multilayer (over 50 layers) laser printed the ziggurat shaped object shown in [Figure 4.32] which exceeded 5mm build height without significant layer defects [211]. To the author's knowledge this is the first sample in the public domain which exceeds the theoretical build stack height limit as calculated by Kumar and Dutta [261]. The sample was produced from the same developmental epoxy based-toner used for the EMB sample, which when paired with a suitable carrier had a charge distribution with a

mean q/d value of $-2.83 \text{ fC}/10 \text{ }\mu\text{m}$ and between 3.1 and 2.2 % of positively charged particles (measured using a q/d meter, EPPING GmbH, Germany). The sample was made by a semi-automated method where five layers were printed using a dual component non-conductive laser printer (CTG 900, CTG PrintTEC GmbH, Germany) and then fused offline for 5 minutes in an oven at 155-160°C; the sample (and ceramic tile substrate) was remounted on the printer to repeat the cycle for each subsequent set of five layers [211]. (© Society for Imaging Science and Technology [236], referencing style and punctuation updated).

The samples produced by CTG (by EMB and laser printing), provided evidence that multilayer laser printing could be achieved independent of transfer field strength, indeed even in the absence of a transfer field. These results instilled the confidence to build a new test rig for automating the process.

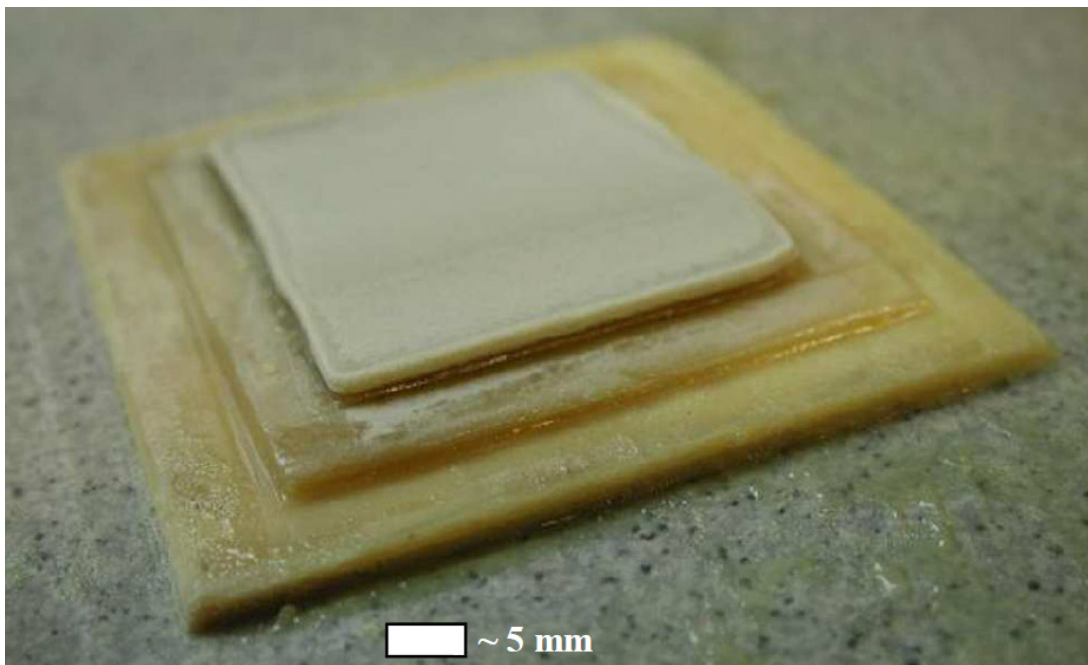


Figure 4.32 – Laser printed ziggurat shaped object exceeding the 3mm theoretical height limit for conventionally transferred laser printing (© Society for Imaging Science and Technology [236] also available without modification from [211])

4.4.5.3. *Selective Laser Printing (SLP) Development Rig*

The encouraging results paved the way for the production of a new development rig with support from the European Union Framework 6 Custom-fit project (No: 507437). The rig was the result of collaboration between De Montfort University (UK), CTG PrintTEC GmbH (Germany), Marcam Engineering GmbH (Germany, now owned by Materialize) and MCP (subsequently MTT Technologies Ltd, and now Renishaw PLC Additive Manufacturing Products Division, all in the UK). The process which the new rig automated was initially called Plastic Powder Printing (PPP) but has been known as Selective Laser Printing (SLP) since early 2009 [304]. The development SLP rig (without its covers on) is shown in Figure 4.33.



Figure 4.33 – *Selective Laser Printing (SLP) development rig being fabricated at MTT Technologies Ltd (now Renishaw PLC Additive Manufacturing Products Division)*

CTG PrintTEC GmbH miniaturized their CTG 900 industrial laser printer (which was based on a 900mm long photoreceptor) down to a 431.8mm (17") photoreceptor resulting in the CTG-1C17-600 (CTG PrintTEC, Germany). The first and third printer of this model made by CTG were installed on the SLP development rig. The same two-component development and non-electrostatic transfer systems were used in order to ensure comparable performance to the CTG 900. The printers featured 600 dpi LED print heads (no lasers were used in these printers) using discharge area development (DAD) enabling high resolution printing of a wide range of non-conductive toners/powders.

Marcam Engineering GmbH developed an interface for slicing models and sending uncompressed single bit bitmaps at 600 dpi resolution to the CTG printers.

With input from De Montfort University (including contribution from the author who had a research appointment at the university at that time), MTT Technologies Ltd (now Renishaw PLC Additive Manufacturing Products Division) was responsible for fabricating the motion system and integrating the CTG printers. The machine was designed with an 0.5m³ build volume which was transported on a platform, along a ball screw-driven X-axis which had a stroke of 6m, thus accommodating a plethora of printer and heater configurations.

The scale of the investment and effort directed to the SLP development rig made it one of the primary focal points of and outputs from the Custom-fit project.

The toner material development was the primary responsibility of De Montfort University and was steered by the demonstrator parts selected by the Custom-fit project. The remit of the project was to print customized rider-specific motorcycle seats and helmet inserts. The former for improving the comfort on long rides, the latter for improving how closely the helmet liner conformed to the head of a specific motorcycle rider in the interest of safety. In both cases a “rubber-like” material was specified.

The successful printing of multilayer objects up to 3mm was achieved using an adapted laser sintering material called Somos 201 (3D Systems, CA, USA). Somos 201 has a proprietary formulation, but analysis revealed that its chemical composition may be primarily polybutylene terephthalate (PBT) or similar [61].

This material was not a proper toner material and was well outside the regime of conventional toner formulation (which is normally acrylic or polyester based and somewhat spherically shaped with an average particle diameter of 5-15 μ m as discussed in §3.2) [61]. The Somos material was a significant departure from conventional toner in chemistry, size distribution, and shape which attracted scepticism that it could be printed. One possible reason why the Somos particles were able

to be printed may be that the sharp points on toner particles allowed the concentration of the surface charge which resulted in high proximity charge as explained by Schein, et al. [155].

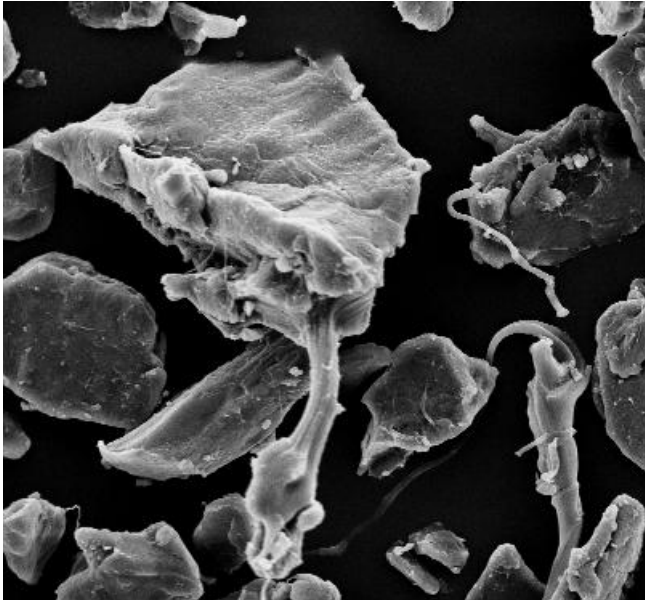


Figure 4.34 – SEM image of Somos 201 [61]

The use of Somos 201 with its irregular shape (See Figure 4.34) and chemistry was enabled by first a) classifying it with a d_{50} 32 μm diameter average particle size (measured by laser diffraction) and then b) surface coating it with 0.5 wt.% of fumed silica FCA using high shear mixing as per the Banerjee and Wimpenny method [58]. The surface coating also improved the negative charging tendency of the powder, when paired with a suitable carrier, from a mean charge to particle diameter ratio q/d of -1.3 fC/10 μm to -2.6 fC/10 μm with less than 1% of positively charged particles (measured using a q -test charge spectrometer, Epping GmbH, Germany) as shown in the charge distribution (Figure 4.35).

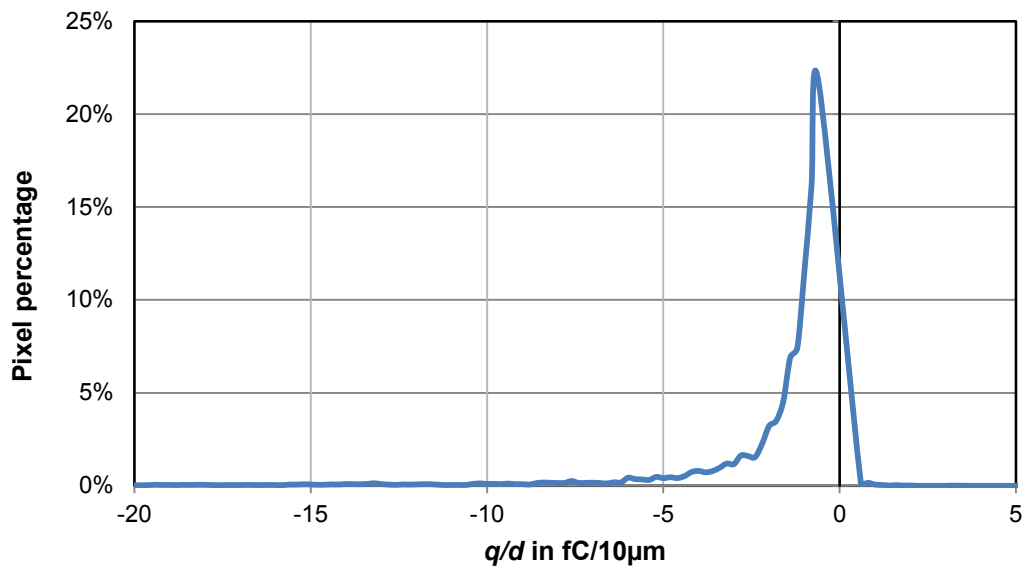


Figure 4.35 – Charge distribution of classified Somos 201 powder with 0.5 wt.% of FCA

SLP samples were produced according to the following general procedure:

1. A glass substrate on the build platform was pre-heated using the medium wave infra-red heater in excess of 150°C. Once the temperature achieved steady-state on the glass platform, the printing cycle was commenced.
2. The glass substrate passed under the infrared heater. It was then allowed to cool to between 115-130°C when operated manually and more precisely (115-120°C) once automated.
3. It was then advanced at a constant speed, which was synchronized to the surface speed of the final transfer roller of the printer.
4. The glass substrate then received a developed image, estimated to be ~15µm thick, from the final transfer roller using heat and pressure.

5. The platform was lowered a few millimetres in Z and returned to its cycle start position in X.
6. Once at the cycle start position the Z-axis was driven back up to its previous height minus a specified height to allow for the thickness of the deposited layer (generally between 10-20 μ m).
7. A new image was then loaded into the printer memory, which initiated a new print cycle beginning with driving the platform under the infrared heater.
8. This process was repeated for each additional layer.
9. (Note: the time required to produce each layer was approx. 1 to 1.5min)

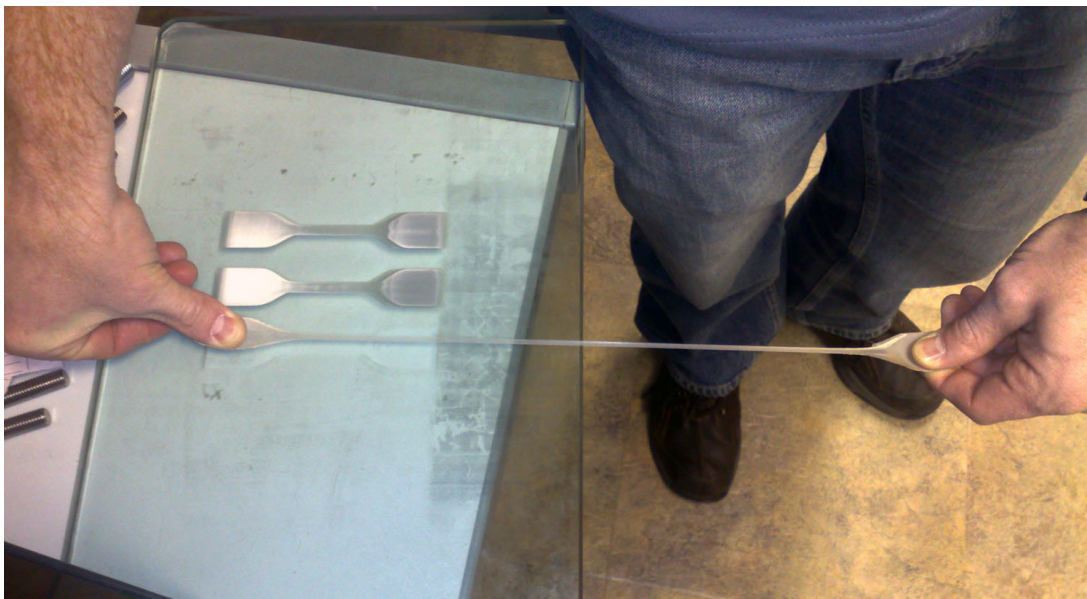


Figure 4.36 – Removal from platform and stretching of a Somos 201 tensile specimen

This process successfully produced tensile test specimens (Figure 4.36), but despite repeated attempts, it was not possible to build parts in excess of 3mm high due to a spectrum of height limiting defects, similar

to those experienced by other researchers [236, 244]. Additionally, the material proved prone to hot offset causing premature failure of the OPC [235].

Due to the improvements made to the SLP process over time, including the automating of temperature sensing, the manufacturing details for individual samples produced can be found in §6.1.1. Also more details about the SLP rig, its components, features, and cycle timings can be found in §5.3 and §5.4.

Therefore, although bespoke helmet inserts were designed and their fabrication attempted, they were never used for their intended purpose because the designed build height could not be achieved.

Additionally, due to the fact that many of the samples were produced in the last weeks of the Custom-fit project, most of them were not fully analysed, except as part of this PhD research in §6.1.2.

Despite the encouraging mechanical properties demonstrated by the SLP process [235, 260], the height limitation and defects experienced were unsatisfactory. Above all, the question of why tall samples were produced successfully by CTG PrintTEC GmbH (§4.4.5.2) in a semi-automated manner, but had not been duplicated by the SLP rig, remained (which is explored further in §6.1). Suspected causes for defects included non-uniform heating and/or non-uniform application of pressure. However,

the lack of a substantive explanation for the underperformance of the SLP development rig *provided the impetus for the current PhD research.*

4.4.5.4. *Laser Printed Electronics*

The SLP development rig was used for digital printing of electronics materials in a two-year feasibility study, “Laser Printed Electronics” project: TP11/HVM/6/I/AB280K supported in part by the UK Technology Strategy Board.

The remit of the project supported further characterization and development of novel toner materials; however it did not embrace further work to overcome the height limitations. Of particular interest was the understanding of materials gained through the use of a two-stage curing epoxy which was sintered using infrared radiation in-process (on the SLP development rig) and then cross-linked by exposure to ultraviolet radiation off-line in order to form protective resists, legend materials, etc. The understanding derived from this project has been summarized in publications elsewhere and is noted here primarily for completeness [18, 95].

4.4.6. *Stratasys*

Six US patent applications were filed, two of them granted [305, 306] at the time of this writing, to Stratasys Inc. which marks their formal interest in the potential of EP for AM.

Each patent employs an adaptation of the tackification method in order to transfer/transfix and consolidate laser printed powder layers. One embodiment illustrates a two-step heating and consolidating pattern where it appears that the layer is partially melted on the surface of a transfer roller and then heated again using a flat platen or transfusion plate when it is added to the consolidated layers [305]. Additional embodiments add a cooling step intended to keep the polymer from deforming once transferred/transfixed.

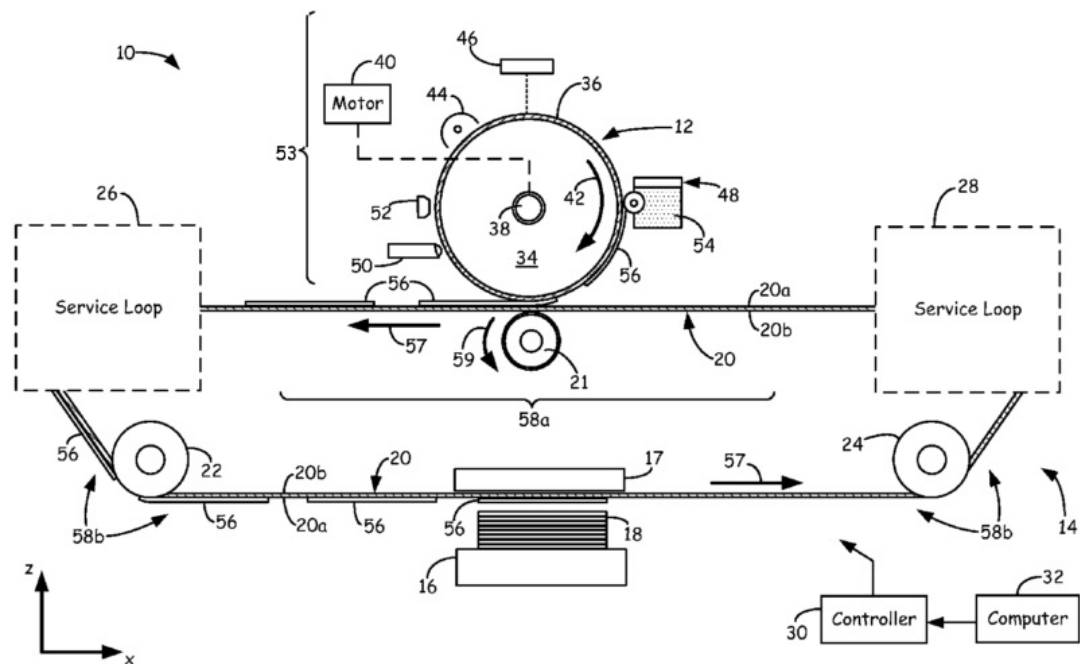


Figure 4.37 – Drawing of an EP based 3D printer utilizing service loops for a transfer belt [306]

The patented features are not explicit modifications to EP process fundamentals, but claim protection for engineered features: specifically an embodiment for bidirectional rotation of a photoreceptor [305], presumably to reduce the size of the equipment; and also for service

loops to manage the speed of a transfer belt as shown in Figure 4.37. There is no public information currently available about the intentions of Stratasys, although it is clear from the inventors listed that consultants with a high level of 2D printing expertise have been involved in the patent process.

Incidentally, the author had contact with and extensive technical disclosure in March 2010 (under the protection of a mutually signed 4-year non-disclosure agreement) with the organization behind the new patents assigned to and filed by Stratasys in September of 2012. The U.S. Provisional Application No. 61/538,491 entitled "Layer Transfusion for Electrophotography-based Additive Manufacturing" from which the 6 filed applications draw priority was filed on Sep. 23, 2011, but no further details have been published. It is strongly suspected that the timing and content of the author's confidential disclosure was a significant catalyst contributing to the recent IP activity by Stratasys.

4.4.7. Critical Review of Non- electrostatic Transfer Approaches

The plethora and relative success of research based on non-electrostatic transfer approaches provides an indicator that a general awareness of the field strength limitations of conventional transfer has been established in the research community. The lack of genuine evidence of reliable and repeatable stacking of toner layers suggests that the height limiting factors are still not understood or overcome.

Bynum – Without evidence of experimental work, it is difficult to comment on Bynum’s activities, apart from the comprehensive and logical approach he details in his patents.

Grenda – Grenda’s known publication [291] does not share specifics about any technical challenges he encountered while producing the first 3D parts made directly from EP. Owing to the small size of the sample parts made, it is unclear if Grenda ever encountered defects similar to those who used electrostatic transfer means, or whether they were not publicized. At any rate, challenges experienced by subsequent researchers tacitly imply that his transfer approach was not fundamentally devoid of similar limitations.

Cormier – Cormier’s research was pioneering in the field of colour science applied by EP in three-dimensional space, however the height of his samples did not reveal additional insights in order to overcome the height limitation and defects experienced by other researchers.

Metal Printing Process – MPP as developed by Sintef demonstrates that at least 25mm high and defect free parts can be produced using ionography and metal powders. It is noteworthy to acknowledge that this was achieved using considerably higher in-process pressures (at high temperature) than has ever been attempted before or since as far as the author is aware. Sintef’s attempts to use EP to build up layers of ceramic powder demonstrates a) the versatility of EP in being able to deposit a

wide range of materials; and b) evidence of similar height limitations experienced by other researchers.

Wimpenny and Banerjee (scoping) – The early scoping trials undertaken by Wimpenny and Banerjee show understanding of the technical barriers to toner material development and also creativity in devising the repulsive transfer and demonstrating it in addition to tackification transfer approaches. The lack of samples exceeding 1-2mm in height make it uncertain whether or not they had overcome factors limiting sample height, or not.

CTG PrintTec GmbH – The samples produced by CTG using a tackification approach are the tallest samples known in the public domain produced by EP and related techniques. They provide assurance that with the correct combination of heat and pressure, toner layers can indeed be stacked to heights well in excess of the theoretical 2-3mm limit. The amount of pressure exerted on these samples exceeded that of conventional office-based laser printing (and also the amount of pressure intended to be exerted by the SLP development rig).

Selective Laser Printing – It has been said of the SLP rig that as far as 3D printing development goes, “never has such a large test rig produced so little.” The lack of tall and large samples produced by the SLP development rig attests to the fact that the critical factors enabling success for the CTG produced samples were either incorrectly translated

across, or that there were unidentified enabling factors inherent in the CTG process, but absent from SLP.

Among the suspected causes for defects was non-uniform heating and or non-uniform application of pressure. Additionally, the scaling down of the CTG printers, and the resources consumed by teething problems, may have contributed to the difficulties in realizing expected outputs.

There was no reconciliation between the “tall” samples produced by CTG and the lack thereof using what was apparently the same printing and fusing techniques, albeit in an automated fashion, on the SLP rig. (This issue is explored specifically in §6.1). *The lack of reconciliation was the specific driver which ultimately led to the current research.*

Perhaps better listed as a criticism of the other techniques, the non-contact heating method employed on the SLP rig may have contributed to early recognition of defects arising later on in other approaches (such as those explained in §4.3.2.1). It is surmised that the early stages of defect formation may have been masked by contact heating sources, and only became evident later when the cumulative effect was larger.

Laser Printed Electronics – Although the height of samples in this research does not directly inform the current research, it does inform the likely outcome of a proposed solution to the defect problem. The two stage (IR + UV) cured epoxy samples provide evidence contrary to the claim by Güttler et. al. (§4.3.1.2) that chemically bonding layers together

could successfully overcome surface defects arising from repeated thermal fusing [262].

Stratasys – Judging only from the patents, it is difficult to assess the viability of what Stratasys proposes and whether or not an appropriate strategy is in place to break through the defects arising in multilayer printing by EP.

4.5. Others Who Have Considered EP and Related Techniques for AM

In addition to those already mentioned in this chapter, several other researchers have considered or announced their intention to use EP in the context of AM; however, insufficient information is available to categorize their endeavours by transfer means. They will be presented here chronologically for completeness.

Johnson described several digital printing processes relevant to 3D fabrication and in particular “Particle Deposition Fabrication” which is similar to Bynum’s proposition [307]. Cormier reviewed this technique summarizing an essential difference from Bynum’s approach in that particle transfer, or deposition, is achieved electromagnetically (rather than electrostatically), by activating electrodes in a matrix which induce the toner to jump off of the drum [293]. Furthermore, the need for magnetic toners precludes its relevance to this work, since the magnetic

content would contravene the objective for a “pure” thermoplastic AM process. No evidence of its implementation has been found.

Williams et al. [16] considered the capabilities of electrostatic printing using a morphology matrix acknowledging the potential benefits of direct material deposition and the potential for “patterning” (multi-material grading of) 2D layers. In the end they did not pursue EP enumerating concerns including potential, “...porosity of printed part, the quality of adherence of the support powder to the build powder, and issues dealing with non-conduction powders (such as ceramics)” [16].

As mentioned by Güttler et al. a patent claiming that chemically binding layers together could overcome the “corrugating” effects of repeated thermal fusing [262]. No empirical evidence that the originators of this concept ever implemented this approach has been found. However, the use of thermally curing epoxy in the Laser Printed Electronics project did overlap the claimed territory (albeit for electronics applications), but did not yield satisfactory evidence to support their claim (§4.4.5.4).

Matthew Benning undertook a PhD project (University of Newcastle upon Tyne, UK) implementing EP for AM, however there is not enough detail in the public domain to confirm the final machine architecture or transfer step employed [308].

4.6. Summary and Analysis of Prior Art

In order to facilitate comparison, the foregoing AM research initiatives which utilized direct deposition by EP (§4.3-4.4) are summarized by approach and then by difficulties encountered. The summaries are presented in tabular format and then followed by a brief discussion. In the tables, approaches have been listed in the same sequence as earlier set out in this chapter. Where information was not available (or easily deducible) the table has been left blank.

Table 4.1 – Summary of AM Approaches Utilizing EP for Direct Deposition

Who	Toner type; and material	Nominal toner diam.; layer thickness (μm)	Develop- ment	Transfer method	Substrate material	Fusing – when?	Fusing method:	Cycle time (seconds)
Güttler 2010 [262]	Non-conductive; polymer		Single- component	Conventional electrostatic transfer	Glass	Each layer	Heated roller	
Kumar 1999 [273]	Non-conductive; polymer		Single- component	Top surface charging		Each layer	Heated roller	
Kumar 2003 [261]	Non-conductive magnetic; Polymer matrix (styrene/2- ethylhexylacrylate/butyl methacrylate/methyl methacrylate based polymer) with an iron oxide core	5; 20	Single- component (Canon)	Top surface charging	Aluminium plate	Each layer	Radiant heater abandoned and replaced with Mica strip heater held at 180°C.	20
Kumar 2004 [272]	Non-conductive magnetic; "Polymer powder consisting of styrene with various additives, including ferrous oxide"	5; 5 (after first few layers which are thicker)	Single- component (Canon)	Top surface charging (1K VDC), Transfer roller required to minimize back transfer.	"Thin layer of polymer sheet covering the aluminium platform"	Each layer	strip heater	
Wimpenny and Banerjee [211]	Non-conductive non- magnetic; "standard toner of Lexmark C510"		Single- component (Lexmark)	Repulsion	Paper	Each layer	IR radiant heater	
Grenda [291]	Non-conductive; polymer			Tackification	Non-conductive	Each layer	Flat heater	
Cormier [60, 293]	Non-conductive magnetic and non-magnetic polymer; standard toner + other polymer powders	10-15;	Single- component (HP)	Tackification	PVOH and paper	Each layer	Heated roller	<5
Sintef - MPP [62, 63, 229]	Non-conductive non- magnetic; Ceramic powder (as a support material)		Two- component	Tackification (extreme heat and pressure)	Conductive die	Each layer	Furnace	
CTG PrintTec [211, 236, 244]	Non-conductive non- magnetic; Epoxy powder	35;	Two- component	Tackification	Ceramic tile	Every 5 layers	Oven	~10min
Wimpenny - SLP [235, 260]	Non-magnetic; Classified and coated Somos 201	32 μm ; estimated at 15 μm	Two- component	Tackification	Glass plate	Each layer	IR radiant heater	30-70

Table 4.2 – Summary of Challenges Encountered

Who	Max Z height achieved	Change in deposition thickness	Thicker edges	Heat discharges the powder	Back transfer	Sparking during transfer	Surface quality deterioration	Support powder tested	Difficulty with co-deposition
Güttler 2010 [262]	<1mm						Yes		
Kumar [181, 261, 272]	1-2mm (no defects) ~5mm	Yes	Yes	Yes	Yes	Yes	Yes	Yes	Yes
Wimpenny and Banerjee [211]	<2mm						Yes	Yes	
Sintef - MPP [62, 63, 229, 309]	~2-3mm		Yes					Yes	Yes
CTG PrintTec [211, 236, 244]	~10mm				Yes	No		Yes	
Wimpenny - SLP [235, 260]	~3mm	Suspected	Yes		Yes (on finer particles)	No	Yes	Yes	

4.6.1. AM Endeavours Using Direct Deposition by EP

This section discusses observations from Table 4.1.

Toner (type and material) – The prior art has been dominated by the use of “standard” non-conductive magnetic toners. This was likely driven by the availability and simplicity of using single component development stations. By virtue of using “standard” toners, a logical choice for ensuring consistent and reliable printing, the materials tested have been largely styrene or polyester-based polymer matrices, including iron oxide/magnetite (where magnetic toner is required). Of particular note is the pure ceramic toner which was deposited by Sintef in the MPP process. This is the only example known to the author where pure ceramics have been deposited. *Interestingly, the use of conventional toners in two-component development stations has not featured significantly in research to date.*

Toner (diameter and deposited thickness) – The size range of the toners had an average diameter of 5-15 μm which often correlates to the age of the printers used (newer high-resolution printers tend to use finer toners – See §3.2.4) [95]. Generally the deposited layer thickness of toners correlates to between half and two thirds of the average toner diameter (when assuming development of a mono layer of toner) [18]. In particular Kumar et al. note a substantially thicker deposition for initial layers. The possibility that layers diminish in thickness with increasing height (as correlated to a reduction in transfer field strength) has been hypothesized, *but empirical evidence is not conclusive.*

Development – As mentioned in connection with the toner type, single component development has been the mainstay of research to date, with only recent emergence of two-component development in order to facilitate the printing of less conventional toner materials.

Transfer method – As discussed extensively in this chapter, there has been a clear trend away from electrostatic transfer methods (due to the inherent self-insulating tendency) *toward the use of heat and pressure* (aka tackification) because by that method there is no theoretical limitation to the number of layers that can be stacked.

Substrate material – a wide variety of conductive and non-conductive substrates have been used. Obviously, after the first deposited layer the build surface is made from toner, thereby limiting the influence of the initial substrate to non-contact effects.

Fusing frequency – Except in the case of the samples produced by CTG, each layer is fused immediately after deposition. Since the height of the samples produced by CTG is anomalous, therefore *the influence of the timing of fusing on its height deserves investigation*.

Fusing method – With the exception of the trials undertaken under the direction of Wimpenny, all in-process heating was performed when the substrate was held under pressure. Since the CTG samples were fused offline, *the influence of non-contact heating (i.e. when sample is not held*

under pressure) also deserves investigation. Additionally, the possibility exists that samples produced using contact heating methods may actually mask defects which can be elucidated more easily using non-contact heating, but this needs further substantiation.

Cycle time – The speed at which these processes work on a layer by layer basis determines their productivity. Although most of these processes have not been optimized for speed, it is clear that the research trend over time has been *less focused on the layer cycle time and more focused on understanding the process.*

4.6.2. AM by EP Challenges

This section discusses observations from Table 4.2.

Maximum Z height achieved – The most obvious shortcoming of prior endeavours is the lack of samples with unlimited Z height growth. With the exception of the samples produced by CTG, no other initiative (in the public domain) has been able to produce defect free samples in excess of 2-3mm high. ***This is the critical challenge which must be overcome in order to unlock the potential of EP in AM.*** Although unlimited height deposition is the objective, in practice achieving 10-100mm height drastically increases the practical use of this process across a variety of classical AM applications.

Change in deposition thickness – Only categorically observed by Kumar et al., inconsistent layer thickness may indicate an inability to

consistently contribute to the height of a part. For processes with transfer steps based on electrostatics, diminishing layer thickness correlates with and seems to be caused by reduced transfer field strength. However, this phenomenon was also suspected on the SLP process, which is based on tackification. If this were the case, it would be difficult to explain in the same way because no transfer field is applied at the transfer step. *This issue deserves further investigation.*

Thicker edges – As explained in §3.4.3.1, the fringe field effects (non-electroded development and insulating magnetic brush development) on a photoreceptor results in more efficient development at the edges of an image than in the centre. This is a known issue in EP as described and evaluated by ASTM standard F2036 – 05^{e1} [201]. Although modern printer systems have “solved” this issue for conventional printing of text and images, it is a phenomenon which needs revisiting in order to ensure precision layers for 3D printing. Three different research groups observed this phenomenon and while it is an important challenge to overcome, it will not receive extensive attention in this work because strategies for overcoming this problem have already been explored elsewhere (§3.4.3.1) [212, 213]. Furthermore, *this issue is overshadowed by the prerequisite need to enable unlimited height deposition.* Where this was not observed, it may have been masked by the use of substantial heat and processing pressure.

Heat discharges the powder – Only Kumar et al. note that the heat from the fusing process aided “discharging” the deposited layers of toner.

There is no published evidence of any empirical work on the electrostatics downstream of the transfer process and scant mention of theoretical or empirical work about what effect toner charge has after transfer. *This needs characterizing.*

Back transfer – The presence of any toner remaining on the printer rollers after the transfer step is undesirable. Furthermore, multilayer deposition increases the opportunity for back transfer (§3.4.5), where deposited toner can be picked up again by the printer rollers which causes excessive wear and or damage to the printer components. Several researchers experienced undesirable adhesion of toner materials to the photoreceptor which in one case was solved (or at least managed) by the installation and use of a final transfer roller [181]. Even with a final transfer roller, there is still a substantial *risk of back transfer which should be monitored in-process.*

Electrostatic breakdown during transfer – Kumar et al. note the propensity of electrostatic breakdown (sparking) when the transfer field strength in the nip (or pinch point between two rollers, often where toner is transferred) is too high (§3.4.4.1). Using a non-conductive substrate and a transfer method not reliant on electrostatics circumvents this issue.

Surface quality deterioration – In several cases the surface quality of the layers deteriorated over time. It is not entirely clear if this issue occurred in a single layer and then was exaggerated or exacerbated by subsequent layer deposition because the process is not “self-healing.”

On the other hand, surface defects may grow in severity as a symptom of another issue which grows in magnitude with the accumulation of layers.

Either way this issue needs further investigation.

Support powder tested –Virtually all research intending to use EP as a deposition means in AM proposes the use of an alternative support material. The results from several researchers who undertook trials on support materials have been published. The exploration of support materials is a good indicator of the progress made on the fundamentals of the process development. This issue needs attention, but only after unlocking unlimited Z-height growth of parts.

Difficulty with co-deposition – There are only two cases which published results concerning the co-deposition of build and support materials using EP. In each case there was a degree of challenge associated with simultaneously managing the behaviour of different materials in close proximity. This issue is also critical to the successful implementation of EP in AM, but again *yields to the priority of achieving unlimited height deposition.*

4.7. Conclusions

This chapter has highlighted unknown foundational knowledge which is required in order to effectively use EP for AM. Despite the lack of

definitive success for many researchers, most maintain a lingering optimism that one day someone will achieve success.

For convenience, the areas for further investigation as highlighted in this chapter are listed below (along with sections where corresponding work has been undertaken):

- ***Understanding required to enable unlimited height deposition (overarching theme)***
 - *See §6.1*
- *Understand limitations on electrostatic and non-electrostatic transfer (including use of heat and pressure-based transfer steps)*
 - *See §7.1-7.2*
- *Empirical evidence that the layer thickness is reduced as the height of stacked layers increases*
 - *See §6.1.4*
- *The cause of surface quality degradation*
 - *Largely due to residual toner charge, depleted field strength and non-uniform pressure in the transfer nip, See Table 7.34, Table 8.18, Table 8.16, Figure 9.6*
- *Influence of fusing frequency (if any) on defect generation*
 - *None observed in this work*
- *Influence of non-contact heating and whether contact heating methods mask defects in their early development stages*
 - *§7.1.3*
- *Characterizing the effect of heat on toner charge*

- *Not fully undertaken in this work, however evidence indicates that fusing does not fully neutralize toner §7*
- *The use of two-component development for AM*
 - *See §5.2, §7-9*
- *Monitoring and minimizing back transfer*
 - *Table 8.18*

Experimental Work

5. Toners and Printing Apparatuses

This chapter marks the end of the literature review and a change of focus toward experimental work.

The most significant contribution to this research by Renishaw PLC, as the industrial sponsor, was providing unlimited access and substantial modification to the Selective Laser Printing (SLP) rig (which was constructed approximately one year before the commencement of this PhD, at the end of the European Union Framework 6 Custom-fit Project No: 507437, as explained in §4.4.5). Additionally, the sponsor was already actively developing AM systems for metal powders and desired to offer a complementary product to its customer base for high integrity AM of engineering polymers (with multiple colours and graded material potential as a bonus).

Basing a PhD on the SLP rig was advantageous in some ways and problematic in others. On the one hand, it was a singular opportunity to work on such a unique piece of equipment. On the other hand, what one gains in terms of time, cost savings and preliminary understanding by adopting an existing test rig, one gives up in flexibility (and suffers headaches associated with the teething issues of new developments). By

using the SLP rig, the author inherited a chain of decisions related to the machine architecture and process without the full understanding of their implications, *which only came with hindsight*.

This chapter explains what the author accepted, modified and rejected from the SLP rig and associated materials throughout the research and why. Now writing with the benefit of hindsight, the SLP rig provided a means to develop crucial understanding in toner printing to advance this area irrespective of its shortcomings.

5.1. Toner Materials

The commercial drivers set an expectation for new toners based on engineering thermoplastics (See objectives in §1.2). This created a tension between the commercial priorities (to use new developmental toners made in lab scale batches) and the rigour required by the academic priority to maximise confidence in experimental outcomes (by reducing potential sources of variation by using fully characterized standard toners, produced at production scale). Additionally, the iron oxide, magnetite and related content in magnetic or conductive toners was regarded by the industrial sponsor as an undesirable contaminant for polymer parts (See objectives in §1.2), and has been known to increase brittleness [211], thereby encouraging use of non-conductive non-magnetic toners.

Investigation of non-conductive non-magnetic toners for AM has been predominantly undertaken by Wimpenny and Banerjee [58, 59, 211, 297, 299]. Although Wimpenny and Banerjee demonstrated that a wide variety of materials were amenable to printing by EP, only two non-standard toner-like materials were developed sufficiently to produce parts above 1mm in height: a proprietary thermosetting epoxy resin and a proprietary thermoplastic elastomer toner made from Somos 201 (a commercially available Selective Laser Sintering powder). Owing to the Somos 201-based powder causing damage to the printer components (§4.4.5.3), its use was discontinued at the end of the Custom-fit project [235], leaving only the epoxy toner as a candidate for this work.

Using the epoxy toner was desirable because a) it had been used by CTG to produce the only defect-free samples in excess of 3mm and b) its larger average particle size (35 μ m) enabled better volume deposition efficiency than conventional toners which are typically 6-12 μ m in diameter (in spite of the fact that it did not result in thermoplastic parts). When paired with an appropriate 80 μ m diameter carrier it had a mean charge to particle diameter ratio q/d of -2.83 fC/10 μ m with between 2.2% and 3.1% of positively charged particles (measured using a q/d meter, EPPING GmbH, Germany) and a charge distribution as shown in Figure 5.1.

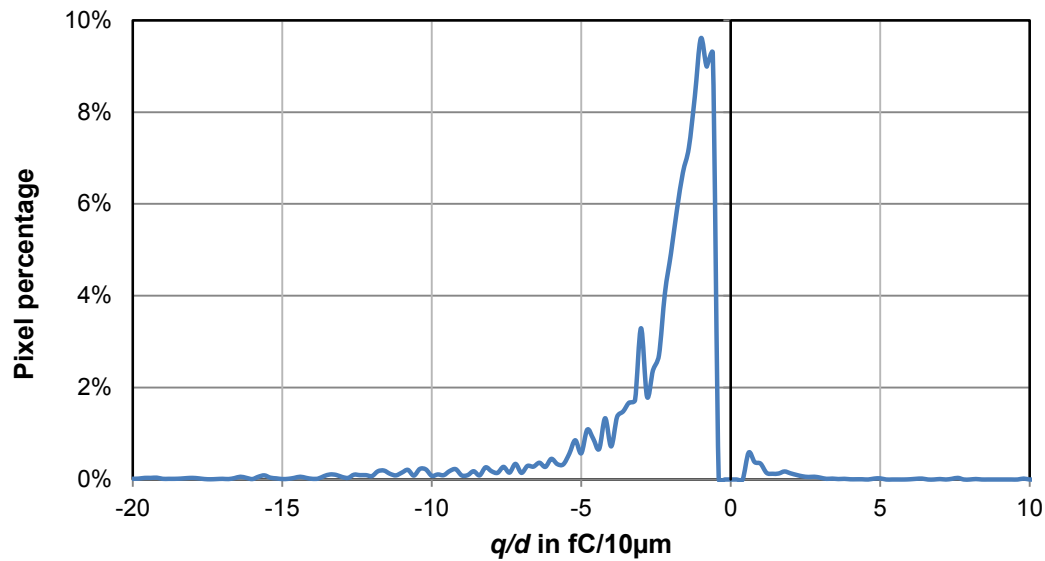


Figure 5.1 – Charge distribution of thermosetting epoxy toner

Owing to a critical need to overcome the part defects historically arising in the SLP process (which was the highest commercial and research priority), it was determined that this investigation would exclude new engineering thermoplastic toner development (which is reported separately by Rupesh Chudasama of De Montfort University). Furthermore, in order to eliminate the possibility that defects were induced by the developmental nature of the epoxy toner, a conventional polyester toner (PolyJZ, Samsung, Japan) was used in tandem with it to provide a consistent benchmark for comparison. The polyester toner had an average particle size diameter of $9\mu\text{m}$ and when paired with an appropriate carrier, the toner had a mean charge to particle diameter ratio q/d of $-5.21\text{ fC}/10\mu\text{m}$ with between 1.6% and 1.8% of positively charged particles (measured using a q/d meter, EPPING GmbH, Germany) and a charge distribution as shown in Figure 5.2.

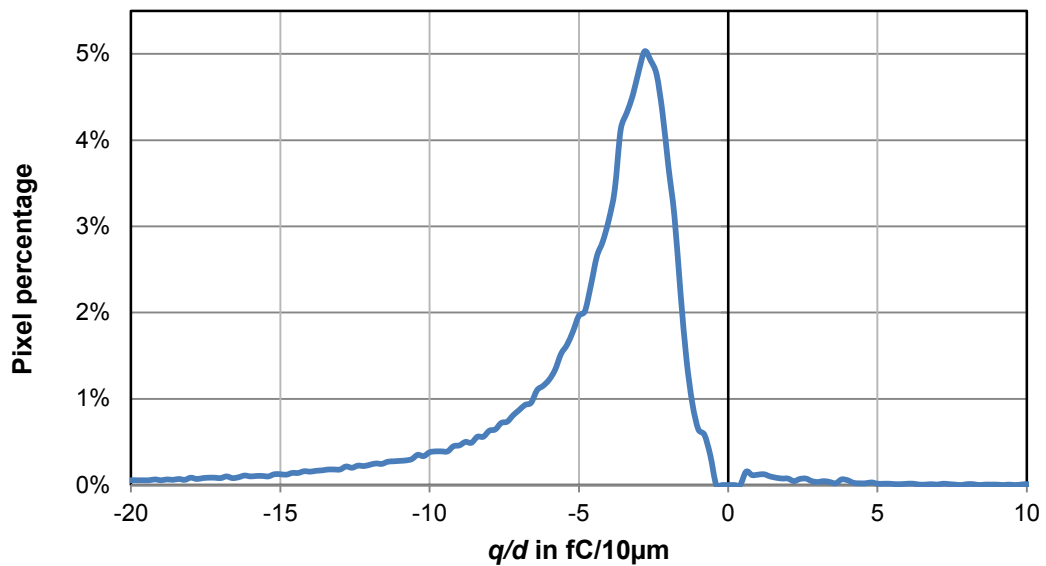


Figure 5.2 – Charge distribution of Samsung PolyJZ polyester toner

The use of a) the standard polyester toner and b) the epoxy based toner satisfied both the academic and the highest commercial priorities.

5.2. Development

The desire of the sponsor to ultimately print a range of pure thermoplastics reinforced the inherited decision to use a two-component printer with non-conductive non-magnetic toner. The historic determination to investigate two-component development for the foundational SLP work (§4.4.5) was summarized as follows:

It was decided to undertake all further laser printing trials using a commercial dual component printer as this provides increased flexibility in terms of toner type and moreover the thickness of the deposited layer is much greater... [211].

The author concurs with the ethos behind selecting two-component development which was the prime development method used for the trials of this work. In addition to supporting the work for this PhD, the use of two-component development paved the way for follow-on work by enabling wide flexibility for non-conductive toner formulation. Two-component printing enables more efficient charging which is required for high speed printing (hundreds of pages min^{-1}) [310], which aligns to a second objective of this work (§1.2).

The use of two-component development rendered the prior work on magnetic toners by Cormier and Kumar (as reviewed in §4.6) as only marginally relevant, and therefore their work could not be used as a sound benchmark for experimental work based on non-conductive toners.

The carrier beads for two-component development of the toners/toner-like materials used in the SLP process were initially selected, tested, and supplied by CTG PrintTEC GmbH in collaboration with ZEAC and Powdertech International.

5.3. Printer Selection

Using EP in the context of AM implicitly requires the stacking of flat layers. Furthermore, the desire to use heat for fusing them required a rigid build substrate. Therefore a printer was required that could print onto flat rigid substrates (to avoid heat induced distortion). In prior

research which used single component development, the printer architecture allowed the adaptation of existing print engines/printers to print onto flat substrates; however since the architecture of two-component development-based printers is more complicated, this was determined not to be a practical work around.

Due to these constraints, some preliminary work was undertaken on a variety of commercial single and two-component printers using flexible substrates (§6.3).

The decision to use non-conductive toner charged by a magnetic carrier (§5.1) made the use of a two-component printer (§5.2) capable of printing onto a rigid substrate mandatory. After extensive searching, only the CTG900 (CTG PrintTEC, Germany) was found to fit that description, which led to the development of a smaller CTG-1C17-600 printer (based on a 17" developer) as part of the Custom-fit project (§4.4.5.3). To date this is still *the only laser printer* (of any development system) known to the author that prints onto rigid substrates. Further details about this printer are included in the next section. For completeness, Delphax Systems produces a printing system which is capable of printing onto flat rigid substrates, but it uses ionography rather than EP.

5.4. Sample Shape and Size

The focus of sample production in previous work (§4.4.5) was dominated by the printing of tensile and related specimens for establishing the

mechanical properties of the printed materials, however little attention was given to standard evaluation methods for laser printing.

All of the current standards for evaluation of EP printers and copiers as maintained by ASTM Committee F05 on Business Imaging Products (and especially Subcommittee F05.04 on Electrostatic Imaging Products) were reviewed early in this work. The standards with some relevance to the needs of this research included:

- ASTM F360 Standard Practice for Image Evaluation of Electrostatic Business Copies
 - The standard sets forth principles which help maintain repeatability in the following standards. It does not propose specific sample sizes or shapes.
- ASTM F875 Standard Test Method for Evaluation of Large Area Density and Background on Office Copiers
 - F2036 is equivalent to this standard as applied specifically to printers, therefore this standard was not used.
- ASTM F2036 Standard Test Method for Evaluation of Larger Area Density and Background on Electrophotographic Printers
 - This standard was used for reasons explained below.
 - The most current version at the commencement of this PhD was used: ASTM F2036-05^{e1} (Note: the "-05^{e1}" indicates that 2005 was the last official balloted version and since then there has been one editorial change).
- ASTM F807 Standard Practice for Determining Resolution Capability of Office Copiers

- There was no equivalent standard specific to printers, so this standard was relevant. The approach proposed was used during scoping trials (only with higher optical resolution evaluation), but studying resolution was not core to the needs of this research, therefore it was not used extensively.

Owing to the problematic non-uniformity of print density and surface quality on SLP samples, *ASTM F2036-05^{E1} Standard Test Method for Evaluation of Larger Area Density and Background on Electrophotographic Printers* [201] was selected as the most appropriate means of evaluating SLP prints. F2036 calls for five squares of equal size to be printed on an A4 area where four squares are placed near the corners and one in the centre of the page (See Figure 6.12). Four additional squares with only the border printed are used for measuring undesired toner printed onto the background. This standard was used for samples during a significant portion of the scoping trials (§6). As the trials progressed, the printed portions of the standard sample pattern were upscaled (thereby reducing the number of square areas that could be printed at a time) to give larger areas for evaluation (as needed for the field mill §5.7.1.2), but maintained a nominally square sample shape (for example, see §7.1.2 and Sample 7-6 onward). To pre-empt premature aging of the photoreceptor, printing patterns were limited to less than the circumference of the photoreceptor (as described in 3.4.2) when using developmental toner compositions.

5.5. Sample Set Populations and Analysis

In the experimental chapters the processing conditions for each set of samples is described and typically illustrated with an image of one of the representative samples from that set. Each set is labelled sequentially using the chapter number in which the sample is first described followed by a hyphen and a serial number (for example Sample 7-26 refers to the 26th sample in chapter seven).

5.5.1. Sample Set Population Size

The preferred minimum sample set population size for this work was five repetitions at each experimental condition described.

It was not always possible to reach a minimum of five repetitions when evaluating legacy samples (§6.1) (due to limited supply) or for multilayer samples produced for scoping or screening purposes (due to practical limitations).

When it was not possible or practical to produce five repetitions, two repetitions with repeated and averaged measurements were strived for. For example the set represented by Sample 7-12 included 6 repetitions of at least 20 layers, but only the final two repetitions involved printing ~200 layers per sample. Where fewer than five repetitions are presented, the author acknowledges that further repetitions are needed to establish statistical significance. However, considering results in the context of the

same results realized in additional sample sets (with similar experimental conditions), partially substantiates and provides a holistic overview of the landscape of defects discussed herein.

As the research presented herein matured, a minimum of five samples was always produced.

5.5.2. Representation of Error in Graphs

Each graph presented includes error bars except where noted. The standard representation for the magnitude of positive and negative error bars for averaged values in a sample set was equal to:

$$\frac{\sigma}{\sqrt{n}} \quad (5-1)$$

Where:

σ is the standard deviation of the measured error

n is the number of samples

Where sample data collection was not automated, the magnitude of the error bars was increased based on an estimated experimental error (typically 5V for the surface potential measurement by field mill and 0.01mm for sample height measurement). Additionally, where error bar magnitude was calculated below the standard error (manufacturer's published device accuracy) of the measurement device, or interpolated values were plotted, a magnitude equal to the standard error has been used (for example, see Figure 7.11).

5.6. Sample Substrates

A standard substrate material and thickness was desired for this research, which could support a range of fusing temperatures without distortion or posing fire or other hazards. After reviewing the variety of substrates which had been successfully used on the SLP rig prior to this research including: glass sheets, varieties of commercial tiles and epoxy laminates, it was determined that a ceramic substrate would be used.

In this work, toner printing during the scoping trials (§6) was undertaken primarily on several variations of paper. The remaining samples were predominantly printed on 1mm thick rigid fired alumina-based ceramic substrates (ADS96R, CoorsTek, CO, USA) with some exceptions as noted. The three standard sizes of ceramic substrates used were 120 x 120 x 1mm (from §7), 114.5 x 114.5 x 1mm with rounded corners (from §8.2), and 94.5mm diameter x 1mm (§9) supplied according to the CoorsTek design standards and specifications [311]. The ceramic substrates had a minimum density of 3.72 g/cm³, an ϵ_r of 9.5, a dielectric strength of 23.6 kV/mm, and a volume resistivity of $>10^{14}$ @ 25°C [311].

5.7. Explanation of the Selective Laser Printing (SLP) Development Rig

Throughout the duration of this project the SLP rig went through a series of changes as understanding of the process improved. This section outlines three milestone states of the rig.

5.7.1. Stage 1 – As Built in Custom-fit (Early 2009)

The SLP test rig was used for scoping trials (§6) and substantiating defect causes (§7) without appreciable changes from the state it achieved by the end of the Custom-fit project (which concluded in early 2009) as shown in Figure 5.3. For the purposes of this research, additional instrumentation was added to the rig to better understand and characterize the process, as shown in Figure 5.4 and explained hereafter.

The framework for the motion components of the SLP rig became the structure upon which all other components were mounted. The machine was designed with a 0.5m³ build volume which was transported on an aluminium platform, along a ball screw-driven X-axis (6m stroke). The speed of the platform was synchronised to the surface speed of the final transfer rollers (5m/min) of the printers. The addition of post-print measurements lengthened the required travel for the platform and increased the cycle time. Typical cycle times are shown in Figure 5.5, with further explanation of timing implications as each component of the rig is described below.



Figure 5.3 – Selective Laser Printing (SLP) development rig as built in the Custom-fit project

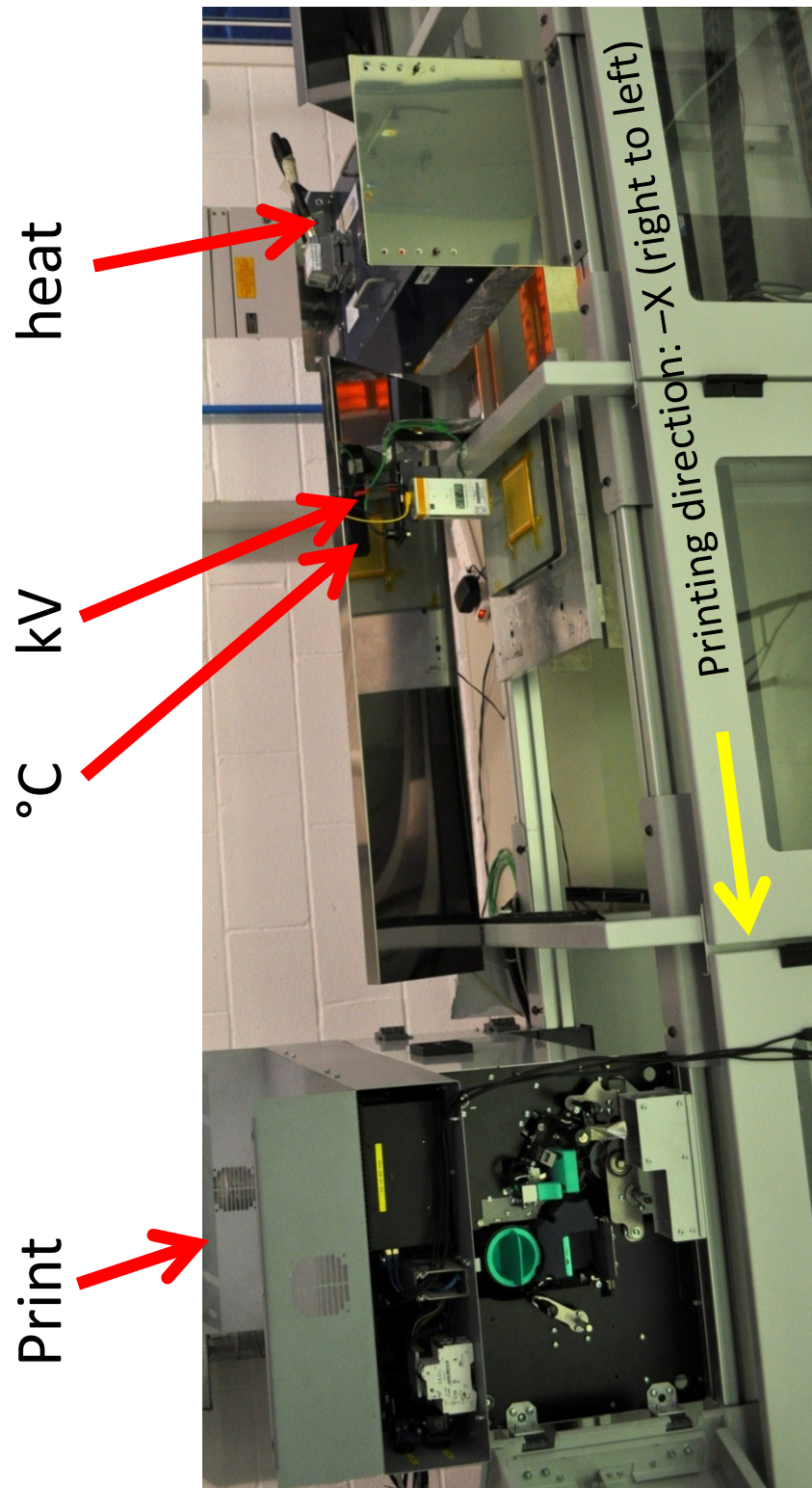


Figure 5.4 – SLP rig showing major components and instrumentation added for this PhD (note: print sequence is from right to left)

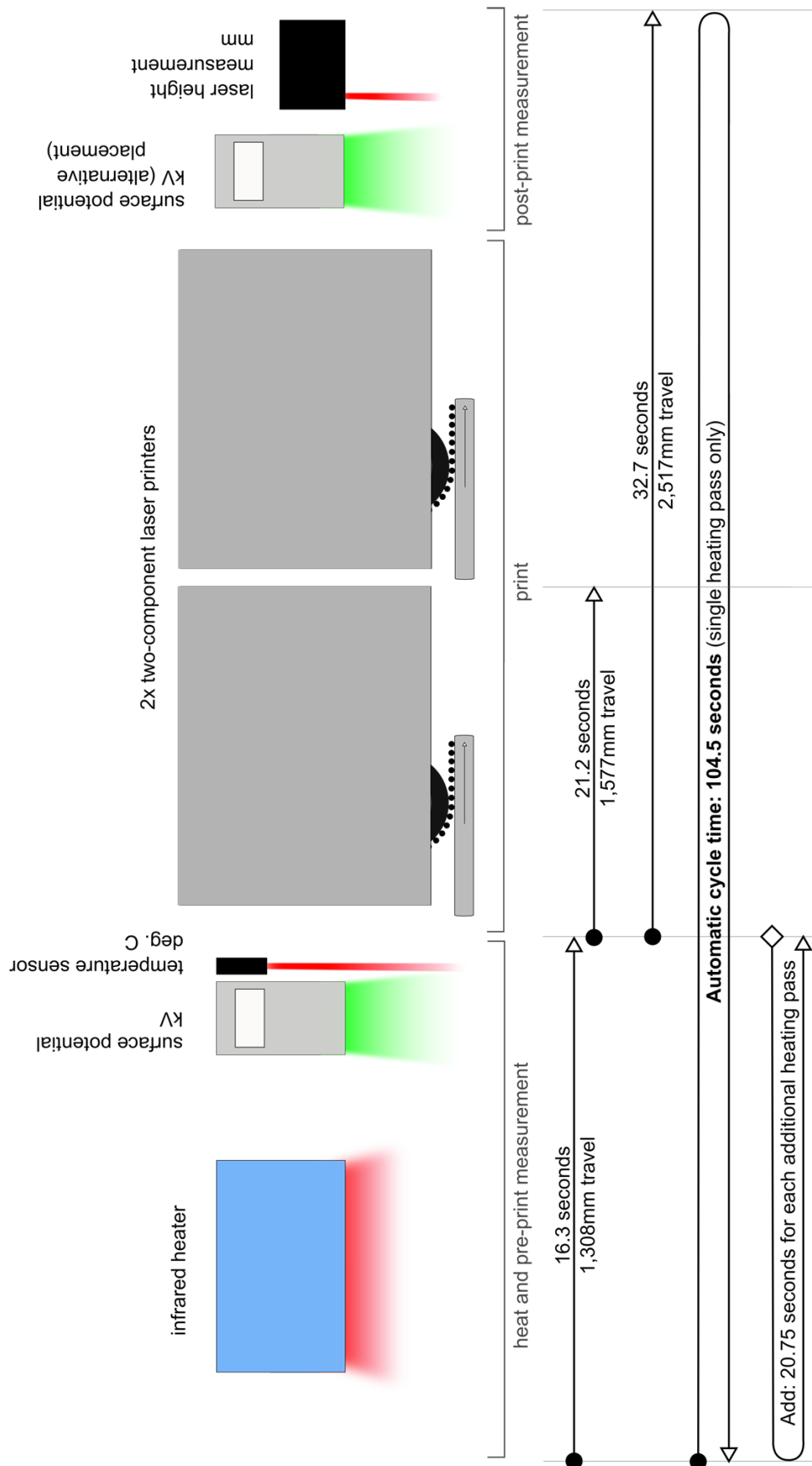


Figure 5.5 – Stage 1 SLP rig schematic layout showing instrumentation and typical cycle timings (note: print sequence is from left to right)

The major components and instruments used on the SLP rig as shown in Figure 5.5 are now described from left to right.

5.7.1.1. *Infrared Heater and Temperature Sensor*

A 12 kW medium/long wave (5-25 μ m) infrared heater (Flare FSMw, Infrared Systems, UK) mounted with the banks of heating elements perpendicular to the platform motion (Figure 5.6 left) was used for all trials in §6-7 except where noted. Banerjee tested a range of stand-off distances and demonstrated that a 128mm heater stand-off distance resulted in the best mechanical properties; therefore this was the basis for the stand-off used on the SLP rig for these trials. [211].

A 12 kW short wave (1-3 μ m) infrared heater (Solar H2, Infrared Systems, UK) mounted with the heating elements approximately parallel to the platform motion (except where noted) was also used in some trials as noted. Heater element orientation relative to sample motion (solid arrows) is shown in Figure 5.6. Heaters are approximately 500mm wide.



Figure 5.6 – Default orientation and print direction (looking up from underneath) of sample passing under medium wave (left) and short wave (right) infrared heaters

For some trials the orientation of the heater was rotated 90 degrees (Figure 5.16) in order to assess any influence of the heating element orientation on defect formation as noted.

Between layers, the platform would move at 5m/min underneath the heater and then stop for a couple of seconds underneath an "infrared thermosensor" (infrared thermometer) (ES1B, Omron, Japan) which measured the average surface temperature in the centre area of the sample to an accuracy of $\pm 2^{\circ}\text{C}$ between 110-120 $^{\circ}\text{C}$ using a reference temperature of 115 $^{\circ}\text{C}$. When a different target temperature was used, the reference temperature was re-set and the raw input voltages were adjusted accordingly.

If the surface temperature was within the specified operating window (typically between 110-120 $^{\circ}\text{C}$ depending on the toner), then the platform would automatically advance to the printers. Temperature control was essential to achieve a successful transfixing step.

If the temperature was too high, the platform would dwell underneath the thermosensor until the temperature had dropped to within the specified operating window (to prevent hot offset and or back transfer) and then continue on to the printers.

If the surface temperature was too low, then the platform was driven back to the cycle start position and then proceeded forward underneath the heater, stopping again underneath the thermosensor. This was done

to ensure the surface was softened and tacky enough to achieve a reliable transfixing step (thus avoiding cold offset). Repeating the heating portion of the print cycle added another 21 seconds for each cycle. In order to minimize the print cycle time, the heater intensity was adjusted in order to raise the surface temperature to within the processing window with a single pass under the heater (after the temperature of the platform and substrate had stabilized at the beginning of each build). In order to protect the photoreceptor in the printer, the build surface was not allowed to proceed to the printer above 135-140°C.

The thermosensor was initially calibrated using a thermal imaging camera as documented by Banerjee [211] and then maintained in calibration throughout the duration of this research by routine use of an infrared thermometer (Model N85FR, Precision Gold, Rotherham, UK).

5.7.1.2. Surface Potential Measurement

The surface potential of the printed toner layers was measured in-process at the same position as the surface temperature using a field mill device (JCI140 Static Monitor, Static Direct Limited, England).

The field mill device is designed to measure the strength of an electrical field. The JCI140 was designed to output its measurements as the average surface potential (net charge imbalance) over a relatively large area from a fixed stand-off distance of 100mm. The device does not require line of sight and even has some sensitivity behind the rear of the device, giving a nearly spherical effective measurement volume. Only

one field mill was used during this research, however it was used in different positions (as shown in Figure 5.5) including before, after (Figure 5.13) and even mounted in between the two printers.

5.7.1.2.1. Field Mill Sensitivity Analysis and Calibration

The JCI140 Static Monitors are calibrated at the factory (Chilworth Technology Ltd, UK) using an A3 (297x420mm) or larger conductive plate charged to a confirmed 1,000V with a current of 100 μ A or less [312]. In order to use this device to measure samples of smaller area, the monitor was calibrated using a 1mm thick piece of aluminium with the same area as the printed samples charged at various reference voltages using a high voltage power supply (Model 477-304, Brandenburg, UK). The voltage charge on the plate was independently checked with a multi-meter (Model 77-4, FLUKE, Washington, USA) equipped with 40KV high voltage probe (Model TT-HVP40, Testec).

The monitor's sensitivity to differing areas of charge was measured by charging four sizes of aluminium plate at a constant +1,000VDC while on top of an insulating foam box and measuring the surface potential detected at the recommended 100mm stand-off distance. In order to minimize interference from the surrounding area on the field mill, it was suspended from a table. Figure 5.7 shows the measurement setup for the smallest and largest samples measured.

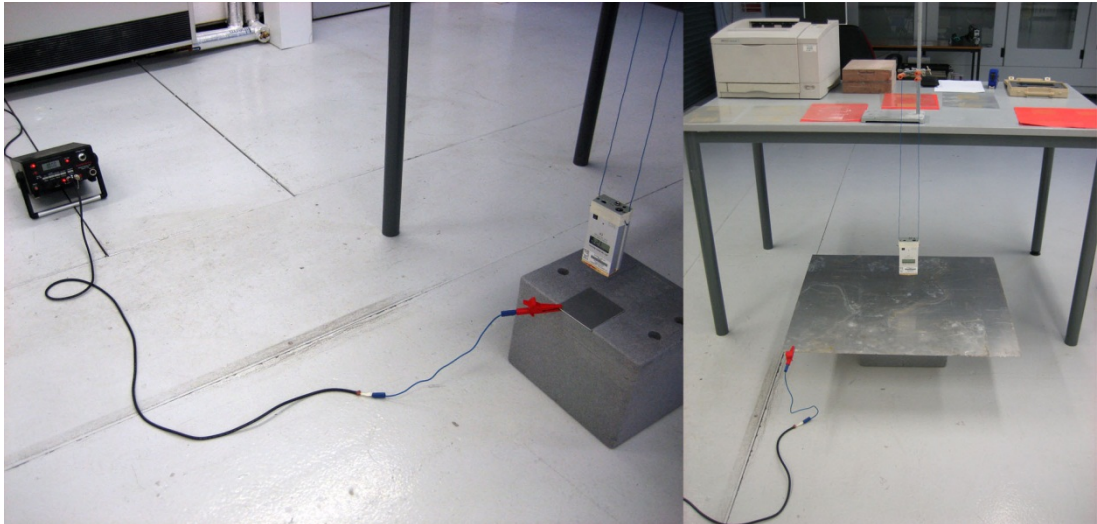


Figure 5.7 – Setup for measuring the sensitivity of the field mill to charged area

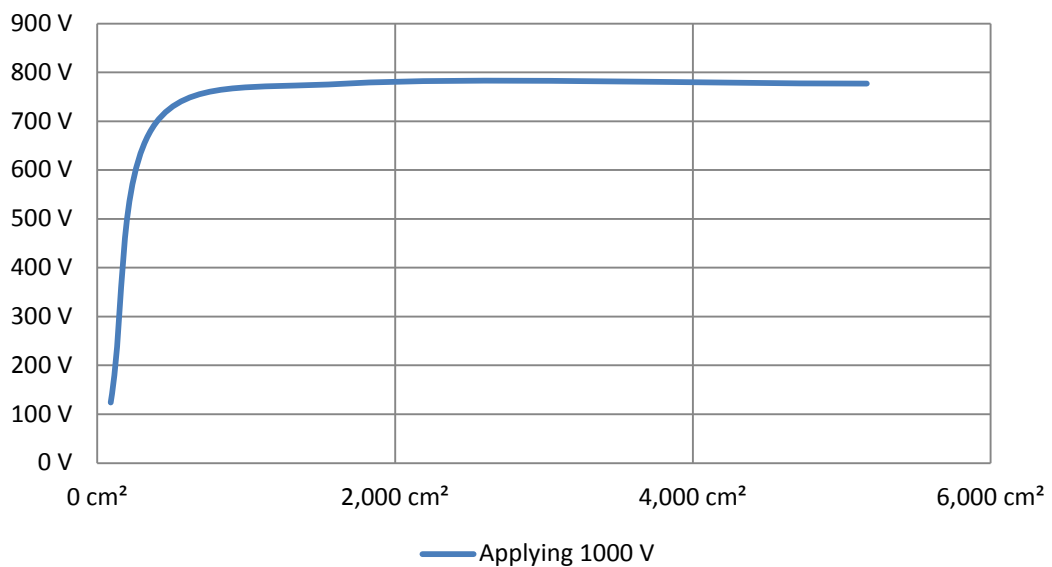


Figure 5.8 – Surface potential measured by field mill vs. charged area

The measurements were very stable and are plotted in Figure 5.8 which show that the monitor’s linear region correlated to samples with areas above 1,000cm². The monitor had a tendency to under measure the actual voltage applied by approximately 25%.

This result indicated that the JCI static monitor with a 100mm stand-off was appropriate to measure samples above 1,000cm², however the solid printed area on samples produced to ASTM F2036 were much smaller, with only 5 solid printed areas of 6.25cm² (= 31.25cm² total area). Scaling up the pattern so that each printed square was approximately 100cm² still placed the size well below the ideal range for the static monitor, therefore its sensitivity to the stand-off distance was evaluated as a method to improve the accuracy and reliable of the surface potential measurement.

The surface potential of a square aluminium plate with an area of 144cm² was charged to +3,000VDC using the same power supply as before and measured using stand-off distances from 10 to 200mm in 10mm increments (± 2 mm accuracy with better than $\pm 10\mu\text{m}$ repeatability). The voltage for this trial was increased from +1,000VDC (standard practice for the JCI140 calibration on a large area) to +3,000VDC to correlate with the magnitude of voltage and reduced sample area required for the experimental work (where the presence of a 1mm thick ceramic build substrate [§5.5], above the charged plate would attenuate the effective field strength at the top surface of the substrate as shown in §7). The measurements were made using the field mill mounted on the SLP rig to measure a charged aluminium plate on top of a stack of ceramic plates (See Figure 5.9 inset image), which isolated it from the build platform. The measurements were repeated four times, twice with the field mill running on battery power and twice with the field mill running from an external power supply. The results from the trials were averaged and

plotted in Figure 5.9. The readings were so consistent that the maximum error (equal to $\sigma/n^{1/2}$, where $n = \#$ of samples) of any measurement was ± 24.7 , which was so small that error bars were omitted from the graph (because they would not have been visible anyway). The two data points which measured nearest to +3,000VDC are labelled in the graph at stand-off distances of 50 and 60mm respectively. Mathematical interpolation between the two gives a theoretical 52.5mm stand-off for accurate surface potential reading. This new stand-off distance was validated by repeated surface potential measurements over multiple days which were always within 1% of 3,000VDC. A stand-off distance of 52.5mm was used for all experiments unless noted.

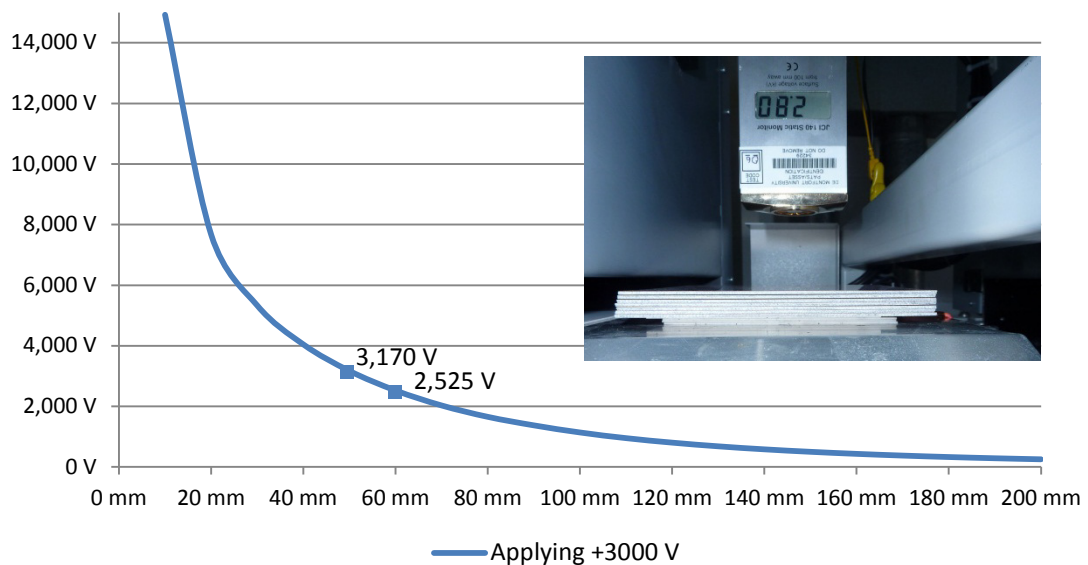


Figure 5.9 – Surface potential (of a fixed area) measured by field mill vs. stand-off distance

5.7.1.3. Pulsed DC Corona Device

For some samples (§7.2.3), a pulsed DC corona device (Meech 976 pulsed DC corona pin emitters with 977 control, Meech International, UK) was used to “shower” the build surface with up to 80% positive or 80%

negative ions (according to Meech it is not possible to only emit one polarity of ions since the corona process breaks apart air molecules giving both positive and negative ions). The device was typically used with a 250mm stand-off distance and 12 kV, 8 Hz, 75% positive or negative output. This was installed on its own frame in between the heater and printers as shown (vertical yellow arrow) in Figure 5.10. When this device was installed on the rig, the field mill device was always re-mounted between or behind the printers (to avoid affecting its readings, diagonal blue arrow).

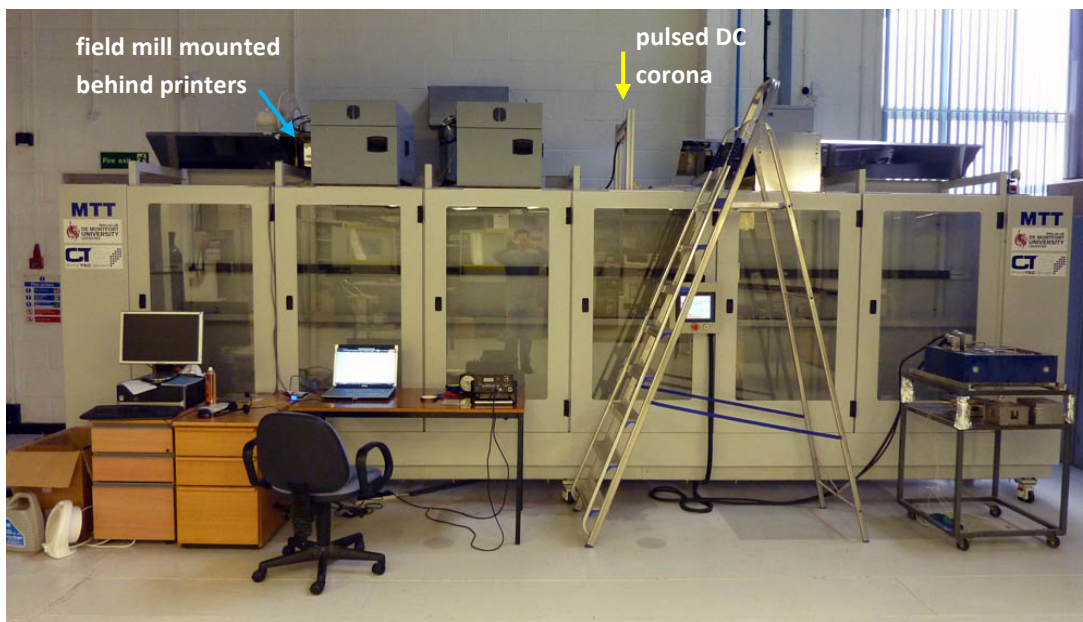


Figure 5.10 – Pulsed DC corona device installed on the SLP rig with the field mill located after the printers (platform motion is from right to left in this image).

5.7.1.3.1. ESD Audit and Ion Calibration

Susan Leahey of Renishaw PLC performed an Electrostatic Discharge (ESD) Audit on the rig at the end of September, 2011. She used a field mill with built-in charge plate (JCI145 charge plate, Chilworth Technology Ltd, UK) positioned at the height of the sample to check the calibration of

the ionizing bars from each corner of the platform and one somewhat central location close to where the sample normally sits. She found that when set for 50:50 ion balance (50% positive, 50% negative) that the readings in all positions charged to a negative value. At 80:20 positive bias all readings were found to be positive. The ionizers were then recalibrated 64:36 positive bias in order to actually achieve a neutral ion balance at the sample position on the platform. This will have biased earlier readings, especially since the field mill was found to have a -43V residual charge (also corrected, but probably less important given the large values that had been measured). Furthermore, she determined that the bars had a variation of $\sim 400V$ from one end to the other. This made the calibration valid for only one location on the platform. Due to the variations, it was determined that a different ion source should be used for neutralizing (§5.7.2.1) and charging (§5.7.2.3) in stage 2.

One additional point from the audit was that the use of non-ESD type Kapton tape could be problematic. It was tested immediately following peel off resulting in a voltage exceeding 10kV/m.

5.7.1.4. Two- component Printers

Two two-component printers (CTG-1C17-600, CTG PrintTEC, Germany) were mounted above the build platform. The printers featured 600 dpi LED print heads (no lasers were used in these printers) and OPCs which developed images using discharge area development (DAD) in negatively charging toners. Either printer or both could be used in each cycle. Unless otherwise noted, normally the first printer was loaded with the

build toner and the second printer (when used) was designated for support material to produce the samples reported in this research.

The printers were used at the default printing speed of 5m/min (resulting in cycle times as shown in Figure 5.5) with capability to run at twice that speed. At the default printer speed of 5m/min a typical cycle time using all of the instrumentation (and no dwell between layers) was ~ 105 s (Figure 5.5). A shorter cycle was possible if the printer(s) was used without the post-print measurement. In that case the travel in the printing portion of the cycle is reduced to 1,577mm and 21.2s making the overall cycle time (with a single heating pass) 50.3s. The plethora of high speed EP printing devices in the market indicates potential for much faster cycle times (normally one or two orders of magnitude faster); however optimizing the processing speed of the SLP rig was not the primary focus of this research.

These printers featured a patented conditioning roller (which is akin to a "toning roller" in some printers) which helped achieve development of thicker layers (up to 80 μ m) on the photoreceptor.

Typical voltages used in the printers are shown in Figure 5.11, although the voltages were fine-tuned based on the different materials printed.

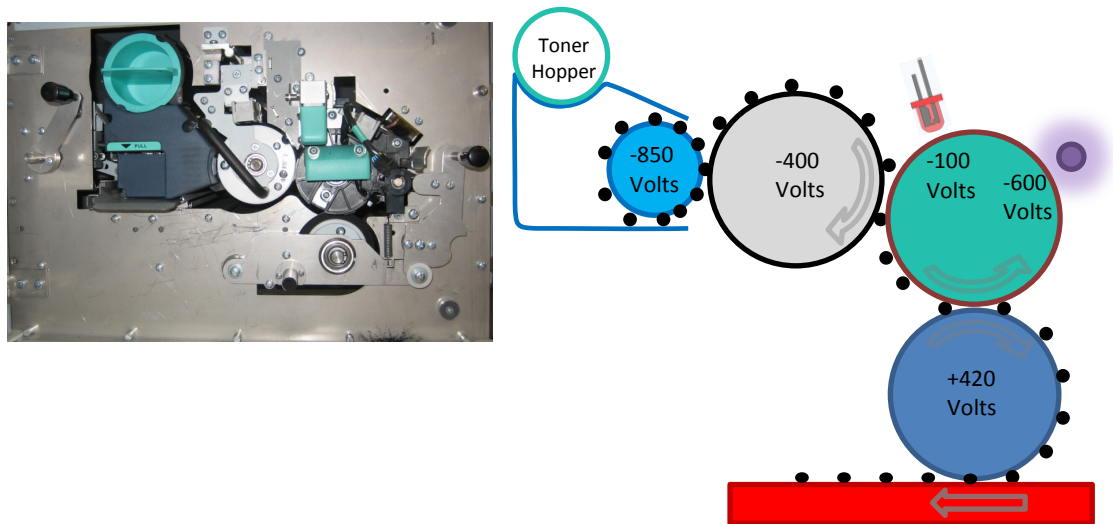


Figure 5.11 – CTG PrintTec GmbH printer configuration with typical voltages

The gap between the platform and final transfer roller was adjusted to be an interference fit (in order to apply some pressure) according to the manufacturer's recommendation using a sheet of A4 80 gram paper as a pseudo-slip gauge which was able to be removed without tearing. The pressure in the nip between the platform and the 80mm dia. final roller (See Figure 5.12) created a nominal nip width of 2.5mm with an average pressure of $126 \pm 9\text{kPa}$ ($\sim 1.29\text{ kg/cm}^2$), as measured by pressure sensitive film and pressure analysis software (Pressurex & Topaq, Sensor Products Inc., USA).

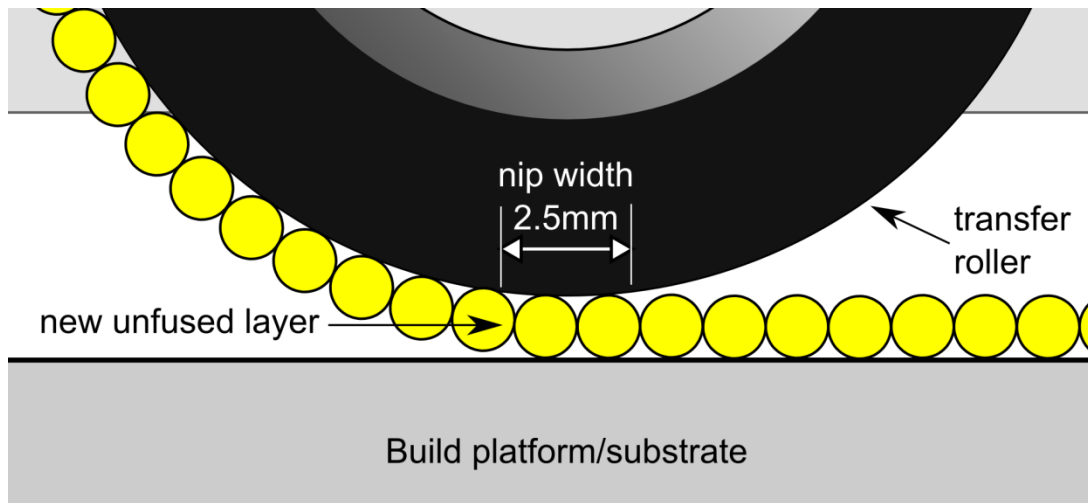


Figure 5.12 – Detailed illustration of the pressure applied during the transfer step

5.7.1.4.1. *User Adjustable Printer Settings*

The printers and control software were designed to have a high degree of adjustability. A printer setup for the conventional polyester toner used in this research (§5.1) is shown in Table 5.1 and explained below.

Table 5.1 – Typical Printer Settings: Polyester Toner

<i>Gaps:</i>	Gap: doctor blade	0.95 mm
	Angle of the magnetic brush	6
	Gap: Developer to conditioning roller	1.2 mm
	Gap: Conditioning roller to OPC (door side)	1.2 mm
	Gap: Conditioning roller to OPC (driven side)	1.3 mm
<i>Voltages:</i>	Developer bias voltage	-950 VDC
	Conditioning roller voltage	-450 VDC
	Charged OPC surface potential	-720 VDC
	Exposed residual OPC surface potential	-100 VDC
	Transfer roller voltage	+420 VDC
<i>Layer Height:</i>	Distance platform drops for each layer	5 μ m

The **doctor blade gap** is a physical measurement of the gap between the doctor blade and the magnetic roller in the developer. It is typically about ten-twelve times the diameter of the carrier beads being used.

The **angle of the magnetic brush** can be adjusted to align to a series of unlabelled notches (where recording convention for this work is that notch 1 is fully anti-clockwise, 6 is in the centre, and 11 is rotated fully clockwise), which influences the shape that the magnetic brush is presented to the OPC. CTG PrintTEC GmbH recommended that angle be left in the centre (6) position and left unchanged.

The **gap between the developer and conditioning roller** was determined by a pair of physical spacers that were mounted on each end of the conditioning roller.

The **gap between the conditioning roller and the OPC** was determined by an adjustable wheel in a slot on each end of the roller. There was no reference for the position of the wheel; therefore convention for this research was to measure its position from the bottom of the wheel to the bottom of the slot. This measurement does not represent the actual gap in between the rollers, but it was the most accessible measurement. Each wheel was adjustable independently from the other. Therefore this value is listed for the door side (where the operator had access to load and unload the imaging components after opening the hinged door) and the driven (far) side (where the drive mechanisms are for the rotating imaging components).

The magnetic **developer roller** was biased with a voltage of typically -800 to -900 VDC in order to induce the toner to jump onto the **conditioning roller** which was typically biased about -450 to -550VDC. The **OPC surface potential** was charged to -720VDC using a scorotron (§3.4.1) (where the conductive screen was biased to -720 by connecting it to ground through Zener diodes). The -720 surface charge prevented toner from jumping onto the surface of the OPC from the conditioning roller, except where it had been exposed. Exposure theoretically reduced the OPC surface potential to 0V, but in practice it retained a **residual charge** of approximately -100VDC. The **transfer roller** was typically charged around +400 to +450VDC in order to induce the toner to jump onto it from the OPC. Although the platform/substrate in the Custom-fit project were not charged, some experiments in §7 onwards did use a charged plate under the substrate as noted. After each print, the platform was dropped by a fixed amount to accommodate the increasing layer height and maintain contact with the final transfer roller.

5.7.1.5. Deposited Layer Height Measurement

Following material deposition via printing, the platform paused underneath a laser height measurement sensor (Smart Monitor ZS-HLDS10-2M with controller ZS-HLDC11A, Omron, Japan) as shown in Figure 5.13 and fed the measurement back directly to the programmable logic controller (PLC) driving the SLP rig. A laser stripe (3.5mm x 60µm) was directed at the centre of the sample and averaged the surface height within the area of the laser stripe to within 1µm. Although the sample being measured exceeded the recommended operating temperature of

55°C the dwell underneath it was only a few seconds (just long enough to get a stable reading) therefore the sensor never approached that temperature.

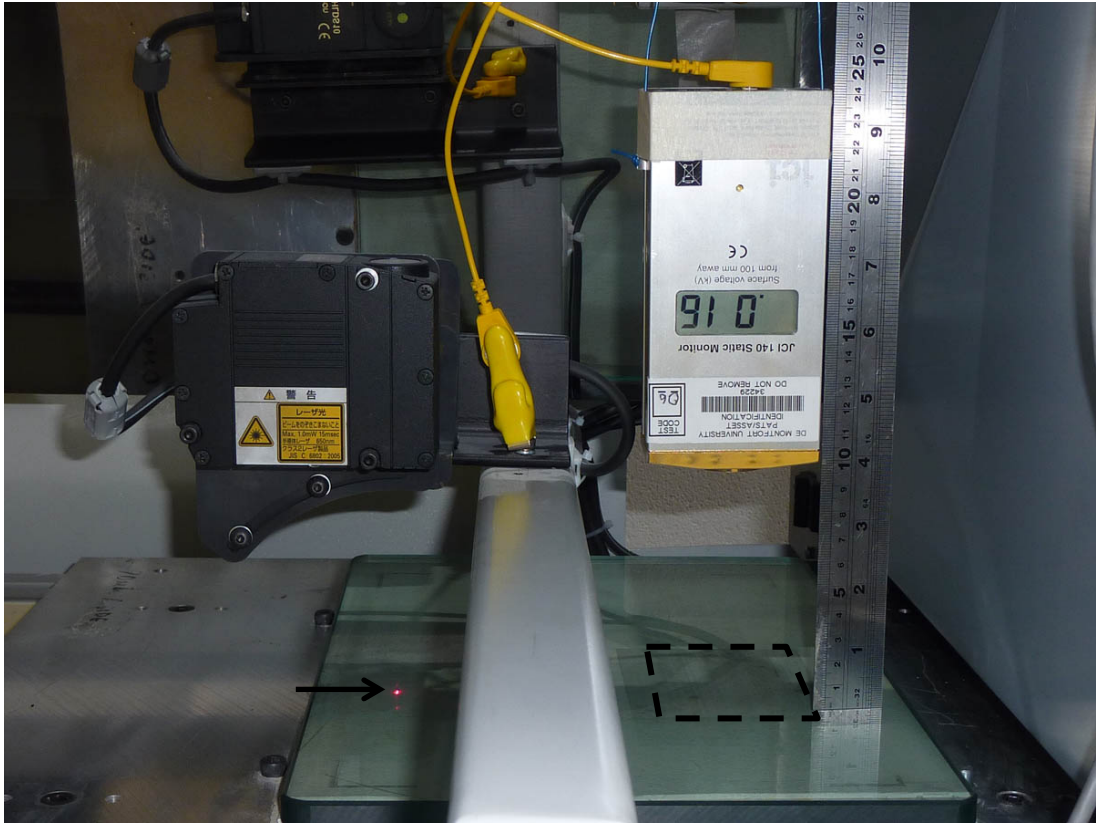


Figure 5.13 – View of the laser stripe used for height measurement (arrow on left); and alternate position for the field mill after the 2nd printer (initially installed at its recommended stand-off distance)

Unfortunately the cantilever design of the build platform was not rigid enough to take full advantage of the accuracy of this height measurement sensor. The worst-case displacement at the unsupported end of the platform was more than 150 μ m when tested with loads on par with the force exerted by the final transfer roller. This relegated the height measurements recorded to being indicative of the build trend, but the absolute accuracy of any reading could not be depended upon from layer to layer.

5.7.1.6. *Ambient Temperature and Humidity (not shown)*

The ambient temperature and relative humidity were recorded prior to each set of experiments using a hygrometer (Model 408-6109, RS Components, UK) which was corroborated using a temperature and humidity meter (Model 971, Fluke, Washington, USA). Owing to the assessment of Whitney et al. [163] (as discussed in §3.3.2) and the difficulty of controlling relative humidity, it was simply recorded and not manipulated (except where noted) for this research.

5.7.1.7. *Platform and Substrate Arrangements*

During Custom-fit the SLP samples were deposited onto a substrate consisting of a sheet of safety glass approximately 12mm thick (as shown inset in Figure 7.1). Glass was desirable because of its smooth surface and thermal mass. The smooth surface promoted good surface quality for early layers and it was relatively easy to peel finished samples off of it. Furthermore, after it was pre-heated (prior to beginning deposition), the thermal mass of the substrate helped maintain elevated sample temperature between heating cycles.

The glass substrate was supported by a cantilevered flat aluminium platform (Figure 5.25) earth bonded to the frame of the test rig. In order to help achieve a more uniform pressure distribution, some compliance was built into the platform by sandwiching a couple of layers of 2mm-thick silicone rubber matting between the glass substrate and the aluminium platform (as shown in Figure 7.6).

5.7.2. Stage 2 – After Refurbishment of Printers

The level of effort associated with the teething issues of building the SLP rig strongly discouraged changes to the printers or the rig, however in time it was evident that aversion to modifications was preventing future progress.

The changes were primarily motivated by understanding gained from trials in §7; namely, that residual (imbalance of) toner charge was inhibiting surface quality in successive layer deposition. Also the printers were refurbished in order to eliminate issues that had arisen during the research, and to incorporate changes for improving printer performance and longevity as recommended by the manufacturer.

The SLP test rig in its Stage 2 form was used for evaluating charge neutralization (§8) as shown in Figure 5.3. Additional instrumentation was added to better understand and characterize the process as shown in Figure 5.14 and explained hereafter. The printer components and instrumentation which did not change from the Stage 1 rig are not repeated here.

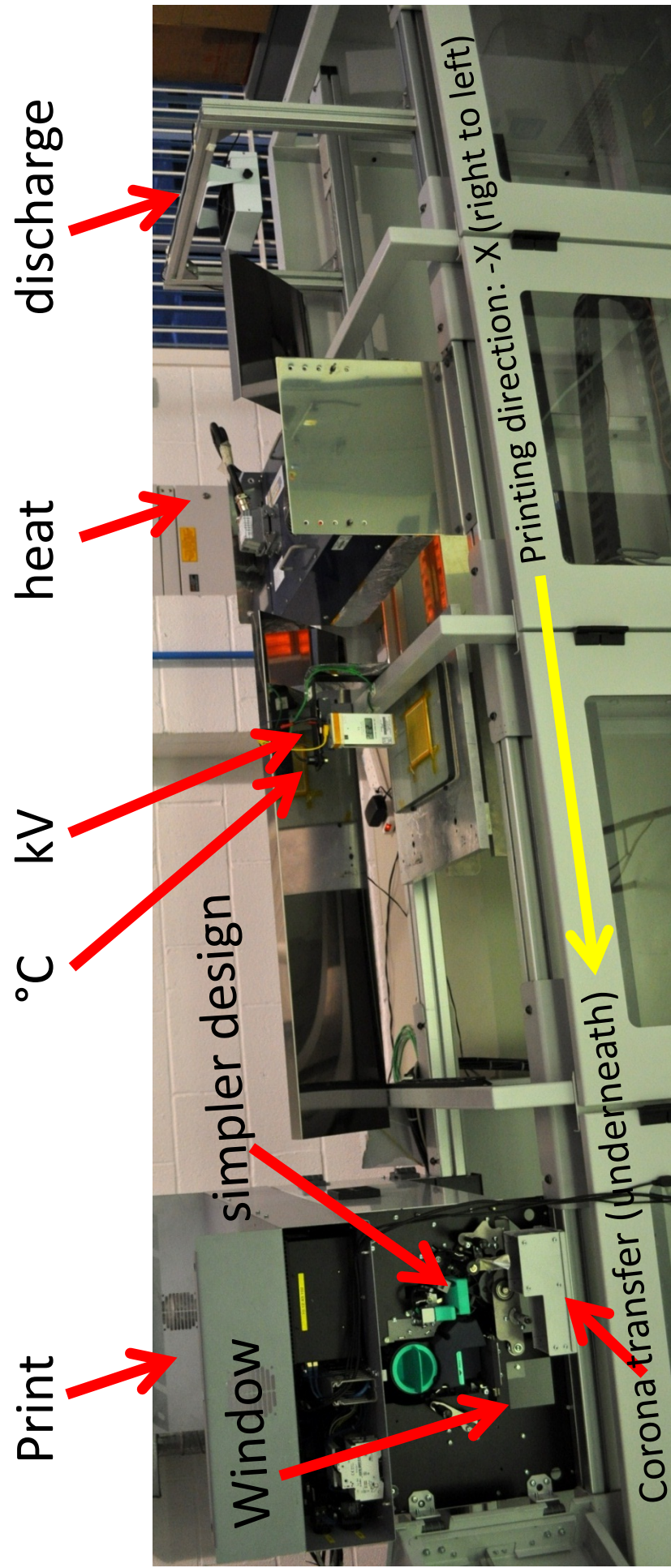


Figure 5.14 – SLP rig showing major components and instrumentation added for Stage 2 of this PhD (note: print sequence is from right to left)

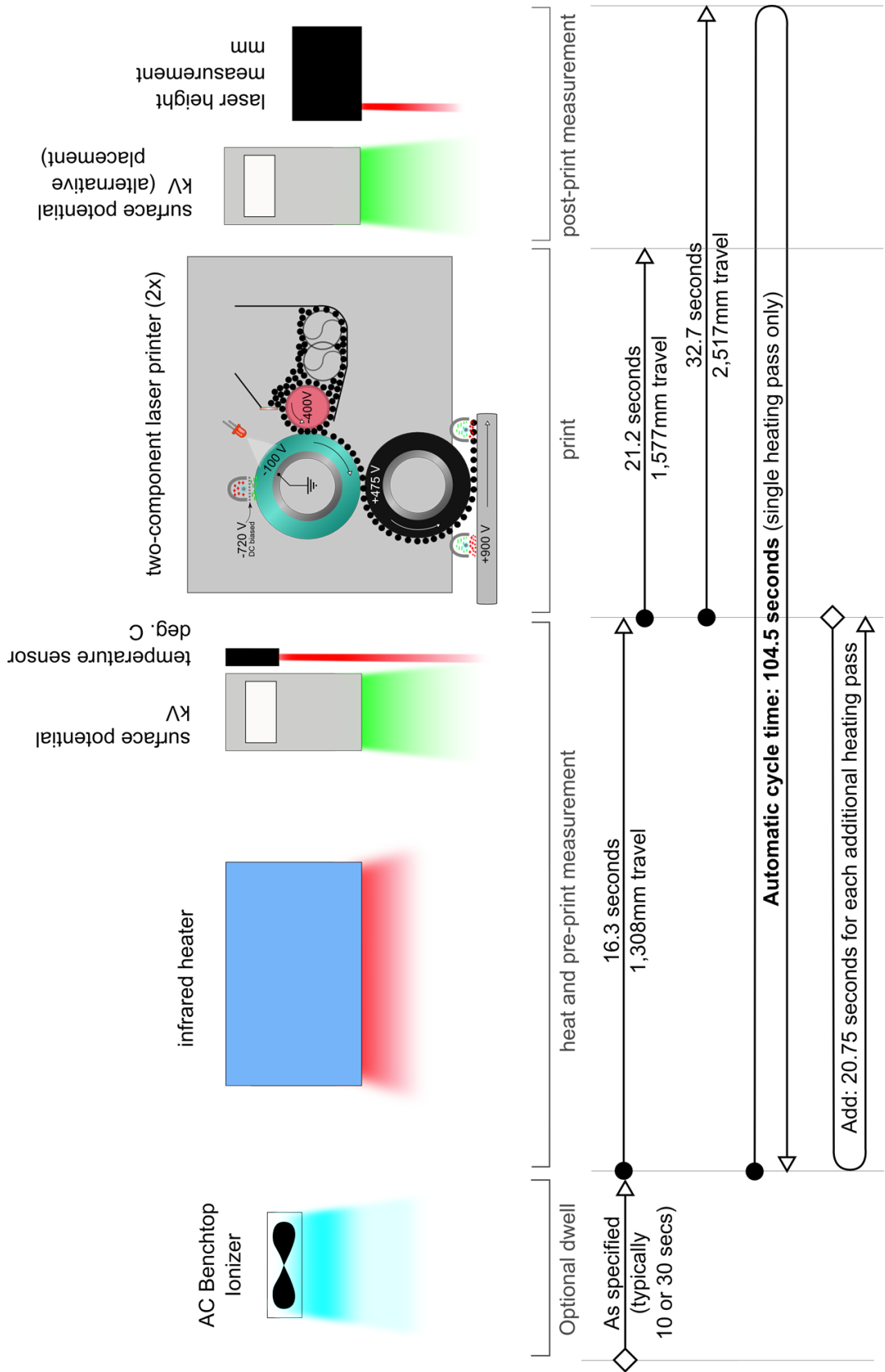


Figure 5.15 – Stage 2 SLP rig schematic layout showing instrumentation and typical cycle timings (note: print sequence is from left to right)

The major components and instruments which were changed on the SLP rig as shown in Figure 5.15 include the following:

5.7.2.1. AC Fan Ionizer

A high frequency air (fan) ionizer (KS21H, Killstat, UK) was installed above the cycle start position in order to neutralize any charge imbalance before printing the next layer. Varying dwell times, typically from 10 to 30s, were used in order to sufficiently neutralize deposited toner after each layer. The stand-off distance was set to ~225mm after consulting with the manual from the manufacturer.

5.7.2.2. Heater Orientation

In the Stage 1 configuration, the samples were passing beneath the medium wave heater such that the seam between the banks of heating elements reduced the heating on a portion of the sample resulting in non-uniform heating (See Appendix C). Therefore, it was determined that rotating the heater through 90 degrees (elements parallel to the platform motion) achieved more uniform heating (Figure 5.16).

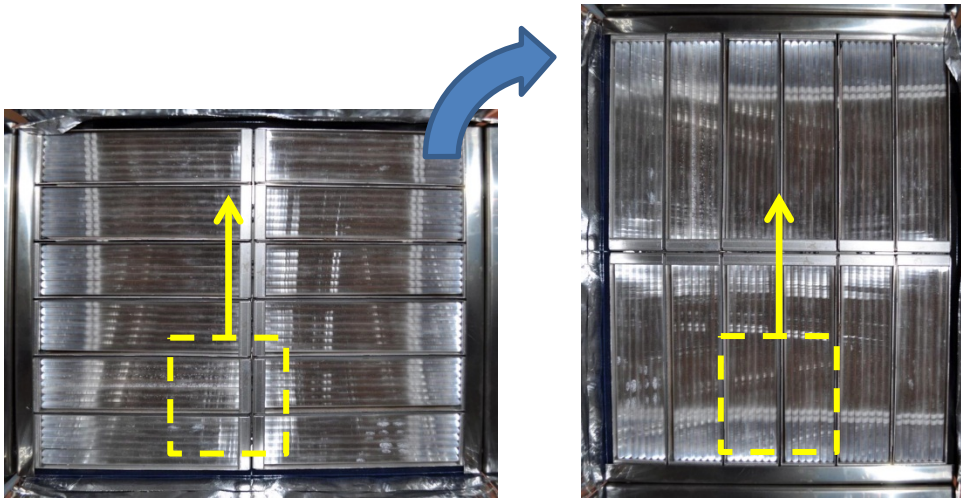


Figure 5.16 – Rotation of medium wave infrared heater to improve heating uniformity

5.7.2.3. Two- component printers

The printers were removed from the SLP rig and shipped one at a time to CTG PrintTEC GmbH (Germany) for refurbishment. Three fundamental changes were made to the printers. First, transfer corotrons (with 8 parallel high voltage wires) were added to the underside of the printers just prior to and after the final transfer roller in order to saturate the print surface/substrate with positively charged ions (Figure 5.17).

Second, the conditioning roller was removed from the printers in favour of a more conventional (and simpler) printing configuration because as the conditioning roller aged, it introduced inconsistencies in the print quality. Third, a small rectangular window was made in the sidewall of the printer (Figure 5.18) allowing observation of the backside of the final transfer roller and corotrons after it. The total duration of the refurbishment was approximately 9 months.

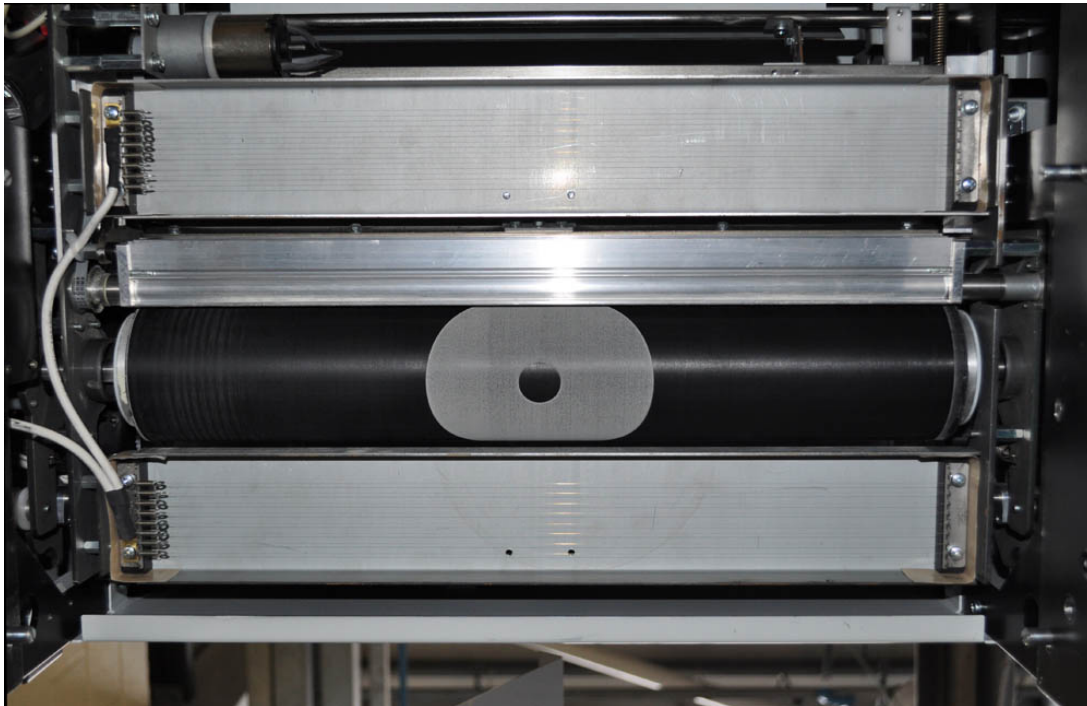


Figure 5.17 – View of the underside of the refurbished CTG PrintTEC GmbH printers showing corotron devices before and after the final transfer roller

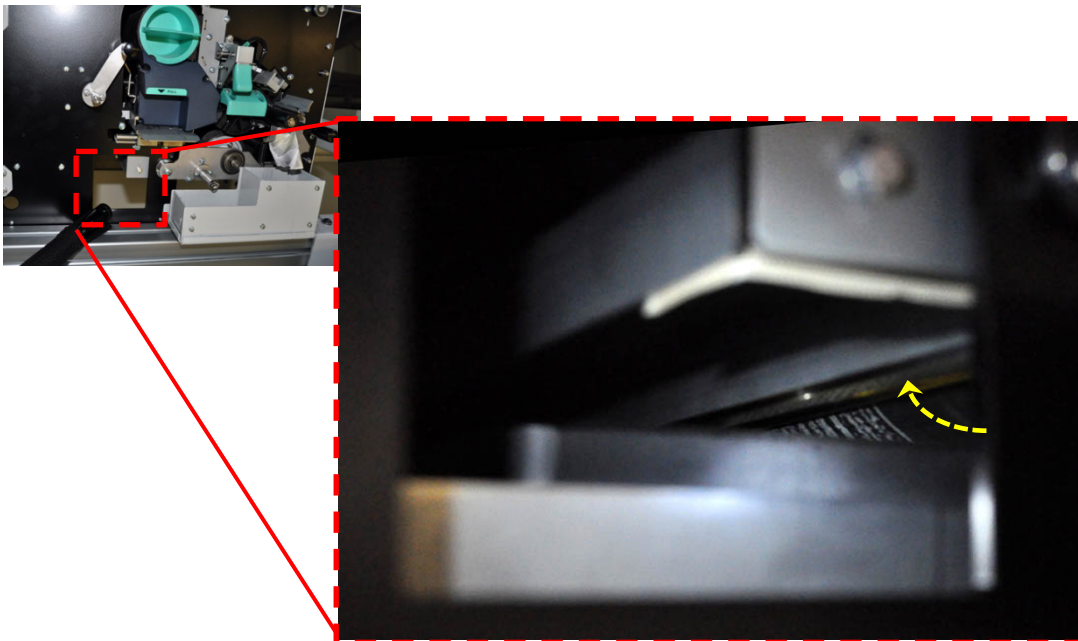


Figure 5.18 – Viewing window in the refurbished printers (left), and view through the window showing the back of the transfer roller (right); arrow shows roller rotation (print direction is right to left)

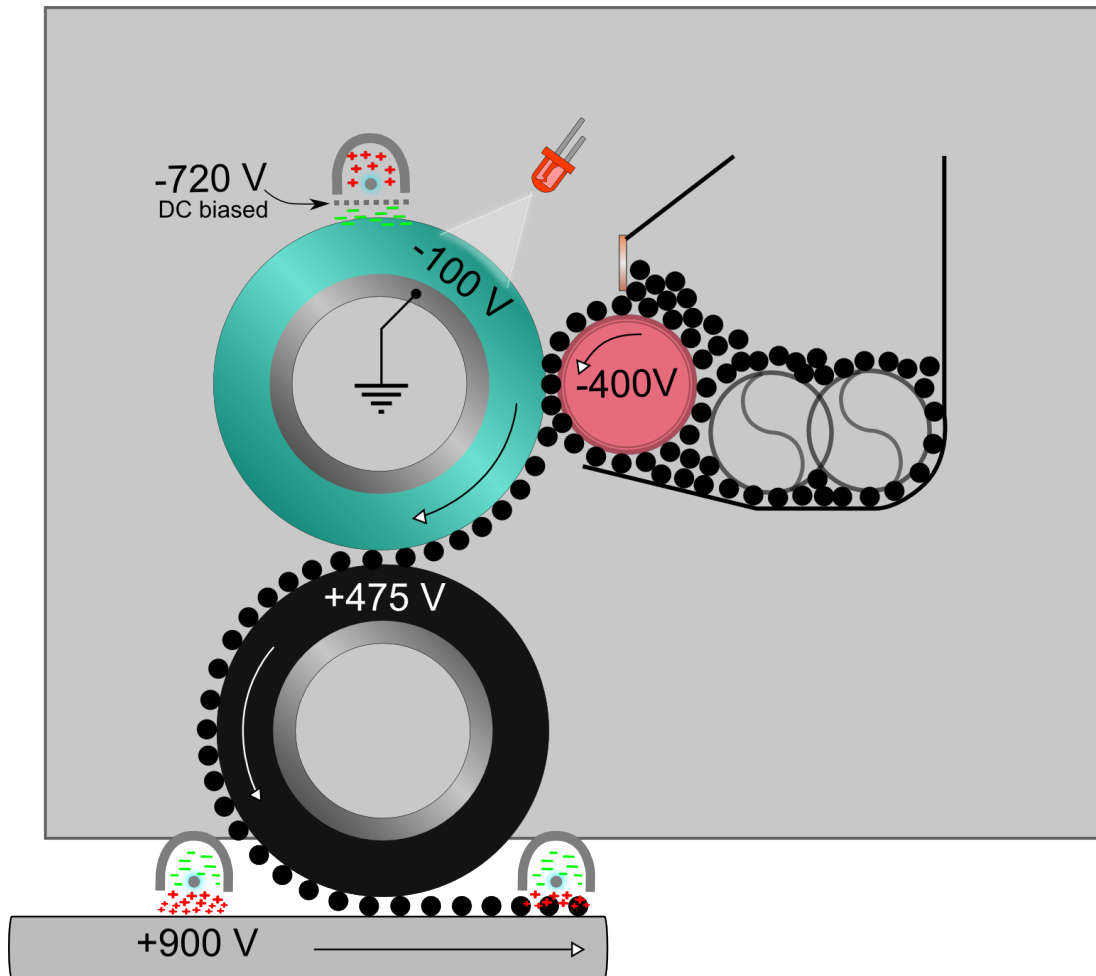


Figure 5.19 – Typical voltages used inside the CTG GmbH printers after refurbishment

Typical voltage settings for the refurbished printers are illustrated in Figure 5.19:

- The magnetic roller is biased with -400V
- The screen in front of the corotron (making the device a scorotron) which charges the OPC is DC biased using Zener diodes to -720V.
- The OPC core is grounded.
- Theoretically the OPC surface should go to ground as well (where the light hits it), however in practice a small residual charge (-100V) remains after 40 μ s exposure to the LED print head.
- The final transfer roller is charged to +475V

- The transfer corona can be used to saturate the upper surface with positive ions within the voltage range of 0 to 5,700 VDC.
- The build surface then relies on tackification forces for transfer. Or to achieve electrostatically favourable transfer it is biased with at least +900V using either the corotrons or by charging a conductive plate on top of the platform, but insulated from it (and typically underneath the non-conductive printing substrate).

5.7.2.3.1. User Adjustable Printer Settings

A printer setup for the epoxy “toner” used in this research (§5.1) is shown in Table 5.2 and explained below.

Table 5.2 – Typical Printer Settings: Epoxy Toner

<i>Gaps:</i>	Gap: doctor blade	0.65 mm
	Angle of the magnetic brush	6
	Gap: Developer to OPC	(not user adjustable)
<i>Voltages:</i>	Developer bias voltage	-400 VDC
	Charged OPC surface potential	-720 VDC
	Exposed residual OPC surface potential	-100 VDC
	Transfer roller voltage	+475 VDC
	Transfer corona (active printer)	0 VDC
	Transfer corona (2 nd printer)	+5,700 VDC
<i>Layer Height:</i>	Distance platform drops for each layer	10 µm

5.7.2.4. Platform and Substrate Arrangements

After the discovery and substantiation of residual charge, the aluminium cover for the platform was removed (Figure 7.6) in order to prevent charge from leaking away and thus improve the signal-to-noise ratio for

measuring the surface potential by field mill. The stack of ceramic substrates was used directly on top of the original glass substrate (Figure 5.20). Figure 5.21 shows the substrate behaviour in the nip.

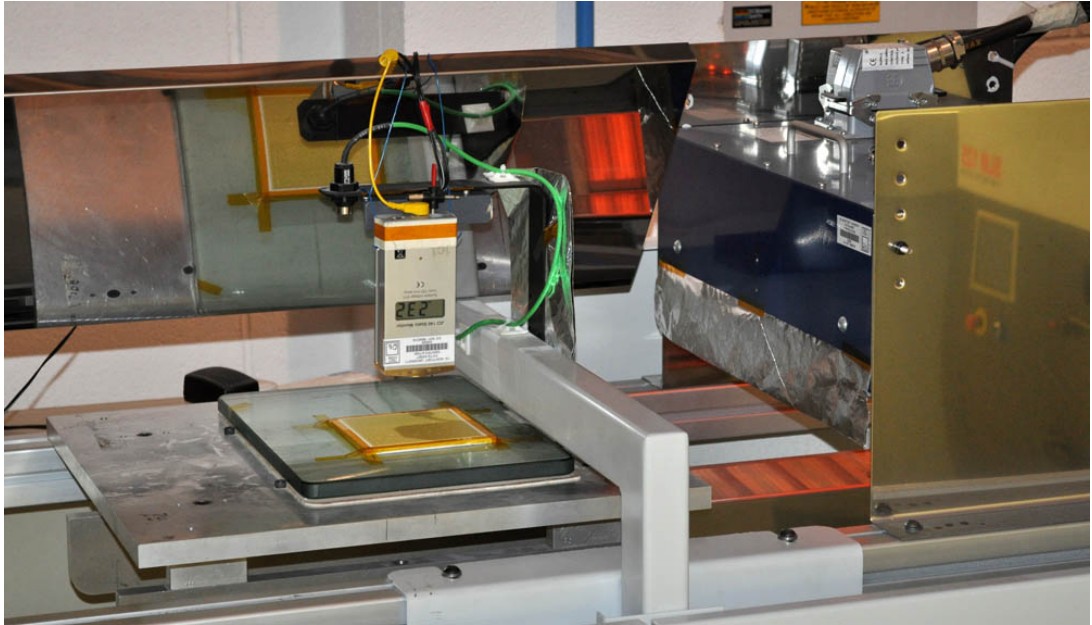


Figure 5.20 – Stage 2 SLP rig platform supporting a stack of ceramic plates on top of the original glass substrate on silicone matting

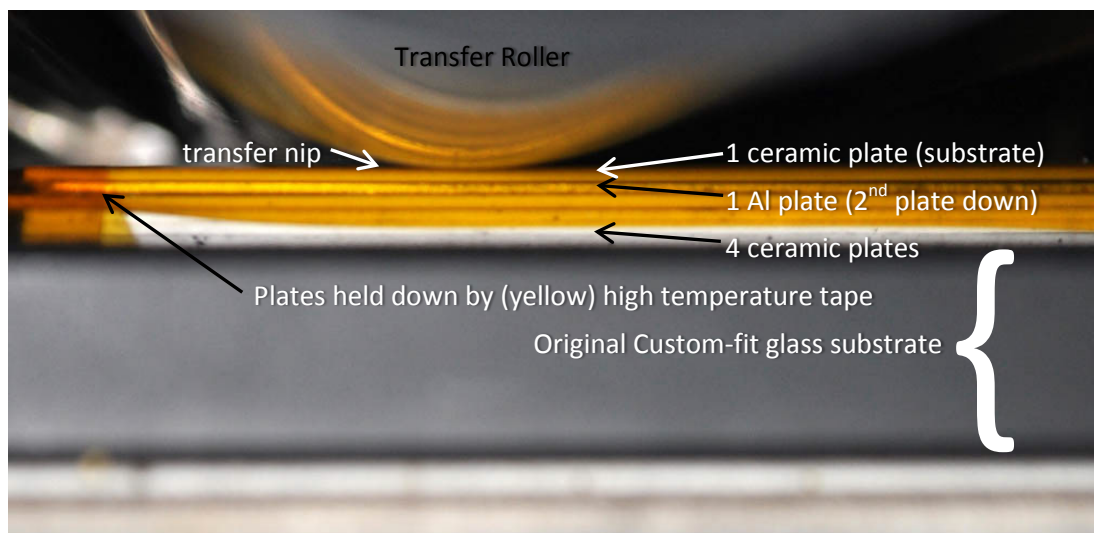


Figure 5.21 – Close up view of a typical substrates stack (including charge plate) on the platform as it passes under the transfer roller

5.7.3. Stage 3 – Print to Ground and Build Sleeve

5.7.3.1. Two- component printer with shifted voltages

In response to the understanding gained from experimental work reported in §8, the printer voltages were shifted in order to be able to print to ground for the first part of the experimental work reported in §9. In order to be able to create an electrostatically favourable transfer to ground, it was necessary to shift the voltages 900V more negative at each step of the EP process resulting in voltages as shown in Figure 5.22.

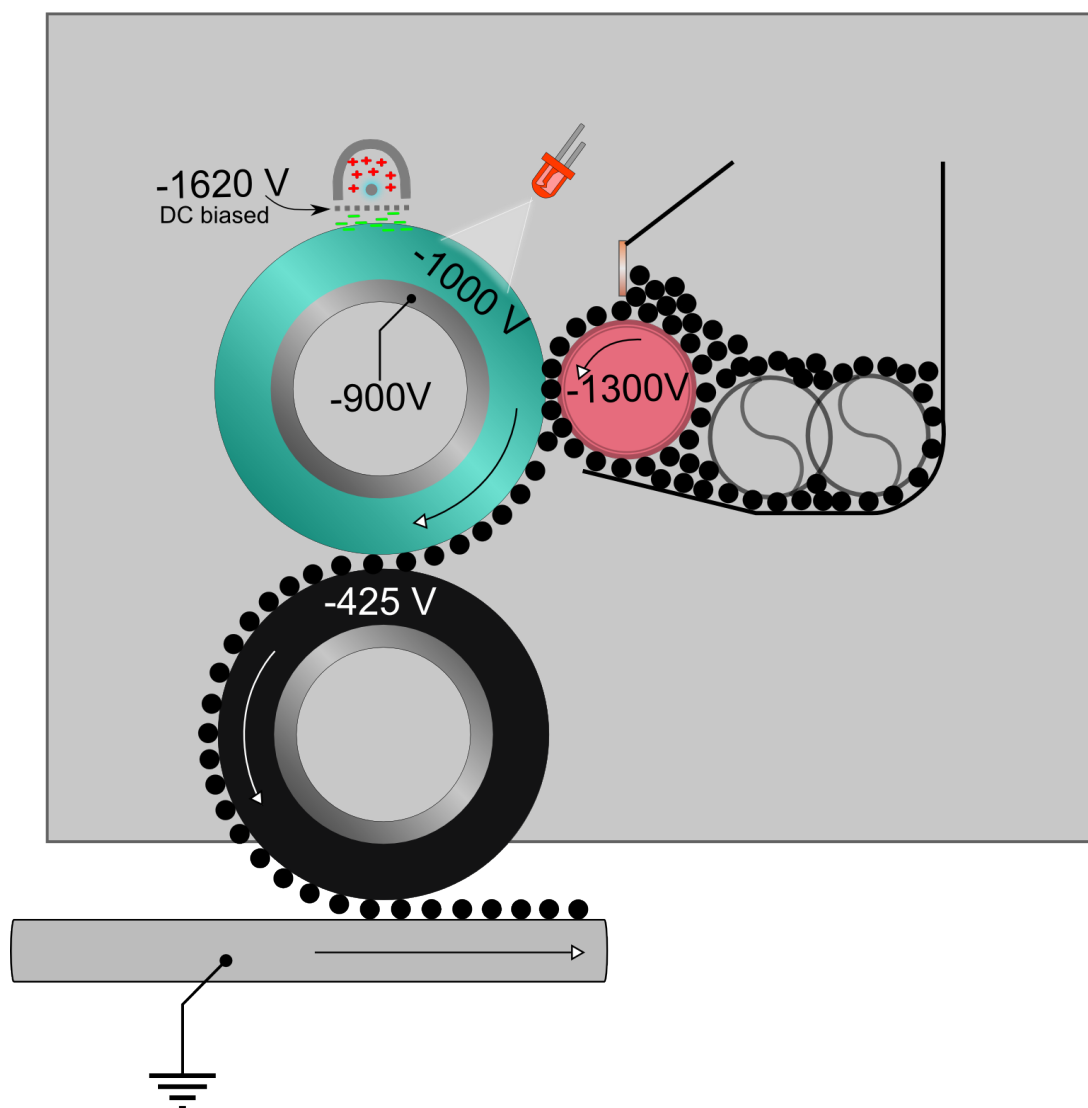


Figure 5.22 – Voltages shifted -900 V so the CTG GmbH printers would print to ground

Typical voltage settings for the printers after the voltage shift (Figure 5.22) are as follows:

- The magnetic roller is biased with -1300V
- The screen of the scorotron which charges the OPC is DC biased using Zener diodes to -1620V.
- The OPC core is held at \sim -900V (it drifts \sim 100V under load)
- In practice the OPC surface has a small residual charge so its potential is estimated to be -1,000V after a 40 μ s exposure.
- The final transfer roller is charged to -425V
- The build platform is grounded which provides an electrostatically favourable potential in order to induce the toner to transfer off of the final transfer roller.

These shifts were only possible by hijacking (by rewiring) the power supplies from within the first and second printers as shown in Table 5.3.

Table 5.3 – Summary of 1st Printer Voltage Shift and Rewiring

<i>Voltage Destination (in 1st printer)</i>	<i>Stage 2 Default (V)</i>	<i>-900V shift (V)</i>	<i>How was the additional -900V supplied?</i>
Developer Bias voltage	-400	-1,300	From 2nd printer OPC corona power supply
OPC Corona Charge	-6,000	-6,000	Used default power supply
OPC Surface Charge (limited by the screen voltage using Zener diodes)	-720	-1,620	More Zener diodes added
OPC Core - connected voltage	0 (GND)	-900	From 2nd printer bias power supply
OPC Core - potential after exposure (OPC residual charge)	-100	-1,000	(Not directly controlled)
Transfer Roller voltage	+400	-425	From 1st printer bias power supply
Platform voltage (for electrostatically favourable transfer)	+900	0V	None required

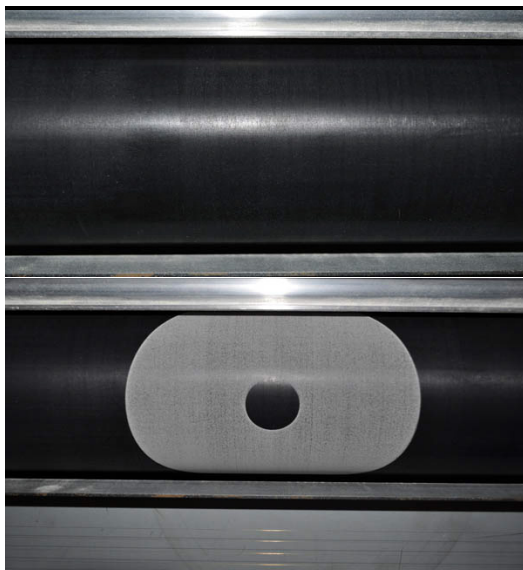
This undertaking was substantially risky to the imaging components in the printers and was pursued with caution. The 55th configuration trialled (after the use of many alternative power supplies and parameters) suitably achieved this (as shown in Table 5.4). It is important to note that this was only possible because the OPC chemistry only transports positive charge, therefore biasing the OPC electrode (the conductive Al core) to -900V did not cause negative charge injection or compromise its performance [313].

For the purpose of defect illustration, photos of the image quality on the final transfer roller (all taken from the same distance using the same camera with 1/60 shutter speed, F-stop of 4.5, ISO 200, zoom of 24x, and a flash) showing progress toward and including the configuration in Table 5.3 are shown in Table 5.4.

Table 5.4 – Progress Toward Printing with Voltage Shift

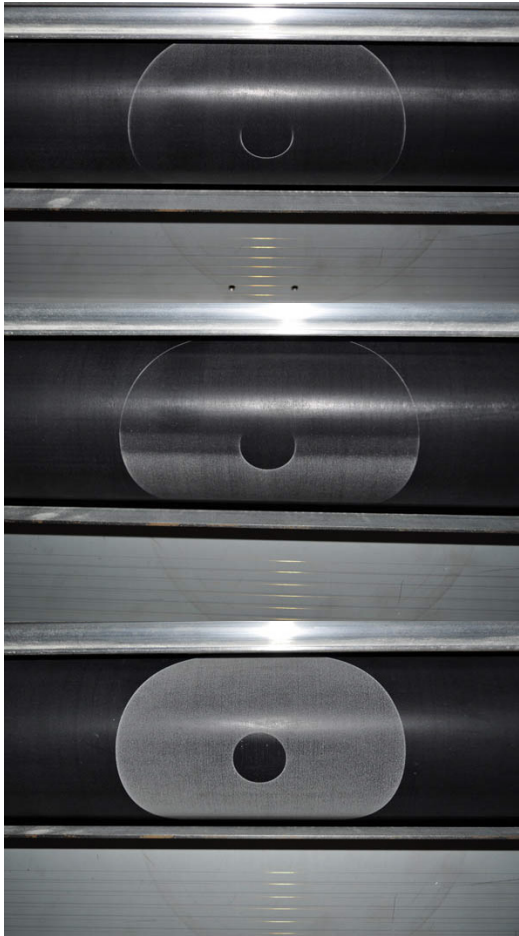
Results:

Discussion:



a Clean final transfer roller (for reference)

b Baseline print (again for reference) with settings used as per the Stage 2 SLP rig



c Only fringe field development was the outcome of experiments where the OPC core voltage was left floating (unconnected), or where power supplies were not adequate resulting in voltage drift so severe that the outcome was essentially the same.

d With some power supplies partial fill or graded density in the image was evident. This may be explained by the power supply initially being able to hold the bias, but over time, drifting caused diminished or discontinued transfer.

e Image density of transfer with shifted voltages as per configuration in Table 5.3. Comparing this density to b, it is slightly less dense, but is sufficient for proof of concept.

Figure 5.23 – Examples of development quality on the transfer roller (including defects) experienced during the 55 trials toward achieving high density printing to ground

For the latter portion of §9, the printers were returned to their original wiring state and voltages operated as per the Stage 2 rig (§5.7.2.3).

5.7.3.2. Enclosed build sleeve and Z-axis stiffening

The work to enclose the build volume and stiffen the Z-axis as described in this subsection was undertaken by the Additive Manufacturing Product Division (AMPD) of Renishaw PLC at the request of the author. The original flat open platform (Figure 5.25 left) was replaced with an enclosed cylindrical build sleeve (100mm inside diameter) to support the bottom and walls of the build in-process. The new cylindrical platform

incorporated locations for pressure sensors and a gimbal design for adjusting the platform to be level with the final transfer roller. This new design also centred the build platform exactly in the middle (the Y direction as determined by ISO/ASTM 52921 [314]) of the build volume (previously placement had favoured one side to conveniently mount the instruments while avoiding impingement on the stainless steel viewing). After installation of the new build sleeve, all instrumentation was adjusted to the same centre accordingly (Figure 5.24).

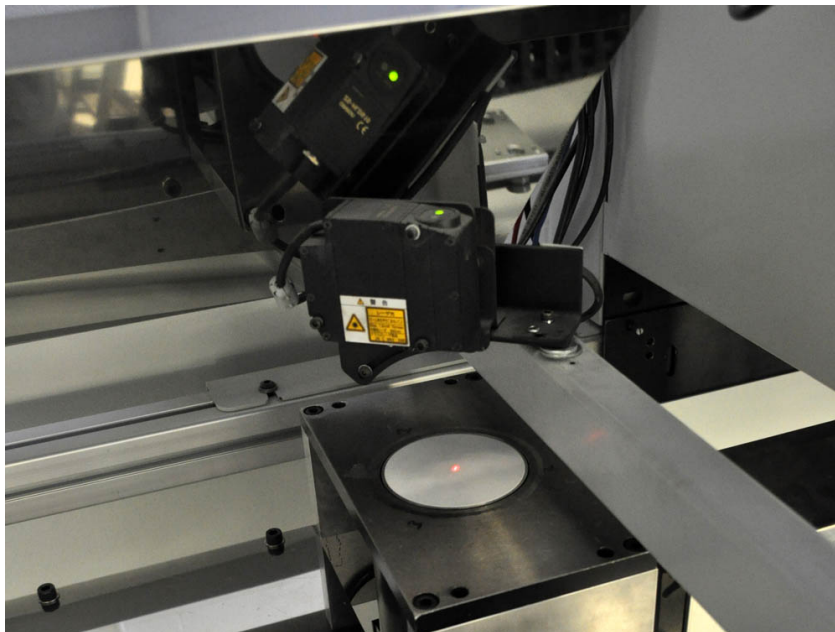


Figure 5.24 – Adjusted position of the laser height measurement device (partially under the stainless reflecting surface) in order to be centred on the new cylindrical build volume

The smaller build volume, and its location nearer to the Z-axis base, dramatically reduced the “diving board” effect observed on the cantilevered platform (See Appendix B), which improved the accuracy and repeatability of measurement from the laser height sensor.

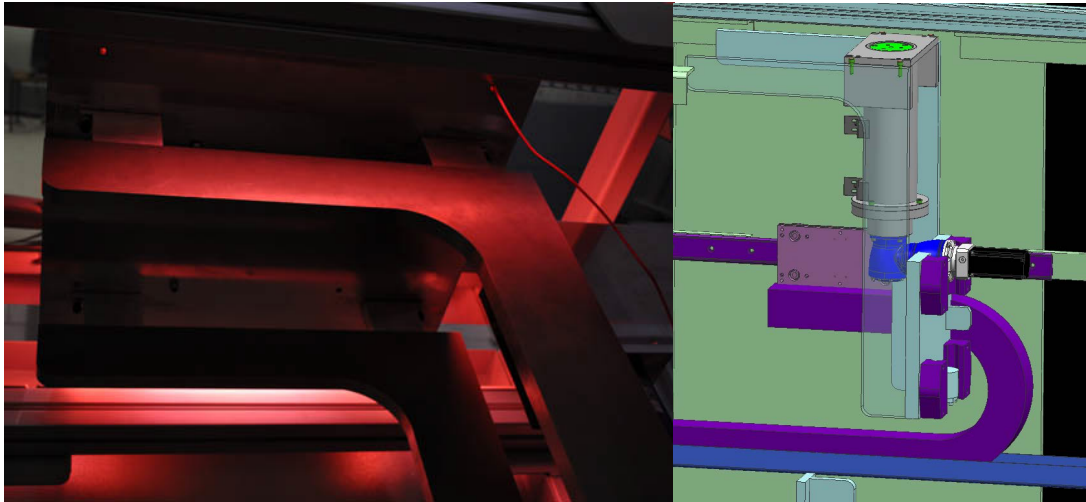


Figure 5.25 – Original cantilevered platform (left); redesigned build sleeve (right)

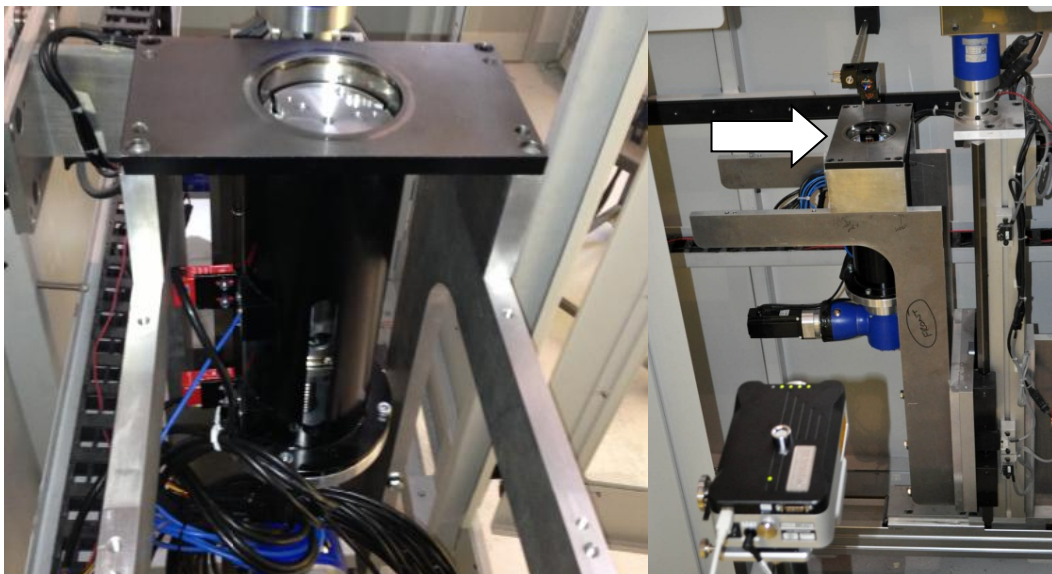


Figure 5.26 – Views of the build sleeve as designed and installed in the SLP rig by Renishaw PLC

5.8. Explanation of the Electro- Magnetic Brush Evaluation Rig (EMBER) test rig

Although the SLP rig provided a means of two-component printing onto rigid substrates, it was difficult to disambiguate the transfer/adhesion effects (of contact, heat, and pressure; i.e. tackification) from

electrostatic forces from the transfer field (§3.4.4). In order to evaluate electrostatic transfer in the absence of contact or pressure, a small single component test rig was built (by the author) which used a jump gap (entirely electrostatic) transfer as shown in Figure 5.27.

Since the EMBER-based study embraced observing electrostatic transfer in isolation, image development (and therefore a photoreceptor) was not required. Using the components from a printer inside a CNC machine enabled testing after the fashion of EMB powder coating (See §4.4.5.2) therefore it was named the Electro-Magnetic Brush Evaluation Rig (EMBER).

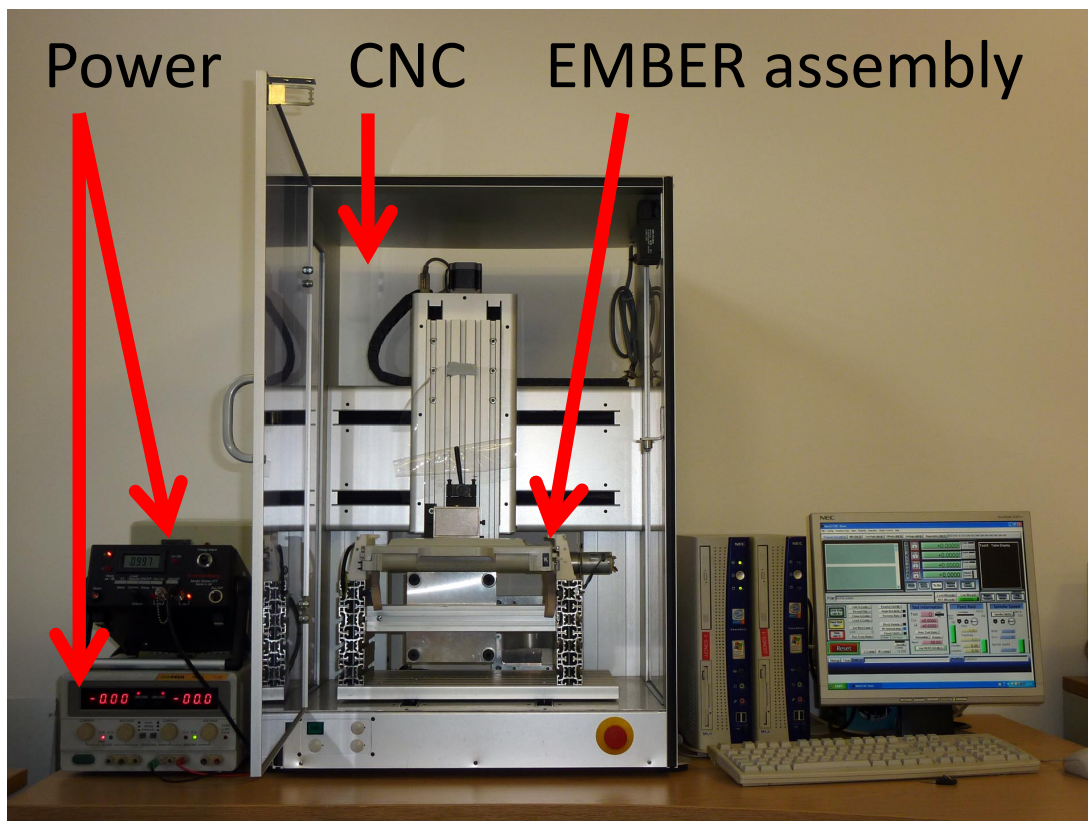


Figure 5.27 – EMBER rig for testing electrostatic transfer effectiveness

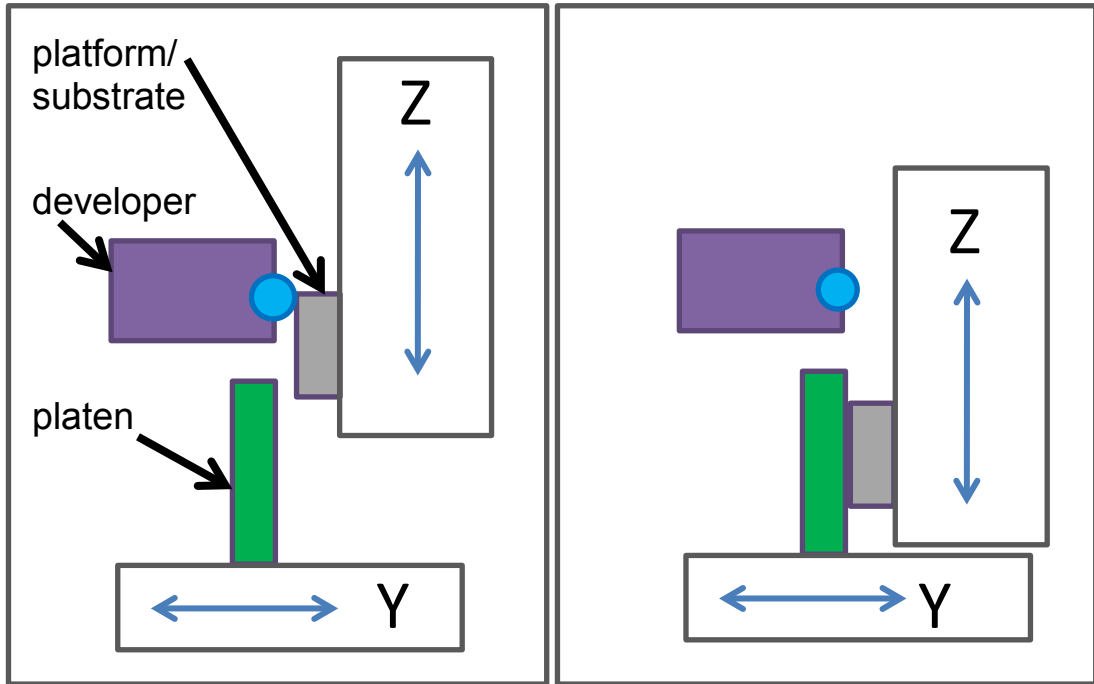


Figure 5.28 – EMBER rig schematic showing printing mode (left); and optional compacting/consolidation step (right)

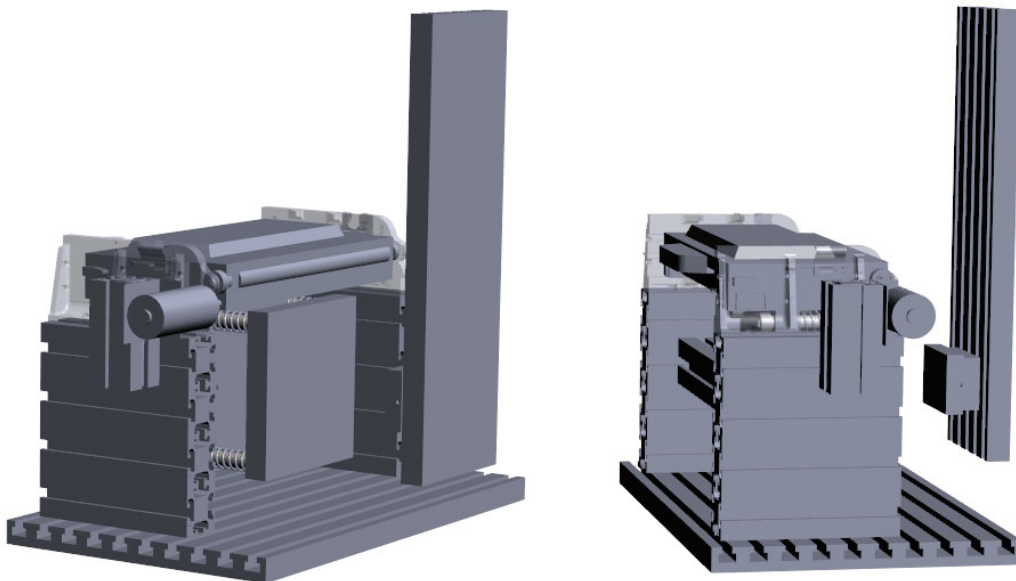


Figure 5.29 – EMBER CAD model showing the developer & platen (left); and platform (right)

Figure 5.28 shows a schematic illustration of the EMBER rig without its structural framework. Building on results from previous research [211]

the integrated developer and toner cartridge from a Lexmark C510 printer (20K1403, Lexmark, KY, USA) was selected to charge the toner. For these trials, the standard black non-conductive toner which came loaded in it was used. In order to utilize the developer in its intended horizontal orientation (and demonstrate new machine concepts), this rig was designed to deposit layers which grew parts "sideways" in a direction parallel to the ground (note axes in Figure 5.28 are labelled as per the CNC machine host, and do not conform to ISO/ASTM 52921 [314]). A mounting framework inspired by the critical internal features of the printer was laser sintered in nylon and secured to an aluminium extrusion frame to the table of the desktop 3-axis CNC machine (Prototype from Proma, Isel, Germany). Custom printing routines were manually written in g-code and executed using adapted Mach3 software (Version3.043.022, Artsoft, USA). A spring-loaded platen which could be heated using a rear-side mounted flat mica strip heater 220W 70x75mm (615-1722, RS Components, England) was also built into the rig, although it was not used for these trials unless noted. In order to achieve non-contact fusing (and therefore avoid masking any defect formation with pressure/contact effects) a hot air gun ((DW340 Type 2, DeWALT, Maryland, USA) was used to achieve the target fusing temperature which was monitored manually using a non-contact thermometer (MiniTemp A01195, Raytek, CA, USA).

The developer roller was typically charged to between -700 to -3,000V using a high voltage supply (Model 477-304, Brandenburg, UK) although it was adjusted based on the initial gap (~0.1-0.2mm) between the

developer and substrate (or when a non-conductive substrate, the gap between the developer roller and ground). This voltage was determined by measuring the Lexmark C510 printer during the normal print cycle using a multi-meter (Model 77-4, FLUKE, Washington, USA) equipped with 40kV high voltage probe (Model TT-HVP40, Testec). The maximum voltage on the roller core averaged over several print cycles was: -675.3V with a standard deviation of 26V.

The roller was driven by a variable speed 35mm diameter motor with integral 47:1 gearbox (970D, RS Components, England). The speed of the developer roller was maintained above 400rpm (8-9VDC) to match the rotation speed in normal operation in the Lexmark C510 as measured by a mechanical (average of 395 rpm with standard deviation of 7) and optical tachometer (average of 417rpm with standard deviation of 0.6).

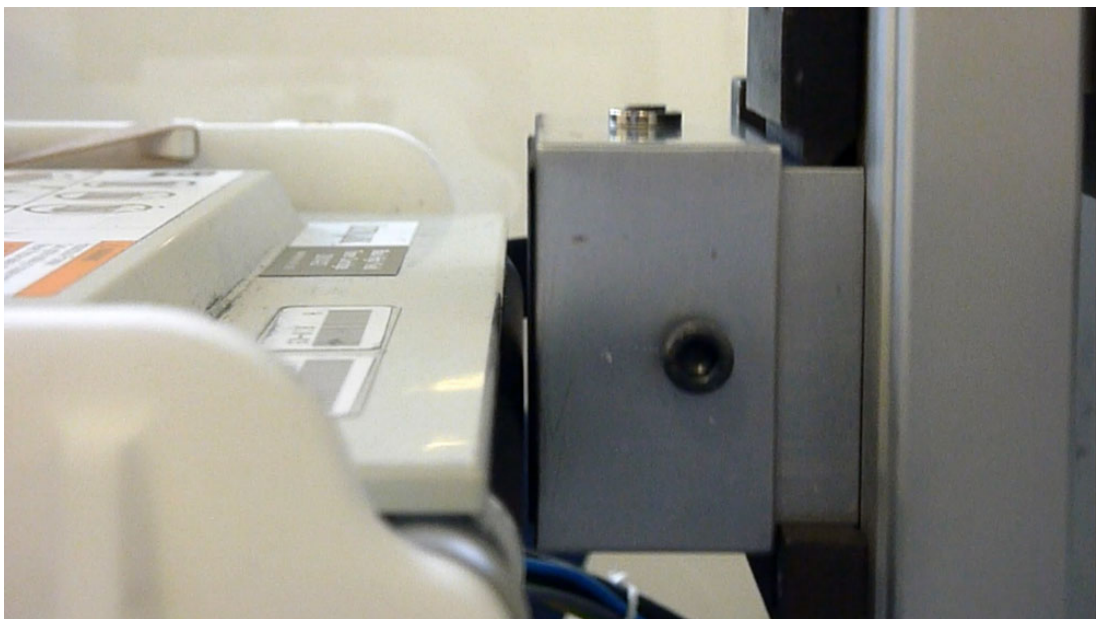


Figure 5.30 – EMBER rig transfer step close up: showing an 0.2mm gap between the developer and substrate during a deposition cycle

The print "platform" accommodated 45x70mm substrates. The substrates were sheared steel plate (held in place magnetically) or laser cut acrylic held in place using double sided tape. An adjustable "collar" or sleeve could be used to support the sides of builds which grew over 1mm. The platform was mounted into the machine such that the build face was vertical (perpendicular to the ground, Figure 5.30). It was removable with the substrate still in place, which facilitated analysis of the build without disturbing the layers/substrate (such as for evaluation of charge using a gold leaf electroscope, Figure 5.31).

The temperature and relative humidity inside the machine were monitored for each set of experiments using a hygrometer (Model 408-6109, RS Components, UK).

5.8.1. Surface potential measurement

Although a surface potential measurement device was not mounted in the EMBER rig, it was possible to remove the build platform and measure the deposited toner on the substrate using the field mill static monitor from the SLP rig or a gold-leaf electroscope (Model 10498, STE, England) as shown in Figure 5.31. The principle upon which this latter device operates is illustrated in Figure 5.32.



Figure 5.31 – Gold-leaf electroscope for detecting net charge imbalance showing no charge (left) and net charge on an acrylic substrate (right)

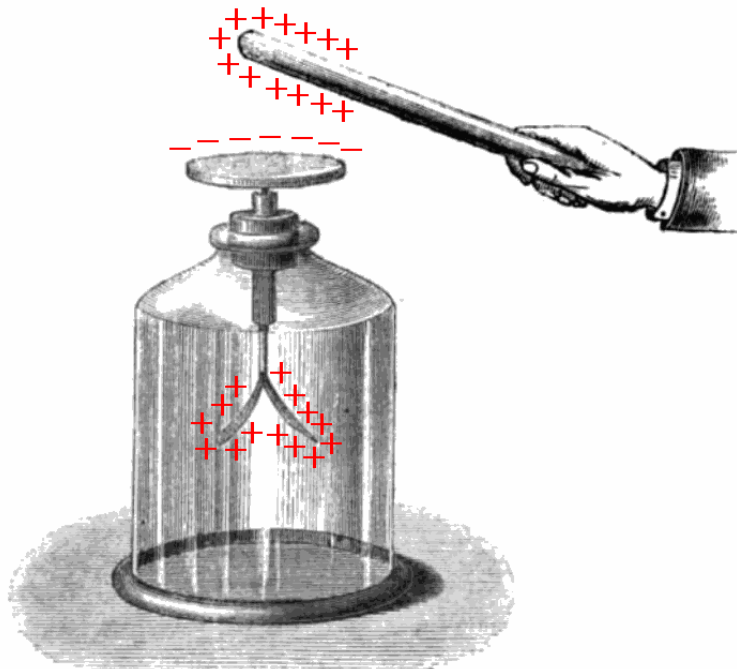


Figure 5.32 – Inducing charge separation in a gold-leaf electroscope [315]

The presence of charge near a conductive plate induces charge separation in the plate (§3.2.1.1.1) and vertical shaft with gold leaves attached to it (this assembly is isolated from ground using a cork stopper in a glass bottle). In this case, the positive charge in the wand attracts the outer shell electrons from the assembly, leaving the two gold leaves (opposite the charge source) depleted of electrons and therefore with a localized positive charge. Since both leaves have the same charge, they repel each other giving a mechanical and thus visual indication of the charge near the plate.

This chapter has set the backdrop to discuss the experimental work undertaken in the remaining chapters.

6. Scoping Trials

This chapter reviews early exploratory experiments and scoping trials which helped to define and prioritize subsequent in-depth experimental work.

The natural place to begin exploratory trials was where previous research left off. The first focus of this chapter was to analyse samples which were produced at the very end of the Custom-fit project (EU FP6 Integrated Project, Contract no. 507437), but were never adequately analysed. Next, the capability and feasibility of using EP in an inert atmosphere was explored for comparison with competing AM techniques for thermoplastics (such as polymer powder bed fusion). Preliminary trials on a variety of printers and toners were then undertaken in order to vet the inherited SLP methods and materials, and understand potential opportunities.

6.1. Further Analysis of Legacy Samples

In order to establish a broader foundation for the experimental work in this and subsequent chapters, further analysis on existing samples was performed. Several sequestered samples were made available courtesy of Wimpenny and the Custom-Fit project.

The legacy samples were produced by SLP (§4.4.5.3) or EMB powder coating (See §4.4.5.2) techniques *without* an electrostatically assisted final transfer. In contrast to the samples produced using the SLP rig during the Custom-fit project, those produced by the EMB coating process exceeded the theoretical height limit of 1-3mm as proposed by Kumar and Dutta [261].

The intent of analysing the samples was to observe any differences in the layer formation (consistency of surface quality and deposited thickness) between the SLP and EMB samples to identify factors that may have contributed to the improved build height of the EMB produced sample.

6.1.1. Manufacture of Legacy Samples

All samples described in this section were produced previous to the commencement of this study.

Sample 6-1 The Largest Volume SLP Sample from Custom-fit

Sample 6-1 (Custom-fit sample 081125.10:17), shown in Figure 6.1, was a bespoke helmet insert, and the largest volume sample produced using the SLP Rig during the Custom-Fit project. It was printed using a toner prepared from Somos 201 and fused at 120-130°C onto a glass build platform according to the SLP build process described in §4.4.5.3 [61]. The sample was abandoned after more than 200 prints because it should have had a flat upper surface with uniform height (thickness) across the entire specimen, and it did not [316]. A “corrugated” effect had

developed at its upper surface with ridges and valleys parallel to the platform motion and perpendicular to the final transfer roller applying the powder onto the substrate [316].

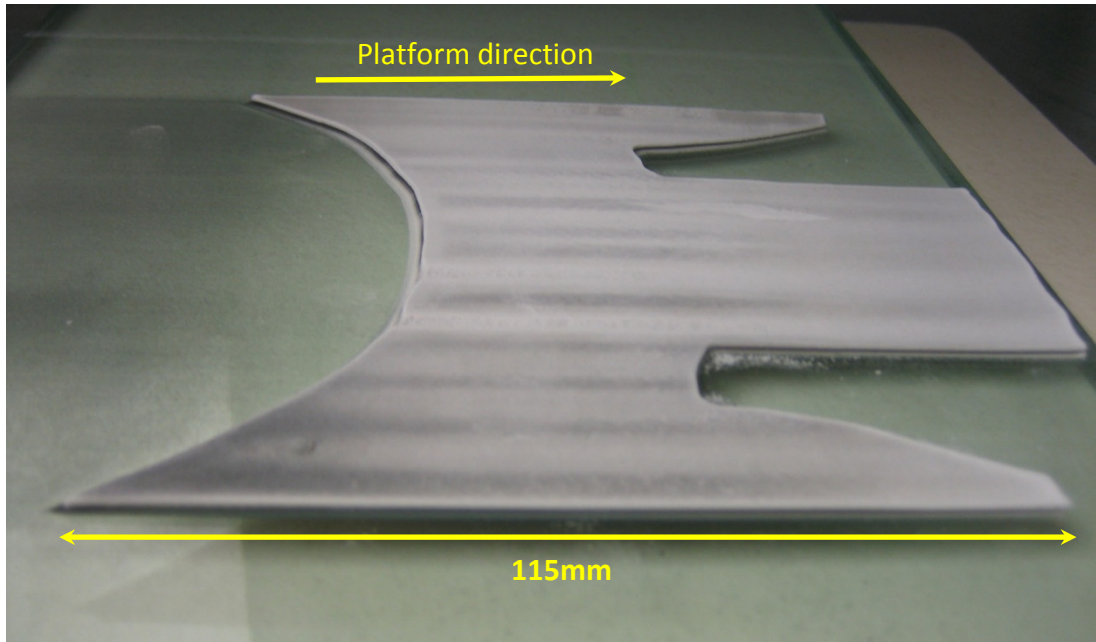


Figure 6.1 – Sample 6-1, a bespoke helmet insert (the largest volume SLP sample produced in the Custom-Fit project)

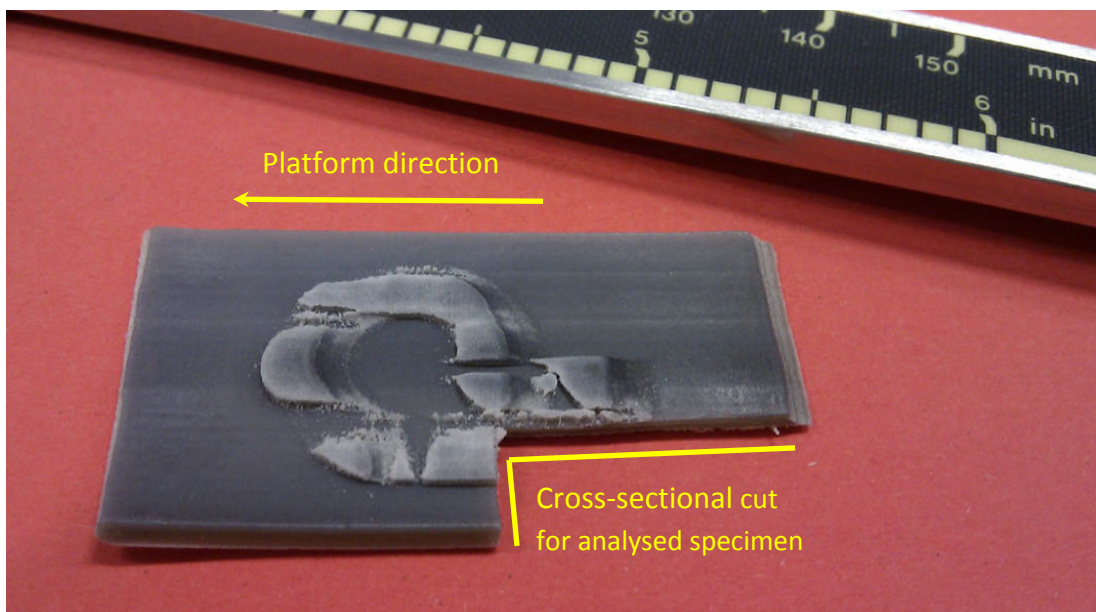


Figure 6.2 – Sample 6-2, the tallest SLP sample from the Custom-Fit project (© Society for Imaging Science and Technology [244])

Sample 6-2 The Tallest SLP Sample from Custom-fit

Sample 6-2 (Custom-fit sample 081125.15:11), shown in Figure 6.2, was produced on the SLP rig using a toner prepared from Somos 201 and fused at 120-130°C [61] as per the build process described in §4.4.5.3. The intent of the sample was to benchmark the maximum sample height that the SLP rig was capable of at that time. No taller sample was produced on the SLP rig during the Custom-Fit project.

The rectangular base was initially printed to a height of approximately 1.6mm in just under three hours when the printing process was stopped due to waviness or corrugation at the upper surface of the part which arrested uniform increase in sample thickness. After a cooling period of one hour, printing was resumed [316]. The top surface of the model was reheated slightly in excess of 130°C and an additional ~0.7mm was added in the semi-legible form of a smeared Custom-fit logo. Ultimately, the continually deteriorating upper surface quality obliged the researchers to abort the build. Regrettably, no count was made of the number of printed layers (as the build process was only semi-automated at that time), however, it was estimated (based on print cycle time) that it was in excess of 150 on the initial build with at least an additional 60 prints on the resumed build. Based on the estimates, the average layer thickness would have been around 10µm, however the researchers suspected that the layer thickness may have been greatest in the initial layers and diminished throughout the build [316].



Figure 6.3 – Sample 6-3, EMB sample from Custom-Fit project exceeding the theoretical height limitation proposed by Kumar and Dutta in [261]

Sample 6-3 EMB Sample Exceeding the 3mm Height Limit

Sample 6-3 (Custom-fit 080000.00:00), shown in Figure 6.3, was made by the modified EMB powder coating process by CTG PrintTEC GmbH (Alsdorf, Germany) as described in §4.4.5.2 using epoxy powder deposited onto an aluminium substrate.

Unfortunately the tallest laser printed sample in the public domain (Figure 4.32) was not available for further analysis.

6.1.2. Analysis of Legacy Samples

All analysis performed on the legacy samples was undertaken as part of this research.

Sample 6-1 (the largest volume SLP sample) – was inspected using a structured white light 3D scanner (Model ATOS, GOM GmbH, Braunschweig, Germany) and analysed using GOM Inspect v7 SR2

software. It is noteworthy that the rubber-like compliance of this material precluded the use of contact surface roughness measurement (such as Talysurf) without damaging the sample, therefore it was avoided.

Sample 6-2 (tallest SLP sample) – A cross-sectional cut from Sample 6-2 produced a specimen including the layers deposited in both the initial and resumed build (as shown in Figure 6.2) which was mounted in epoxy (Epo-thin, Buelher UK, Coventry, UK), and ground and polished using 9, 3 and 1 μ m grinding media in preparation for optical microscopy (Model DM4000 M, Leica Microsystems CMS GmbH, Wetzlar, Germany) and SEM (Model Σ IGMA, Carl Zeiss SMT AG, Oberkochen, Germany). In preparation for examination by SEM, the samples received a carbon sputtered coating and silver dag. A generous amount of silver dag was required on the upper surface around the area to be viewed to help dissipate charge (as evident in Figure 6.11).

Sample 6-3 (EMB sample) – A cross-sectional specimen was fractured off of one end of Sample 6-3 which was mounted in epoxy (Epo-thin, Buelher UK, Coventry, UK), and ground and polished using 9, 3 and 1 μ m grinding media in preparation for optical microscopy (Model DM4000 M, Leica Microsystems CMS GmbH, Wetzlar, Germany) and SEM (Model Σ IGMA, Carl Zeiss SMT AG, Oberkochen, Germany).

6.1.3. Results and Discussion of Legacy SLP Sample Analysis

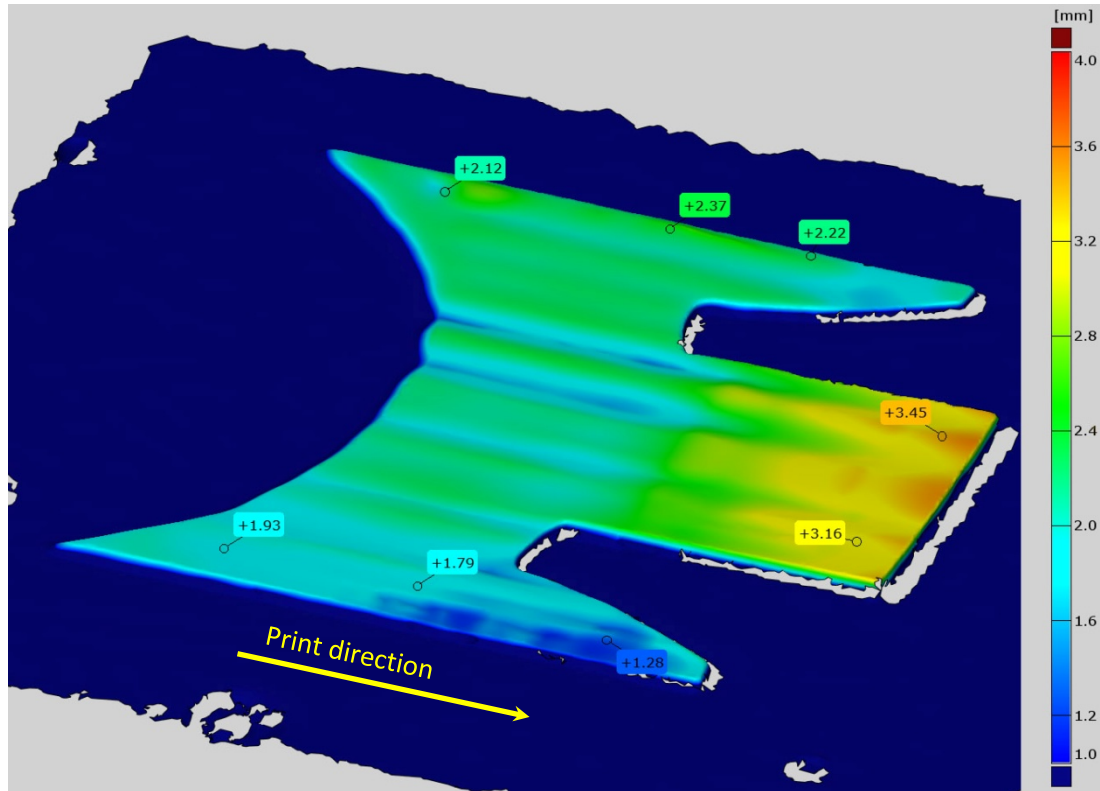


Figure 6.4 – Result from dimensional analysis of Sample 6-1 (largest volume SLP sample)

Sample 6-1 (largest volume SLP sample) – Figure 6.4 shows the magnitude of waviness which had developed at the upper surface of Sample 6-1 was in excess of 2.0mm from crest to trough. The magnitude was so great that it made conventional surface roughness evaluation (such as Talysurf or vertical scanning interferometry) unpractical. It further revealed that the print height fluctuations were not concentrated only at the edges, as has been documented by previous researchers [120, 201, 261, 271, 317], but were distributed generally across the entire upper surface with the deepest troughs located toward the centre of the sample and parallel to the print direction. This distribution of

defects means that it is unlikely they were caused by solid area fringing fields (§3.4.3.1).

Sample 6-2 (tallest SLP sample) – Figure 6.5 shows a side by side 200x optical microscope and 200x SEM image of the cross-section (images from the upper portion of the sample near the middle of the longest cross-sectional cut shown in Figure 6.2) of the mounted specimen taken from Sample 6-2. In both images, the most obvious feature is the interface between the initially deposited layers and those deposited after the build was resumed. Figure 6.6 shows this interface in greater context and labels where the initial build stopped and the resumed build began.

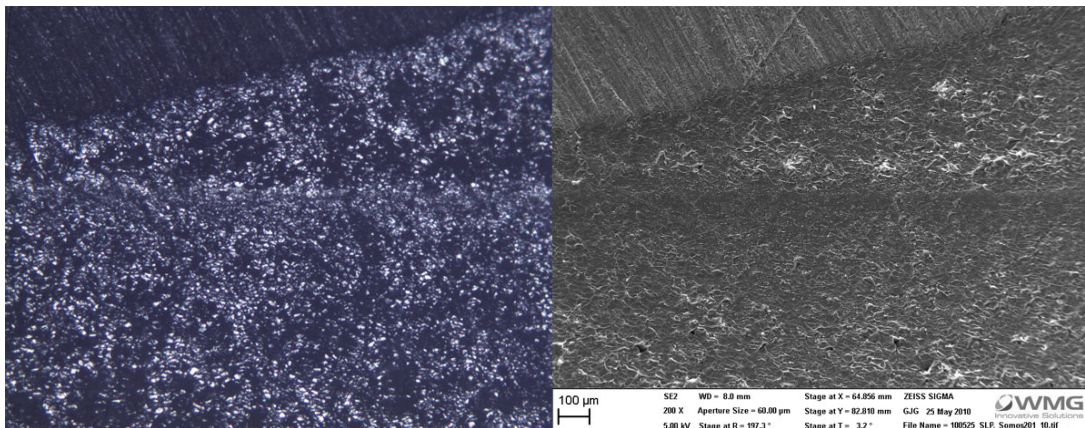


Figure 6.5 – Optical and SEM (both at 200x) comparison of the resumed build interface on Sample 6-2 (tallest SLP sample)

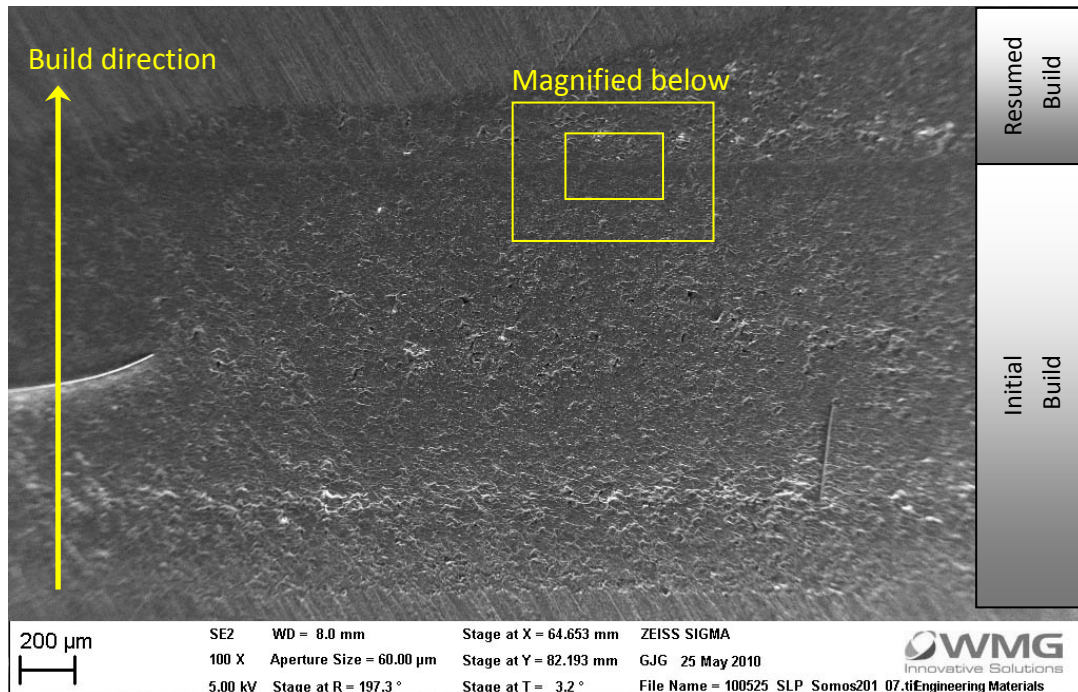


Figure 6.6 – SEM (100x) of cross-section from Sample 6-2 (tallest SLP sample) showing the layers which were deposited initially and those deposited in the resumed build

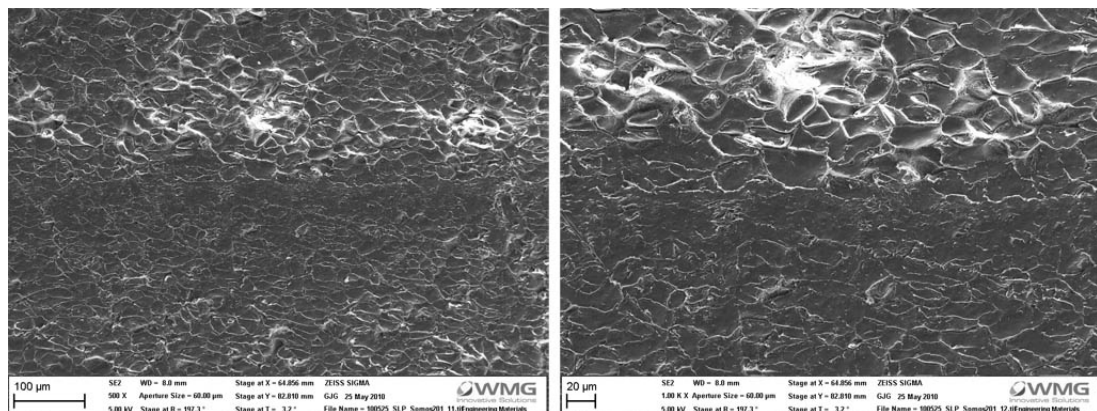


Figure 6.7 – SEM of the interface between the initial and resumed build in Sample 6-2. Left image at 500x and right image at 1,000x

Examining the interface at 500x and 1,000x magnification (Figure 6.7) reveals larger grains in the reheated layer(s) which typifies the crystallization tendencies of PBT based materials [318].

Although some stratification is evident in the sample (presumably due to the variability of the operator dependent thermal management) apart from the aforementioned interface, it was not possible to identify the interface between individual layers. Unfortunately, it seems that the recrystallized grain size exceeded the layer deposition thickness and therefore precluded the measurement of individual layer thickness consistency [318-320].

It is noteworthy that the compliance or rubber-like nature of the Somos 201 material may have contributed to reducing or eliminating any evidence of non-uniform application of pressure during the production of the sample. Additionally, the relatively low toner charge (compared to conventional toners) may have enabled development of thicker layers on the photoreceptor as explained by equation (3-9).

6.1.4. Results and Discussion of EMB Sample Analysis

Sample 6-3 (EMB sample) – The most noteworthy feature identified in the optical and SEM inspection of the cross-section of Sample 6-3 was the presence of three rows of spherical particles as shown in Figure 6.8. Unfortunately, as with the SLP specimens it is not possible to identify individual layers in the fused epoxy.

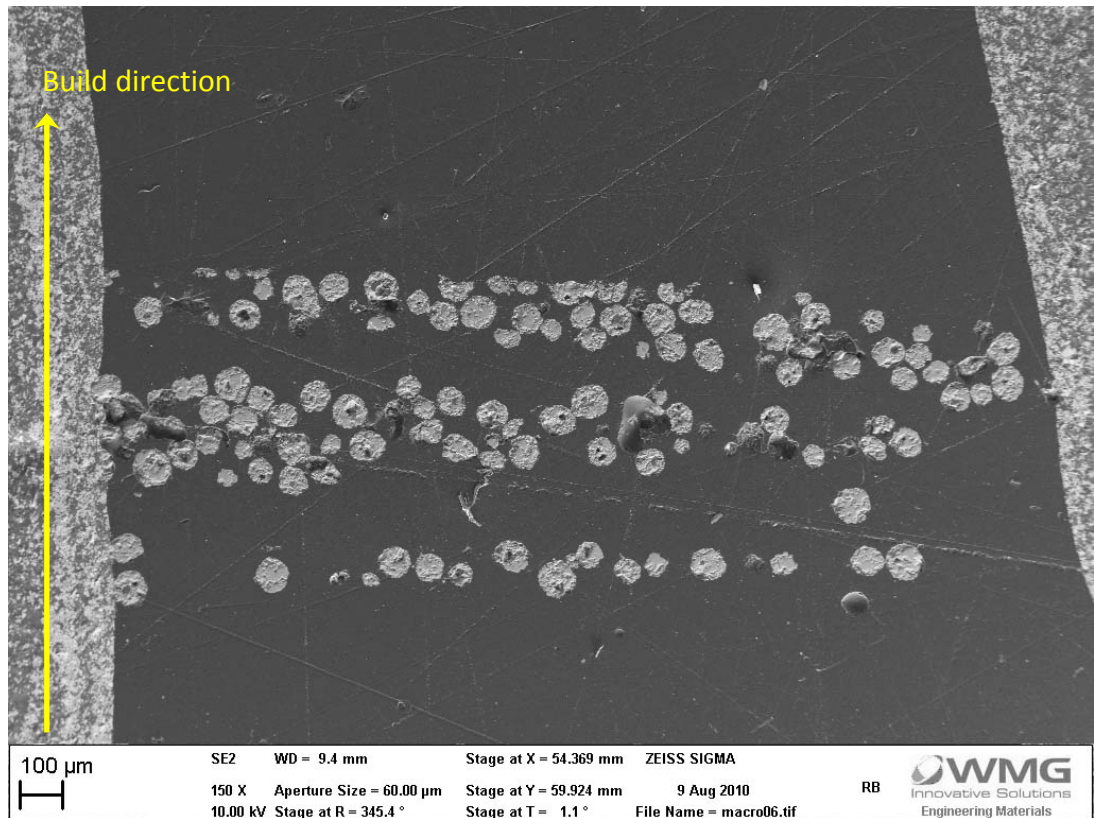


Figure 6.8 – SEM image of cross-section through Sample 6-3 produced by EMB technique

Logically, the most likely source of particle contamination in the layers was the carrier particles which can inadvertently be transferred out of the printer along with the toner particles if the field strength between rollers is too high, due to excessive voltage or the roller gaps being set too narrow [321].

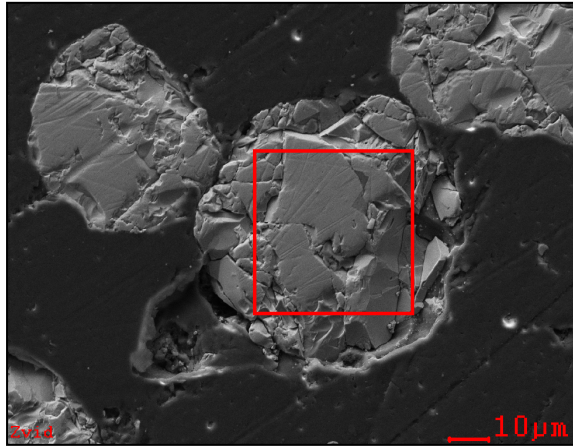


Figure 6.9 – EDS of contamination particle found in Sample 6-3 (EMB sample)

Table 6.1 – EDS of contamination in Sample 6-3

Element	Orbital	Wt%	At%
O	K	19.94	53.44
Nd	M	33.76	10.04
Si	K	01.29	01.96
Fe	K	45.01	34.56
Matrix		Correction	ZAF

Energy dispersive X-ray spectroscopy (EDS) analysis of the contamination (see Figure 6.9) indicated a significant oxygen, neodymium and iron content as shown in Table 6.1 which correspond to typical magnetically permeable core compositions [322, 323] and the manufacture’s data sheet [324]. Furthermore, particle sizes observed in the images correlate to the specified 60-80 μ m average particle size for carrier to be used with the epoxy powder [324].

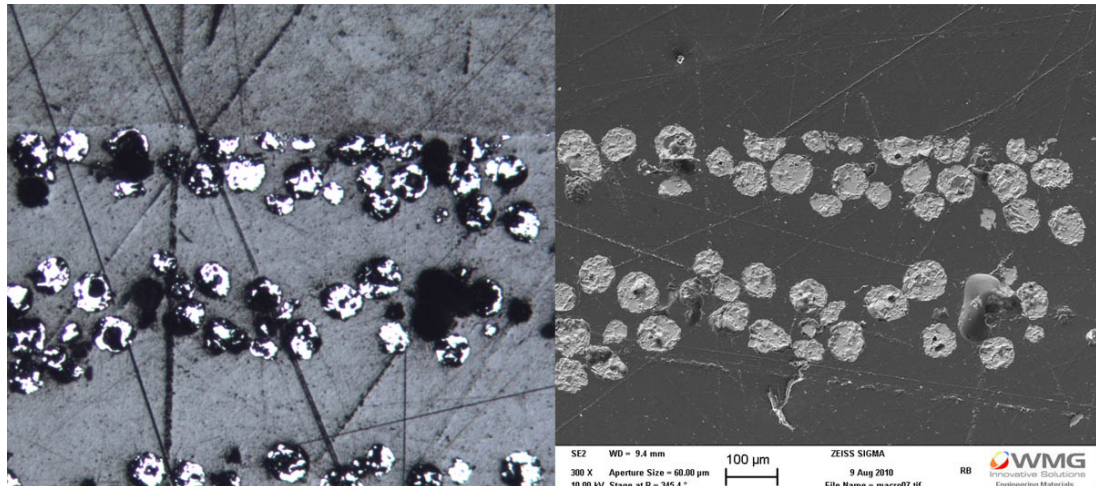


Figure 6.10 – Optical and SEM comparison (both at 300x) of the contamination particles in Sample 6-3 (EMB sample)

The optical portion of Figure 6.10 shows a change in colour above the carrier contamination which may indicate an interruption to the deposition process resulting in two distinct thermal histories (similar to the interface between the layers printed initially and layers printed after resuming the build in the tallest SLP sample as shown in §6.1.3). This coupled with the absence of carrier particles in subsequent layers suggests that the build process was interrupted in order to adjust printer parameters (transfer voltage or roller gaps) to avoid further contamination of printed layers. This adjustment would be standard practice when such contamination is experienced according to Schoenberger [321].

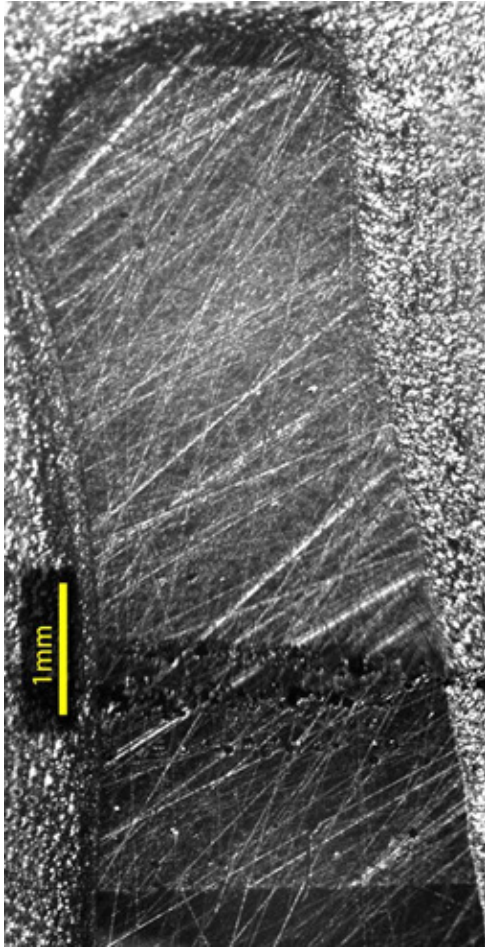


Figure 6.11 – Carrier banding evident in Sample 6-3 (EMB sample)

Both logic and analysis point to the conclusion that the contamination was carrier particles. Proceeding on this basis supports further observations about individual layer formation. Assuming these carrier particles were printed in three consecutive layers, Figure 6.8 reveals that each layer was between 100 and 200 μm thick and not perfectly uniform in flatness or thickness. Although the thickness is outside the range of controlled EMB coating [302], it follows that if the field strength were sufficient to draw carrier beads off of the magnetic

roller, then it could also have developed layers which were thicker than expected. Figure 6.11 also indicates that the contaminated layers (visible as a dark pitted band in the lower third of the sample) were not perfectly parallel to the substrate, or the top surface.

6.1.5. Conclusions From Legacy Sample Analysis

The analysis of the legacy samples yielded a number of general conclusions common to all samples and others specific to each manufacturing method.

Drawing from the results of all three samples supports the following general conclusions:

- When the thermal management was consistent, the solidification behaviour of epoxy and PBT made it difficult to identify individual layers after deposition and solidification using conventional optical microscopy and SEM.
- Therefore no evidence to either confirm or deny that the height of each layer decreased as the build grew further away from the grounded platform as hypothesized was observed.
- Where surface quality defects were introduced they were exaggerated with each subsequent layer until they covered an estimated 40% of the surface, making the deterioration of surface quality an inhibitor for overall height growth.
- The sample charging which occurred in the SEM prior to the more generous application of silver dag highlights that the non-conductive materials used in toner accumulate charge which is not quickly depleted.

The following conclusions can be drawn from the results of samples produced by SLP: Sample 6-1 (largest volume SLP sample) and Sample 6-2 (tallest SLP sample).

- The surface quality of samples produced by SLP began deteriorating after the sample exceeded 1mm high (Figure 6.4), as predicted by Kumar and Dutta [261].
- Since the corrugation defects were distributed generally on the upper surface (See Figure 6.3 and Figure 6.4) (and not just at the

edges), the defects cannot have been caused by fringe fields (§3.4.3.1) developing at the edges of large solid area development.

The following conclusions are supported by the results of analysing Sample 6-3 which was produced using the EMB coating process.

- Taking the pitch of the rows of carrier particles (See Figure 6.5) in the EMB sample as the average layer thickness indicates that the EMB sample was composed of far fewer layers than either of the SLP samples. If the height inhibiting factor(s) relate to the number of layers deposited, then we cannot assume that the EMB process is immune to the same phenomenon that is limiting the SLP samples.
- The thickness of each layer developed is much thicker than the monolayer or double monolayer typical of laser printing.

6.1.6. Unanswered Questions from Legacy Sample Analysis

The analysis of legacy samples also identified many unanswered questions which corroborated questions arising from the literature survey (§4.7) which led the direction of this research.

Although the transfer method used for all the legacy samples was theoretically the same, the difference in deposited height between SLP and EMB produced samples leaves the following questions unanswered:

1. Was one of the primary factors influencing layer thickness and stack height something induced by the use of a photoreceptor (which was used in SLP, but was not used in EMB)? (See §7.3)
2. Was the difference of heating influential?
 - a. Heating method: infra-red heater versus oven (See Appendix C)
 - b. Target layer consolidation temperature: 120°C (infra-red) versus 150°C (oven)
3. What was the effect of the substantially lower contact pressures used in the SLP process compared to the EMB process? (See Appendix B)
4. Did an inherent difference in the toner material (particle size, dielectric constant, etc.) influence its deposited height? (See Sample 8-5, Sample 8-14)
5. Was the longer time delay between layers (due to off-rig oven heating of layers) or the associated manual handling of the sample influential? (See §4.4.5.2)
6. Were the surface imperfections a result of charge? (See §7.1.2.1)
 - a. What happened to the surface potential as parts were being built (i.e. is each layer being fully neutralized)? (See §7.1.2 below onwards)
 - i. How does heating influence that charge, if present?
 - b. Was a surface charge accumulation on the substrate inhibiting the transfer of fresh toner onto it (possibly in proportion to the amount of toner already accumulated). (See §7)

- i. If that is the case, can surface quality (lack of roughness) be used as a proxy for accumulated charge imbalance? (See §7.2)
7. Why was the surface waviness parallel to the platform direction?
 - a. Could the waviness be a result of photoreceptor, or transfer roller imperfections? (See Appendix B)

6.2. Assessing the Performance of EP in Inert Atmospheres

In order to produce polymers with the maximum mechanical properties (as laid out in the objectives of this research §1.2), it was critical that they be fused in optimum conditions. Owing to the standard practice of operating powder bed fusion in an inert environment, such as nitrogen or argon, the sponsor desired to determine whether EP would work in an inert atmosphere. The size and scale of the SLP rig or even a large office dual component printer (such as the Ricoh Aficio CL7000) made it impractical to put them in a vacuum chamber, however it was determined that a small desktop laser printer could be.

These trials were reported in detail in the last half of a conference paper by the author under the heading "Deposition in Inert Environments" which is reprinted in the Annex: Additive Manufacturing by Electrophotography: Challenges and Successes [260].

The primary finding was that for corona based charging functions to work in the printer, a gas medium is required so it can be ionized into its

component parts. It was shown that the printer could feasibly operate in a nitrogen environment if necessary.

This trial provided valuable insight into the nature of the charging processes in EP, however it was determined that ambient operation was preferred if viable. Since the mechanical performance of specimens made on the SLP rig in ambient conditions was on par with injection moulded properties [260], it was determined that operation without an inert atmosphere would be pursued for the duration of this research.

6.3. Evaluating Printers

Owing to the defects and height limitation of samples produced previously on the SLP rig (using what were essentially prototype printers, §4.4.5.3) pertinence required evaluation of multilayer printing on alternative printers in order to establish whether the problems experienced were specific to the prototype nature of the printers or to toner-based systems generally. The printer exploration also facilitated the exploration of toner candidates (§6.4). For this purpose both single and two-component printers were used in these scoping trials.

6.3.1. Two- component Printer Evaluation

Two two-component printers (Aficio CL7000, Ricoh Company Limited, Japan) were used for evaluating multilayer and alternative toner material printing for comparison with the CTG PrintTEC GmbH printers on the SLP rig.

6.3.1.1. Multilayer Height Limit of Printing on Paper

Demonstrations such as the one described herein have doubtless been repeated dozens of times as an early feasibility check when considering the potential of EP for functional multilayer printing.

Sample 6-4 Multilayer Two-component Print on Paper

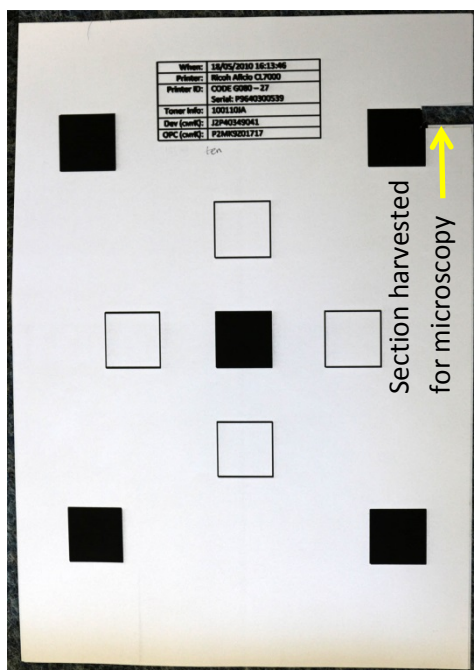


Figure 6.12 – ASTM F2036 pattern printed on paper; an example from the Sample 6-4 series (Multilayer Printing on Paper)

Sample 6-4 is an example from a series of samples printed using a Ricoh Aficio CL7000 (Ricoh Company Limited, Japan) on 80 gram paper using a commercially available aftermarket black toner with ceramic pigments (normally printed onto transfer paper and then transferred to decorate ceramic and glass objects) (C-CLC, ZEAC, Switzerland). Reasons

for using a non-standard toner are explained in §6.4.1. The ASTM F2036

pattern was printed 1,2,3,4,5,10 and

15 times on each sheet of paper by feeding the sheets of paper through the printer multiple times (Figure 6.12). Attempts to re-circulate the paper more than 15 times resulted in paper jams. After printing, a cross-sectional cut was made through the solid printed areas and evaluated using optical microscopy. Measuring print thickness using a CMM was also considered, however it was difficult to measure single layer differences in

print thickness in prior research [212], so it was not pursued. Cross-sectional optical microscopy of the samples printed once and fifteen times is shown in Figure 6.13 for side by side comparison. A cross-section through a representative sample for each repetition in the entire series is shown in Figure 6.15 (Note: lines and white boxes in this figure show measurements made by optical microscopy which are graphed in Figure 6.14).

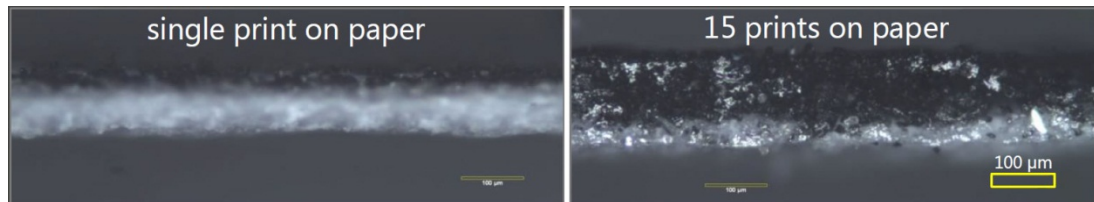


Figure 6.13 – Cross-sectional optical microscopy from the Sample 6-4 series, comparing the stack height between single (left) and 15 layer prints (right) (© Society for Imaging Science and Technology [244])

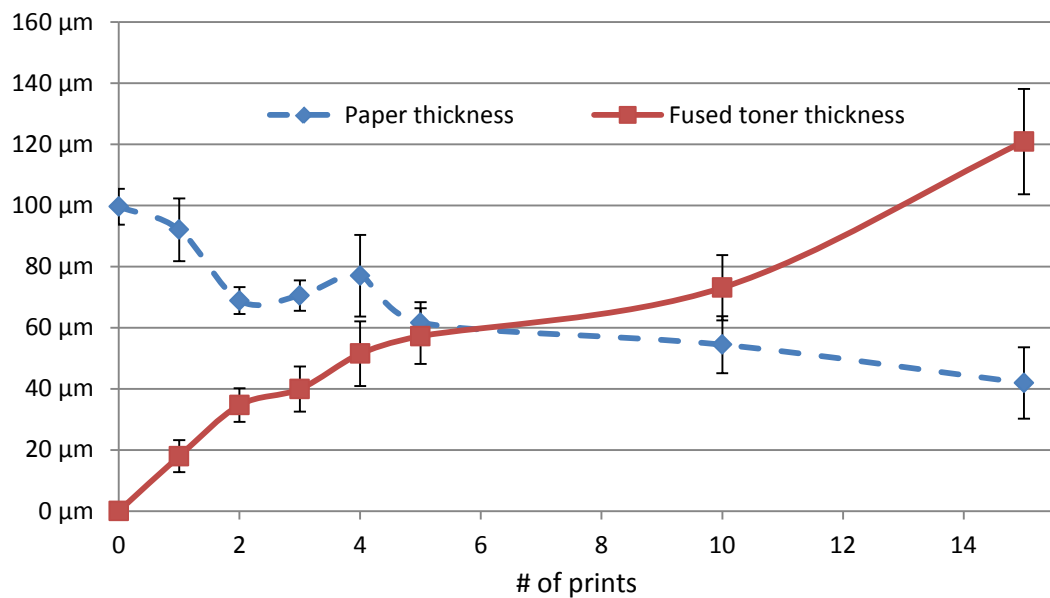


Figure 6.14 – Graph of the Sample 6-4 series showing the paper thickness versus the fused toner thickness

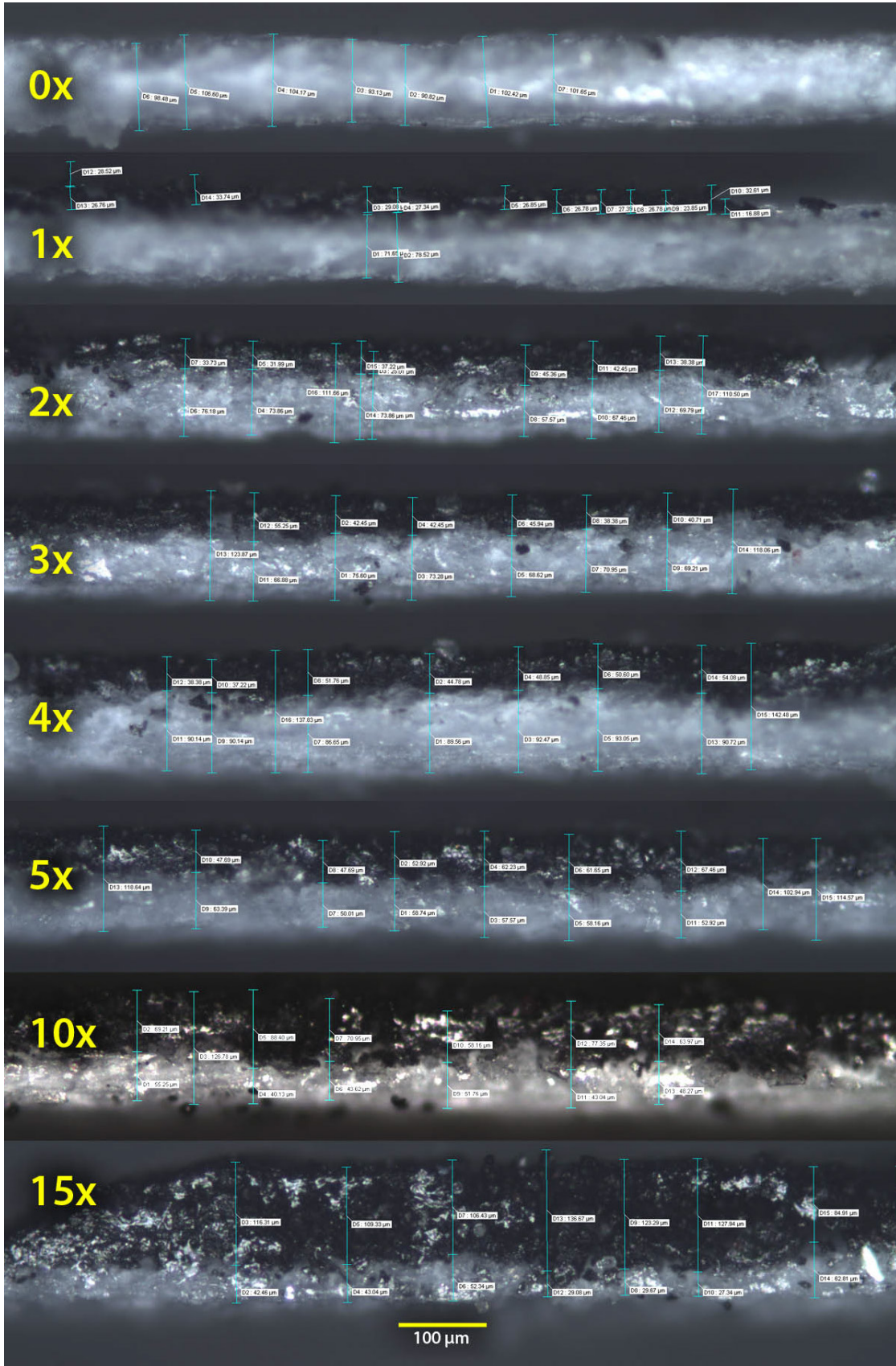


Figure 6.15 – Cross-sectional optical microscopy comparison of the fused toner height from the entire series of Sample 6-4 at 1,2,3,4,5,10 and 15 prints (Note: lines and boxes in this figure show optical microscopy measurements graphed in Figure 6.14)

A single printed layer resulted in an average print thickness of $17.9 \pm 0.3\mu\text{m}$ while fifteen accumulated layers of toner resulted in fused toner thickness of $120.9 \pm 0.9\mu\text{m}$ as shown in Figure 6.13.

Figure 6.14 is a graph showing the change in paper thickness versus the thickness of the toner fused on it as the number of prints increased. The error bars are \pm the standard deviation (because the standard representation of $\pm\sigma/n^{1/2}$ made the error too small to be seen on the graph). It is noteworthy that the thickness of the paper was reduced from $99.5 \pm 0.8\mu\text{m}$ down to $41.9 \pm 0.6\mu\text{m}$ over the course of 15 prints. The reduction in thickness was predominantly caused by the heat and pressure applied during the fusing process (§3.4.4.3). This downward trend is also reminiscent of the drop in mass experienced by Banerjee when recirculating paper through the printer multiple times [211]. Banerjee attributed this mass reduction to the vaporization of moisture in the paper. The observed reduction of paper thickness in this case may also be an additional manifestation of the same dehydration phenomenon.

The increasing toner thickness was expected, however, the initial five layers printed indicated a trend of diminishing contribution to the cumulative height with each additional layer. This could be explained by diminishing field strength in the transfer nip, owing to the added material, which acts as an insulator to the field strength (as discussed in §4.3.1.3). This early trend reinforces the suspicion formed in prior research that layer thickness may diminish with increasing height (at

least for conventional electrostatic transfer). A researcher at Sintef (§4.4.4) confirmed similar observations when they printed ceramic support material in the MPP process [309]. At a minimum, it indicates that this type of a trend is not specific to the two-component printers used on the SLP rig.

If this trial had been undertaken only from 1 to 5x printed layers, then the discussion would be over. However, the samples printed 10 and 15 times do not continue the same trend of diminished rate of contribution to toner height. The exact cause of the apparent recovery to a more stabilized contribution to toner height by each layer printed for the latter two samples is unclear. It may be attributed to improved fusing efficiency, due to elimination of moisture in the paper. Alternatively, it may be a false measurement which the methodology is susceptible to. For example, the greater thickness of fused toner may have sheared during sectioning to give the impression of being thicker than it really is at the cross-section. Measuring the cross-section of the paper without overlying toner (the unprinted areas) on the sample printed 15x averages $68.8 \pm 2\mu\text{m}$ (compared to $42 \pm 3\mu\text{m}$ with overlying toner as plotted in Figure 6.14) reinforcing this notion, however it needs further substantiation. Otherwise it could have been caused by factors not anticipated in this study.

It was envisaged that these unanswered questions could be resolved by subsequent trials on the SLP rig where paper (including the moisture it is prone to absorb) would not be a factor, change in part thickness would be

measured each layer (§5.7.1.4.1), and the number of layers deposited would not be limited to 15.

6.3.1.2. *Post- print Assembly and Consolidation*

Having demonstrated the maximum deposition thickness of fused toner possible on paper using a conventional printer (as shown in the previous trial), and indications from the previous trial that reinforce the self-limiting nature of conventional electrostatic transfer (§4.3.1.3), it was deemed judicious to explore an alternative (indirect) approach to produce parts from toner. This section is an aside to the remaining body of research presented herein.

The question of whether using an indirect printing route, where the layers would be printed using conventional printers and then stacked (assembled) and consolidated (fused or laminated) together into a part after printing, would be possible or practical was considered. This seemed to be a logical strategy for circumventing the field strength associated height limitations of direct layer-on-layer printing worth exploring. This trial was undertaken in connection with exploring potential ceramic-based toners as discussed in §6.4.1. For that reason, feasibility was evaluated for developing a furnace firing regime in which a stack of paper (or at least the coating layer from transfer paper) with laser printed green ceramic layers on each page could be burned away (eliminating the paper and organic materials) and sinter the remaining ceramic into a solid fired body.

6.3.1.2.1. *Repeatability of Image Registration*

The initial investigative step toward post-print assembly was to establish the repeatability of image registration on A4 paper, to understand the accuracy of alignment between layers that was possible with stacked sheets of paper.

To assess the repeatability of image registration, the same series produced for the previous trial was assessed using optical microscopy of the top surface at the corners of each of the four hollow boxes printed as part of the ASTM F2036 pattern.

Figure 6.16 compares a single print to the deviation in image registration of 15 prints layered on top of each other for the bottom right hand corner of the lower square in the pattern. The average line width nearly triples from $265 \pm 7\mu\text{m}$ after a single print to $781 \pm 7\mu\text{m}$.

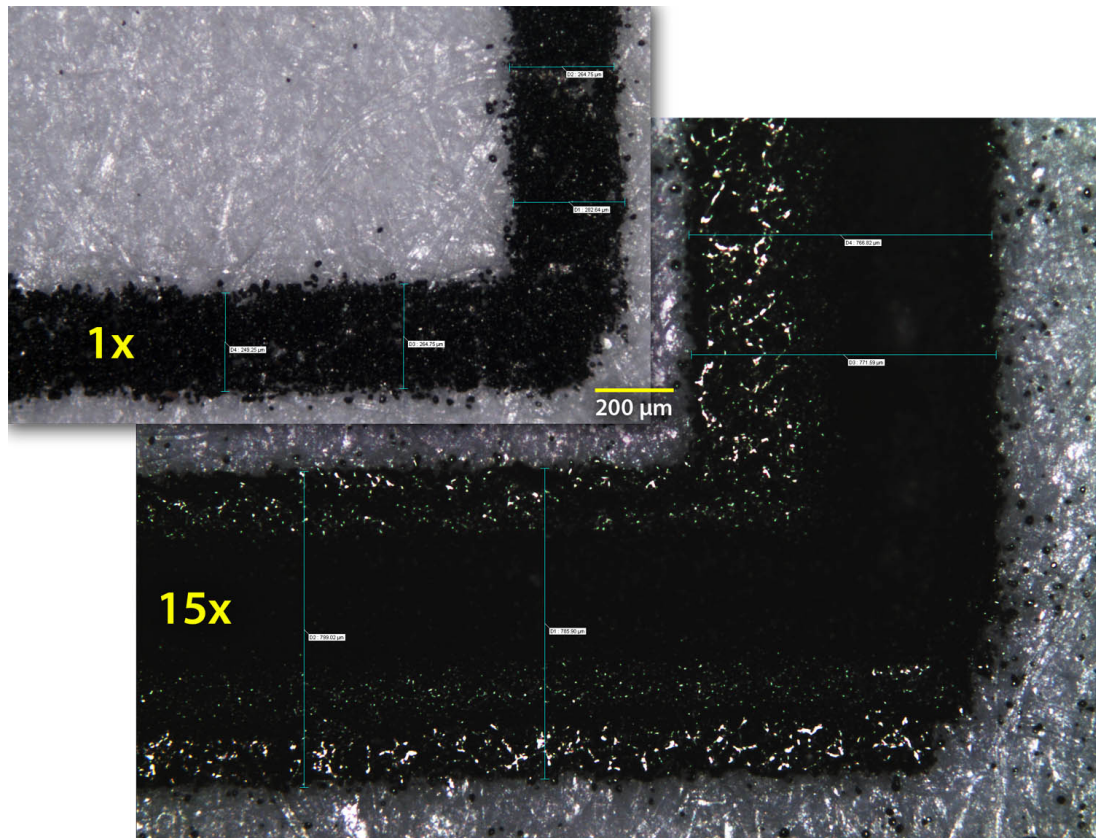


Figure 6.16 – Optical microscopy images from the Sample 6-4 series showing the deviation in image registration when the paper is recirculated 15 times

This preliminary study showed the locating of a $265\mu\text{m}$ wide feature within a $780\mu\text{m}$ wide boundary indicates a maximum shift of $515 \pm 14\mu\text{m}$ which points to an approximate placement repeatability of $258 \pm 7\mu\text{m}$ from a nominally defined position, which was deemed sufficient for further assessment.

6.3.1.2.2. Transfer, Stack and Sinter Commercial Ceramic Toner

Following on from the repeatability study (§6.3.1.2.1), a preliminary trial considering the feasibility of post-print assembly and consolidation was undertaken.

Sample 6-5 Post-print Stacking and Sintering of Transfer Paper

The same printer and toner were used to print the same pattern on 130g transfer paper (fotocal decal paper, Tullis Russell Coaters, UK). The transfer paper used had a coating of water soluble wax to facilitate removal of the printed ceramic toner for application onto any desired substrate. After printing, the solid squares in the ASTM F2036 pattern were cut out, the backing removed by partially dissolving the wax with water, and then applied to an 0.5mm thick alumina substrate (similar to the §5.5 specification) in single and double stacks (Figure 6.17).

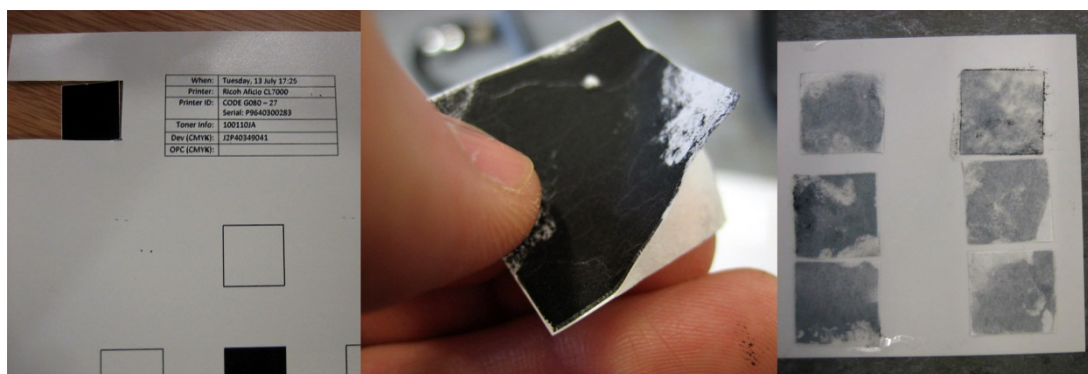


Figure 6.17 – Images showing the post-print assembly steps for Sample 6-5 prior to firing

In order to simulate the difficulty of outgassing through overlying layers, a second sheet of 0.5mm thick ceramic (alumina) was placed on top of the sample and put inside a furnace (Griffin Electric Furnace with Eurotherm controls, Griffin and George Limited, UK). The sintering profile from room temperature initially was a ramp rate of $1^{\circ}\text{C min}^{-1}$ up to 500°C and then $5^{\circ}\text{C min}^{-1}$ up to $1,000^{\circ}\text{C}$ (the maximum temperature of the furnace) and then held for 12 hours. After the 12 hour dwell at $1,000^{\circ}\text{C}$ the furnace was switched off and allowed to cool to room

temperature. The conservative initial ramp rate was intended to facilitate drying and allow safe burn out of binder and organics as used in previous research [325]. Although sintering a fully dense alumina typically requires a maximum temperature above 1300°C [326, 327], the maximum sintering temperature was limited by the availability of furnaces with suitable extraction to handle the relatively large outgassing expected during burnout. In spite of the limited maximum temperature, previous research [328] indicates that burnout of organics and relative densities up to 65% are possible at 1,000°C, which was sufficient for proof of concept in this case.

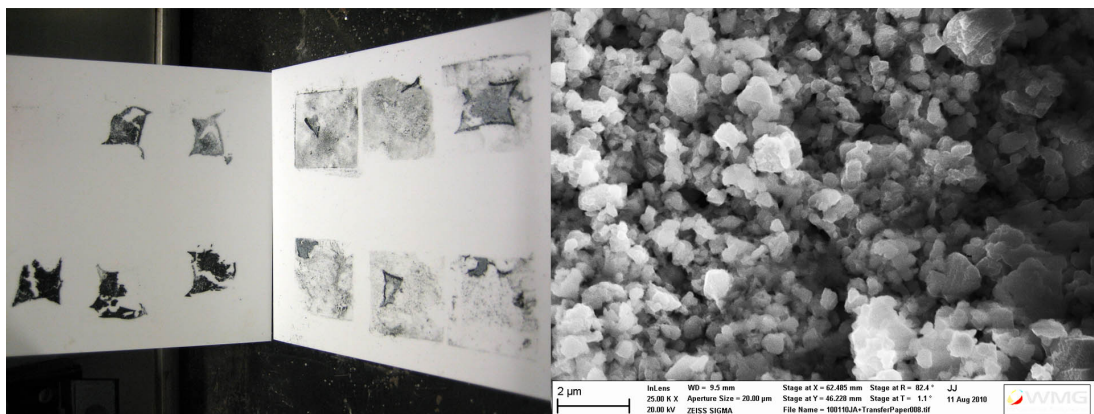


Figure 6.18 – Sample 6-5 after firing (left) and SEM image of resulting body (right)

After the furnace cooled, the sample was removed and the upper plate removed for visual inspection. A small fractured sample was carbon coated by sputtering and examined using a scanning electron microscope (SEM) (Model ΣIGMA, Carl Zeiss SMT AG, Oberkochen, Germany) in in-lens secondary electron (SE) mode, WD = 9.5mm, 20.0 kV and 25,000x magnification.

Figure 6.18 shows the results after firing which did not indicate a clean burnout (trapped ash content), nor any necking of the alumina particles to indicate the early stages of sintering (perhaps due to insufficient proximity with each other). The results of this trial were so poor, that the notion of burning away intermediate layers in between ceramic layers was called into question.

Table 6.2 – EDS of Fired Portion of Sample 6-5

Element	Orbital	Wt%	At%
O	K	33.97	58.16
Al	K	12.52	12.71
Si	K	05.68	05.54
Ca	K	01.05	00.72
Cr	K	11.78	06.21
Fe	K	15.52	07.61
Co	K	19.47	09.05
<i>Matrix</i>		Correction	ZAF

EDS analysis of a fired portion of Sample 6-5 (Table 6.2) showed the presence of oxygen and aluminium, but substantial wt.% of other elements suggested sources of “contamination”, at least partially explained by the inclusion of magnetic pigment to achieve the black colour. Further toner analysis (reported in §6.4.2.1) suggested that the toner lacked sufficient density of ceramic content to result in a solid body.

6.3.1.2.3. Stack and Sinter Bulk Alumina Between Transfer Paper

The toner analysis and understanding gained from Sample 6-5 led to the conclusion that the commercial “ceramic” toner did not have sufficient ceramic content to facilitate printing of green parts which could be sintered into a monolith. Therefore the next trial used pure alumina powder, with thicker layer deposition, to evaluate the feasibility of post-print assembly and sintering.

Sample 6-6 Stack and Sinter Bulk Alumina between Paper

Prior to preparing a pure ceramic as a toner (which is reported in §6.4.1), a bulk deposition (not printed) of alumina powder (CT 19 FG Calcined Alumina, Almatis, USA) with average particle size of $\sim 6\mu\text{m}$ onto transfer paper was undertaken by wetting paper squares and then “dipping” them into the ceramic powder to coat them with alumina powder. Two stacks, three squares high (ceramic coated side down) were assembled onto a ceramic plate, pressed with a 0.5kg weight, and allowed to dry. The assembly was then fired using the same regime and equipment as before (§6.3.1.2.2).



Figure 6.19 – Sample 6-6 assembled stack (left) and result after firing (right)

After the furnace cooled, the sample was removed and the upper plate removed for visual inspection. Portions of the sample were lightly sintered together but highly fragile, while the remainder was essentially a powder cake. A sample of one of the sintered portions was carbon coated by sputtering and examined using the SEM in in-lens SE mode, WD = 9.5mm, 20.0 kV and 10,000x magnification as shown in Figure 6.20.

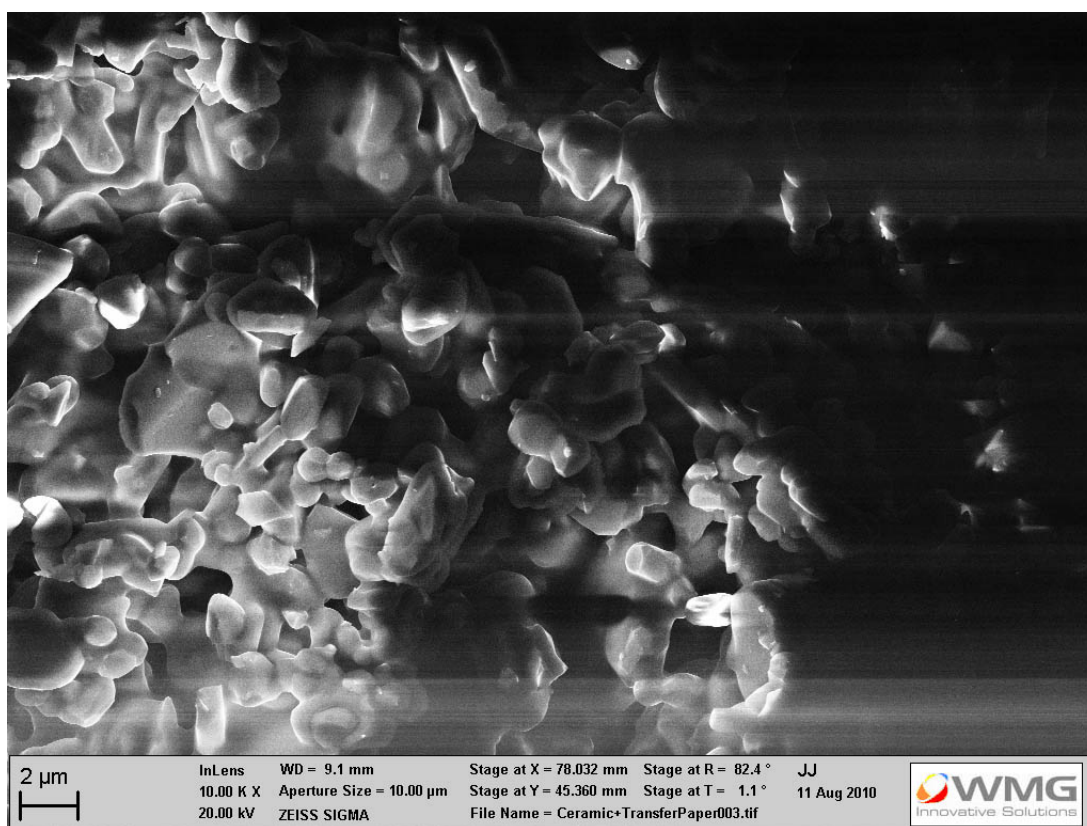


Figure 6.20 – SEM of a sintered portion of Sample 6-6 showing light necking

The SEM image confirms that the maximum sintering temperature was too low to achieve a substantial degree of particle consolidation; however necking and particle rounding are evident. The aberrations in the SEM image indicate the sample material had poor conductivity.

EDS analysis of the lightly sintered portion of Sample 6-6 (Table 6.3) showed the dominant presence of oxygen and aluminium as expected with traces of chlorine (Cl) and silver (Ag). The chlorine probably came from the bleaching process in the paper.

Table 6.3 – EDS of Fired Portion of Sample 6-6

Element	Orbital	Wt.%	At%
O	K	47.45	61.04
Al	K	48.11	36.69
Cl	K	03.65	02.12
Ag	L	00.79	00.15
<i>Matrix</i>		Correction	ZAF

These results indicated the possibility of achieving post-print assembly and firing of ceramics; however confirmation of this potential would require sintering at higher temperatures.

6.3.1.3. Conclusions from Two- Component Printer Trials

These trials undertaken on an office based two-component laser printer have confirmed behaviour observed on the SLP rig two-component printers (CTG PrintTEC GmbH), including variation in the layer height when directly printing layer-on-layer. These results indicate that changing layer thickness was not specific to the CTG PrintTEC printers only. The paper thickness reduction attributed to dehydration effects was also observed.

In order to fully assess the varying layer height phenomenon, it is necessary to print more than 15 consecutive and stacked layers onto a substrate, thereby necessitating the need to use the SLP rig or some alternative means of achieving the same.

In light of the transfer challenges, the feasibility of a two-step process for printing layers using conventional printers and then executing a post-print assembly and consolidation step was undertaken. Despite the fact that this represented a logical strategy for circumventing the field strength associated height limitations of direct image-on-image or layer-on-layer printing, it proved more difficult in practice than originally envisaged.

6.3.2. Single Component Printers

Although the flexibility of two-component printing was desirable in the SLP process (§5.2), the empirical and iterative nature of pairing toner with appropriate carriers made screening of large varieties of materials for toner impractical. Therefore, single component printing was used for initial screening of candidate toner materials as described in the remainder of this chapter.

6.4. Exploring a Range of Toner Composition

The potential flexibility of toner formulation for laser printing provided an opportunity to revisit prior toner materials and explore further materials not yet researched up to this point. Of particular interest was the

potential to print ceramic. Where candidate materials showed early potential, they were screened by a combination of evaluation techniques including: optical microscopy, tribocharging affinity trials (to determine if the material preferentially charged positively or negatively), differential scanning calorimetry (DSC analysis), Raman spectroscopy, particle size distribution (PSD) analysis, and in a few cases X-ray diffraction analysis (XRD). Owing to the narrowed focus of the research reported after this point, treatment of materials evaluation will be abbreviated.

6.4.1. Conventional toner

Although conventional toners have been demonstrated by prior researchers to be too brittle for producing 3D objects [58, 211], their well characterized attributes and consistent printing performance made them the ideal material for benchmark trials. Therefore, virtually every experiment in this research was benchmarked against the manufacturer's standard black toner (even though it would be demonstrated repeatedly that it was indeed too brittle to be a viable material for 3D parts; See Sample 7-12). Of particular relevance was the conventional polyester toner (PolyJZ, Samsung, Japan) as described in §5.1.

6.4.2. Ceramics

The successful printing by EP of pure ceramic powders as a support material by other researchers [63, 229, 296] (See §4.4.4), indicated the potential for using ceramic as a build material in the SLP process which is explored herein. The envisaged process was to use the SLP development rig to print a green ceramic body which would then be post-fired as

described in §6.3.1.2. Most ceramics preferentially tribocharge positively according to experimental work and virtually all triboelectric series [65-68] (See also discussion about ceramic toners in §3.2.1.1).

6.4.2.1. Commercial “Ceramic” Toner

A commercial toner (C-CLC, ZEAC, Switzerland) formulated for digitally decorating ceramic tiles was used as the benchmark for evaluating the possibility of ceramic toners. The toner had been optimized to charge negatively for use in commercial two-component printers using the factory default print engine voltages and fusing (as used for trials in §6.3.1). A replacement toner cartridge and developer for the printer (Aficio CL7000, Ricoh Company Limited, Japan) were obtained, loaded with the aftermarket toner and carrier, and fitted into the printer as prescribed by the toner manufacturer. The print quality with the aftermarket ceramic toner was virtually indistinguishable from the manufacturers standard black toner, however trying to produce a sintered 3D body from it proved difficult as shown by Sample 6-5. It was estimated that the ceramic content in the toners was 40 to 70 wt.%. Owing to the heterogeneous mixing and multitude of materials in the toner matrix, estimating its vol.% was more difficult.

In order to further understand the toner, Raman spectroscopy (inVia Reflex Raman microscope, Renishaw PLC, UK) was undertaken by Dr. Tim Batten, Raman applications specialist at Renishaw PLC, at the request of the author. The samples were excited using 514nm and 785nm laser excitation with lateral spatial resolution of 0.7 μ m and 1.2 μ m respectively

(determined by the Raleigh criteria). Optical images were obtained of each sample using a 100x objective lens.

In Raman spectroscopy, some materials fluoresce strongly at certain wavelengths producing what is normally an undesirable large spectral background, which is mitigated by changing the laser source. However, in this case the fluorescing of the polymer matrix enabled the visualization of the ceramic particles in the matrix of the toner as shown in Figure 6.21.

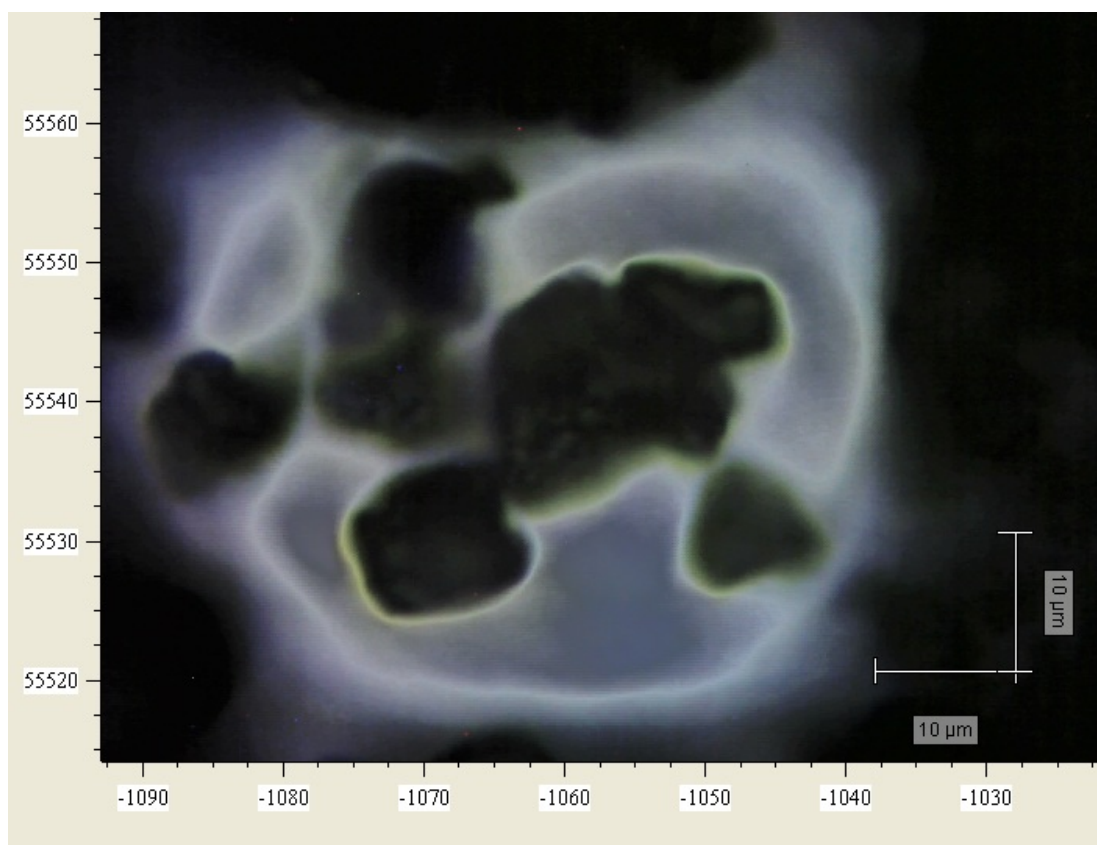


Figure 6.21 – Optical image during Raman spectroscopy of commercially available “ceramic” toner exhibiting a strong fluorescence background

The results of the Raman spectroscopy were not ideal due to the low signal-to-noise ratio (caused by the black colour, spherical shape, small size/thickness, low level of crystallinity in the polymer matrix and propensity to burn at higher laser powers), however the unanticipated fluorescing provided a vital insight to the relatively low vol.% of ceramic content in the toner. This assessment does not preclude the possibility of producing toner with higher ceramic loading (particularly if pre-treatment of the ceramic particles were undertaken, as is the state-of-the-art for preparing conductive toners [101]). Based on the spectroscopy results, the toner used for these trials would be best described as a “polymer matrix toner incorporating ceramic pigments.” The large proportion of polymer is likely what enables this toner to charge negatively (when alumina normally charges positively), thereby making it compatible with the widest spectrum of printers in the market today (§3.4.2).

6.4.2.2. *Ceramic Powder as a Negative Single Component Toner*

Despite the positive charging affinity of alumina, the effective deposition of negatively charging commercial alumina-based toner in §6.3.1.2.2 left the question of whether pure or surface treated alumina would print as a negative toner. To test this possibility, samples of alumina powder (CT 19 FG, Almatix, USA) were prepared for printing as a negative toner in a mono-component printer (Laserjet 5, Hewlett Packard, CA, USA) as described below. The ceramic powder had an average particle size of $\sim 6\mu\text{m}$ and was selected within the range of the intended toner size for the printer, yet on the lower end of the range owing to the higher density

of the ceramic over conventional toner (thus providing the most favourable charge to mass ratio for development).

Sample 6-7 Pure Alumina as a Negative Toner

A 50g sample of alumina was loaded into a Laserjet 4/5 toner cartridge modified to enable easy refilling by Banerjee and Wimpenny [211] as shown in Figure 6.22. Then the ASTM F2036 pattern was printed onto red A4 paper (colour chosen to give contrasting background for the white ceramic powder) in the laboratory at 22.4°C and 45% relative humidity (RH).



Figure 6.22 – Loading pure ceramic into a LaserJet 5 cartridge (left); and the resulting print on paper, Sample 6-7 (right).

The ceramic powder was not printed onto the paper in the pattern sent to the printer. Some ceramic powder was deposited onto the paper, but it was toward one edge (Figure 6.22) which seemed to correlate with where the powder had leaked out into the printer rather than where any latent electrostatic image had been. Sample 6-7 did not indicate that pure ceramic toner would print as a negatively charging single component

toner. The printer and toner cartridge were cleaned prior to attempting the next sample.

Sample 6-8 Surface Coated Alumina as a Negative Toner

The alumina powder was surface coated with 0.5 wt.% amorphous fumed silica FCA (CAB-O-SIL TG-308F, Cabot, USA) using a high torque mixer (CKL Multimix, Malaysia). The alumina powder was oven dried at 140°C for 4 hours during which time the mass reduced by 0.31 grams (from 150 to 149.69 grams). Then a 50g sample was loaded into the toner cartridge/printer and the same pattern was printed on the same paper as before, with the lab at 21.9°C and 48% RH. In order to be able to further visualize the deposited ceramic, this material was also printed on transparent film with text label (visible in Figure 6.23).

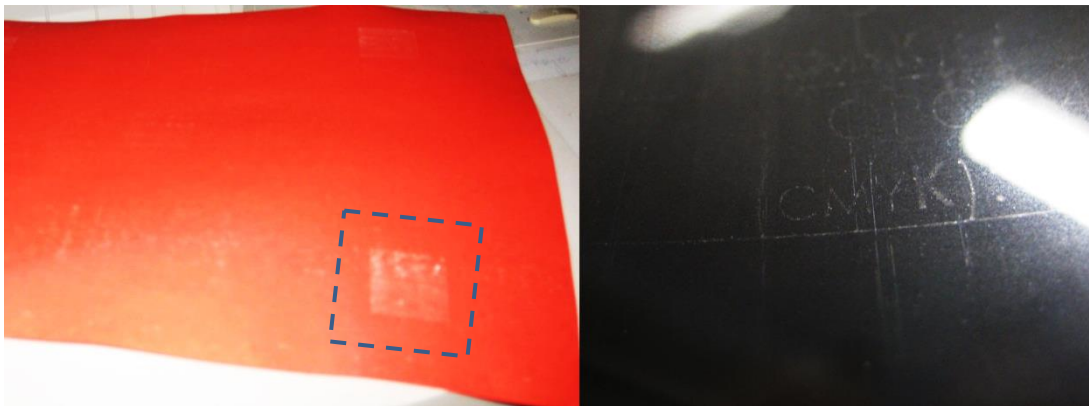


Figure 6.23 – Surface coated alumina printed on paper (inside dashed rectangle) as Sample 6-8 (left); and text printed on overhead transparency (right).

The results of this trial are shown in Figure 6.23. Although the image density is very weak, deposition on the electrostatic latent image is apparent on both the red paper and overhead transparency film.

The modest success of Sample 6-8 indicates that some ceramic materials do have the potential to be developed into toners.

Based on the carrier composition used in the research by Boivie et al., it can be deduced that they were using a dual component printer for positive toners [62]. Therefore, this was the *first time that pure ceramic powder had been laser printed using single component development* to the author's knowledge.

6.4.2.3. Ceramic Powder as a Positive Mono Component Toner

Following on from the unexpected success of Sample 6-8, a trial to use the alumina powder as a positively charging toner was undertaken.

Sample 6-9 Surface Coated Alumina as a Positive Toner

In order to use alumina as a positive toner, it was necessary to obtain a printer with a photoreceptor intended for positively charging toners. Although a printer with an amorphous silicon photoconductor was desired, in the end a less expensive option was selected.

The alumina powder was prepared identically to the previous trial (Sample 6-8), was loaded into a printer (HL10H, Brother Industries, Japan) and printing attempted as a positive toner.

Unfortunately, the trial was unsuccessful with no visible deposition of ceramic powder onto the paper. It could be argued that the surface

coating with fumed silica was an inhibitor in this printer and that a positive metal oxide, such as titanium oxide, should have been used in this case. For that reason, it could be argued that these trials should be repeated.

Owing to the prerequisite need to be able to improve the print quality and increase the height limitation, further investigation of ceramic powders as toners was discontinued.

6.4.2.4. *Sand & Sugar*

Both sand and sugar represented candidate materials for build and support respectively, and both preferentially tribocharge positively (with a few exceptions). In particular the sugar was desired as a support material because of its low cost, wide availability and solubility in water. The particle size of these materials was considered and the sand was even classified by sieving. Although it had a poor yield with 97% of the particles above 100 μ m, its low cost and high availability made use of the smaller particles possible for research purposes (and further particle size reduction to improve the yield for pilot scale use was deemed viable). Preliminary work toward converting these materials into toner-like powders for printing was abandoned as the gravity of the transfer/height limitation issues began to be understood.

6.4.3. Legacy Toner Materials Revisited

In order to provide a smooth transition from prior research to this current research, several materials which had been previously printed were assessed for continuing use on the SLP rig.

6.4.3.1. *Somos 201*

The original batch of Somos 201-based toner had originally been classified into several very narrow PSDs (including removal of all the fines), for in-depth analysis of the influence of particle size on its performance. This material printed acceptably well for thousands of print cycles, without noticeable adverse effects on the printing components. The second batch of Somos 201-based toner, which damaged the printer components (§4.4.5.3) was nominally specified with the same PSD; however it is not clear whether the fines were removed. In addition to this possible difference, the carrier was changed and the fusing temperature was increased by 5-10°C.

In an attempt to establish if the fines had been removed, the author sent a sample from the second batch away for a PSD analysis by laser diffraction (Cilas 1064 particle size analyser, Cilas, France). The percentile particle diameters (d_5 , d_{50} , d_{95}) for the second batch of toner were 1.86, 32.16, and 62.96 μm . The results from the second batch were nearly identical to the PSD values from the first batch which were 1.63, 32.02, and 63.00 μm . In both cases, the percentage of particles below 5 μm was approximately 10%. From these results it is unclear whether a difference in the fines was not detected or not present. Without further

means to reduce the risk of damaging the printer components, the use of this material was not reinstated for the current research, despite the tolerable printing performance (from the first batch) and exceptional mechanical properties of the fused parts [235, 260].

6.4.3.2. Epoxy

The epoxy-based toner used in early feasibility studies for the Custom-fit project (§4.4.5.2) and also in the Laser Printed Electronics project (§4.4.5.4) was evaluated and is suitable and relevant for this research. Therefore a new batch of this toner was ordered with the characteristics described in §5.1.

6.4.4. High Performance Polymers

A range of high-performance polymers, including amorphous and semi-crystalline engineering polymers (ABS, PC, PVA) and high temperature polymers (PEEK, PAI, PTFE), was explored in parallel to the research reported herein and reported elsewhere by Rupesh Chudasama.

6.5. Conclusions

These trials highlighted the lack of understanding surrounding the defects and height limitation experienced on the SLP rig. Furthermore, the flexibility of the laser printing process and its compatibility with a wide range of toner formulations has been demonstrated. The promising preliminary work on new toner candidates was overshadowed by the need to understand and remedy the cause(s) of the defects produced by

the SLP process and the inherent sample height limitations. This focus had priority for the remainder of the research reported herein over expanding the range of toner materials because, if they could not be printed with sufficient integrity and height, then the utility of their development would be precluded.

7. Discovery and Substantiation of Defect Causes

As summarized in §4.6, in the previous attempts to use EP for AM, the limited Z height deposition highlights the greatest barrier to using laser printing (i.e. EP) for 3D applications. Building on the understanding gained from the literature review (§2-4) and the scoping trials (§6) the focus narrowed to study of the potential causes of height limiting surface defects arising in the parts produced by the SLP process.

Experimental work in this chapter was undertaken using the SLP test rig in its Stage 1 configuration (§5.7.1) using a commercially available black polyester (thermoplastic) toner (PolyJZ, Samsung, Japan) (§5.1). The initial subsection of this chapter (§7.1) experimentally characterizes the SLP process (and defects arising from) using a non-electrostatic transfer. Subsequent subsections detail minor modifications to the process in order to experimentally demonstrate electrostatic transfer (§7.2), the influence of residual toner charge (§7.1.4 and §7.2 onward), and the influence of pressure uniformity on defect behaviour.

7.1. Using Non- electrostatic Transfer

One of the most perplexing phenomena experienced during early SLP trials, using a non-electrostatic transfer method (§4.4.5.3 and Figure 5.12), was the formation of defects typically associated with reduced transfer field strength in electrostatic transfers (§4.6).

This behaviour first led to trials to confirm that the defects were not unique to the developmental toner-like materials used, and then to explore and characterize the processing conditions suspected to contribute to defect formation.

7.1.1. Defects Using Conventional Toner

Although the same commercial polyester toner (PolyJZ, Samsung, Japan) used in these trials, had been used during former research (§4.4.5.3), its use was limited to preliminary printing for alignment and calibration of the CTG PrintTec GmbH printers during installation on the SLP rig. Therefore, it was not known if it would suffer from defects similar to those observed with multilayer printing of the other developmental toner-like materials previously used on the SLP rig. Therefore, initial trials were undertaken to observe its behaviour.

Sample 7-1 Registration Trials with Commercial Toner

In order to minimize potential sources of variation, the commercial black polyester-based toner was loaded into the printer (pre-mixed with carrier beads for 20min and then loaded directly into the developer) and printer settings (voltages and gaps) were optimized by CTG Print TEC GmbH in

Germany and then the developer unit was shipped to the UK. After in-person training by the manufacturer, the toner hopper (used to replenish the toner-carrier developer mix) was filled and the printer/voltage settings were fine-tuned based on the manufacturer's recommendations to the values shown in Table 7.1.

Table 7.1 – Printer Settings: Commercial Polyester Toner

<i>Gaps:</i>	Gap: doctor blade	0.85 mm
	Angle the magnetic brush	6
	Gap: Developer to conditioning roller	1.00 mm
	Gap: Conditioning roller to OPC (close side)	1.85 mm
	Gap: Conditioning roller to OPC (far side)	1.00 mm
<i>Voltages:</i>	Developer bias voltage	-950 VDC
	Conditioning roller voltage	-450 VDC
	Charged OPC surface potential	-720 VDC
	Exposed residual OPC surface potential	-100 VDC
	Transfer roller voltage	+420 VDC
<i>Layer Height:</i>	Distance platform drops for each layer	10 μ m

Once the printers were optimized for the toner, the platform was levelled to match the transfer roller. Due to variation in the glass and the relatively low compliance of the transfer roller (hardness of 60 Shore A coated with an 0.5mm thick fluoropolymer sleeve), it was not possible to achieve uniform pressure across the entire build platform area. The "best fit" enabled uniform nip pressure across approximately three quarters of the platform (as is evident in the inset image in Figure 7.1).

The final step of preparation to print samples was to synchronize the printer with the motion of the platform. This sample was used to align

the print onto the substrate. The pattern printed was a rectangle with crop marks in the corners of the substrate. The substrate was heated to 110°C and the result of several of prints (including a small shift) is shown in Figure 7.1 with inset image of the entire substrate. The arrow indicates printing direction for all subsequent samples unless otherwise labelled.

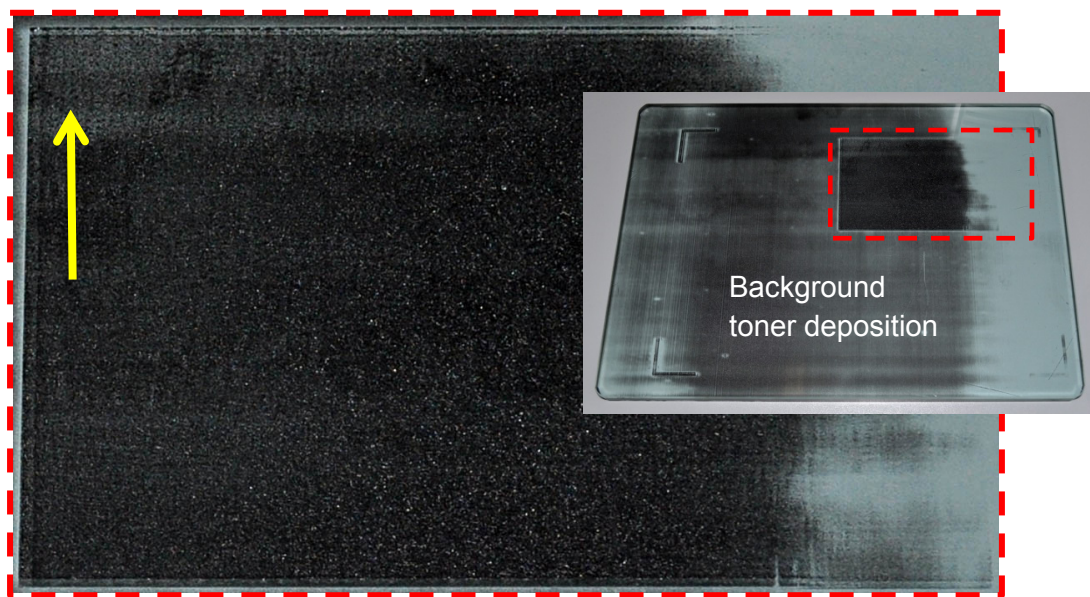


Figure 7.1 – Large detail of the deposition from registration trials (Sample 7-1) with view of the entire substrate inset; yellow arrow indicates the printing direction

The results show very little deposition on the right side of the sample/substrate which may illustrate low (or possibly the absence of) contact pressure. This is reinforced by the clearly printed crop marks in the corners on the left side while those on the right are scarcely distinguishable. The relatively large amount of background deposition globally deposited on the glass (labelled on inset image in Figure 7.1) indicates the potential for further optimization of the printing parameters. The small shift in the print alignment can be noticed when looking at the left edge of the detail of the sample. Most significantly, the printed

rectangular area (indicated within a dashed border) showed early signs of texturing or pitting.

The texture of the printed solid area was evocative of the defects experienced and described by other researchers. Together with subsequent samples, this sample indicated that the defects experienced were not unique to developmental toners. Furthermore, it confirmed that even with a non-electrostatic transfer, defects seemed to be related to those experienced when using electrostatic transfer.

This outcome warranted further exploration of defects and underscored the question of whether charge was among their causes.

7.1.2. Characterizing Surface Potential

Building on the outcomes from preliminary printing, including Sample 7-1, it became apparent that producing samples which facilitated the observation and evaluation of defect formation and exaggeration (including defects which typify the shortcomings of electrostatic transfer approaches as discussed in §4.3) was paramount.

A 20 layer sample pattern was devised (Figure 7.2) in order to enable evaluation of surface quality, consistency of deposited layer height, and surface potential. It was based on up-scaling the solid area pattern from ASTM F2036 (§5.4) to nearly fill the 120x120x1mm ceramic substrate (ADS96R, CoorsTek, CO, USA). The larger printed area facilitated field measurement as an indicator of surface potential by field mill (as

explained in §5.7.1.2.1). Furthermore, it was determined to shift the print pattern 5mm every layer in order to leave a portion of each printed layer exposed. This shift was planned for two reasons: a) to allow observation of defect formation and exaggeration with each additional layer (if any) and b) to facilitate measurement of the contribution of each layer to the cumulative sample thickness.

The surface potential of the sample was measured in-process, after each layer was printed using a field mill device. Furthermore, the cumulative toner deposition thickness was measured using digital callipers (CD-6"CS, Mitutoyo Corp, Japan) in the centre of the exposed 5mm strip for each of the 20 layers. For each sample set, the average surface potential (primary Y-axis) and cumulative toner thickness (secondary Y-axis) are plotted for each layer (X-axis) with \pm error bars equal to the standard representation of error (§5.5.2) for this work of $\sigma/n^{1/2}$ (n samples).

The samples in this sub-section were produced using the print pattern as described above, with standard commercial black polyester toner (PolyJZ, Samsung, Japan) printed with settings shown in Table 5.1. The samples were printed onto individual ceramic sheets which were taped onto the large glass substrate (inset image in Figure 7.1) using 12mm wide high temperature tape (Kapton tape, RS Components, UK) (as shown in Figure 5.14). The samples have been named retrospectively to facilitate the discussion. A summary of sample preparation and results is included in Table 7.2 and then a more in-depth explanation of the results from each sample follows.

Table 7.2 – Experimental Regime for Surface Potential Characterization

<i>Sample:</i>	<i>Unique Preparation Steps:</i>	<i>Result:</i>
Sample 7-2	None (as described above)	Defect exaggeration observed; Surface polarity swapped
Sample 7-3	10 min dwell between layers	Surface potential “relaxes” with time
Sample 7-4	Grounded conductive platform	Defects continued
Sample 7-5	Printed only blank images	Substrate charged positive
Sample 7-6	Grounded conductive substrate & platform; constant area print	Defects continued; field mill measured zero

Sample 7-2 Baseline for Sample with 5mm Shift Print Pattern

Sample 7-2, as shown in Figure 7.2 (showing area ~80x80mm), is representative of the set of samples produced as described at the beginning of this subsection. Each layer was fused using the infrared heater to a target temperature of 115°C (not 150°C as published elsewhere [236]). The ambient conditions when the sample was produced were 24.0°C and 40% RH.

Figure 7.3 shows the average surface potential versus the average cumulative toner thickness for the set of samples represented by Sample 7-2. The author has explained elsewhere [236], that initially the average surface potential decreased to a minimum of $-0.18 \pm 0.02\text{kV}$ at layer 2, and then followed an upward trend to a maximum of $0.39 \pm 0.01\text{kV}$ at layer 19. The upward trend of the surface potential (with a maximum value of 0.105 mm at layer 19) correlated with the average cumulative

print thickness. The average thickness per layer was $5.5 \pm 1.1\mu\text{m}$ for all samples.

(Intentional page break to allow image and graph on the next page to be viewed at the same time)



Figure 7.2 – Surface quality of Sample 7-2 where successive prints (with each layer shifted 5mm to the right), were transferred layer-on-layer using only heat and pressure

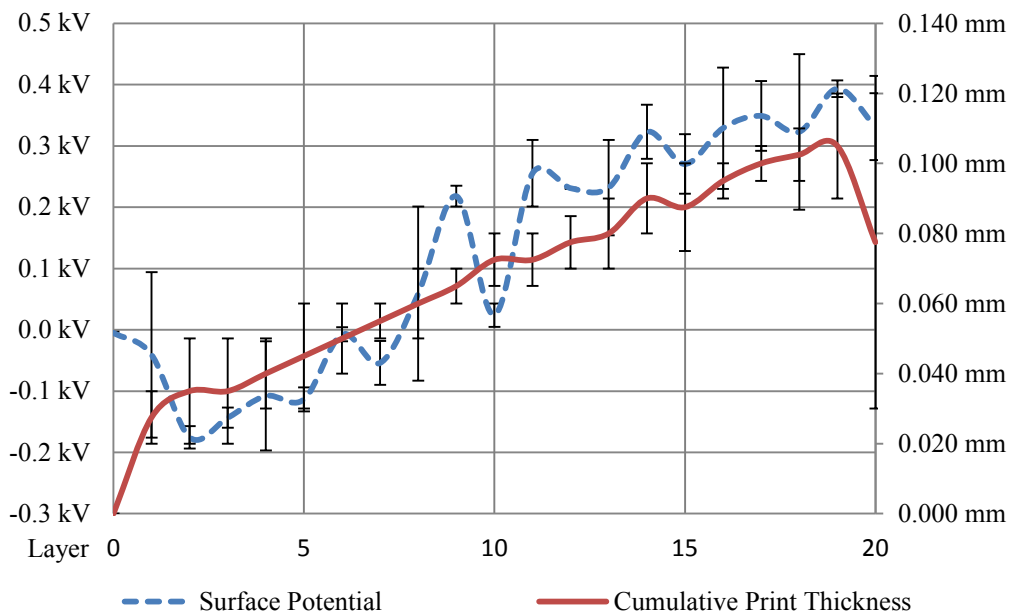


Figure 7.3 – Graph of average post-print surface potential vs. average cumulative maximum print thickness for set of samples including Sample 7-2 (© Society for Imaging Science and Technology from [236])

This sample provides a clear illustration of surface defect initiation and propagation which correlated with the addition of successive overlying layers. The left side of Sample 7-2 (Figure 7.2), where only a few layers were printed, had a surface roughness of less than $1\mu\text{m Ra}$ (measured using white light interferometry, WYKO NT2000, PZ-06-CS-SF, Mikro Precision Instruments, USA); yet it was so degraded on the far right-hand side of the sample (where up to 20 layers were printed), that it was impractical to measure [236]. The defects developed around layers 7-8, which correspond to when the average surface potential changed from negative to positive [236].

Sample 7-3 10min Delay Between Layers

In order to simulate one of the key differences between the legacy SLP (Sample 6-1, Sample 6-2) and EMB (Sample 6-3) produced samples (discussed in §6.1), it was determined that a 10min dwell between layers should be introduced.

Sample 7-3, as shown in Figure 7.4, is representative of the samples produced as described for the prior sample, except with a 10min delay between each layer. The surface potential was measured immediately after (as with Sample 7-2) and following a 10 min delay (immediately before the next print). Each layer was fused using the infrared heater to a target temperature of 115°C . The ambient conditions when the sample was produced were 21.9°C and 43% RH.

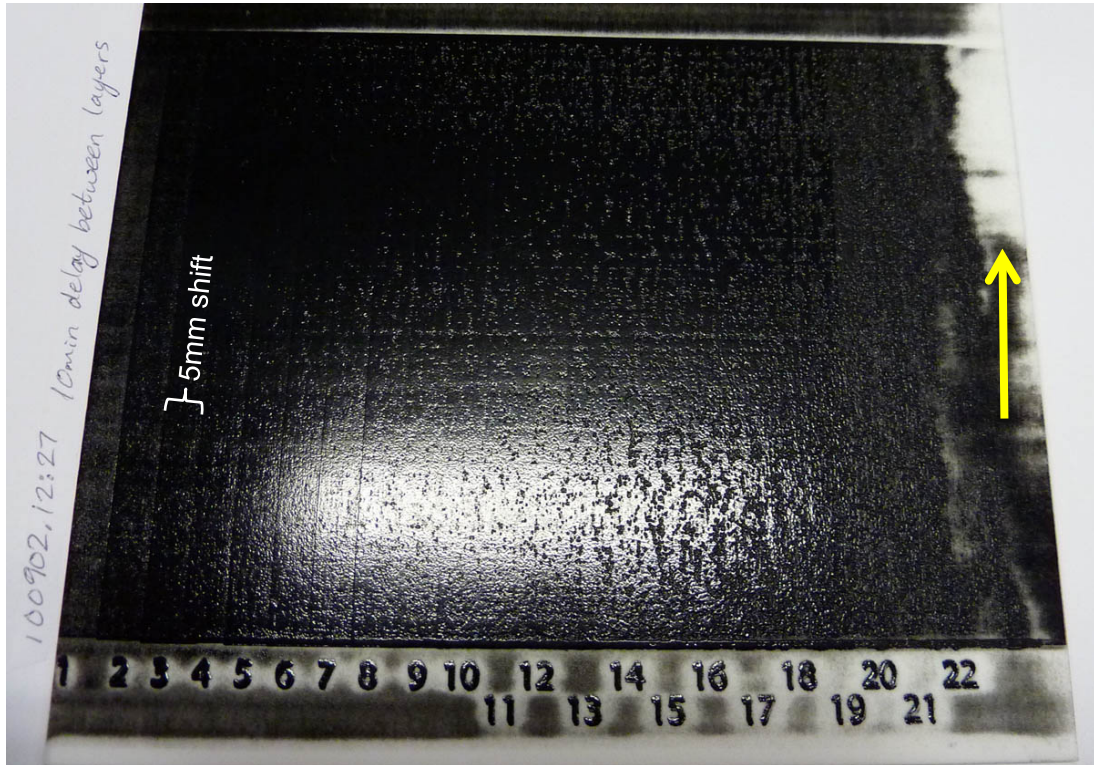


Figure 7.4 – Surface quality of Sample 7-3 where a 10 min delay was introduced between successive prints (with each layer shifted 5mm to the right)

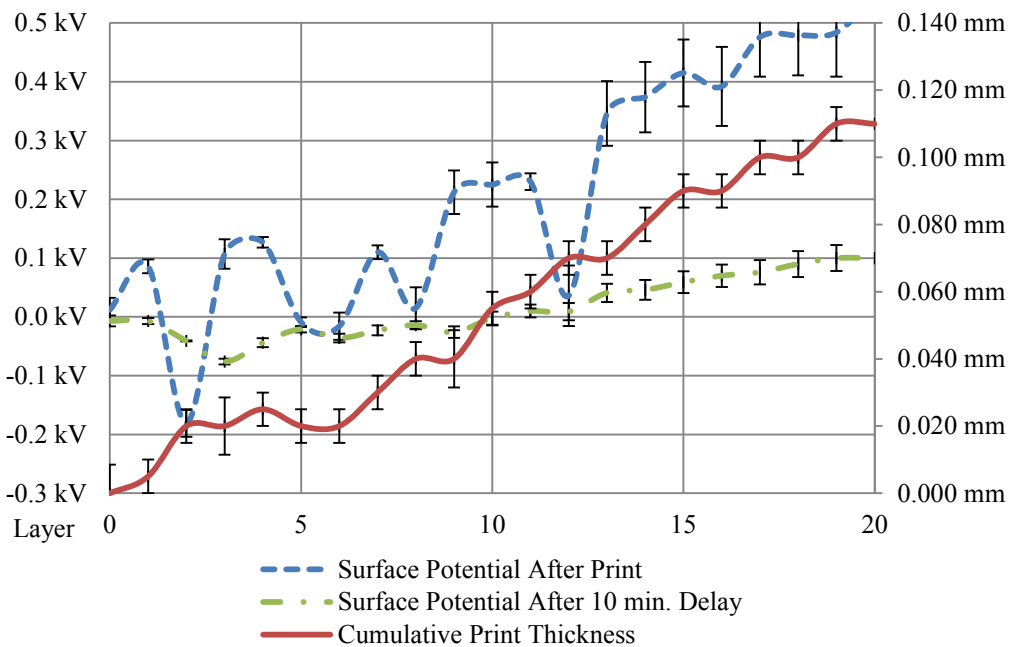


Figure 7.5 – Graph of post-print surface potential and surface potential after 10min delay vs. average cumulative maximum print thickness for Sample 7-3

Figure 7.5 shows the sample surface potential immediately after (blue dashed line) and 10min after printing (green dashed and dotted line) versus the cumulative toner thickness for the samples represented by Sample 7-3. The author has also reviewed this sample in detail elsewhere [236], but in summary, the surface potential of Sample 7-3 measured immediately following the print and after a 10min delay, initially decreased to $-0.18 \pm 0.01\text{kV}$ and $-0.08 \pm 0.01\text{kV}$ (layer 2 and layer 3 respectively). Then it followed an upward trend peaking at $0.55 \pm 0.08\text{kV}$ and $0.10 \pm 0.02\text{kV}$ (layer 20 for both). The surface potential after the 10min delay had a significantly reduced magnitude and was much less variable. The average cumulative print thickness correlated with the upward trend of the surface potentials, with a maximum value of $0.11 \pm 0.01\text{mm}$ at layer 19 and an average layer thickness of $5.5 \pm 1.3\mu\text{m}$. Its surface roughness and appearance were nearly identical to Sample 7-2 (in Figure 7.2) with surface degradation first evident around layers 5-6, (correlating to when the surface potential changed from negative to positive), and then increased with the number of layers deposited [236].

This sample reinforces the earlier illustration of surface defect initiation and propagation which correlated with the addition of successive overlying layers. Never-the-less, the 10min delay appears to have provided an opportunity for charge relaxation in between prints. This did not noticeably mitigate the surface quality degradation however, which initially begins on the left with a surface roughness of just under $1\mu\text{m Ra}$

(essentially the same as Sample 7-2) and degrades so much toward the right hand side of the sample, that it is impractical to measure.

Sample 7-4 Grounded Conductive Platform

Increased familiarity with the field mill measurements, made it apparent how easily the field mill would detect and “average in” the field from charge from anywhere in its vicinity. Therefore, any (nonconductive) surfaces which could be charged were removed or covered with a conductive material. Owing to the platform configuration (which had been designed to accommodate a relatively thick glass substrate) and the difficulty of levelling the platform to the printers, the large glass substrate was left in place and an aluminium cover was made to go over it. The aluminium cover (Figure 7.6) was designed to allow the compliance of the rubber matting to help achieve more uniform pressure distribution (§5.7.1.7), while still maintaining contact with the grounded platform (to ensure any charge arriving at its surface would instantaneously be neutralized). The addition of this conductive cover plate obliged the use of a stack of substrates on top of it to provide a large enough gap to prevent sparking from the transfer roller.

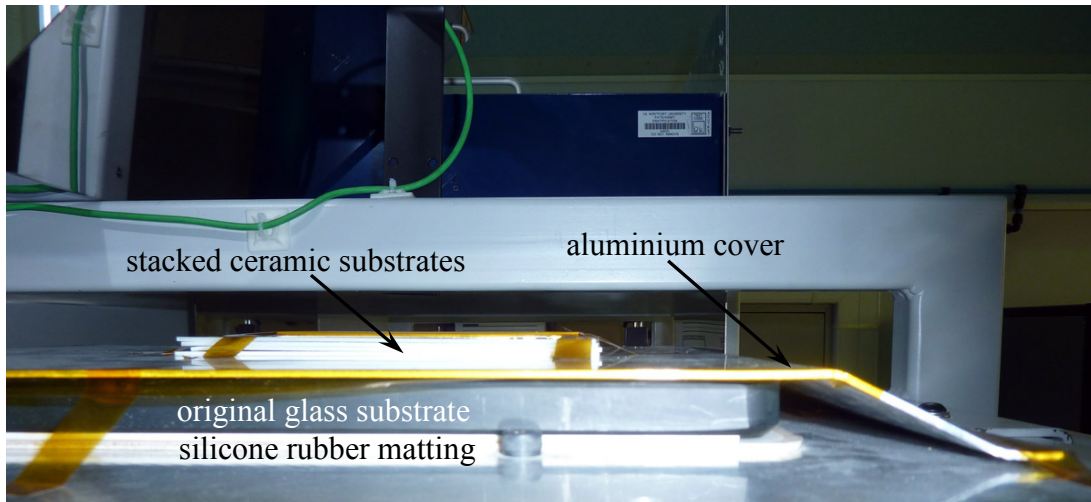


Figure 7.6 – Image showing the conductive aluminium cover plate used to cover the nonconductive former glass substrate and silicone matting

Each layer of Sample 7-4 was printed according to the same settings as for Sample 7-2 and fused using the infrared heater to a target temperature of 120°C (increased slightly to account for the lower thermal mass of the substrate). The ambient conditions when the sample was produced were 21.0°C and 46% RH.

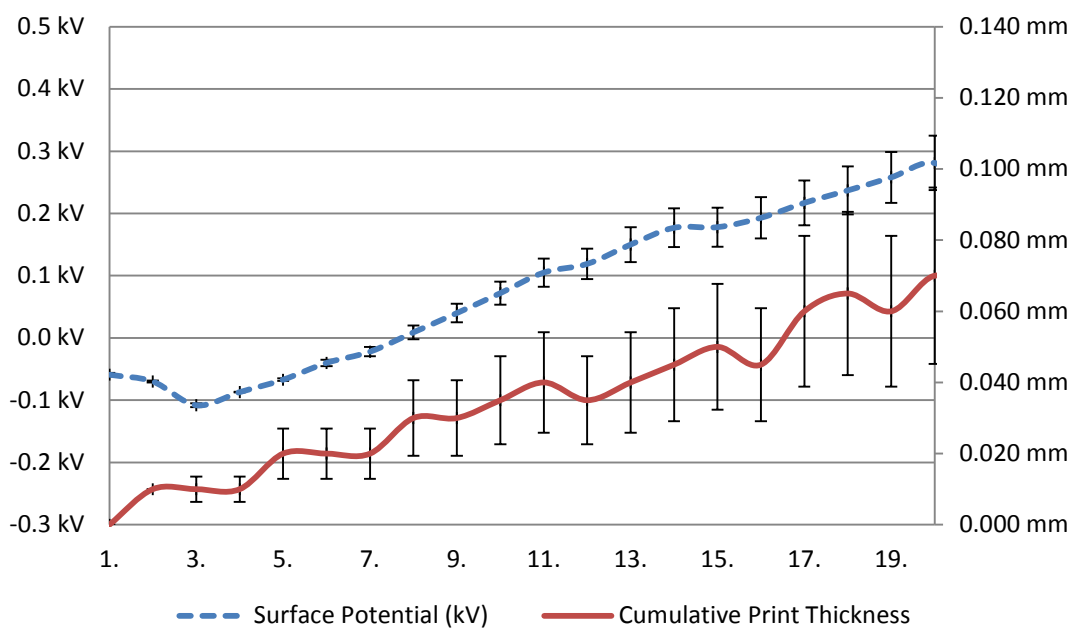


Figure 7.7 – Graph of post-print surface potential vs. cumulative maximum print thickness for Sample 7-4

Figure 7.7 shows the post-print surface potential vs. cumulative maximum print thickness for Sample 7-4. The surface potentials were measured immediately following the print, which initially decreased to -0.11 ± 0.01 kV (at layer 3) and then followed an upward trend, peaking at 0.281 ± 0.04 kV (at layer 20). This maximum surface potential is approximately half of the maximum for Sample 7-3 (measured immediately after the print) indicating that perhaps prior readings were subject to augmentation by charge not on the sample area itself. The surface roughness followed in the same pattern as the prior samples, but the maximum cumulative thickness was only 0.70 ± 0.02 mm with an average layer thickness of 3.8 ± 1.3 μ m, which may indicate that the substrate change may have influenced the transfer efficiency. The close correlation between rising surface potential and increasing print thickness was not logically explained (as discussed in §7.1.2.1). Therefore, further consideration and analysis was undertaken on this sample. The conundrum was resolved by Figure 7.8 which plots the surface potential against the area printed in each layer. Note: the variation in the dimensions of the printed area was so small that error bars are not visible (not accounting for the reduction of area due to defects).

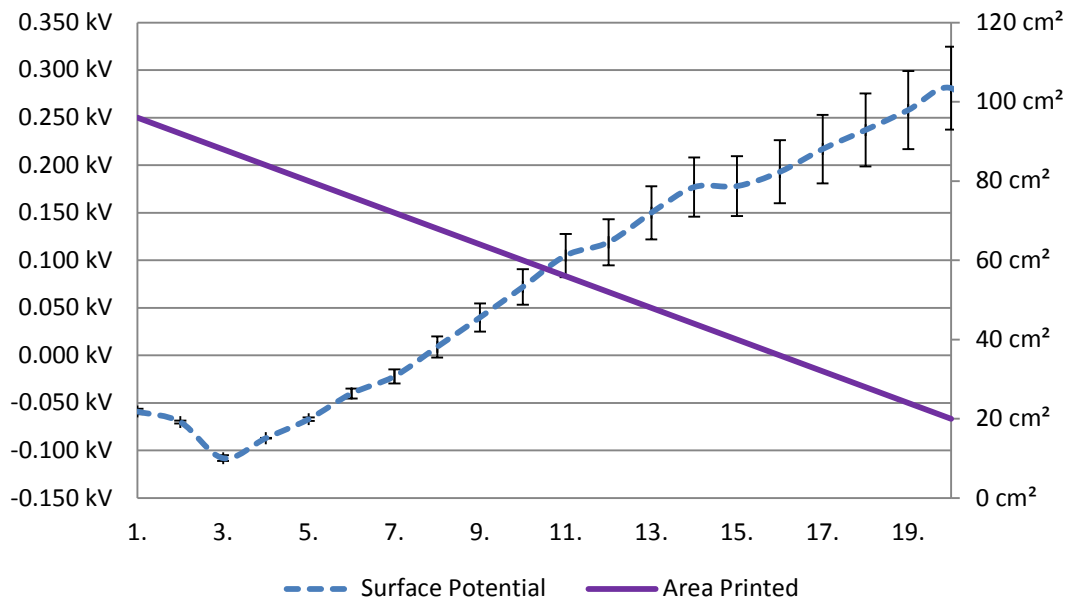


Figure 7.8 – Graph of post-print surface potential vs. the area printed for each layer

The printed area for all samples in this subsection so far have started by printing toner onto an area of 96cm² at layer 1 and then printed an area reduced by 4cm² (for each 5mm shift) so that by layer 20, only an area of 20cm² was deposited with toner. The surface potential was inversely proportional to the printed area for Sample 7-4 and has been for all samples printed using the 5mm shifted pattern.

Sample 7-5 Print Blank Images First

The measured surface potential of the foregoing samples all followed a trend toward increasing positive surface potential, therefore attention turned to the final transfer roller which was the only obvious source of positive charge in the entire system. In order to assess if contact with the transfer roller was causing an increase in the surface potential of the sample, the substrate of Sample 7-5 was 'printed' with a blank print (and the platform was not continuously indexed down with Z-axis steps in

order to keep the substrate in contact with the transfer roller) 20 times and the surface potential was recorded. Following the "dry run" of 20 prints, a sample with the same baseline settings as Sample 7-2 was produced (including original substrate configuration) with a target fusing temperature of 115°C. The ambient conditions when this sample was produced were 24.0° C and 40% RH.

Sample 7-5 appears virtually identical to Sample 7-2 with the same print sequence, coverage, and defect pattern and is therefore not shown here.

Figure 7.9 plots the surface potential measured immediately after the blank 'print' and normal print of each layer in Sample 7-5. Obviously the first 20 blank 'prints' did not result in any thickness accumulation on the substrate, however the latter 20 prints did and are plotted on the secondary axis of the same graph.

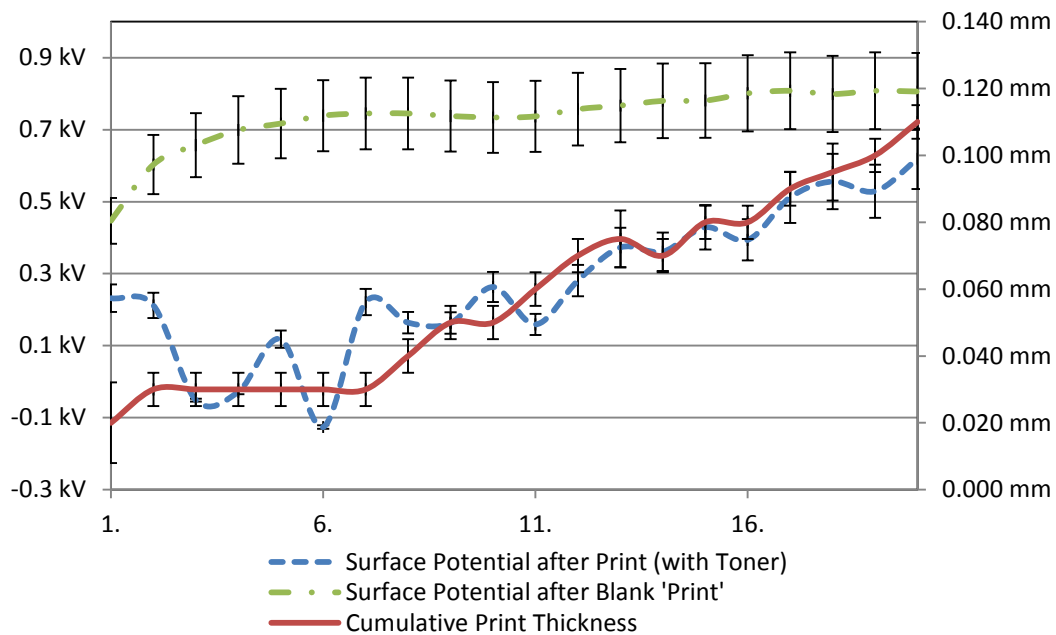


Figure 7.9 – Graph of post-print surface potential of Sample 7-5 following 20 consecutive blank 'prints' and then a surface potential vs. average cumulative maximum print thickness printed immediately afterwards on the same substrate

The surface potential after the blank 'prints', begins at $0.45 \pm 0.06\text{kV}$ after layer 1 (essentially equal to the 450V set point for the transfer roller charge, as shown in Table 5.1), then it approaches nearly $0.80 \pm 0.10\text{kV}$ by layer 5 where the value then almost plateaus and finishes near its maximum at $0.81 \pm 0.11\text{ kV}$ after layer 20.

The surface potential after the normal prints (with toner) started off at $0.23 \pm 0.04\text{kV}$ after layer 1 (down from $\sim 0.80\text{ kV}$ before the print) and then drop as low as $-0.13 \pm 0.01\text{kV}$ (layer 6), before climbing to $0.62 \pm 0.08\text{ kV}$ after layer 20.

In addition to printing blanks images onto the substrate, this trial was repeated with air gap "prints" (with a gap of $\sim 1.5\text{mm}$ between the

substrate and transfer roller) without any change to the surface potential measured by the field mill (varied less than 1V throughout). Following the air gap "prints", a print was made which had a surface potential of -0.114 ± 0.016 kV.

Sample 7-6 Grounded Conductive Substrate and Platform

The possibility that the substrate material significantly influences the surface potential of the sample (as discussed in relation to Sample 7-5 in §7.1.2.1), prompted Sample 7-6 which is representative of samples made on grounded conductive substrates (aluminium plate the same size as the ceramic substrate) directly in contact with the grounded conductive platform (as shown in Figure 7.6). It was envisaged that coupling the toner to ground would help any charge imbalance to leak away more quickly than by using a 10min dwell (Sample 7-3). Additionally, the 5mm shift was discarded in order to print the same area (96cm^2) layer-on-layer directly on top of each other (without any shift), to improve the measurement of surface potential (and avoid repeated contact by the transfer roller with areas left exposed due to the shift). Apart from these two changes, this sample used the same printer settings as Sample 7-2. Due to the lack of absorption of medium wave infrared radiation by aluminium (and therefore virtually no thermal mass in the substrate to help maintain sample processing temperature), the deposited toner layers were heated to a target temperature of 150°C . This high temperature was an exception to the normal limits which protect the OPC (§5.7.1.1), since it was estimated that the initial toner layers would cool to approximately 135°C before contacting the transfer

roller (due to their low thermal mass). Sample 7-6 was fabricated in ambient conditions of 21.0°C and 46% RH.

Due to the conductivity of the substrate, some sparking between the transfer roller and substrate occurred during the printing cycle. Where sparking occurred, a defect in the shape of an "eye" developed. Consolidated toner formed the centre "pupil" of the defect, but the radial area surrounding it was devoid or depleted (Figure 7.10) of toner deposition. The surface quality suffered as with previous samples; however the pitting defects had a finer resolution and more uniform distribution.

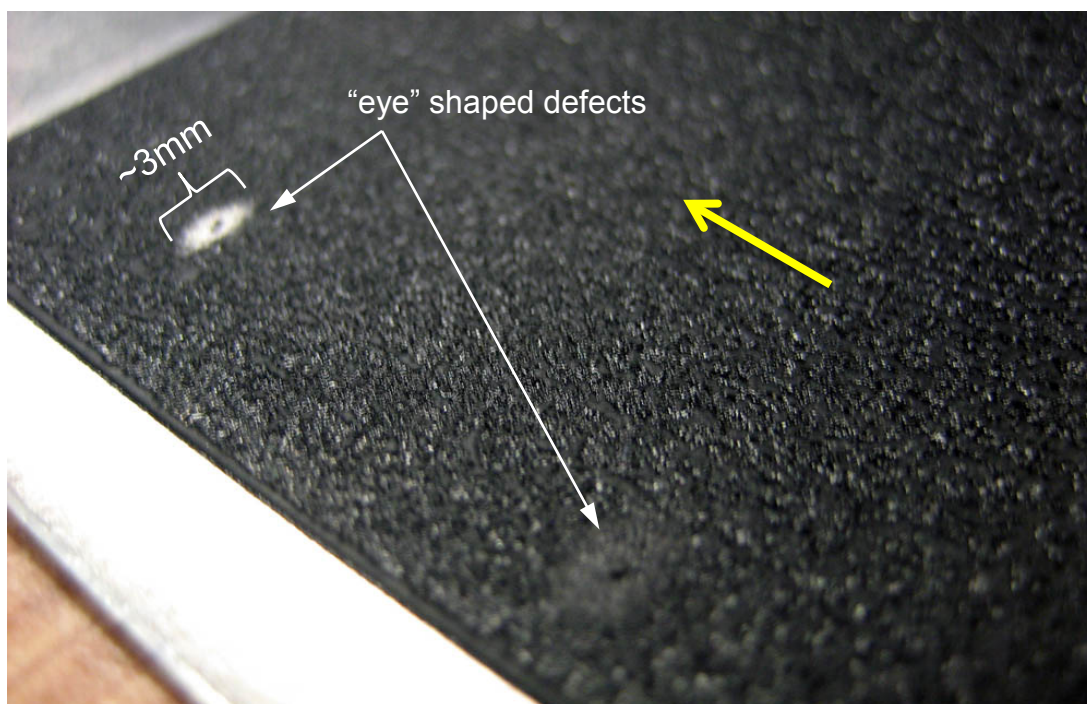


Figure 7.10 – Image of the surface quality and "eye" shaped defects of Sample 7-6

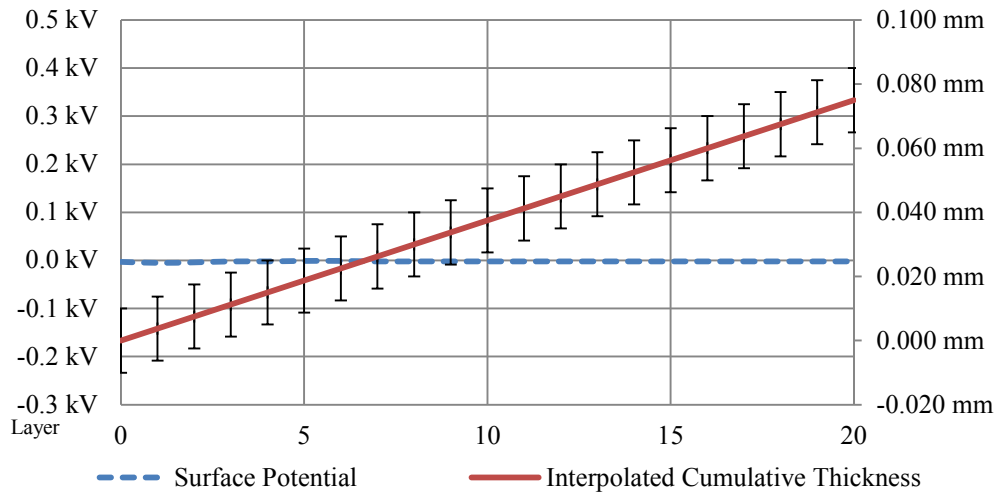


Figure 7.11 – Graph of post-print surface potential vs. average interpolated cumulative thickness for Sample 7-6

Figure 7.11 shows the post-print surface potential versus the interpolated cumulative thickness for Sample 7-6. Since the same area is repeatedly printed one on top of another, there is no opportunity to measure the individual contribution to layer thickness post-process and unfortunately the laser height measurement in-process was not reliable (§5.7.1.5). Therefore, in order to compare this sample to previous samples, a linearly interpolated layer thickness is plotted (based on the total height of the finished sample divided by the number of layers printed). This sample achieved a height of 0.08 ± 0.01 mm (with an average interpolated layer thickness of $3.8 \pm 2\mu\text{m}$). Furthermore, the field mill did not detect the presence of charge outside the range of $\pm 10\text{V}$ for any of the twenty layers which is why error bars are not visible in the graph (Figure 7.11). This led to the question of whether any charge imbalance was present (i.e. was it leaking away to ground) or whether it was simply not being detected (for some unknown reason, identified retrospectively in §7.1.2.1). At layer 20, a sheet of paper was added to the top of the

stack to test if the toner was still transferring across the nip and onto the sample.

The result of placing the sheet of paper over the 19 consolidated layers was that no toner was deposited above them. Furthermore the paper stuck to the underlying layers, which when removed provided a record of the uppermost layer of resulting surface texture from pitting defects.

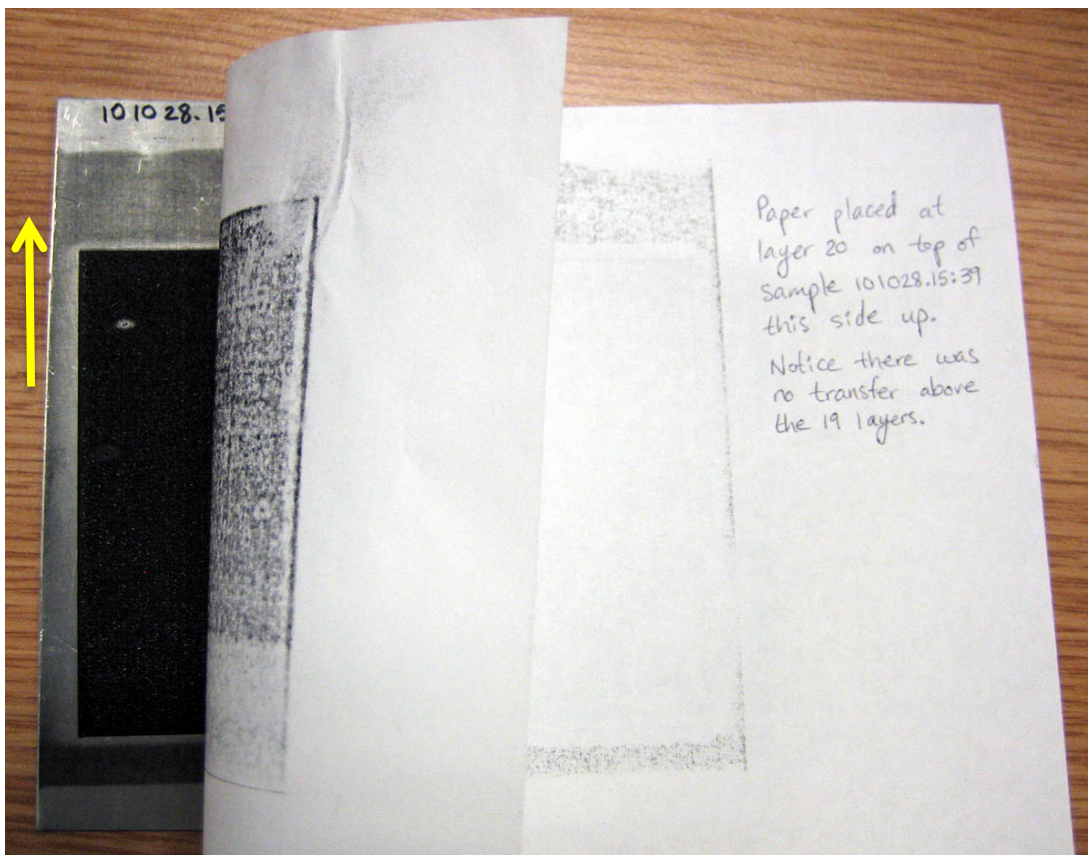


Figure 7.12 – Result of placing a sheet of paper on top of Sample 7-6 for layer 20

For the convenience of the following discussion (§7.1.2.1), Table 7.3 summarizes the results from the sets of experiments for characterizing the surface potential when printing toner with non-electrostatic transfer methods.

Table 7.3 – Summary of Surface Potential Characterization Results

<i>Sample:</i>	<i>Min/Max Surface potential (kV):</i>	<i>Max cumulative thickness (mm):</i>	<i>Average layer thickness (μm):</i>
Sample 7-2	-0.18 ± 0.02/0.39 ± 0.01	0.11 ± 0.02	5.5 ± 1.1
Sample 7-3 (after 10min)	-0.18 ± 0.01/0.57 ± 0.08 -0.08 ± 0.01/0.10 ± 0.02	0.11 ± 0.01	5.5 ± 1.3
Sample 7-4	-0.11 ± 0.01/0.281 ± 0.04	0.07 ± 0.02	3.8 ± 1.3
Sample 7-5 (blank 'prints')	-0.13 ± 0.01/0.62 ± 0.08 0.45 ± 0.01/0.81 ± 0.11	0.11 ± 0.01	5.5 ± 1.3
Sample 7-6	-0.01 ± 0.01/0.00 ± 0.01	0.08 ± 0.01	3.8 ± 2.3

7.1.2.1. Discussion of Surface Potential (Non- electrostatic Transfer)

This subsection discusses the results of each set of samples described in the previous subsection and their significance.

Sample 7-2 provided early critical evidence of defect formation and exaggeration. Although the defects were reminiscent of those experienced by field strength limited transfers, there was not reliable evidence that the thickness added to the stack by each layer was diminishing as the cumulative height increased. Admittedly, the density of the layers deteriorated (due to increased defects) and the height range observed for this sample was only 0.1mm (an order of magnitude lower than the thickness at which Kumar et al. observed defect formation). However this may indicate that the non-contact heating method enabled earlier manifestation of these defects. These results indicate that surface

defect magnitude increases with rising surface potential (which also correlated with increased cumulative sample height). The surface potential trend from negative to positive polarity was surprising, since each printed layer deposited additional negatively charged toner particles. Furthermore, it was around the transition point from negative to positive polarity that defect formation became evident. To the author's knowledge, *this was the first time that the surface potential of multilayer printing was systematically measured.*

Sample 7-3 provided strong evidence that the 10min delay allowed for charge relaxation (Figure 7.5). However, the reduction in charge did not correlate with a noticeable reduction in surface defects or deposited layer height. Due to the bluntness of the field mill, it was unclear whether the potential measurement represented a surface charge consisting of a uniform polarity or whether it was an average of a mosaic of areas with alternating polarity/charge density, as has been observed by some researchers [179]. Owing to the relatively large effective measurement volume of the field mill, it was determined to eliminate chargeable nonconductive surfaces in the vicinity of the sample which may have been having a confounding effect on readings.

Sample 7-4 reinforced the notion that prior field mill readings included detection of charge outside of the sample area. The close correlation between surface potential and increasing layer height would have been logical had the surface potential been increasingly negative with each print (due to the addition of negatively charged toner); however the

increasing positive surface potential was not logical, which led to further consideration of this phenomenon. Since the initial image covered virtually the entire width of the ceramic substrate, the shifting motion actually reduced the area of toner deposited with each layer. Plotting the surface potential against the printed area revealed that the amount of negative toner deposited on the substrate was reduced with each layer (as plotted in Figure 7.8). This provided some explanation of why the negative charge contribution from incoming toner was perhaps harder to detect, but it did not explain the source of increasing positive charge which led to the following trial.

Sample 7-5 demonstrated that the first blank 'print' left a surface potential (447V) essentially equal to the charge of the transfer roller (450V). The upward trend thereafter and stabilization around 800V clearly indicates that repeated contact with the transfer roller increases the positive surface potential of the substrate. The highest substrate potential measured in the experimental work so far of $0.81 \pm 0.11\text{kV}$ was reached (layers 17 and 19). In the absence of toner, this positive charging may have been assisted by the tendency for alumina-based ceramic to tribocharge positive (§6.4.2). Regardless of any triboelectric "assist" due to the substrate material, without the presence of negative toner it stands to reason that the substrate would achieve a higher positive charge than with it. The question of interaction with the substrate prompted the idea to use a conductive substrate in the following trial. Interestingly, the defect behaviour of the toner was not visibly different from Sample 7-2; perhaps emphasizing that the

accumulated surface potential was neutralized (at least in part) or masked with the layers of toner added to it. This said, it still reached the highest surface potential ($0.62 \pm 0.11\text{kV}$) of any sample with toner so far, indicating that perhaps the effects of the early charge injection from the transfer roller were not entirely eliminated or covered over. It is noteworthy that the cumulative toner height seemed to be stagnant from layers 2-7. If this were the result of the substrate charging, one would assume that additional positive charge would attract negative toner to it, rather than retard its accumulation and growth. Regardless of the reason it seemed delayed, it still attained the same cumulative height as prior samples of $0.11 \pm 0.01\text{mm}$. This sample served as a confirmation of the source of positive charge, which when combined with understanding of the reduced toner area being deposited (evident from the Sample 7-4 analysis) provides a compelling explanation of the surface potential trend toward a positive polarity (at least when averaged overall as read by the field mill).

The "eye" shaped defects of Sample 7-6 can be explained by the high temperature of the spark which promoted toner fusing in the central "pupil" area of the defect. The spark also neutralized the surrounding area (presumably on the transfer roller and the substrate), thereby eliminating any potential difference (field) and thus discouraging toner transfer. The slightly improved homogeneity of the defects may be an indication that the conductive substrate promoted homogenization of residual toner charge (due to the inevitable redistribution of its outer shell electrons in response to the accumulated toner charge). In addition

to these defects, the use of a grounded conductive substrate provided definitive electrostatically adverse conditions (negative toner cannot be induced to leave a roller charged to +420VDC for ground by electrostatics alone) for toner transfer, which probably accounts for the lowest cumulative print height so far of 0.075 mm.

Initially, the lack of a reading by the field mill for Sample 7-6 was unexpected and difficult to understand. However, subsequent consideration indicated that the measurement of the field was being suppressed because virtually all of the flux was being coupled to ground (analogous to solid area development without an electrode, as shown in Figure 3.25a). This essentially created an internal field only, and thus cloaked it from the field mill. The inability to measure charge as an indicator of surface potential, made the future prospects of understanding its correlation with defects very difficult. This issue will be re-visited in subsequent sections of this work (See §8.2.1).

Without a valid method to characterize the charge, the sheet of paper added at layer 20 (Figure 7.13), provided evidence for critical insights into what happened during the fabrication of Sample 7-6.

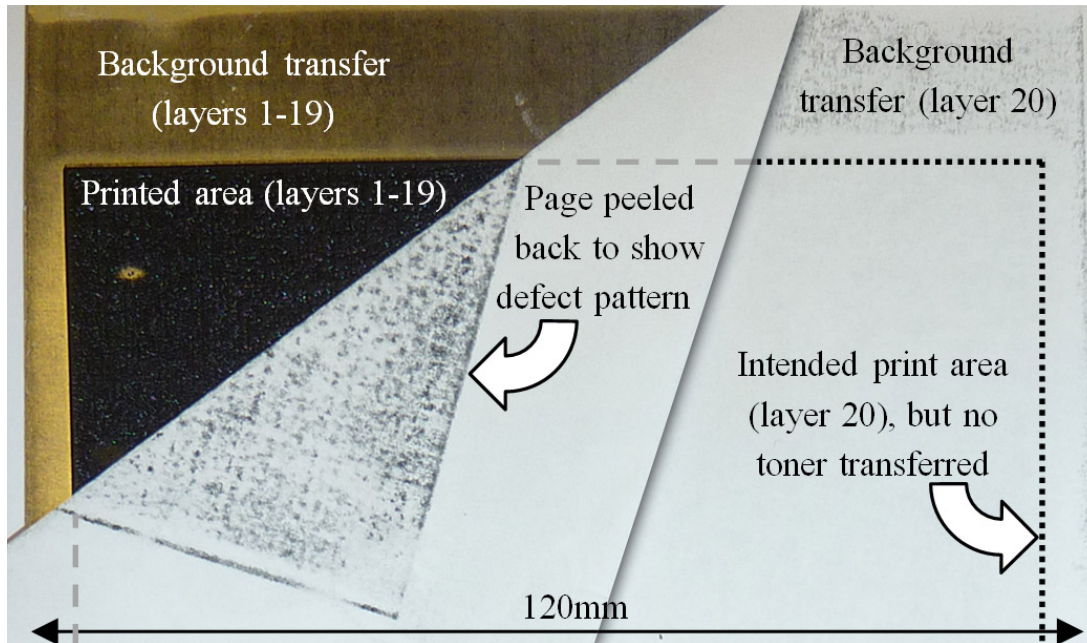


Figure 7.13 – Sheet of paper as placed on top of Sample 7-6 during the printing of layer 20. Note: toner transferred near to the image stack as background (upper right hand corner), but not directly over it; this is evidence that residual toner charge in the image stack was repelling incoming toner. Also, the paper is folded back to show the defect pattern on the top surface of the sample. (Note: image adapted from [236] with shadow of folded back paper edge enhanced for better reproduction)

Although the field mill did not indicate that any charge was present on the substrate, the toner pattern deposited on the paper did. The author has discussed this sample in detail elsewhere [236], but essentially the dashed rectangular outline in Figure 7.13 indicated the area where toner was expected to be printed onto the paper, but was not. Despite the fact that the developed toner image did not transfer, some toner was transferred as background onto other areas of the paper. The toner that was transferred onto the background (Figure 7.13) is evidence that a) there was toner on the transfer roller and that it was electrostatically able to b) transfer onto the paper around the image stack, but c) not directly over it [236]. Since the primary difference between the area where the toner transferred and where it did not, was the presence of the image stack, this supports the hypothesis that incoming toner in the new

layer was repelled (despite the contact pressure) due to the accumulation and retention of like sign charge in the consolidated image stack. In spite of the fact that no transfer field was explicitly being used in the transfer nip, an electrostatic force (field) seems to have been exerted by the accumulated toner, which prevented additional toner transfer from the developed image. It is proposed that surface defects are another (albeit less severe) manifestation of this same phenomenon [236].

This latter sample reinforces the hypothesis that one of the primary factors contributing to defect formation is the unmanaged presence of charge imbalance in the consolidated toner layers. It is important to note that this hypothesis of residual toner charge inhibiting further toner transfer was reached independently of a similar notion written by Kumar Das in 2004 (See §4.3.2). The independence of discovery, yet agreement of consequence, contributes to the strength of the evidence supporting this hypothesis.

In light of the defect patterns observed in all samples in this subsection, it is noteworthy to mention a phenomenon used for production of images by surface deformation (effectively microscale 3D reliefs, sometimes called "frosted photoplastic" from "frost development" because the deformation/wrinkles appear similar to a frosted piece of glass [329]), rather than selective deposition of toner (as in conventional EP), by *thermoplastic xerography* which is reviewed and summarized by Thourson [204]. Thermoplastic xerography was inspired by the early thermoplastic recording methods which used a cathode ray tube (CRT) to

selectively charge a thermoplastic in a vacuum, “and thereafter softened by the application of heat or solvents thereto so that such thermoplastic layer would deform in response to the charges deposited thereon” [329]. After the thermoplastic re-solidified, it became a permanent record of the charge pattern deposited [329]. Thermoplastic xerography replaced the need for a CRT and vacuum by using conventional EP methods to create a latent image applied to a thermoplastic powder [204, 330]. Once the thermoplastic powder was charged, it was softened (as with the prior method), allowed to deform and then solidify, in order to form a 3D relief pattern (as shown in Figure 7.14) potentially useful for holograms, data storage, etc. [331-334].

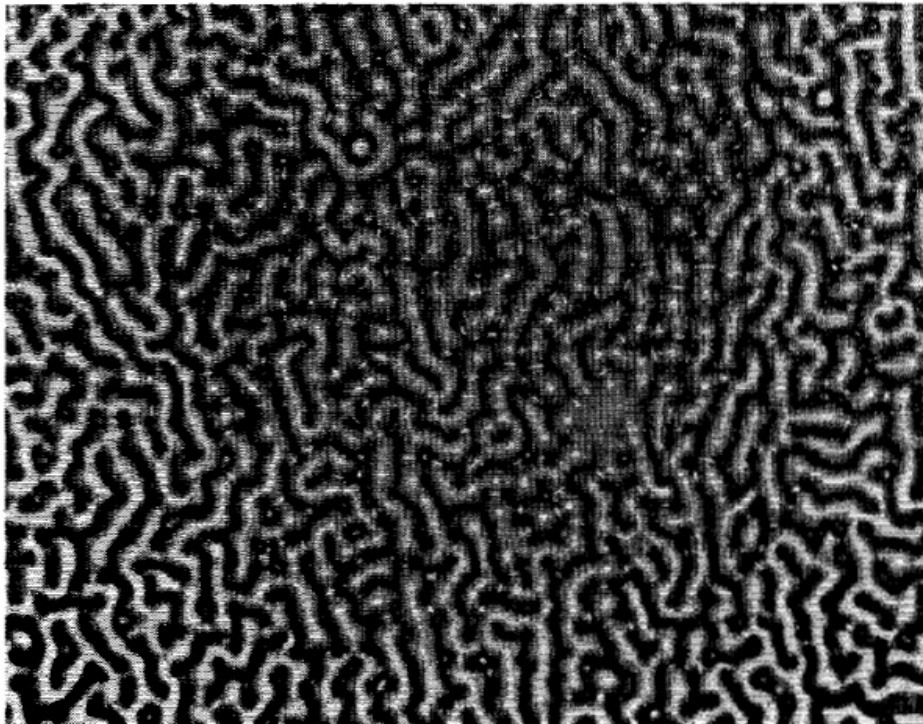


Figure 7.14 – Photomicrograph of developed thermoplastic surface from [204]. The size of the deformation cells is about $2\mu\text{m}$.

Heurtley explained that the relief pattern occurred due to the, "results from viscous flow which takes place between areas of substantial charge density difference due to differential fluid pressure in the thermoplastic layer below the charges and the lateral component of the electric vector on the charges at the boundary between each of such areas" [329]. Heurtley further describes the deformation as follows:

...ridge-like deformation would occur at areas of sharp difference in the charge density of the applied charge pattern whereby the overall response of the thermoplastic layer or the deformation pattern obtained was related to the differences in the charge density of adjacent areas rather than the absolute charge density of each portion of the thermoplastic layer [329].

Although the scale of deformations in thermoplastic xerography is different than the defects manifest in samples of this work, it confirms that thermoplastic deformation can be the result of charge - especially during softening and solidification behaviour. Furthermore, the layer of thermoplastic powder used in thermoplastic xerography is reported to be only 1-6 μ m thick [329], while the cumulative layer thickness in the current samples is \sim 10-50 times that thickness when the defects are manifest, therefore it is not unreasonable to question if the defects would scale with the toner thickness (and potentially the magnitude of charge). Assuming that were the case, Heurtley's explanation would indicate that the surface pitting/corrugation pattern on the current samples may indicate transitions between alternating domains of charge polarity, again

potentially reinforcing the notion that dielectric materials can be a charge mosaic [179].

Interestingly, the use of colloidal particles in a polymer matrix has also been used for an analogous process to thermoplastic xerography, where in the presence of a field, the polymer matrix is brought to a softened condition allowing the colloidal particles to align, which can be permanently frozen in if the polymer is allowed to solidify [335]. This phenomenon will be important to discussions in §8.1.3, but is mentioned here in the context of thermoplastic xerography.

Having elucidated that charge was a likely contributor to defect formation; a couple of additional factors deserved attention, prior to determining the direction for additional work.

7.1.3. Considering Surface Energy and Pressure

Another factor considered potentially significant in defect formation was surface energy to improve surface "wetting" which was the basis for the next trial [336, 337].

Sample 7-7 Plasma Treated Toner Layers

Since the observed defects did not develop during the initial layers, it was determined that if a surface energy was discouraging adhesion/wetting of incoming/fused toner, it was most likely the consolidated toner build surface that would pose a problem. Therefore, a preliminary trial was undertaken by printing five layers on a ceramic

substrate using the same settings as Sample 7-4. The substrate then underwent atmospheric plasma treatment by Graham Porcas, a director at Plasmatreat UK. There were three tracks of different treatment: a) a single pass with a 1kW plasma system at 10 m/min with a 50 mm rotating nozzle at a 10mm standoff distance; b) single pass with a 20mm nozzle; and c) same as b, but with three passes. Using test inks, it was determined that the surface energy had been raised to >72 mN/m which substantially increased adhesion/wetting.



Figure 7.15 – Photomicrograph of developed thermoplastic surface from [204]. The size of the deformation cells is about $2\mu\text{m}$.

Despite the smooth initial deposition of early layers (visible at the top of Figure 7.15), printed layers overlying all three areas of the plasma treated surface developed defects similar to those seen on earlier

samples. It was unclear whether the plasma treatment was helpful for the first layer deposited, but at any rate there was no noticeable benefit after several additional layers of toner were deposited. Although plasma treating each layer was considered (and could be beneficial to manage charge; see Sample 7-32), it was not pursued due to the potential oxidation/aging effects on the polymer [338], low likelihood that surface energy would improve toner transfer, and the cost.

The potential to use higher fusing pressures (above 250 ksi) was also considered as a means to “muscle” past defect formation, (especially since it had been one of the factors enabling production of Sample 6-3 EMB Sample Exceeding the 3mm Height Limit). After some preliminary trials, it was determined that the CTG printers were not engineered to exert sufficient pressure (the transfer rollers were deflecting in the middle). Additionally, parts subjected to that much pressure at elevated temperatures would experience significant deformation (as shown by the edges of the part in Figure 6.3) without appropriate support strategies (probably requiring the enclosure of the build volume inside a build sleeve; See §5.7.3.2). Finally, based on the experience of prior research (§4.6), it seemed that increasing pressure alone may only defer the manifestation of defects and mask their root cause(s). Therefore it was determined to continue in the short term to characterize the defects with suspected causes (in particular charge) aiming to establish causation.

7.1.4. Summary of Defects Arising with Non-electrostatic Transfer

Based on the observations in §7.1, it seems apparent that charge is likely a significant contributing factor to the defects observed, even when a non-electrostatic transfer method is used (because charge is still introduced from the toner particles and transfer roller). Due to the idiosyncrasies and limited resolution of charge measurement described heretofore, it was still unclear how the real surface potential (not just what has been measured) and surface quality correlate, despite evidence from thermoplastic xerography that indicates that the surface defects are a manifestation of differences in charge density and possibly polarity.

7.2. Using Electrostatic Transfer

The hypothesis that charge was a significant factor contributing to defect formation (as elucidated from experimental work in §6-7.1) led to the need to further explore and substantiate how charge influences the defects. Since the presumed presence of toner charge implicitly created fields, it was determined to consider the effect of explicitly induced fields (as in electrostatic transfer) to improve understanding.

The limitations of measuring charge imbalance using a field mill (as illustrated by Sample 7-6) created a dilemma of how to characterize charge in further experimental work in order to pursue this hypothesis. Alternative charge measurement devices were considered and their effectiveness assessed (including a non-contact electrostatic voltmeter,

see Sample 8-14). Owing to the relatively long lead time needed to obtain access to alternative methods, it was determined to continue use of the field mill (avoiding the use of conductive substrates, which undermine its ability to detect the field). Furthermore, it was presumed that the defects were a proxy for residual charge (imbalance) in the consolidated toner layers, which exerted a repulsive force on incoming toner as indicated by Sample 7-6. If that were the case, then defects arising due to unfavourable electrostatic conditions should, in theory, be corrected by electrostatically favourable conditions. For that reason, this subsection examines if the defects were diminished by the use of electrostatic transfer methods.

7.2.1. Theoretical Modelling of Height Limitation

Kumar et al. have published formulas [261, 271] describing the height limitations of conventional electrostatic transfer (as illustrated by Figure 4.13). Using electrostatic transfer methods to better understand toner behaviour, provided an opportunity to leverage these formulas to obtain further insight. In particular it was desirable to compare the toner used in this study with Kumar's formulas. Additionally, the question arose of whether it could ever be practical to produce samples 100mm high using conventional electrostatic transfer.

Kumar's equation to determine the electric field at the interface between the printed (consolidated) toner layers and the fresh incoming toner layer (based on a parallel plate model) is as follows [261]:

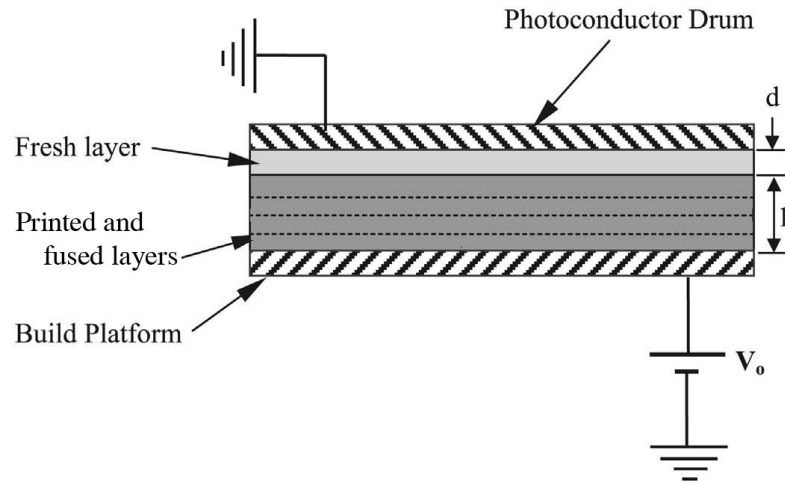


Figure 7.16 – Parallel plate illustration of powder transfer from photoconductor to build platform [Adapted from 261]

$$E_f|_{x=p+} = \frac{K_p}{K_f p + K_p d} \left[V_0 + \frac{\rho_p p^2}{2\epsilon_0 K_p} - \frac{\rho_f d^2}{2\epsilon_0 K_f} \right] \quad (7-1)$$

Where:

p is print height

d is the thickness of the fresh layer of toner

E_f is field strength

V_0 is a DC voltage applied to the build platform

ϵ_0 is the permittivity of free space

K_p is the relative permittivity of the printed layers of powder

K_f is the relative permittivity of the fresh layer of toner

ρ_f is the charge per unit volume in the fresh toner layer

ρ_p is the charge per unit volume in the printed toner layer

Solving for V_0 gives:

$$V_0 = \frac{E_f(K_f p + K_p d)}{K_p} + \frac{\rho_f d^2}{2\epsilon_0 K_f} - \frac{\rho_p p^2}{2\epsilon_0 K_p} \quad (7-2)$$

Substituting the same values that Kumar used [261], as summarised in Table 7.4, and assuming a required transfer field of 3MV/m (just insufficient to cause breakdown, §3.4.4.1), the platform voltage required in order to print from 0 to 100mm high is plotted in Figure 7.17.

Table 7.4 – Values for Figure 7.17

E_f	3,000,000	V/m
p	0 to 0.001	m
V_0	(Figure 7.17)	V
ϵ_0	8.85E-12	F/m
ρ_f	-2.26	C/m ³
ρ_p	0	
K_f	3	
K_p	3	
d	0.00002	m

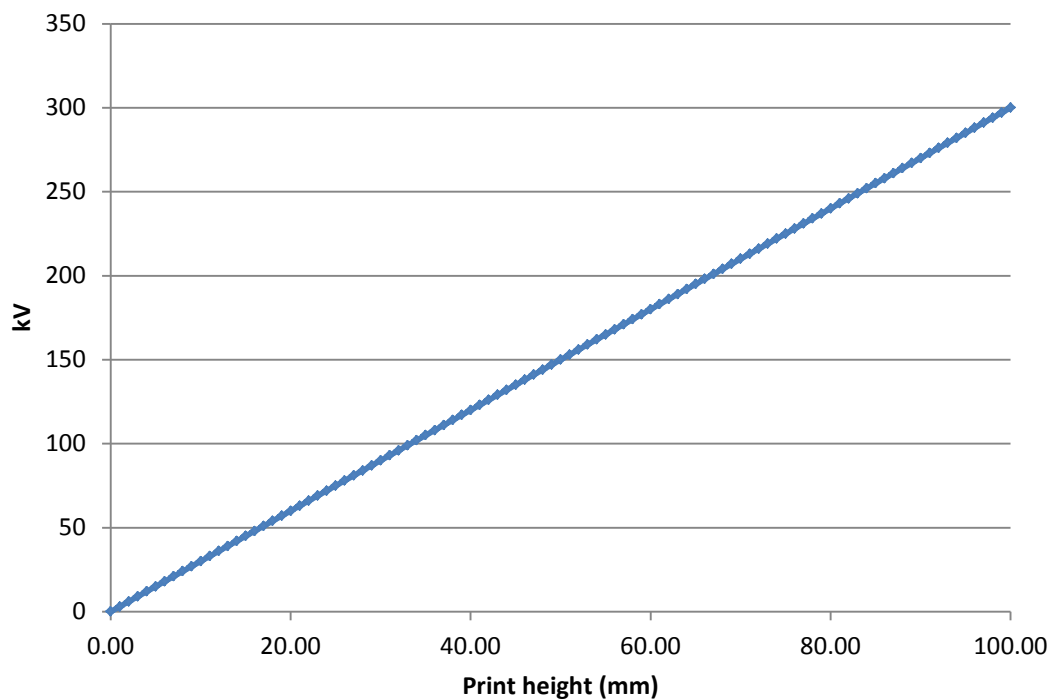


Figure 7.17 – Required platform voltage to maintain a 3MV/m transfer field strength at the top surface of a given part height (using conventional transfer) based on Equation (7-2).

Using the values in Figure 7.17 as a guide, realizing classical AM applications (with parts printed up to 100mm high) would require a voltage source of 300kV in order to ensure sufficient transfer field

strength according to Kumar's assumptions and formulas. Handling voltage at this magnitude was not deemed to be safe or practical in this context. In addition to the safety issues, it would pose unacceptable risk for damaging the imaging components. Furthermore, the field strength would not be uniform at the build surface due to the changing proportions of build/support material in the build (which changes with the part geometry), and random variations in the toner composition/consolidation resulting in fluctuations in the dielectric constant (§3.4.4.2).

Reviewing the values that Kumar's used in his equation reveals that he did not expect the fused toner layers to have any volume charge ($\rho_p = 0$). Even in his final report in December 2003, where he uses an updated formula for field strength calculations (Eq. 1 in [271]), the assumed charge per unit volume in the fused powder layer was 0 C/m³. It seems that the realization that the toner may have been retaining residual charge was not obvious to other researchers [211, 262, 277], and came only with hindsight to Kumar et al. as reported most succinctly by one of his master's students, Kumar Das [181]. It may not be surprising that detection of residual toner charge when using an electrostatic transfer method could be difficult; however *the assumption that fused toner has no charge per unit volume contravenes the evidence observed in the early experimental results of this work.*

Working on the hypothesis that residual toner charge is retained, Kumar's original values (Table 7.4) were substituted into his original equation

(7-1), except that the value for the charge per unit volume of the fused printed toner (ρ_p) was set as a percentage (0, 10, 25, 50, 75, and 100%) of the fresh toner value ($\rho_f = -2.26\text{C/m}^3$) [261]. The resulting plot of electric field strength (at the interface between the printed and fresh toner layer) versus the deposited toner thickness is shown in Figure 7.18, where the dashed black line assumes no charge per unit volume for the printed (and fused) toner as originally published [261].

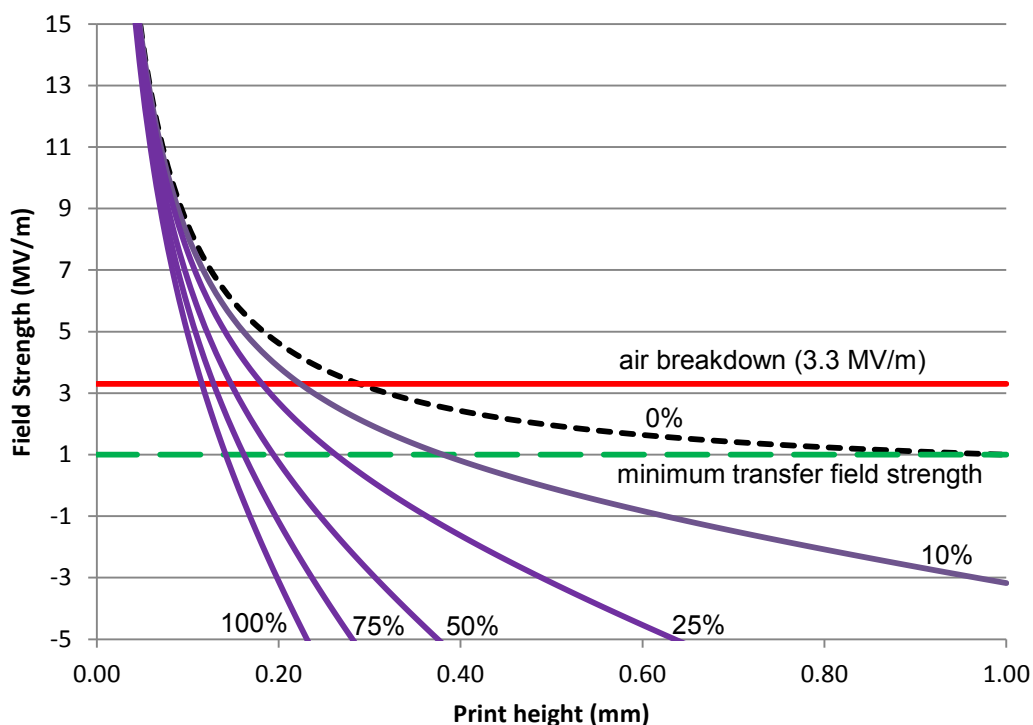


Figure 7.18 – Electric field strength versus deposited print thickness, using Equation (7-1) with the charge per unit volume of the fused toner equal to 0-100% of the fresh toner value used by Kumar and Dutta [261].

The upper horizontal (red) line indicates the maximum upper field strength before air breakdown (assuming no concentrating effects due to sharp geometry). Since the charge on the platform can be adjusted lower than 1,000V (and indeed was at 0V for all of the trials in §7.1) this can easily be compensated for. The lower horizontal (green) line indicates the

minimum field strength needed to transfer toner. Once the transfer field drops below this threshold, the electrostatic force exerted on the toner is not strong enough to overcome the electrodynamic forces holding the toner in place (§3.3.1.2, §3.4.4); therefore any toner transfer method must work to overcome these forces. Furthermore, once the field strength drops below zero it is no longer electrostatically favourable for toner to transfer (irrespective of the electrodynamic forces). The curving lines each indicate the field strength at the printed toner height with the indicated percentages of the fresh toner charge per unit volume assumed for the printed (fused) layers. The original graphed calculation by Kumar [261] (shown in Figure 7.18 with a dashed black line), which was based on the assumption that the fused toner loses all of its charge, does not drop below the minimum field strength until toner is printed 1mm high. However, when considering possible residual toner charge the field strength drops below acceptable levels much earlier.

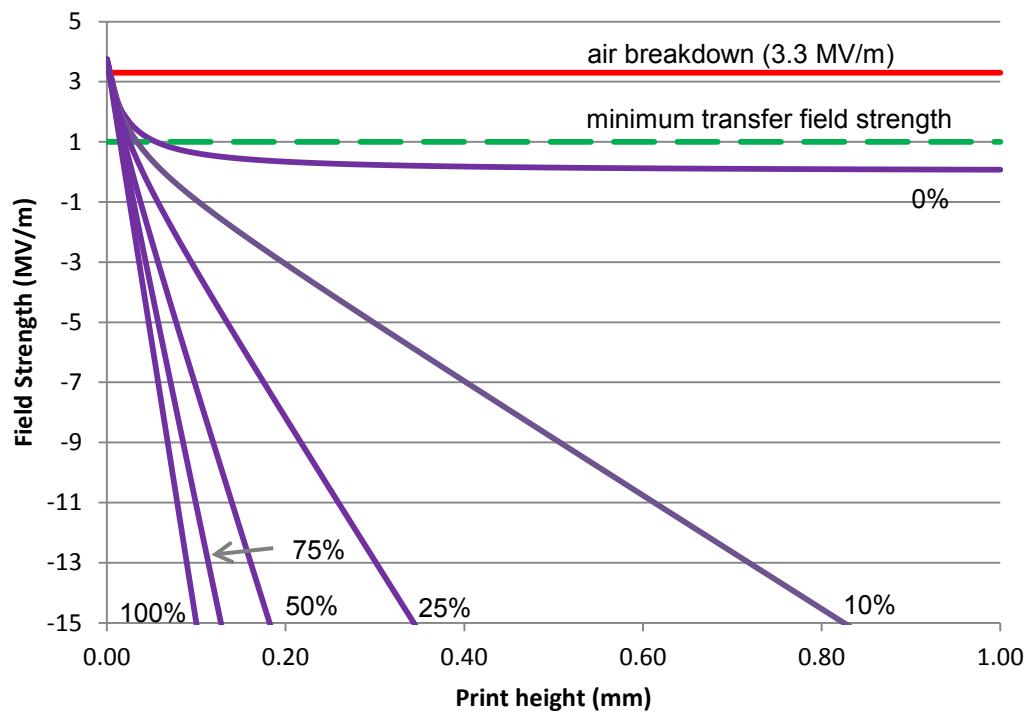


Figure 7.19 – Electric field strength versus deposited print thickness, using Equation (7-1) with the charge per unit volume of the fused toner equal to 0-100% of the fresh commercial polyester toner value and no voltage applied to the platform.

Substituting the values corresponding to the commercial polyester toner as listed in Table 7.5 (with the platform voltage reduced to 0V) into Equation (7-1) the field strength at the build surface for the §7.1 trials is plotted in Figure 7.19 as a function of print height. The charge per unit volume for the fresh polyester toner was calculated by converting the mean particle diameter from the measured

Table 7.5 – Values for Figure 7.19

E_f	(Figure 7.19)	V/m
ρ	0 to 0.001	m
V_0	0V	V
ϵ_0	8.85E-12	F/m
ρ_f	-10	C/m ³
ρ_p	0 to 100% ρ_f	
K_f	3	
K_p	3	
d	0.00002	M

mean q/d (-5.21 fC/10 μ m, §5.1) to a charge per unit volume ratio (assuming an ideal sphere for toner particle shape) of -5.21 fC/524 μ m³, then converting units to C/m³.

Despite the intention for tackification to achieve a 'non-electrostatic' transfer, assuming some toner charge is retained after fusing, Figure 7.19 indicates that the polarity of the field will swap to be the same polarity as the accumulated toner reaches a height of between 0.030 and 0.060mm (assuming a residual toner charge of 100% and 10% of the charge per unit volume of the fresh toner respectively). That means once the polyester toner printed height exceeds 0.060mm (with no platform voltage), the adhesion/tackification forces would need to be strong enough to overcome the repulsive transfer field strength (and electrodynamic forces) in order to realize high quality transfer of layers.

The new output from this model (due to the assumed residual toner charge) provides some basis for re-evaluating all alternative transfer methods (including repulsion).

It is noteworthy that the calculated thickness range (0.030-0.060mm) corresponds to the initial formation of defects in Sample 7-2 (and virtually all of the samples in §7.1).

Despite this correlation, further evidence was needed to confirm defect causation, which was the motivation for the following trials.

For completeness, multi-physics electrostatic modelling in 2D and 3D (COMSOL version 4.1.0.88, COMSOL AB, Sweden) was undertaken to expand upon the above equations. Although the visualisation was helpful, the assumptions lacked any experimental basis – in particular the presence, magnitude, and decay rate of residual toner charge were not yet substantiated. Additionally, the methodology for measuring these values experimentally (using a field mill) was not deemed robust. Therefore this approach was deferred (and not resumed within the scope of this work) until a more significant body of experimental measurements could be made to help validate an appropriate model.

7.2.2. Conventional Electrostatic Transfer

In order to further substantiate the theory that the defects were caused by electrostatics, trials were undertaken to evaluate if the repulsive effect of the suspected residual charge in the consolidated toner could be counteracted with an explicitly created transfer field (over a limited distance §4.3.1.3).

In order to test this theory, the SLP platform was further adapted by adding a conductive plate immediately underneath the ceramic substrate which was connected by wire (Figure 7.20) to a high voltage power supply (Model 477-304, Brandenburg, UK). In order to insulate the charged plate from the grounded platform (and prevent sparking), it was placed on a stack of 4 ceramic substrate plates (4mm high) which sat on top of the grounded conductive platform (as described for Sample 7-4).

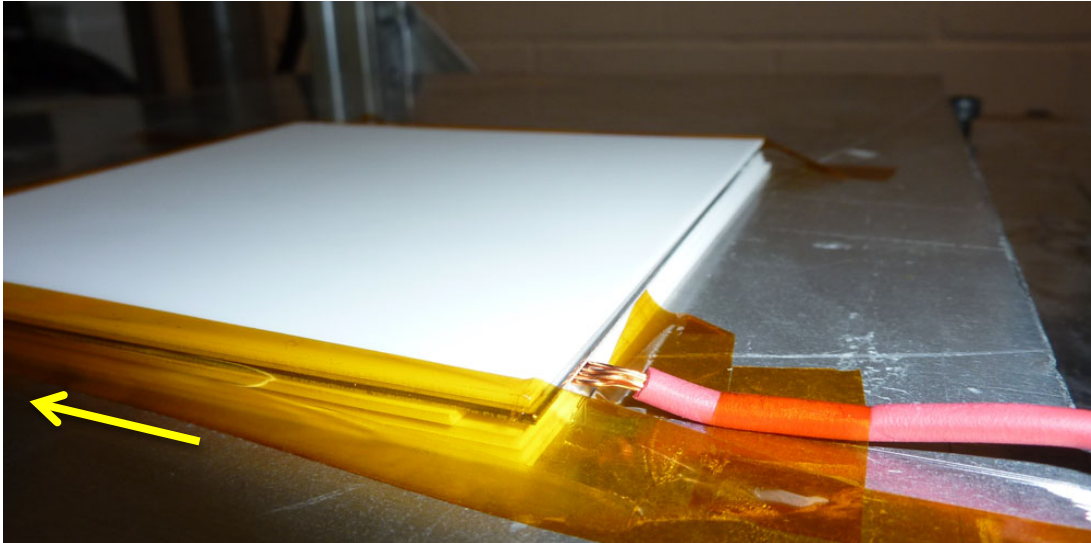


Figure 7.20 – Substrate and platform configuration enabling an aluminium plate to be charged with a high voltage wire to effect electrostatic transfer methods

7.2.2.1. Effect of Breakdown on Deposition

One of the early defects noticed was when printing occurred in a transfer field that exceeded the breakdown strength of air (noticeable because sparks could be heard and sometimes seen).

Sample 7-8 First Layer Defects

Sample 7-8 illustrates the defects arising in the first layer when applying a 3,000V charge to the plate underneath the 1mm-thick ceramic substrate. This voltage was sometimes sufficient for breakdown to occur in the first (or sometimes second) layer printed, which resulted in defects as shown in Figure 7.21 and Figure 7.22 (using polyester and epoxy toner respectively). After the first couple of layers of toner were deposited, no further breakdown occurred (probably due to increased toner thickness and dielectric strength). Due to the shape and pattern of these defects, they were called “fish scaling.”

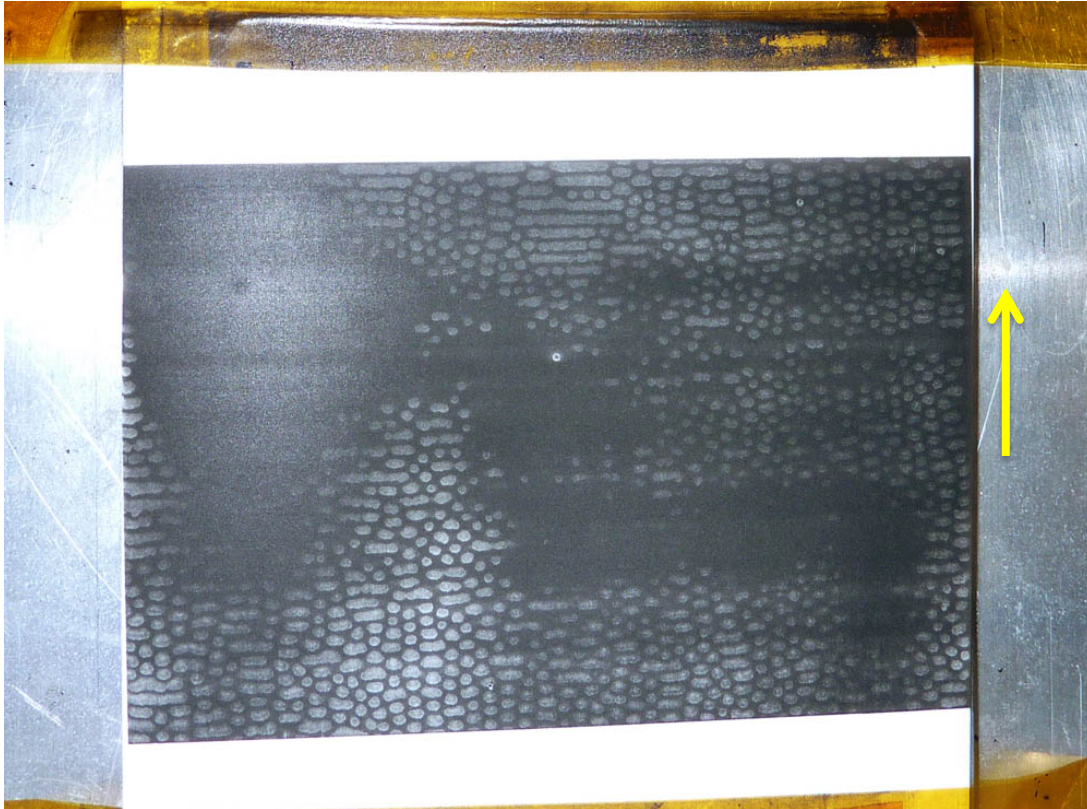


Figure 7.21 - "Fish scaling" defects in polyester toner layer due to air breakdown

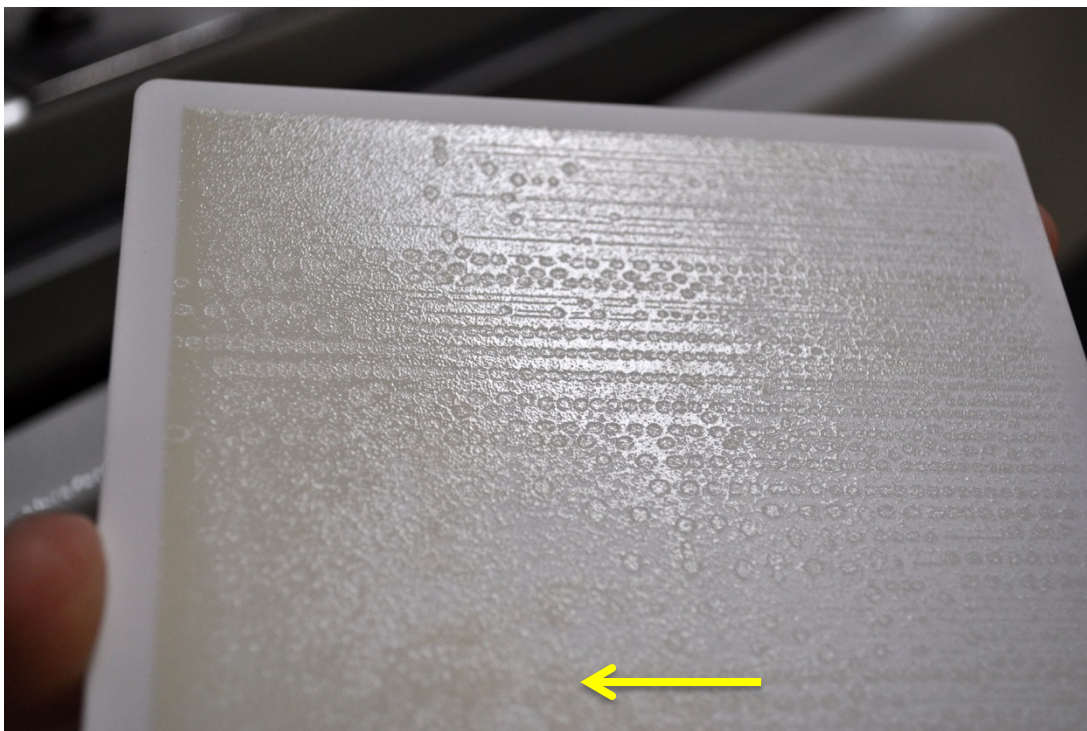


Figure 7.22 - "Fish scaling" defects in epoxy toner layer due to air breakdown

These round and oval defects ~2-2.5mm in diameter seem to relate to the "eye" shaped defects on Sample 7-6, except that: there was no "pupil" in the centre of them, and the surrounding area was not completely barren of toner. The slightly different features of this defect from the "eye" could be accounted for by use of the non-conductive substrate which did not allow electron flow in the same way. Evidence that these defects were the result of breakdown, included the strong smell of ozone (produced during breakdown) during and immediately following their production. Additionally, by reducing the voltage on the charged plate by 500V for the first print of each sample, the fish scaling pattern was avoided. Where fish scaling occurred, continued printing usually covered over this pattern. Although fish scaling was possible with other electrostatic transfer methods, it most frequently occurred with conventional electrostatic transfer. The alignment of defect patterning did not always correlate with the print direction (see yellow arrows in Figure 7.21 and Figure 7.22).

7.2.2.2. Counteracting the Repulsive Effect of Residual Charge

This subsection is based on the hypothesis that the consolidated toner body was retaining some charge, and therefore exerting a repulsive field on incoming toner. Here samples are produced in similar way to those in §7.1, except that an explicitly applied transfer field was used in order to counteract the suspected repulsive field, exerted by the consolidated toner layers.

The samples in this section conform to the following preparation, except as noted. They were printed with standard commercial black polyester toner (PolyJZ, Samsung, Japan) printed with settings shown in Table 5.1, except the conditioning roller voltage used was -550V, adjusted to improve image density. The same rectangular area was printed 20 times layer-on-layer (without any shift) onto a 120x120x1mm ceramic substrate (ADS96R, CoorsTek, CO, USA) which sat directly on top of the charge plate (Figure 7.20). The substrate and stack supporting it were held down using 12mm wide high temperature tape (Kapton tape, RS Components, UK) (as shown in Figure 7.30). The surface potential of the sample was measured in-process, after each layer was printed using a field mill device, with the lower platform covered with aluminium (Figure 7.6) to improve the signal-to-noise ratio. The toner deposition thickness was measured using digital callipers (CD-6"CS, Mitutoyo Corp, Japan) at the corners. For each sample set, the average surface potential (primary Y-axis) and cumulative toner thickness (secondary Y-axis) are plotted for each layer (X-axis) with \pm error bars equal to $\sigma/n^{1/2}$ (n samples) (§5.5.2). Where interpolated values are plotted, error is based on equipment accuracy/repeatability.

The samples have been named retrospectively to facilitate the discussion. A summary of sample preparation and results is included in Table 7.6 and then a more in-depth explanation of the results from each sample and discussion follows. In Table 7.6, the transfer voltage refers to the charge applied to the charge plate. The '# of layers' is the number of images printed layer-on-layer. The last column refers to the number and total

thickness of (1mm thick) ceramic plates above the charge plate. For expediency, the results are summarized in tabular format and verbiage is reserved for the discussion.

Table 7.6 – Experimental Regime using Conventional Electrostatic Transfer

<i>Sample:</i>	<i>Transfer Voltage:</i>	<i># of Layers:</i>	<i>Distance from 1st Layer to Charge Plate</i>
Sample 7-9	800V	20	1mm
Sample 7-10	1600V (½ of the sample only)	20	1mm
Sample 7-11	3,000V	20, 40, 60	1mm
Sample 7-12	3,000V, 2500V	176, 229	1mm
Sample 7-13	3,000V	20	2mm

Sample 7-9 First Conventional Transfer

The rationale for the following preparation parameters (Table 7.7) was to undertake a conservative first conventional electrostatic transfer. The $\sim 400\text{V}$ increase in voltage for the transfer step (over the transfer roller) was in line with similar increases between EP steps inside the printer (Figure 5.11), and posed a minimal threat to damaging the imaging components of the printer.

Table 7.7 – Sample 7-9 Preparation and Results

	<i>Value:</i>	<i>Description:</i>
Sample Preparation	18.3°C, 53% RH	Ambient conditions during build
	140°C	Target fusing temperature
	800V	Transfer voltage
	20	# of Layers
	1mm (1 plate)	Distance from 1st printed layer to the charge plate
Results	0.15 ± 0.03/0.21 ± 0.04	Min/Max Surface potential (kV)
	0.10 ± 0.01	Max height (mm):
	4.8 ± 1	Average interpolated layer thickness (μm)
	Pitting, but with reduced pitting in some areas	Description of Defects

Note: The surface temperature dropped $\sim 20^\circ\text{C}$ (to $\sim 100^\circ\text{C}$) after each print

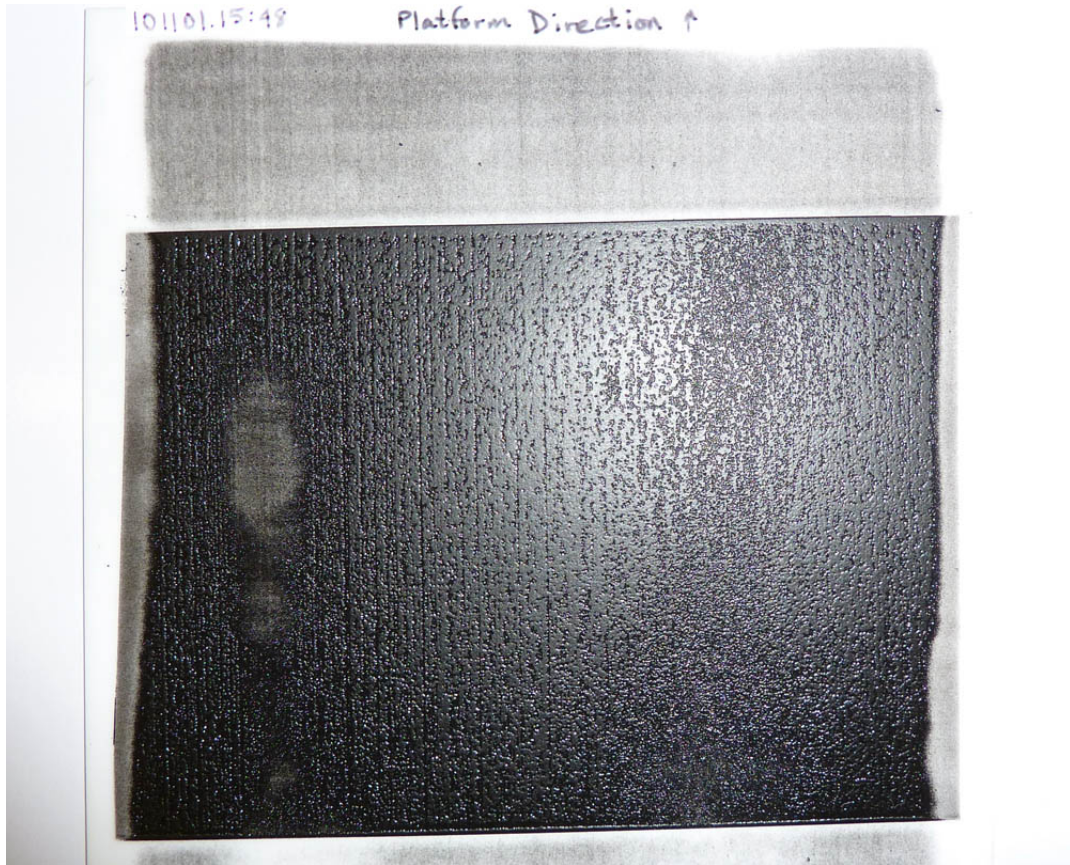


Figure 7.23 – Image of Sample 7-9 (800V transfer voltage) with general pitting, but some areas of reduced pitting

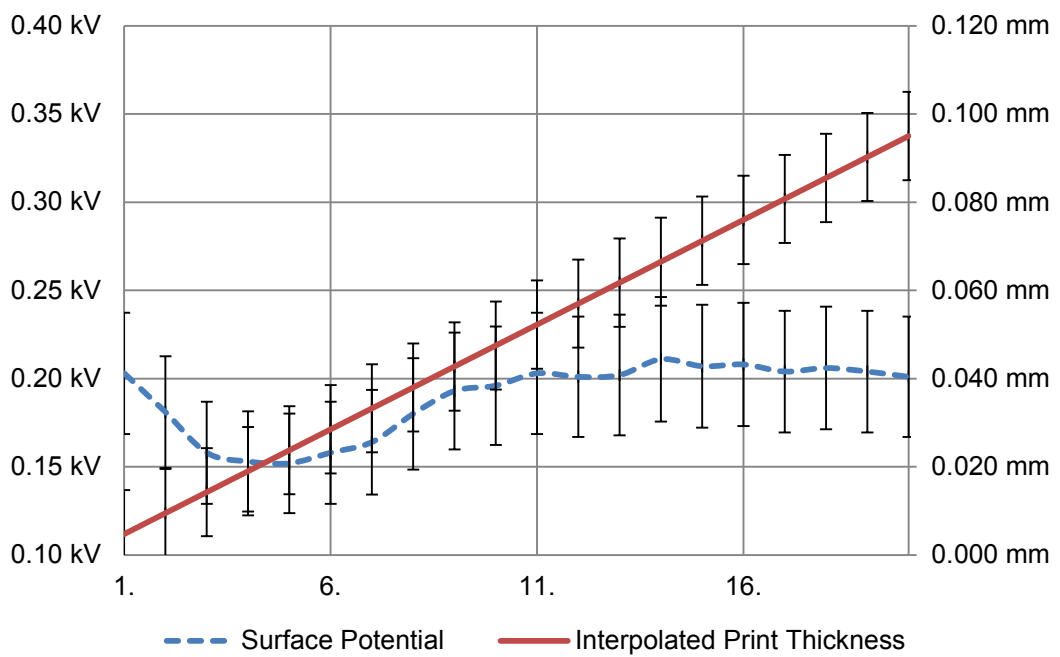


Figure 7.24 – Graph of post-print surface potential vs. average interpolated cumulative thickness for Sample 7-9

Sample 7-10 Half Conventional/Half Tackification Transfer

The rationale for the following preparation parameters (Table 7.8) was to provide a better frame of reference to evaluate the effect of the conventional transfer field on the surface defects by placing the charged plate under only half of the sample and leave a non-conductive support under the remaining sample area (Figure 7.25).

Table 7.8 – Sample 7-10 Preparation and Results

	<i>Value:</i>	<i>Description:</i>
Sample Preparation	19°C, 45% RH	Ambient conditions during build
	140°C	Target fusing temperature
	0V (½ of the sample)	Transfer voltage
	1600V (½ of the sample)	
	20	# of Layers
1mm (1 plate)	Distance from 1st layer to the charge plate	
Results	0.16 ± 0.03/0.36 ± 0.05	Min/Max Surface potential (kV)
	0.10 ± 0.01 (no charge)	Max height (mm):
	0.12 ± 0.01 (1600V)	
	5.5 ± 1 (no charge)	Average interpolated layer thickness (µm)
	5.8 ± 1 (1600V)	
General pitting (no charge) Less pitting (1600V)	Description of Defects	



Figure 7.25 – Charge plate configuration for Sample 7-10 (note: the exposed area on the charged plate shown here was covered during printing to avoid breakdown)

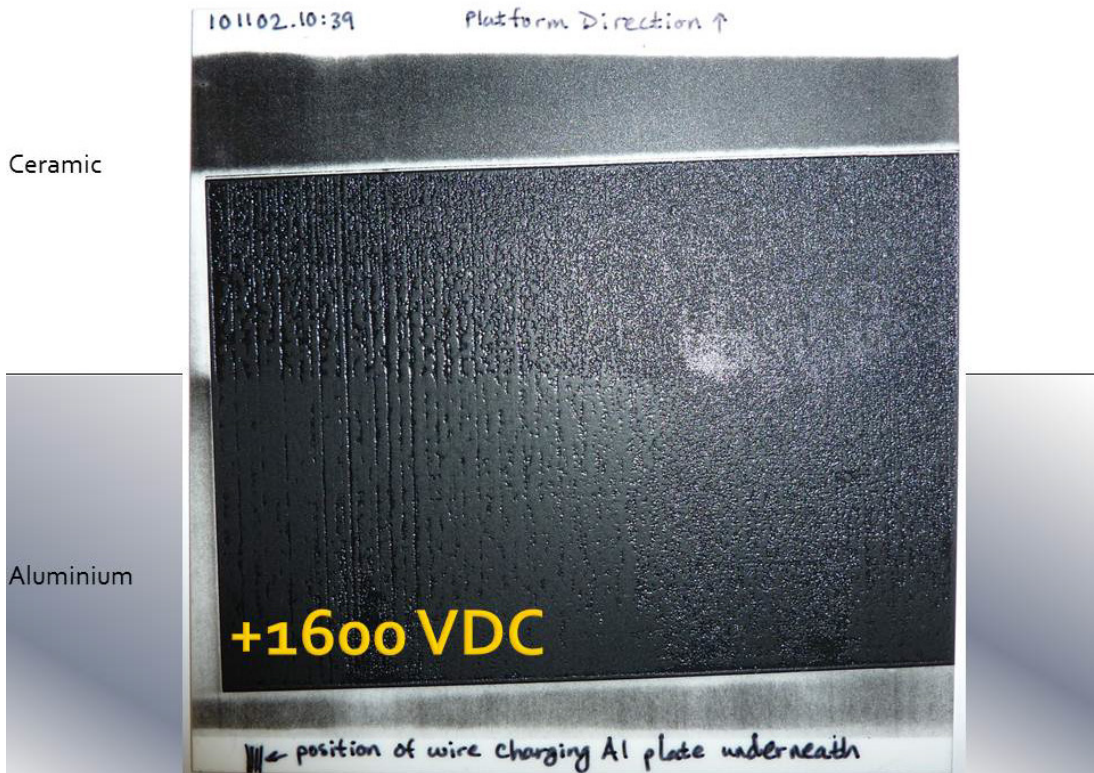


Figure 7.26 – Image of Sample 7-10 with significantly reduced pitting in areas above the charged plate

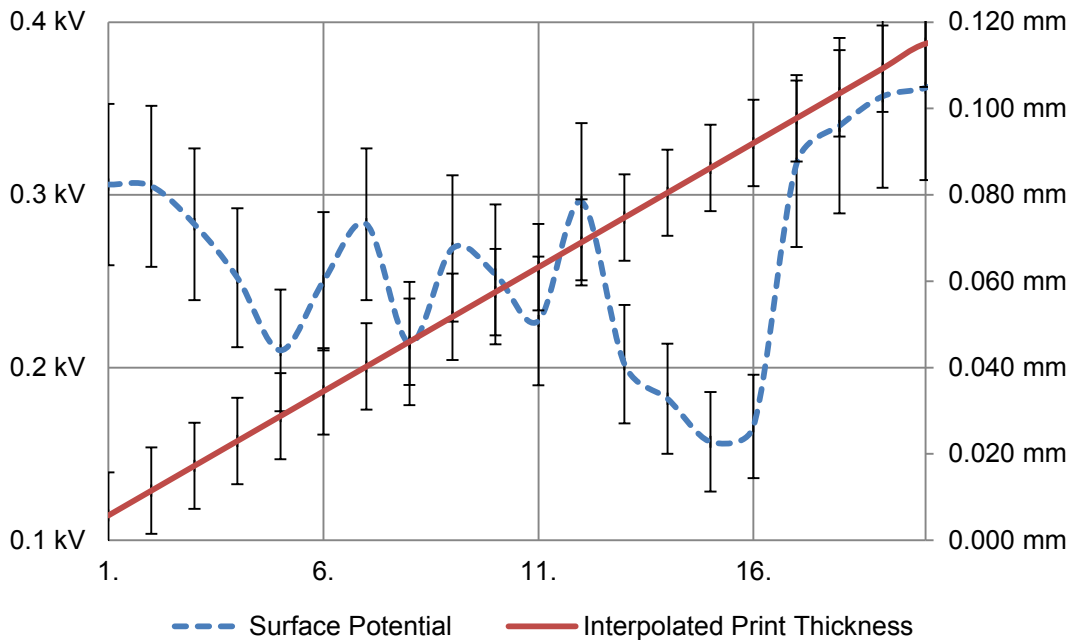


Figure 7.27 – Graph of post-print surface potential vs. average interpolated maximum cumulative thickness (for the half over the charged plate) for Sample 7-10

Sample 7-11 Maximum 3,000V Transfer

The rationale for the following preparation parameters (Table 7.9) was to see if the high voltage power supply (maximum capacity: 3kV) was able to achieve a defect-free 20-layer high sample.

Table 7.9 – Sample 7-11 Preparation and Results

	<i>Value:</i>	<i>Description:</i>
Sample Preparation	19°C, 45% RH	Ambient conditions during build
	140°C	Target fusing temperature
	3,000V (entire sample)	Transfer voltage
	20	# of Layers
	1mm (1 plate)	Distance from 1st printed layer to the charge plate
Results	0.37 ± 0.05/0.66 ± 0.09	Min/Max Surface potential (kV)
	0.16 ± 0.01	Max height (mm):
	7.8 ± 1	Average interpolated layer thickness (µm)
	No pitting, <1 µm Ra	Description of Defects

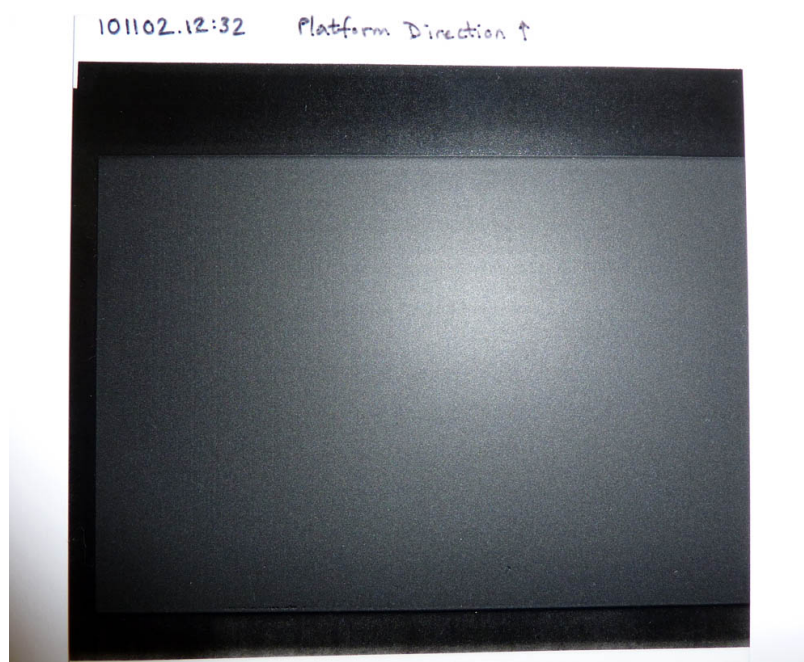


Figure 7.28 – Image of Sample 7-11, without pitting defects

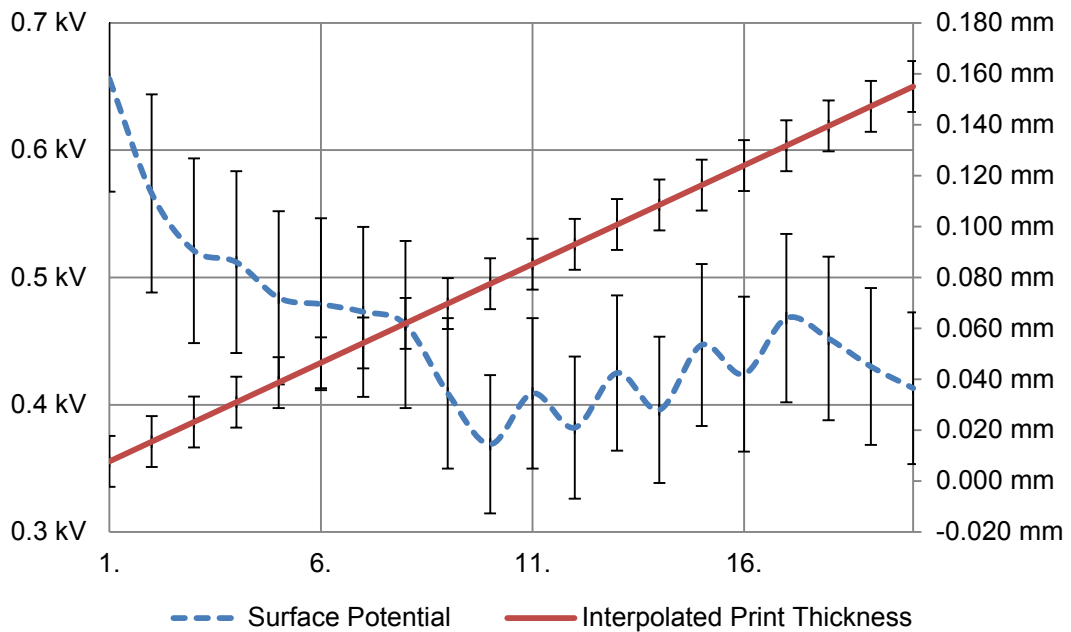


Figure 7.29 – Graph of post-print surface potential vs. average interpolated cumulative thickness for Sample 7-11

After successful defect-free printing at 20 layers, samples were produced using the same settings with 40 and 60 layers, achieving maximum thicknesses of 0.30 ± 0.01 and 0.41 ± 0.01 mm respectively and similar surface potentials. The 40 and 60 layer samples had an average interpolated layer thickness of 7.5 ± 1 and 6.8 ± 1 μm respectively. Samples were normally executed in automated cycles of 20 layers which were then manually re-initiated.

Sample 7-12 Print All Day Long

The elimination of defects in Sample 7-11 evoked a desire to test how long defect-free layers could be added to a sample. Therefore, it was determined that printing with the same settings as the last sample would commence and not cease until defects formed. Additionally, the surface potential measurement was taken just prior to the print in order to

assess how the surface potential of the sample affected the transfer. The preparation parameters and summary of results are show in Table 7.10.

Table 7.10 – Sample 7-12 Preparation and Results

	<i>Value:</i>	<i>Description:</i>
Sample Preparation	13.4°C, 30% RH 23% RH	Ambient conditions during build
	140°C	Target fusing temperature
	3,000V 2500V	Transfer voltage
	176 229	# of Layers
	1mm (1 plate)	Distance from 1st printed layer to the charge plate
	Results	1.82 ± 0.06/3.01 ± 0.10 1.60 ± 0.06/2.58 ± 0.09
0.87 ± 0.02 0.75 ± 0.06		Max height (mm):
4.9 ± 1 3.3 ± 1		Average interpolated layer thickness (µm)
No pitting, <1 µm Ra Multiple rows of pits		Description of Defects

After an entire day of work including preparation (~1.5 hrs.) and over five hours of printing (176 layers), no substantial defects were evident on the sample (Figure 7.30), therefore it was determined to repeat the same experiment using a plate voltage of 2,500V. The area printed was also increased to 132cm² in an attempt to print virtually every exposed area of the ceramic substrate to improve field mill readings. After another day of printing (229 layers in approximately seven hours), defects were becoming established on the second sample (Figure 7.31).

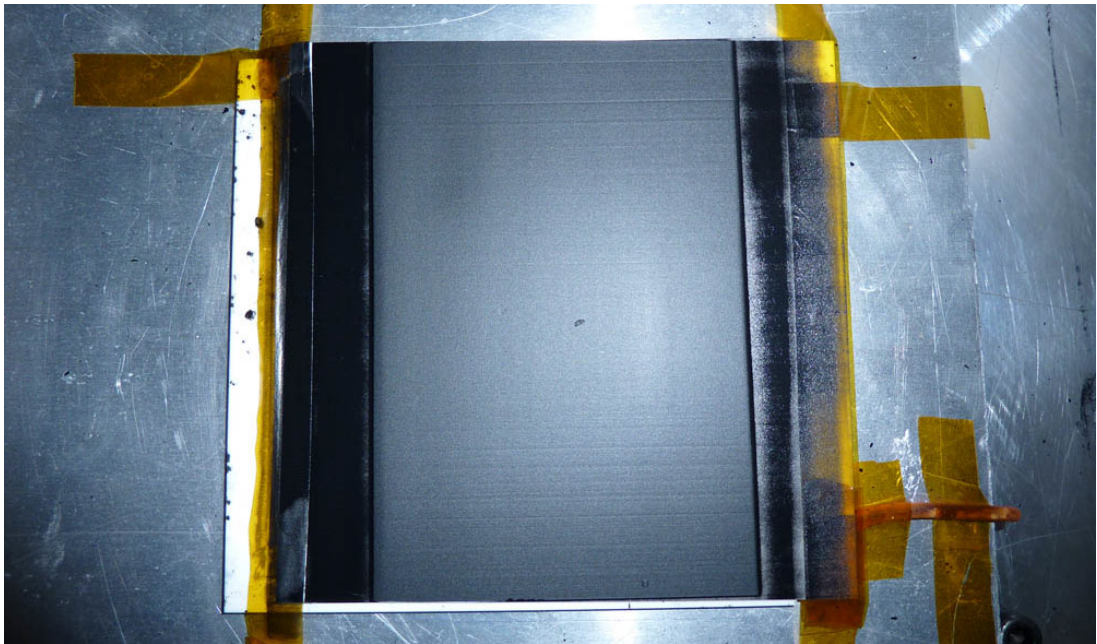


Figure 7.30 – Image of Sample 7-12 with 176 layers and very few surface defects as built on the SLP rig (before removal from platform); print direction was to the left

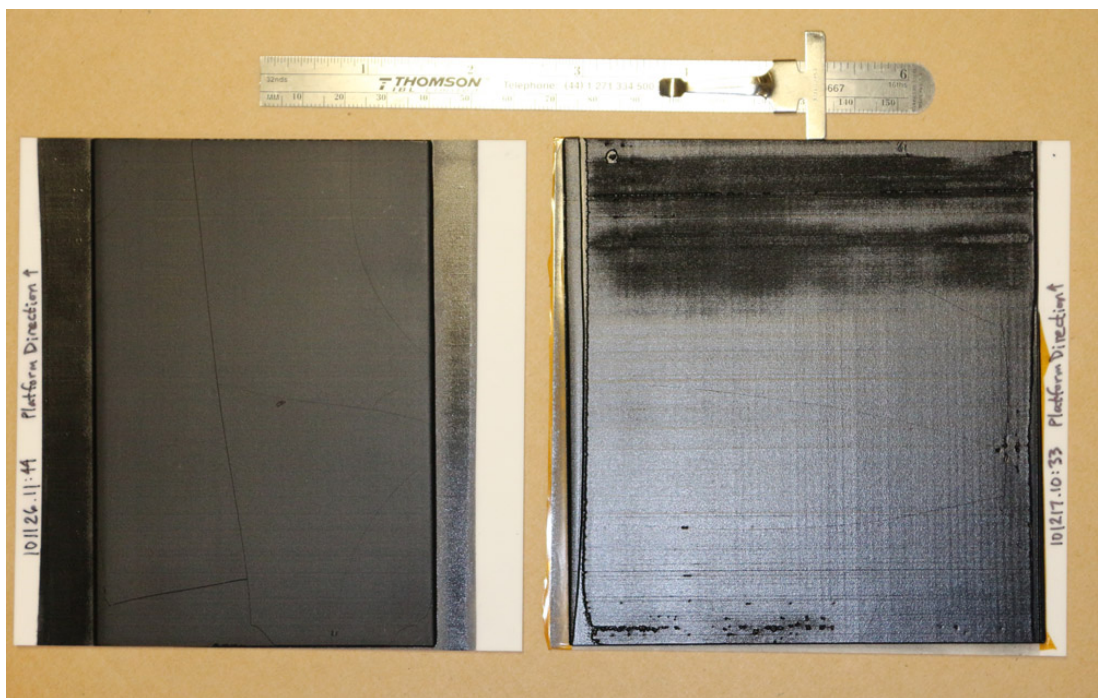


Figure 7.31 – Image comparing repetitions from Sample 7-12: 176 layers printed with transfer voltage of 3,000V (left) vs. 229 layers printed with transfer of 2,500V (right)

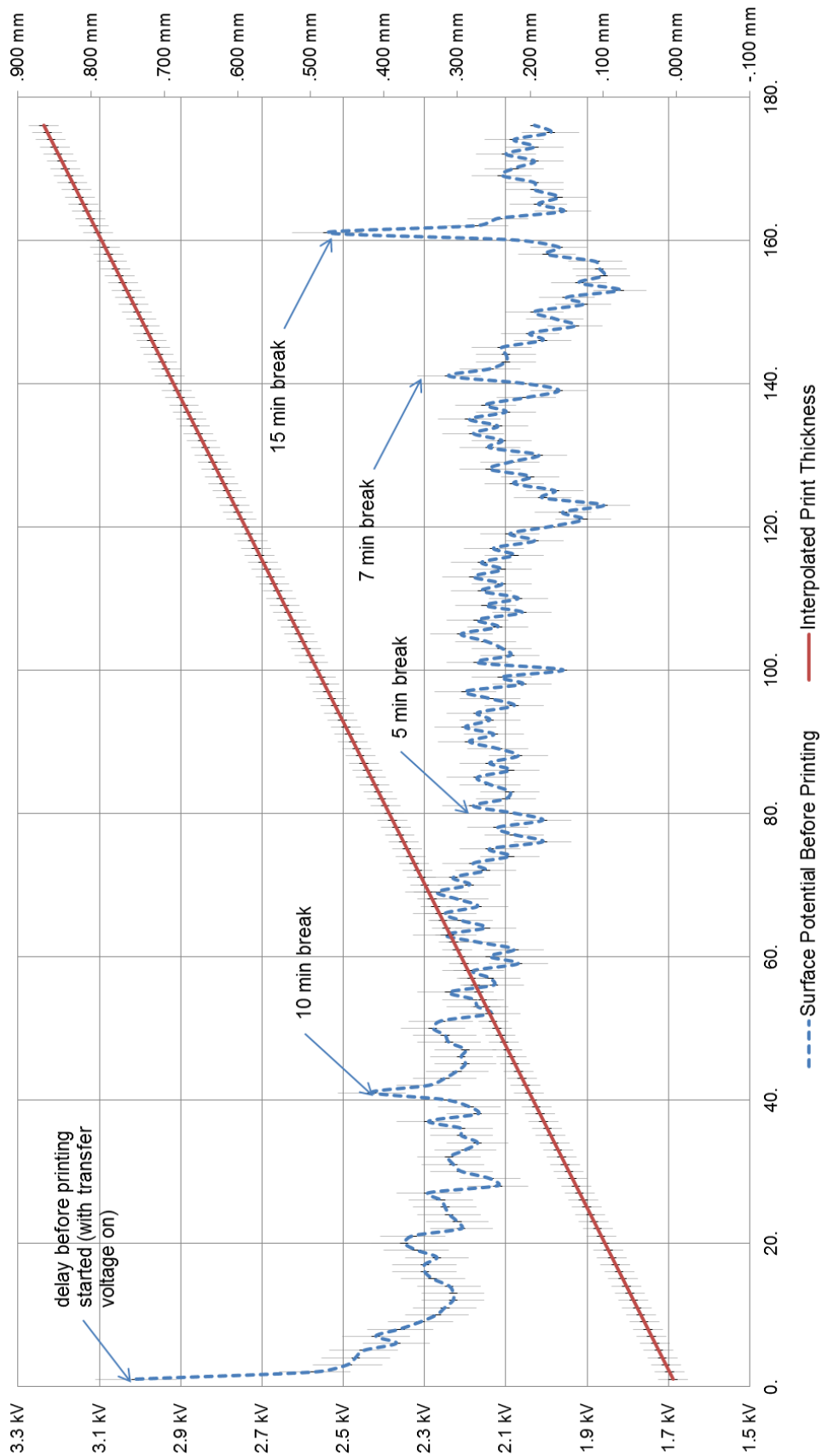


Figure 7.32 – Graph of pre-print surface potential vs. average interpolated cumulative thickness for Sample 7-12

Sample 7-13 Doubling the Distance to the Counter Electrode

This sample was undertaken to observe defect behaviour when simulating printing in excess of 1mm.

Since cracking on the top layer (as/after the samples cooled) of the prior samples prevented resuming the build, an additional sheet of ceramic was inserted above the charge plate so that the initial build surface was 2mm away from the charged plate (twice as far as all previous samples), which is essentially the counter electrode to the charged transfer roller. (Note: the additional 1mm of ceramic had no measurable volume charge; therefore it was not capable of reversing the polarity of the field or exerting any repulsive force on the incoming toner. However, the ceramic's higher ϵ_r of 9.5 [compared to ~ 3 for polyester toner] simulated the magnitude of the additional field attenuation [approaching 10MV/m] due to residual charge [albeit without the negative polarity], as approximated using equation (7-1) and assuming a 7% residual toner charge in the consolidated toner).

Apart from the 2mm distance from build surface to the charge plate, the print settings were the same as for Sample 7-11 with additional parameters listed in Table 7.11. The surface potential was measured after each print.

Table 7.11 – Sample 7-13 Preparation and Results

	<i>Value:</i>	<i>Description:</i>
Sample Preparation	18.3°C, 53% RH	Ambient conditions during build
	140°C	Target fusing temperature
	3,000V	Transfer voltage
	20	# of Layers
	2mm (2 ceramic plates above the charged Al plate)	Distance from 1st printed layer to the charge plate
Results	0.09 ± 0.02/0.58 ± 0.08	Min/Max Surface potential (kV)
	0.14 ± 0.01	Max height (mm):
	7.0 ± 1	Average interpolated layer thickness (µm)
	Substantial pitting	Description of Defects

Once the printing was complete, the surface potential with the transfer voltage on was $0.57 \pm 0.08\text{kV}$. Upon turning the transfer voltage off, the surface potential of the sample dropped to $-0.32 \pm 0.03\text{kV}$.

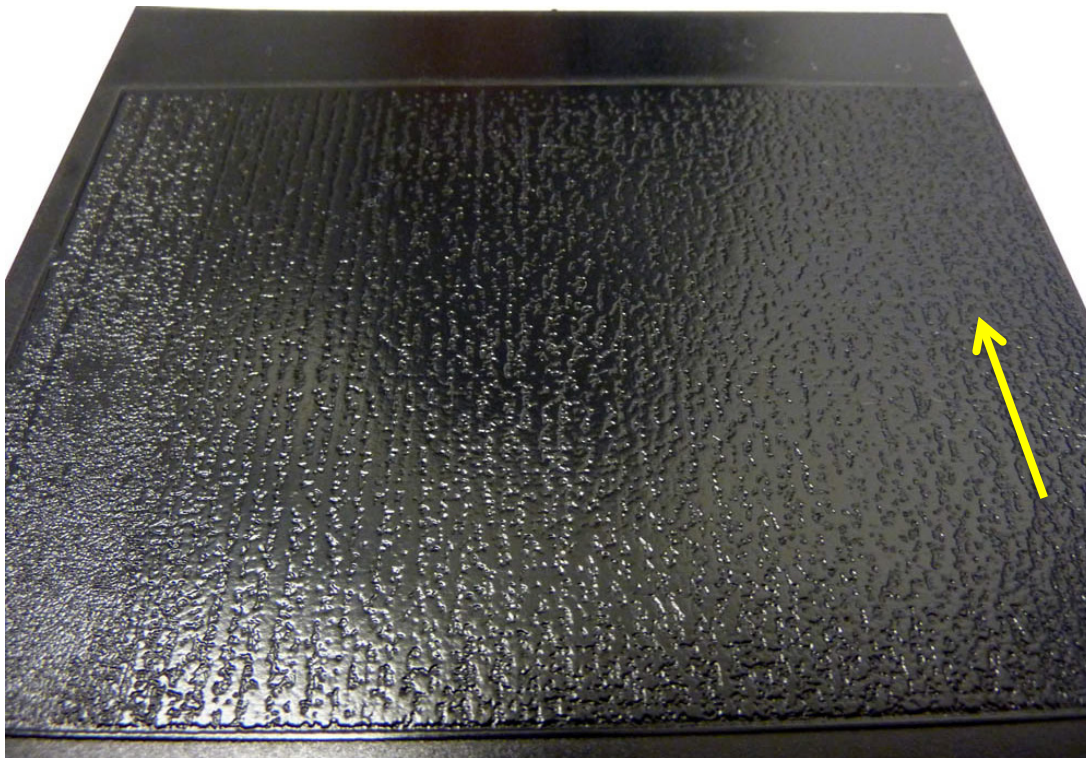


Figure 7.33 – Image of Sample 7-13, exhibiting general pitting defects and low deposition area on the left

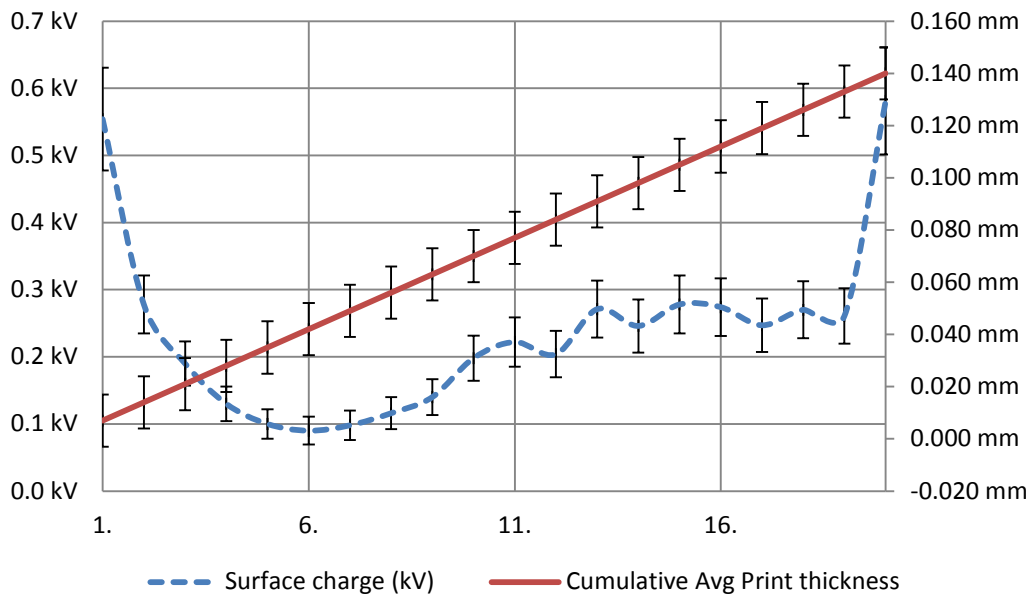


Figure 7.34 – Graph of post-print surface potential vs. average interpolated cumulative thickness for Sample 7-13

Table 7.12 – Summary of Conventional Electrostatic Transfer Results

Sample:	Max height (mm)/ (# of layers):	Transfer Voltage (V)	Average Interpolated Layer Thickness (μm)	Description of Defects
Sample 7-9	0.10 ± 0.01 (20)	800	4.8 ± 1	General pitting
Sample 7-10	0.10 ± 0.01 (20)	0	$5.5 \pm 1\mu\text{m}$	Reduced pitting above 1600V
Sample 7-11	0.16 ± 0.01 (20)	3,000	7.8 ± 1	None
	0.30 ± 0.01 (40)	3,000	7.5 ± 1	A few rows of pits
	0.41 ± 0.01 (60)	3,000	6.8 ± 1	A few rows of pits
Sample 7-12	0.87 ± 0.02 (176)	3,000	4.9 ± 1	Only 1 small pit
	0.75 ± 0.06 (229)	2,500	3.3 ± 1	Multiple rows of pits
Sample 7-13	0.14 ± 0.01 (20)	3,000	7.0 ± 1	General pitting

7.2.2.2.1. Discussion of Counteracting the Repulsive Effect

Sample 7-9 had a large area of low deposition on the left, possibly due to insufficient pressure in the transfer nip. The sample generally suffered from pitting; however in the centre of the sample the pitting was moderately reduced. It was unclear if the reduced pitting was due to the transfer field or possibly higher nip pressure in that area. Reviewed in the context of all of the samples, it appears that this was the effect of a relatively weak (yet helpful) transfer field. The dip in surface potential during the first 9 layers (lowest at layer 5) may be the effect of incoming negatively charged toner (transferred most efficiently in the early layers when the transfer field strength would have been the strongest). These results instilled the confidence to double the transfer voltage (on the charge plate) to 1,600V for the next sample.

Sample 7-10 provided the first compelling evidence suggesting that the transfer field significantly improved the surface finish of the printed toner. The maximum printed toner height was nearly the same, the primary difference was that the sample half above the charge plate had significantly reduced surface roughness. The charge measurement of this sample was almost certainly skewed by the half and half transfer field which was in effect averaged out in the field mill measurements. Due to the improvements in surface quality with increased voltage, the voltage was almost doubled again to 3,000V for the next sample.

Sample 7-11 was the first sample in this study which did not exhibit pitting defects. Interestingly it was also the first sample to exhibit a

definitive downward surface potential trend. This downward trend may be accounted for because of the transfer efficiency which continually supplied the consolidated layers with fresh negatively charged toner (which simultaneously may have been increasing the negative residual charge and also insulating the field mill from the field of the positively charged transfer plate). This sample set exhibited a linear increase in height from 20 to 40 layers printed (0.16 to 0.30mm), but dropped off a little from 40 to 60 layers (adding only 0.11mm more), possibly due to diminished field strength. The 20-layer sample is virtually defect-free, while the 40 and 60 layer samples exhibit a few rows of minor pitting on one side (perhaps due to lower nip pressure), but most of the surface is the same as the 20-layer sample. This sample set raised the question of how far it would be possible to continue printing defect free layers, which led to the next trial.

Sample 7-12 provided confirmed evidence that reducing the field strength reduces the layer thickness because even with 53 additional layers (229-176), the sample printed with a transfer voltage of 2,500V was 0.12mm (0.87-0.75) shorter than the sample printed with a transfer voltage of 3,000V. It then follows that as the print height/thickness grows, the critical field strength at the build (upper) surface decreases. Therefore the average layer thickness must be reduced as the layers stack up. This leads to the conclusion that in order to maintain a consistent printed layer thickness, the voltage should be actively controlled to maintain consistent transfer field strength at the build surface. This formed a core concept in a patent application [339].

Sample 7-12 also had a generally downward surface potential trend during the first 40 or so layers. The reduction of transfer voltage to 2,500V at first produced results similar to 3,000V, however over the course of the printing, defects began to arise and grow which can be seen on its final upward facing surface (Figure 7.31). It is noteworthy that neither sample extended beyond 1mm high (in line with Kumar's calculations [261]) despite spending two entire days printing. This led to the question of what would happen when printing more than 1mm high which led to the next sample. Originally, it was envisaged that printing could be resumed the next day, however over night the samples cracked preventing this. The cracking was almost certainly the result of the unmanaged thermal stresses on the brittle toner material during cooling. Speculatively, the cracking may have also been contributed to by the density of same sign electrostatic forces essentially trying to separate themselves from each other.

Another phenomenon became evident with Sample 7-12. Since it was necessary to take some breaks throughout the hours of printing (which was performed in sets of 20 prints), the extra time which elapsed during those breaks enabled the surface potential to "recover" toward the voltage of the applied field strength (Figure 7.32). Breaks which lasted longer than 3 min have been labelled on Figure 7.32. The longer the break duration, the surface "recovered" to higher potential as measured by the field mill. (Note, the transfer voltage was left on during the breaks.) Excluding the effects from longer breaks, there seems to be a

cyclical rise and fall in the surface potential over time. Speculatively this may be explained by the accumulation of potential until charge flows briefly (accelerating charge recombination) and then it begins to cyclically accumulate again.

Sample 7-13 repeated the same area of low deposition on the left as seen in other samples, probably due to insufficient pressure in the transfer nip. Otherwise, the sample was generally covered with pitting defects, some in rows parallel to the platform motion (Figure 7.33). The overall height was 0.02mm lower than the (20-layer) Sample 7-11 which was processed identically except for the 1mm difference in the distance between the counter-electrode and the build surface. This makes the reduced height and surface defects attributable to the reduced field strength (due to the larger gap between the voltage sources, Figure 4.13).

The reduction of pitting defects in every sample produced in this subsection has correlated with increased transfer field strength. Conversely, the reduction of field strength has enabled defect formation (Sample 7-12b, Sample 7-13). The average interpolated layer thickness increased and decreased with transfer field strength. That is not to say that the samples grew in height linearly (it was simply represented that way because there was not enough data to represent it otherwise), but it does confirm the overall trend.

The samples in this subsection collectively provided compelling evidence that the pitting surface defects can be corrected by electrostatics. *This fact is strong evidence that pitting arises largely due to electrostatic causes.*

7.2.2.3. *Using Intermediate Conductive Layers*

Since the results in the last section (§7.2.2.2) demonstrated the potential to suppress defects with sufficient transfer field strength, the practicality of one way to achieve that was explored in this subsection. Since the primary factors affecting field strength are voltage and distance (Equation (3-10)), and high voltage was deemed impractical to use (§7.2.1), innovations to reduce the distance were explored. Building on the information from Sample 7-13, the potential to include intermediate conductive layers in the part that could be charged was assessed. For example, if a conductive layer was included every 0.5mm and was charged to create a transfer field, it would effectively reduce the maximum distance that a field had to permeate accordingly. The concept would be to “leap frog” from one intermediate conductive layer to the next to limit the distance between counter electrodes to less than 1mm. Although the practicalities were potentially dubious and it would contravene the desire for “pure” thermoplastic parts, its potential as an option was deemed worthy of preliminary exploration.

7.2.2.3.1. *Feasibility of Printing onto Conductive Substrates*

The first test for this concept was to explore how to print onto conductive layers. Based on experience with Sample 7-6, it was known that a

grounded substrate would create breakdown (sparking), however it was unclear if printing could be done directly onto an isolated conductive material. Al foil was used to test this idea. 20-layer samples were printed onto ceramic substrates partially covered with Al foil.

Sample 7-14 Printing onto Taped Down Al Foil

This sample was made with print settings similar to Sample 7-11 and yielded results as shown and discussed in Table 7.13.

Table 7.13 – Sample 7-14 Results and Discussion

<i>Results:</i>	<i>Discussion:</i>
 <p data-bbox="296 1440 845 1561"><i>Figure 7.35 – Sample 7-14 with surface pitting above the foil and defect-free surface elsewhere</i></p>	<p data-bbox="845 1104 1415 1462">The surface quality above the Al foil was severely pitted except just before the second piece of tape (high temperature Kapton tape) where a small bulge formed and no toner was deposited on the backside of the bulge. The bulge stuck up a little more than the rest of the sample and would discharge on the SLP rig during the print cycle, so the next sample was not taped in back.</p>

Sample 7-15 Printing onto Glued and Taped Al Foil

This sample was prepared as for Sample 7-14, except the transfer voltage was reduced to 800V (to avoid sparking) and the foil was mounted with spray adhesive to avoid creating a bulge and only one

piece of tape was used to keep the leading edge down. Results and discussion follow in Table 7.14.

Table 7.14 – Sample 7-15 Results and Discussion

Results:



Discussion:

In process the foil, despite being isolated from the high voltage, was prone to discharge on the SLP rig at the safety gate (shown at left) like the prior sample. This gate was located just before the printers and intended to ensure nothing (except for the build substrate) passed underneath the printers.

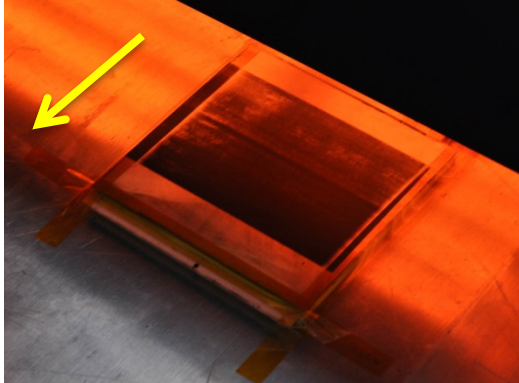
The surface quality above the Al foil was severely pitted. This indicated that isolated conductive substrates may not be amenable to receiving printed toner directly.

Figure 7.36 – Sample 7-15 showing sparking during sample preparation (above) and global surface quality defects (below)

Sample 7-16 Printing onto Al Plate with Low Voltage

Since each case of breakdown had occurred on a raised portion of Al foil for each of the preceding samples of this subsection, a sample was printed using the same settings as Sample 7-15, except that the toner was printed directly onto the Al transfer plate. Results and discussion follow in Table 7.15.

Table 7.15 – Sample 7-16 Results and Discussion

<i>Results:</i>	<i>Discussion:</i>
 <p data-bbox="327 891 821 974"><i>Figure 7.37 – Image during the fusing of Sample 7-16, showing defects forming in early layers deposited on the Al plate</i></p>	<p data-bbox="890 443 1409 728">Although the low voltage reduced the magnitude of breakdown, it was not prevented because of the direct contact between the transfer roller and conductive substrate. Due to the breakdown in combination with the poor quality deposition, only a few layers were printed on Sample 7-16, and then it was discontinued.</p> <p data-bbox="890 766 1409 1052">The poor quality deposition on the trailing edge of the sample (upper right as in Figure 7.37) may be due to the fact that the potential in the plate had been depleted by early/continued contact with the transfer roller. The poor deposition on the left side of the sample was attributed to low pressure in the contact nip.</p>

Although there were no high points for breakdown to preferentially occur on this sample, the poor density results discouraged continuing (even though surface pitting defects were not yet formed).

Sample 7-17 Printing onto Al Foil Covered by Tape

This sample was prepared as for Sample 7-14, except a small piece of foil was completely covered with a piece of high temperature tape to keep it from discharging. Results and discussion follow in Table 7.16.

Table 7.16 – Sample 7-17 Results and Discussion**Results:****Discussion:**

Figure 7.38 – Sample 7-17 defect free deposition over substrate and foil covered with insulating tape (on left side)

The rectangular piece of tape covering a rectangular piece of foil can be seen on the left side of the Figure 7.38.

The surface quality all around was defect free and $<1\mu\text{m Ra}$. This indicated that isolated conductive substrates covered with a non-conductive layer can be printed over.

The samples in this subsection indicated that it would be necessary to cover isolated conductive surfaces prior to printing onto them (using a conventional transfer field) in order to prevent discharge.

7.2.2.3.2. Feasibility of the “Leap Frogging” Concept

Having understood the conditions required for printing over conductive substrates, the next test was whether the “leap frogging” concept would work. One concern was that intermediate conductive layers could further “shield” the build surface from the transfer field.

Instead of trying to print many layers and the conductive layer, initial tests were undertaken to simulate 0.5mm thick printed material with conductive layers. This was performed by printing onto the unclad side of single-sided 1 ounce ($\sim 35\mu\text{m}$ thick) copper-clad FR-4 glass-reinforced epoxy board (Kingboard Laminates Ltd, Hong Kong supplied by Quartz

TSL Ltd, UK). This was printed onto with the copper side facing down (labelled as Intermediate Layer 0.5mm FR4 single, "IL0.5mmFR4Cu↓" or simply "IL" for short) in a stack with the high voltage coupled to the foil layers.

Sample 7-18 Printing onto a Stack of Copper-clad Board

This sample was printed onto a stack of IL0.5mmFR4Cu↓ from 1 to 4mm high (2 to 8 IL stacked) with the charge plate coupled by foil to the copper layer 1mm down from the build surface (Figure 7.39). The print settings were the same as for Sample 7-14, except the transfer voltage was set to 2,500V (to avoid 1st layer "fish scaling" defects and account for the different dielectric strength of the epoxy board). The results and discussion follow in Table 7.17.

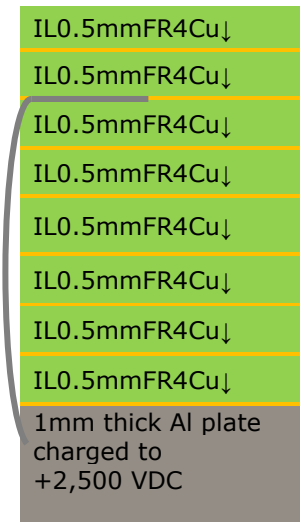


Figure 7.39 – Illustration of transfer voltage coupling for Sample 7-18

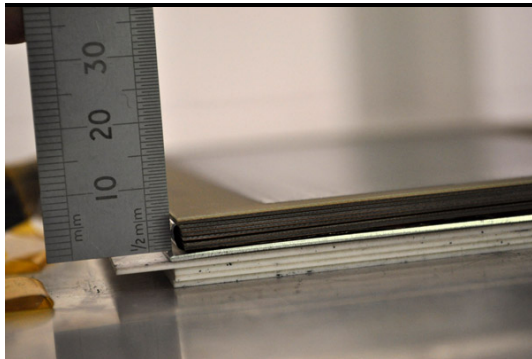
Table 7.17 – Sample 7-18 Results and Discussion*Results:*

Figure 7.40 – Sample 7-18 defect-free deposition over 4mm high

Discussion:

By leap frogging the foil coupling to the intermediate conductive layers, defect-free printed layers were deposited over 4mm high (4mm of intermediate layers + the thickness of the printed layers). This was expected, but demonstrates one way to circumvent to the height limitation published by Kumar and Dutta [261].

It appears this method can build parts of unlimited height without compromising surface quality.

This set of samples demonstrated the viability of the leap frogging concept and its potential to produce “tall” parts by EP.

7.2.2.3.3. Capacitive Coupling of Intermediate Conductive Layers

Combining the understanding that isolated conductive layers allow field to “pass through” them without causing shielding effects (Sample 7-17) with the leap frogging concept (Sample 7-18) led to trials to capacitively couple intermediate layers to the charge plate.

Sample 7-19 Capacitively Coupling to Conductive Layers

This sample was prepared with the same printer settings as for Sample 7-13, except that instead of separating the charge plate and transfer roller with two ceramic substrates, two ceramic substrates with an isolated 1mm thick Al plate in between them were used (as drawn on the back of Sample 7-19 shown in Figure 7.42). In addition, the surface potential was measured before and after the print, as plotted below

(Figure 7.41). The results are shown and compared to Sample 7-13 in Table 7.18.

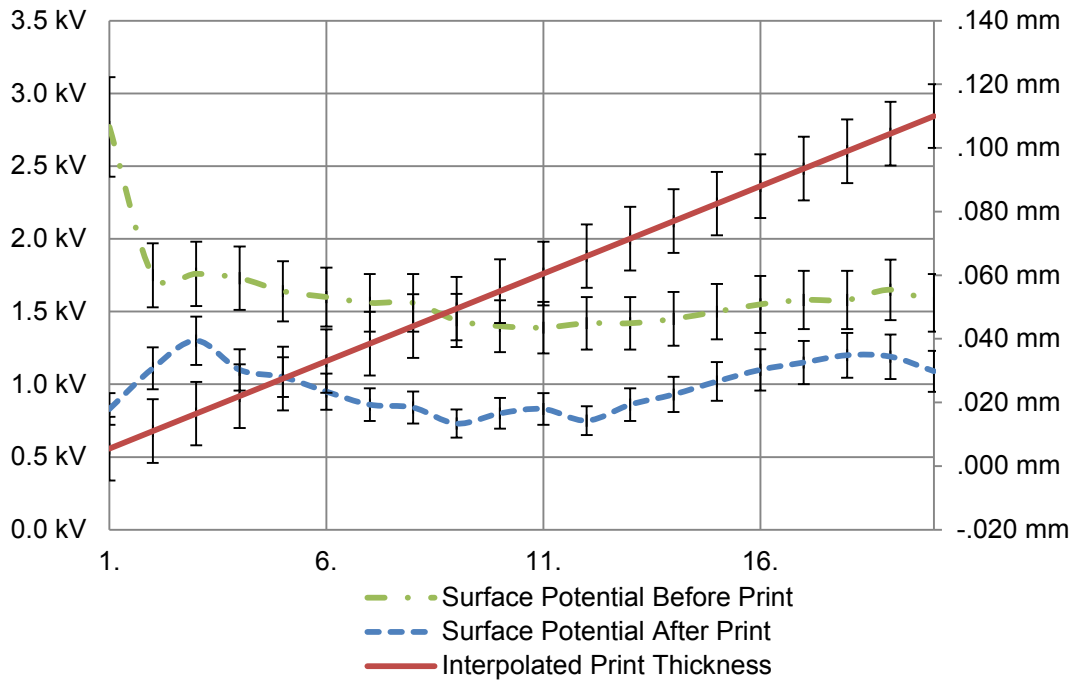


Figure 7.41 – Graph of pre- and post-print surface potential vs. average interpolated cumulative thickness for Sample 7-19.

Table 7.18 – Sample 7-19 Results Compared to Sample 7-13

Results: (Sample 7-13 for comparison)

Sample 7-19

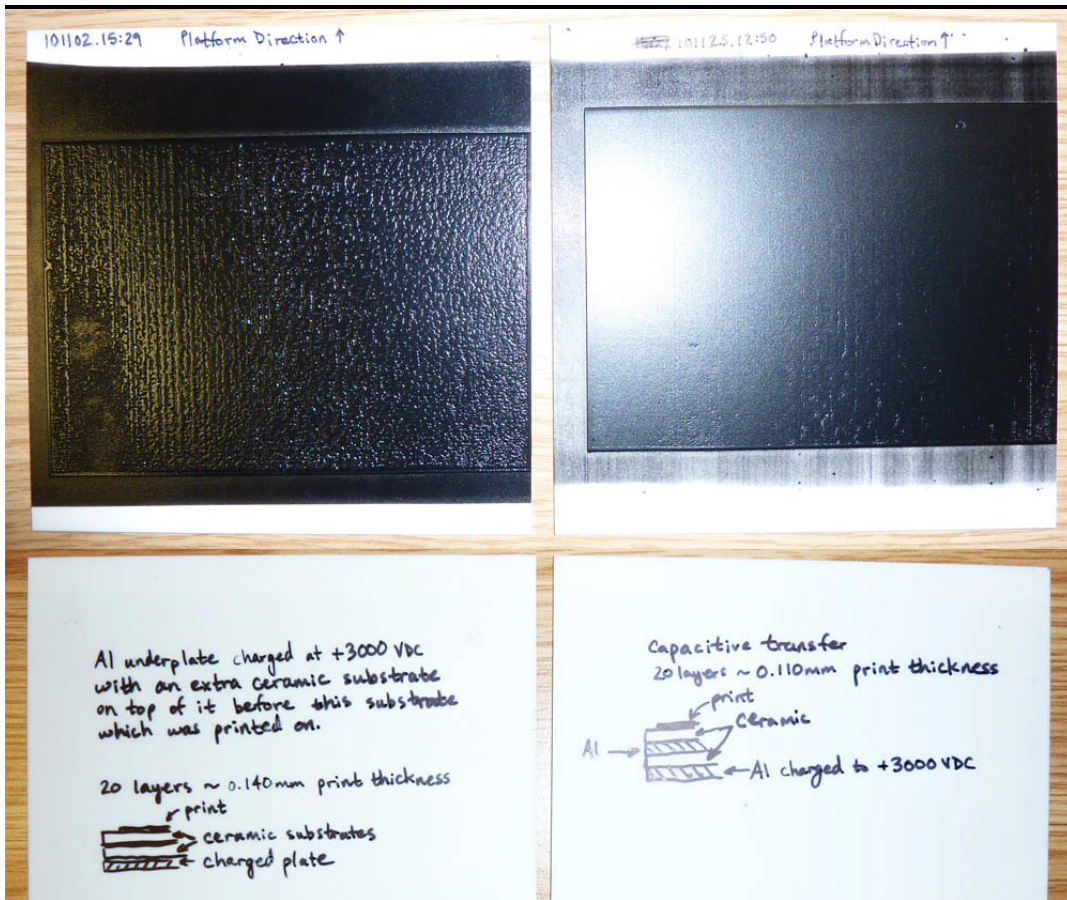


Figure 7.42 – Showing Sample 7-13 compared to the reduced defects in Sample 7-19

0.14 ± 0.01 Print thickness

0.11 ± 0.01 Print thickness

Discussion:

As previously discussed (§7.2.2.2.1), the transfer field used to print Sample 7-13 spanned 2mm of ceramic substrate and resulted in a pitted upper surface after 20 layers deposited.

The transfer field used to print Sample 7-19 spanned a total of 3mm (2mm of ceramic + 1mm of isolated Al plate) and resulted in only mild dispersed pitting. Although the toner height is not as high as for Sample 7-13, the Al plate appears to have had a “homogenizing” effect on the surface roughness. Furthermore, Figure 7.41 shows that the effect of printing each toner layer drops the surface potential by approximately 0.5kV. This graph helps to quantify how much the added (negatively charged) toner reduced the surface potential, even with the field mill measuring a positive bias overall (due to the transfer field).

This same trial was repeated with alternating conductive and non-conductive layers up to 8mm high. In each case, the presence of the conductive layers reduced the surface roughness; although the overall toner thickness was reduced until defects did arise. This indicates that the field strength cannot be propagated indefinitely by capacitive coupling. One of those additional samples is compared with Sample 7-19 (on the left) in Figure 7.43.

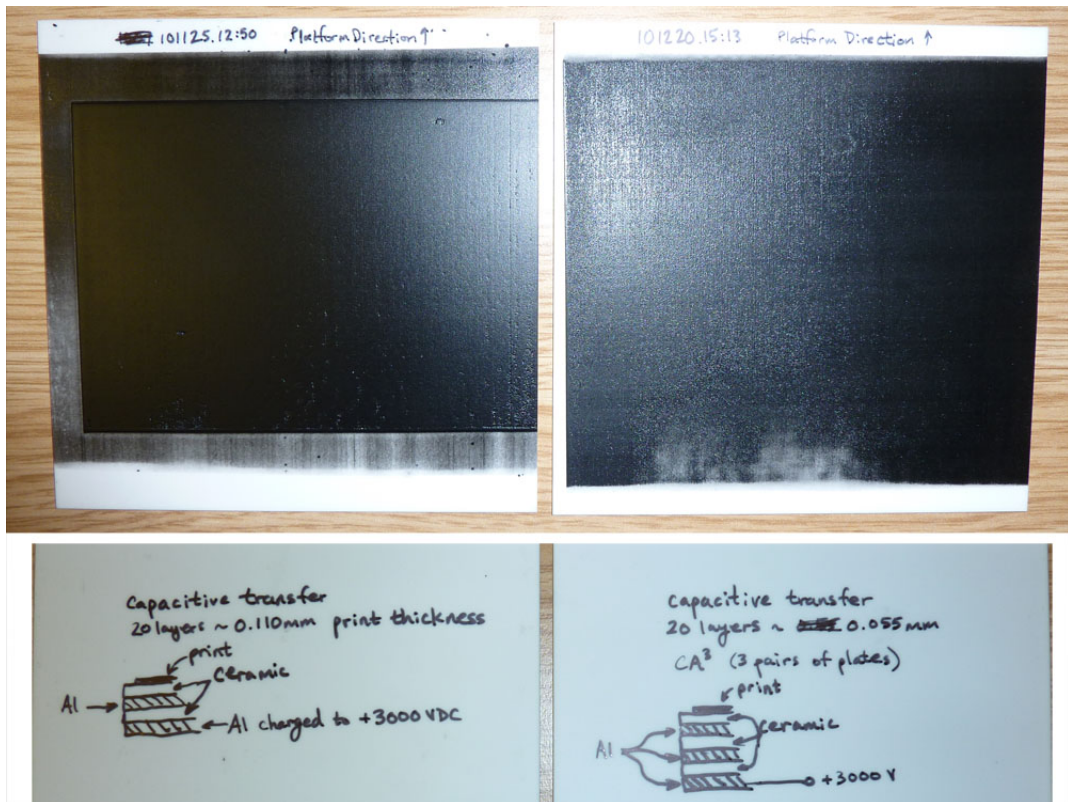


Figure 7.43 – Comparing Sample 7-19 (left) with a sample build on top of a 2mm taller capacitively coupled stack (right)

These samples provided evidence that the wire/foil coupling to the intermediate conductive layers could still be effective with less regularity (than every 0.5mm), therefore the need for a practical method for adding foil layers was explored.

7.2.2.3.4. Feasibility of Adding Conductive Layers In-process

In order for this approach to be viable, a practical way of depositing conductive layers was required. Although these trials were undertaken without awareness of related approaches, they are analogous to the proposed process by Honjo (§3.2.1.3) of adding a conductive agent or coating to a consolidated toner layer (Figure 3.11) in order to make photoconductive toner work effectively [104], and a similar practice used to treat substrates for digital fabrication of circuit boards [94, 95].

Sample 7-20 Embedding Wires

One approach was to embed parallel wires into the part as it was built. If embedded with the right pitch, they could theoretically carry the transfer voltage (acting as the counter electrode to the transfer roller) and increase the transfer field at the build surface. Apart from the substrate arrangement, the printer settings were the same as for Sample 7-14. The results are shown and discussed in Table 7.19.

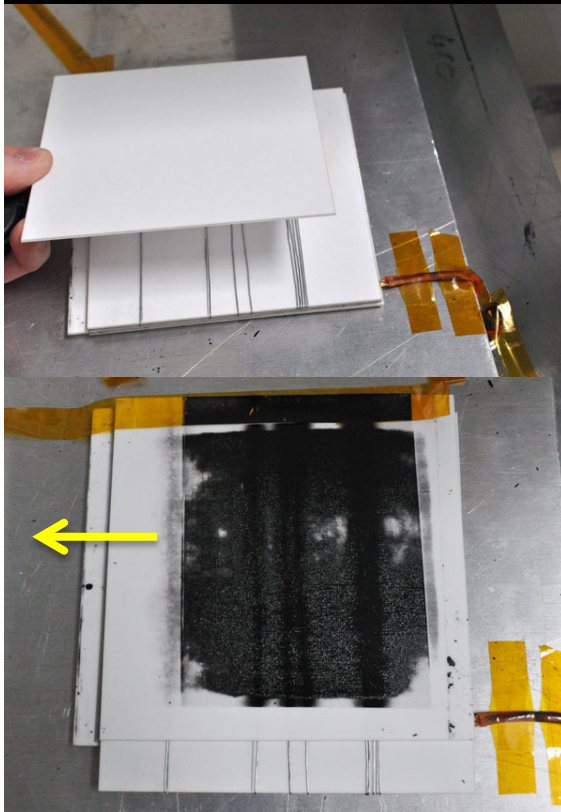
Table 7.19 – Sample 7-20 Results and Discussion*Results:*

Figure 7.44 – Sample 7-20 showing wires carrying transfer voltage (above) and resulting deposition pattern (bottom)

Discussion:

0.4mm bare steel wire was wound around a ceramic plate at various pitches. Where it wrapped around the back side of the plate, it was in direct contact with the charge plate which was charged to 3,000V.

The resulting toner transfer onto the substrate was low in defects immediately over the wire, but suffered from pitting defects everywhere else. The density of parallel wires required to achieve relatively homogenous transfer made this approach of questionable practicality, not to mention a substantial contaminant). (Even though it could impart significant reinforcement to the part's mechanical properties.)

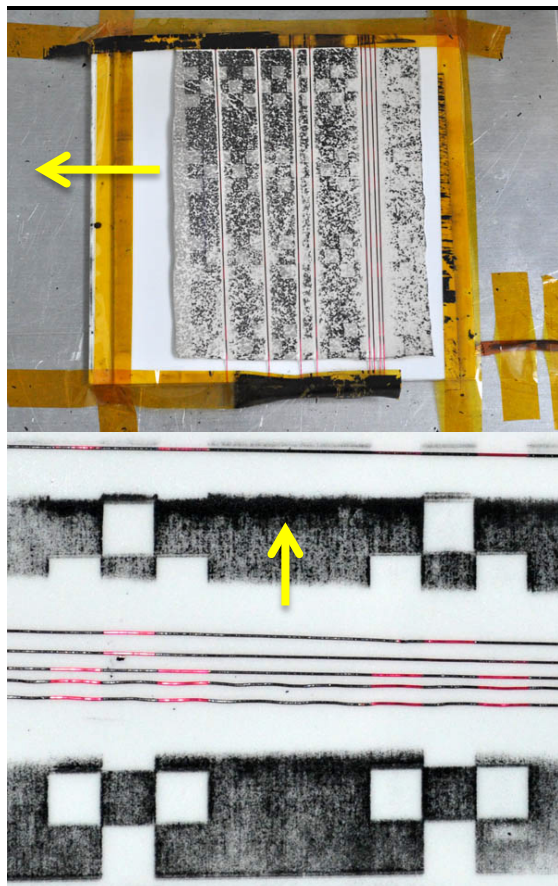
Sample 7-21 Insulated Wires at the Build Surface

Despite the questionable practicality of the approach used for Sample 7-20, a related approach was undertaken to observe the effect of transfer voltage carrying wires at the build surface of the part. To achieve this, a 2mm thick silicone rubber matt (to simulate underlying toner layers and keep the wire from preventing contact in the transfer nip) was placed on a ceramic substrate and both were wrapped with a 0.25mm diameter insulated copper wire (357-716, RS Components, UK) as shown in Figure

7.45a. Another sample was made without the silicone rubber matt (Figure 7.45b). No explicit connection from the insulated wires to the charge plate was made because the wires were charged inductively. The print settings were as for Sample 7-14, except the standard print image was partially checker boarded to provide better contrast for observing the effect of the wires, and the charge plate was set to +800V (a lower potential to avoid breakdown). The ambient conditions were 20.4°C and 36% RH. The results are presented and discussed in Table 7.20.

Table 7.20 – Sample 7-21 Results and Discussion

Results:



Discussion:

The resulting toner transfer onto the substrate with the silicone matting was high in defects virtually everywhere, except on the insulation of the wire itself (visible in b). All of the toner appears to have been scavenged from the area near to the wires. Lengths of wire which received toner are coated all the way around (360°) which reinforces the notion of electrostatic toner scavenging.

The sample without a silicone matt had virtually no deposition near the wires. This was likely due to the scavenging effect of the charged wires and also to the lack of contact in the transfer nip (due to the gap created by the wire diameter). The print pattern transferred to the wires and all the way around them—more evidence of non-line of sight deposition. Deposition in between the sets of parallel wires suffers from early signs of surface pitting.

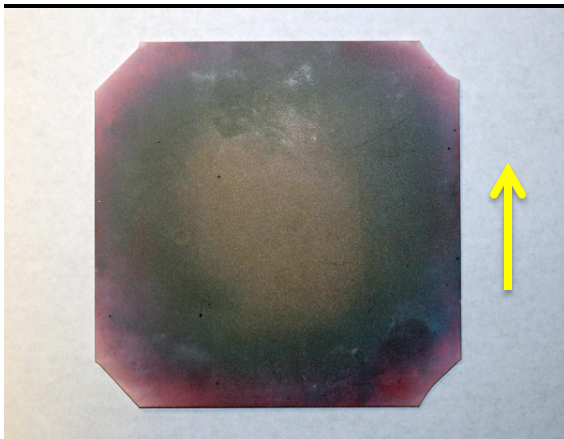
Figure 7.45 – Sample 7-21 with red insulated wires at the build surface carrying the transfer voltage, charged inductively showing a) good deposition on wires and poor deposition on silicone and b) detail of the same on a sample without silicone matt

Although Sample 7-21 confirms that using wires at the build surface to attract a homogenous layer of toner was unpractical, it provided the first evidence in this study that conventional EP transfer is not necessarily a line of sight deposition process (similar to powder coating). Further evidence of this was observed with samples produced on the EMBER rig as shown in §7.3.

Sample 7-22 Gold Sputtering

After preliminary experimentation with imitation gold (~20µm thick Al with a few angstroms of Au coated on both sides) foil (Gold imitation leaf, Nazionale, Italy), it was determined to attempt to Au sputter a toner layer and then use it instead of the charge plate for printing. Apart from the Au on the substrate/no charge plate, the printer settings were the same as for Sample 7-14. The results are presented and discussed in Table 7.21.

Table 7.21 – Sample 7-22 Results and Discussion

<i>Results:</i>	<i>Discussion:</i>
	<p>A ceramic substrate (with corners broken off to fit into the cylindrical vacuum chamber) was placed in a sputterer (SC515, Biorad, England) and a ~20nm layer of Au was deposited thereon using a plasma current of 25mA. The deposition density was reasonable in the centre, but suffered toward the edges. The resistance over 50mm was ~100 Ohms (in centre). The gold side was placed in contact with a wire carrying 3,000V.</p>

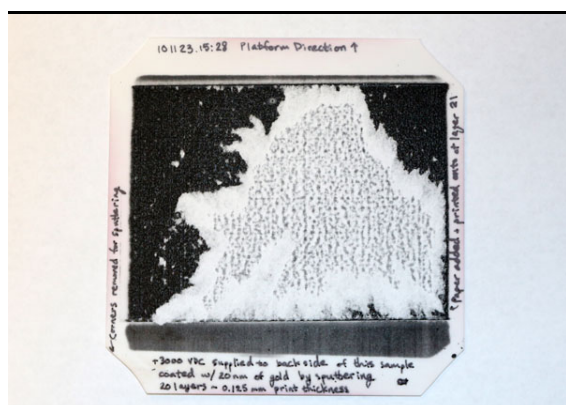


Figure 7.46 – Sample 7-22 showing poor surface quality deposition throughout 20 layers including onto a sheet of paper

The resulting toner transfer onto the substrate suffered from severe pitting defects everywhere. It was so bad that at layer 20, a sheet of paper was added to the top to see if toner was still transferring. It appears that the density of the Au was not high enough for it to behave like a continuous conductive layer and therefore did not provide an adequate transfer field, even though some toner did transfer onto the paper. When attempting to remove the paper it tore as shown at left. The cost/complexity of this approach discouraged its pursuit.

Sample 7-23 Conductive Polymer Layers

In order to remain focused on the aims and objectives of this work, it was desirable to move away from metals entirely and use a material with properties closer to the bulk toner, therefore a moderately conductive polymer: poly(3,4-ethylenedioxythiophene)-poly(styrenesulfonate) (PEDOT:PSS) (PH 1000, Heraeus Clevis GmbH, Germany) with a specific conductivity of 90 kS/m was trialled [340].

Table 7.22 – Sample 7-23 Results and Discussion

Results:

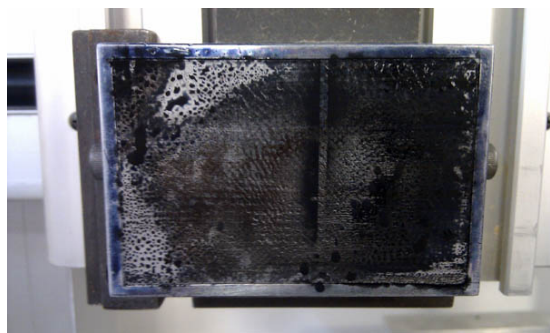


Figure 7.47 – Sample 7-23 showing poor wetting/application of PEDOT:PSS onto a substrate prior to toner deposition

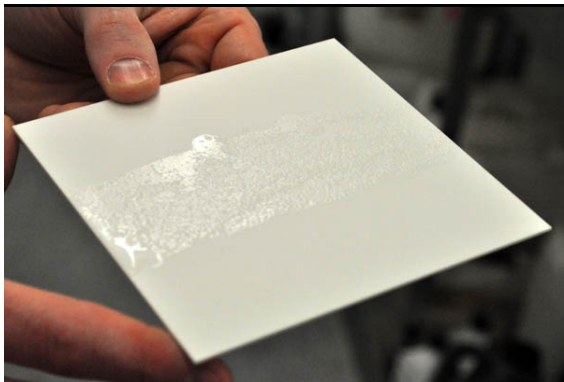
Discussion:

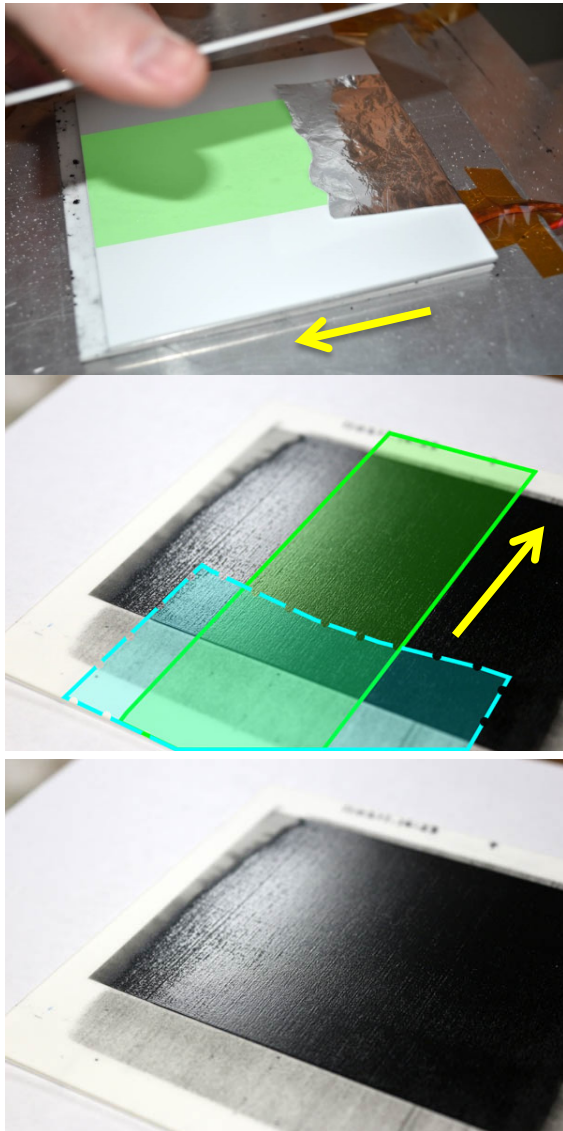
In the first instance, the PEDOT:PSS was sprayed onto a polymer covered substrate (45x70mm) loaded into the EMBER rig (\$5.8) using an air brush. Unfortunately, complications including poor surface wetting and difficulty attaining the desired conductivity discouraged pursuit of this approach. However, it represents an approach which may be considered in the future.

Sample 7-24 Brine Layers

Even more desirable than using a polymer is the use of a “temporary” conductive layer. This was initially tested by wetting the surface to see if water alone would impart enough conductivity to serve as a temporary conductive layer and then be allowed to evaporate away. Unfortunately, water alone was not conductive enough so dry salt (NaCl) was attempted hoping that the ionic bonding would allow for ionic charge exchange, enabling sufficient conductivity, but it was not. Therefore a brine solution (of salt mixed with a small amount of water) was applied down the centre of a ceramic substrate and charged through foil connected to the high voltage charge plate. The substrate for printing was placed above it (before it was dry) and printing commenced using the polyester print setting as before with fusing @ 125°C.

Table 7.23 – Sample 7-24 Results and Discussion

<i>Results:</i>	<i>Discussion:</i>
	<p>First, a wet brine solution was applied to the centre third of a ceramic plate intended to act as a conductive layer to impart the transfer field through an overlying sample substrate.</p>



This image shows the substrate that the toner will be printed onto being set upon the brine solution (covering the brine area highlighted in false colour green to help identify where it is). The arrow indicates the print direction.

Here in false colour is indicated the location of the foil (light blue with dashed outline) and brine solution (green) on the underside of the sample. Surface defects can be seen in the lower left hand corner of the sample.

The area which was over the charged foil has significantly improved surface quality. The central area over the brine solution only nearly maintains the same surface quality as the area over the foil. Pitting defects affect the right and left hand side of the sample. The effect of the brine is subtle, but noticeable. This is early evidence that brine may be used to conduct transfer voltage.

Figure 7.48 – Sample 7-24 showing a) application of brine solution onto the ceramic plate underlying the sample substrate, b) foil coupling to the brine solution (false coloured in green), c) resulting deposition with false colour indicating the position of the underlying foil (blue) and brine solution (green), d) photo showing reduced defects in sample centre

Of the approaches presented in this subsection, the brine solution looks most promising to extend the effective range of conventional electrostatic transfer. However, it is preferable if this step can be avoided entirely and an alternative transfer means (which does not require additional steps or special conditions) can be realized capable of unlimited height deposition.

7.2.3. Variations on Top Charging

This subsection builds on the foundation laid by Kumar et al. (§4.3.2.1) and aims to eliminate the need to introduce a conductive layer into the part.

Sample 7-25 Top Charging with Positive Pulsed DC Corona

In order to provide a frame of reference for comparison, a top charging approach as proposed by Kumar was undertaken, albeit with non-contact fusing, polyester toner material, and a pulsed DC corona device (Meech 976 pulsed DC corona pin emitters with 977 control, §5.7.1.3). In order to provide a high intensity of ions (yet ensure the ions arrived with uniform density) the corona device was used at a 250mm stand-off distance (near the minimum recommended stand-off distance) with 12kV at 8 Hz (both set as per the manufacturer's instructions), with 75% positive output (nearly the maximum of the device, with polarity opposite to the toner) [341]. Apart from the corona device, this trial was undertaken with the same printing parameters as Sample 7-2. The initial intention was to neutralize toner charge, rather than create an opposite polarity surface charge per se. The results are presented and discussed in Table 7.24.

Table 7.24 – Sample 7-25 Results and Discussion

Results:

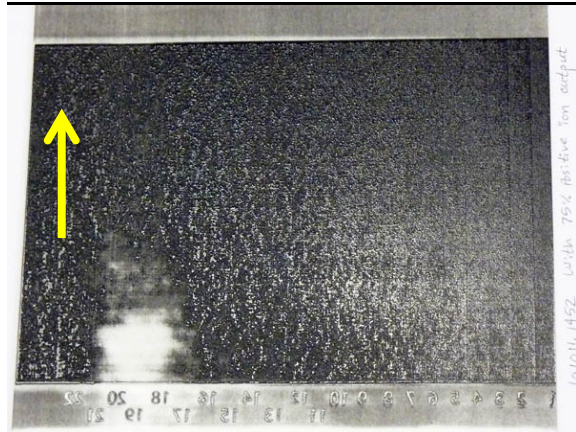


Figure 7.49 – Sample 7-25 showing extensive surface defects without any noticeable improvement due to the positive ions; the arrow indicates the print direction

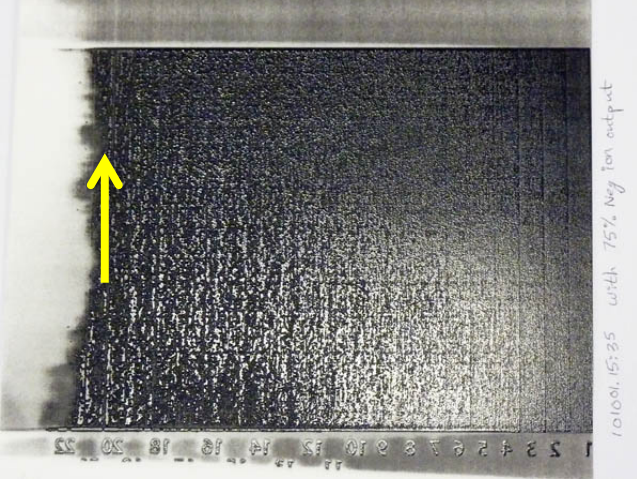
Discussion:

The large unprinted area in the lower left-central side is attributed to low contact pressure in the transfer nip. Apart from that the surface suffers from quite severe pitting after the first ~ 5 layers (virtually identical to Sample 7-2) with a max cumulative height of $0.11 \pm 0.01\text{mm}$. Defects arise dramatically earlier than Kumar reported [261, 271], but in line with Figure 7.19. This may be explained by the higher toner charge, lower fusing temperature and non-contact heating.

Sample 7-26 Top Charging with Negative Pulsed DC Corona

Owing to the unsatisfactory surface quality of Sample 7-25, the same conditions were used, except that the pulsed DC corona device was used with a 75% negative output (nearly the maximum negative polarity of the device). Although this was the same polarity as the toner, it was hoped that a difference (better or worse) could be affected, observed, and measured from this change. The results are presented and discussed in Table 7.25.

Table 7.25 – Sample 7-26 Results and Discussion

Results:	Discussion:
 <p data-bbox="304 936 943 1025"><i>Figure 7.50 – Sample 7-26 showing extensive surface defects without any noticeable improvement due to negative ions</i></p>	<p data-bbox="975 477 1401 925">The large unprinted area is now on the entire left edge, again attributed to low contact pressure in the transfer nip. Apart from that, the surface suffers from severe pitting after the first ~5 layers with a max cumulative height of $0.07 \pm 0.01\text{mm}$. The 0.04mm reduction in height may be explained by the ions being the same polarity as the fresh toner which therefore enhanced any repulsive effect.</p>

The research outcome from Sample 7-25 and Sample 7-26 is that the presence of a high density of free charge (ions) in proximity with a surface does not necessarily mean that the surface will retain enough charge to contribute to critical transfer field strength. For that reason the next set of trials were undertaken.

Sample 7-27 Top Charging with Field Attracted Positive Ions

Owing to the unsatisfactory surface quality of the two preceding samples, it was determined that a field would be used to attract positive ions (needed to help transfer negatively charged toner) onto the build surface prior to the printing cycle. The same printing conditions as Sample 7-11 were used, except that the charged plate was charged with -3,000V only while passing under the DC corona device set to an 80% positive output

(the maximum positive polarity of the device). Once the platform passed the corona device the charged plate was switched off and toner transfer was achieved by tackification plus the electrostatic assist by the surface charge on the build surface (i.e. top charging) with results in Table 7.26.

Table 7.26 – Sample 7-27 Results and Discussion

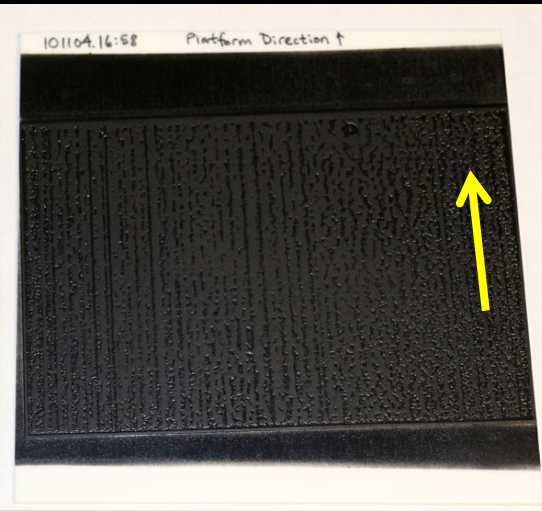
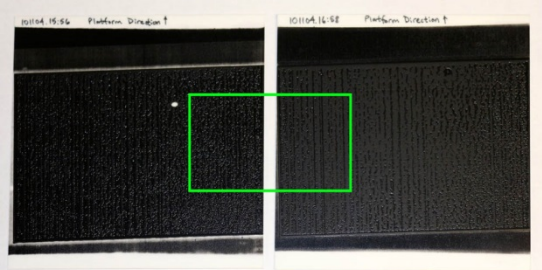
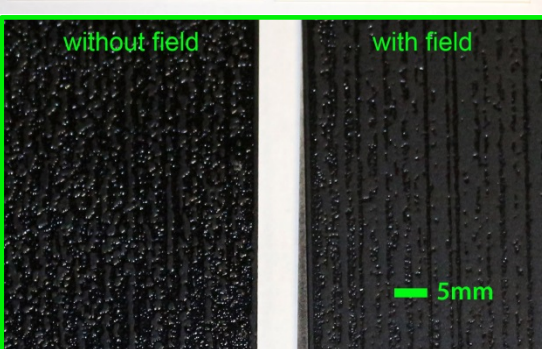
Results:	Discussion:
	<p>Moderate surface pitting is evident; however it is mitigated (and appears similar to the half of Sample 7-10 which was over the charge plate @1,600V). Comparing the defects on this sample to those of the former two (the areas with a 20 or nearly 20 layers) this sample is significantly improved. The maximum sample height was $0.16 \pm 0.01\text{mm}$. In order to have a like for like comparison, another sample was produced with identical settings, except that no field was used to assist ion attraction.</p>
	<p>These images show Sample 7-27 (right) compared to a sample prepared identically (left), except that no field was used to attract the ions. The sample made without the field was a similar height ($0.15 \pm 0.01\text{mm}$), but the surface defects were more pervasive as shown most clearly in the lower detail image (c) at left. This reduction of surface defects provides evidence that a field is helpful to “transfer” ions as well as (and in order to) transfer toner. It also may explain why top charging is dependent on the build surface distance from ground/the counter electrode.</p>
	<p>c</p>

Figure 7.51 – Sample 7-27 showing a) reduced surface pitting; b) this sample (right) compared to another sample prepared identically, except without ions; c) detail comparing the two samples showing improved surface quality with field attracted ions

Despite the improvement demonstrated by using the field to attract ions, the power supply was at maximum capacity (3,000V) therefore it was not possible to pursue this approach with a stronger field in order to attempt to produce a defect-free sample. The difficulty of having enough field strength to transfer the toner in a defect-free way may be explained by Dan Hays' assertion that tribocharging is twice as effective as corona charging (§3.4.1.1) [54].

It is noteworthy that following these trials, the pulsed DC corona was audited and found to lack ion balance uniformity across its length. This meant that surface potentials were likely less negative by an estimated 50-150V (depending on their location on the platform) than measured. This does not invalidate the work, but it does create a larger potential window of error in the measurements. This lack of reliability in the ionizers provided motivation for the changes to the printers realized for stage two of the rig (§5.7.2.3).

The differences in this method (non-contact fusing at a relatively low temperature and higher toner tribocharge) compared to Kumar's may account for the earlier appearance of defects and hopefully additional insights. It is proposed that Kumar's contact fusing approach may have deferred the detection of these defects.

7.3. Pressure- free Electrostatic Transfer

The results and discussion in §7.1-7.2 presented strong evidence that residual toner charge was not being eliminated with fusing, and that its influence was one of the primary causes for fish scaling and pitting defects. Up to this point, it has not been possible to definitively disambiguate defects arising due to non-uniform pressure from residual toner charge. Therefore, a small test rig called EMBER (§5.8), was devised and built by the author (independent of Renishaw) which enabled toner transfer exclusively by electrostatics (in the absence of pressure). This section overviews experiments and understanding gained using the EMBER rig.

Sample 7-28 Conventional Electrostatic Transfer onto Conductive Substrates

In order to provide a baseline for tests on the EMBER rig, samples were produced using a conventional electrostatic transfer. First, a 1.17mm steel substrate was mounted onto the platform and the collar/sleeve was positioned to help retain it in place, yet be 0.5mm further from the developer (so toner would preferentially jump to the substrate rather than the collar). Next, following standard practice with the EMBER rig, the alignment of the platform to the developer roller was checked to be parallel, and the gap between the two was set to be 0.20mm ($\pm 10\mu\text{m}$). The EMBER rig settings were used as per Table 7.27, with an automatic layer deposition cycle (which moved the substrate past the developer roller twice to maximise deposition between fusing operations). Between each layer deposition cycle, the newly deposited toner was manually

fused to the target fusing temperature of $\sim 100^{\circ}\text{C}$ using low pressure hot air from a heat gun. The results are presented and discussed in Table 7.28.

Table 7.27 – Sample 7-28 Preparation Parameters

	<i>Value:</i>	<i>Description:</i>
Sample Preparation	18.9°C, 40% RH	Ambient conditions inside the machine
	-1,250 to -3,000V	Developer roller bias*
	0.20mm	Transfer gap
	1.17mm steel	Substrate

*Although transfer was possible at -1,250V and 2,000V, the higher voltage allowed the use of a larger gap between the developer roller and platform which made the process less sensitive to non-uniform deposition.

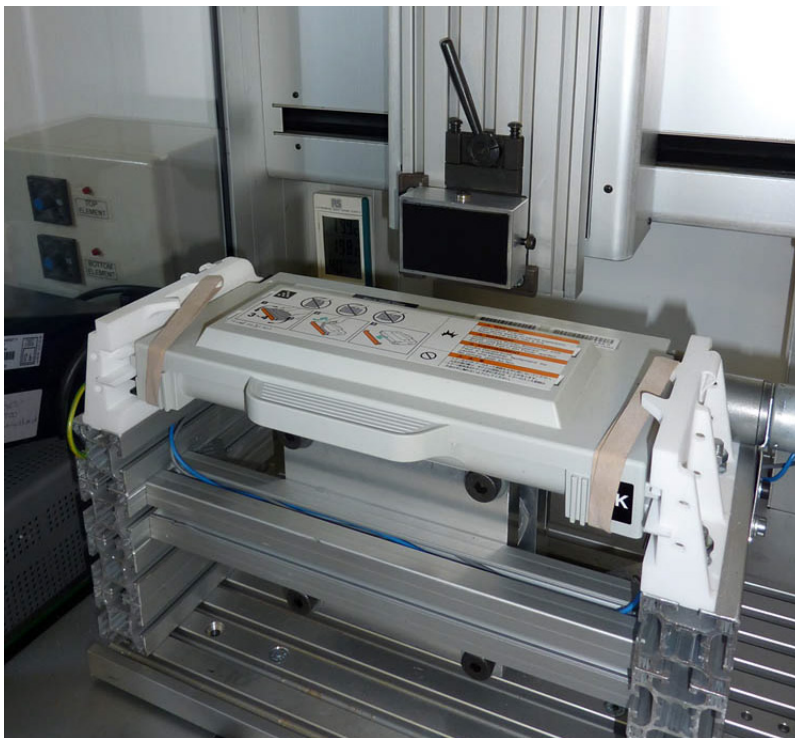


Figure 7.52 – Image of the EMBER rig just after a printing cycle to deposit black toner onto the substrate. For more information on the EMBER rig, see §5.8

Table 7.28 – Sample 7-28 Results and Discussion*Results:*

Figure 7.53 – Sample 7-28 showing the layer fusing step with hot air gun (above), and the resulting fused surface quality (below)

Discussion:

Toner transferred and fused uniformly (see layer beneath the heat gun) for the first layer (-1,250V). Attempting to transfer more toner, the voltage was set to -2,000V which caused breakdown, therefore the gap was increased to 0.34mm. After the sparking, ridges began to appear on the surface, parallel to the rotation of the roller. These ridges are attributed to increased roller diameter due to “arc welding” toner onto it where the sparks occurred. The layers leading up to layer 8 resulted in lower density of toner transfer (presumably due to reducing field strength); therefore at layer 9 the voltage was set to -3,000V and the gap at 0.58mm. Furthermore, cracking occurred in some of the layers (visible just to the lower left of the specular reflection) due to toner brittleness. The average thickness after 20 layers was 0.20 ± 0.03 mm. This increase in layer thickness compared to Sample 7-11 (20-layer) may be for two reasons. First, there was no ceramic substrate to attenuate the field strength, and second, the voltage and gap were adjusted throughout the build to provide maximum field strength but without (intentional) breakdown. The high and low areas of toner deposition did not correlate with proximity to the magnetized areas on the platform.

Samples prepared in this way provided clear evidence that the EMBER rig was capable of electrostatic toner transfer (without pressure), and the effects of diminishing field strength. It provided a good benchmark for exploring what happened when the build surface was more distant from the counter-electrode/ground which led to the following trials.

Sample 7-29 Conventional Electrostatic Transfer onto Non-conductive Substrates

Following on from Sample 7-28 two changes were made. First, in order to simulate printing onto a plurality of fused layers (without any residual toner charge), a 9.7mm thick non-conductive high impact polystyrene substrate was attached to the platform using double-sided tape with the collar/sleeve positioned to be as far away from the build surface as possible (so that it could not have any electrostatic influence on the toner transfer). Second, the deposition cycle program was altered so that the substrate was moved past the developer roller in different locations to avoid substrate patterning from the breakdown-caused roller defects. The standard neutralization practice for non-conductive substrates (undertaken prior to printing) was to swab the area generously with isopropyl alcohol (IPA) using a cotton swap coupled to ground and allow the IPA to evaporate. As per Sample 7-28, the platform parallelism with the developer was checked and the transfer gap was set. The settings in Table 7.29 were used with fusing at $\sim 130^{\circ}\text{C}$ (high temperature due to lack of Al heat transfer). The results are presented in Table 7.30.

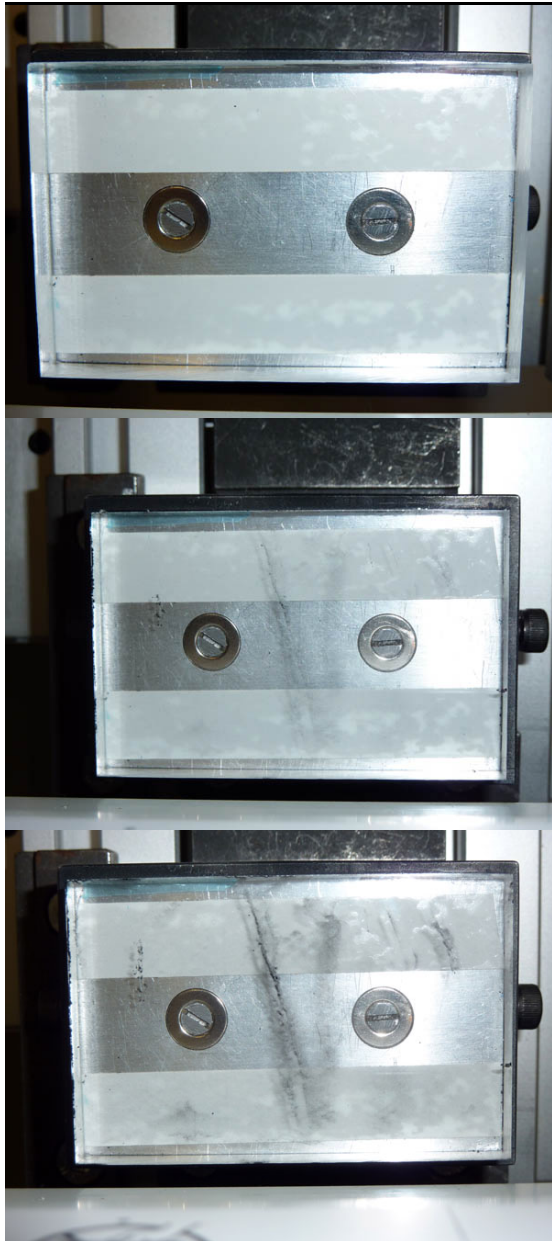
Table 7.29 – Sample 7-29 Preparation Parameters

	<i>Value:</i>	<i>Description:</i>
Sample Preparation	19.4°C, 47% RH	Ambient conditions inside the machine
	-1,000 to -3,000V	Developer roller bias
	0.20mm	Transfer gap
	9.7mm clear polystyrene	Substrate

Table 7.30 – Sample 7-29 Results and Discussion

Results:

Discussion:



a With the developer roller bias at -1,000V, no toner transfer was evident.

b With the bias at -2,000V, a very light non-uniform deposition of toner (approximately in the shape of a "V") was evident in the middle of the substrate. The substrate was not cleaned before making a further attempt with increased voltage.

c With the bias at -3,000V, slightly more toner transferred in the middle of the substrate making the pattern first seen above (b) more visible and adding light deposition to a few additional areas.

Figure 7.54 – Sample 7-29 showing a) no toner transfer after printing using a developer bias of -1,000V, b) very light toner transfer using a developer bias of -2,000V, c) slightly darker transfer when using -3,000V bias

The series of conventional electrostatic transfer settings demonstrated with Sample 7-29 provides clear evidence that its effectiveness is

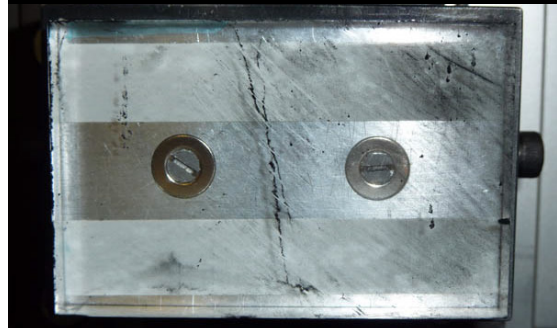
diminished with increased distance between the two potentials (the biased developer roller and grounded platform in this case). Therefore alternative transfer means were needed in order to enable AM by EP.

Sample 7-30 Top Charging by Tribocharging

Owing to the difficulty of using corona generated ions to enable top charging/discharging (§4.3.2.1, §7.2.3), a trial was undertaken to evaluate if tribocharging the build surface (initially the build substrate) to facilitate toner transfer was viable.

A sample was produced with the same settings as Sample 7-29, except that before each deposition cycle, the right hand side of the substrate was manually rubbed with a 0.05mm thick PTFE sheet (536-4012, RS Components, UK) for ~7s. The ambient conditions were 21.8°C, 40% RH. The results are presented and discussed in Table 7.31.

Table 7.31 – Sample 7-30 Results and Discussion

<i>Results:</i>	<i>Discussion:</i>
	<p>a The first deposition after the initial rub was faint. For this reason, it was not fused, but rubbed again with the PTFE, this time harder.</p>



The second rub resulted in a far more substantial deposition including round voids (See Sample 7-32) where no toner transferred. This was the first definitive evidence that tribocharging a surface could assist with toner attraction onto that surface.

14 fused layers resulted in substantial coverage of the right side (max height 0.100 ± 0.01 mm), although the surface quality was bumpy, perhaps evidence of non-uniform charge. As the layers increased in thickness the gap was increased to maintain clearance. Also, latter layers only added toner to the raised areas, not the valleys.

Figure 7.55 – Sample 7-30 showing a) the toner transferred after the first rubbing, b) more substantial deposition after the second rubbing, c) toner deposition and texture after 14 fused layers.

This set provided strong evidence that tribocharging did alter the surface charge which facilitated transfer. However, the non-uniform tribocharging (and resulting non-uniform deposition) was not amenable to unlimited height deposition, therefore further alternatives were explored.

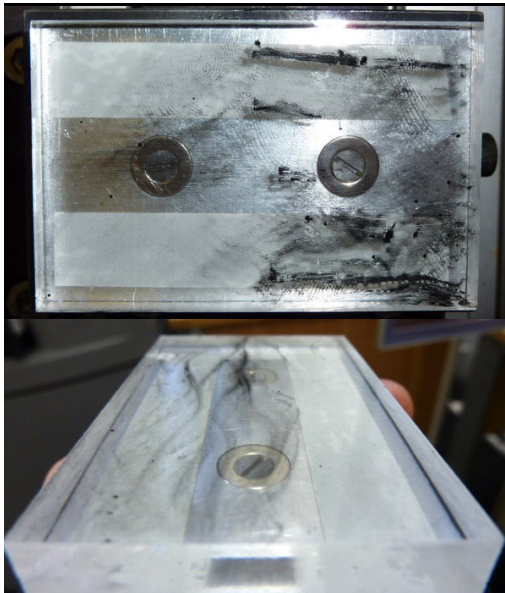
As an aside, further exploration of this principle was undertaken using the SLP rig where film was effectively laminated onto a toner layer (similar to Sample 8-2) and peeled off which resulted in surface potentials approaching -10kV as measured by the field mill. Continued work on this approach was discouraged because the field mill indicated that the surface potential dropped in less than a second to near ground. In hindsight, this reading may have been the result of field suppression as experienced and explained with Sample 7-6. Therefore this approach (with swapped surface polarity) may warrant further investigation.

Sample 7-31 Selective Contact Charging of the Substrate

Essentially, this sample was intended to use a selective charging method which was a practical and more powerful alternative to Hungarian physicist Paul Selenyi's directed beam of ions (§3.1.2)[39]. This method was inspired by Hays' demonstrator of "writing charge" using contact charging of an insulator [54]. It was produced in the same way as Sample 7-29, except that before deposition the right half of the substrate was contacted to a piece of metal charged to +3,000V in horizontal passes. The ambient conditions were 19.4°C, 47% RH and the results are presented in Table 7.32.

Table 7.32 – Sample 7-31 Results and Discussion

Results:



Discussion:

Horizontal swathes of toner deposition are evident which correspond to the areas contacted with high voltage. Interestingly, some finger prints were also developed on the substrate. The deposition uniformity is the challenge with this approach.

Seeking alternative charge application devices, this sample was repeated with pre-print charging via contact with a carbon brush charged to +3,000V. The left half of the sample shows corresponding deposition, but still does not achieve a uniform deposition.

Figure 7.56 – Sample 7-31 showing toner deposit after contacting the substrate with high voltage using a piece of metal (above), and the resulting toner deposit after contacting the substrate with high voltage using a carbon brush (below)

Additional application methods were attempted including flooding the area with electrified water (with and without a film ovetop to spread it evenly) and IPA, however deposition was not uniform.

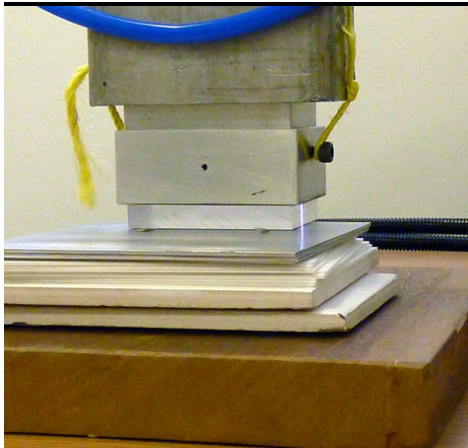
Sample 7-32 High Voltage Global Contact Charged Sample

Pursuing a uniform surface charging method to enable unlimited height deposition, the entire substrate was charged between a charged plate (electrode) and the grounded platform and then printed using the same settings as Sample 7-29. The ambient conditions were 20.9°C and 55% RH. The results are presented and discussed in Table 7.33.

Table 7.33 – Sample 7-32 Results and Discussion

Results:

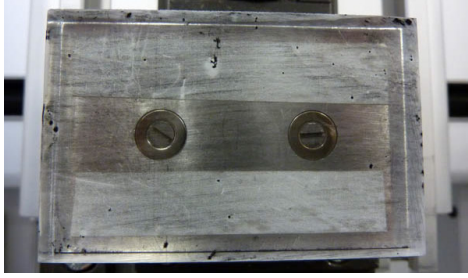
Discussion:



- a Prior to deposition on the EMBER rig, the sample was placed for 30s on +12kV charged plates (sat on top of a ceramic tile stack on a wooden base). The EMBER platform is being pushed down onto the plates using an estimated 5kg Al weight which is grounded. Sparks can be seen traveling from the charged plate through the substrate to ground.



- b The deposition following the exposure to high voltage was full of rounded areas without any toner deposition whatsoever. These "bubbles" seem to have been caused by breakdown which radially neutralized outward from a point on the substrate, thus removing any electrostatic attraction for the toner. This seems to be an extreme manifestation of fish scaling and is evident on Sample 7-30 as well.



Minimizing sparking eliminated the toner "bubbles" but resulted in a lower density deposition. This little deposition does not have the potential to accumulate the thickness required for 3D parts.

Figure 7.57 – Sample 7-32 showing a) substrate pre-print treatment in a high voltage field which induced breakdown; b) toner deposition including "bubble" defects; c) repeat of treatment with lower field strength eliminated "bubbles" but resulted in a lower density of toner deposition

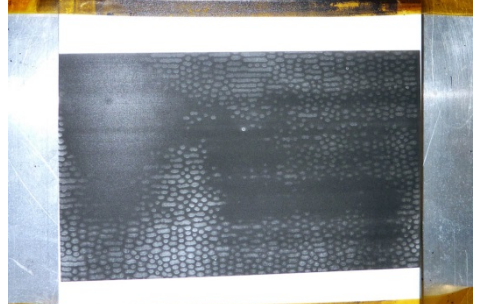
Another set of samples similar to Sample 7-32 were undertaken where additionally the surfaces of the samples were neutralized using an AC bench-top ionizing fan between each layer. Scarcely any toner transferred at all. This result strengthens the explanation that the observed "bubbles" of no toner deposition resulted from neutralization of the substrate.

The samples in §7.3 have reiterated the challenges of field strength limitation and toner deposition uniformity experienced in the earlier subsections of this chapter. Due to these trials, it has been confirmed that the difficulties are present even in the absence of pressure. Furthermore, they have extended the illustration of defects including the discussed "bubble" defect which is the result of radial charge neutralization in the substrate due to breakdown.

7.4. Summary and Conclusions

This chapter has identified and substantiated at least 4 types of defects arising in samples made by EP as summarized in Table 7.34.

Table 7.34 – Summary of Defects Substantiated in §7

<i>Defects:</i>	<i>Description:</i>
	<p>Pitting – Virtually every sample that was transferred when the transfer field (implicit or explicit) was electrostatically unfavourable suffered from surface pitting defects. These are explained most often by the reduction of field strength due to too little voltage/too large of a distance and/or the repulsive effect on incoming toner from the accumulation of like sign charge in the consolidated toner layers.</p>
	<p>Fish scaling (§7.2.2.1) – This is a pattern observed when transfer field strengths marginally achieve localized breakdown in a pattern that is distributed across the sample surface. It is typically only observed on the first layer of SLP samples, since subsequent layers do not achieve breakdown (due to additional thickness/toner insulation).</p>
	<p>Bubbles – The absence of toner deposition in rounded patterns with the appearance of “bubbles” is caused by severe breakdown which neutralizes the surface radially from the spark through the substrate, thus removing any electrostatic attraction for the toner. This has been observed prominently on Sample 7-32, Sample 7-30, etc.</p>
	<p>Ridges – The defects arising on Sample 7-28 were caused by non-uniformities in the developer roller diameter. The excess diameter was caused by permanent accumulation of toner (akin to hot offset) due to the thermal result of breakdown (arcing).</p>

Most importantly *the correlation of surface defects with the surface potential has been measured and published for the first time.* This correlation has been substantiated as causation for the pitting surface

defects by the use of equations showing unfavourable electrostatic transfer conditions as well as a plethora of samples with and without contact/pressure in the transfer nip. The control of residual toner charge will be an on-going theme throughout the rest of this work.

This newly substantiated principle was the basis for the experimental work in Chapter 8 and formed core elements of the patent applications filed [339, 342] in connection with this PhD.

8. Approaches to Controlling Charge

As Schein observed, increased understanding of the physics of a process promotes technical innovation [238]. The results and discussion in §7.1-7.3 presented strong evidence that residual toner charge is not eliminated by fusing, and that its influence is one of the primary causes for fish scaling and pitting defects. With this increased understanding came the motivation to experiment with, and innovate, methods to manage the residual toner charge. This chapter reviews experimental work for both accumulating and neutralizing residual toner charge.

8.1. Accumulating Residual Toner Charge

In order to further substantiate the hypothesis that residual toner charge causes defects, direct evidence of the presence of residual charge was needed (in addition to the heretofore proposed evidence using surface pitting defects as a proxy for residual charge).

8.1.1. Unexpected Evidence of Residual Charge

Early evidence for residual charge was observed in Sample 7-12, which after being produced was left on the platform of the SLP rig (with the rig in a powered down condition) for 18 days. Upon removing the sample,

the Al charge plate was electrostatically held to the underside of the sample, which required a noticeable physical exertion to remove it. The electrostatic attraction was still strong enough after a couple of minutes to hold the charge plate up against gravity as shown in Figure 8.1.

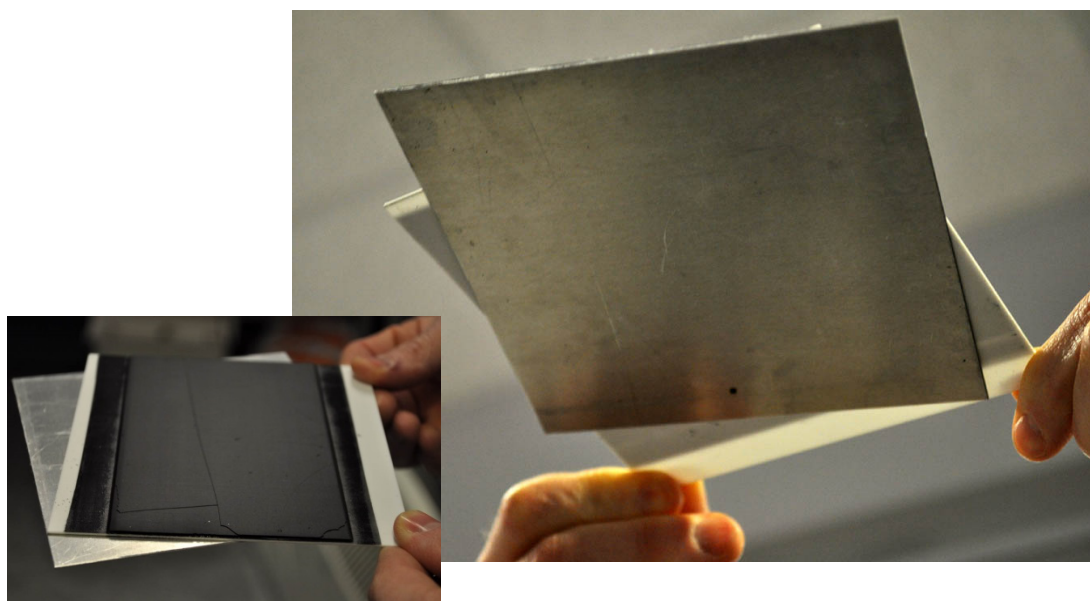


Figure 8.1 – Large image (right) viewing the underside of the charge plate clinging electrostatically to Sample 7-12 upon removal from the SLP rig 18 days after it was made. Overlaid on the left is a small image of the same, viewed from above.

After approximately 5 minutes of handling the sample and charge plate, the attraction between the two diminished until it could no longer be felt. This behaviour was repeated for the rest of the sample set represented by Sample 7-12, albeit with a shorter time delay between producing the sample and removing it from the SLP rig.

The ability to hold up the conductive plate represented a substantial residual charge on both the sample and conductive plate. The diminished attraction upon handling was almost certainly due to charge leaking away

from the Al plate to ground, using the human body as the path to ground. Presumably, the toner still retained a substantial amount of residual charge because it did not have a path to ground since it was held only by the ceramic substrate. Furthermore, since the toner was not conductive, any contact in one area could not drain charge quickly from other areas of the sample. Despite any charge retained in the toner, once the Al plate was neutralized, it was no longer attracted to it. This may be an analogy for understanding why the toner was not attracted onto a neutralized substrate (See Sample 9-2, Sample 9-4) despite the potential of the transfer roller.

The residual charge observed when removing Sample 7-12 from the platform was unexpected because of the long delay between printing and removing the sample from the platform. It provided evidence that the polyester toner was capable of trapping charge for extended periods.

The reduction of charge on the Al plate due to handling for Sample 7-12, prompted re-consideration of the reasons why *Sample 6-3 EMB Sample Exceeding the 3mm Height Limit*, was able to exceed the 3mm height limitation. It is possible that the extensive manual handling during the fabrication of this legacy sample (§6.1.1, §4.4.5.2) promoted charge neutralization which avoided surface defect formation. In combination with the manual handling, the time delay between layers for fusing (which required removal from the rig and placement in the oven), and dwell at elevated temperature in the oven, may have also promoted charge recombination (neutralization) inside the sample layer by layer.

These observations (in addition to the three cited in §6.1.5) could help explain differences in preparation and outcome between the EMB and legacy SLP produced samples. This reasoning eventually led to efforts to neutralize charge layer by layer.

8.1.2. Intentional Charge Trapping

With the understanding that charge was being trapped in toner layers, came the desire to manage it. Initially, easier observation of its effects was desired, therefore this subsection describes experiments to intentionally trap charge.

Sample 8-1 Macroscale Simulation of Residual Toner Charge Decay

Sample 8-1 illustrates the duration of the effects of residual charge at macroscale by using a small wooden child's toy filled with plastic beads (with an estimated 2mm diameter) observable through an acrylic window (Figure 8.2 inset). When this toy was gently rotated end over end, beads contacting the acrylic window would fall back into the bottom of the toy due to gravity. However, when shaken vigorously for ~30s (tribocharging), some of the beads would electrostatically cling to the inside of the upward facing acrylic window. Sample 8-1 was placed on the author's desk in a climate controlled office in mid-Oct 2011 with a sheet of paper blocking any direct sunlight (simulating conditions for toner inside a 3D laser printed part) [343]. It was photographed regularly and the number of beads clinging onto the acrylic window were counted and plotted against time in Figure 8.2.

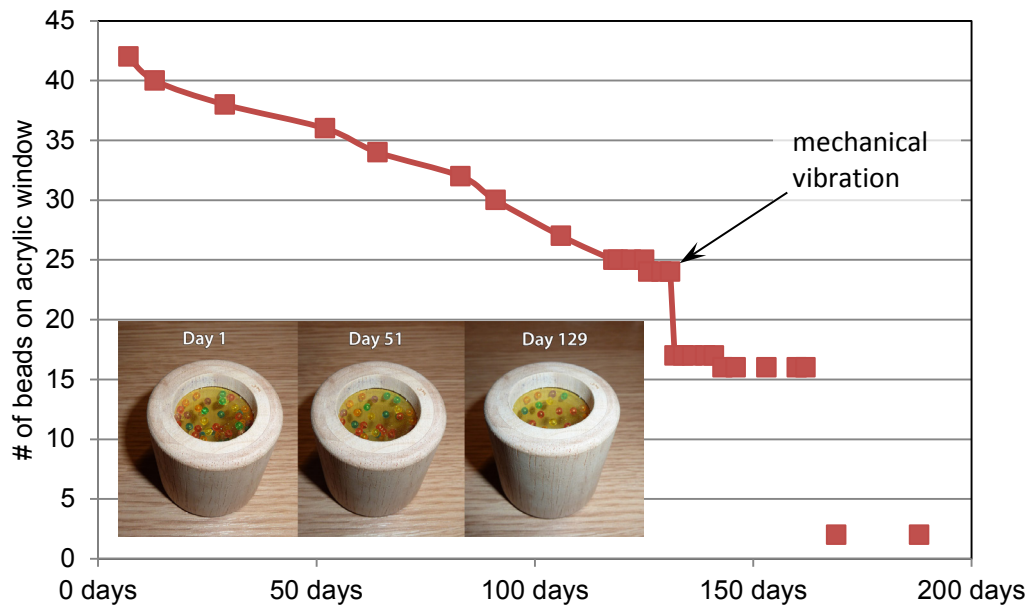


Figure 8.2 – Plot showing the drop off rate for the tribocharged beads electrostatically suspended from the acrylic window of Sample 8-1; periodic photos of beads inset

Figure 8.2 shows the duration that the beads hung from the acrylic window during the undisturbed period. On day 132 a mechanical vibration (caused by something dropping on the table) affected 7 beads. Between day 168 and 169 a large number of beads fell, possibly due to another vibration. The portion of the graph prior to the table vibration appears to be relatively linear and provides some basis that the residual charge can last for at least months, if not more.

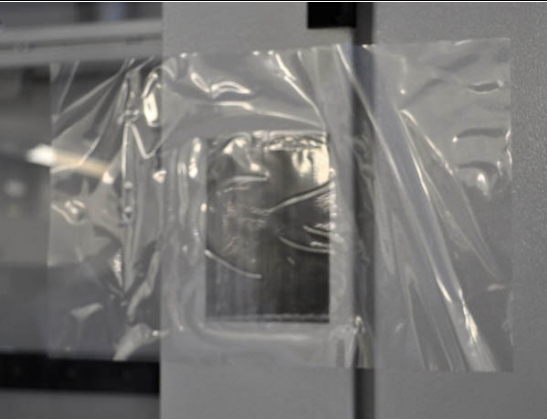
While this experiment provided an easy to observe analogy, there were several differences to consider. Most importantly, the 2mm diameter bead size afforded a much smaller total surface area for charging than micron-scale toner would have for the same volume. If the same volume were filled using the polyester (9 μ m diameter) toner (ignoring the shape change due to fusing), the ratio of the total particle surface areas

(assuming idealized spheres of a single size and uniform packing densities) would be 1:222. From this ratio it can be assumed that the macroscale demonstration is a best case scenario representing relatively low surface/volume charge and that the cumulative residual charges for micron-scale toner would likely be higher by a couple of orders of magnitude. Also, the act of fusing toner presumably entraps its surface charge inside and between layers (Figure 8.11), in a similar way that oxide layers on feedstock powders get entrapped in metal-based AM processes [18].

Sample 8-2 Print onto Film

Building on the understanding gained by the earlier samples in this chapter, it was desirable to measure and observe multiple polyester toner layers. For this purpose, Sample 8-2 followed on from Sample 7-16 with the same pattern, setup, and print settings as before, except that the charge plate and initial toner layers were covered with a 0.05mm thick PTFE film substrate (536-4012, RS Components, UK). The results and discussion follow in Table 8.1.

Table 8.1 – Sample 8-2 Results and Discussion

<i>Results:</i>	<i>Discussion:</i>
 <p data-bbox="304 801 853 920"><i>Figure 8.3 – Sample 8-2 clinging to the side of the SLP rig; the film substrate wrinkled during processing which precluded further layer deposition</i></p>	<p data-bbox="890 369 1414 696">Although Sample 8-2 was intended to be a multilayer print, substrate wrinkling during processing made further layer deposition unpractical. Therefore only one layer was printed. Although it was difficult to measure its potential by field mill (due to field suppression, see discussion re: Sample 7-6), the film readily clung to the side of the SLP rig.</p> <p data-bbox="890 725 1414 920">Despite the ability to electrostatically cling, it is not clear how much of this charge arose due to the presence of the toner, and how much was generated when the film was peeled off of the charge plate.</p>

Sample 8-3 Printing onto Tape

In light of the sample/substrate wrinkling which occurred with Sample 8-2, the target substrate was changed to 12mm-wide high temperature tape (Kapton tape, RS Components, UK) as used to hold samples in place since trials in §7.2.2.2. Two pieces of tape were added to a ceramic substrate (inside the green rectangles as indicated on Figure 8.4) and the substrate processed as per Sample 7-11 with ambient conditions of 25.1°C and 40% RH. The results and discussion follow in Table 8.2.

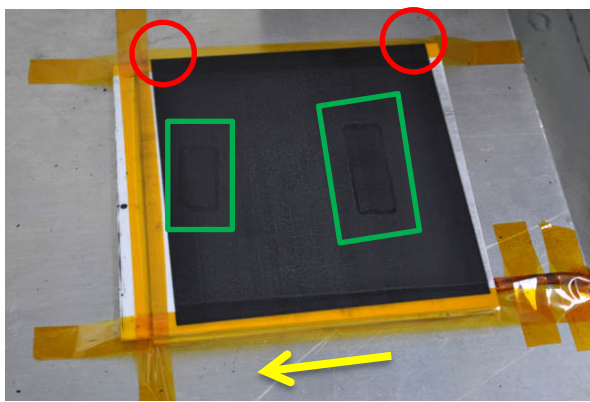
Table 8.2 – Sample 8-3 Results and Discussion**Results:**

Figure 8.4 – Fabrication of Sample 8-3, printing over Kapton tape (entirely covering two pieces of tape inside rectangles and covering only a portion of the tape in the circled corners)

Discussion:

Sample 8-3 printed toner layers onto high temperature tape added to a ceramic substrate. The result of using a conventional electrostatic transfer field, generated between the transfer roller and charge plate at 3,000V, was a multilayer sample low in surface defects. Upon removing the sample from the charge plate, the surface potential measured by field mill approached -2kV. Unfortunately, when trying to remove the tape from the substrate, the force required to peel it off caused virtually all of the toner to flake off. The toner flakes were too fragile to handle.

Although the toner flakes which came off of the tape were highly charged, they were so brittle that attempts to handle them fractured them into fine shards.

Sample 8-4 Toner on Tape

Although Sample 8-3 failed for its intended use, several printed portions of tape $\sim 12 \times 12\text{mm}$, especially near the corners (circled in Figure 8.4) were harvested from the length of tape holding down the substrate which comprise Sample 8-4. The toner did not flake off of the tape when it was unpeeled from the ceramic because: a) it was only half stuck down to the ceramic; b) the unprinted length allowed the initial peeling to start without disturbing the toner; and c) it was carefully peeled off at a less severe angle. Once unpeeled, the tape was folded back on itself (so the adhesive surfaces stuck to each other and were not exposed) and cut to enable handling. In order to prevent charge neutralization from

grounding though handling, the sample was held by the Kapton area using tweezers (Figure 8.5b). The results are presented and discussed in Table 8.3.

Table 8.3 – Sample 8-4 Results and Discussion

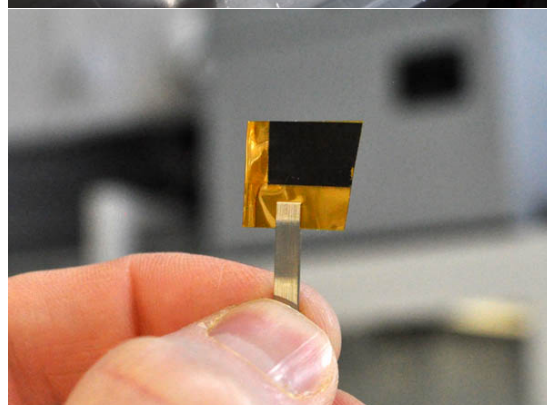
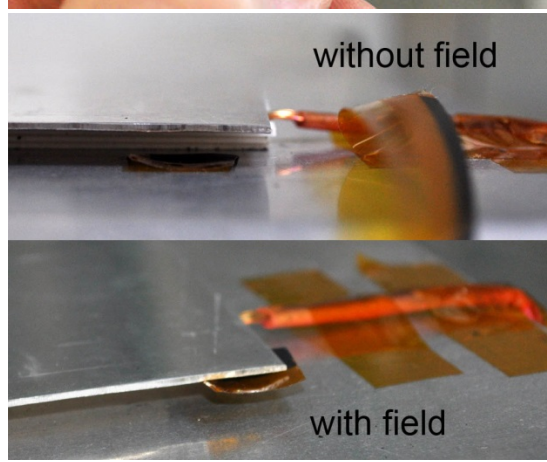
<i>Results:</i>	<i>Discussion:</i>
	<p>a Unpeeled high temperature tape from Sample 8-3.</p>
	<p>b Portion of the length of tape shown in a) which was folded back on itself to become Sample 8-4. This sample weighed 0.025g.</p>
	<p>c Since the sample was too small to be measured using a field mill, its behaviour was observed in a field. The charged plate was shifted approximately 10mm so it was overhanging the grounded substrate with a 4mm gap between them. Several specimens of tape with toner printed on them were placed on the grounded substrate underneath the charge plate. When a transfer voltage of +3,000V (0.75MV/m field strength) was turned on, the tape lifted up to the charge plate.</p>

Figure 8.5 – a) Unpeeled tape which secured Sample 8-3; b) harvested section with tape folded back on itself and cut; c) physically lifting the tape up using a field

Interestingly, after this sample had been attracted on to the charge plate, it would remain suspended after the transfer voltage was switched off. The reasons for this deserve further investigation, but preliminarily may be attributed to electrodynamic forces. Reversing the polarity on the charge plate repelled it back to the grounded substrate. This behaviour was consistently observed over the course of an hour. With lower field strength it was possible to rock the sample back and forth by switching the field on and off. The re-oriented position was only stable with the field on and as soon as it was switched off, gravity would return it to a resting position.

Sample 8-4 provided a clear demonstration that one effect of residual charge in toner material was mechanical motion in a field. This was achieved using a new substrate material which eliminated the possibility that the ceramic substrate used heretofore was somehow storing or contributing to the residual charge in prior samples (especially Sample 7-12). The unprinted areas of the tape were contacted (and thus charged) positively by the final transfer roller. The polarity of any charge retained in the tape from contact with the transfer roller would have been repelled by the positive charged plate, rather than attracted to it. These results were confirming evidence of the hypothesis that fused toner was retaining charge and prompted more detailed trials to determine if patterns of charge could intentionally be written into parts.

Sample 8-5 More Toner on Tape

Sample 8-5 comprises follow on samples prepared as for Sample 8-4, except as noted, in ambient conditions of 22.6°C and 25% RH. Care was taken when folding the tape back on itself (covering the adhesive) to provide flat specimens. The specimens shown in Figure 8.6 were harvested from the tape which was used to hold down Sample 7-20. An additional control sample made from new tape (D) was added to this set of samples, which had not been through the printing process (Figure 8.6c). The resulting specimens are characterized in Table 8.4. These specimens were tested with a range of field strengths (0.13, 0.19, 0.25, 0.31, 0.38, 0.44, 0.50, 0.56, 0.63, 0.69, 0.75 MV/m) with illustration of preparation and results with discussion in Table 8.5 onwards.

Table 8.4 – Summary of Sample 8-5 Specimens

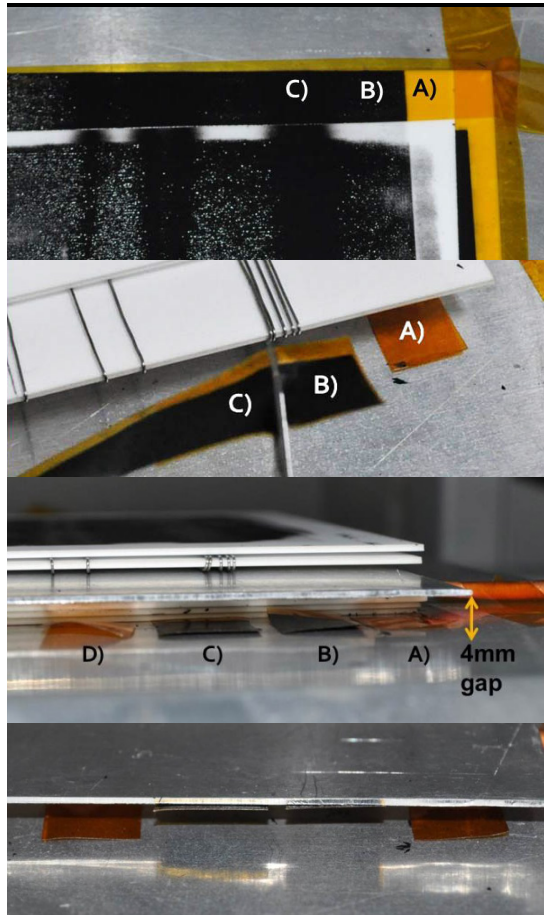
<i>Specimen</i>	<i>Total (tape + toner) mass (g)</i>	<i>Volume of deposited toner (mm³)</i>	<i>Calculated mass of toner (g)</i>	<i>Estimated total fresh toner charge in each specimen (C)</i>
A	0.026 ± 0.001	0	0	0
B	0.027 ± 0.001	3.75 ± 0.2	0.005	-3.73 × 10 ⁻⁸
C	0.031 ± 0.001	2.84 ± 0.2	0.004	-2.82 × 10 ⁻⁸
D	0.023 ± 0.001	0	0	0

Since the mass of the deposited toner was close to the limit of the scale, its volume was measured and the mass of the toner was calculated based on the density of the toner. Also, the total fresh toner charge in each

specimen was calculated by multiplying the volume by the charge per unit volume as calculated for Table 7.5.

Table 8.5 –Sample 8-5 Results and Discussion

Results:



Discussion:

The harvested areas of tape used to produce the specimens are labelled here. A) went through the print cycle, but received no toner, B) was printed without a strong transfer field and C) was printed in a strong field (0.75 MV/m).

The tape was removed from the sample and cut in order to provide specimens corresponding to the capital letters in the image at left. A backing was added to cover the adhesive for each.

The samples were placed in a 4mm gap between the charged plate above and the grounded platform below.

The samples with toner consistently lifted with a positive transfer field for 1.5 hours on the first day in field strengths over 0.69 MV/m. The samples were periodically tested over the next 8 days.

Figure 8.6 – a) Areas harvested for Sample 8-5; b) harvesting the specimens; c) specimen placement without a field; d) B and C lifting due to the field

The first time the field was applied (0.75 MV/m), D lifted. Thereafter, D never lifted regardless of the field strength or polarity applied. This can be explained as being the result of surface charge due to tribocharging from unpeeling the tape off of the roll, which quickly decayed (see Sample 7-30 aside).

On the first day, specimen B was the most responsive to the field, while specimen C was less easily moved. This can be explained by one or more of the following: the 0.9mm³ less toner deposit, the lower toner-to-total specimen mass ratio, and the lower field strength used when depositing the toner layers.

After tests on day one, specimens B and C were left suspended from the charge plate with the power off overnight. In the morning both were still clinging to the charge plate. Overnight, specimen B (with more toner on it) curled, possibly due to thermal contraction of the toner as it cooled. In the morning and afternoon of day two, the specimens were tested again using the full range of field strengths with results as shown in Table 8.6.

Table 8.6 – Results of Sample 8-5 Specimens on Day 2

Specimen	0.13-0.25 MV/m	0.31-0.44 MV/m	0.50-0.63 MV/m	0.69-0.75 MV/m
A	-	-	-	-
B	Re-oriented	1 corner lifted	1 corner lifted	Lifted
C	Re-oriented	Re-oriented	Lifted	Lifted
D	-	-	-	-

On day two, specimen C was more responsive, possibly because the curved surface of specimen B reduced the effect of the field on it. For field strengths from 0.69 to 0.75 MV/m both samples lifted (sometimes a

gentle airflow helped release them from the substrate). The specimens were tested over the next week and became gradually less responsive. The last time the sample would lift (using the maximum 0.75 MV/m field strength) was 8 days after it was first printed.

This sample set provided evidence that charge is retained for a relatively short time for tribocharged surfaces without volume charge (such as by peeling tape or Sample 8-12), compared to high resistivity bodies with volume charge (resulting from fusing individual tribocharged particles, for example). It gave preliminary indication of the profile of charge decay using micron-scale toner which confirmed the trend of the 2mm beads in Sample 8-1. As Dan Hays has emphasized, “nature abhors imbalance” and therefore charge recombines over time [54]. It was not clear, however, how long the charge could be retained, especially in the bulk of samples with 100’s of fused layers.

This sample also demonstrated the potential for using a field in combination with volume charge to produce mechanical motion. This is clear evidence indicating its potential for transduction.

Sample 8-6 Volume Charged Cantilever

The results of Sample 8-5 led to the desire to assess how long fused toner can retain a volume charge and explore geometries for mechanical motion. A portion of a two-year old “failed” legacy tensile specimen created using the SLP rig during the Custom-fit project (§4.4.5.3), which developed surface defects, was tested as Sample 8-6 as shown in Figure

8.7. The sample was made from Somos 201 based toner (§4.4.5.3) and had been stored in the bottom of a drawer for two years prior to testing.



Figure 8.7 – “Failed” tensile sample from the Custom-fit project; the circled portion was used as Sample 8-6

The defects created a long narrow cantilevered feature (approximately 1 x 3 x 20mm) (circled in Figure 8.7). The sample was placed in between the 4mm gap in such a way that the end of the cantilevered portion was elevated above the rest of the sample with the field off (Figure 8.8a). Its behaviour was then repeatedly observed in both negative (Figure 8.8b) and positive (Figure 8.8c) fields of 0.75 MV/m field magnitude. The results are presented and discussed in Table 8.7.

Table 8.7 – Sample 8-6 Results and Discussion

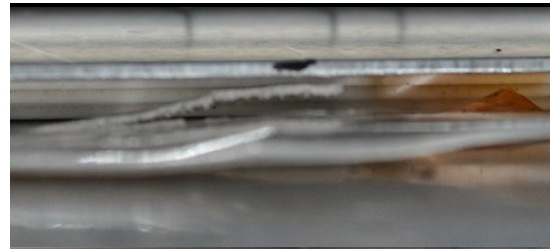
Results:	Discussion:
	<p>a Sample 8-6 is shown with the cantilever in an elevated position without any field. The gap between the charge plate and the highest portion of the cantilever is approximately 0.5mm (as shown at left).</p>
	<p>b In a negative field of 0.75 MV/m, the cantilever was attracted to the plate and it lifted to touch it. This position is shown with a close up image (above) and also with a wide shot (below).</p>
	<p>c In a positive field of 0.75 MV/m the cantilever was repelled from the charge plate toward ground. The gap created by the repulsion was approximately 1mm.</p>

Figure 8.8 – Sample 8-6 in a 4mm gap with a) no applied field, b) with a field of -0.75 MV/m, and c) with a field of 0.75 MV/m applied

Given the magnitude of movement in this sample, it could best be described as micromechanical motion. It provided clear evidence of residual charge after two years of storage (without being in any other container/bag to protect it from ambient conditions in the drawer). The relatively small magnitude of motion relative to its size indicates that the retained charge was probably quite weak. The evidence of charge

provided motivation to measure the retained charge in other legacy samples.

Given that the Somos 201 toner was negatively charged for printing, the fact that the cantilever was attracted to the plate charged to -3,000V was unexpected. The opposite response in the positive field confirmed that the cantilever had a positive residual charge. One possible explanation for this was that the repeated contact with the transfer roller, especially near to a defect area where toner was not being deposited, could have injected some positive charge through contact (similar to the effects observed with Sample 7-5).

Alternatively, working on the assumption that opposite polarity charges can be stable in close proximity, as asserted by Baytekin et al. [179], the observed patterns of pitting could conceivably map to different polarity charge domains arising in the part during production. The cantilevered feature may be a positive charge rich domain on the sample; whereas the adjacent defect area may have been a domain of negative charge. Speculatively, the borders between these domains could conceivably form in patterns analogous to lipids in bilayers, liposomes, or micelles [344].

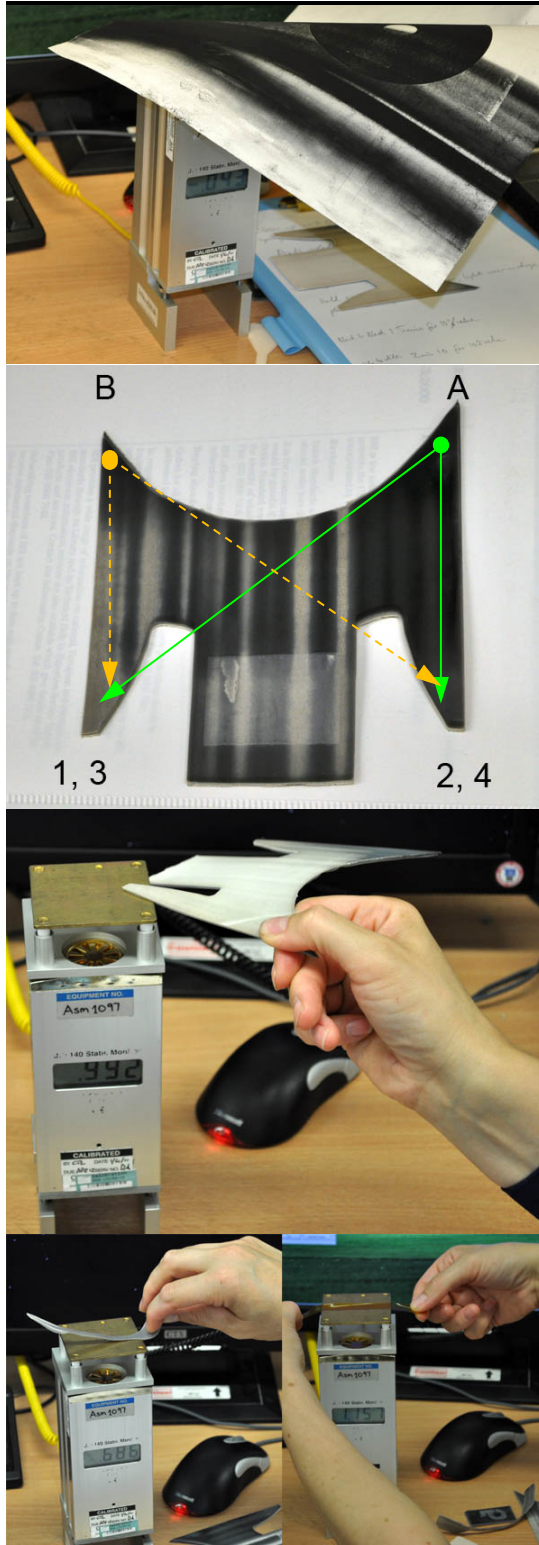
A further theory attributes the positive charge to charge migration over time, after the production of the sample. Given that the volume resistivity of the material was somewhat static dissipative (as shown by Sample 8-7, and measured in conjunction with Sample 8-14), limited migration of charge over time is feasible. It may be possible that positive

charge ingress occurred over time in the outward areas of the part (including the cantilever), in order to counterbalance the inner core of negative charge (which was decaying more slowly due to the inward location).

Unfortunately, the resolution of the field mill does not readily enable evaluation of these three theories, which must be regarded as conjecture until further investigation with higher resolution measurement devices can be undertaken (Sample 8-14).

Sample 8-7 Measuring Residual Charge in Legacy Samples

The evidence of residual charge after two years in Sample 8-6 provided an impetus to measure additional legacy samples. In order to measure residual charge, the expertise and equipment of Susan Leahey, ESD expert at Renishaw PLC, were hired for one day onsite. The primary device used to measure residual charge was a field mill with built-in charge plate (JCI145 charge plate, Chilworth Technology Ltd, UK). Initially Sample 6-1 was assessed. The further assessment of residual charge in legacy samples is referred to as Sample 8-7. After assessment of residual charge, the ability to discharge the isolated charged plate from 1,000V down to 10% (100V) through the body of the part was assessed with results and discussion as shown in Table 8.8.

Table 8.8 – Sample 8-7 Results and Discussion**Results:****Discussion:**

First, the samples were placed directly on top of the built-in charge plate and the total average residual charge was measured. For a single layer print on paper (left) the residual charge was -43V (detected on the area of the plate). For Sample 8-7, the residual charge was -30V. Most of the two year old legacy SLP samples had a residual charge between -30 and -50V.

This is an image of the test procedure used for trials 1-4, where A and B were the corners held by Susan Leahey and 1-4 indicate the point of the part (Sample 6-1) in contact with the charged plate.

Next, the charged plate was raised to 1,000V and then isolated. Then while wearing a grounded wrist strap, Sample 8-7 was held at corner A (for points 1, 2), and corner B (for points 3, 4) and another corner was placed in contact with the charged plate. The time it took to discharge through the part was measured. The discharge times (m:ss) for 1-4 are as follows: 2:00, 1:30, 2:10, 1:55.

Additional legacy samples were assessed with similar results to the first. The high temperature tape used to hold the samples down was also assessed and found to be prone to high charging (from peeling, resulting in field strengths of 10kV/m) and decay rates of many hours to days.

Figure 8.9 – Sample 8-7 showing a) residual charge testing; b) the strategy for testing the static dissipation of the material; c-d) testing

The residual charge on all of the samples tested had a negative polarity which was expected because it matched the initial toner charging polarity during sample production. The magnitude ranged from $-196 \pm 20\text{V}$ (Sample 6-3) to approximately $-50 \pm 7\text{V}$ for rest of the samples. The reduction of magnitude from the surface potential during fabrication may be representative of decay during the ensuing two+ years, or as hypothesized for the last sample (Sample 8-6), positive charge ingress may have been induced to offset and reduce the negative residual charge trapped deep in the sample core.

The longer discharge time ($\geq 2\text{m}$) between opposite corners indicates that the discharge time increases with the length of the discharge path (geometry dependence), as expected. This provides some assurance that the resistivity of the material has a degree of consistency throughout the part. Most importantly, this behaviour indicates the static dissipative behaviour of the material (corroborated with bulk resistivity measurements, see Sample 8-14), which supports the possibility that positive charge could ingress into the outward features of the part.

In addition to the Somos 201-based legacy samples, bulk fused 10mm thick discs of epoxy and polyester toners were tested (as per Figure 8.9c), but were found to be insulative (no reduction in surface potential could be detected over the $>7\text{m}$ trial duration).

The result of placing charged (newly peeled off the roll) high temperature tape on the charge plate did not discharge it significantly (only 1%) after

5m. This indicated that the Kapton film (which the tape was made from) was highly resistive and if charged during sample production, could retain charge for hours or days. This could be skewing field mill measurements intended to be indicative of the surface potential of the sample due to residual toner charge.

The samples in this subsection provided clear evidence of the potential to pattern volume charge in 3D in laser printed objects (making them electrets by virtue of the trapped charge) by controlling the placement and charge on toner particles when fused. *This was the first time that a method was demonstrated for digitally patterning the charge density in electrets (in all three dimensions)*, enabling opportunities to optimize electrets for transduction, micromechanical motion, data storage, etc. This work became the basis for filing GB patent application number 1213585.1 and subsequent PCT application PCT/EP2013/065694 [342].

8.1.3. Proposed Model of Charge Trapping

The foregoing experimental work provided the basis for a new conceptual model describing the probable location of charge in the volume of 3D laser printed objects. For context, a simple initial model is described first.

Based on the standard practice of modelling toner as a point charge [86, 108, 158], in combination with legacy assumptions that residual charge is neutralized during fusing (as per Kumar et al., §7.2.1), the state of understanding prior to this work has been summarized graphically using a simplified model of toner charge as shown in Figure 8.10.

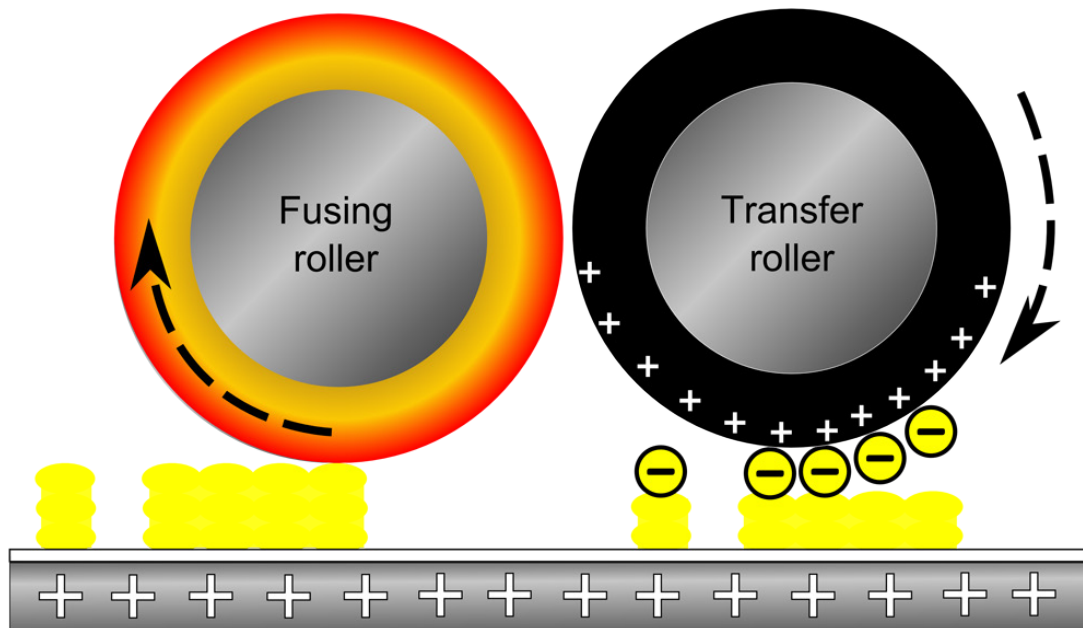


Figure 8.10 – Simplified model of toner charge based on the assumption that residual toner charge is neutralized during fusing

The substantiation of lingering residual toner charge (after fusing, §7-8.2), in combination with the understanding that charge is not distributed uniformly on the toner surface (§3.2.4.4), led to a *new improved conceptual model proposed by the author* in Figure 8.11.

Due to the concentration of rubbing force on the raised surface features (high spots) of individual toner particles, a non-uniform distribution of surface charge is generated by tribocharging. Toner particles then align to the flux of the transfer field according to their individual non-uniform charge distributions (similar to how colloidal particles are electrostatically aligned in a field [335], or how sand is oriented electrostatically as it is glued to sandpaper [345]). This results in the highest density of unbalanced charge at the upper and lower surface of the toner particle essentially comprising charge rich “polar cap” regions on toner particles

prior to fusing (Figure 3.16, §3.2.4.4). After fusing, the charge remains most densely concentrated at the upper and lower boundaries of the fused layer. As overlying layers are added, charge is trapped in situ resulting in the development of charge rich interlayers as illustrated in Figure 8.11. Although some excess charge is also certainly trapped (intralayer) at the boundaries between laterally adjacent toner particles as they fuse, the concentration is significantly less due to particle re-orientation in the transfer field.

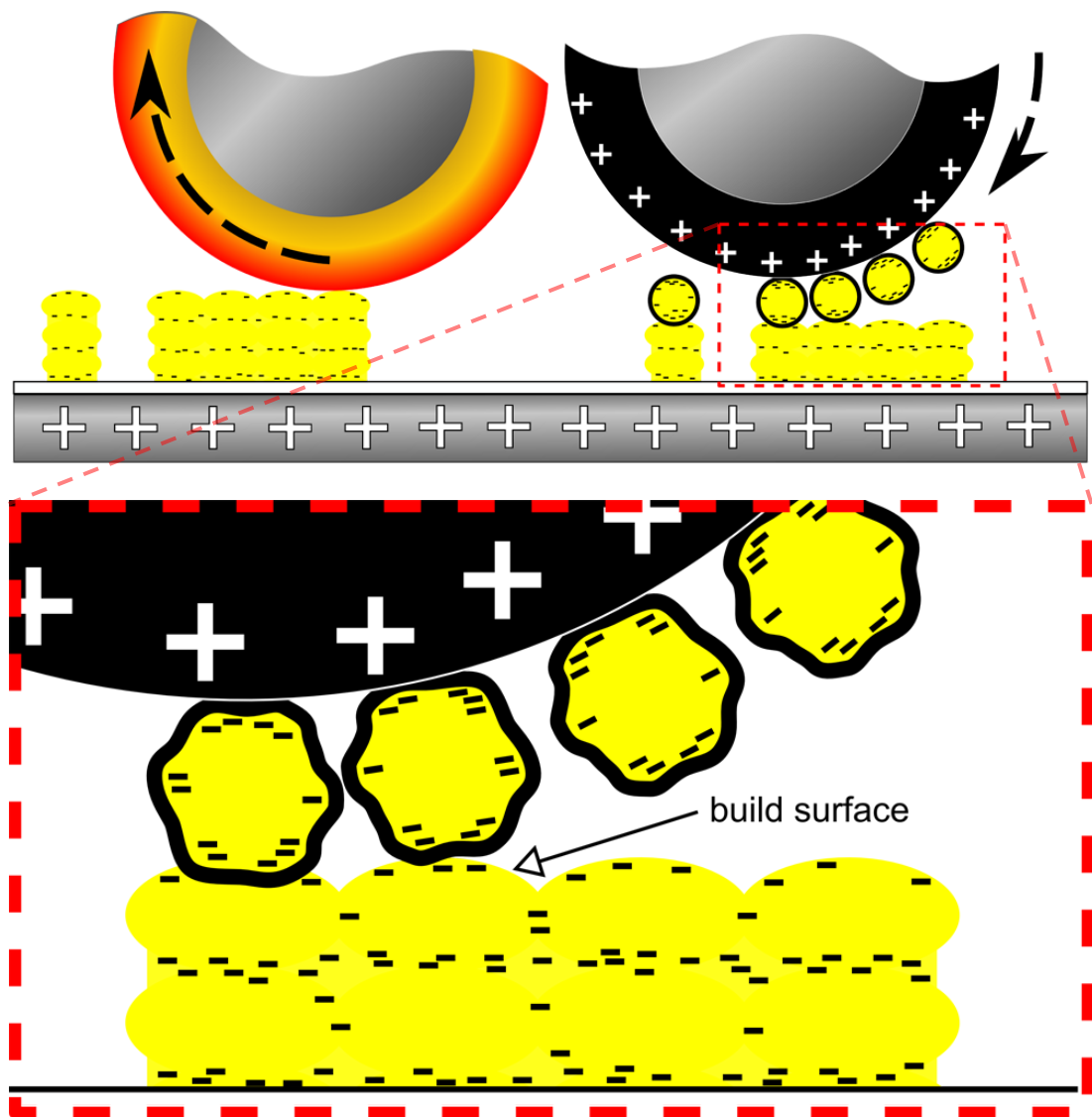


Figure 8.11 – Improved conceptual model of charge trapping, showing non-uniform shape and charge distribution of toner prior to fusing, and charge rich interlayers thereafter

This improved model of residual charge distribution provides an explanation for failed prior transfer attempts and a new foundation for progress toward AM by EP. For example, it explains why prior attempts to neutralize 3D laser printed layers by direct contact with a grounded conductive plate were ineffective [181]. The plate did not provide a path for electrons to escape (neutralization), especially from the lower “polar cap region” of the fused toner because it was embedded into the underlying build surface. This also explains why top charging ion treatments (§4.3.2) were not fully effective in achieving charge recombination, due to the lack of access to the charge on the underside of each fused toner layer.

8.2. Approaches to Charge Neutralization

Building on the improved residual charge model (Figure 8.11), new methods for neutralizing volume charge were trialled. From this point forward, all trials were undertaken using the SLP rig in its Stage 2 form (§5.7.2) using epoxy “toner” (§5.1), printed in a square print pattern 110cm^2 (fitting just inside the radii on the ceramic substrates §5.5) with printer settings listed in Table 5.2 unless noted.

8.2.1. Preliminary Exploration of Neutralizing Methods and Measurements

The following trials were undertaken to assess the effectiveness of the following neutralization strategies.

Sample 8-8 Neutralize by Contact with Grounded Al Plate

Although Kumar Das reported contacting the upper surface of printed layers to a conductive grounded plate to neutralize it without success [181], this was performed on samples printed using the SLP rig with the same result.

This duplicated result confirmed that physical contact to the upper surface of the toner alone would be unlikely to neutralize residual toner charge.

Sample 8-9 Neutralize by High Voltage Discharge Through a Body

Recognizing the need to neutralize charge entrapped in the body of the sample, further samples were produced similar to Sample 7-32 where the voltage was intentionally used to create breakdown through the multilayer body and therefore promote charge recombination and neutralization. The resulting surface potential was not uniform; therefore this approach was not pursued further.

Sample 8-10 Neutralize by AC Discharge Through a Body

Theoretically, the use of AC voltage to neutralize individual layers could be effective; however the transfixing/transfusing action of the SLP rig was not amenable to this approach without undue risk to the printers.

Preliminary attempts to adapt the SLP rig to print onto an intermediate transfer substrate where AC neutralization could be undertaken resulted in unsatisfactory transfer (Table 8.9); therefore AC neutralization was not

further attempted. This approach was not pursued, due primarily to the SLP printer architecture, however, it represents an opportunity for further work.

Table 8.9 – Sample 8-10 Results and Discussion

Results:

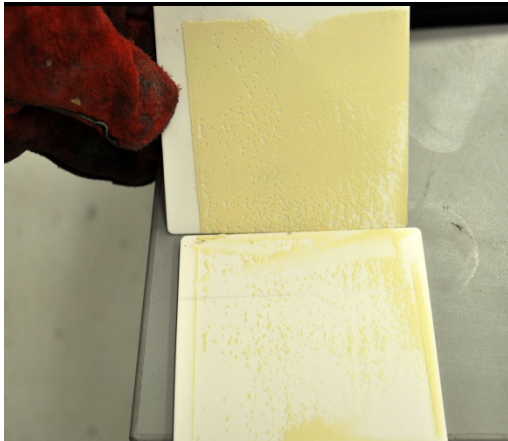


Figure 8.12 – Early attempt to transfer from an intermediate substrate (lower plate) onto the final receiver (upper plate)

Discussion:

Preliminary attempts to transfer the toner layer onto an intermediate substrate (lower plate in Figure 8.12), used with and without PTFE coating, resulted in defective transfer onto the final receiver (upper plate). Therefore AC discharge of the layer was not attempted.

Since the neutralization methods for passing through a body were not successfully implemented, attention turned to the potential of removing charge using surface treatments which had a penetrating effect, or at least could provide some counterbalancing surface charge to the residual charge submerged in the consolidated toner, thus resulting in a net zero charge on the consolidated body.

Sample 8-11 Neutralize by Immersion in a Liquid

Seeking to maximize the surface area contacted and avoid the non-uniformities arising from uneven contact/pressure in Sample 7-30 (and possibly with Sample 8-8), neutralization by immersion in a water-based

liquid was attempted. The motivation behind it was reinforced because of the moderate success of using a brine solution to prepare Sample 7-24 (and also retrospectively strengthened by further literature discovered after these trials as reported in §4.3.2.2, §3.2.1.3, and §4.3.4.2).

Table 8.10 – Sample 8-11 Results and Discussion

Results:



Figure 8.13 – Attempted neutralization by immersion in water

Discussion:

A sample prepared as for Sample 8-4 was immersed in water for 30s as shown at left. The trial was also repeated using a grounded conductive container of water.

In both cases, after the sample dried, it could be lifted up to the charge plate using a field strength of 0.75MV/m

This result (with a 20 layer sample) indicated that the residual interlayer charge was not accessible for neutralization by immersion in liquid. This result (and the practical difficulties of handling liquids in-process) discouraged further trials using higher conductivity liquids, such as liquid mercury which has been used to add or remove charge *to the surfaces* of dielectrics/insulators [346]. Therefore, ion sources were next considered to neutralize charge.

Sample 8-12 Neutralize Surfaces by AC Fan Ionizer

Due to the non-uniform nature of the pulsed DC pin ionizers (§5.7.1.3.1), an AC fan ionizer (§5.7.2.1) with an output of $0 \pm 5V$ was used for neutralizing charge. Preliminary experimentation exposing tribocharged acrylic EMBER build substrates (without toner on them) to the ionized air flow for 10s totally neutralized the surface as shown by the gold leaf electroscope (Figure 8.14; cf. Figure 5.31 right). This neutralization method was next used on printed toner layers.



Figure 8.14 – Acrylic substrate neutralized by AC fan ionizer

Sample 8-13 Neutralize by AC Ionizer before Fusing

Based on the improved model of residual toner charge (Figure 8.11), in combination with the outcome of Sample 8-8, it seemed that the ideal time to neutralize charge would be prior to fusing, before charge entrapment could occur and the surface area was reduced. Therefore a sample was made where the initial toner layer was printed, but without pre-heating the substrate (to avoid transfixing or transfusing the toner during transfer). After printing, it was moved underneath the AC fan ionizer (Figure 5.14) for 30 seconds and then under the heater. When the substrate exited from the heaters, the toner layer was mostly gone. This outcome was repeated several times. Careful observation revealed that the toner was being blown off of the substrate by the fans which cooled

the heating elements. Since this never happened with prior trials, it can be assumed that as long as the toner retained its charge, it was held in place electrostatically, but when the charge was neutralized, it was dislodged from the substrate and blown away by the air flow.

This result confirmed that the AC ion treatment was effective at removing toner charge (prior to fusing), however as a consequence the toner layer was expunged. This problem is similar to the dilemma that Schein observed regarding AC corona having the potential to neutralize, but simultaneously contaminating the printed layers in most transfer arrangements [37]. Further work using the AC fan ionizer for neutralizing toner layers after fusing is reported in §8.2.2.

Sample 8-14 Non-contact Electrostatic Voltmeter Measurements

Part of the further work recommended by Susan Leahey of Renishaw after Sample 8-7 was to engage the services of Dr. Jeremy Smallwood, primary consultant and investigator of Electrostatic Solutions Limited (UK). Dr. Smallwood was contracted to undertake a site visit and perform some surface potential measurements with alternative measurement devices. While on site, Sample 8-14 was produced with only a single layer (and no fusing) on the SLP rig and the surface potential was measured by field mill as done previously. Next, the sample was measured off-rig (requiring 30-60s to relocate it) by Dr. Smallwood using a high impedance non-contact electrostatic voltmeter (Model 347, Trek Inc., USA) with a 10mm diameter probe at a ~5mm stand-off distance.

The surface potential as measured by the field mill was -514V. The surface potential on the sample as measured by the non-contact electrostatic voltmeter varied from 233V at the edges to more than -3,000V (the meter is only rated for a maximum of $\pm 3,000\text{V}$) in the centre.

Table 8.11 – Sample 8-14 Results and Discussion

Results:

Discussion:



a Scanning the probe over the surface of the Sample 8-14 revealed surface potential in excess of -3,000V in the central areas of the sample. The voltage dropped to $\sim -1,000\text{V}$ after 1min of measurement.

b Measurements taken toward the edges of the sample where the high temperature tape was used to secure the substrate resulted in a positive surface potential as shown at left.

Figure 8.15 – Non-contact electrostatic voltmeter measurement of the surface potential on Sample 8-14 in different areas

These measurements provided the first insight into the X-Y spatial variation of residual charge imbalance on the surface. It confirmed that the field mill is a very “blunt” instrument which averages all charge imbalance in its vicinity. It also corroborated the observation by Susan Leahey (Sample 8-7) that the use of (non-ESD) high temperature tape is skewing the intended field mill measurement of the toner layers only and

should be avoided in future. This may also indicate that previous readings using the field mill assumed to primarily be measuring the surface potential of the toner layer were underestimates. Observing the sample surface potential decay for 1m (\approx to the takt time between layers in an automated SLP print cycle) indicates that, in some cases, residual toner charge trapped by successive overlying layers may be upwards of 30% of the fresh toner charge (or more), but this requires further study.

In addition to the non-contact electrostatic voltmeter measurements, Dr. Smallwood assessed the resistivity of bulk fused toner materials using a resistance meter (Model 152-1, Trek Inc., USA). Although the assessment was not comprehensive, it indicated that Somos 201 had a resistivity on the order of 10^{11} , while the polyester and epoxy used in this study exceeded 10^{13} (which was the limit of his measuring equipment).

Sample 8-15 Neutralize by Flame

Discussion with Dr. Smallwood about the difficulties experienced with the imbalanced ion output of the pulsed DC ionizing pin emitters (§5.7.1.3.1), led to the suggestion of considering the use of flame to neutralize toner charge. This notion resonated with the historical use of flame (which generates a balance of positive and negative ions, as well as buckyballs) to neutralize electrostatic charges by P. Selenyi in his 1930's electrographic recording system, which led to the first facsimile image [54, 347, 348]. Therefore, another sample was prepared as for Sample 8-14, except that after it was measured using the non-contact electrostatic voltmeter, a flame from a lighter was quickly passed over its

surface (at an estimated rate of 150-250mm/s to avoid burning/oxidizing the polymer) and the potential was measured again.

Table 8.12 – Sample 8-15 Results and Discussion

Results:



Figure 8.16 – Neutralizing the surface potential on Sample 8-15 using a flame

Discussion:

Passing a flame over the surface of Sample 8-15 reduced the surface potential from over -3,000V to less than 5% of that value in ~10s.

Although the practicalities of safely using flame to treat powder layers made this method second choice to ion neutralization methods, it provided a simple method for neutralizing charge which did not blow the toner off of the substrate (like the AC fan ionizer did on Sample 8-13).

The samples in this subsection provided improved insight into how to neutralize charge in multilayer samples.

8.2.2. Layer by Layer Neutralization

The difficulty of removing trapped charge from a 3D body encouraged neutralizing the residual charge of each layer prior to the addition of further layers. The following trials were undertaken to evaluate the effectiveness of the subset of methods selected from §8.2.1.

Although prior attempts to use coronas for top charging had failed (§4.3.2, §7.2.3), the refurbished printers had two exceptionally high power corotron devices (Figure 5.17) for charging the substrate before and after the final transfer. It was unknown if the higher power corona would provide a penetrating effect into the polymer layers. It was also unknown what effect AC neutralizing each layer followed by top charging would have. Therefore a 2x2 experimental matrix was set out as follows in Table 8.13:

Table 8.13 – Matrix to Evaluate Neutralization by Transfer Corona and AC Ionizer

		AC Ions 100%		AC Ions OFF
Transfer Corona* = 0V		Sample 8-17		Sample 8-16
Transfer Corona = 5,700V		Sample 8-18		Sample 8-19

* this refers to the transfer corona of the 1st printer (as used during the final transfer of toner in these trials)

Sample 8-16 Baseline Sample without Neutralization

Baseline samples were produced using a tackification transfer according to the standard pattern (Table 5.2) without any neutralization treatments (apart from the corona of the 2nd printer after the print used to neutralize deposited toner charge as per Table 5.2). Due to the light colour of the toner, target fusing temperatures were raised to $145 \pm 5^\circ\text{C}$ (without recalibrating the thermal sensor on the SLP rig). The ambient conditions for Sample 8-16 were 17°C and 37% RH and the results are presented and discussed in Table 8.14.

Sample 8-17 Neutralize by AC Ions Only

Samples were prepared as for Sample 8-16 except that after each print, the platform was positioned underneath the AC fan ionizer for 30s to promote upper surface neutralization prior to the addition of the next layer. The ambient conditions for Sample 8-17 were 21°C and 36% RH and the results are presented and discussed in Table 8.14.

Sample 8-18 Neutralize by AC Ions and Transfer Corona

Samples were prepared as for Sample 8-16 except that just preceding and following the toner deposition, the platform and build surface were exposed to the built-in corona devices charged to +5,700VDC. Also, as for Sample 8-17, after each print, the platform was positioned underneath the AC fan ionizer for 30s to promote upper surface neutralization prior to the addition of the next layer. The ambient conditions for Sample 8-18 were 19°C and 43% RH with results presented and discussed in Table 8.14.

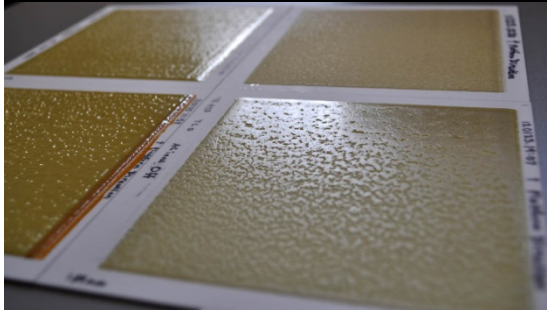
Sample 8-19 Neutralize by Transfer Corona Only

Samples were prepared as for Sample 8-16 except that just preceding and following the toner deposition, the platform and build surface were exposed to the built-in corona devices charged to 5,700VDC. The ambient conditions for Sample 8-19 were 18°C and 45% RH with results presented and discussed in Table 8.14.

Table 8.14 – Results and Discussion for Sample 8-16 to Sample 8-19

Results:

Discussion:



The best surface quality of all four samples was achieved along one edge of Sample 8-16 as shown in this image where the reflected light reveals reduced surface pitting on the upper edge (probably where the nip pressure was highest).

Figure 8.17 – Sample 8-16 shown in the lower right hand side of this image with reduced surface pitting along the top edge.

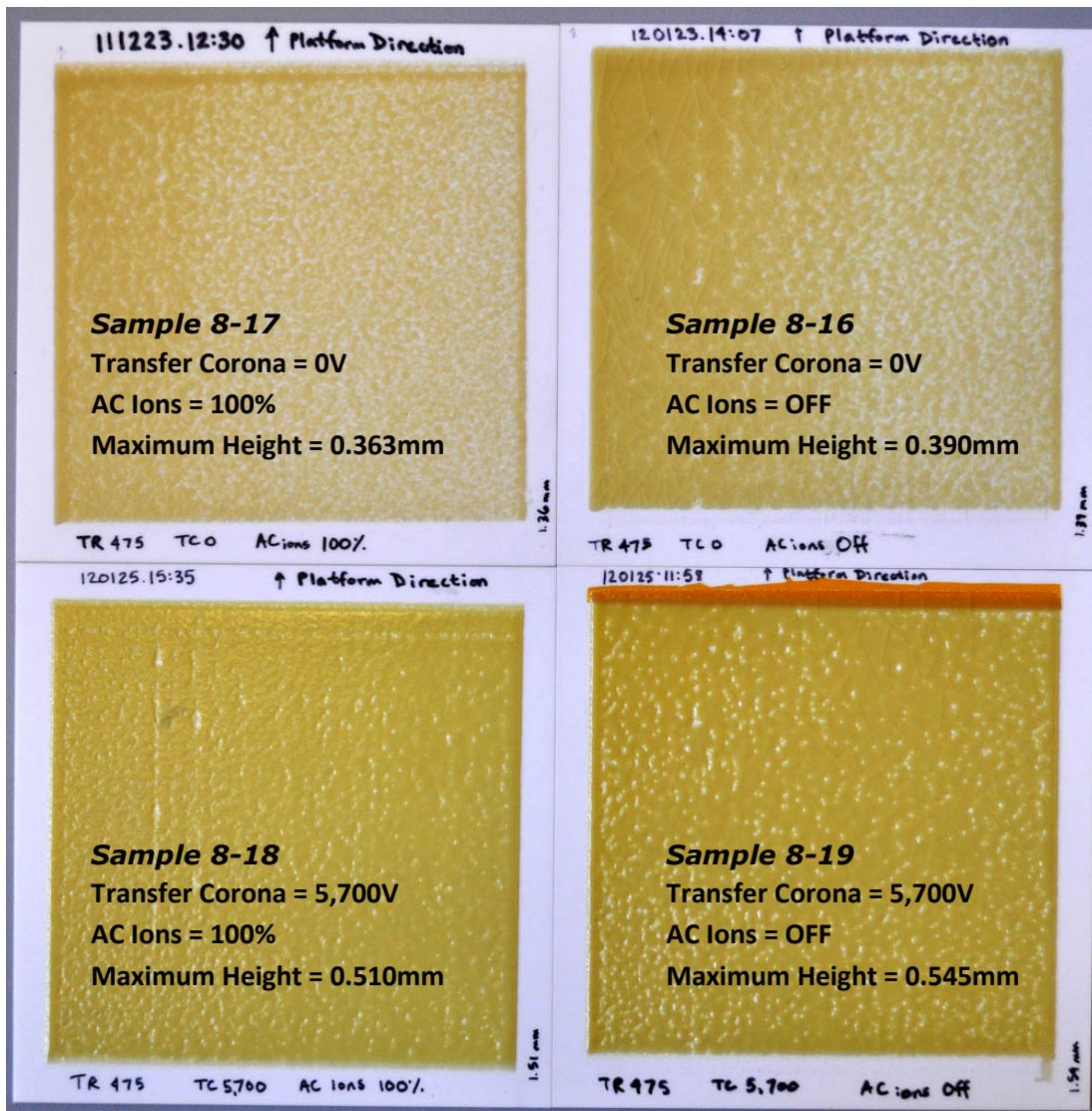


Figure 8.18 – Four samples showing the effect of neutralization by ac fan ionizer and use of transfer corona

The tallest build was Sample 8-19 which used only transfer corona and achieved 0.545mm, although it had substantial surface pitting defects. The shortest build height was Sample 8-17 which was neutralized only by AC ions and was 0.363mm high.

Interestingly, the best surface quality was achieved by the left edge of Sample 8-16 (also shown in Figure 8.17) which did not receive any additional neutralization treatment. Unfortunately some cracking resulted in this sample as it cooled due to thermal contraction.

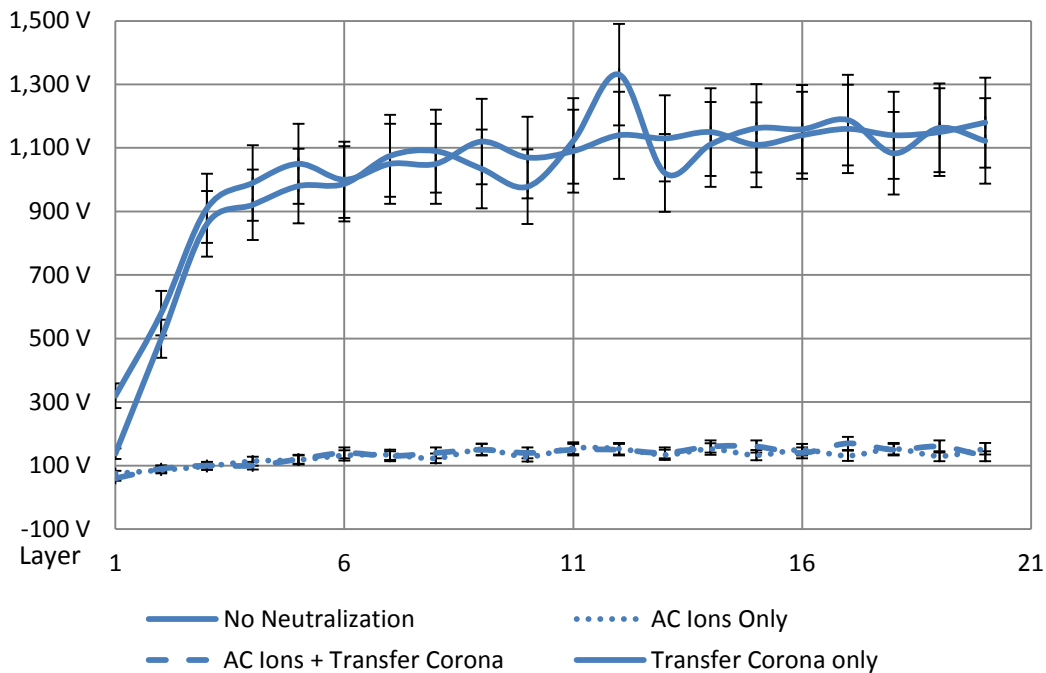


Figure 8.19 – Graph showing the surface potential before each layer printed for all four samples illustrating the effect of neutralization by AC fan ionizer and transfer corona

This graph reveals that the AC ionizer had the best neutralizing effect on each sample and that, in fact the transfer corona charged the sample rather than only neutralizing it. Logically, Sample 8-19 which had the tallest build also had the highest average surface potential. Surprisingly, Sample 8-16 which received no “neutralizing” treatment and was built almost half as high, sustained an average surface potential almost equal to Sample 8-19.

As with samples made from polyester, these results confirmed the need for electrostatically favourable conditions in order for a consistent tackification transfer. Despite the intention for neutralization to eliminate pitting, both of the samples with an order of magnitude reduced surface

potential (due to the AC ionizer) experienced noticeably more defects than those with higher surface potential.

Although improved deposition rates (Sample 8-18, Sample 8-19), and good surface quality (Sample 8-16) were desired, the latter takes precedence over the former since maintaining a defect-free build surface is the only way to continue to build increased uniform part height. For that reason, further work is built on the approach used by Sample 8-16.

Sample 8-20 Blank Prints then No Neutralization

Observing that the best surface quality resulted from samples which had a high positive surface potential (Figure 8.19), an approach similar to the one used for Sample 7-5 was employed. Sample 8-20 was produced as for Sample 8-16, except that prior to printing, three blank "prints" were made. This was an attempt to raise the initial surface potential prior to printing (as was the case for Sample 7-5) and thus avoid defect formation in the first few layers while the potential was ramped up (Figure 8.19).

The result was reduced deposition (0.290mm height) and worse surface quality (more pitting) than for Sample 8-16. This may be due to an anomaly in the thermal management which was corrected for the next set of trials. Rather than re-run this sample, the use of a conventional transfer field provided higher assurance of raising the surface potential and was therefore deemed better for proving this concept, however the approach attempted for Sample 8-20 may have merit for future research.

Sample 8-21 Prime by Conventional Transfer, No Neutralization

Following the same line of thinking as for Sample 8-20, to prevent defects from forming in the first few layers, Sample 8-21 was printed using conventional transfer (transfer plate voltage = 2,000V) for the first three layers. This was done in order to “prime” the surface with a high quality toner layer which could be used for tackification thereafter. Following the first three layers, the charge plate was turned off and the remaining 17 layers were printed as for Sample 8-16. Ambient conditions were 18°C and 39% RH and the results are shown in Table 8.15.

Table 8.15 – Sample 8-15 Results and Discussion

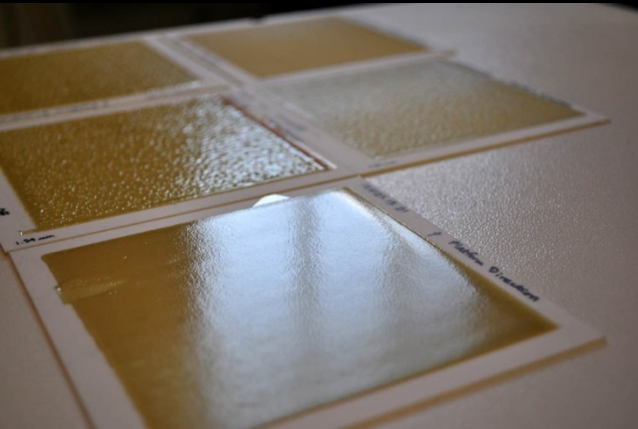
<i>Results:</i>	<i>Discussion:</i>
	<p>The height of Sample 8-21 was 0.50mm and the surface was free from pitting defects as shown in Figure 8.20. Also, the surface potential scarcely dropped below 1,500V (including the first three layers).</p>

Figure 8.20 – Smooth defect-free surface of Sample 8-21

Building on the success achieved with Sample 8-21, this sample was repeated with 60 layers (instead of only 20). The ambient conditions were 18°C and 29% RH and the results appeared identical to Figure 8.20 after twenty layers had been printed. At layer 29 “valleys” started forming and a small amount of toner in the same pattern as the valleys

(which had not been deposited on the build surface) could be seen on the back side of the transfer roller. By layer 46 a significant amount of toner was visible on the backside of the roller as shown in Figure 5.18 and waviness (a series of ridges and valleys) was apparent on the sample itself. Although the frequency/pitch of the ridges and valleys was higher, these defects were reminiscent of the waviness defects observed in Sample 6-1 (§6.1.3). After that the uppermost area of the ridges began to develop pitting defects similar to those observed on the polyester samples. The result is shown in Table 8.16.

Table 8.16 – Results and Discussion: 60-layer Sample 8-21

<i>Results:</i>	<i>Discussion:</i>
	<p>Although the 60-layer version of Sample 8-21 was over 1mm high, it suffered from waviness (ridges and valleys) and also surface pitting which was most noticeable on the ridges.</p>

Figure 8.21 – 60 layer version of Sample 8-21 showing ridges and surface pitting defects

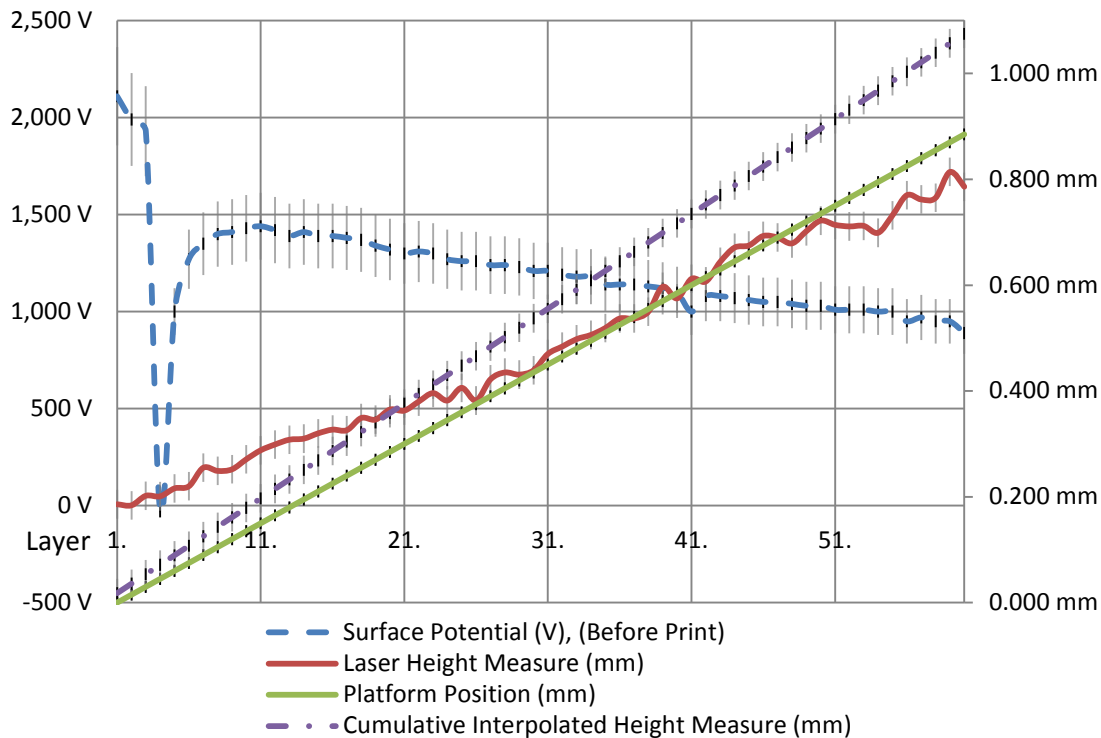


Figure 8.22 – Graph of the surface potential versus the build height during the production of the 60 layer version of Sample 8-21

Figure 8.22 shows a trend of reduced surface potential over time which correlates with the formation and exaggeration of defects in the 60 layer version of Sample 8-21. The early dip in surface potential was caused when the charge plate for conventional transfer was switched off. The first noticeable defect formation was at layer 29 which coincides with the surface potential dropping below 1,200V.

Most importantly, the 60 layer version of Sample 8-21 provided clear evidence that the transfer corona was serving as a top charging transfer method (§4.3.2) and not merely a neutralization technique. While this underscores the need to maintain an electrostatically favourable potential for any transfer method to work consistently (as discussed in §7.1.2.1), it also means the results are field strength limited. Therefore these results demonstrate that as the layer stack grows away from ground, the build surface potential will be reduced accordingly. For this reason, the work in §9 was re-focused on transfer methods which theoretically were not inherently field strength limited.

The sequence in which defects arose on this sample may be instructive. The fact that waviness was first manifest prior to surface pitting may indicate that residual charge was not the primary cause of the waviness defects. This notion is reinforced by the relatively slow decline of surface potential ($\sim 11\text{V}$ per layer between layers 10-60) observed in this sample. Sample 6-1 provides more supporting evidence, which similarly exhibited substantial waviness, but only limited surface pitting. This is logical when considering the lower resistivity of the Somos 201 material (as shown by measurements made in conjunction with Sample 8-14), which would have made it less susceptible to residual charge accumulation (and pitting caused therefrom), but provided no immunity to other factors such as non-uniform nip pressure (as considered in Appendix B). This notion merits further consideration for future work.

Lastly, it is noteworthy that this is the first sample where multiple indicators of in-process height measurement are plotted, facilitating comparison: the platform position, the laser height measurement. For reference, the interpolated cumulative thickness (based on dividing the final measured thickness by the number of layers) is included. As can be seen in Figure 8.22, none of them can be considered to have high accuracy, but they all follow the same trend. This imparted enough confidence in the laser height measurement to use it in the next sample set.

Sample 8-22 Conventional Transfer with Flame Neutralization

Due to the potential for confounding effects in earlier samples in this subsection, the effect of neutralizing residual toner charge by flame was examined in isolation. The hope was that the flame neutralization would eliminate any repulsive effect from the accumulated layers thereby achieving a measurable improvement in transfer efficiency. To achieve this, 10-layer samples were produced as for Sample 8-21 with four exceptions. First, the transfer corona from the 2nd printer was switched off; second, a conventional transfer (ramped up transfer voltage from 2,250V to 3,000V, as shown in Figure 8.23) was used for all 10 layers; third, no heat was used for fusing/tackifying; and fourth, flame was used to neutralize residual toner charge with two regimes. In one regime, flame was used to neutralize the charge immediately after each print (layerwise) by passing over the entire surface of the layer (as per Sample 8-15). In the second regime, the flame treatment was applied after all 10 layers had been printed. The surface potential just prior to printing each layer was measured by field mill and then measured after the charge plate was switched off (in layer 11 position) and after the last flame neutralization treatment (in layer 12 position). The results are presented and discussed in Table 8.17.

Table 8.17 – Results and Discussion for Sample 8-22

Results:

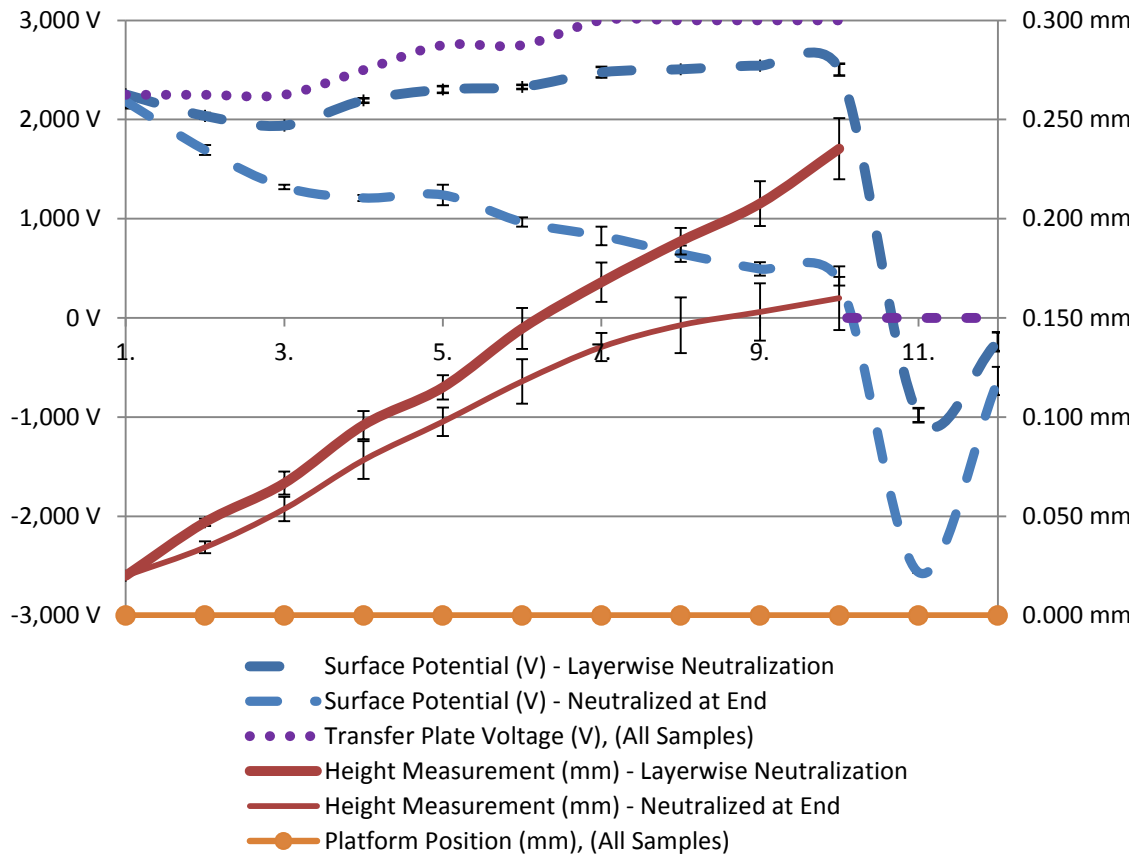


Figure 8.23 – Graph of the surface potential and laser height measurement for the two sets of different flame neutralization regimes of Sample 8-22



Figure 8.24 – Photo of Sample 8-22 which was flame neutralized each layer (left) and another which was flame neutralized only after all 10 layers were deposited (right)

The results in Figure 8.23 indicate that layerwise neutralization maintains a more constant surface potential, resulting in improved build height (in line with the premis for this trial). However, upon examining the samples it was clear that layerwise neutralization reduces the printed layer quality and consistency as shown in Figure 8.24. The reasons for these defects are elucidated in Table 8.18.

The discrepancy between the graphed instrument readings and the visual inspection of the surface quality of Sample 8-22 led to a repeat of the trial where each sample was weighed after each print – a measurement only made practical due to the decision to omit thermal fusing for this sample set. The results are graphed in Figure 8.25.

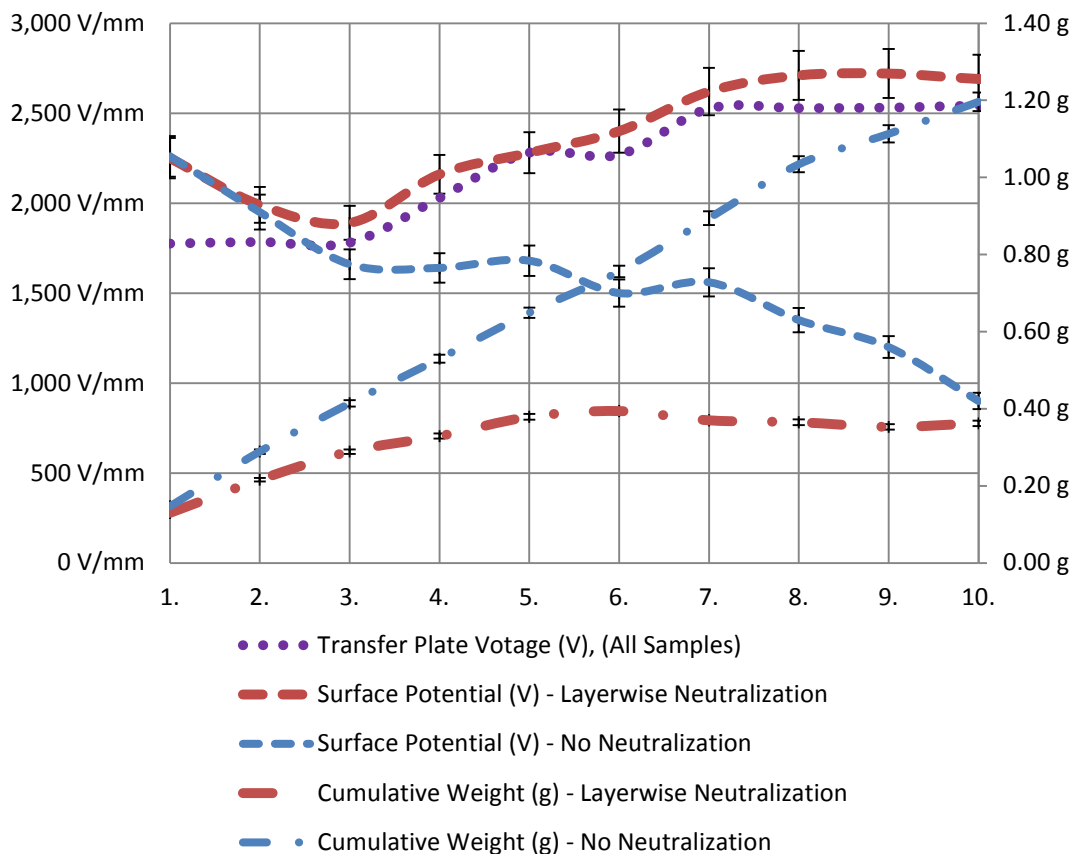


Figure 8.25 – Graph of the cumulative toner weight added for each layer in the repeat of Sample 8-22 showing much lower deposition rate for samples neutralized layerwise

The graph shows that the samples without layerwise neutralization (and thus dropping surface potential) were receiving more toner by weight, despite measuring a lower height on the laser height measurement. This indicates that the toner which had not been neutralized was packed more densely, probably due to the effect of the transfer field, as explored further in Sample 8-23. The steady deposition rate of the sample which was not receiving layerwise neutralization treatment prompted a repeat of this trial with 40 layers to see if the deposition rate would remain constant. It was determined that flame neutralization would only be done if or when the deposition rate began to plateau. Neutralization was done three times for this sample at the surface potentials labelled in the graph (Figure 8.26).

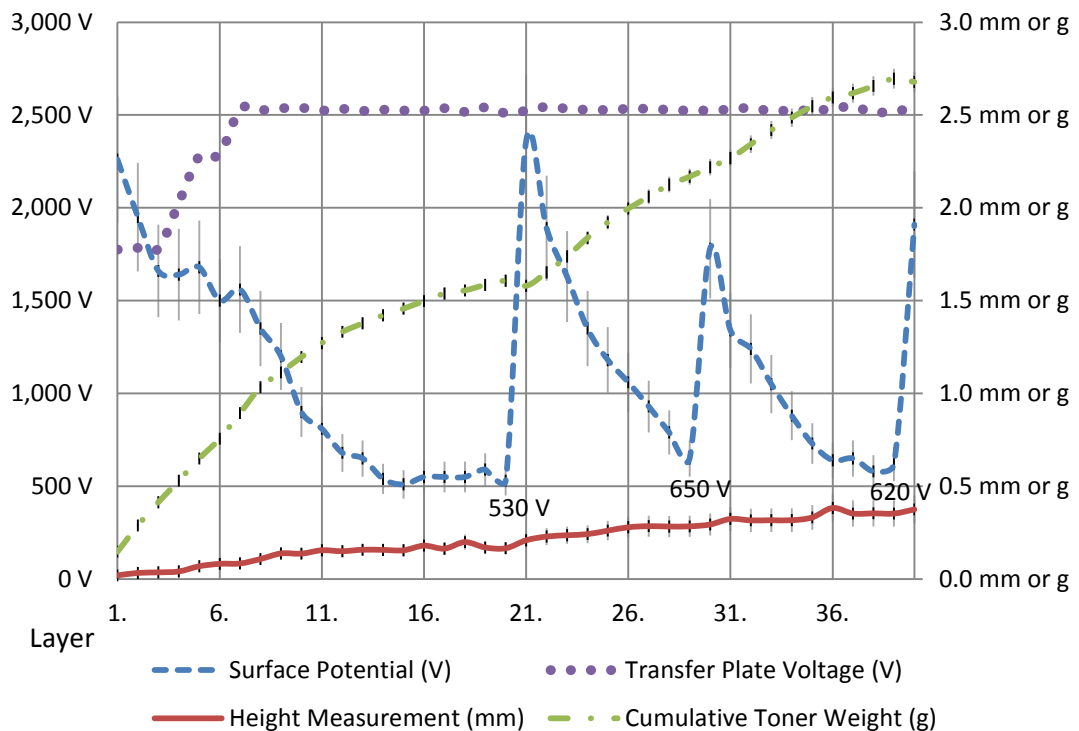


Figure 8.26 – Graph of a repeat of Sample 8-22 prepared without flame neutralization except for three instances when the surface potential troughed at 530, 650, and 620V as labelled on the graph.

Although the deposition rate for the sample without layerwise flame treatment was constant for the first 10 layers (Figure 8.25), the deposition rate began to diminish as soon as the surface potential dropped below $\sim 1,000\text{V}$ (Figure 8.26). The deposition rate started to plateau until the first flame treatment at layer 20, which revives the surface potential and deposition rate. This was repeated again with flame treatment just prior to layer 30 and 40.

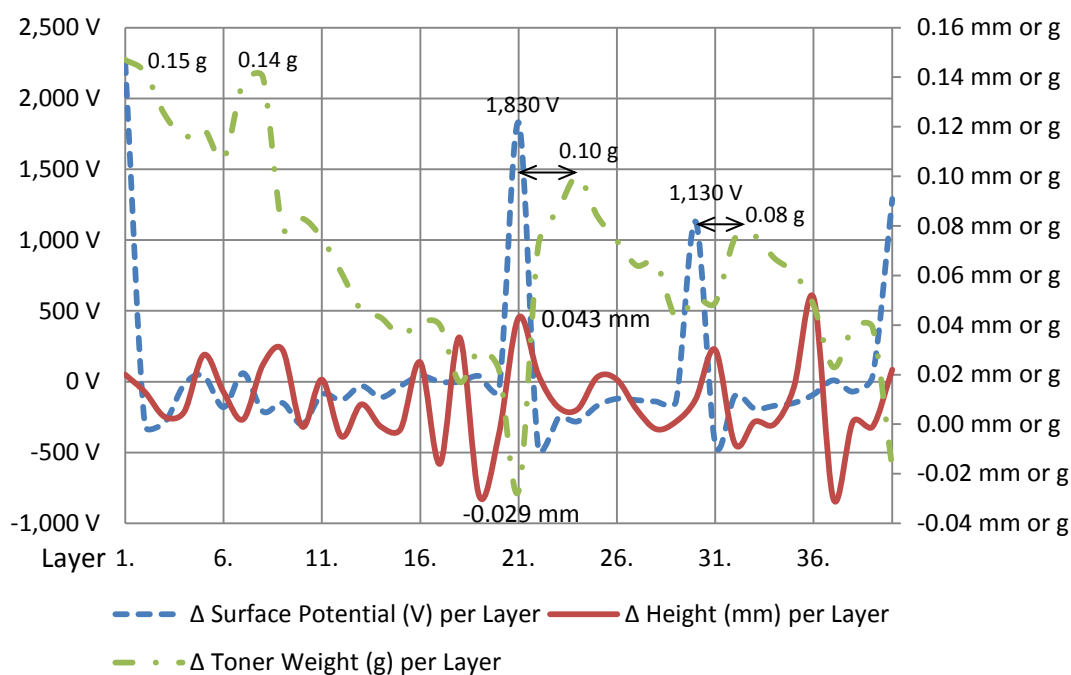
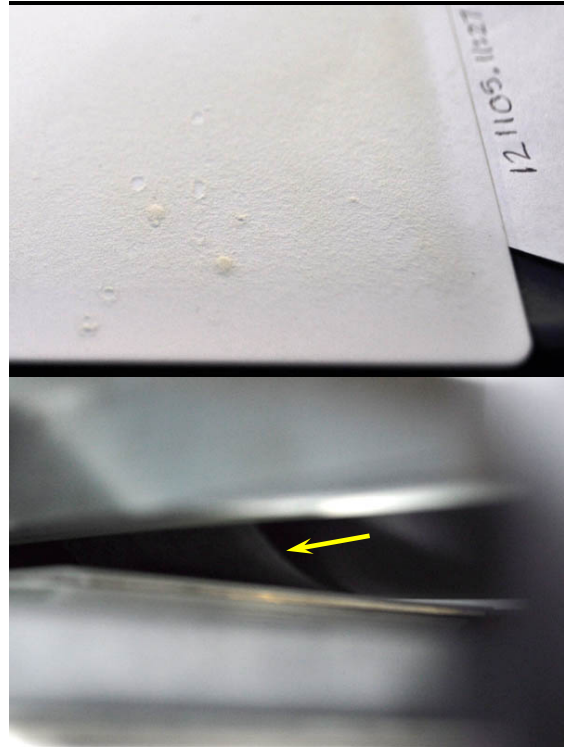


Figure 8.27 – Differential plot of the graph in Figure 8.26 showing the change in (Δ) surface potential, height, and weight effected by each layer deposited

The differential plot in Figure 8.27 shows the influence of flame neutralization on the surface potential and the toner deposition rate. Although the treatment is useful to revive both, each “recovery” peak of the deposition weight per layer is diminished in magnitude, possibly due to the reduced field strength. Unfortunately this sample only had 40 layers, therefore it was not possible to see the effect on deposition rate

of the surface potential recovery at layer 40 (which was stronger than at layer 30). *This is clear evidence that after 10 layers the repulsive effect of the accumulated (unfused) toner layers is limiting transfer efficiency.* Interestingly, the deposition rate did not achieve peak recovery immediately after the flame treatment, but was deferred a few layers (as indicated with horizontal double-headed arrows in Figure 8.27). This may be explained by the unfused (and unfixed) state of the toner, which after neutralization was not being held in place electrostatically and therefore was leaving the sample based on evidence presented in Table 8.18.

Table 8.18 – Evidence of Toner Leaving 40-layer Sample 8-22

<i>Results:</i>	<i>Discussion:</i>
	<p>Snowballing – After flame neutralization, toner behaviour called “snowballing” was observed on toner layers. It is proposed that by removing the toner charge, the particles then agglomerated into miniature balls which were displaced from their position on the sample as shown at left. It is also proposed that Figure 8.24 left is a severe manifestation of the same.</p> <p>Back transfer – Examination of the back side of the transfer roller during printing was not clean (black) as it should have been. Toner was visible along the entire width of the rectangular print pattern (yellow arrow) which was intended for the substrate, but was continuing on the transfer roller (to the waste bin). This was compelling evidence of back transfer.</p>
<p><i>Figure 8.28 – Evidence of toner leaving the 40-layer Sample 8-22 by snowballing (above) and back transfer (below)</i></p>	

The virtually constant occurrence of the above behaviours explains the reason why there was no increase to net weight for samples which were neutralized layerwise (without fusing) after the first 5 layers (Figure 8.25).

Sample 8-23 Pseudo-Piezoelectric Behaviour of Toner

The unfused 40 layer toner stack created in Sample 8-22 was used further to explore if the density of the stack was affected by the presence or absence of a transfer field. The sample was positioned underneath the laser height measurement device and the transfer voltage (3,000V) was switched on for 2min and then off for 2min for four cycles as shown in Figure 8.29. The height measurement was recorded just prior to each change to the transfer voltage.

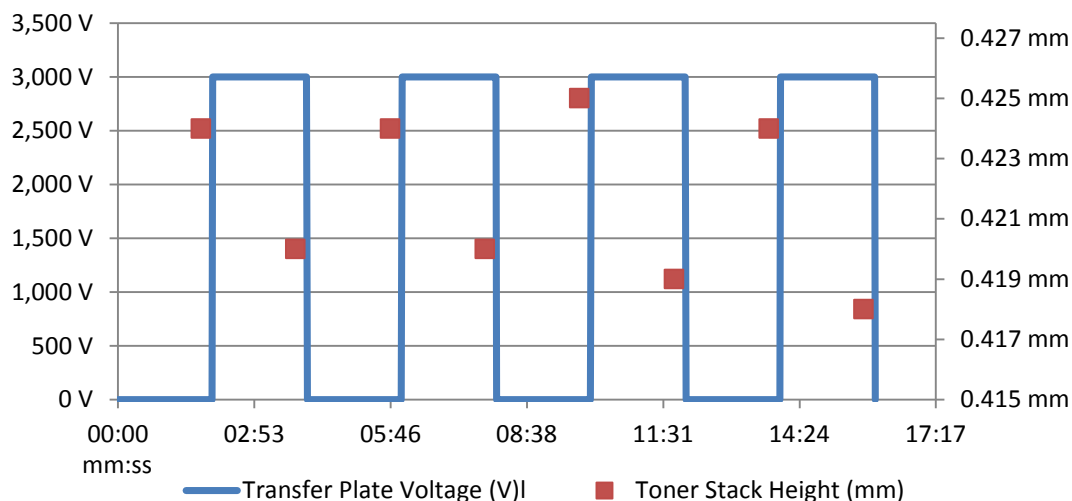


Figure 8.29 – Height of unfused 40-layer toner stack measured with and without 3,000V on the charge plate over time

Sample 8-23 oscillated in height an average of $4.8 \pm 0.3\mu\text{m}$, contracting to an average of $419 \pm 0.8\mu\text{m}$ when the field was on and growing to an average of $424 \pm 0.4\mu\text{m}$ with the transfer plate voltage switched off. This pseudo-piezoelectric behaviour confirms the potential for a field to increase the density of the build stack (especially in the presence of a counter electrode such as the transfer roller). This behaviour in unfused toner is an indicator that similar behaviour would be possible in a consolidated multilayer sample with residual charge, as is acknowledged by the literature about electrets [76, 192, 349].

8.2.3. Discussion of Neutralization Approaches

Although the trials in this chapter have each been discussed individually, several overarching themes deserve mentioning here.

First, the reduction of surface area due to fusing makes charge neutralization challenging, especially since large proportions of charge are immediately embedded into the underlying build surface (due to the transfixing/transfusing design of the SLP rig) making them difficult to access by non-penetrating neutralization methods.

The architecture of the printers makes fully penetrating neutralization methods difficult to implement in-process without causing undue risk to the printers. This obliges use of neutralization methods which effect change on the outer surfaces, but in each of these trials the surface potential (or at least the field mill) was affected by the passage of time and change of sample surface temperature. It is supposed that the

surface neutralization methods have enabled attraction of enough charge to achieve a net charge balance on the body (or at least a localized net zero charge at the surface, based on Sample 8-6), but no serious endeavour has been made to understand the interaction between the intralayer and interlayer charge recombination with the surface potential. It is suspected that this interaction of volume and surface charges accounts for variations in surface potential with time and temperature, and deserves further investigation. Although significant progress in understanding toner-to-toner interactions before fusing has been made in the last decade (§3.3.1.2, §3.4.4), this could expand to embrace a fused multilayer image-on-image context including implications arising due to the presence of substantial residual toner charge.

Although the influence of pressure uniformity is not core to this study, the ridges and valleys arising on the later repetitions of Sample 8-21 prompted some preliminary trials as reported in Appendix B. The outcome of those trials was that pressure uniformity had a large influence on layer quality when electrostatic conditions in the transfer nip were unfavourable and was far less important when electrostatic conditions were favourable. These trials contributed to the improvements made to the SLP rig in its Stage 3 format (§5.7.3).

8.2.4. Summary and Conclusions

The evidence provided by the samples in this subsection clearly shows that residual toner charge is a contributor to defects in 3D laser printed objects made in thermosetting epoxy toner materials (and all materials

tested in this work). It is necessary to neutralize residual toner charge to avoid defect formation when stacking more than 8-29 layers image-on-image (depending on the resistivity of the toner material).

It also shows that charge neutralization actually contributes to unfavourable electrostatic conditions for many transfer approaches which stunts height growth and promotes defect formation. Although several effective neutralization methods have been demonstrated in this chapter, AM by EP cannot be achieved with neutralization alone. Therefore the focus of §9 will be to simultaneously address the neutralization of residual toner charge and maintain electrostatically favourable conditions at the build surface in the transfer nip. The understanding derived from the experimental work up to this point formed the basis for patent application GB1109045.3 and subsequent PCT application [339].

9. Assimilating Charge Neutralization and Electrostatic Transfer

Chapter 8 successfully demonstrated residual toner charge neutralization, however neutralized toner alone did not unlock the potential for unlimited defect-free builds (§8). This chapter is dedicated to simultaneously achieving electrostatically favourable transfer and simultaneously eradicating residual toner charge from the consolidated body.

The Stage 3 SLP rig (§5.7.3) with epoxy toner was used in the experiments undertaken in this chapter unless otherwise noted. The same ceramic build substrate material was used (§5.5), only it was cut into a circular shape and for some trials it was painted with grey or black paint to give improved contrast. Holding down the ceramic substrates with tape was avoided entirely to improve charge measurement (Sample 8-14, §5.7.1.3.1). The OPC was replaced due to wear induced fatigue during the preliminary trials (Sample 9-1). About two-thirds of the sample production and analysis reported in this chapter was undertaken by Rupesh Chudasama under the direction of (and sometimes executed jointly with) the author. This provided Chudasama an opportunity to collect nip pressure data (from the sensors installed in the Stage 3 platform) for his research and gain familiarity with operating the SLP rig.

9.1. Conventional Electrostatic Transfer to 0V

Building on the understanding that residual toner charge neutralization in Sample 8-22 was undermining electrostatic toner transfer, a way of electrostatically transferring to 0V (ground) was sought. In that way, after printing, the deposited toner could be neutralized (before or after fusing) without unfavourably affecting the surface potential and compromising the transfer quality of additional layers.

The first transfer method considered was conventional electrostatic transfer, due to its maturity and consistency. It was envisaged that conventional electrostatic transfer to 0V could simultaneously achieve a highly reliable transfer and also be amenable to layerwise neutralization. In preparation for these trials, the voltages in the printers were shifted to be 900V more negative as explained in §5.7.3.1.

Sample 9-1 Print onto Grounded Conductive Substrate

Preliminary printing onto conductive Al substrates was undertaken to demonstrate the viability of the shifted voltage printing with satisfactory results. Early printing also enabled the alignment of the platform (now mounted on an adjustable gimbal) to the final transfer roller and timing adjustments for synchronising the print with the new platform position. It was found that leaving the platform 5mm above the surrounding flange improved transfer (it appeared that the transfer roller was grounding out on the surrounding conductive flange when the platform was left flush with the flange). One unexpected outcome of the new build sleeve and platform was that the magnitude of the field mill measurements was

reduced (probably due to the reduced area of the print and also because of all the grounded conductive metal in the vicinity). Printing onto non-conductive substrates was undertaken next.

Sample 9-2 Print onto Non-conductive Substrate (Near Ground)

Sample 9-2 is representative of the 10-layer samples (set of 5) which were printed onto the ceramic substrate held in the shallow recess on the new build platform with shifted voltages (Table 5.3) and layerwise flame neutralization. The ambient conditions during production of Sample 9-2 were 17.1°C and <20% RH. Variation in density was observed in the printed layers which was consistent in all five samples produced, as shown in Table 9.1.

Table 9.1 – Sample 9-2 Results and Discussion

<i>Results:</i>	<i>Discussion:</i>
	<p>Distinct circular areas of virtually no toner deposition appeared in all of the layers deposited on each sample.</p> <p>Inspection revealed that the areas of non-deposition correlated with the location of the counter bores in the underlying platform. This indicates that the conductive grounded platform was affecting (improving) the toner deposition at the build surface above it. The absence of deposition above the counter bores suggests that a non-conductive surface (at 0V), may not be able to attract toner electrostatically, even from a higher potential.</p>

Figure 9.1 – Sample 9-2 showing areas of non-deposition (above), which correlated to counter bores in the underlying platform (below)

The correlation of low density deposition with the counter bores provided strong evidence that the toner deposition was substantially improved by proximity to ground. In order to assess how effective transfer (with shifted voltages) would be with minimal influence from ground, a non-conductive spacer (machined from laminated resin board, Tufnol, UK) was made to move the substrate 13.5mm further away from the grounded platform (Figure 9.2).



Figure 9.2 – Non-conductive spacer which lifted the ceramic substrate 13.5mm above the grounded platform.

Sample 9-3 Print onto Non-conductive Substrate (Away from Ground)

A set of samples was produced as for Sample 9-2, except that the sample substrate was placed on top of the spacer. The results are presented and discussed in Table 9.2.

Table 9.2 – Sample 9-3 Results and Discussion

<i>Results:</i>	<i>Discussion:</i>
	<p>Deposition on Sample 9-3 was of poor density (only visible as the darker area on the upper half of the sample shown at left) and very sensitive to uniform pressure in the nip (see further agreement with pressure sensitivity in Appendix B).</p> <p>The reduction in toner deposition density is obvious when compared with Sample 9-2.</p>
<p><i>Figure 9.3 – Sample 9-3 showing reduced deposition (above) and compared to Sample 9-2 (below)</i></p>	

The results from Sample 9-3 indicate that transferring onto a non-conductive substrate, even when it is fully neutralized (0V) is not effective unless it is within close enough proximity (typically a few mm) to a ground plane in order to develop critical transfer field strength at the build surface.

Sample 9-4 Transfer Corona Near and Away from Ground

In order to assess if transfer corona (+5,700V) would improve the deposition, four sets of five samples were made and weighed. One set as for Sample 9-2, the next prepared in the same way except adding transfer corona. The last two sets were prepared as for Sample 9-3, except one of them was made with transfer corona. The results are presented in Figure 9.4 and Figure 9.5 and discussed thereafter.

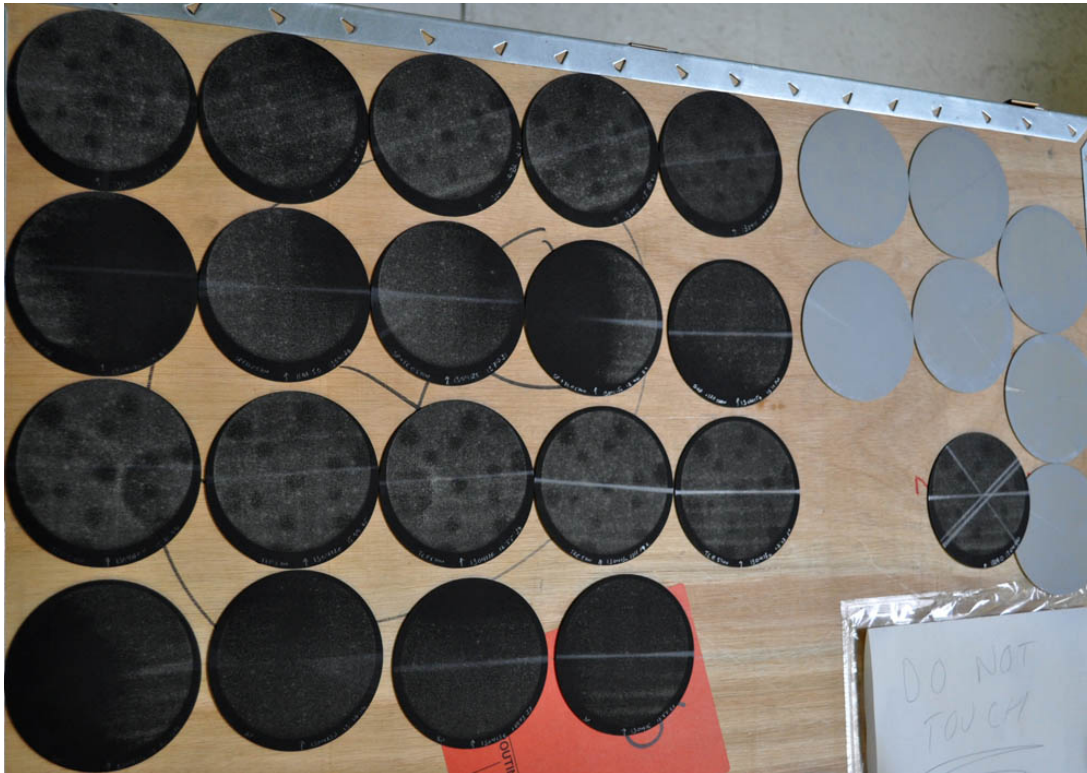


Figure 9.4 – Sample 9-4 sets laid out in rows

The sample sets appeared very similar to their respective forbearers and any visual differences from the use of transfer corona were subtle.

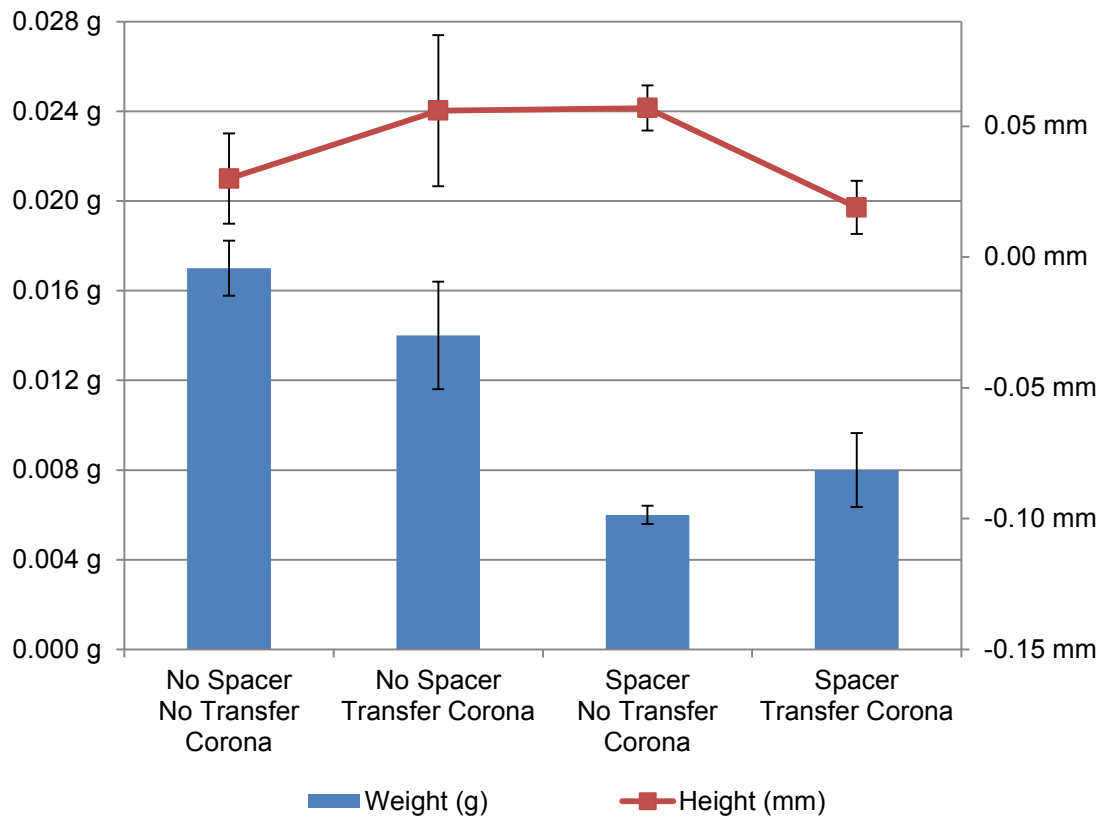


Figure 9.5 – Weight and height of sets in Sample 9-4

The result of adding transfer corona actually reduced deposition weight when the sample was produced near to the grounded platform, but improved deposition weight when on the spacer. The sample height appears to have behaved in an analogous way to Sample 8-22, where transfer corona increased the height near to ground (probably providing a neutralizing effect and thus reducing the force of the field between the transfer roller and the grounded platform on the toner) and reduced it for the sample made on the spacer (possibly providing some electrostatic fixing force in the absence of a transfer field).

9.1.1. Discussion of Printing to “Ground”

The results from the trials in §9.1 indicate that ground is not merely a location of 0V potential. Had that been the case, then the flame neutralized non-conductive substrates would have been able to electrostatically attract toner uniformly irrespective of their distance from a conductive ground plane. Instead, the ceramic substrates acted like an isolated island of floating potential with limited ability to exert influence on the toner electrostatically.

The data suggests that a conductive grounded plate actually serves as a behemoth sump which constantly accepts, donates, and homogenizes charge. It is required to serve as a counter electrode to the transfer roller in order to generate an electric transfer field for conventional transfer. Its proximity within a few mm also appears to be needed in order to attract a high density of ions onto the upper surface of a non-conductive material for highly effective top charging (as also shown by Sample 7-27).

The inability of a neutralized non-conductive substrate to electrostatically attract dense toner layers was prefigured by Sample 7-12 (see discussion in §8.1.1), but it was only apparent with corroborating results (Figure 9.5) and hindsight.

These results have largely come full circle since §4.6, highlighting limitations of the electrostatic transfer methods attempted, and

highlighting the possibility that tackification (or other non-electrostatic transfer methods) may still hold promise. However, there is at least one remaining electrostatic transfer method which deserves reconsidering, which comprises the next section of this chapter.

9.2. Feasibility of Repulsion with Neutralization

The inability of a neutralized non-conductive substrate to electrostatically pull toner onto it prompted re-evaluation of the proposed repulsion transfer technique (§4.3.3) with some improvements. Theoretically combining residual toner neutralization with repulsion would provide a transfer method capable of stacking defect-free layers indefinitely. The full exploration of this possibility would require substantial changes to the SLP rig (which is out of scope for this work); therefore this subsection only undertakes preliminary feasibility trials.

Since the shifted voltages did not result in electrostatic transfer onto non-conductive layers, the printers were changed back to their original wiring and voltages as used in the Stage 2 SLP rig (Table 5.2) for these trials.

Sample 9-5 Defects from Touching the Underside of the Substrate

During the production of the latter repetitions of Sample 8-22 some defects developed while handling the samples to get them to the scales. Initial attempts to remove the substrates from the charge plate caused

disturbances to the toner layers, therefore the toner deposited onto the ceramic substrate and charge plate were subsequently removed as one unit and carried back and forth to the scale between print cycles. Despite the care used, occasionally defects in the form of a flower or fan pattern (indicated with dashed line in Figure 9.6) developed as a result of handling. Observation revealed that these defects occurred when a finger contacted the underside of the charge plate and toner was repelled away from it. Further patterns were “drawn” using a finger to confirm causation of the disturbances.

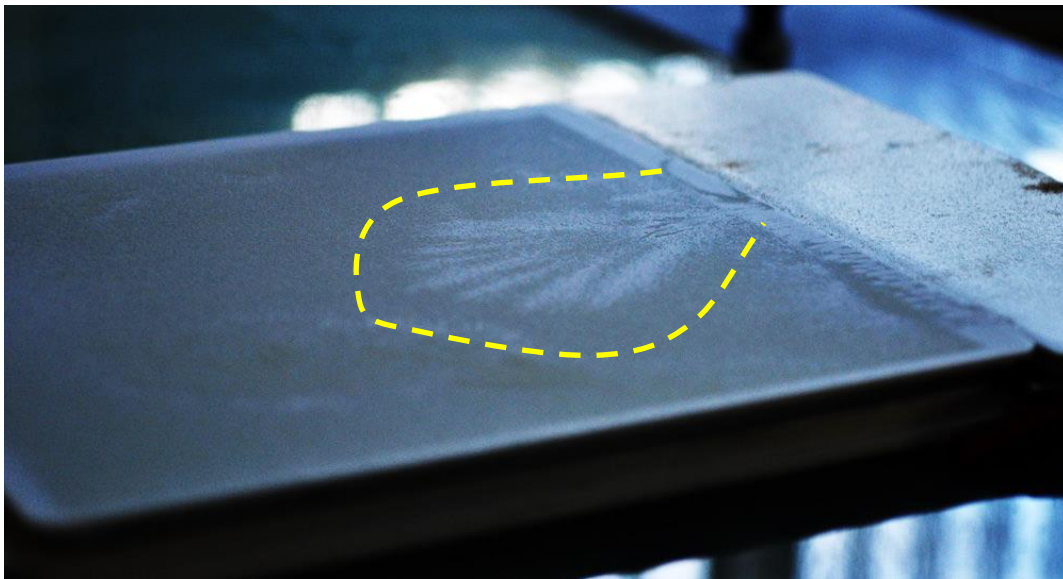


Figure 9.6 – Defect in a flower or fan pattern which was caused by a finger contacting the underside of the substrate-charge plate pair

Sample 9-6 Intentionally Repelling Toner Off the Substrate

Following Sample 9-5, several samples were printed, the charge plate removed (which disturbed some toner), and intentional finger contact was made with the bottom of the substrate to observe if the toner would jump off as with Sample 9-5. The results are shown in Figure 9.7.

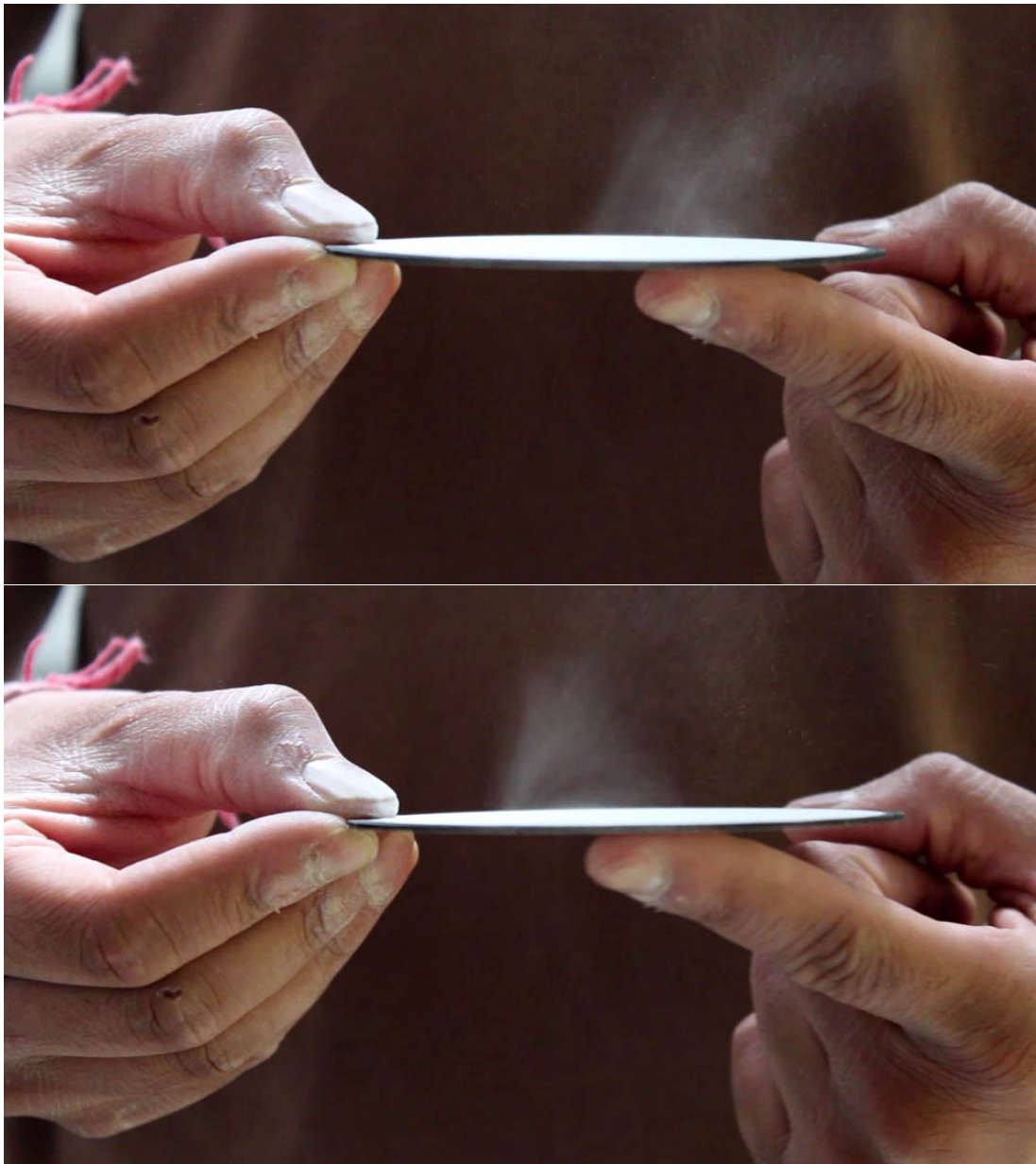


Figure 9.7 – Sample 9-6 showing toner intentionally repelled off of the substrate by a finger contacting the underside of the substrate

The toner was caused to jump as far as several cm (Figure 9.7 top) and was also observed making arcing motions (Figure 9.7 bottom) reminiscent of a solar prominence (or coronal helmet streamer) [350]. This motion was presumably initiated by the charge on the finger. The magnitude of the toner motion provided evidence that repulsion can have

the strength to overcome the electrodynamic force holding toner to the substrate.

Sample 9-7 Repulsion with and without a Counter Electrode

The preceding samples prompted a desire to examine the effect of a repelling field at a microscopic level. Therefore it was planned that if a charge plate could be used for conventional electrostatic transfer, it could also be used to demonstrate the principle of repulsion. Therefore in order to affect a repulsion transfer with the Stage 3 platform/build sleeve, a PTFE spacer was made which also incorporated a charge plate. The charge plate was isolated from the platform and connected to a high voltage supply (Model 477-304, Brandenburg, UK). One and two layer samples were produced using settings as per Table 5.2 (without the 2nd printer corona) and including a conventional electrostatic transfer (using the charge plate = +3,000V) to maximise the thickness of the toner layers. After the layer(s) was deposited, the polarity of the voltage on the charge plate was turned off for a few seconds (this was required to swap output polarity) and then reversed to -3,000V in order to repel the toner (which was tribocharged negatively). The result on the edge of the cylindrical ceramic substrate (painted black) was observed at 20x magnification using a digital microscope (VMS-001, Veho, UK) with plastic housing (to avoid affecting the experiment electrostatically) and is shown in Figure 9.8 (Note: these images are different and inspection near the red arrows reveals toner removal that was obvious when seen as a dynamic event).

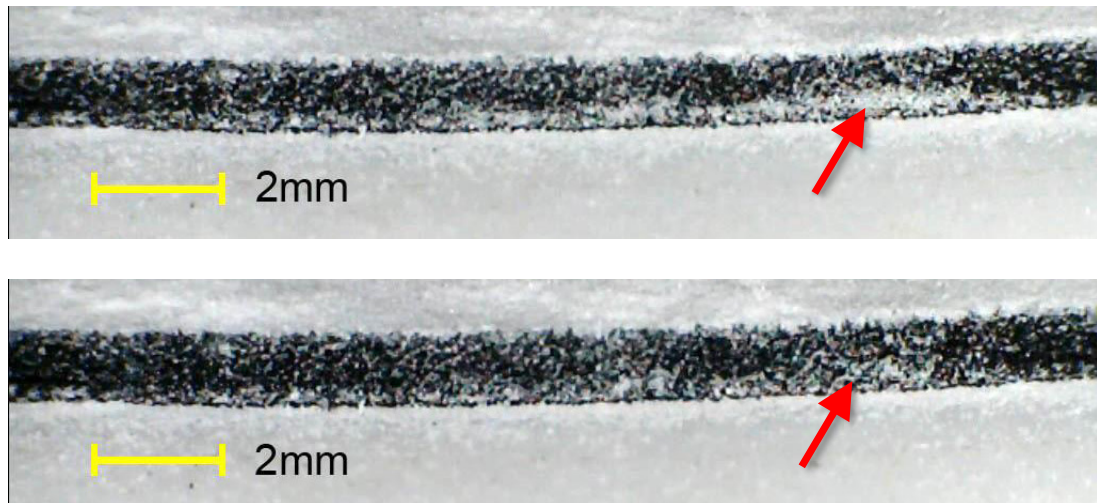


Figure 9.8 – Sample 9-7 showing the edge of a sample substrate (painted black) as printed with white epoxy toner (above) and the same edge after toner has been repelled off (see area by arrows) by using the charge plate at $-3,000V$ without a counter electrode

The reduction of toner on this sample was most obvious at the edges of the sample (probably because they are just above the edges of the underlying charge plate). Without a counter electrode this result is to be expected since the fringing fields probably provided the most influence on the toner, similar to historic performance of cascade or other non-electroded development methods (§3.4.3.1).

Producing more samples and reversing the polarity of the charge plate in the presence of a grounded socket head cap screw (used as a counter electrode to the charge plate) produced toner movement in the large solid area of development as well as at the edges as shown by the toner accumulation on the screw in Figure 9.9.

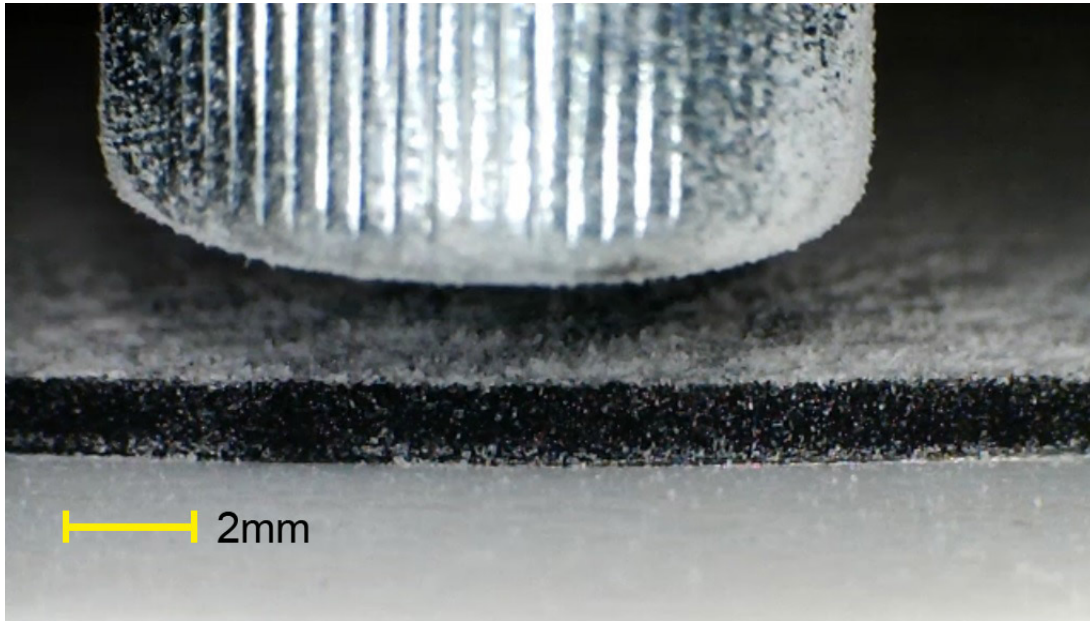


Figure 9.9 – Sample 9-7 shown with the underlying charge plate at -3,000V causing toner to collect on a grounded socket head cap screw (acting as the counter electrode)

9.2.1. Discussion of Repulsion Feasibility

The samples in §9.2 provided preliminary indicators that toner can be repelled off of substrates using the same polarity of charge, with or without a counter electrode. Only a small proportion of the printed toner on these examples was repelled off, which may indicate that the efficiency of repulsion needs substantial improvement to become a practical transfer method. As yet, no attempt has been made to calculate whether the majority of the toner population has high enough charge to be repelled using a field which does not instigate air breakdown, however this is advisable for future work. Furthermore, pursuit of this approach would necessitate re-investigation of issues including solid-area development (or in this case solid-area repulsion) and significant adaptations made to the printing hardware.

The results in this chapter indicate that electrostatic approaches such as conventional or top charging transfer cannot be efficiently undertaken when distanced more than a few mm from a ground plane. These results confirm preliminary feasibility that repulsion transfer combined with residual charge neutralization may provide a more robust and elegant development method than tackification alone.

10. Conclusions and Further Work

A recent UK government sponsored study highlighted imminent and industrially relevant needs for AM, including improved process speed, lower system and material costs, a wider selection of polymer materials, and improved mechanical properties of AM processable polymers [351]. Fully leveraging the speed, economies of scale, and materials of 2D digital printing technologies in 3D printing is one strategy for fulfilling those needs [20]. Digital printing techniques also have the potential to answer the growing aspiration for printed functionality, which can require the simultaneous deposition of multiple materials with volume scalability (§2.4-2.5). The aim of this work was to investigate the viability of using laser printing, one of the most mature 2D printing techniques, for 3D printing and AM to meet those needs. In depth analysis of the stacking and consolidating of laser printed toner layers as presented herein revealed substantial untapped potential and commensurate technical challenges.

This thesis records the largest body of experimental work concerning the use of laser printing to directly build multilayer objects above the microscale since the work of Dr. Ashok V. Kumar et al. of the University of Florida, conducted from the late 1990's until approximately one decade ago (§4.3.1.1, §4.3.2.1).

Kumar's research activities were suspended because the maximum height of defect-free printed objects achieved by stacking and laminating laser printed toner layers did not exceed a couple of millimetres [270]. The reason for the height limitation was retrospectively surmised to be charge build up which undermines the final transfer step; however no supporting empirical evidence was forthcoming [181]. After arriving at a similar hypothesis independently, this work provides compelling quantitative empirical and theoretical evidence to confirm that the stacking of conventionally laser printed and fused toner layers inherently results in accumulation of like toner charge until it becomes disabling for 3D applications. Historically the presence and role of residual toner charge in consolidated multilayer printed toner bodies have been drastically underestimated (Figure 8.10, §7.2.1). This work led to a new proposed model to identify the behaviour and effects of residual toner charge, as presented in Figure 8.11. When left unmanaged, residual charge accumulation undermines both explicitly electrostatic transfer methods (§4.3, §7.2) and so called 'non-electrostatic' transfer methods (§4.4), which have been demonstrated to be implicitly electrostatic (§7.1). This can be explained by the accumulating residual toner charge counteracting the transfer field. This often results in critically diminished transfer field strength which can no longer attract fresh incoming toner. In severe cases it actually reverses the polarity of the transfer field as shown in Figure 7.18 and Figure 7.19, and ultimately repels fresh incoming toner layers. Thus reduction in transfer field strength below a critical level allows defects to develop and arrests height growth. This

knowledge sets the stage for overcoming the height limitation of the SLP process which was the first core objective of this work.

The understanding that unmanaged residual toner charge is a primary cause of surface/layer defects has enabled substantial progress toward disambiguating and understanding the root causes of a spectrum of defects arising in parts produced by the SLP process (as summarized in Table 7.34). Identifying the primary defect causes has been a gateway for answering early research questions raised in §4.7 and §6.1.6 and fulfils the second core objectives of this research (§1.2).

Analysis of legacy SLP samples in the early stages of this PhD confirmed indications that laser printing has the potential to directly print microscale thermoplastic powder into consolidated macroscale laminated objects with mechanical properties on the order of injection moulding; in line with the third core objective of this work [235, 260].

In the final analysis, it is asserted that in time, and with sufficient resources (which will doubtless come in step with market growth), the technical challenges which currently inhibit the use of laser printing and EP-derived approaches in macroscale 3D applications will be overcome, thus achieving the final objective of this work. This will enable the definitive establishment of EP in its own niche in the 3D digital fabrication landscape, co-existing with inkjet (and other complimentary digital deposition technologies) by merit of its superior volume scalability and inherent technical advantages (§3.5).

10.1. Summary of Novelty

By comparison with the state of prior art available in the public record (as reviewed in §4.6 and §3.5), this work encompasses a number of novel trials, steps, and approaches as follows.

Firstly, the majority of the experimental work in this PhD was undertaken using the SLP development rig – the only operational AM device/system which uses “flat bed” two-component laser printers for depositing build and support materials known worldwide, as described in §5.7. This provided the opportunity and motivation to make the first in-depth analysis of a selection of the earliest SLP produced parts (§6.1), as well as the first measurements of residual toner charge imbalance in multilayer EP printing (§7.1.2 onward).

In order to empirically confirm the presence of residual toner charge, intentional retention of net charge imbalance in coalesced tribocharged particles was demonstrated for the first time (§8.1). This achievement provided the basis for demonstrating the first feasible method for digitally patterning the charge density in electrets (in all three dimensions) (§8.1.2). These activities together with corresponding neutralization strategies constituted the first holistic intentional management of residual toner charge (§7-8) in functional and 3D printing.

Evidence of residual toner charge prompted re-evaluation of prior modelling assumptions by Kumar. Thus, the first mathematical modelling of consolidated toner assuming a non-zero residual charge is presented herein (§7.2.1).

In order to reduce and eliminate defects, a host of never-before-tried variations on transfer methods were attempted, and their effectiveness was evaluated (§5.7, §7.2, §7.3, §8.2, §9.1, §9.2).

In confirmation of suspected layer thickness variation, Sample 7-12 from this work yielded the first definitive empirical evidence that layer thickness diminishes with increasing height of layer stack for electrostatic transfer methods (as expected) and for tackification transfer approaches where residual toner charge is present and unmanaged (reinforcing the counterproductive effect that residual toner charge has on building up layers).

The need to simultaneously address residual toner charge neutralization and electrostatically favourable transfer was publically acknowledged and attempted for the first time (§9).

This was the first time that pure ceramic was printed by a single component developer-based printer and sintered thereafter (§6.4.2.2).

The SLP rig first introduced non-contact heating for AM by EP. This work revealed that the implementation of this fusing method enabled early

identification of defects which were masked by other fusing methods (§7.1.3).

10.2. Summary of the Contribution to Knowledge:

The result of novelty is new knowledge. This sub-section summarizes some of the new knowledge which corresponded with the novelty embraced by this study.

Perhaps most important was the discovery and substantiation that residual toner charge is not eliminated by fusing, but is resident in the consolidated toner body until it leaks out at a charge decay rate dependent on depth of charge trapping and the volume resistivity of the toner material (§7-9), possibly in conjunction with other factors. Furthermore, it has been demonstrated that the residual charge attains sufficient strength not only to impede electrostatic transfer methods (as is logical), but also to undermine heat and pressure transfers by effecting a repulsive force on incoming toner (§7). This knowledge has been summarized graphically to show the legacy understanding of and a newly proposed improved conceptual model describing how residual charge (due to non-uniform toner charging in a field) is distributed within a printed 3D body (§8.1.3).

The foregoing knowledge has been obtained through the development and use of three methodologies for evaluating the influence of residual

toner charge in image stacks. First, analysis of surface roughness was used as a proxy for charge retention (§7.2). Second, the surface potential can be estimated by measuring the field it generates via a field mill device (§7.1.2). Third, the surface potential can be measured directly by using a non-contact (high impedance) electrostatic voltmeter (Sample 8-14).

With methodologies for measuring residual toner charge it was possible to assess the effectiveness of methods for actively managing and neutralizing charge as reported in §7-9.

The major defects arising in parts made by the SLP process have been characterized and their causes identified (Table 7.34, Table 8.18, Table 8.16, Figure 9.6), including disambiguation of the effects of residual toner charge, depleted transfer field strength and non-uniform pressure in the transfer nip.

It is noteworthy that, much of the foregoing knowledge has already been disseminated via the research outputs listed in the front matter.

10.3. Future Work

The outcomes of this research provide optimism for the future of EP in digital fabrication which provides an impetus for future work in the following recommended areas:

Simulation and Modelling

This work establishes the need to modify the assumptions and improve modelling methods of toner in order to anticipate and understand the implications of stacking toner layers in 3D. The following needs should focus future modelling efforts:

- Modelling of the electrostatics of multilayer toner layer stacking including the accumulation of residual toner charge is needed (following on from §7.2.1). The approach, may be patterned after the approach of Kemp and Whitney (for example see [162, 164, 219]). Alternatively or in addition, the modelling may focus on more visual 3D computer multi-physics modelling and simulations.
 - Key factors for the model should include Coulombic attraction due to the transfer field, electrodynamic (including van der Waals) attraction between layers and repulsive forces arising from residual toner charge. Quantified net forces on the particles would be invaluable in order to compare with and validate against empirical measurements.
 - Additionally, the residual toner charge should be varied as a function of the toner's initial charge, charge decay time (prior to fusing), volume resistivity, shape and surface area change due to fusing, the number and thickness of stacked layers (to account for the repulsive field exerted by the

consolidated underlying toner layers following on from Sample 9-4, etc.).

- Process understanding could be further enhanced by including additional factors in the modelling such as the quantitative effects of pressure in the nip, and non-Coulombic or vdW based adhesion of the material (such as so called “tackification” or “stickiness”).

Process Characterization

A wide variety of transfer conditions have been evaluated herein. The majority of these have primarily been evaluated to assess the influence of residual charge on defects by the use of a field mill. This lays the foundation for improved methodologies for more exhaustive/exact characterization of residual toner charge and in-depth evaluation of the influence of other processing conditions (such as the uniformity of nip pressure) on the quality of parts produced by SLP. Specific suggestions for follow-on process characterization trials include the following:

- Firstly, a statistically significant body of work measuring the surface potential of each layer directly using an improved surface charge measurement device such as a non-contact high impedance electrostatic voltmeter (following on from Sample 8-14) should be undertaken to establish higher confidence in the residual toner charge characterization (which is acknowledged to be an approximation in this work due to the limitations of the field mill device used for the majority of the measurements).
- In parallel with managing the electrostatics of the process, the uniformity of nip pressure, and any defects arising in its absence,

including waviness (as hypothesized by analysing the 60 layer version of Sample 8-21), should be characterized and addressed.

- Further measurements should be made to indicate the likelihood of the migration of charge from the centre of a fused toner body toward the outer surfaces (accounting for changes in surface potential over time) as intimated in §8.2.3 and subsequently hypothesized in the discussion.
 - Understanding the migration and rate of flow of charge, if any, could inform material engineering to enable a toner which would charge acceptably to be printed (patterned electrostatically), yet be less susceptible of charge retention.
- The effect of temperature (in the fusing range of the polymer) on surface potential/volume charge of consolidated toner layers needs further characterizing (§8.2.3) to assess what contribution, if any, the fusing process contributes to charge relaxation/recombination.
- Further characterization of charge neutralization methods is prerequisite to avoiding charge initiated defects. Methods for consideration should include:
 - Use of high energy particles or waves (ultraviolet, X-rays, gamma rays, etc.) which are capable of penetrating into polymer layers to at least a depth equal to the toner diameter in order to neutralize residual charge trapped at the build surface and the lower “polar cap” area of said toner particles (following on from §8.2).
 - Exploring AC or an alternative through-layer neutralization methods applied to layers on an intermediate transfer

member prior to its lamination onto the build (following on from Sample 8-10) may also yield a practical means of managing residual toner charge.

- A prime transfer method candidate from the author's perspective would be a tackification transfer including a repulsion transfer "assist" to help detach the toner from the imaging members in the printer together with layerwise neutralization (following on from trials in §9.2), in order to prevent residual toner charge from instigating defects in layers.

Materials Development

The modification of toner properties (including volume resistivity) by refinement of toner formulation represents a largely unexploited opportunity (which was deprioritized after §6.4 in order to focus on understanding the cause of defect formation) to overcome the residual charge impediment to stacking defect-free layers indefinitely.

- Materials which are not as conductive as metals, but which are electrostatically dissipating (such as polymer materials filled with carbon nano tubes) may avoid the problems of trying to transfer conductive particles (§3.4.4.3) while evading the transfer limitations of nonconductive materials (§4, §6-9).
- Conversely, intentional charge trapping (following on from §8.1.2) could reveal further understanding to enable unlimited defect-free toner transfer, and also advance the production of digitally printed electrets outright.

- Characterizing the density and duration of stored charge should be studied and correlated to the material properties and SLP processing conditions in order to enable applications for both retention and dissipation of charge.
- Compatible combinations of build and support materials (which can be consolidated in close proximity into the same part) need to be prioritized in future work.

Hardware

The SLP rig has provided a means to develop crucial understanding of the process parameters needed for effective multilayer toner printing; however, in due course its shortcomings will need to be rectified to ensure reliability and repeatability of the process and its outputs. The next major hardware revision may consider the following:

- Assess, and if needed, improve the quality of the final transfer rollers to ensure uniform pressure in the nip (See Appendix B).
- Assess the rigidity of the latest platform improvements (§5.7.3) and the angle of its contact with the final transfer rollers.
- Convert one of the printers to be able to print materials which naturally tribocharge with a strong positive polarity. This will expand the pool of potential build and support material options.
- Expand the charging capacity and efficiency of the printers to charge materials with a wider spectrum of potential and also to be able to acceptably charge a wider range of materials.
 - This may be achieved by implementing the use of Kodak developer technology with hard ferrite carriers constituting a

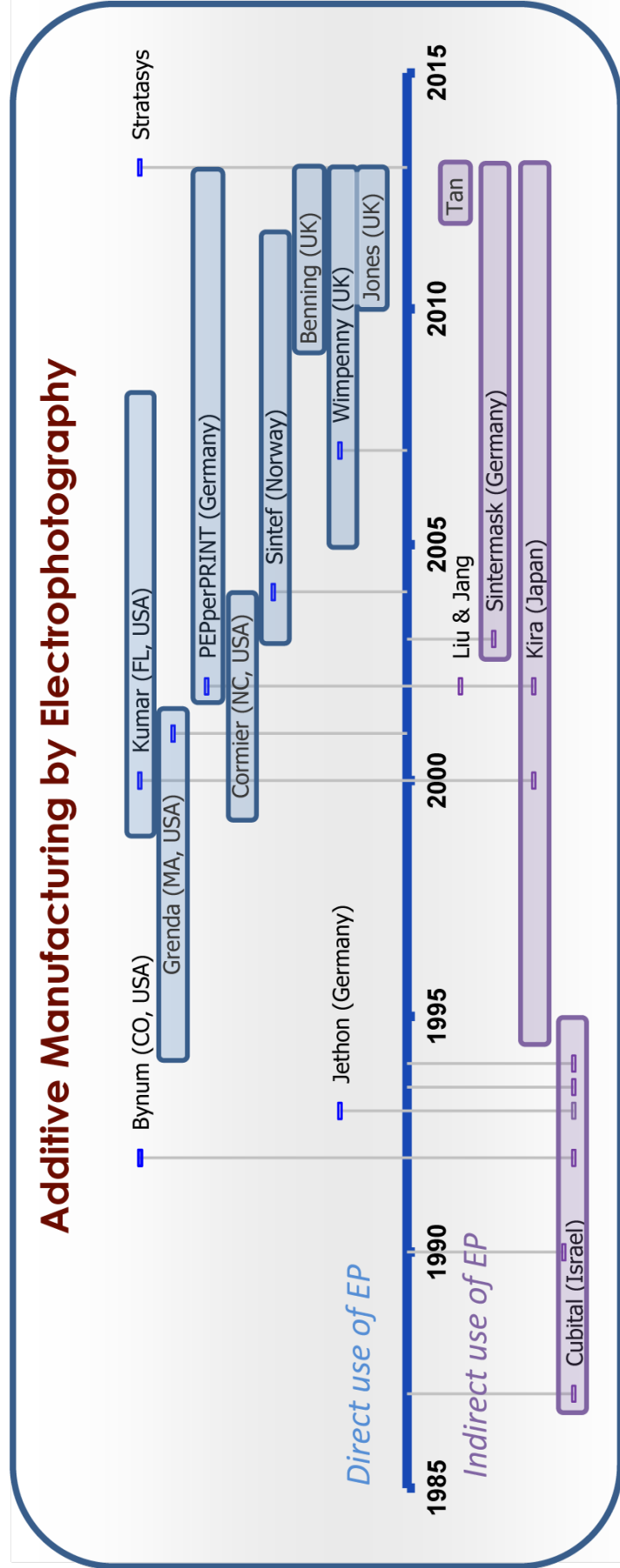
conductive magnetic brush (to improve development density on the photoreceptor, §3.4.3) with independently adjustable rollers.

- It may be advisable to consider the use of more durable photoreceptors such as those made using ceramic or ceramic-like amorphous silica (for their high wear and temperature resistance). This could open the processing window without incurring undo risk for the imaging components.
- If required, an intermediate transfer member may be used to provide top and bottom access to neutralize through the thickness of each layer prior to lamination onto the image stack (in a similar approach to Sample 8-10, but in a layerwise manner).

This concludes the future recommendations. Thank you for your interest in this work.

Appendix A:

Timeline of AM and EP Convergence



Appendix B: Elucidating the Influence of Pressure Uniformity

The nature of the original SLP rig construction made alignment of the platform to the printers difficult (Figure 7.1). Although several improvements have been made over time, non-uniform pressure has plagued many if not most of the samples produced during this research. The recurring pattern of waviness (ridges and valleys) defects in the later repetitions of Sample 8-21 prompted exploration of where these defects originated.

Owing to the waviness (ridge and valley pattern) defects observed on the back side of the transfer roller (Figure 5.18), the question arose as to whether those defects may originate inside the printer. In order to assess that possibility, the printer was stopped at various positions mid-print and the image quality observed and photographed (Figure 10.10).

Since the defects were not present on the OPC or the transfer roller, they must have originated at the transfer nip. One theory for why this would be is that the compliance of the roller may be variable and therefore produce the defects observed. In order to assess any density differences, the transfer roller was CT scanned. Unfortunately the resolution of the

data was not sufficient to detect relatively subtle density variability in the rubber coating of the roller.

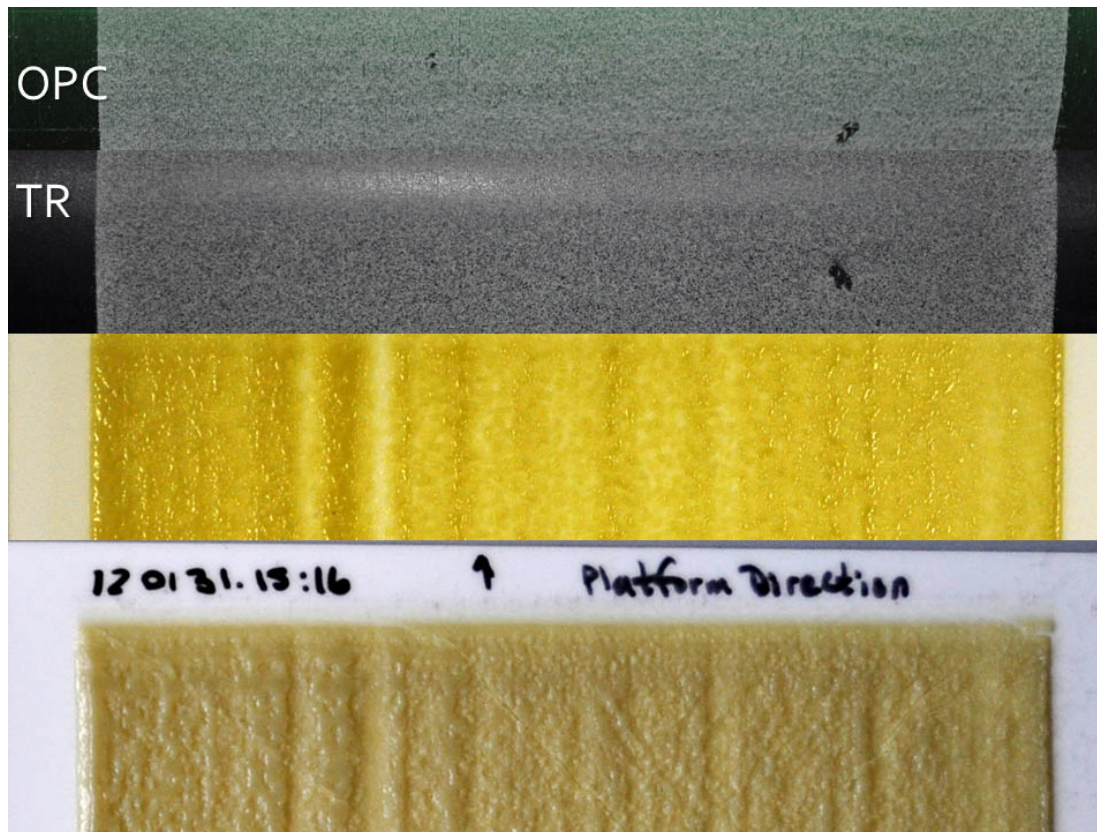


Figure 10.10 – Overlapping photographs showing the same toner image on each imaging member from the OPC to the transfer roller (TR) to two different samples both with the same waviness defect pattern

The fact that these samples started off with high quality surface finishes (Figure 8.20) indicates that any transfer roller aging or defects did not introduce defects early on. This leads to the conclusion that any non-uniformities in the roller density did not introduce defects while the conditions in the nip were electrostatically favourable. As soon as the conditions became marginal, defects started to appear. By the time conditions in the nip were electrostatically unfavourable, substantial defects were manifest.

Since the prospect of using tackification (with layer by layer neutralization) was strong, the nip pressure was further characterized. Renishaw arranged for a site visit by Tekscan where dynamic pressure readings could be made in the nip. The scanner confirmed the suspected low pressure on one side of the sample substrate (Figure 10.11 left) which was corrected by using a shim in order to provide some pressure across the entire width of the substrate (Figure 10.11 centre). Despite the improvements, substantial non-uniformity in the nip was still inherent in this highly dynamic application of pressure (Figure 10.11 right).

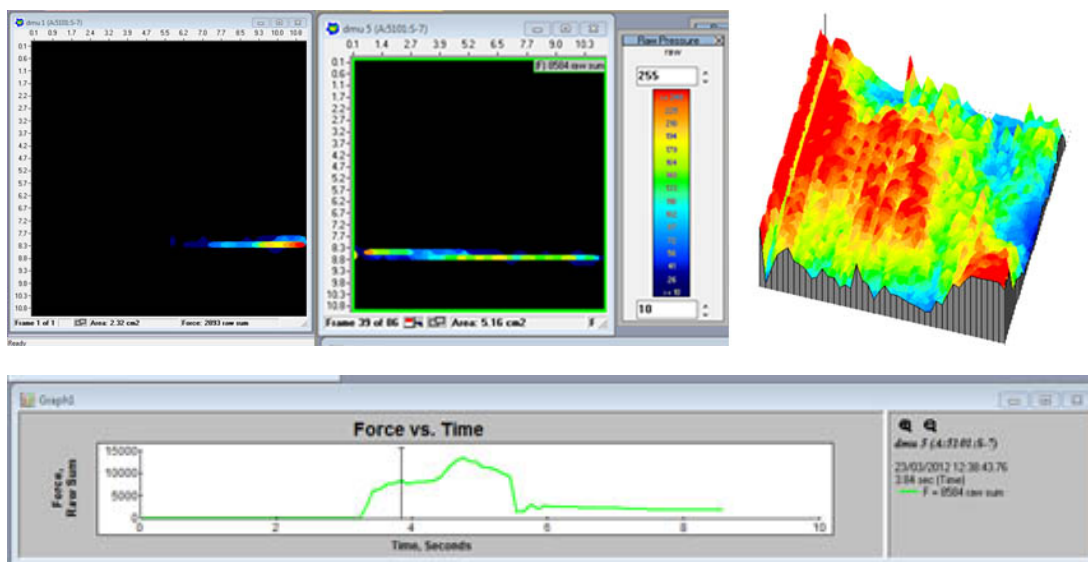


Figure 10.11 – Tekscan pressure sensor readings showing non-uniform pressure (left); improved distribution (middle); a map of entire substrate after improvement (right); and a force vs. time plot (below)

As the platform travelled past the transfer roller, the pressure rose substantially about half way along the travel (Figure 10.11 bottom). This was likely a manifestation of the cantilevered platform (Figure 5.25 left), which deflected easily initially and then became stiffer closer to the supported end.

This preliminary characterization informed and justified the design and fabrication of a new build sleeve and platform with in-process pressure measurement for the Stage 3 SLP rig (§5.7.3).

Appendix C: The Influence of the Heater on Defect Formation

The fact that the seam in the mounting framework of the heating elements was parallel to the waviness defects (Figure 10.12) in Sample 8-21 led to the question of whether the orientation, wavelength, or uniformity of the heaters were affecting the formation of waviness or other defects in the samples.



Figure 10.12 – Image showing the medium wave length heater elements aligned to the waviness defects

In order to assess these concerns both the short wave and medium wave printers were used to produce samples with their elements parallel and perpendicular to the samples (Figure 5.16).

The orientation of the printers was not found to be a significant factor as the defects always ran parallel to the platform motion. Also both wavelengths tested with the epoxy toner were absorbed easily and no difference was observed in the samples.

Some variation in heating uniformity was observed with the elements, therefore the heater was rotated to have its elements parallel to the print direction which reduced the non-uniformity as reported in §5.7.2.2. This however, occasionally caused overheating of the samples which introduced accuracy issues.

Although geometric accuracy has not been a significant feature of the SLP research reported herein, it has not been ignored altogether. In the early stages of printing, pre-heating the substrate (to store heat in it [see §5.7.1.7]) helped homogenize the layer temperature and prevent cooling (and accompanied thermal contraction) between heater passes. As the parts grew, they had the propensity to overheat (unless the heat input was reduced) and lose their geometric definition because of their susceptibility to flow (in a softened state) induced by pressure of the nip. The ambient temperature was also raised by the use of the 12kW heaters to the point that it began to affect the electronics of the laser printers after 35-40 consecutive prints. Early in the SLP rig testing (during the

Custom-fit project, §4.4.5.3), the use of fans was initiated to cool by convection. As a more controllable solution, several means of “quenching” each polymer layer in-process were devised. One of these was to maintain the entire build volume well below the melt temperature and if possible below the glass transition temperature (contrary to current polymer powder bed AM processes which maintain a temperature near to the melting point [352-355]) of the polymer being processed. This cooling was intended to promote early thermal contraction in layers after the thermal input was several layers distant from them. In this way it was hoped that a gradient of heat in the upper areas of the build stack could be controlled and thereby the accuracy of parts could be managed in a similar fashion to how metal AM processes are (where the build volume is maintained well below the build material melt temperature). Unfortunately, a convenient and energy efficient means of maintaining a large difference between the polymer processing temperature and ambient build volume was not forthcoming, so instead an alternative method of contacting each layer with a chilled (water cooled) roller was proposed. In this way the endotherm and exotherm could be controlled layer by layer (including in the centre of the part where heat was most prone to accumulate). Unfortunately the necessity to understand residual toner charge took precedence for resource before this work could be undertaken; therefore as a stop-gap, build surfaces were covered with sacrificial/support material to prevent overexposure and overheating. These innovations are included here in the hope that they may provide utility or inspiration for future work.

Appendix D: Two Interesting Facts

About Electrophotography

Here are a couple of points which did not fit into the body of the thesis for consideration:

- When paper jammed in Xerox's 914 it was very susceptible to catching on fire from the 350°F (177°C) supplied by the fuser to melt the toner. Furthermore, anyone attempting to put out the fire with a water-based fire extinguisher was likely to get electrocuted from the high voltage power supplies; therefore it was deemed necessary for every machine to be supplied with a CO₂ fire extinguisher. Don Clarke, the product manager, protested that he could not sell a product so likely to cause a fire that it required a "fire extinguisher built right into it!" A compromise was then offered in which the fire extinguisher was renamed a 'scorch eliminator.' Thereafter, every 914 was supplied complete with a scorch eliminator installed as standard [41].
- One very dry winter those who would be standing by the early copy machines to pick up printed stacks of paper would be shocked by ~10cm (4-inch) long sparks. Understandably this did not find favour with the workers [39]. This fact attests to the ability of printed toner on paper to store a large amount of charge.

Appendix E: 3D Photocopying

Poster

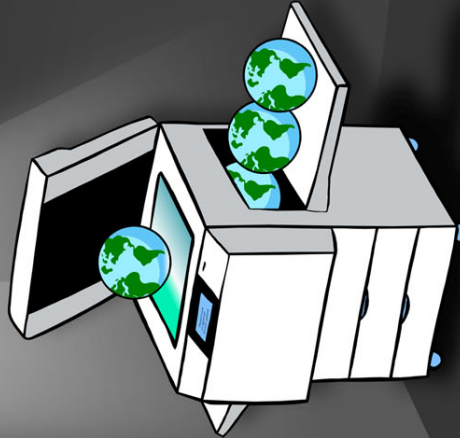
The poster on the following page was prepared for this PhD and was awarded 1st Prize from the University of Warwick Science Faculty at the university-wide Warwick Post-graduate Poster Competition (2011). The poster was then advanced to the 6th annual Vitae Midlands Hub Regional Poster Competition (2011) where it also won 1st Place against 77 competing posters (each winners from their respective universities in the Midlands) as judged by 50 judges from across the Midlands. This is the highest award for any post-graduate poster competition nationwide.

Following the poster is a copy of the poster summary submitted for the competition.

3D Photocopying

Jason B. Jones - j.b.jones@warwick.ac.uk
 Supervisor: Greg Gibbons

THE UNIVERSITY OF
WARWICK



From 2D to 3D:
 Repeatedly printing and fusing layers of toner results in a growing stack which can take virtually any shape.

MTT
 TECHNOLOGIES GROUP

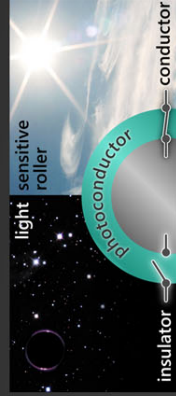
EPSRC
 Engineering and Physical Sciences
 Research Council

The Concept:

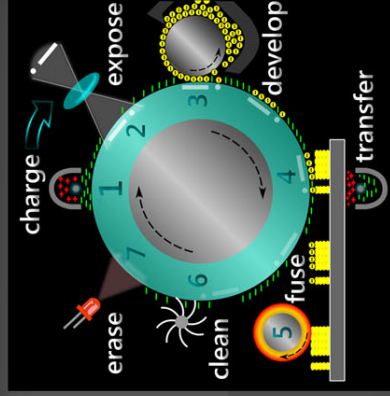
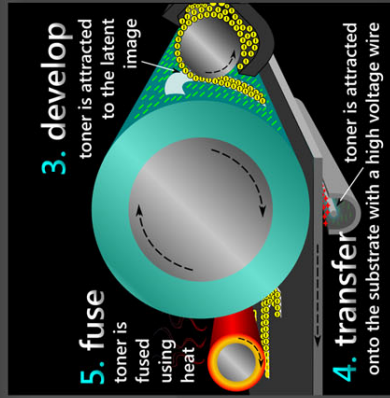
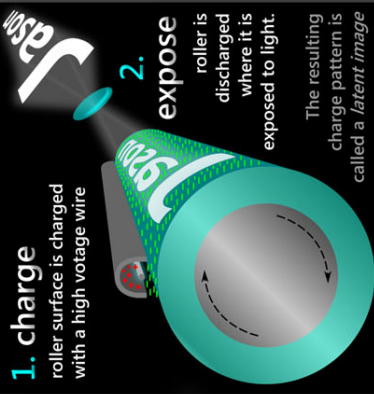
Imagine putting the same sheet of paper through your photocopier over and over again to build a 3D object.



Materials:



Process:



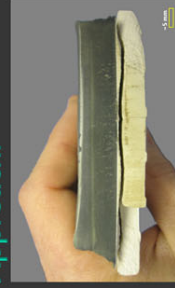
Challenge:



Kumar attempted 3D photocopying, but found that with each new layer the transfer step was less effective. The non-conductive toner acted as an insulator, which created air pockets and limited the process to ~2mm high[1]

The object of this research is to overcome this height limitation.

Approach:



Banerjee and Wippeny demonstrated greater height was possible using only heat and pressure (rather than electrostatics) to transfer layers in a powder coating process.[2]

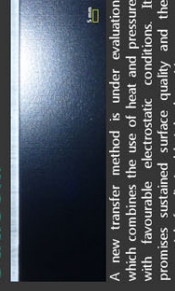
Adapting a photocopy machine to transfer using only heat and pressure theoretically should enable printing to an unlimited height.

Early Results:



Using a development rig (inset picture above) it was demonstrated that successive prints transferred one upon another using only heat and pressure. As for (a) the surface quality (~1 µm Ra) but quickly degraded (for right) which curtailed height accumulation. This result is evidence that the role of electrostatics has been underestimated.

Outlook:



A new transfer method is under evaluation which combines the use of heat and pressure with favourable electrostatic conditions. It promises sustained surface quality and the potential of unlimited height deposition.

Acknowledgements:

This research is gratefully undertaken with support from The University of Warwick, MTT Technologies Group Ltd, and the Engineering and Physical Sciences Research Council

3D Photocopying

by Jason Jones - j.b.jones@warwick.ac.uk

The University of Warwick

Pressing a button on your computer which automatically creates a physical product has been the fascination of science-fiction for decades.

3D printing is a recent phenomenon in manufacturing technologies making that dream a reality. Objects are made by “printing” a series of miniature mosaics which are stacked and laminated together into practically any shape. The process is akin to automating the assembly of millions of microscopic LEGO® bricks.

Modern photocopying is a proven method for digitally placing highly complex patterns (or mosaics) of fine particles onto paper. However, due to limitations in photocopying physics it has never been successfully upscaled for 3D printing [1-3].

The current research has identified the underlying problems, applied for a patent on a new method to enable *3D photocopying* and built bespoke hardware for further trials [4]. Leveraging the strengths of photocopying for 3D assembly promises to deliver a cost-effective and efficient 3D replication technology.

1. Cormier, D., J. Taylor, and H. West, *An Investigation of Selective Coloring with 3-D Laser Printing*. Journal of Manufacturing Processes, 2002. **4**(2): p. 148-152.
2. Kumar, A.V. and A. Dutta, *Investigation of an electrophotography based rapid prototyping technology*. Rapid Prototyping Journal, 2003. **9**(2): p. 95-103.
3. Kumar Das, A., *An Investigation on the Printing of Metal and Polymer Powders Using Electrophotographic Solid Freeform Fabrication*, in *Department of Mechanical and Aerospace Engineering 2004*, University of Florida: Gainesville, Florida. p. 177.
4. Jones, J., et al., *Additive Manufacturing by Electrophotography: Challenges and Successes*, in *NIP26: International Conference on Digital Printing Technologies and Digital Fabrication 2010*2010: Austin, Texas. p. p. 549-553.

References

1. Carlsson, B., *The development and use of machine tools in historical perspective*. Journal of Economic Behavior & Organization, 1984. **5**(1): p. 91-114.
2. Boothroyd, G., *Design for assembly—The key to design for manufacture*. The International Journal of Advanced Manufacturing Technology, 1987. **2**(3): p. 3-11.
3. Boothroyd, G., *Product design for manufacture and assembly*. Computer-Aided Design, 1994. **26**(7): p. 505-520.
4. Beckerle, L.D., *US Patent 3,428,503 Three-dimensional Reproduction Method*. 1969, United States Patent and Trademark Office.
5. Takada, M., *US Patent 4,404,684 Object solid figure recognizing method and apparatus*. 1983, United States Patent and Trademark Office.
6. Hull, C.W., *US Patent 4,575,330 Apparatus for production of three-dimensional objects by stereolithography*. 1986, United States Patent and Trademark Office.
7. Hull, C.W., *US Patent 4,929,402 Method for production of three-dimensional objects by stereolithography*. 1990, United States Patent and Trademark Office.
8. Deckard, C.R., *US Patent 4,863,538 Method and apparatus for producing parts by selective sintering*. 1989, United States Patent and Trademark Office.
9. Forderhase, P.F., C.R. Deckard, and J.M. Klein, *US Patent 5,252,264 Apparatus and method for producing parts with multi-directional powder delivery*. 1993, United States Patent and Trademark Office.
10. Crump, S.S., *US Patent 5,340,433 Modeling apparatus for three-dimensional objects*. 1994, United States Patent and Trademark Office.
11. Crump, S.S., *US Patent 5,121,329 Apparatus and method for creating three-dimensional objects*. 1992, United States Patent and Trademark Office.
12. Kruth, J.P., M.C. Leu, and T. Nakagawa, *Progress in additive manufacturing and rapid prototyping*. CIRP Annals - Manufacturing Technology, 1998. **47**(2): p. 525-540.
13. Levy, G.N., R. Schindel, and J.P. Kruth, *Rapid Manufacturing and Rapid Tooling with Layer Manufacturing (LM) Technologies, State of the Art and Future Perspectives*. CIRP Annals - Manufacturing Technology, 2003. **52**(2): p. 589-609.
14. Hopkinson, N., R.J.M. Hague, and P.M. Dickens, eds. *Rapid Manufacturing: An Industrial Revolution for the Digital Age*. Vol. 1. 2006, John Wiley & Sons: Chipperham, Wiltshire, UK. 76.
15. Gibson, I., D.W. Rosen, and B. Stucker, *Additive Manufacturing Technologies: Rapid Prototyping to Direct Digital Manufacturing*. 2010: Springer.
16. Williams, C.B., F. Mistree, and D.W. Rosen. *Towards the Design of a Layer-Based Additive Manufacturing Process for the Realization of Metal Parts of Designed Mesostructure*. in *Solid Freeform Fabrication Symposium*. 2005. Austin, Texas, USA.
17. ASTM, *F2792 – 10^{E1} – Standard Terminology for Additive Manufacturing Technologies*, in *10.04 Electronics; Declarable Substances in Materials; 3D Imaging Systems*. 2010, ASTM International: West Conshohocken, PA, USA.
18. Jones, J.B., et al. *Printed Circuit Boards by Selective Deposition and Processing*. in *22nd Solid Freeform Fabrication Symposium*. 2011. Austin, TX, USA: University of Texas.

19. Wohlers, T.T., ed. *Wohlers Report 2013 Additive Manufacturing and 3D Printing State of the Industry Annual Worldwide Progress Report*. 2013, Wohlers Associates, Inc.: Fort Collins, CO, USA.
20. Jones, J.B., et al., *SME Technical Paper TP12PUB36: Gateways Toward Dissimilar Multi-material Parts*, in *RAPID 2012 and 3D Imaging Conferences & Exposition*. 2012, Society of Manufacturing Engineers: Atlanta, GA, USA.
21. Christensen, C.M. and M.E. Raynor, *The Innovator's Solution: Creating and Sustaining Successful Growth*. 2003: Harvard Business Press.
22. Joo, D.-I. and S.-J. Kim. *Commercialization of Inkjet Printing Technology as an Alternative Fabrication Route for Large Area Devices*. in *NIP26: International Conference on Digital Printing Technologies and Digital Fabrication*. 2010. Austin, Texas, USA.
23. Slot, M. *Printing as Digital Fabrication Technology*. in *6th International Conference on Additive Manufacturing*. 2011. Loughborough University, UK.
24. Stasiak, J.W., *SC21-M4: An Introduction to Digital Fabrication: Methods, Materials, and Applications*. 2012, Society of Imaging Science and Technology: Springfield, VA, USA. p. 53.
25. Malone, E., et al., *Freeform fabrication of zinc-air batteries and electromechanical assemblies*. *Rapid Prototyping Journal*, 2004. **10**(1): p. 58-69.
26. Malone, E. and H. Lipson, *Freeform fabrication of ionomeric polymer-metal composite actuators*. *Rapid Prototyping Journal*, 2006. **12**(5): p. 244-253.
27. Malone, E., M. Berry, and H. Lipson, *Freeform fabrication and characterization of Zn-air batteries*. *Rapid Prototyping Journal*, 2008. **14**(3): p. 128-140.
28. Kadara, R.O., et al., *Manufacturing electrochemical platforms: Direct-write dispensing versus screen printing*. *Electrochemistry Communications*, 2008. **10**(10): p. 1517-1519.
29. Khatri-Chhetri, P., et al. *Printed Fuel Cell Electrodes with Engineered Porosity*. in *IS&T's NIP27 and Digital Fabrication 2011*. 2011. Minneapolis, MN: IS&T.
30. Kaufmann, U., et al., *Free form fabrication of 3D-ceramic parts with inkjet-printing*. *Industrial Ceramics*, 2008. **28**(1): p. 45-51.
31. De Hazan, Y., et al., *High solids loading ceramic colloidal dispersions in UV curable media via comb-polyelectrolyte surfactants*. *Journal of Colloid and Interface Science*, 2009. **337**(1): p. 66-74.
32. Perelaer, J., et al., *One-step inkjet printing of conductive silver tracks on polymer substrates*. *Nanotechnology*, 2009. **20**(16): p. 165303.
33. Sridhar, A., D.J. van Dijk, and R. Akkerman, *Inkjet printing and adhesion characterisation of conductive tracks on a commercial printed circuit board material*. *Thin Solid Films*, 2009. **517**(16): p. 4633-4637.
34. Özkol, E., et al., *Development of high solid content aqueous 3Y-TZP suspensions for direct inkjet printing using a thermal inkjet printer*. *Journal of the European Ceramic Society*, 2009. **29**(3): p. 403-409.
35. Derby, B., *Inkjet printing ceramics: From drops to solid*. *Journal of the European Ceramic Society*, 2011. **31**(14): p. 2543-2550.
36. Ren, M., et al., *Inkjet Printing Technology for OPV Applications*. *Journal of Imaging Science and Technology*, 2012. **56**(4): p. 40504-1-40504-5.
37. Schein, L.B. *The Outlook for Electrophotography, the Best Known Modern Application of Electrostatics*. in *AVS 53rd International Symposium & Exhibition*. 2006. San Francisco, California.
38. Smith, W., *Effect of Light on Selenium During the Passage of An Electric Current*. *Nature*, 1873. **7**: p. 303.

39. Owen, D., *Copies in seconds: how a lone inventor and an unknown company created the biggest communications breakthrough since Gutenberg: Chester Carlson and the birth of the Xerox machine*. 2004, New York: Simon & Schuster Paperbacks.
40. Brooks, J., *Profiles: XEROX XEROX XEROX XEROX*, in *New Yorker*. 1967.
41. Ellis, C.D., *Joe Wilson and the Creation of Xerox*. 2006, Hoboken, New Jersey: John Wiley & Sons, Inc.
42. Carlson, C.F., *US Patent 2,221,776 Electron photography*. 1940, United States Patent and Trademark Office.
43. Carlson, C.F., *Electrophotography*. 1942, US Patent 2,297,691.
44. Xerox, *Astoria 10-22-38 (The first xerographic image)* 1938, Xerox Images Library Xerox Newsroom.
45. Xerox, *914: First automatic office copier to make copies on plain paper* 1959, Xerox Images Library Xerox Newsroom.
46. Rimai, D.S., et al., *Electrophotography as a means of microfabrication: the role of electrodynamic and electrostatic forces*. *Comptes Rendus Chimie*, 2006. **9**(1): p. 3-12.
47. Xerox, *Telecopier 200: First laser, plain-paper fax machine*. 1975, Xerox Images Library Xerox Newsroom.
48. Xerox, *Xerox 9700: First xerographic laser printer* 1977, Xerox Images Library Xerox Newsroom.
49. Mason, P., *Digital Manufacturing and the Primary Digital Print Technologies*, J.B. Jones, Editor. 2011: UK.
50. Commission., G.B.M.a.M., *Indirect electrostatic photocopiers : a report on the supply by manufacturers and importers of indirect electrostatic photocopiers in the United Kingdom*. Cm ; 1693. 1991, London: H.M.S.O.
51. Rimai, D.S., P. Alexandrovich, and D.J. Quesnel, *Effects of submicrometer particulate silica addenda on the adhesion of micrometer-size particles to a polyester-composite substrate*. *The Journal of Adhesion*, 2003. **79**(11): p. 1041-1066.
52. Schaffert, R.M. and C.D. Oughton, *Xerography: A New Principle of Photography and Graphic Reproduction*. *Journal of the Optical Society of America*, 1948. **38**(12): p. 991-998.
53. Živcová, Z., E. Gregorová, and W. Pabst, *Porous alumina ceramics produced with lycopodium spores as pore-forming agents*. *Journal of Materials Science*, 2007. **42**(20): p. 8760-8764.
54. Hays, D.A. *SC10-S3: Electrostatics and Particle Adhesion in Electrophotography*. 2011. Society for Imaging Science and Technology.
55. Zobrist, B., *Toner Technology 3 - Raw Materials*, in *Toner Technology Training*. 2009: Stone, UK.
56. Law, K.Y., *Organic photoconductive materials: recent trends and developments*. *Chemical Reviews*, 1993. **93**(1): p. 449-486.
57. Weiss, D.S. and M. Abkowitz, *Advances in Organic Photoconductor Technology*. *Chemical Reviews*, 2009. **110**(1): p. 479-526.
58. Banerjee, S. and D.I. Wimpenny, *Laser Printing of Polymeric Materials*, in *Solid Freeform Fabrication Symposium*. 2006: Austin, TX, USA.
59. Banerjee, S. and D.I. Wimpenny, *Laser Printing of Soluble Toner for Rapid Manufacturing*, in *Annals of DAAAM for 2008: Proceedings of the 19th International DAAAM Symposium - Intelligent Manufacturing & Automation: Focus on Next Generation of Intelligent Systems and Solutions*, B. Katalinc, Editor. 2008, DAAAM Int Vienna: Wien. p. 1551-1552.

60. Cormier, D., J. Taylor, and H. West, *An Investigation of Selective Coloring with 3-D Laser Printing*. Journal of Manufacturing Processes, 2002. **4**(2): p. 148-152.
61. Wimpenny, D.I., S. Banerjee, and J.B. Jones. *Laser Printed Elastomeric Parts and their Properties*. in *Solid Freeform Fabrication Proceedings*. 2009. Austin, TX, USA: The University of Texas.
62. Boivie, K., et al., *Issues of Incremental Graded Metallic Materials by the Metal Printing Process, MPP, in Additive Layered Manufacturing: From Evolution to Revolution*, I. Drstvenšek and S. Dolonšek, Editors. 2008, University of Maribor, Faculty for Mechanical Engineering: Maribor. p. 79-98.
63. Boivie, K., *Technical Discussion re: MPP during Visit to Sintef*, J. Jones, Editor. 2009: Trondheim.
64. Beckwith, D., *Technical Discussion re: Ceramic toner & carrier*, J. Jones, Editor. 2010: Leicester.
65. Diaz, A.F. and D. Fenzel-Alexander, *An ion transfer model for contact charging*. Langmuir, 1993. **9**(4): p. 1009-1015.
66. Diaz, A.F. and J. Guay, *Contact charging of organic materials: ion vs. electron transfer*. IBM J. Res. Dev., 1993. **37**(2): p. 249-259.
67. Fuhrmann, J., *Contact electrification of dielectric solids*. Journal of Electrostatics, 1978. **4**(2): p. 109-118.
68. Oguchi, T. and M. Tamatani, *Contact Electrification in Inorganic Binary Compounds*. Journal of The Electrochemical Society, 1986. **133**(4): p. 841-847.
69. Ribes, C., et al. *Preparation of Chemically Prepared Toners (CPT) by Polymerisation for Ceramic Decoration*. in *IS&T's NIP27 and Digital Fabrication 2011*. 2011. Minneapolis, Minnesota, USA: Society for Imaging Science and Technology.
70. Zobrist, B., *Technical Discussion re: Ceramic Toner*, J. Jones, Editor. 2009: Leicester.
71. Crowley, J.M., *Electrostatic fundamentals*, in *Handbook of electrostatic processes*, J.-S. Chang, A.J. Kelly, and J.M. Crowley, Editors. 1995, CRC Press: New York.
72. Encyclopædia Britannica, *Dielectric*, in *Encyclopædia Britannica Online*. 2013: <http://www.britannica.com/EBchecked/topic/162630/dielectric> [22 Oct 2013].
73. Onsager, L., *Electric Moments of Molecules in Liquids*. Journal of the American Chemical Society, 1936. **58**(8): p. 1486-1493.
74. Onsager, L., *Electrostatic Interaction of Molecules*. The Journal of Physical Chemistry, 1939. **43**(2): p. 189-196.
75. Athenstaedt, H., *Pyroelectric and Piezoelectric Properties of Vertebrates*. Annals of the New York Academy of Sciences, 1974. **238**(1): p. 68-94.
76. Eguchi, M., *XX. On the permanent electret*. Philosophical Magazine Series 6, 1925. **49**(289): p. 178-192.
77. Encyclopædia Britannica, *electric susceptibility*, in *Encyclopædia Britannica Online*. 2013: <http://www.britannica.com/EBchecked/topic/182768/electric-susceptibility> [22 Oct 2013].
78. Viman, L. and C.M. Vancea. *PCB design considerations for wireless Data Logger used for thermal validation system*. in *Design and Technology in Electronic Packaging (SIITME), 2011 IEEE 17th International Symposium for*. 2011.
79. Anon., *permittivity*, in *Collins English Dictionary – Complete and Unabridged*. 2003, HarperCollins Publishers.
80. Lewin, W., *Dielectrics & Polarization (Lecture #8)*, in *8.02 Electricity and Magnetism, Spring 2002*. 2013, (Massachusetts Institute of Technology: MIT OpenCourseWare) License: Creative Commons BY-NC-SA.
81. Encyclopædia Britannica, *dielectric constant*, in *Encyclopædia Britannica Online*. 2013: <http://www.britannica.com/EBchecked/topic/162637/dielectric-constant> [22 Oct 2013].

82. The Editors of Encyclopædia Britannica, *dielectric constant*, in *Britannica*. 2013.
83. Watts, C.M., X. Liu, and W.J. Padilla, *Metamaterial electromagnetic wave absorbers*. *Advanced Materials*, 2012. **24**(23): p. OP98-OP120.
84. Wynants, D.L. *DK or Dielectric Constant or Relative Permittivity or ϵ_r , What is it, Why is it Important, and How Does Taconic Test for It?* 2011.
85. Konrad, A. and M. Graovac, *The floating potential approach to the characterization of capacitive effects in high-speed interconnects*. *Magnetics, IEEE Transactions on*, 1997. **33**(2): p. 1185-1188.
86. Zobrist, B., *Toner Technology 1 - Physics and Chemistry*, in *Toner Technology Training*. 2009: Stone, UK.
87. Arbatti, M., X. Shan, and Z. Cheng, *Ceramic-polymer composites with high dielectric constant*. *Advanced Materials*, 2007. **19**(10): p. 1369+.
88. Tan, D. and P. Irwin, *Polymer Based Nanodielectric Composites*. GE Gobal Research Center, USA, 2005: p. 115-132.
89. ASTM, *D149 – 09 Standard Test Method for Dielectric Breakdown Voltage and Dielectric Strength of Solid Electrical Insulating Materials at Commercial Power Frequencies*, in *10.01 Electrical insulation and electronics*. 2009, ASTM International: West Conshohocken, PA, United States.
90. Enis, T., et al., *Enhancement of dielectric strength in nanocomposites*. *Nanotechnology*, 2007. **18**(32): p. 325704.
91. Neusel, C. and G.A. Schneider, *Dependence of the breakdown strength on thickness and permittivity*, in *11th IEEE International Conference on Solid Dielectrics*. 2013: Bologna, Italy.
92. ASTM, *D257 – 07 Standard Test Methods for DC Resistance or Conductance of Insulating Materials*, in *10.01 Electrical insulation and electronics*. 2007, ASTM International: West Conshohocken, PA, United States.
93. UL IDES, *Volume and Surface Resistivity - ASTM D257 Plastic Test Standard*, in *UL IDES > Resources > Plastic Material Properties > Electrical*. 2013.
94. Büttner, D. and K. Krüger. *Improving Performance of Laser-Printed Conductive Silver Lines*. in *IMAPS/ACerS 8th International Conf. on Ceramic Interconnect and Ceramic Microsystems Technologies*. 2012. Erfurt, Germany: IMAPS/ACerS.
95. Jones, J.B., et al., *Laser Printing Circuit Boards and Electronics*. *Journal of Imaging Science and Technology*, 2012. **56**(4): p. 040503-1 – 040503-11.
96. Takeda, F., H. Tosaka, and K. Tomita, *US Patent 5,527,657 One-component magnetic toner for use in electrophotography*. 1996, United States Patent and Trademark Office.
97. Büttner, D., et al. *Laser Printing of Conductive Silver Lines*. in *IS&T's NIP26 and Digital Fabrication 2010*. 2010. Austin, Texas: IS&T.
98. Büttner, D., W. Diel, and K. Krüger. *Digital Printing of Conductive Silver Lines: Comparison between Inkjet and Laser Printing*. in *12th Eur. Ceram. Soc. Conf.* 2011. Stockholm, Sweden: European Ceramic Society.
99. Büttner, D., et al., *Laser Printing of RFID Antenna Coils on Ceramic in 2011 IMAPS/ACerS 7th International Conference and Exhibition on Ceramic Interconnect and Ceramic Microsystems Technologies*. 2011: San Diego, California, USA.
100. Büttner, D., et al., *Electrophotographic Printing of RFID Antenna Coils on Cofired and Postfired Ceramics*. *Journal of Microelectronics and Electronic Packaging*, 2011. **8**: p. 58-65.
101. Büttner, D., W. Diel, and K. Krüger. *Pre-Treatment of Silver Particles as a Basis for Functional Toner*. in *IS&T's NIP27 and Digital Fabrication 2011*. 2011. Minneapolis, Minnesota, USA: IS&T.

102. Martin, T.I. and L.A. Reeves, *US Patent 7,285,303 Powder material for electrostatic application to a substrate and electrostatic application of the powder material to a substrate*. 2007, United States Patent and Trademark Office.
103. Walker, A. and D.F. Baldwin, *Initial investigations into low-cost ultra-fine pitch solder printing process based on innovative laser printing technology*. Electronics Packaging Manufacturing, IEEE Transactions on, 1999. **22**(4): p. 303-307.
104. Honjo, S., *US Patent 3,764,312 Electrophotographic Process*. 1973, United States Patent and Trademark Office.
105. Morimoto, T., et al., *US Patent 4,701,389 Photoconductive toner*. 1987, United States Patent and Trademark Office.
106. Van Allan, J.A., et al., *US Patent 4,165,984 Electrophoretic migration imaging process*. 1979, United States Patent and Trademark Office.
107. Goto, H., et al., *The image forming process of photoconductive toner*. Applied optics, 1969. **8 Suppl 1**: p. 124-124.
108. Schein, L.B., *Electrophotography and Development Physics*. Revised 2nd ed. p. cm. ed. 1992, Morgan Hill: Laplacian Press. 362.
109. Zobrist, B., *Toner Technology 7 - Toner Production*, in *Toner Technology Training*. 2009: Stone, UK.
110. Kiatkamjornwong, S. and P. Pomsanam, *Synthesis and characterization of styrenic-based polymerized toner and its composite for electrophotographic printing*. Journal of Applied Polymer Science, 2003. **89**(1): p. 238-248.
111. Konica Minolta *Polymerized Toner —an Innovative Choice*. The Creation of New Value Konica Minolta CSR Report 2010, 2010.
112. Neilson, I. *Toner Technologies*. 2004.
113. Hasegawa, J., N. Yanagida, and M. Tamura, *Toner prepared by the direct polymerization method in comparison with the pulverization method*. Colloids and Surfaces A: Physicochemical and Engineering Aspects, 1999. **153**(1-3): p. 215-220.
114. Yamana, S. *High-Speed Color Laser Printing*. in *IS&T's NIP20: International Conference on Digital Printing Technologies*. 2004.
115. Paine, A.J., K.J. O'callaghan, and A. Rudin, *US Patent 5,455,315 Emulsion polymerization processes and toners thereof*. 1995, United States Patent and Trademark Office.
116. Chudasama, R., J.B. Jones, and D.I. Wimpenny, *Synthesis of an Electrophotographic Toner for Additive Manufacturing*, in *DAAAM International Scientific Book 2012*, B. Katalinic, Editor. 2012, DAAAM International: Vienna Austria.
117. Sánchez, L., et al., *Influence of operation conditions on the microencapsulation of PCMs by means of suspension-like polymerization*. Colloid and Polymer Science, 2008. **286**(8-9): p. 1019-1027.
118. Kokal, S. and M. Wingrove. *Emulsion Separation Index: From laboratory to field case studies*. in *SPE Annual Technical Conference and Exhibition*. 2000.
119. Tan, J.S., et al. *Palm Oil-based Bio-Resin for Toner*. in *NIP28: International Conference on Digital Printing Technologies and Digital Fabrication 2012*. 2012. Quebec City, Canada: Society of Imaging Science and Technology.
120. Bartscher, G., et al., *Comparison of the electric fields of electrophotography and contact electrography*. Journal of Electrostatics, 2001. **53**(4): p. 295-310.
121. Manjooran, N.J., A. Kumar, and W.M. Sigmund, *Development of a liquid toner for electro-photographic solid freeform fabrication*. Journal of the European Ceramic Society, 2006. **26**(13): p. 2459-2465.
122. Iida, A., et al., *Digital Fabrication Using High-resolution Liquid Toner Electrophotography*. Journal of Imaging Science and Technology, 2007. **51**(5): p. 465-472.

123. Mazumder, M.K., et al., *Measurement of particle size and electrostatic charge distributions on toners using E-SPART analyzer*. Industry Applications, IEEE Transactions on, 1991. **27**(4): p. 611-619.
124. ASTM, *F 577 – 03 Standard Test Method for Particle Size Measurement of Dry Toners*, in *15.09 Paper; Business Imaging Products*. 2003 (2009), ASTM International: West Conshohocken, PA, USA.
125. Weiner, B.B. *White Paper: What is a Continuous Particle Size Distribution?* 2011.
126. Mitchell, J.P., *Particle standards: their development and application*. Kona, 2000. **18**: p. 41-59.
127. Park, H. and S. Park, *New Approaches to Characterize and Reduce the Number of Ultrafine Particles from a Laser Printer*. Journal of Imaging Science and Technology, 2013. **57**(1): p. 10502-1-10502-7.
128. Freeman, G.R. and N.H. March, *Triboelectricity and some associated phenomena*. Materials Science and Technology, 1999. **15**(12): p. 1454-1458.
129. Iversen, P. and D.J. Lacks, *A life of its own: The tenuous connection between Thales of Miletus and the study of electrostatic charging*. Journal of Electrostatics, 2012. **70**(3): p. 309-311.
130. Tkachenko, E.Y. and S.G. Kozachkov, *Possible contribution of triboelectricity to snow-air interactions*. Environmental Chemistry, 2012. **9**(2): p. 109-115.
131. Latham, J., *The electrification of snowstorms and sandstorms*. Quarterly Journal of the Royal Meteorological Society, 1964. **90**(383): p. 91-95.
132. Walton, O.R., *Review of Adhesion Fundamentals for Micron-Scale Particles*. Kona Powder and Particle Journal, 2008. **26**: p. 129-141.
133. Keith Watson, P. and Z.-Z. Yu, *The Contact Electrification of Polymers and the Depth of Charge Penetration*. Journal of Electrostatics, 1997. **40-41**(0): p. 67-72.
134. Kok, J.F., *Understanding wind-blown sand and the electrification of granular systems*. 2009, The University of Michigan.
135. Karner, S. and N. Anne Urbanetz, *The impact of electrostatic charge in pharmaceutical powders with specific focus on inhalation-powders*. Journal of Aerosol Science, 2011. **42**(6): p. 428-445.
136. Nash, R., M. Grande, and R. Muller. *The effect of toner and carrier composition on the average and distributed toner charge values*. in *NIP14*. 1998. IS&T.
137. Wada, M., et al., *Developing Device and Image Forming Apparatus Having the Same*, U.S.P. Office, Editor. 2010, KYOCERA MITA CORPORATION: USA.
138. Hutcheson, B., *Carrier Design for Pulverized & Polymerized Toner*, in *Toners and Photoreceptors Conference*. 2006, The Tiara Group, LLC.
139. Diaz, A.F. and R.M. Felix-Navarro, *A semi-quantitative tribo-electric series for polymeric materials: the influence of chemical structure and properties*. Journal of Electrostatics, 2004. **62**(4): p. 277-290.
140. Nakayama, K., *Tribocharging and friction in insulators in ambient air*. Wear, 1996. **194**(1-2): p. 185-189.
141. Nash, R.J., M.L. Grande, and R.N. Muller, *CCA Effects on the Triboelectric Charging Properties of a Two-Component Xerographic Developer*. Journal of Imaging Science and Technology, 2002. **46**(4): p. 313-320.
142. Šupuk, E., et al., *Tribo-electrification of active pharmaceutical ingredients and excipients*. Powder Technology, 2012. **217**(0): p. 427-434.
143. Webers, V.J., *Measurement of triboelectric position*. Journal of Applied Polymer Science, 1963. **7**(4): p. 1317-1323.
144. Wiles, J.A., et al., *A Tool for Studying Contact Electrification in Systems Comprising Metals and Insulating Polymers*. Analytical Chemistry, 2003. **75**(18): p. 4859-4867.

145. Law, K.-Y., et al., *Investigation of the Contact Charging Mechanism between an Organic Salt Doped Polymer Surface and Polymer-Coated Metal Beads*. Chemistry of Materials, 1995. **7**(11): p. 2090-2095.
146. Bailey, A.G., *Charging of Solids and Powders*. Journal of Electrostatics, 1993. **30**: p. 167-180.
147. Benda, J.A. and W.J. Wnek, *A Model for Magnetic Brush Development in Xerographic Machines*. Industry Applications, IEEE Transactions on, 1981. **IA-17**(6): p. 610-618.
148. Harper, W.R., *Contact and frictional electrification*. 1967: Laplacian Press.
149. Gutman, E. and G. Hartmann, *Triboelectric properties of two-component developers for xerography*. Journal of imaging science and technology, 1992. **36**(4): p. 335-349.
150. La Marche, K.R., *Electrostatic instabilities, charging and agglomeration in flowing granular materials*. 2008: ProQuest.
151. Hasbrouck, R., *Mitigating lightning hazards*. Science and Technology Review, 1996.
152. ASTM, *F1425 - 06 Standard Test Method for Determining the Tribocharge of Two-Component Developer Materials*, in *15.09 Paper; Business Imaging Products*. 2006, ASTM International: West Conshohocken, PA, USA.
153. Küttner, A. and R.H. Epping. *Theory and Practice of a Small Toner-Charge-Spectrometer*. in *IS&T's NIP14*. 1998. Toronto, Canada: IS&T.
154. Noras, M.A. *An apparatus for the charge-to-mass and charge-to-diameter measurements on powders*. in *Journal of Physics: Conference Series*. 2008. IOP Publishing.
155. Schein, L.B., et al., *Experimental verification of the proximity theory of toner adhesion*. Journal of Imaging Science and Technology, 2004. **48**(5): p. 417-425.
156. Nash, R.J. *Impact of Digital Xerography on Toner/Carrier Designs*. in *8th Annual Toner & Imaging Chemicals Conference*. 2005. St. Pete Beach, Florida: Information Management Institute, Inc.
157. Vanbesien, D.W., et al., *US Patent 20,120,308,925 Hyperpigmented black low melt toner*. 2012, United States Patent and Trademark Office.
158. Hays, D.A., *Toner Adhesion*. The Journal of Adhesion, 1995. **51**(1-4): p. 41-48.
159. Mizes, H., et al., *Small particle adhesion: measurement and control*. Colloids and Surfaces A: Physicochemical and Engineering Aspects, 2000. **165**(1-3): p. 11-23.
160. Castle, G.S.P. and L.B. Schein, *General model of sphere-sphere insulator contact electrification*. Journal of Electrostatics, 1995. **36**(2): p. 165-173.
161. Czarnecki, W.S. and L.B. Schein, *Electrostatic force acting on a spherically symmetric charge distribution in contact with a conductive plane*. Journal of Electrostatics, 2004. **61**(2): p. 107-115.
162. Kemp, B.A. and J.G. Whitney, *Electrostatic adhesion of multiple non-uniformly charged dielectric particles*. Journal of Applied Physics, 2013. **113**(4): p. 044903-044903-6.
163. Whitney, J.G., *Toner Charge and Environmental Interactions with Toner Adhesion*, in *NIP27: International Conference on Digital Printing Technologies and Digital Fabrication*. 2011, Society for Imaging Science and Technology: Minneapolis, Minnesota. p. 136-139.
164. Whitney, J.G. and B.A. Kemp. *Toner Adhesion Measurement*. in *IS&T's NIP26 and Digital Fabrication 2010*. 2010. Austin, Texas: Society for Imaging Science and Technology.
165. Schein, L.B., *Recent advances in our understanding of toner charging*. Journal of Electrostatics, 1999. **46**(1): p. 29-36.
166. Whitney, J.G. *Toner/Transfer Member Adhesion Response to Environment-Induced Material Property Changes, and Their Impact on Transfer Fields*. in *NIP28*:

- International Conference on Digital Printing Technologies and Digital Fabrication*. 2012. Quebec City, Canada: Society for Imaging Science and Technology.
167. Havas, P., *On theories of gravitation with higher-order field equations*. *General Relativity and Gravitation*, 1977. **8**(8): p. 631-645.
 168. Rimai, D.S., D.S. Weiss, and D.J. Quesnel, *Particle adhesion and removal in electrophotography*. *Journal of Adhesion Science and Technology*, 2003. **17**(7): p. 917-942.
 169. Srinivasan, S.A. and P.S. Alexandrovich, *Electrophotographic toner surface treated with silica mixtures*. 2001, Google Patents.
 170. Lazzarotto, L., et al., *The effects of processing bath parameters on the quality and performance of zinc phosphate stearate coatings*. *Surface and Coatings Technology*, 1999. **122**(2-3): p. 94-100.
 171. Tomas, J., *Mechanics of particle adhesion*, PhD in *Department of Process Engineering and Systems Engineering*. 2006, Otto-von-Guericke University: Universitätsplatz 2, D-39106 Magdenburg, Germany. p. 92.
 172. Noll, C.G., *Electrostatic Charge Elimination Techniques*, in *Handbook of electrostatic processes*, J.-s. Chang, A.J. Kelly, and J.M. Crowley, Editors. 1995, Marcel Dekker, Inc.: New York.
 173. Hoshino, Y., et al., *Review of Toner-Based Printing Technologies and Fundamentals of Toner Charging Mechanism*. *Journal of Imaging Science and Technology*, 2010. **54**(5): p. 050201-5.
 174. Krein, P.T. and K.S. Robinson, *Printers*, in *Handbook of electrostatic processes*, J.-s. Chang, A.J. Kelly, and J.M. Crowley, Editors., Marcel Dekker, Inc.: New York.
 175. Mazumder, M.K., et al., *Twenty-first century research needs in electrostatic processes applied to industry and medicine*. *Chemical Engineering Science*, 2006. **61**(7): p. 2192-2211.
 176. Weiss, D.S., B.R. Benwood, and D.L. Troendle, *Corona Charging Characterization of Organic Photoreceptors*. *Journal of Imaging Science and Technology*, 2007. **51**(6): p. 520-524.
 177. Ientilucci, E., *Fundamentals of Xerography*. 1994, Feb.
 178. Pietrowski, K. *SC20-M3: Charging Systems and Dependent Processes in Electrophotography*. in *Digital Fabrication 2010* 2010. Austin, Texas: Society for Imaging Science and Technology.
 179. Baytekin, H.T., et al., *The Mosaic of Surface Charge in Contact Electrification*. *Science*, 2011. **333**(6040): p. 308-312.
 180. Thomas III, S.W., et al., *Controlling the Kinetics of Contact Electrification with Patterned Surfaces*. *Journal of the American Chemical Society*, 2009. **131**(25): p. 8746-8747.
 181. Kumar Das, A., *An Investigation on the Printing of Metal and Polymer Powders Using Electrophotographic Solid Freeform Fabrication*, Masters of Science in *Department of Mechanical and Aerospace Engineering* 2004, University of Florida: Gainesville, Florida. p. 177.
 182. Kasap, S. and P. Capper, *Springer handbook of electronic and photonic materials*. 2006: Springer.
 183. Wikipedia. *Laser printer*. 2010 [14 May 2010]; Available from: http://en.wikipedia.org/wiki/Laser_printer.
 184. Williams, R.M., *"Introduction to Electron Transfer" adapted from "Fullerenes as Electron Accepting Components in Supramolecular and Covalently Linked Electron Transfer Systems"*, PhD. 1996: Amsterdam.
 185. Seino, K., et al., *Photoinduced and Dark Discharge Mechanisms of High Gamma Photoreceptors*. *Journal of Imaging Science*, 2010. **54**(6): p. 60502-1-60502-9.

186. Tokarski, Z., Y.-J. Ahn, and S.-Y. Jung, *Investigations of Charge Migration and Charge Trapping in Fatigued Organic Photoconductors*. Journal of Imaging Science and Technology, 2013. **56**(6): p. 60501-1-60501-11.
187. Liu, C.-y., et al., *High-density nanosecond charge trapping in thin films of the photoconductor ZnODEP*. Science, 1993. **261**(5123): p. 897-899.
188. Lidiard, A.B., *The Mott-Littleton method: an introductory survey*. Journal of the Chemical Society, Faraday Transactions 2: Molecular and Chemical Physics, 1989. **85**(5): p. 341-349.
189. Mott, N.F. and M.J. Littleton, *Conduction in polar crystals. I. Electrolytic conduction in solid salts*. Transactions of the Faraday Society, 1938. **34**: p. 485-499.
190. Coudray, C. and G. Blaise, *Charge trapping induced electromechanical energy*. Journal of Applied Physics, 1996. **80**(9): p. 5248-5255.
191. MacDonald, B.A. and B.G. Fallone, *Charge decay of electrets formed by ionizing radiation in air*. Journal of Electrostatics, 1993. **31**(1): p. 27-33.
192. Bamji, S.S., K.J. Jao, and M.M. Perlman, *Polymer electrets corona charged at high temperature*. Journal of Electrostatics, 1979. **6**(4): p. 373-379.
193. Prime, D. and S. Paul, *Overview of organic memory devices*. Philosophical Transactions of the Royal Society a-Mathematical Physical and Engineering Sciences, 2009. **367**(1905): p. 4141-4157.
194. Xiao, F.F., *Permanent Magnets in Xerographic Systems*, in *Permanent Magnet Systems Conference*. 2000: Atlanta, GA, USA.
195. Hays, D.A., *Electrical Properties of Conductive Two-Component Xerographic Developer*. Industry Applications, IEEE Transactions on, 1987. **IA-23**(6): p. 970-974.
196. Folkins, J.J., *Intermediate conductivities-the crossover function for insulative and conductive two-component magnetic brush development in electrophotography*. Industry Applications, IEEE Transactions on, 1988. **24**(2): p. 250-255.
197. Scharfe, M., *Electrophotography principles and optimization*. Vol. 3. 1984, Letchworth, England: Research Studies Press.
198. Hays, D.A., *Electrical properties of insulative two-component magnetic brush development*. Journal of imaging technology, 1989. **15**(1): p. 29-38.
199. Cheng, Y.C. and G.C. Hartmann, *Electrographic development: An electrostatic calculation*. Journal of Applied Physics, 1980. **51**(5): p. 2332-2337.
200. Berg, W.F. and K. Hauffe, eds. *Current problems in electrophotography*. 1972, Walter de Gruyter: Berlin. 387.
201. ASTM, *F 2036 – 05^{E1} Standard Test Method for Evaluation of Larger Area Density and Background on Electrophotographic Printers*, in *15.09 Paper; Business Imaging Products*. 2009, ASTM International: West Conshohocken, PA, USA.
202. Neugebauer, H., *Electrostatic Fields of Xerographic Images*, in *Xerography and Related Processes*, J. Dessauer and H. Clark, Editors. 1965, Focal Press: London.
203. Neugebauer, H.E.J., *Development Method and Modulation Transfer Function of Xerography*. Appl. Opt., 1967. **6**(5): p. 943-945.
204. Thourson, T.L., *Xerographic development processes: A review*. Electron Devices, IEEE Transactions on, 1972. **19**(4): p. 495-511.
205. Chang, J.-S., A.J. Kelly, and J.M. Crowley, eds. *Handbook of electrostatic processes*. 1995, CRC Press: New York, NY. 768.
206. Gundlach, R.W., *US Patent 2,777,418 Apparatus for developing a powder image on a xerographic plate*. 1957.
207. Fraser, L.J., D.G. Parker, and J.L. Scaletta, *US Patent 3,950,089 Coated roll for magnetic brush development and cleaning systems*. 1976, United States Patent and Trademark Office.

208. Mott, G.R. and H.E. Clark, *Mechanical shield to protect magnetic core in xerographic developing apparatus*. 1965, US Patent 3,219,014.
209. Schein, L.B., *Electrophotography*, in *Handbook of electrostatic processes*, J.-S. Chang, A.J. Kelly, and J.M. Crowley, Editors. 1995, CRC Press: New York.
210. Mahadevan, P., *Analysis of Layer Development and Fusing for 3D Laser Printing*, Masters of Science in *Industrial Engineering*. 2003, North Carolina State University. p. 87.
211. Banerjee, S., *Development of a Novel Toner for Electrophotography based Additive Manufacturing Process*, PhD in *Department of Engineering*. 2011, De Montfort University: Leicester, UK.
212. Raut, S.S., *Investigation of Layer Thickness Uniformity of Laser Printing*, Masters of Science in *Department of Engineering*. 2009, De Montfort University: Leicester, UK.
213. Fay, J.E., Jr., *Electrostatic Analysis of and Improvements to Electrophotographic Solid Freeform Fabrication*, Masters of Science in *Department of Mechanical and Aerospace Engineering* 2003, University of Florida: Gainesville, Florida. p. 110.
214. Ermenc, J.J., *Interview of Chester F. Carlson, the Inventor*. *NYL Rev.*, 2000. **44**: p. 247.
215. Yzmo, *Xerographic photocopy process en.svg*. 2007, Wikipedia Creative Commons.
216. Cook, W.P., G.A. Denton, and D.D. Dreyfuss, *Traveling Wave and Vertical Toner Transfer*, U.S.P. Office, Editor. 2000, Lexmark International, Inc.: USA.
217. Mizes, H., J. Beachner, and P. Ramesh, *Optical Measurements of Toner Motion in a Development Nip*. *Journal of Imaging Science and Technology*, 2000. **44**(3): p. 210-218.
218. Pai, D.M. and B.E. Springett, *Physics of electrophotography*. *Reviews of Modern Physics*, 1993. **65**(1): p. 163.
219. Kemp, B.A. and J.G. Whitney. *Analytical Modeling of Electrostatic Toner Adhesion*. in *NIP27: International Conference on Digital Printing Technologies and Digital Fabrication*. 2011. Minneapolis, Minnesota: Society for Imaging Science and Technology.
220. Paschen, F., *Ueber die zum Funkenübergang in Luft, Wasserstoff und Kohlensäure bei verschiedenen Drucken erforderliche Potentialdifferenz*. *Annalen der Physik*, 1889. **273**(5): p. 69-96.
221. Nelsen, D.E., et al. *Design and Test Results for a Robust CMOS VLSI Input Protection Network*. in *Electrical Overstress-Electrostatic Discharge Symposium Proceedings*. 1986. Las Vegas, NV, USA: EOS/ESD Association, Incorporated.
222. Detig, R.H. and D.C. Eberlein, *Electrokinetic imaging: A new electrostatic printing process for liquid toners*. *Digital Fabrication 2006, Final Program and Proceedings*. 2006, Springfield: Soc Imaging Science & Technology. 103-106.
223. Bonisch, S., W. Kalkner, and D. Pommerenke, *Modeling of short-gap ESD under consideration of different discharge mechanisms*. *Plasma Science, IEEE Transactions on*, 2003. **31**(4): p. 736-744.
224. Hamamoto, R., et al. *Effect of Transfer Roller Surface Profile on Discharge Mark*. in *NIP27 International Conference on Digital Printing Technologies*. 2011. Minneapolis, Minnesota: Society for Imaging Science and Technology.
225. Cassidy, A., M. Grant, and N. Provasas, *Modelling dielectric heterogeneity in electrophotography*. *Modelling and Simulation in Materials Science and Engineering*, 2004. **12**(1): p. 91-107.
226. Tong, C.H., T. Wu, and N. Provasas, *Modelling the role of paper microstructure in electrophotography*. *Modelling and Simulation in Materials Science and Engineering*, 2006. **14**(8): p. 1447-1464.

227. Cho, A.Y.H., *Contact Charging of Micron-Sized Particles in Intense Electric Fields*. Journal of Applied Physics, 1964. **35**(9): p. 2561-2564.
228. Speardock, *The Shuttling Ball (Electrical Charge/Discharge Demonstration)*, in *The Mysterious Shuttling Ball Physics Experiment*. 2013, Youtube.
229. Boivie, K.M., R. Karlsen, and C. Van der Eijk. *Material Issues of the Metal Printing Process, MPP*. in *17th Solid Freeform Fabrication Symposium*. 2006. Austin, TX: University of Texas.
230. Tyagi, D. *SC20-M3: Fusing Technologies and Toner Materials Relationships*. in *NIP28: International Conference on Digital Printing Technologies and Digital Fabrication*. 2012. Quebec City, CA: Society for Imaging Science and Technology.
231. Komuro, H., et al., *US Patent 7,133,634 Circulating body and fixing device*. 2006, United States Patent and Trademark Office.
232. Farrow Michael, M., G. Miller Allen, and M. Walsh Anne, *Surface Chemistry of Business Papers: Electron Spectroscopy for Chemical Analysis Studies*, in *Colloids and Surfaces in Reprographic Technology*. 1982, American Chemical Society. p. 455-474.
233. Suzuki, T., et al., *US Patent 7,324,778 Fixing device including heating roller and pressure roller*. 2008, United States Patent and Trademark Office.
234. Kikuchi, H., et al., *US Patent 7,254,362 Fixing device, image forming apparatus using the fixing device, and heat insulating member*. 2007, United States Patent and Trademark Office.
235. Jones, J.B., D.I. Wimpenny, and G.J. Gibbons, [*In Press, Accepted Manuscript*] *Additive Manufacturing Under Pressure*. Rapid Prototyping Journal, 2013. **20**(6).
236. Jones, J.B., D.I. Wimpenny, and G.J. Gibbons. *The Influence of Residual Toner Charge on 3D Laser Printed Objects*. in *IS&T's NIP28 and Digital Fabrication 2012* 2012. Quebec City, Canada: Society for Imaging Science and Technology.
237. Noguchi, H., *Next Generation Inkjet Printer and Potentiality*. Journal of Printing Science and Technology, 2011. **48**(1): p. 027-036.
238. Schein, L.B., *Role of Technical Innovation in the Physics of Electrophotography*. Journal of Imaging Science and Technology, 2010. **54**(2): p. 020201.
239. Buskirk, W.A., et al., *Development of a high-resolution thermal inkjet printhead - HP DeskJet printer - technical*. Hewlett Packard Journal, 1988. **55**.
240. Hoath, S.D., O.G. Harlen, and I.M. Hutchings, *Jetting behavior of polymer solutions in drop-on-demand inkjet printing*. Journal of Rheology, 2012. **56**(5): p. 1109-1127.
241. Jung, S., et al., *A New Method to Assess the Jetting Behavior of Drop-on-Demand Ink Jet Fluids*. Journal of Imaging Science, 2011. **55**(1): p. 10501-1-10501-6.
242. Martin, G.D., S.D. Hoath, and I.M. Hutchings, *Inkjet printing - the physics of manipulating liquid jets and drops*. Journal of Physics: Conference Series, 2008. **105**(1): p. 012001.
243. Zobrist, B., *Toner Technology 6 - Quality Control*, in *Toner Technology Training* 2009: Stone, UK.
244. Jones, J.B., G.J. Gibbons, and D.I. Wimpenny. *Transfer Methods toward Additive Manufacturing by Electrophotography*. in *IS&T's NIP27 and Digital Fabrication 2011*. 2011. Minneapolis, Minnesota, USA: Society for Imaging Science and Technology.
245. Pomerantz, I., et al., *US Patent 4,961,154 Three dimensional modelling apparatus*. 1990, United States Patent and Trademark Office.
246. Pomerantz, I., et al., *US Patent 5,031,120 Three dimensional modelling apparatus*. 1991, United States Patent and Trademark Office.

247. Pomerantz, I., B. Ben-Ezra, and G. Shamir, *US Patent 5,139,338 Method and apparatus for volumetric digitization of 3-dimensional objects*. 1992, United States Patent and Trademark Office.
248. Zur, A., *US Patent 5,157,423 Apparatus for pattern generation on a dielectric substrate*. 1992, United States Patent and Trademark Office.
249. Pomerantz, I., et al., *US Patent 5,263,130 Three dimensional modelling apparatus*. 1993, United States Patent and Trademark Office.
250. Cohen, N., et al., *US Patent 5,287,435 Three dimensional modeling*. 1994, United States Patent and Trademark Office.
251. Pomerantz, I., et al., *US Patent 5,519,816 Three dimensional modeling apparatus*. 1996, United States Patent and Trademark Office.
252. efunda *Rapid Prototyping: SGC*. 2012.
253. Morita, S. and K. Sugiyama, *US Patent 6,056,843, Sheet lamination modeling method and sheet lamination modeling apparatus*. 2000, United States Patent and Trademark Office.
254. Morita, S. and K. Sugiyama, *US Patent 6,413,360 Sheet lamination modeling apparatus*. 2002, United States Patent and Trademark Office.
255. Prinz, F.B., et al., *JTEC/WTEC Panel Final Report on Rapid prototyping in Europe and Japan*. 1997, Rapid Prototyping Association of the Society of Manufacturing Engineers.
256. Liu, J.H. and B.Z. Jang, *US Patent 6,376,148 Layer manufacturing using electrostatic imaging and lamination*. 2002, United States Patent and Trademark Office.
257. Larsson, R., *US Patent 6,531,086 Method and device for manufacturing three-dimensional bodies*. 2003, United States Patent and Trademark Office.
258. Sintermask GmbH, *Image of the masking process*. 2012.
259. Tan, Y.E. and C.K. Chua. *An additive manufacturing method based on xerography*. 2012. Leiria.
260. Jones, J.B., et al. *Additive Manufacturing by Electrophotography: Challenges and Successes*. in *IS&T's NIP26 and Digital Fabrication 2010*. 2010. Austin, Texas: Society for Imaging Science and Technology.
261. Kumar, A.V. and A. Dutta, *Investigation of an electrophotography based rapid prototyping technology*. *Rapid Prototyping Journal*, 2003. **9**(2): p. 95-103.
262. Güttler, S., et al. *Electro Photography ("Laser Printing") an Efficient Technology for Biofabrication*. in *IS&T's NIP26 and Digital Fabrication 2010*. 2010. Austin, Texas, USA: Society for Imaging Science and Technology.
263. Kumar, A.V. and A. Dutta, *Electrophotographic Layered Manufacturing*. *Journal of Manufacturing Science and Engineering*, 2004. **126**(3): p. 571-576.
264. Dutta, A., *Study and Enhancement of Electrophotographic Solid Freeform Fabrication*, Masters of Science in *Department of Mechanical and Aerospace Engineering* 2002, University of Florida: Gainesville, Florida. p. 124.
265. Karunakaran, K.P., et al., *Low cost integration of additive and subtractive processes for hybrid layered manufacturing*. *Robotics and Computer-Integrated Manufacturing*, 2010. **26**(5): p. 490-499.
266. Kumar, A., *US Patent 6,066,285 Solid Freeform Fabrication Using Powder Deposition*, in *United States Patent and Trademark Office*. 2000, University of Florida: USA. p. 9.
267. Kumar, A., *Electrophotographic Solid Freeform Fabrication*. 1999, University of Florida, Mechanical and Aerospace Engineering: Gainesville. p. 11.
268. Kumar, A.P., et al., *Nanoscale particles for polymer degradation and stabilization—Trends and future perspectives*. *Progress in Polymer Science*, 2009. **34**(6): p. 479-515.

269. Kumar, A.V. *Powder deposition and sintering for a two-powder approach to solid freeform fabrication*. in *Solid Freeform Fabrication Proceedings, August, 1998*. 1998.
270. Kumar, A.V., *Technical Discussion re: State of Electrostatic SFF at the University of Florida*, J. Jones, Editor. 2010: Leicester.
271. Kumar, A.V., *Electrophotographic Solid Freeform Fabrication*. 2003, University of Florida, Mechanical and Aerospace Engineering: Gainesville. p. 40.
272. Kumar, A.V., A. Dutta, and J.E. Fay, *Electrophotographic printing of part and binder powders*. *Rapid Prototyping Journal*, 2004. **10**(1): p. 7-13.
273. Kumar, A.V. and H.X. Zhang, *Electrophotographic powder deposition for freeform fabrication*. *Solid Freeform Fabrication Proceedings*, 1999: p. 647-653.
274. Güttler, S., et al., *Electrophotography---An Efficient Technology for Biochip Fabrication*. *Journal of Imaging Science and Technology*, 2011. **55**(4): p. 040306.
275. Stadler, V., et al., *Combinatorial Synthesis of Peptide Arrays with a Laser Printer*. *Angewandte Chemie International Edition*, 2008. **47**(37): p. 7132-7135.
276. Grunze, M., et al., *Surface-modified layer system*. 2004, United States Patent and Trademark Office.
277. Wimpenny, D.I. and S. Banerjee, *Electrostatic printing method and its use in rapid prototyping*. 2008: Great Britain.
278. Zimmer, M., et al., *Device for Applying Decors and/or Characters on Glass, Glass Ceramics and Ceramics Products*, U.S.P. Office, Editor. 2002, Schott Glas: USA.
279. Jethon, R., *Dreidimensionale Formkörper beliebiger Form und Verfahren zur Herstellung derselben*, B.D.D. PATENTAMT, Editor. 1993: Germany.
280. Schoenberger, A., *Technical Discussion re: Producing Epoxy Samples using EMB Technology*, J. Jones, Editor. 2010: Leicester.
281. Jacobs, H.O., S.A. Campbell, and M.G. Steward, *Approaching nanoxerography: The use of electrostatic forces to position nanoparticles with 100 nm scale resolution*. *Advanced Materials*, 2002. **14**(21): p. 1553-+.
282. Barry, C.R., et al., *Printing nanoparticle building blocks from the gas phase using nanoxerography*. *Applied Physics Letters*, 2003. **83**(26): p. 5527-5529.
283. Barry, C.R., et al., *Printing nanoparticles from the liquid and gas phases using nanoxerography*. *Nanotechnology*, 2003. **14**(10): p. 1057.
284. Barry, C.R., J. Gu, and H.O. Jacobs, *Charging Process and Coulomb-Force-Directed Printing of Nanoparticles with Sub-100-nm Lateral Resolution*. *Nano Letters*, 2005. **5**(10): p. 2078-2084.
285. Seemann, L., A. Stemmer, and N. Naujoks, *Selective deposition of functionalized nano-objects by nanoxerography*. *Microelectronic Engineering*, 2007. **84**(5-8): p. 1423-1426.
286. Jacobs, H.O. and C. Barry, *US Patent 7,232,771 Method and apparatus for depositing charge and/or nanoparticles*. 2007, United States Patent and Trademark Office.
287. Detig, R.H., *US Patent 7,094,627 Process for the manufacture of large area arrays of discrete components*. 2006, United States Patent and Trademark Office.
288. Bynum, D.K., *Automated manufacturing system using thin sections*, in *United States Patent 5,088,047*, U.S.P. Office, Editor. 1992: USA.
289. Priyadarshi, A., et al., *Manufacturing multi-material articulated plastic products using in-mold assembly*. *The International Journal of Advanced Manufacturing Technology*, 2007. **32**(3): p. 350-365.
290. Bynum, D.K., *Apparatus for Forming a Three-Dimensional Reproduction of an Object from Laminations*, in *United States Patent 5,127,037*. 1992: USA.

291. Grenda, E., *3D Laser Printing – The Next Generation of Rapid Prototyping Systems?*, in *AUTOFACT*. 1997: Detroit, MI.
292. Grenda, E.P., *US Patent 6,206,672 Apparatus of fabricating 3 dimensional objects by means of electrophotography, ionography or a similar process*. 2001, United States Patent and Trademark Office.
293. Cormier, D., et al. *Experiments In Layered Electro-Photographic Printing*. in *Solid Freeform Fabrication Proceedings, August, 2000*. 2000. Austin, Texas, USA.
294. Mahale, T.R., *Three Dimensional Electrophotographic Printing through Layered Manufacturing: An exploration into personal fabrication*, Masters of Science in *Industrial Engineering*. 2003, North Carolina State University. p. 154.
295. Karlsen, R. and J. Reitan. *Metal Printing - Development of a New Rapid Manufacturing Process for Metal and Ceramic Objects*. in *International Conference on Advanced Research in Virtual and Rapid Prototyping*. 2003. Leiria, Portugal.
296. Kolnes, Ø., et al. *Metal Printing Process - Challenges and Potentials*. in *Digital Fabrication 2005*. 2005. Baltimore, MD, USA.
297. Banerjee, S. and D.I. Wimpenny. *Rapid Manufacturing of Thermoplastic Parts by Laser Printing in International Conference on Polymers & Mould Innovations*. 2007. Ghent Belgium.
298. Jones, J.B. and D.I. Wimpenny. *Customised Rapid Manufactured Parts: Technology and case studies from the Custom-Fit project*. in *20th International Solid Freeform Fabrication Symposium*. 2009. Austin, TX, USA: University of Texas.
299. Banerjee, S. and D.I. Wimpenny, *Feasibility of Laser Printing based Rapid Manufacturing of 3D Plastic Parts [unpublished work in author's possession]*. 2008, De Montfort University. p. 22.
300. Kloppers, P. *EMB status update*. in *43rd ECCA Autumn Congress*. 2009. Brussels, Belgium.
301. Handels, J.W.H., et al., *Process for coating a substrate with a powder paint composition*, U.S.P.a.T. Office, Editor. 2002, DSM N.V., Michael Huber Munchen GmbH.
302. Kress, J. and Sis. *Powder coating using electromagnetic brush technology*. in *IS&T's NIP23 and Digital Fabrication 2007*. 2007. Society of Imaging Science and Technology.
303. Zobrist, B., *Technical Discussion re: Producing Epoxy Samples using EMB Technology*, J. Jones, Editor. 2010: Leicester.
304. Jones, J.B. and D.I. Wimpenny, *Envisiontec, Selective laser printing and Voxeljet*, in *Wohlers Report 2009*, T.T. Wohlers, Editor. 2009, Wohlers Associates Inc.: Fort Collins, CO, USA. p. 66-67, 75, 88.
305. Hanson, W.J., et al., *US Patent 2013/0077996 A1 Electrophotography-Based Additive Manufacturing System with Reciprocating Operation*. 2013, United States Patent and Trademark Office.
306. Hanson, W.J., et al., *US Patent 2013/0077997 A1 Electrophotography-Based Additive Manufacturing System with Transfer-Medium Service Loops*. 2013, United States Patent and Trademark Office.
307. Johnson, J.L., *Principles of Computer Automated Fabrication*. 1994, Irvine, CA, USA: Palatino Press. 156.
308. Benning, M.J. and K.W. Dalgarno. *The conceptualisation of a novel electrophotographic Rapid Prototyping system*. in *Postgraduate Conference 2009*. 2009. Newcastle University, Newcastle Upon Tyne, UK: Newcastle University.
309. Boivie, K., *Transfer and Part Thicknesses of Ceramic Printed by the MPP Process*, J.B. Jones, Editor. 2010: UK.

310. Zobrist, B., *Toner Technology 2 - Printer Technology*, in *Toner Technology Training*. 2009: Stone, UK.
311. CoorsTek, *CoorsTek Design standards and specifications for Thick Film ceramic substrates H0801 8510-1537 Rev B*. 2008, CoorsTek: Grand Junction, CO, USA.
312. Anderson, R., *Personal communication re: calibration and wiring of the JCI 140 Static monitor*, J.B. Jones, Editor. 2010: UK.
313. Weiss, D.S., *Correspondence re: Question about holding the OPC core at a negative voltage*, J.B. Jones, Editor. 2013: Coventry, UK.
314. ISO/ASTM, *ISO/ASTM 52921:2013(E) Standard Terminology for Additive Manufacturing—Coordinate Systems and Test Methodologies*. 2013, ISO/ASTM: West Conshohocken, PA, USA.
315. Thompson, S.P., *Fig 12 from Elementary Lessons in Electricity and Magnetism (modified for Wikipedia)*. 1881, New York: MacMillan.
316. Jones, J.B., *Technical Discussion: Selective Laser Printing Specimen, "Going for height" on 25 November 2008*, J. Jones, Editor. 2010: Coventry.
317. Teshigawara, T., H. Tachibana, and K. Terao, *Simulation of toner depositing process in Xerographic image studies*. Industry Applications, IEEE Transactions on, 1988. **24**(2): p. 232-237.
318. Righetti, M.C. and A. Munari, *Influence of branching on melting behavior and isothermal crystallization of poly(butylene terephthalate)*. Macromolecular Chemistry and Physics, 1997. **198**(2): p. 363-378.
319. Nadkarni, V.M., V.L. Shingankuli, and J.P. Jog, *Blends of thermoplastic polyesters with amorphous polyamide. I. Thermal and crystallization behavior*. Polymer Engineering & Science, 1988. **28**(20): p. 1326-1333.
320. Runt, J., et al., *Crystallization of poly(butylene terephthalate) and its blends with polyarylate*. Macromolecules, 1992. **25**(7): p. 1929-1934.
321. Schoenberger, A., *Industrial Laser Printer Training*, J. Jones, Editor. 2008: Alsdorf, Germany.
322. Lambert, P.M., *WO 2001088621 A1 Magnetic carrier particles*. 2001, Google Patents.
323. Saha, B.S., *US Patent 4,855,206 Rare earth containing magnetic carrier particles*. 1989, United States Patent and Trademark Office.
324. Powdertech, *Material Safety Data Sheet*. 2010, Powdertech: Kashiwa-shi, Japan
325. Kristoffersson, A. and E. Carlström, *Tape casting of alumina in water with an acrylic latex binder*. Journal of the European Ceramic Society, 1997. **17**(2-3): p. 289-297.
326. García, D.E., et al., *Fast firing of alumina*. Journal of the European Ceramic Society, 1995. **15**(10): p. 935-938.
327. Bocanegra-Bernal, M.H., et al., *Fracture toughness of an [alpha]-Al₂O₃ ceramic for joint prostheses under sinter and sinter-HIP conditions*. International Journal of Refractory Metals and Hard Materials, 2009. **27**(4): p. 722-728.
328. Xue, L.A. and I.W. Chen, *Low-Temperature Sintering of Alumina with Liquid-Forming Additives*. Journal of the American Ceramic Society, 1991. **74**(8): p. 2011-2013.
329. Heurtley, J.C., *US Patent 3,858,973 Methods of Thermoplastic Xerography and Apparatus Therefor*. 1975, United States Patent and Trademark Office.
330. Walkup, L.E., *US Patent 2,825,814 Xerographic image formation*. 1958, United States Patent and Trademark Office.
331. Urbach, J.C., *Thermoplastic hologram recording*, in *Holographic Recording Materials*, H. Smith, Editor. 1977, Springer Berlin Heidelberg. p. 161-207.
332. Heurtley, J.C., *Organized frost: a modulated noise-carrier electrophotographic system*. Appl Opt, 1969. **8 Suppl 1**: p. 137-41.
333. Bickmore, J., et al., *FROSTED PHOTOPLASTIC*. 1963, DTIC Document

334. Glenn, W.E., *US Patent 3,113,179 Method and apparatus for recording*. 1963, United States Patent and Trademark Office.
335. Goldberg, E.P., *US Patent 3,919,938 Permanent electrostatic master*. 1975, United States Patent and Trademark Office.
336. Huiskamp, T., et al., *Maskless Patterning by Pulsed-Power Plasma Printing*. Plasma Science, IEEE Transactions on, 2012. **40**(7): p. 1913-1925.
337. Noeske, M., et al., *Plasma jet treatment of five polymers at atmospheric pressure: surface modifications and the relevance for adhesion*. International Journal of Adhesion and Adhesives, 2004. **24**(2): p. 171-177.
338. France, R.M. and R.D. Short, *Plasma Treatment of Polymers: The Effects of Energy Transfer from an Argon Plasma on the Surface Chemistry of Polystyrene, and Polypropylene. A High-Energy Resolution X-ray Photoelectron Spectroscopy Study*. Langmuir, 1998. **14**(17): p. 4827-4835.
339. Jones, J.B. and G.J. Gibbons, *Additive Building*. 2012, WO Patent 2,012,164,015.
340. CLEVIOS, *CLEVIOS™ PH 1000 Preliminary Specification, Number PD-6119, Issue 0-23.07.2009*. 2009.
341. Meech Static Eliminators, *Model 977CM, Current Monitoring Pulsed DC Controller Manual 12.07.2009, Issue 1*. 2009.
342. Jones, J.B. and G.J. Gibbons, *Improved Electret Manufacture in PCT/EP2013/065694*. 2013.
343. National STEM Centre and the Institute of Physics, *Photoelectric Effect (Physics Demonstration Video)*. 2010.
344. Israelachvili, J.N., D.J. Mitchell, and B.W. Ninham, *Theory of self-assembly of hydrocarbon amphiphiles into micelles and bilayers*. J. Chem. Soc., Faraday Trans. 2, 1976. **72**: p. 1525-1568.
345. Ralston, O.C., *Practical applications of electrostatic phenomena to particulate matter*. American Institute of Electrical Engineers, Part I: Communication and Electronics, Transactions of the, 1956. **75**(2): p. 155-159.
346. Wise, L.G., *US Patent 3,723,274 Method of Electrocoating Using a Plowing Mercury Cathode*. 1973, United States Patent and Trademark Office.
347. Lemley, M.A., *Myth of the Sole Inventor*, The. Mich. L. Rev., 2011. **110**: p. 709.
348. Chenevey, J.L., *Buckyballs*. Potentials, IEEE, 1992. **11**(3): p. 49-51.
349. Paaajanen, M., J. Leikkala, and K. Kirjavainen, *ElectroMechanical Film (EMFi) — a new multipurpose electret material*. Sensors and Actuators A: Physical, 2000. **84**(1-2): p. 95-102.
350. Low, B.C., *Solar activity and the corona*. Solar Physics, 1996. **167**(1-2): p. 217-265.
351. Quarshie, R., et al., *Shaping our National Competency in Additive Manufacturing*. 2012, The Additive Manufacturing Special Interest Group for the Technology Strategy Board: UK.
352. Shi, Y., et al., *Effect of the properties of the polymer materials on the quality of selective laser sintering parts*. Proceedings of the Institution of Mechanical Engineers Part L-Journal of Materials-Design and Applications, 2004. **218**(L3): p. 247-252.
353. Yan, C., Y. Shi, and L. Hao, *Investigation into the Differences in the Selective Laser Sintering between Amorphous and Semi-crystalline Polymers*. International Polymer Processing, 2011. **26**(4): p. 416-423.
354. Zarringhalam, H., et al., *Effects of processing on microstructure and properties of SLS Nylon 12*. Materials Science and Engineering: A, 2006. **435-436**(0): p. 172-180.
355. Zarringhalam, H., C. Majewski, and N. Hopkinson, *Degree of particle melt in Nylon-12 selective laser-sintered parts*. Rapid Prototyping Journal, 2009. **15**(2): p. 126-132.

Annex: Related Publications by the Author

This annex includes the author's version of three conference publications with content that was developed as part of this research. They are included here a) to provide a brief synopsis of this work, b) for the convenience of the reader, and c) to show any excerpts included in this work in their original context as published. The copyright for all three has been signed over to the Society for Imaging Science and Technology.

[260] J. B. Jones, D. I. Wimpenny, G. J. Gibbons, and C. Sutcliffe, "Additive Manufacturing by Electrophotography: Challenges and Successes," in *IS&T's NIP26 and Digital Fabrication 2010*, Austin, Texas, 2010, pp. p. 549-553.

[244] J. B. Jones, G. J. Gibbons, and D. I. Wimpenny, "Transfer Methods toward Additive Manufacturing by Electrophotography," in *IS&T's NIP27 and Digital Fabrication 2011*, Minneapolis, Minnesota, USA, 2011, pp. 180-84.

[236] J. B. Jones, D. I. Wimpenny, and G. J. Gibbons, "The Influence of Residual Toner Charge on 3D Laser Printed Objects," in *IS&T's NIP28 and Digital Fabrication 2012*, Quebec City, Canada, 2012, pp. 327-331.

Note: Due to copyright restrictions, the papers listed here *may not be included in some versions of this work*.